

AD-A242 531



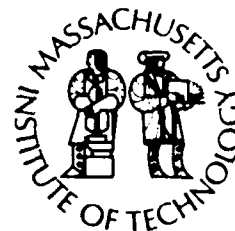
WHOI-89-29

①

Woods Hole Oceanographic Institution Massachusetts Institute of Technology



Joint Program
in Oceanography
and
Oceanographic Engineering



DOCTORAL DISSERTATION

Evolution of Icelandic Central Volcanoes: Evidence from the Austurhorn Plutonic and Vestmannaeyjar Volcanic Complexes

by

Tanya Helen Furman

September 1989

DISTRIBUTION STATEMENT A

Approved for public release;
Distribution Unlimited

WHOI-89-29

**Evolution of Icelandic Central Volcanoes:
Evidence from the Austurhorn Plutonic and
Vestmannaeyjar Volcanic Complexes**

by

Tanya Helen Furman

Woods Hole Oceanographic Institution
Woods Hole, Massachusetts 02543

and

The Massachusetts Institute of Technology
Cambridge, Massachusetts 02139

September 1989

Doctoral Dissertation

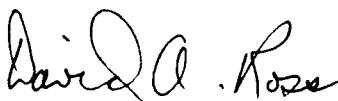
Funding was provided by the Office of Naval Research through the
Massachusetts Institute of Technology.

Reproduction in whole or in part is permitted for any purpose of the
United States Government. This thesis should be cited as:

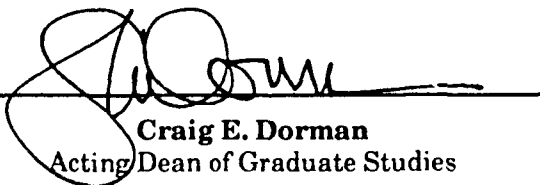
Tanya Helen Furman, 1989. Evolution of Icelandic Central Volcanoes: Evidence from the Austurhorn
Plutonic and Vestmannaeyjar Volcanic Complexes. Ph.D. Thesis. MIT/WHOI, WHOI-89-29.

Approved for publication; distribution unlimited.

Approved for Distribution:



David A. Ross, Chairman
Department of Geology & Geophysics



Craig E. Dorman
Acting Dean of Graduate Studies



91-14716

91 10 31 088

EVOLUTION OF ICELANDIC CENTRAL VOLCANOES:
EVIDENCE FROM THE AUSTURHORN PLUTONIC
AND VESTMANNAEYJAR VOLCANIC COMPLEXES

by

TANYA HELEN FURMAN

B.S.E., Princeton University, 1982

SUBMITTED IN PARTIAL FULFILLMENT OF THE
REQUIREMENTS FOR THE DEGREE OF
DOCTOR OF PHILOSOPHY

at the

MASSACHUSETTS INSTITUTE OF TECHNOLOGY
and the
WOODS HOLE OCEANOGRAPHIC INSTITUTION

February 1989

©Massachusetts Institute of Technology, 1989

Signature of author.....

Tanya Furman
Joint Program in Oceanography, Massachusetts Institute of
Technology and Woods Hole Oceanographic Institution and
Department of Earth, Atmospheric and Planetary Sciences,
Massachusetts Institute of Technology, February, 1989.

Certified by.....

Frank A. Fry
Thesis Supervisor

Certified by.....

Peter S. Meyer
Thesis Co-Supervisor

Accepted by.....

Marcia McNitt
Chairman, Joint Committee for Marine Geology and Geophysics,
Massachusetts Institute of Technology and Woods Hole
Oceanographic Institution

Accession For	
NTIS GRA&I	<input checked="" type="checkbox"/>
DTIC Tab	<input type="checkbox"/>
Unannounced	<input type="checkbox"/>
Justification	
By	
Distribution	
Availability Codes	
Dist	Avail and/or Special
A-1	

EVOLUTION OF ICELANDIC CENTRAL VOLCANOES: EVIDENCE FROM THE AUSTURHORN PLUTONIC AND VESTMANNAEYJAR VOLCANIC COMPLEXES

by

TANYA HELEN FURMAN

There are several aspects of Icelandic magmatism which are not predicted from its geographic position along the mid-Atlantic Ridge. Specifically, local occurrences of primitive or evolved alkalic lavas and abundant silicic magmas are uncommon in a mid-ocean ridge setting. The focus of this study is to use field, petrologic and geochemical data to understand the petrogenesis of these diverse lava types. Two areas have been investigated: the volcanic Vestmannaeyjar archipelago and the hypabyssal Austurhorn intrusive complex. Vestmannaeyjar is located at the tip of a transgressive ridge segment (the eastern neovolcanic zone); the most recent eruption in this area was Eldfell in 1973. Austurhorn is an evolved central volcano in southeastern Iceland which was active approximately 6-7 Ma and has been exhumed by glaciation. In both areas, the relative contributions of fractional crystallization and crustal melting to geochemical trends among cogenetic magmas have been assessed.

The Vestmannaeyjar archipelago is composed of alkalic lavas erupted at the southern end of the active Eastern Volcanic Zone. Recent eruptions include the most primitive (Surtsey) and evolved (Eldfell) compositions found in this area. Time-stratigraphic sample suites from both eruptions were studied to characterize the magmatic environment of Vestmannaeyjar. Compositional trends of lavas from the two eruptions are not consistent with fractionation in a near-surface environment, but rather with moderate pressure evolution of small magma batches. At Eldfell, mugearite lavas can be modeled by 30% closed system fractional crystallization of olivine + plagioclase + clinopyroxene + FeTi oxides from cogenetic parental hawaiite. The phase proportions are consistent with an experimentally determined moderate pressure (~8 kbar) cotectic in mildly alkaline systems (Mahood & Baker, 1986). The Surtsey lavas can be modeled by initial crystallization of orthopyroxene + clinopyroxene followed by removal of olivine + plagioclase + clinopyroxene + FeTi oxides. The presence of clinopyroxene with ~8 wt% Al_2O_3 in xenoliths from Surtsey lavas supports a moderate pressure fractionation scenario. Small variations in radiogenic isotopic ratios require limited source heterogeneity or some component of open system behavior. The alkaline nature of Vestmannaeyjar lavas is a primary feature of the parental basalt in this area, not the result of assimilation of lower crustal melts (cf. Oskarsson et al., 1985; Steinthorsson et al., 1985). Magmagenesis in the Vestmannaeyjar propagating rift tip involves small batches of mantle-derived melts which undergo fractionation in isolated pockets at various depths near the base of the lithosphere beneath southern Iceland.

The Austurhorn intrusion is a hypabyssal complex in southeastern Iceland which represents the exhumed remains of an evolved Tertiary central volcano. Field relations at Austurhorn provide convincing evidence for the existence of shallow Icelandic magma chambers, and allow documentation of the physical processes which accompany volcanic evolution. Initial magmatic activity at Austurhorn was basaltic, with a shallow chamber preserved today as a modally layered gabbro body. Felsic magmas were emplaced from below into the cooling gabbro and adjacent crust. Intrusion of felsic magmas into basalts with varying degrees of solidification produced an extensive net veined complex. Felsic replenishment was infrequent enough that a single large convecting felsic body did not develop. Individual felsic units identified in the field generally form small (<500 m extent) sills. Mafic liquids were available throughout the history of the Austurhorn system; the final phase of basalt intrusion forms a NE-trending dike swarm.

Investigation of mineralogic and geochemical trends among contemporaneous, compositionally diverse liquids from Austurhorn provides new insight into the genesis of evolved basalts and rhyolites at Icelandic central volcanoes. Mafic and felsic samples have comparable ranges in incompatible trace element ratios (Ba/La, La/Nb) and Sr- and Pb-isotopes (O'Nions & Pankhurst, 1973; B. Hanan, pers. commun., 1988) suggesting derivation from a common mantle source. The Austurhorn suite is strongly bimodal, with maximum MgO content 7.8 wt% and a well defined "Daly gap" between 3.5-1.5 wt% MgO. Austurhorn basalts are dominantly transitional tholeiitic, and the associated felsic rocks are metaluminous to mildly peralkaline. The distinctive basalt geochemistry and abundance of silicic rocks at Austurhorn are controlled by the crustal structure of an immature rift. A proposed Tertiary rift axis in central Iceland (along which Austurhorn developed) is parallel to the modern western and eastern volcanic zones in southern Iceland.

The principle finding of this study is that major and trace element systematics within Austurhorn basaltic and silicic sequences are consistent with progressive fractional crystallization of the observed minerals. Quartz normative basalts can be derived from mildly nepheline normative parental liquid (7.8 wt% MgO) by extensive low pressure crystallization. The inferred crystallizing assemblage of olivine, augite, plagioclase, magnetite and ilmenite is consistent with modal mineralogy of the Hvalnesfjall gabbro. The cumulus mineralogy of leucocratic gabbros gives important evidence for fractionation processes in a compositional interval not represented by dikes and sills (i.e., the "Daly gap"). Diversity among the mafic dikes reflects several additional factors: (1) crystallization under conditions of variable oxygen fugacity, (2) separate mantle melting events generating a range of Ce/Yb ratios, (3) contamination of a small number of dikes at depth, presumably by interaction with felsic magmas. Major and trace element trends among most felsic samples can be modeled by fractionation of the observed mineral phases: plagioclase, K-feldspar, clinopyroxene, magnetite, ilmenite, apatite. It is possible that crustal melting augments fractional crystallization in producing Icelandic rhyolites. However, most Austurhorn felsic samples are unlike liquids derived by progressive melting of hydrated basalts. Specifically, the Zr, Sr, La systematics of the felsic rocks are inconsistent with melting of a plagioclase- and amphibole-rich source. One felsic dike with petrographic evidence for in situ anatexis has anomalous trace element abundances and an unusually high proportion of ^{206}Pb is interpreted as a melt of an evolved substrate.

Thesis supervisor: F.A. Frey

Thesis co-supervisor: P.S. Meyer

Acknowledgements

I am deeply indebted to many individuals without whose help and support this thesis would never have been written. Most important among these is Fred Frey, who patiently shared with me his approach and insight into matters both scientific and human. His efforts to teach me both rigor and tact have made me a far better scientist and person. I am particularly grateful for his calm, steadfast faith in me during the final stages of finishing and moving away.

Peter Meyer's friendship and encouragement enabled the Austurhorn project to become a reality. His willingness to talk over ideas at all hours of day or night helped me get through some very rough times. I am very grateful to Henry Dick for keeping me fed and entertained, and for reminding me that anything is possible if your dreams are large enough. Tim Grove introduced me to the joys and struggles of teaching, one of the many pressures, responsibilities and rewards of academia. Sigurdur Steinthorsson first encouraged me to work at Austurhorn - I doubt if either of us guessed it would take so long or go so far.

Field work in Iceland was made possible by permission from Rannsoknarrad Ríkisins during and after my tenure as a Fulbright fellow in Reykjavik. Invaluable logistical support and friendship were given by Thorger Kristjansson and his wife Asa in Hofn, and by Benedikt Stefansson and his wife Valgerdur at Hvalnes. Anna Lisa Gudmundsdottir, Vincent Salters, Dan Tormey and Tom Juster accompanied me into the field; only they and I know how much of a struggle it was at times. Their contributions to this study are much appreciated. Funding for field work in Iceland was provided by the American Scandinavian Foundation, Sigma Xi, the Explorers Club, the Geological Society of America and the SRFC.

Sveinn Jakobsson kindly shared with us samples and unpublished data from the Vestmannaeyjar archipelago as well as much appreciated insight into magmatic processes throughout Iceland. Kye-Hun Park and Barry Hanan obtained several dozen isotopic analyses on Vestmannaeyjar and Austurhorn samples and generously made them available for this study.

Pilalamarri Ila enlightened me in the use of neutron activation equipment and the importance of karma in making machines function properly. Steve Recca, Mike Rhodes and Joel Sparks introduced me to the electron microprobe and XRF, respectively, and did their collective best to help me overcome my fear of computers. Margaret Sulanowska patiently taught me about drafting, CHN analysis and efficiency. I am thankful to these people for their time and expertise.

There are many special friends who encouraged me, suffered through interminable drafts of the thesis and, most importantly, believed in me even when I had lost faith in myself. These include: my officemates Don Hickmott and Kevin Johnson, Ro Kinzler, Song Yan, David Graham, Roger Burns, Peter Tilke, Karen Bartles, Gustaf Nielsson, Joanie McKewen and, especially, Jim Knapp. Thanks also to Bill Odum and the students in EVSC 480 at the University of Virginia for shining a light near the end of this tunnel.

Finally, many thanks are due my family for their love and support as I pursued this dream. My sister, Lydia, and her family helped me adjust to Boston and made it seem like a home. My parents - Robert and Erna Furman - introduced me to volcanoes (and Iceland) at a very young and impressionable age and have stood by me throughout the trials of my "have hammer, will travel" graduate career.



“Þitunð er enn eða kvæð?”

-Þöluspa’

Table of Contents

Abstract	1
Acknowledgements	3
Frontispiece	4
Table of Contents	5
List of Figures	8
List of Tables	10
 Chapter I: Introduction to Icelandic Volcanism	 11
 Chapter II: Petrogenesis of mildly alkaline lavas from Vestmannaeyjar	 25
2.1 Sample collection and description	28
2.2 Analytical techniques	31
2.3 Results	31
2.3.1 Major and trace element geochemistry	31
2.3.2 Radiogenic isotope systematics	38
2.3.3 Oxygen isotope systematics	48
2.4 Discussion	48
2.4.1 Quantitative approach to modeling	48
2.4.2 Evolution of the Eldfell lava series	53
2.4.3 Evolution of the Surtsey lava series	63
2.4.4 Crustal origin of alkali basalts?	77
2.4.5 Melting and melt extraction at depth	81
2.4.6 Estimating the degree of mantle melting	89
2.5 Summary and conclusions	91
 Chapter III: Magmatic evolution of the Austurhorn central volcano	 95
3.1 Tectonic and geologic setting	99
3.2 Field observations: Major intrusive units	103
3.2.1 Previous work	103
3.2.2 Hvalnesfjall gabbro	108
3.2.3 Hvasshjalli granophyre	126
3.2.4 Felsic dikes and sills	133
3.2.5 Basaltic dikes and sills	134
3.2.6 The net veined complex	137
3.2.7 Intermediate, hybrid and commingled rocks	151
3.3 Evolution of the Austurhorn magmatic system	154
3.3.1 Summary of intrusive activity	154
3.3.2 Stage 1: Basaltic differentiation in the shallow crust	158
3.3.3 Chamber isolation: Transitional stage	163
3.3.4 Stage 2: Abundant silicic magmatism	165
3.3.5 Development of the net veined complex	167
3.4 Implications for Tertiary rift zone systematics	170
3.5 Conclusions	174

Chapter IV: Petrogenesis of evolved basalts and silicic magmas at Austurhorn	176
4.1 Geologic background	181
4.2 Analytical techniques	183
4.3 Mineral chemistry	191
4.3.1 Olivine	191
4.3.2 Clinopyroxene	198
4.3.3 Low-Ca pyroxene	201
4.3.4 Amphibole	202
4.3.5 Plagioclase feldspar	203
4.3.6 Potassium feldspar	209
4.3.7 Fe-Ti oxides	209
4.4 Major and trace element geochemistry	209
4.4.1 Sample selection and nomenclature	209
4.4.2 Major element geochemistry	213
4.4.3 Rare earth element geochemistry	221
4.4.4 Trace element geochemistry	227
4.4.5 The ratios Ba/La, La/Nb and P/Ce	232
4.4.6 The ratios Zr/Y and Zr/Hf	241
4.4.7 Radiogenic isotopic data	244
4.4.8 Geochemistry of rhyolite f-61	248
4.5 Distinctive basic compositional groups	252
4.5.1 Mafic pillows	252
4.5.2 Alkaline dikes	257
4.6 Estimates of intensive parameters	260
4.7 Approach to petrogenetic modeling	269
4.8 Petrogenesis of Austurhorn basalts	272
4.8.1 Mafic pillows	272
4.8.2 Alkaline dikes	281
4.8.3 Transitional tholeiitic dikes	286
4.9 Petrogenesis of Austurhorn felsic liquids	291
4.9.1 Models involving fractional crystallization	292
4.9.2 The case against crustal anatexis	298
4.9.3 Petrogenesis of rhyolite f-61	307
4.9.4 Bridging the Daly gap	307
4.10 Conclusions	309
 Chapter V: Mature volcanoes, immature rifts	 313
5.1 Mantle heterogeneity beneath Iceland: Fact or artifact?	315
5.1.1 Oxygen isotope ratios of neovolcanic basalts	316
5.1.2 Oxygen-helium relationships	318
5.1.3 Sr-Nd-Pb relationships	323
5.1.4 Summary of observations	326
5.2 Crustal contamination and overprinting	326
5.3 Speculations: Crustal controls on basalt geochemistry	329
5.3.1 Major element evidence	329
5.3.2 Trace element effects	332
5.4 Silicic magmatism	333
5.5 Nota bene	335

References	336
Appendix I: Representative microprobe analyses of Austurhorn minerals	354
Appendix II: Replicate analyses	368
Appendix III: Petrographic descriptions of representative Austurhorn samples	370
Appendix IV: Temperature and oxygen fugacity for Icelandic samples	372

List of Figures

1.1	Physiography of the north Atlantic	14
1.2	Neovolcanic zones of Iceland	15
1.3	$^{208}\text{Pb}/^{204}\text{Pb}$ vs. $^{206}\text{Pb}/^{204}\text{Pb}$ of Icelandic volcanic centers	18
1.4	Index map of Vestmannaeyjar	21
1.5	Geology of the Austurhorn intrusion	23
2.1	Neovolcanic zones of Iceland	27
2.2	Map of the Vestmannaeyjar archipelago	29
2.3	Lava compositions through time for Eldfell and Surtsey eruptions	30
2.4	Alkalis vs. silica for Vestmannaeyjar lavas	36
2.5	Major element oxide variation diagram	37
2.6	Chondrite-normalized REE patterns	39
2.7a	La/Sm vs. MgO	40
2.7b	La/Yb vs. MgO	41
2.8	Trace element variation diagram	42
2.9	$^{87}\text{Sr}/^{86}\text{Sr}$ vs. La/Sm	46
2.10a	$^{143}\text{Nd}/^{144}\text{Nd}$ vs. $^{87}\text{Sr}/^{86}\text{Sr}$	46
2.10b	$^{208}\text{Pb}/^{204}\text{Pb}$ vs. $^{206}\text{Pb}/^{204}\text{Pb}$	47
2.11	Rb and $\delta^{18}\text{O}$ vs. MgO	49
2.12	Fractional crystallization model for Eldfell	54
2.13	Model REE behavior at Eldfell	58
2.14	Nepheline-olivine-clinopyroxene projection	60
2.15	Schematic crustal cross section beneath Vestmannaeyjar	62
2.16a	CMAS projection from plagioclase	65
2.16b	CMAS projection from clinopyroxene	67
2.17	Model REE behavior at Surtsey	75
2.18	$^{143}\text{Nd}/^{144}\text{Nd}$ vs. Sm/Nd	80
2.19	Mantle melting model: FeO and MgO	83
2.20	Mantle melting model: Projected data	85
3.1	Tertiary intrusions in southeastern Iceland	97
3.2	Physiography of the Austurhorn area	100
3.3	Geology of the Austurhorn area	104
3.4	Map of the net veined complex	106
3.5	Features of Hvalnesfjall gabbro	114
3.6a	Composite diagram of clinopyroxene data	117
3.6b	Composite diagram of feldspar data	118
3.7	Modal mineralogy of Hvalnesfjall gabbro	119
3.8	Modal layering in Hvalnesfjall gabbro	121
3.9	Pegmatoidal pocket in hand sample and thin section	123
3.10	View of Hvasshjalli	127
3.11	Petrographic features of Austurhorn felsic rocks	130
3.12	Poles to dike trends	135
3.13	MgO content of Austurhorn samples	136
3.14	Type 2 granophyre	141
3.15	Mafic pillow from the net veined complex	144
3.16	Petrographic features of Austurhorn mafic pillows	146
3.17	Clasts in granophyre	149
3.18	Planar felsic veins in diabase	152

3.19	Evolution of the magmatic system	156
3.20	Proposed crustal structure beneath Austurhorn	159
3.21	Covariations in plagioclase and clinopyroxene compositions	161
3.22	Calculated densities of liquids and cumulates	162
3.23	Proposed evolution of Icelandic rift zones	171
4.1	Simplified geologic map of the Austurhorn intrusive complex	178
4.2	Sample locality map	193
4.3	Clinopyroxene and olivine compositions (by sample and rock type)	194
4.4	Composite diagram of clinopyroxene data	199
4.5	Plagioclase compositions (by sample and rock type)	204
4.6	Composite diagram of feldspar data	207
4.7	Alkalis vs. silica for Austurhorn samples	211
4.8	Major element oxide variation diagram	214
4.9	Trace element variation diagram	217
4.10	Chondrite-normalized REE data for Austurhorn basalts	222
4.11	La/Sm and Ce/Yb vs. MgO	223
4.12	Chondrite-normalized REE data for Austurhorn felsic rocks	225
4.13	Eu/Eu* vs. Sr	226
4.14	P ₂ O ₅ , La/Sm and Zr vs. La for felsic samples	228
4.15a	La vs. MgO for mafic pillows, dikes and gabbro samples	229
4.15b	Chondrite-normalized REE data for Hvalnesfjall gabbro	230
4.16	Trace element variation diagram for gabbros	233
4.17	Histograms of incompatible element ratios	239
4.18	Zr/Hf and Zr/Y vs. La	242
4.19	Zr/Y vs. Sc for basalts and gabbros	243
4.20	Secular variations in La/Sm and ⁸⁷ Sr/ ⁸⁶ Sr in eastern Iceland	245
4.21	Secular variation in radiogenic Pb in eastern Iceland	247
4.22a	²⁰⁸ Pb/ ²⁰⁴ Pb vs. ²⁰⁶ Pb/ ²⁰⁴ Pb	249
4.22b	Relative proportions of ²⁰⁶ Pb, ²⁰⁷ Pb and ²⁰⁸ Pb	250
4.23a	Projection from plagioclase onto olivine-clinopyroxene-quartz	254
4.23b	Projection from clinopyroxene onto olivine-plagioclase-quartz	255
4.23c	Pseudoliquidus projections for Thingmuli data	256
4.24	Extended Coryell-Masuda diagram	259
4.25	Nepheline-olivine-clinopyroxene projection	262
4.26	Temperature vs. oxygen fugacity	263
4.27	Evaluation of Mg/Mn equilibrium in Fe-Ti oxide pairs	266
4.28	TiO ₂ and FeO* Vs. MgO	267
4.29	Demonstration of elevated P ₂ O ₅ /Hf in alkali-rich dikes	282
4.30	Ce/Yb vs. Ce for Austurhorn samples	290
4.31	Quartz-albite-orthoclase projection of felsic rock data	293
4.32	Eu/Eu* vs. SiO ₂ in felsic rocks	294
4.34	Trace element systematics in melts of hydrothermally altered basalt	304
5.1	Location maps of Iceland and Jan Mayen	320
5.2	Paired oxygen and helium analyses of Icelandic samples	322
5.3	Sr-Nd-Pb relationships among Icelandic samples	324
5.4	Schematic crustal cross section beneath a flank zone volcano	331

List of Tables

2.1	Accuracy, precision and interlaboratory calibration	32
2.2	Major and trace element analyses	33
2.3	Calculation of mineral compositions	52
2.4	Fractionation model for Eldfell lavas	55
2.5	Evaluation of Eldfell model with trace elements	57
2.6	Inverse model for fractionation of Surtsey lavas	69
2.7	Elaluation of inverse model with trace elements	72
2.8	Forward model for fractionation of Surtsey lavas	73
2.9	Evaluation of forward model with trace elements	74
	Appendix	93
3.1	Representative plagioclase analyses	109
3.2	Representative clinopyroxene analyses	111
3.3	Representative olivine analyses	113
3.4	Representative amphibole analyses	129
3.5	Felsic units of the net veined complex	140
3.6	Estimates of intercumulus liquid in gabbro samples	164
4.1	Major and trace element analyses	184
4.2	Pb isotopes in Austurhorn samples	192
4.3	Normative mineralogy of mafic Austurhorn samples	212
4.4	Representative modal analyses	236
4.5	Geochemical characteristics of selected Icelandic basalts	258
4.6	Calculation of mineral compositions	271
4.7	Fractionation model for mafic pillow samples	274
4.8	Experimental and calculated phase assemblages	275
4.9	Partition coefficients used in trace element modeling	277
4.10	Evaluation of basalt fractionation model with trace elements	279
4.11	Fractionation model for mafic dikes	287
4.12	Fractionation model for felsic liquids	296
5.1	Oxygen and helium isotope ratios	317
5.2	Bulk assimilation calculation	328

CHAPTER 1

INTRODUCTION TO ICELANDIC VOLCANISM

Iceland is a prominent feature of the north Atlantic, where it forms an anomalously elevated portion of the mid-Atlantic Ridge [MAR]. It has been the subject of detailed field, geophysical and geologic investigation for over a hundred years, yet its origin and evolution are not well understood. The eruptive products have historically been classified as part of the Tertiary Brito-Arctic or Thulean Province, which encompasses the recent volcanic portions of Greenland, Scotland and Britain. Within the tectonic framework of seafloor spreading, Iceland is located at the intersection of the MAR and the aseismic Greenland-Faeroe Ridge [GFR], where Eocene basalts record earlier activity of the Iceland mantle plume (figure 1.1). Both the MAR and the GFR constitute linear topographic highs; their intersection contributes to the anomalous regional elevation profile of the Iceland plateau. The thickness of the Icelandic crust, up to three times that of normal oceanic lithosphere, also reflects interaction of a "hot spot" or mantle plume with the slowly spreading MAR. Beneath Iceland the mantle-derived magma supply is greater than can be accommodated by the axial spreading velocity, resulting in high volcanic productivity and a thick elevated crustal section.

The MAR crosses Iceland in a complex fashion, forming two parallel rift zones trending NE-SW in southern Iceland and a single spreading axis trending N-S in the north (figure 1.1). Volcanic activity has occurred continuously within these zones since the last magnetic reversal (~700,000 yrs; Cox, 1969) with post-glacial lavas preserved for the past 10,000 years. The structure of the neovolcanic rift zones in Iceland is one of discrete eruptive centers, rather than a continuous zone of extrusion (Jakobsson, 1972). Each volcanic system is composed of a basaltic fissure swarm ~10 km wide and up to 100 km long; individual swarms are arranged en echelon when their trend does not parallel that of the rift zones (figure 1.2; Jakobsson, 1972; Saemundsson, 1974). Localized volcanic constructs, known as central volcanoes, occur within many fissure swarms. They are the only vents for intermediate and acid lavas, and often develop calderas following explosive eruptions (e.g., Askja, Torfajokull, figure 1.2). Central

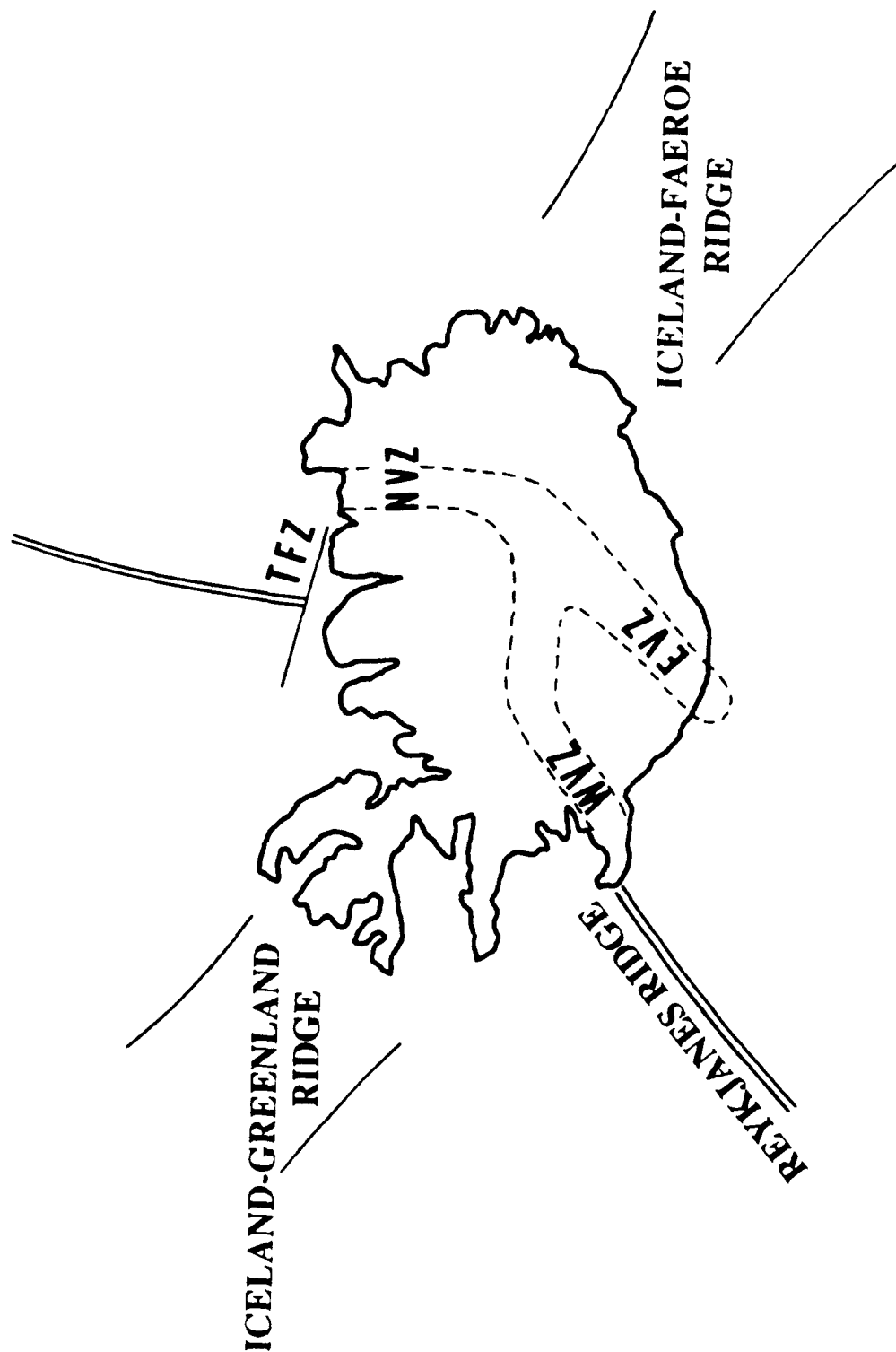


Figure 1.1

Physiography of the Iceland area, north Atlantic. The mid-Atlantic Ridge, represented by the Reykjanes Ridge south of Iceland, has two parallel branches in southern Iceland [WVZ, EVZ] and a single axis in the north [NVZ]. The ridge is offset by the Tjornes Fracture Zone [TFZ] off the coast of northern Iceland. The location of the western and eastern segments of the Greenland-Faeroe Ridge are indicated schematically using the bathymetric data of Talwani & Eldholm (1976).

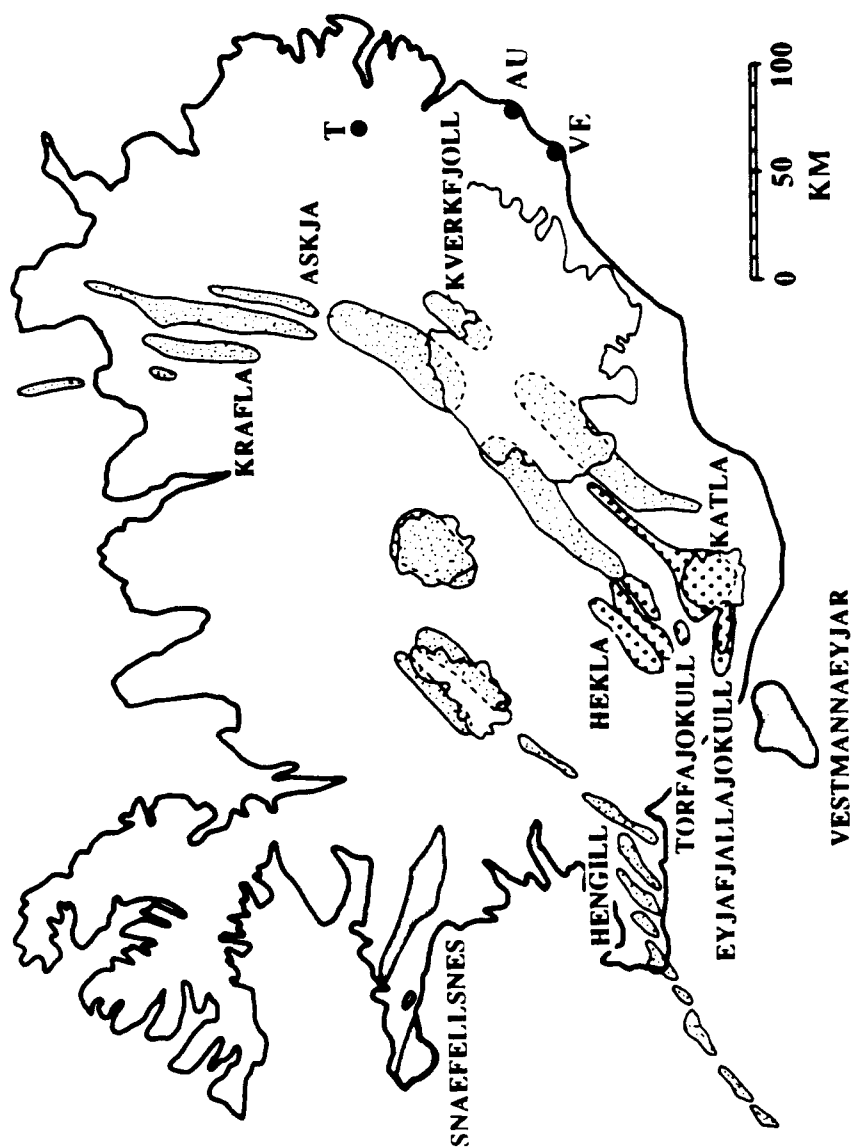


Figure 1.2

The neovolcanic zones are comprised of individual basalt fissure swarms, drawn here after Jakobsson (1979). Stippled regions (e.g., Krafla, Askja, Kverkfjoll, Hengill) are tholeiitic; triangle-patterned areas (e.g., Hekla, Katla, Torfajokull, Eyjafjallajokull) are transitional tholeiitic, often with abundant FeTi-rich basalts and silicic lavas; shaded areas (Vestmannaeypjar, Snæfellsnes) are alkalic. In eastern Iceland, the intrusive complexes Austurhorn (AU) and Vesturhorn (VE) represent the exhumed magma chambers of 6-7 Ma volcanoes geochemically analogous to modern transitional tholeiitic centers. Thingmuli (T) is a ~9 Ma tholeiitic central volcano.

volcanoes form topographic highs during peak eruptive activity but are buried in time by flood basalts from neighboring fissure swarms. Detailed mapping of the Tertiary lava pile in eastern Iceland indicates this style of volcanism has dominated for the past ~16 Ma (Walker, 1960, 1963, 1974; Gibson & Piper, 1972). Many Tertiary sections are deeply dissected by glaciation, revealing intrusive cores of the extinct central volcanoes and their fissure swarms (e.g., Walker, 1963).

Within Iceland, typical mid-ocean ridge [MOR] volcanism is overprinted by both mantle and crustal influences and processes. It is widely accepted that the Iceland mantle plume, which supplies this region with copious basalt magmas, is currently located near Kverkfjoll in the center of the country (e.g., Vink, 1984; figure 1.2). Plume material is geochemically distinct from the mantle source of normal MORB: it is rich in incompatible and volatile elements (e.g., K_2O , light rare earth elements, 3He) as well as radiogenic Sr and Pb and is relatively depleted in radiogenic Nd (Hart et al., 1973; Sun et al., 1975; Kurz et al., 1985). The geochemical effect of the plume (as evidenced by La/Sm ratios and He, Sr, Pb isotopes) is apparent throughout Iceland's neovolcanic zones but diminishes gradually to the south along the Reykjanes Ridge and ends abruptly at the Tjornes Fracture Zone to the north (figure 1.1; Schilling et al., 1983).

The nature of geochemical heterogeneities in the sub-Icelandic mantle is not well understood, and no single model has accounted for all extant trace element and isotopic data. Zindler et al (1979) noted correlations between rare earth element abundances and Sr- and Nd-isotopes in picritic and tholeiitic basalts from the Reykjanes Peninsula and interpreted them as evidence for progressive melting of a geochemically layered mantle. Wood (1981) interpreted geochemical variations within the Reykjanes Peninsula to indicate melting of a veined mantle diapir. In this model, a homogeneous depleted mantle source contains isotopically distinct veins rich in large element lithophile elements. Differential melting of veins and host can lead to variable La/Sm and Sr- and

Nd-isotopic ratios. More recently, Hanan & Schilling (1986, 1987) documented secular variations in Pb-isotopic compositions of the Tertiary flood basalt sequences which do not correlate uniformly with temporal patterns in La/Sm or Sr-isotopes of the same samples (O'Nions & Pankhurst, 1973). These data require the mantle source beneath Iceland to contain at least three isotopically distinct components (Langmuir et al., 1978; Hanan & Schilling, 1987), not strictly a binary mix of normal MORB and plume-type mantle. The range of Pb-isotopic ratios represented by the Tertiary basalts is also found today within the eastern neovolcanic zone (figure 1.3; Park et al., in preparation).

Superposed on these isotopic variations are regional gradients in magma geochemistry which cannot be attributed to mantle processes alone. The northern [NVZ] and southwestern neovolcanic zones [WVZ] are characterized by tholeiitic basalt volcanism with sparse occurrences of silicic lavas (e.g., Hengill, Askja, Krafla, figure 1.2). In contrast, basalts of the eastern neovolcanic zone [EVZ] become progressively alkali-rich to the south away from central Iceland. Tholeiitic basalts are erupted at Grimsvotn, but transitional tholeiitic and FeTi-rich lavas dominate at Katla, Eyjafjallajokull and Hekla, and offshore in the Vestmannaeyjar archipelago all lavas are undersaturated with respect to silica (figure 1.2; Jakobsson, 1972, 1979). Evolved (quartz-normative) basalts and silicic rocks are abundant in central volcanoes of transitional tholeiitic affinity; at Torfajokull rhyolites comprise ~90 vol% of all extrusives.

These variations in basalt chemistry are linked to thermal and structural differences between active rifting segments. The NVZ and WVZ are characterized by a thin crust (8-10 km; Palmason, 1971; Gebrande et al., 1980), high heat flow (up to 160°C/km; Palmason, 1973; Palmason et al., 1979) and well developed extensional features including fissures and fault grabens. In the EVZ, a thicker crust (20-30 km; Palmason, 1971; Gebrande et al., 1980) and lower regional heat flow (~60°C/km; Palmason, 1973; Palmason et al., 1979) are not associated with major fissures or basins.

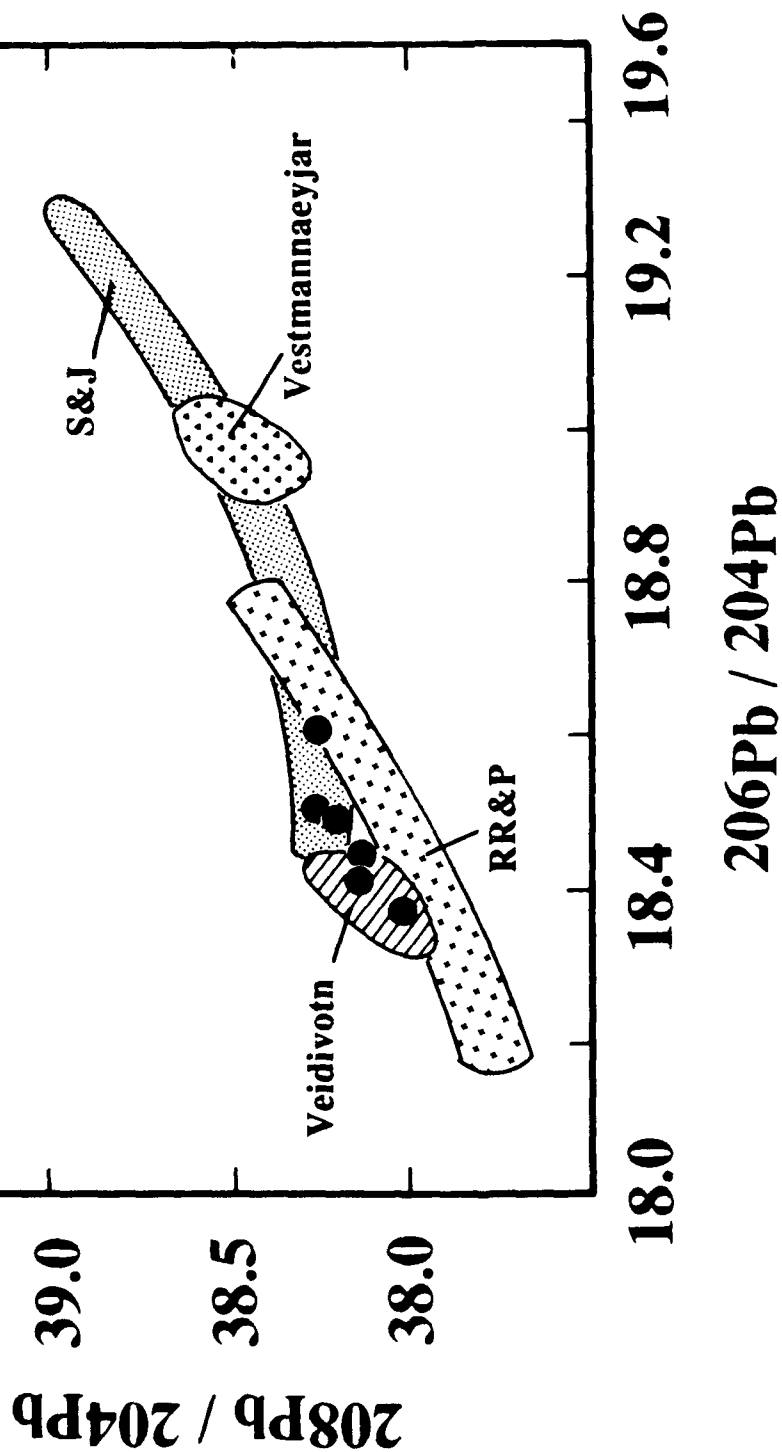


Figure 1.3 Individual Icelandic volcanic centers show restricted ranges in Pb isotopes. Shown here are fields for tholeiitic lavas from Veidivotn (diagonally ruled), alkalic lavas from Vestmannaeyjar (triangle pattern), and mafic and felsic intrusives from Austurhorn (filled circles). The field labeled S&J indicates variation of Pb isotope data in neovolcanic basalts from central and northern Iceland (Sun & Jahn, 1975). Samples from the Reykjanes Ridge and Peninsula (RR&P; Sun et al., 1979) become less radiogenic with increasing distance south of Iceland.

The depth and geometry of differentiating magma bodies also differs between the two neovolcanic zones. Magnetotelluric evidence indicates a zone of partial melt at depths of 8-10 km beneath the mature Reykjanes Ridge and up to 20-30 km beneath the immature EVZ (Beblo & Bjornsson, 1978, 1980; Eysteinsson & Hermance, 1985).

Recent syntheses by Oskarsson et al (1982, 1985) and Meyer et al (1985) have incorporated dynamic aspects of crust-mantle interaction into comprehensive models linking eruptive geochemistry and rift zone evolution. Briefly, the model of Oskarsson and co-workers (1982, 1985; Steinthorsson et al., 1985; Hemond et al., 1987) requires a single parental olivine tholeiite beneath all of Iceland, and attributes variations in lava chemistry to modification of this basalt by melts produced within the hydrothermally altered crust. In contrast, the work of Meyer et al (1985) suggests that geochemically distinct basalts reflect different degrees and depths of mantle melting, followed by crystal fractionation and magma mixing in crustal chambers. Proponents of both models agree that the EVZ displays transgressive volcanism, that is, the propagation of an axial rift segment southward into thick lithosphere.

Two fundamental questions remain, and provide the impetus for the present study. In both cases, the issue of concern is the relative roles of fractional crystallization and crustal assimilation in generating the erupted magmas. The first problem is the origin of alkali basalts, found only in Vestmannaeyjar and the Snaefellsnes peninsula (figure 1.2). Investigations by Sigurdsson (1970) and O'Nions & Gronvold (1973) attributed the alkalic liquids to low degrees of mantle melting at depths greater than those required for MORB volcanism. More recently, Oskarsson et al (1982) and Steinthorsson et al (1985) suggest the alkali basalts contain a nepheline-normative component generated by melting of kaersutitic amphibole at 12-15 km depth within the thickened lava pile. Steinthorsson et al (1985) point out geochemical differences between the two alkalic areas (e.g., Snaefellsnes basalts are enriched in K_2O and radiogenic Sr relative to Vestmannaeyjar lavas) but conclude that contaminated olivine

tholeiites are erupted in both locations. Studies of Icelandic alkalic volcanism have heretofore been hampered by a lack of geochemical data on appropriate sample suites, and these petrogenetic scenarios remain somewhat speculative.

A second focus of this study is the origin of evolved basalts and silicic magmas in central volcanoes. The occurrence of granophyre in southeastern Iceland was noted by Bunsen (1851) in the mid-nineteenth century and has remained enigmatic since that time. Carmichael's (1964) investigation of the Thingmuli central volcano included the first geochemical treatment of this question; he concluded that rhyolites could be derived by extensive fractional crystallization of associated basalts. Subsequent studies by Wood (1978) in eastern Iceland and Sigurdsson & Sparks (1981) at Askja concur with Carmichael's initial result. Isotopic investigation of neovolcanic rhyolites, however, led O'Nions & Gronvold (1973) to suggest that crustal melting was involved in the production of silicic magmas. This work demonstrated that recent rhyolites were sometimes enriched in radiogenic Sr relative to spatially associated basalts. In contrast, mafic and felsic samples from Tertiary centers show no systematic differences in Sr-isotopes (O'Nions & Pankhurst, 1973). Evolved neovolcanic lavas enriched in radiogenic Sr and depleted in ^{18}O (Hemond et al., 1987; Gunnarsson & Marsh, 1988; Gunnarsson et al., 1988) indicate that a crustal or meteoric component influences magma chemistry. In most cases, however, the source, nature and amount of contamination are unclear.

The present study was undertaken to evaluate extant models of rift zone evolution through detailed petrogenetic investigation of two volcanic centers which represent process endmembers in Icelandic magmatism. The first volcanic system is the Vestmannaeyjar archipelago, where alkali basalts are generated beneath thickened lithosphere at the tip of the transgressive EVZ (figure 1.2). Postglacial volcanism in Vestmannaeyjar has generated numerous island and submarine ridges; historic activity includes the eruptions of Surtsey (1963-1967) and Eldfell (1973). There is no evidence for a shallow magma reservoir in this area, although the prominence of Heimaey (figure

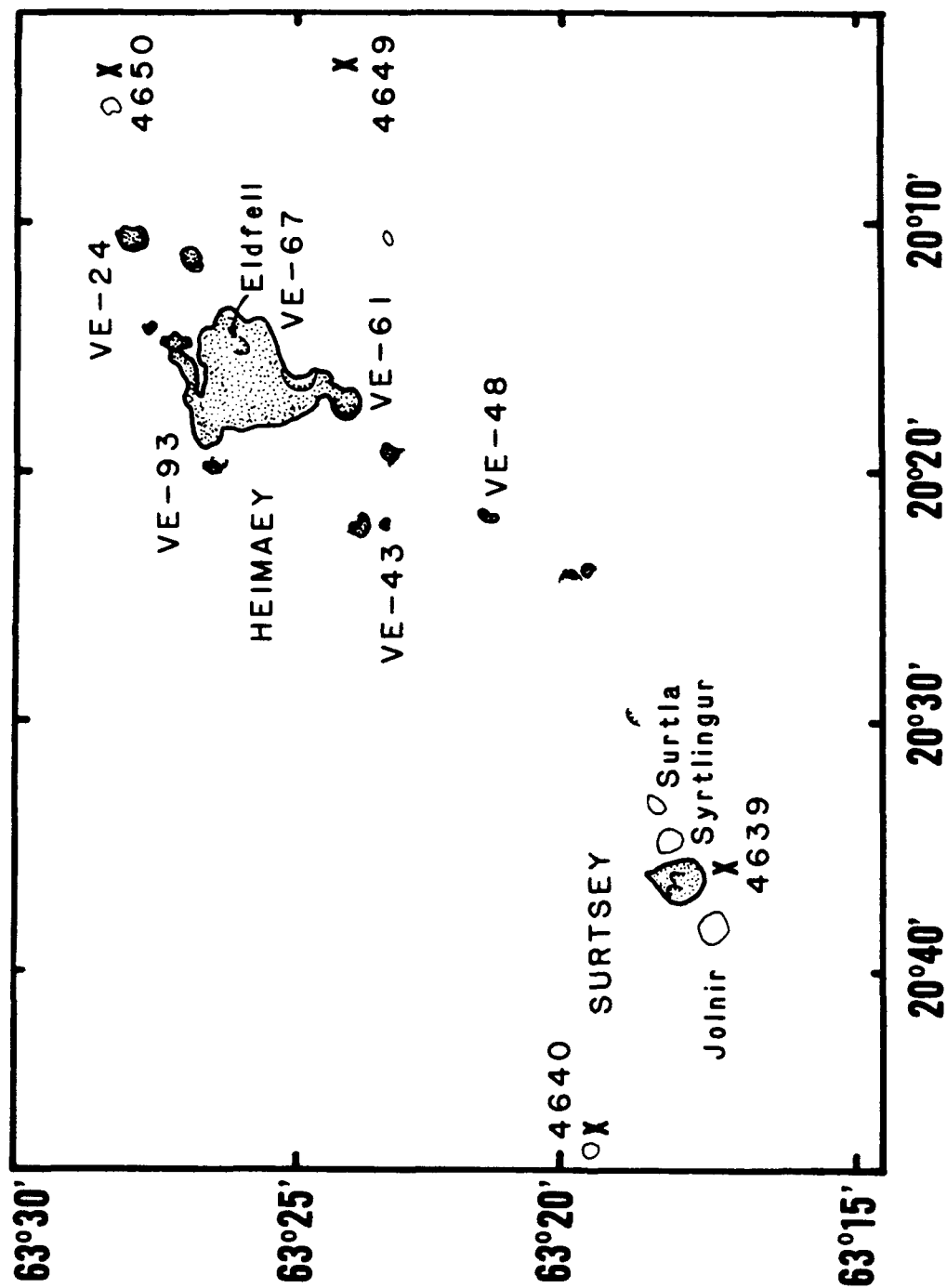


Figure 1.4 Index map of Vestmannaeyjar, southern Iceland, showing islands (shaded) and selected submarine vents (e.g., Surtla, Surtlingur). Sample numbers refer to lavas analyzed in this study (see chapter 2).

1.4) suggests that volcanism is becoming localized through time. Through geochemical analysis of Vestmannaeyjar lavas and xenoliths (chapter 2) I address the magmatic environment of Iceland's youngest alkalic volcanoes.

Another stage of volcanic evolution is revealed in the Austurhorn intrusion, an exhumed mature Tertiary central volcano in southeastern Iceland (figure 1.5). Field relations at Austurhorn indicate the nature of magmatic processes during the final stages of magma chamber activity (chapter 3). Austurhorn magmas ranged from basaltic to rhyolitic and were chemically similar to modern flank zone lavas from Torfajökull and Eyjafjallajökull (Arney, 1978; Jakobsson, 1979; McGarvie, 1984). The intrusion consists of approximately equal volumes of mafic and felsic rock and preserves a wide spectrum of comagmatic interactions. By combining field relations with geochemical and mineralogic analysis of cogenetic liquids and cumulates I assess the relative roles of fractional crystallization, crustal assimilation and magma mixing in determining the chemical signature of erupted liquids. In particular, chapter 4 is devoted to understanding generation of diverse basaltic compositions and silicic magmas in central volcanic complexes.

This comparative study of Vestmannaeyjar and Austurhorn allows an integrated assessment of central volcano evolution in a flank zone environment. A fundamental premise of this work is that neither volcanoes nor rift segments are static features. Volcanic evolution is linked intrinsically to the thermal and magmatic constraints imposed by local extension. In Iceland, transgressive volcanism is slow, and long-lived volcanic centers such as Vestmannaeyjar and Austurhorn may record a single stage of rift zone evolution. The along-axis geochemical gradients observed in Iceland are therefore similar to those found within individual Hawaiian volcanoes, where the changing magmatic environment is also manifest in variations in basalt composition (e.g., Clague & Frey, 1982; Chen & Frey, 1983; Feigenson et al., 1983; Roden et al., 1984). Repeated relocation of Icelandic axial rift segments from Tertiary through recent times

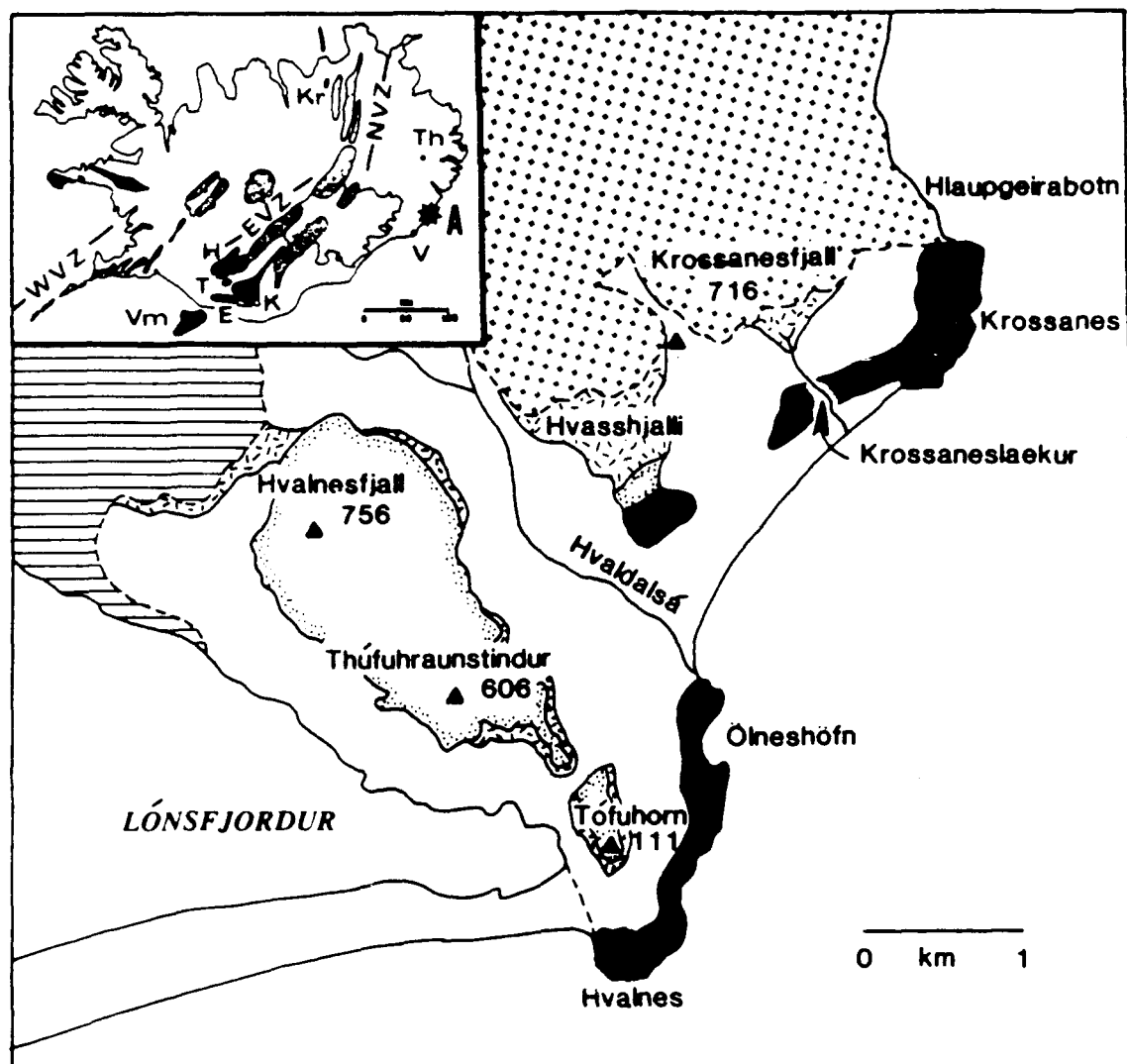


Figure 1.5 Simplified geologic map of the Austurhorn intrusion, SE Iceland. Lavas of the Tertiary Lón (ruled) and Alftafjörður (patterned) central volcanoes host the intrusion. Major rock units identified are: gabbro (stipple outline), granophyre (random dash) and the net veined complex (shaded) (see chapter 3). Mafic and felsic rocks are present in roughly equal proportions at Austurhorn.

(Aronsson & Saemundsson, 1975; Sigurdsson et al., 1978; Helgason, 1984) preserves a 16 million year history of volcano-tectonic evolution and provides insight into the dynamics of extensional magmatism.

CHAPTER 2

PETROGENESIS OF MILDLY ALKALINE LAVAS FROM VESTMANNAEYJAR:

THE ELDFELL (1973) AND SURTSEY (1963-1967) ERUPTIONS

INTRODUCTION

Current volcanism in Iceland occurs in two types of rift environment. Axial rift zones, exposed in the southwest and northeast, are landward extensions of the mid-Atlantic ridge (figure 2.1). These regions are characterized by well-exposed tensional structures (Saemundsson, 1978), high heat flow (up to $160^{\circ}\text{C}/\text{km}$; Palmason, 1973; Palmason et al., 1979), and a crustal thickness similar to that of normal oceanic lithosphere (Palmason, 1971). Flank zones, such as the eastern volcanic zone (EVZ) and the Snaefellsnes peninsula (figure 2.1), typically show poorly-developed extensional features, lower heat flow ($60^{\circ}\text{C}/\text{km}$; Palmason, 1973; Palmason et al., 1979) and a thicker crustal section (20-30 km; Palmason, 1971; Gebrande et al., 1980).

Axial volcanism is similar to that of mature ocean ridge systems. Fissure eruptions of tholeiitic basalt are dominant and more evolved compositions are rarely observed. In contrast, flank zones are characterized by central volcanoes which have calderas or central eruptive vents and contain differentiated lavas, e.g., rhyolites. Alkali basalts are abundant in Snaefellsnes and in the southern portion of the EVZ in Vestmannaeyjar, and Fe-Ti enriched lavas occur in the central EVZ.

The EVZ exhibits systematic changes in geophysical, geochemical and petrologic parameters along its length. In central Iceland it is similar to axial rift zones, but 100 km to the south (near Hekla and Katla) it has flank zone characteristics. The along-axis variations within the EVZ have led to the general interpretation of flank zones as thermally and magmatically immature axial rift zones. More specifically, the EVZ represents a recent rift axis propagating southward from central Iceland, with its tip now located at the Vestmannaeyjar archipelago (Oskarsson et al., 1982; Kurz et al., 1985; Meyer et al., 1985).

In this study we use the chemical compositions of historic and prehistoric Vestmannaeyjar lavas to determine their petrogenesis. Although the archipelago consists of numerous islands and submarine volcanoes it is a single volcanic system, following the

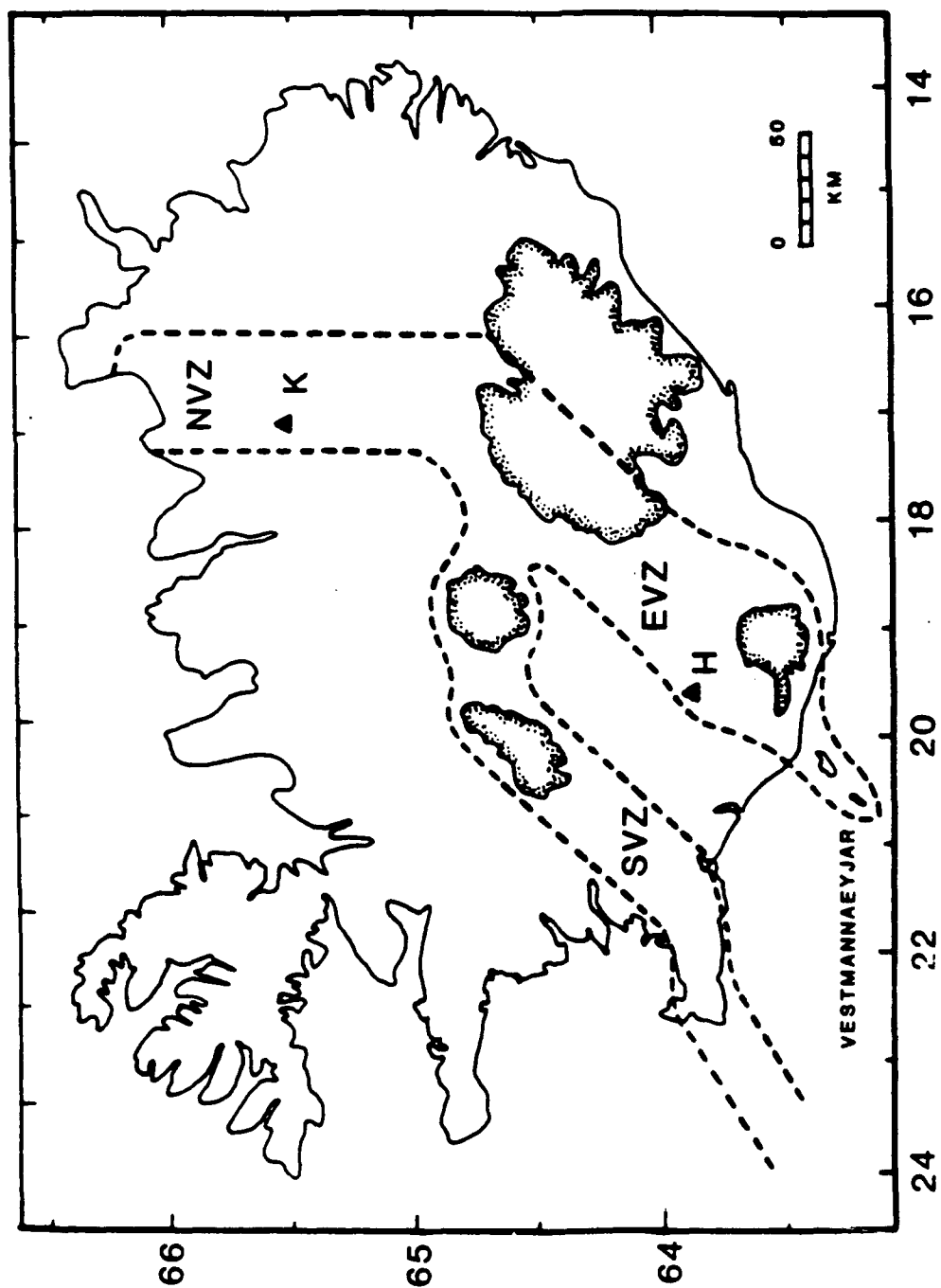


Figure 2.1 Map of Iceland showing the three active volcanic zones. Tholeiites are erupted in the southern [SVZ] and northern [NVZ] rift segments, and the eastern zone [EVZ] is of transitional to alkaline chemistry. The volcanoes Hekla and Krafla are indicated by H and K, respectively.

classification of Jakobsson (1979). Of particular interest are time-stratigraphic samples collected during the Surtsey (1963-1967) and Eldfell (1973) eruptions. We have used these data to model magma evolution within these two suites, specifically to constrain the degree and pressure of fractionation. We conclude that moderate pressure (~5-15 kbar) cotectic crystallization controls the evolution of lavas from both Eldfell and Surtsey. The isotopic characteristics of Vestmannaeyjar lavas support a mantle origin for the parental basalts and indicate that crustal assimilation did not occur during magmatic evolution.

2.1 Sample Collection and Description

Sample descriptions and locations are in Jakobsson (1979) and Jakobsson et al (in prep). Samples analyzed include dredged and subaerial postglacial lavas from throughout the Vestmanneyjar archipelago (figure 2.2). Especially important are time-stratigraphic suites collected during the eruptions of Surtsey (1963-1967) and Eldfell (1973, on the island of Heimaey). The Eldfell suite records five months of continual extrusive activity from a single vent (figure 2.3). Eruption at Surtsey was longer lived but discontinuous, and involved several vents and fissures. Samples from the Surtsey and Eldfell eruptions form the primitive and evolved extremes, respectively, of the entire archipelago. For this reason as well as the relative age control we focused on these samples. All Eldfell and most Surtsey samples were erupted and collected subaerially; exceptions are 4638 from Surtla and 8066 and 8067 from Syrtlingur (figure 2.2).

The majority of Vestmannaeyjar lavas are fine-grained and porphyritic (see Jakobsson et al., 1973, in prep., and Jakobsson, 1979 for petrographic details). The basalts contain up to 12 vol% plagioclase (An_{64-67}) and 12-17 vol% olivine (For_{81-86}) in a groundmass of plagioclase + olivine + augite + titanomagnetite +/- apatite. Phenocrysts in the more evolved basalts are often embayed. Rare megacrysts of plagioclase (An_{50-52}) always show evidence of crystal-liquid disequilibrium. Lavas from the Eldfell

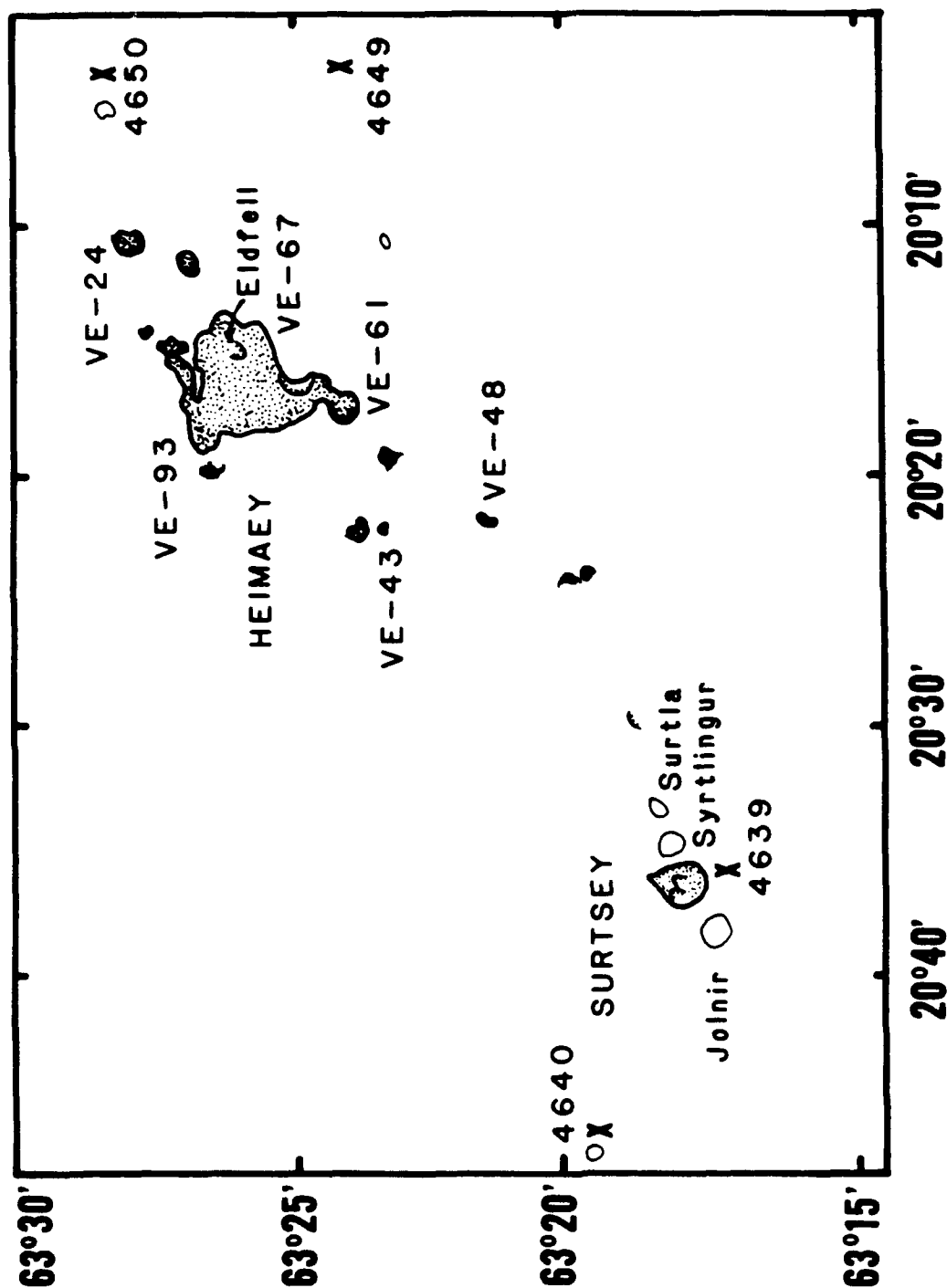


Figure 2.2 Map of the Vestmannaeyjar archipelago, after Jakobsson (1982) showing islands (shaded) and sampled submarine eruptive sites (e.g., Surtla, Syrtlingur, Jólnir). The volcano Eldfell is located on the island of Heimaey. Sample localities correspond to samples in table 2.2; "X" marks approximate sites of dredges.

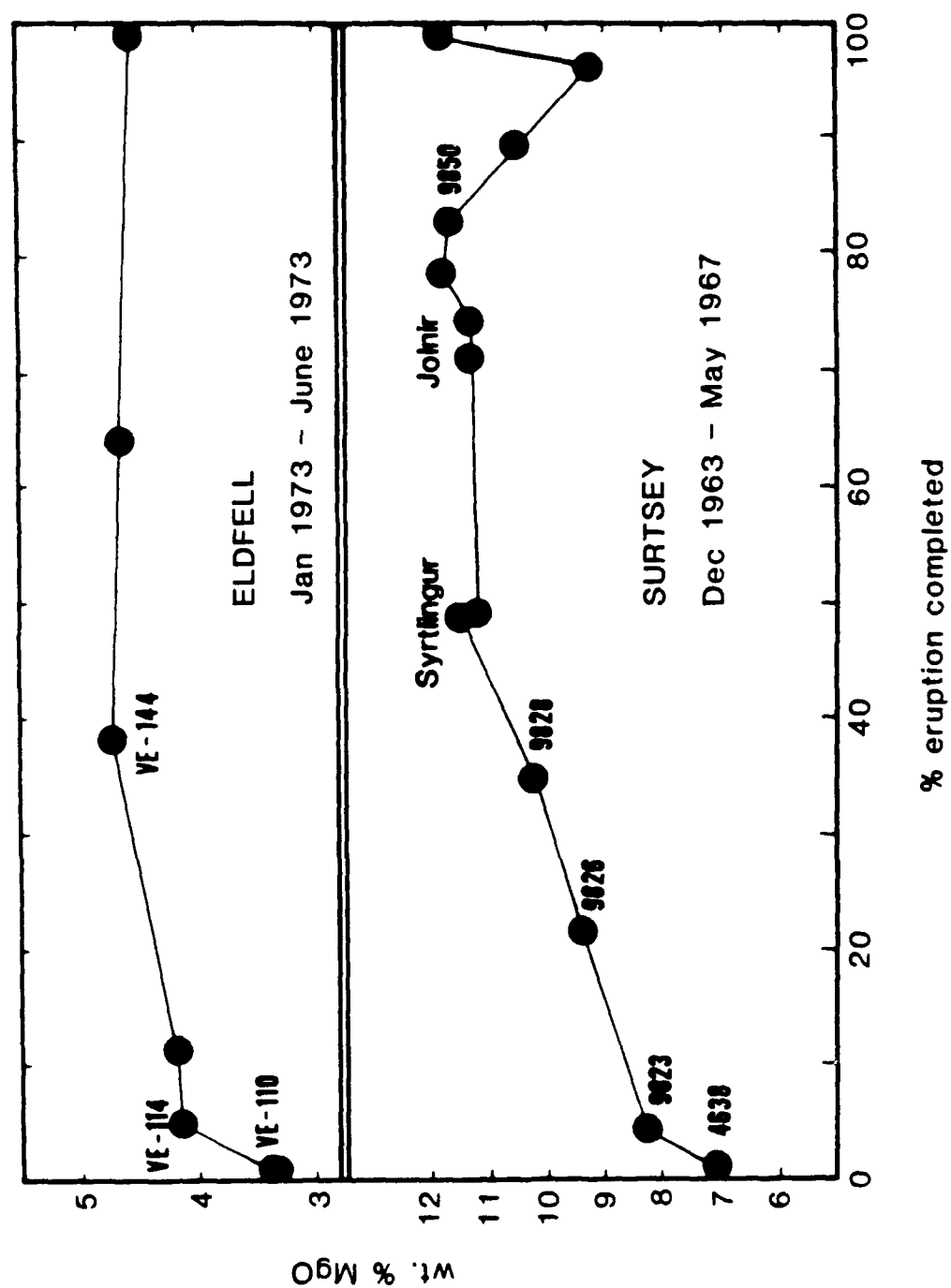


Figure 2.3 Lava composition as a function of time for the Eldfell and Surtsey eruptions. Labeled samples are those used in modeling crystal fractionation.

eruption are not porphyritic and contain up to 40 volume % microphenocrysts (<.15 mm) of olivine, plagioclase and titanomagnetite. Samples chosen for analysis are sparsely phyrlic without plagioclase megacrysts and do not appear to be accumulative.

2.2 Analytical Techniques

Samples reported in Jakobsson (1979) were crushed in a tungsten-carbide (WC) disc mill. Powders of samples from the Surtsey and Eldfell eruptions were prepared by crushing in an agate disc mill. Major element analyses of all samples were performed by x-ray fluorescence (XRF) by I. Sorensen, Copenhagen. Replicate analyses of six samples were done by XRF on fused discs at the University of Massachusetts (Amherst).

Neither interlaboratory bias nor sample inhomogeneity were detected (see table 2.1).

The trace elements Ba, Rb, Ga, Nb, Ni, Pb, Sr, V, Y, Zn, Zr were analyzed by XRF at the University of Massachusetts. Instrumental neutron activation analyses for the rare earth elements (REE), Co, Cr, Hf, Na, Sc, Ta, and Th were done at MIT. Major, minor and trace element data as well as estimates of precision and accuracy are given in table 2.2. A subset of the samples has been analyzed for Sr, Nd and Pb isotopes at Lamont-Doherty Geological Observatory (Park et al, in prep).

2.3 Results

2.3.1 Major and Trace Element Geochemistry

Lavas from Vestmannaeyjar are all of alkaline affinity (figure 2.4). The most mafic Surtsey basalts are hypersthene-normative, while more evolved lavas contain up to 6% normative nepheline. Mg#s ($Mg/(Mg+Fe)$ with total Fe as Fe^{+2}) of Vestmannaeyjar lavas range from 64 to 32, with several samples clustering around Mg# 51 and 62. Major element oxide variation diagrams show generally smooth trends for lavas from throughout the archipelago (figure 2.5). Because of their spatial proximity we first consider all the Vestmannaeyjar lavas as a group. Subsequently, we evaluate

Table 2.1 Accuracy, Precision and Interlaboratory Calibration

Sample	4638		9828		4693		8066		VE-114		VE-144	
	A	B	A	B	A	B	A	B	A	B	A	B
SiO ₂	46.99	47.00	47.03	46.62	47.01	46.66	46.75	46.42	48.40	48.46	47.54	47.06
TiO ₂	2.38	2.41	1.84	1.86	2.04	2.04	1.99	1.97	3.00	3.01	3.18	3.16
Al ₂ O ₃	16.22	16.30	15.14	15.10	13.31	13.36	14.13	14.01	16.27	16.35	16.20	16.10
Fe ₂ O ₃	2.34	13.39	1.35	12.90	2.11	13.01	1.76	12.88	3.90	14.31	2.84	14.99
FeO	9.90	-	10.42	-	10.01	-	10.12	-	9.41	-	11.00	-
MnO	.19	.21	.19	.20	.18	.19	.19	.19	.26	.26	.25	.25
MgO	7.01	7.05	10.17	10.16	11.59	11.43	11.44	11.11	4.09	4.03	4.70	4.66
CaO	9.68	9.60	10.15	10.16	10.80	10.69	10.40	10.36	7.58	7.66	8.33	8.32
Na ₂ O	3.80	3.55	2.92	2.75	2.27	2.15	2.80	2.41	4.93	4.70	4.67	4.20
K ₂ O	.68	.66	.43	.43	.35	.32	.43	.37	1.19	1.17	1.03	.98
P ₂ O ₅	.36	.36	.22	.22	.18	.18	.21	.20	.60	.61	.52	.52
sum	99.65	100.53	99.86	100.40	99.85	100.04	100.22	99.93	99.63	100.57	100.26	100.22

Replicate analyses of samples by XRF in Copenhagen (I. Sorensen, analyst) and at University of Massachusetts (T. Furman, analyst) are denoted by A and B, respectively. Samples 4638-A, 9828-A, 4693-A, 8066-A, VE-114-A and -B, VE-144-A and -B were crushed in tungsten carbide; remaining samples were crushed in agate. Analyses obtained by Furman report all Fe as Fe₂O₃.

INAA Duplicate Analyses

	4638		9823		9826		9828		9850		9839		
La	16.7	17.3	14.5	14.6	12.1	12.3	10.4	10.6	9.0	8.8	8.6	8.6	8.6
Ce	43.1	44.7	37.2	37.1	30.3	32.0	26.2	27.0	22.7	24.0	22.4	23.6	22.5
Nd	23.5	24.2	21.1	21.0	17.3	18.0	15.5	14.9	14.6	14.4	14.1	14.8	14.1
Sm	5.91	6.02	5.33	5.40	4.59	4.90	4.06	4.30	3.87	4.19	4.14	4.24	4.32
Eu	2.07	2.02	1.82	1.84	1.67	1.63	1.47	1.51	1.42	1.42	1.45	1.45	1.45
Yb	2.76	2.98	2.68	2.71	2.44	2.60	2.28	2.39	1.92	1.8	1.99	2.04	2.10
Lu	40	43	40	41	36	37	33	33	28	27	28	28	28
Hf	4.1	4.4	3.7	3.8	3.4	3.4	2.8	3.0	2.7	2.9	2.8	2.8	2.9
Th	2.00	1.27	1.06	0.99	1.08	0.90	0.69	0.79	0.44	0.45	0.42	0.70	0.60
Ta	1.29	1.33	1.17	1.12	1.06	0.98	0.87	0.84	0.73	0.71	0.67	0.65	0.68
Cr	168	167	284	298	391	391	416	432	697	696	675	664	672
Co	45.4	44.8	49.4	50.8	52.8	53.3	55.9	57.7	63.0	63.9	61.0	59.4	60.3
Sc	26.4	26.4	29.5	29.9	30.1	30.3	29.6	30.6	30.3	30.9	32.2	31.8	32.1

Note: One-sigma precision of XRF and INAA (based on replicate analyses) are: major elements (except MnO) <1% (Rhodes, 1983). La, Co, Cr, Hf, Sc, Ba, Rb, Ga, Y, Sr, Ni, V, Zn, Zr <2%; remaining REE, Nb, Ta, MnO 2-5%; Tb, Th, Ni (<20 ppm) 5-10%.

Table 2.2 Major and Trace Element Analyses

	I. Surtsey Lavas										Surtsey Syntingur									
	46/38	98/23	SU-42	98/26	98/28	SU 11	80/66	80/67	98/39	98/42	46/93	98/50	SU 24	98/51	98/53	98/54				
	12/63	2/64	7/64	8/64	2/65	4/65	X/65	X/65	5/66	7/66	8/66	11/66	12/66	12/66	5/67	5/67				
	Surtla	Surtsey	Surtsey	Surtsey	Surtsey	Surtsey	Syrtlingur	Syrtlingur	Johnir	Johnir	Surtsey	Surtsey	Surtsey	Surtsey	Surtsey	Surtsey				
SiO ₂	46.99	47.07	46.7	47.04	47.03	46.4	46.75	46.84	47.25	47.08	47.01	47.04	46.9	47.06	47.12	47.06				
TiO ₂	2.38	2.20	2.1	2.02	1.84	1.6	1.99	2.03	2.07	2.05	2.04	2.02	2.2	2.12	2.18	2.04				
Al ₂ O ₃	16.22	15.69	15.5	15.40	15.14	15.3	14.13	14.17	13.22	13.90	13.31	13.53	14.8	14.52	14.86	13.61				
FeO	9.90	10.11	10.2	9.87	10.42	10.0	10.12	10.44	10.09	9.52	10.01	10.40	9.6	9.74	10.29	10.23				
Fe ₂ O ₃	2.34	2.05	2.0	2.09	1.35	1.8	1.76	1.40	2.10	2.63	2.11	1.59	2.8	2.29	1.65	1.76				
MnO	19	19	18	20	19	17	19	19	18	18	18	19	18	19	18	19				
MgO	7.01	8.22	9.2	9.34	10.17	11.7	11.44	11.10	11.16	11.19	11.59	11.69	10.1	10.48	9.17	11.82				
CaO	9.68	10.15	10.5	10.10	10.15	9.7	10.40	10.50	10.68	10.69	10.80	10.51	9.8	10.33	10.58	10.62				
Na ₂ O	3.80	3.21	3.1	3.00	2.92	2.7	2.80	2.72	2.52	2.53	2.27	2.40	2.9	2.79	2.85	2.45				
K ₂ O	68	60	47	53	43	32	43	41	33	32	35	33	39	41	49	35				
P ₂ O ₅	36	30	32	26	22	21	21	21	19	19	18	19	25	22	23	19				
H ₂ O	25	13	35	19	12	34	38	30	19	38	11	11	30	13	10	21				
sum	99.80	99.92	100.62	100.04	99.98	100.24	100.60	100.31	99.98	100.06	99.96	100.00	100.22	100.28	99.70	100.53				
FeO*	12.01	11.96	12.00	11.75	11.64	11.62	11.70	11.70	11.98	11.89	11.91	11.83	12.12	11.80	11.78	11.81				
Na ₂ X/NAI	3.71	3.27	3.35	3.04	2.89	2.82	2.62	2.52	2.43	2.52	2.39	2.33	2.83	2.72	2.89	2.43				
TiO ₂ /XRF	2.48	2.26	2.09	2.11	1.93	1.59	2.03	2.07	2.13	2.10	2.21	1.96	2.18	2.22	2.20	2.14				
Mg#	51.0	55.1	57.7	58.6	60.9	64.2	63.5	62.8	62.4	62.7	63.4	63.8	59.7	61.3	58.1	64.1				
Rb	13.5	11.4	9.3	10.0	8.3	6.3	6.3	-	5.2	5.9	5.8	5.8	7.1	7.1	7.1	5.8				
Sr	378	340	305	312	291	280	275	285	264	269	283	271	289	298	310	276				
Ba	158	165	123	126	103	89	94	81	72	80	79	70	92	100	96	80				
Sc	26.4	29.7	29.6	30.2	30.1	-	31.1	31.1	32.0	31.8	31.7	30.6	31.3	30.9	30.0	32.1				
V	241	251	250	252	260	202	268	272	275	275	286	256	264	268	263	272				
Cr	168	291	381	391	424	-	583	593	670	651	683	696	506	498	405	684				
Co	451	501	53.6	53.0	56.8	-	59.7	61.7	60.2	59.8	60.5	63.4	57.8	56.9	52.1	62.2				
Ni	112	131	173	176	226	267	290	314	296	306	302	305	233	241	193	292				
Zn	116	108	105	112	115	87	105	107	112	106	111	106	108	112	106	102				
Ga	21.0	21.0	20.0	19.4	20.0	18.7	18.8	-	19.1	18.1	18.8	17.7	20.0	20.1	20.0	17.9				
Ge	31.4	28.6	27.0	26.1	25.0	21.1	23.1	-	23.6	22.8	22.5	21.5	23.9	24.0	25.6	22.3				
Zr	201	173	153	148	131	103	129	129	116	113	121	114	133	131	137	117				
Nb	23.2	19.8	16.9	16.4	15.0	11.2	13.8	12.8	11.4	11.7	12.4	11.9	13.8	13.7	15.2	11.7				
Hf	4.2	3.8	3.3	3.4	2.9	-	3.0	3.0	2.8	2.8	2.8	2.8	3.3	3.1	3.1	2.9				
Ta	1.31	1.14	9	1.02	74	-	8	5	67	6	7	72	8	8	8	6				
Th	1.6	1.0	1.1	1.0	9	-	8	7	6	6	5	4	7	8	8	5				
La	17.0	14.6	12.1	12.2	10.5	-	10.1	9.6	8.6	8.8	8.9	8.9	10.7	10.9	11.2	9.2				
Ce	43.9	37.2	32.2	31.2	26.6	-	26.6	26.8	22.8	23.8	22.8	23.4	26.8	28.0	29.1	23.5				
Nd	23.8	21.0	18.1	17.6	15.2	-	15.8	16.2	14.3	14.8	14.4	14.5	16.5	17.5	17.6	14.5				
Sm	5.96	5.36	4.57	4.74	4.18	-	4.40	4.25	4.23	4.04	4.19	4.03	4.38	4.42	4.51	4.30				
Eu	2.04	1.83	1.59	1.65	1.49	-	1.52	1.48	1.45	1.46	1.44	1.42	1.60	1.59	1.62	1.44				
Gd	1.0	1.0	1.0	1.0	1.0	-	1.0	1.0	1.0	1.0	1.0	1.0	1.0	1.0	1.0	1.0				
Tb	2.87	2.70	2.51	2.52	2.33	-	2.14	2.04	2.04	1.98	2.03	1.90	2.18	2.29	2.37	2.04				
Lu	42	40	37	36	33	-	29	29	28	30	26	28	31	32	33	31				
87Sr/86Sr		70313	70315	70309	70311	70312			70326	70326	70326	70314								
(unpublished)			70315		70326				51301	51301	51302									
143Nd/144Nd			51306	51304	51303	51303						19.18								
206Pb/204Pb		19.01	19.02									15.53								
207Pb/204Pb		15.50	15.53									38.76								
208Pb/204Pb		38.52	38.58																	

II. Eldfell Lavas

	VE-110 23 Jan.	VE-111 23 Jan.	VE-114 30 Jan.	VE-121 8 Feb.	VE-144 22 Mar.	VE-149 1 May	Prestavik June
SiO ₂	50.15	50.7	48.40	48.32	47.54	47.57	47.64
TiO ₂	2.42	2.5	3.00	3.10	3.18	3.16	3.11
Al ₂ O ₃	16.38	16.8	16.27	16.23	16.20	16.16	16.18
FeO	9.82	10.3	9.41	10.25	11.00	11.32	10.72
Fe ₂ O ₃	2.72	2.3	3.90	3.46	2.84	2.62	3.04
MnO	.26	.25	.26	.25	.25	.24	.23
MgO	3.32	3.2	4.09	4.17	4.70	4.64	4.51
CaO	6.94	6.4	7.58	7.96	8.33	8.46	8.41
Na ₂ O	5.34	5.4	4.93	4.81	4.67	4.53	4.60
K ₂ O	1.50	1.3	1.19	1.16	1.03	1.00	1.02
P ₂ O ₅	.72	.64	.60	.59	.52	.52	.52
H ₂ O	.39	.44	.31	.09	.16	.04	.28
sum	99.96	100.23	99.94	100.39	100.42	100.26	100.26
FeO*	12.27	12.37	12.92	13.36	13.56	13.68	13.46
Na ₂ O(NA)	5.27	5.22	4.83	4.74	4.44	4.51	4.44
TiO ₂ (XRF)	2.39	2.26	3.08	2.90	3.14	3.20	3.03
Mg#	32.5	31.6	36.1	35.7	38.2	37.7	37.4
Rb	31.7	31.5	24.5	23.3	20.3	19.9	20.0
Sr	356	367	369	362	365	370	370
Ba	277	419	291	286	236	234	251
Sc	17.3	17.0	21.3	22.5	24.5	24.8	24.1
V	58	53	133	136	200	204	190
Cr	0	1	0	4	7	8	7
Ce	22.7	26.3	28.7	41.4	35.3	36.5	34.8
Ni	7	3	6	5	11	15	13
Zn	146	145	148	129	131	136	122
Ga	26.1	26.2	25.2	25.3	25.2	25.5	25.5
Y	56.7	56.8	50.5	48.7	44.0	43.8	48.7
Zr	398	401	337	310	281	279	275
Nb	45.6	46.4	40.8	36.6	33.7	33.7	32.5
Hf	8.4	8.8	7.0	6.8	6.0	6.3	6.1
Ta	2.6	2.8	2.2	2.2	1.8	1.8	1.8
Th	2.6	3.1	2.3	2.1	1.7	1.7	2.0
La	36.0	35.6	29.6	28.2	25.2	24.9	24.9
Ce	89.7	88.5	74.6	71.7	62.3	63.4	62.1
Nd	47.4	46.4	41.6	37.7	35.2	35.3	34.3
Sm	11.36	10.62	9.97	9.56	8.72	8.72	8.67
Eu	3.40	3.42	3.07	3.03	2.70	2.77	2.69
Tb	1.8	1.7	1.6	1.7	1.4	1.5	1.3
Yb	5.64	5.57	5.00	4.76	4.39	4.26	4.20
Lu	.84	.82	.73	.69	.64	.67	.67
⁸⁷ Sr/ ⁸⁶ Sr		.70314			.70304		
(unleached)		.70315					
¹⁴³ Nd/ ¹⁴⁴ Nd		.51304			.51306		
²⁰⁶ Pb/ ²⁰⁴ Pb	19.02	19.03			18.96		
²⁰⁷ Pb/ ²⁰⁴ Pb	15.54	15.53			15.51		
²⁰⁸ Pb/ ²⁰⁴ Pb	38.58	38.62			38.50		

III Vestmannaeyjar Lavas

	4650	VE-24	VE-93	VE-61	VE-67	4649	VE-43	VE-48	4639	4640	VE-72
	Rufuböðli	Flidacy	Dallfjall	Storhöfði	Hellafell	Hensaklakkur	Brandur	Hellsey	Surtsey	Skarðfelli	Sæfell
SiO ₂	46.66	46.80	46.66	46.71	47.27	46.40	46.49	47.41	46.50	46.24	46.90
TiO ₂	2.82	2.62	3.16	1.81	2.36	2.14	2.17	2.33	2.49	2.27	2.36
Al ₂ O ₃	16.19	15.85	16.19	14.60	16.98	14.77	15.55	17.17	15.88	15.87	15.35
FeO	10.77	8.40	10.77	9.89	9.10	9.71	6.15	8.84	9.93	10.68	9.20
Fe ₂ O ₃	2.26	4.65	2.26	1.31	2.66	1.56	5.73	2.94	2.88	1.76	2.26
MnO	27	17	27	23	15	23	20	25	27	26	19
MgO	5.75	6.07	5.75	10.03	5.38	9.49	9.05	5.86	7.36	8.21	8.67
CaO	9.76	9.88	9.76	12.03	10.43	10.53	10.88	10.47	9.63	9.40	11.08
Na ₂ O	3.60	3.66	4.05	2.36	3.63	2.83	2.67	3.42	3.37	3.78	2.76
K ₂ O	82	67	82	31	70	64	38	67	67	59	54
P ₂ O ₅	31	34	31	05	37	17	28	17	25	25	34
H ₂ O	32	45	22	56	48	97	38	49	56	114	50
sum	99.53	99.56	100.22	99.89	99.51	99.44	99.93	100.02	99.80	100.35	100.15
FeO*	12.80	12.58	12.80	11.07	11.49	11.11	11.30	11.48	12.52	12.26	11.23
Na ₂ (XNA)	4.34	3.59	4.17	2.40	3.75	3.05	3.13	3.37	3.44	3.59	2.89
TiO ₂ (XRF)	-	2.08	2.93	1.76	2.24	2.15	1.67	2.33	2.48	2.30	1.95
Mg#	44.5	46.2	44.5	61.8	45.5	60.3	58.8	47.6	51.1	54.4	59.5
W	148	-	-	-	-	55	-	-	-	10.4	11.3
Rb	-	13.3	20.3	5.2	13.3	10.5	7.6	11.9	11.6	315	328
Sr	-	364	401	256	404	323	329	389	371	122	158
Ba	-	202	246	89	192	138	110	153	169	281	33.7
Sc	34.8	32.6	25.5	38.1	28.1	36.6	36.4	29.4	27.9	242	248
V	-	242	243	279	233	275	238	261	265	213	429
Cr	66	101	28	621	86	522	399	97	199	560	51.5
Co	78.3	47.8	39.1	57.0	41.5	72.3	63.2	43.6	50.1	148	159
Ni	-	42	20	261	41	189	148	49	109	117	82
Zn	-	81	109	127	86	106	80	102	116	191	19.6
Ga	-	23.9	25.5	16.7	22.0	19.6	19.6	22.1	22.6	28.8	29.1
Y	-	32.0	40.4	22.4	30.8	25.9	22.9	28.5	31.4	169	151
Zr	-	176	260	113	176	153	108	175	184	194	168
Nb	-	19.2	32.2	11.1	20.0	19.5	10.9	20.8	20.9	10	38
Hf	5.0	4.2	5.8	2.7	4.3	3.5	2.8	4.0	4.1	1.2	1.2
Ta	2.2	1.3	2.1	7	1.2	1.3	8	1.2	1.4	1.1	1.2
Th	1.4	1.2	2.3	5	1.2	1.0	6	1.3	1.1	14.6	13.8
La	20.9	16.6	25.4	8.6	15.9	14.4	10.3	15.7	15.4	36.3	35.1
Ce	51.9	43.5	61.4	22.8	39.6	36.6	27.3	38.0	39.0	21.1	20.0
Nd	29.6	23.7	32.7	14.4	21.8	20.6	16.3	22.0	21.8	5.21	4.77
Sm	7.83	5.97	7.86	3.99	5.49	5.17	4.38	5.13	5.73	1.86	1.78
Eu	2.50	2.06	2.72	1.39	1.98	1.78	1.55	1.99	1.96	8	8
Gd	9	8	9	8	9	8	8	1.0	9	2.89	2.62
Tb	3.90	3.27	3.51	2.26	2.90	2.60	2.48	2.60	2.96	41	39
Yb	-	46	51	33	40	37	34	36	43	-	-
Lu	56	-	-	-	-	-	-	-	-	-	-
87Sr/86Sr	-	-	70310	-	-	70315	70313	-	70312	70327	70313
(uncalc bed)	-	-	70325	-	-	70345	70329	-	70329	70334	-
143Nd/144Nd	-	-	51305	-	-	51307	51307	-	51305	51302	51302
206Pb/204Pb	-	-	19.00	-	-	19.01	19.01	-	18.90	18.96	18.91
207Pb/204Pb	-	-	15.52	-	-	15.52	15.52	-	15.52	15.53	15.52
208Pb/204Pb	-	-	38.56	-	-	38.51	38.51	-	38.57	38.63	38.47

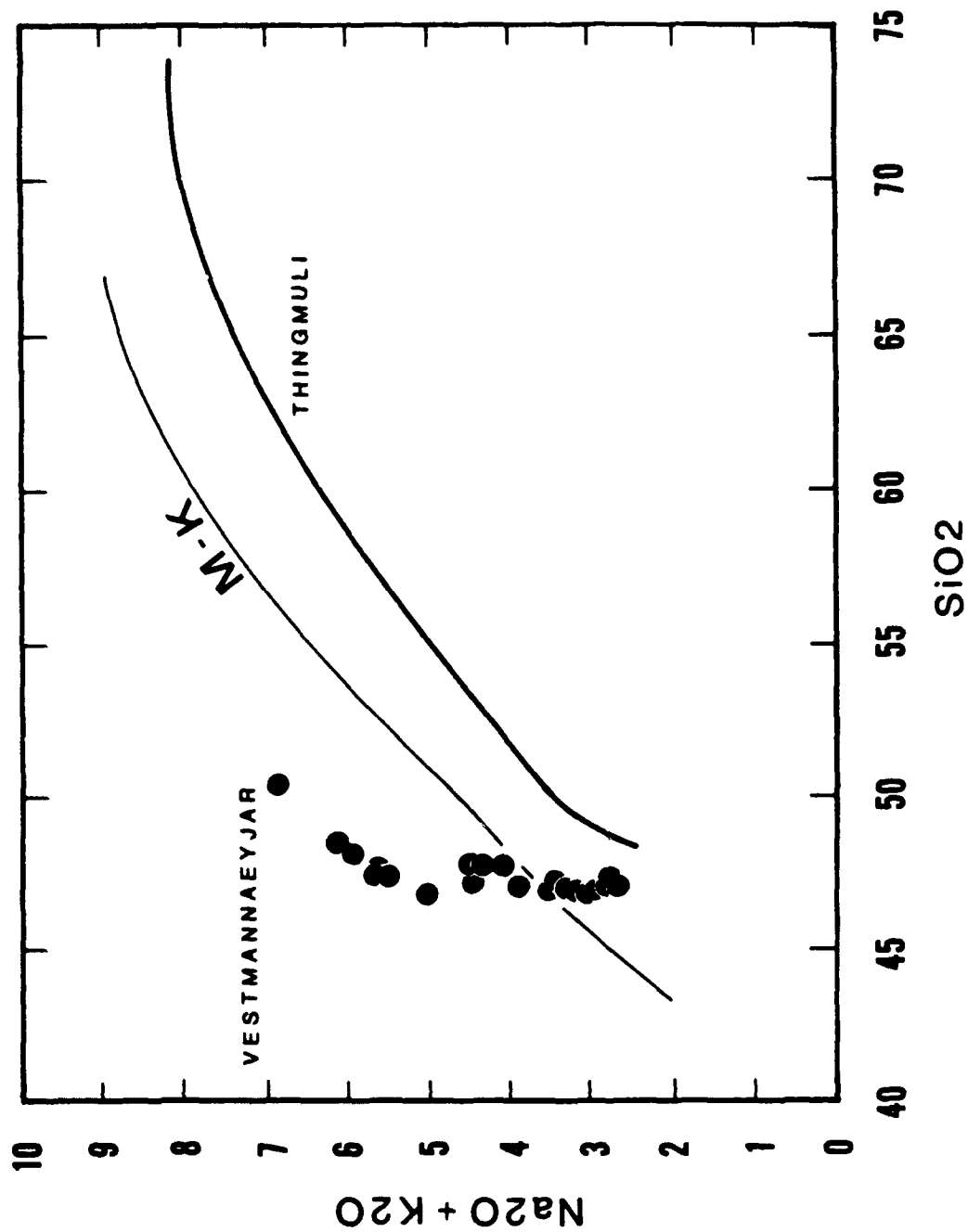


Figure 2.4 Total alkalis versus silica for Vestmannaeyjar samples (filled circles) defines an alkaline differentiation trend. The Hawaiian division line of Macdonald and Katsura (1964) and tholeiitic evolution trend of the Thingmuli central volcano (Carmichael, 1964) are shown for comparison.

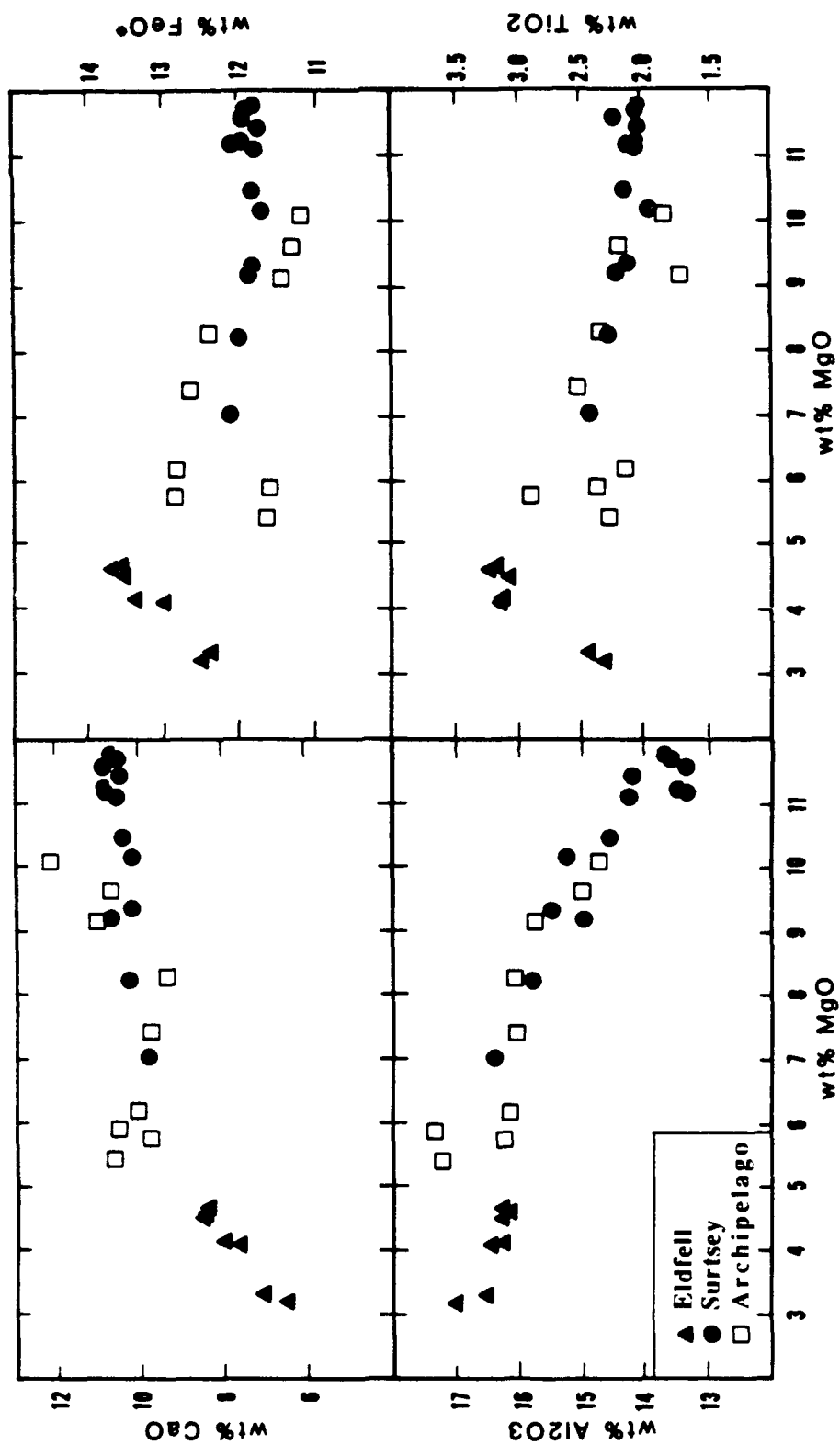


Figure 2.5 Major element oxide variation diagrams show coherent trends among samples from throughout Vestmannaeyjar. Filled circles are samples from Surtsey, filled triangles are from Eldfell, and open squares indicate lavas from the remainder of the archipelago.

quantitatively the role of crystal fractionation in creating compositional variations observed in the Eldfell and Surtsey eruptions.

Chondrite-normalized rare earth element (REE) profiles are quite similar, $\text{La}/\text{Sm}_n = 1.3\text{--}2.1$, throughout the archipelago (figure 2.6), with La/Sm increasing as MgO decreases (figure 2.7a). The Surtsey basalts have LREE abundances of 35–45x chondrites and HREE of 11–18x chondrites, while the Eldfell hawaiites have LREE 100–150x chondrites and HREE 21–30x chondrites. Samples from the remainder of the archipelago have REE abundances comparable to Surtsey basalts. Surprisingly, alkali basalts from Vestmannaeyjar have lower and more uniform chondrite-normalized LREE/HREE than transitional or tholeiitic basalts from more northerly portions of the EVZ (figure 2.7b).

Abundances of the typically incompatible elements P, K, Ba, Rb, Hf, Zr, Ta, Th and Nb are positively correlated; they are negatively correlated with Co, Cr, Ni, Sc and V (figure 2.8). Sr is positively correlated with La in lavas with >5 wt% MgO but is nearly constant in the hawaiites and mugearites (356 to 370 ppm; figure 2.8). These correlations are defined by Surtsey and Eldfell lavas as well as samples from the entire Vestmannaeyjar volcanic system. Samples from throughout the archipelago have nearly constant Nb/Ta (16.4–18.8) comparable to that of MORB and OIB (~17; McDonough et al., 1985). Ba/Rb of Vestmannaeyjar lavas range between 11.2–14.3, similar to the global OIB value of ~12 (McDonough et al., 1985). The Vestmannaeyjar samples also have uniform Zr/Hf (42–46) which is higher than that of MORB and OIB (~36; McDonough et al., 1985), and virtually constant La/Nb (0.766) that is lower than the chondritic value (0.96; Sun & McDonough, in press) but higher than most OIB (~0.6–0.7; Sun & McDonough, in press).

2.3.2 Radiogenic Isotopic Systematics

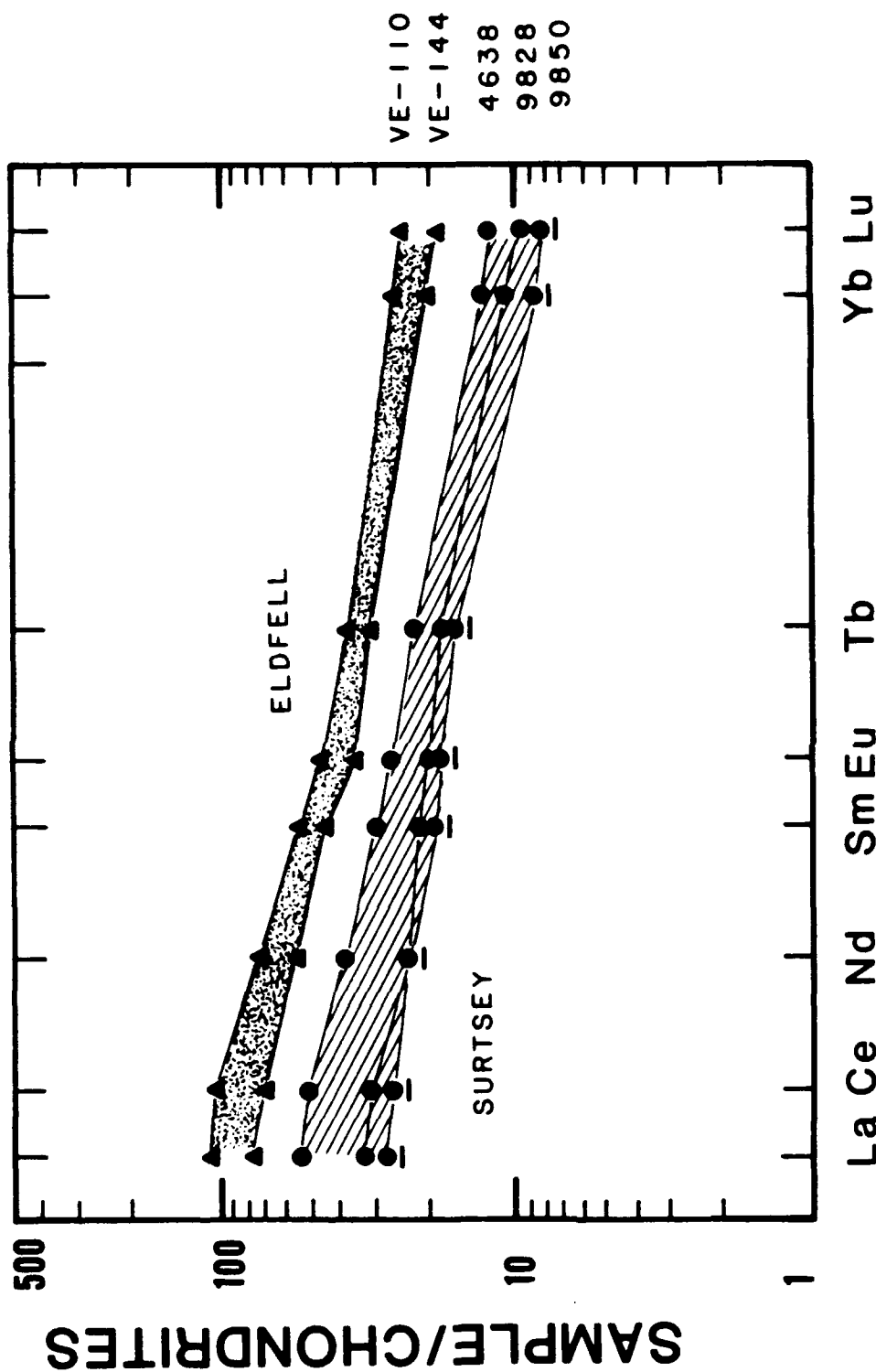


Figure 2.6 Chondrite-normalized REE patterns of Vestmannaeyjar lavas (normalizing values of Boynton, 1966). All 7 Eldfell samples fall in the range defined by VE-144 and VE-110. Samples from the remainder of Vestmannaeyjar lie within the field of 15 Surtsey lavas. The pattern of 9850 is typical of primitive Surtsey lavas. Note that 9850 and 9828 have Nd concentrations within analytic error of one another; sample 9850 has lower abundances of all other REE.

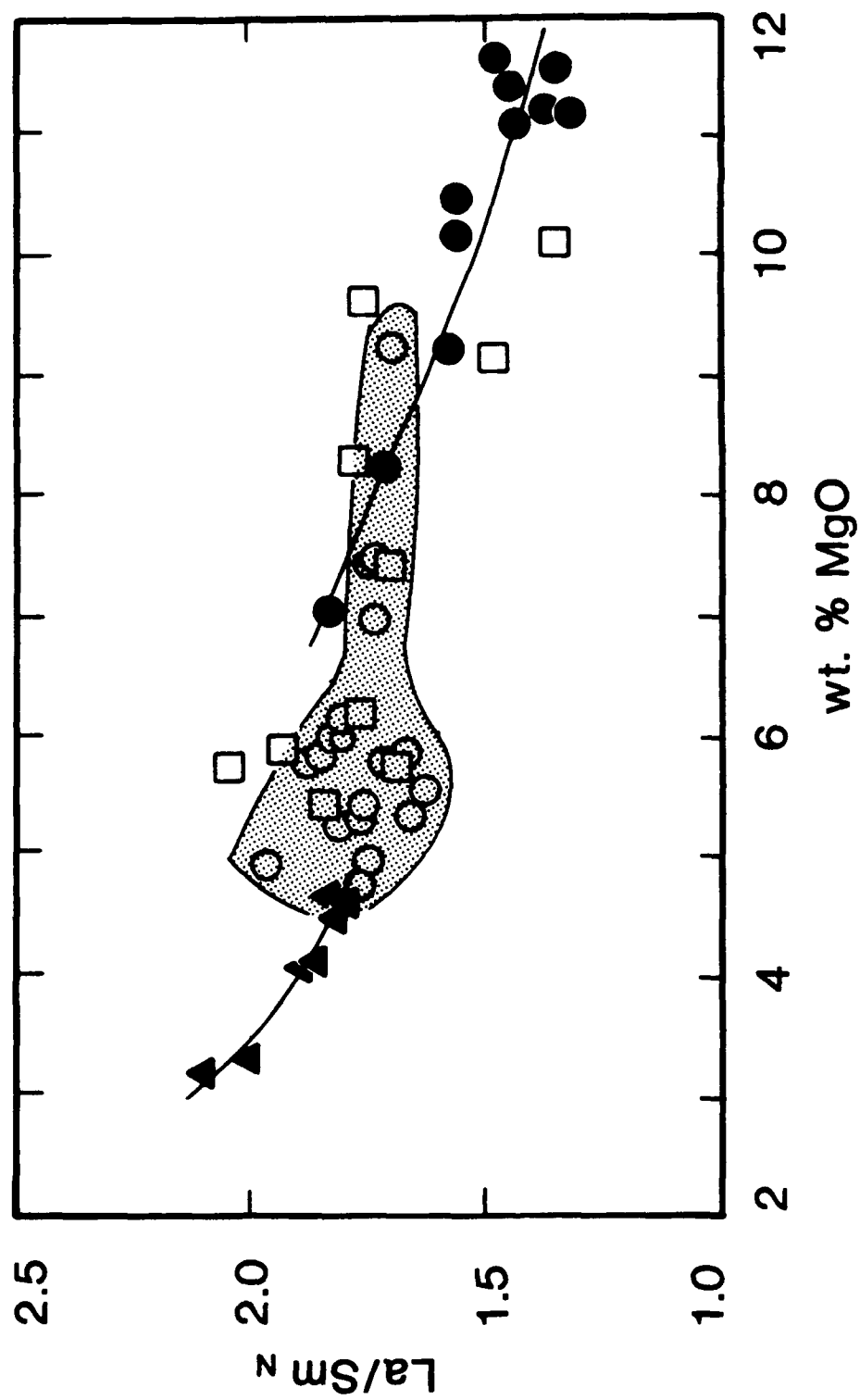
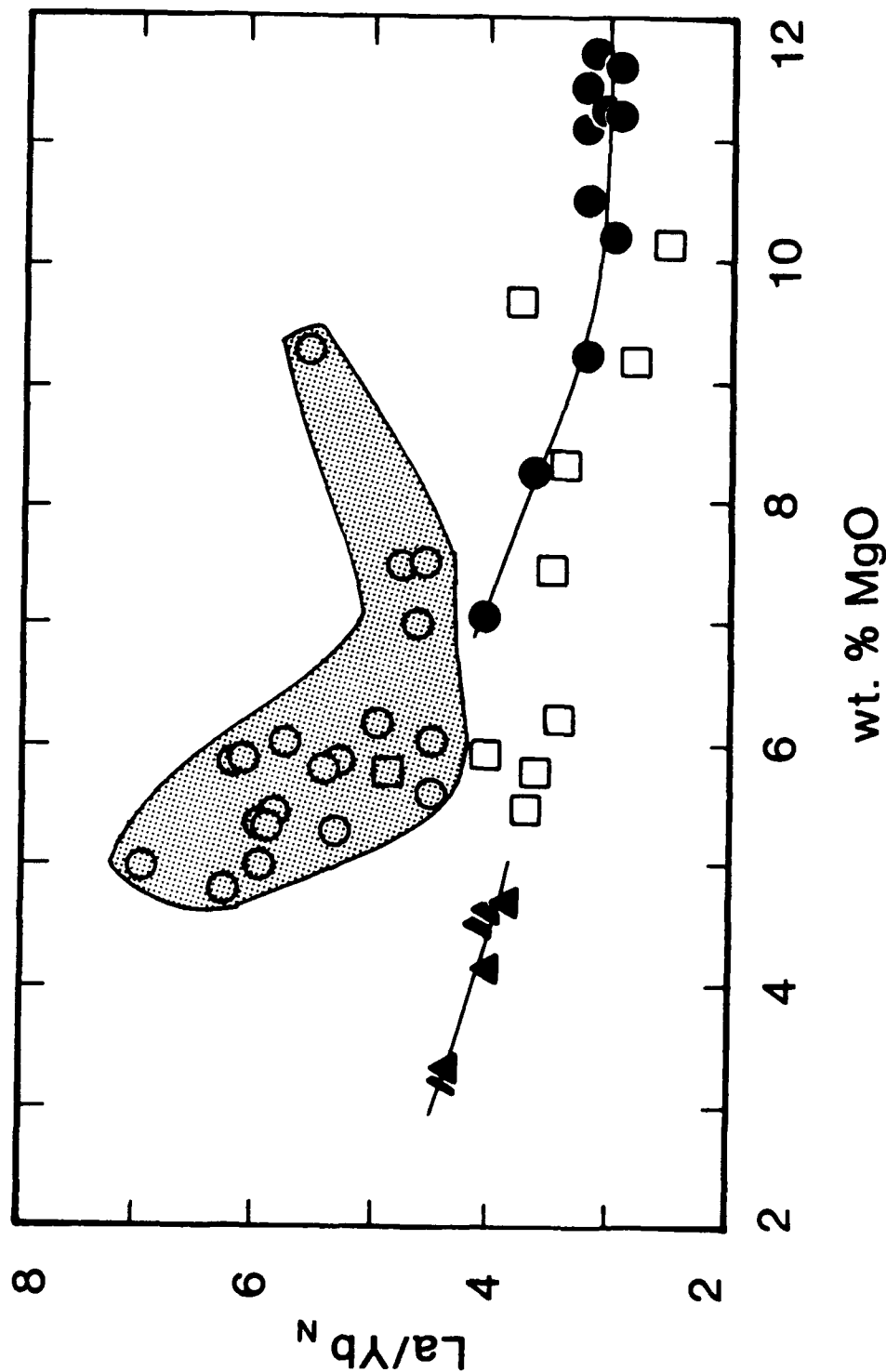


Figure 2.7 (a) Chondrite-normalized La/Sm of Vestmannaeyjar lavas (symbols as in figure 2.5) are comparable to ratios of transitional EVZ basalts (shaded field with open circles; data from Meyer et al., 1985).



(b) Chondrite-normalized La/Yb of Vestmannaeyjar samples show a slight increase with magmatic differentiation. Notice the greater scatter among transitional EVZ samples; the larger range at constant MgO suggests these lavas did not evolve from a common parental basalt. We reanalyzed five samples from Meyer et al (1985) to verify that interlaboratory bias did not cause the difference in La/Yb between Vestmannaeyjar and EVZ transitional basalts. While discrepancies for individual elements ranged from 0 to 24%, La/Sm and La/Yb differed by 3-17%. In all cases with >4% difference, the MIT values are higher than those from URI; therefore the higher ratios in transitional basalts are verified.

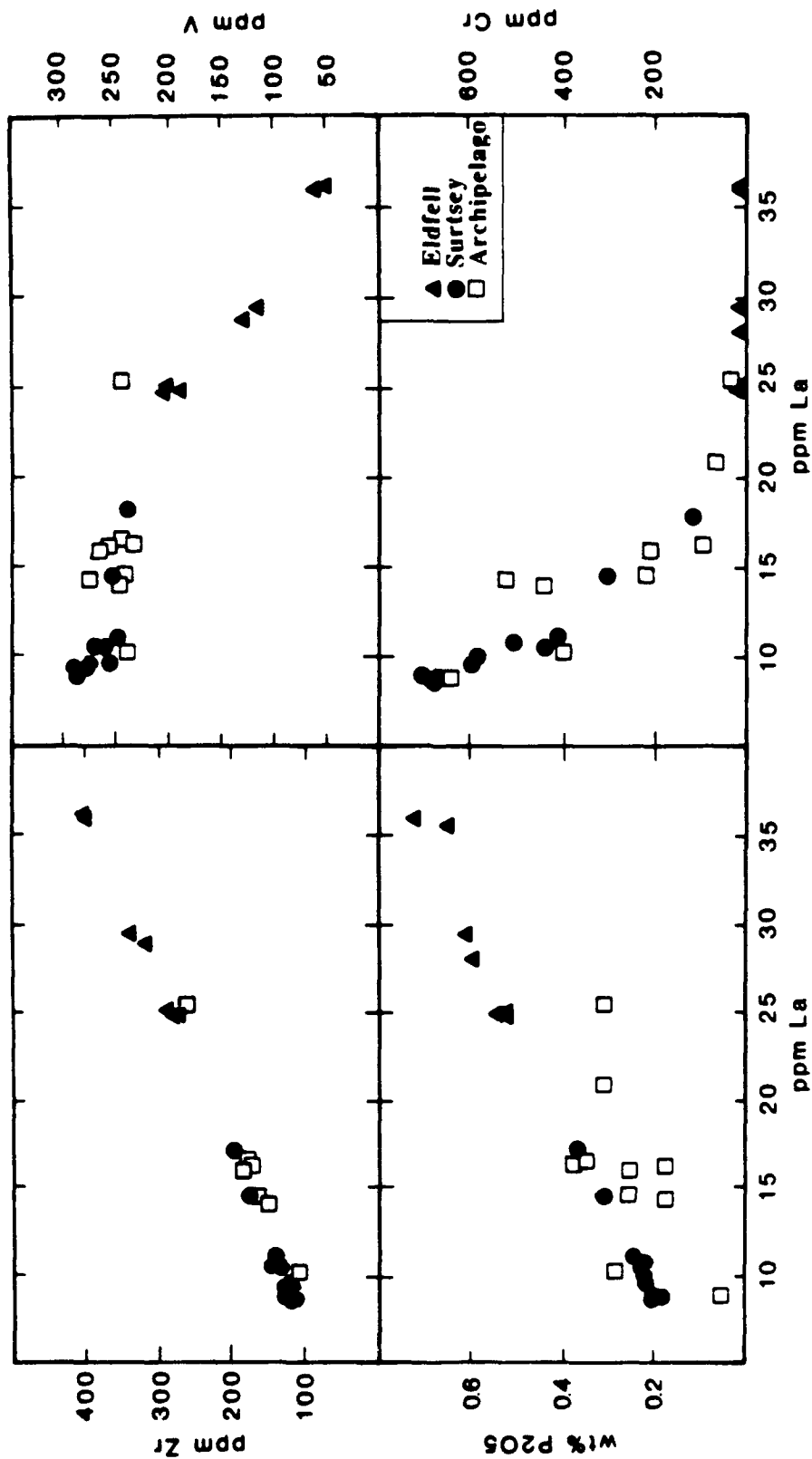
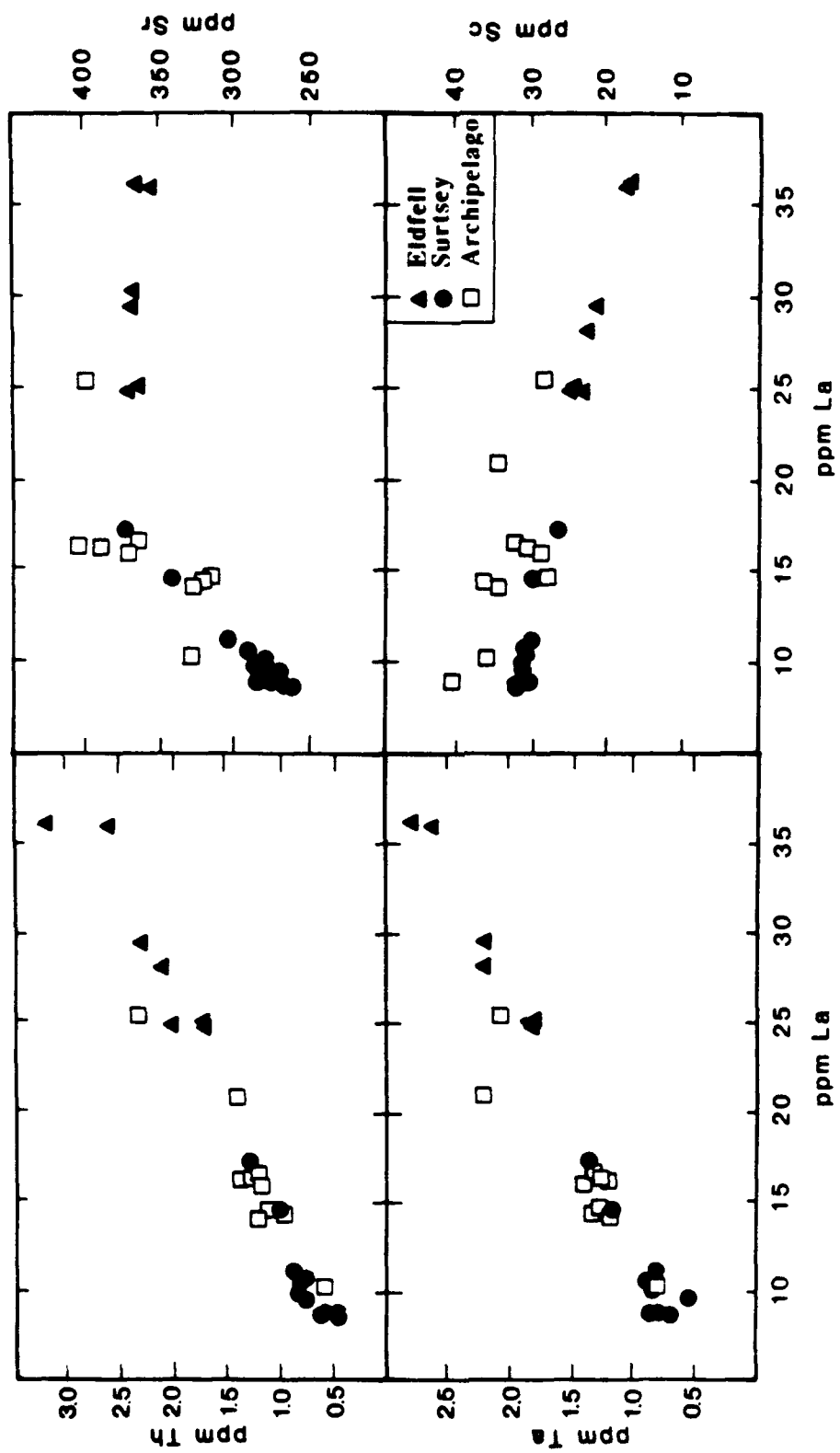


Figure 2.8 Behavior of incompatible (La, Th, Zr, P) and selectively compatible (Sr, Sc, V, Cr) trace elements in Vestmannaeyjar lavas. Symbols as in figure 2.5.



Selected Vestmannaeyjar samples were analyzed for Sr, Nd and Pb isotopes (table 2.2). Eight unleached samples have $^{87}\text{Sr}/^{86}\text{Sr}$ values ranging from 0.70315-0.70345 (all data relative to E&A standard value of 0.70800). The dredged archipelago samples (4639, 4640, 4649) have ratios more radiogenic than the subaerial lavas, suggesting contamination by seawater. Samples leached in acid (16) have $^{87}\text{Sr}/^{86}\text{Sr}$ ratios of 0.70304-0.70327. Two samples analyzed previously by O'Nions et al (1973) have been re-examined in this study (VE-93, VE-111); analyses of the *unleached* powders agree within analytic error in both cases. Despite leaching the samples show minor isotopic variability, although most fall within analytic error of 0.70313. Among lavas from the Surtsey eruption there is a weak negative correlation between $^{87}\text{Sr}/^{86}\text{Sr}$ and $\text{La}/\text{Sm}_\text{N}$, i.e., the MgO-rich lavas are more radiogenic. This correlation may be fortuitous as it is not observed in the remainder of the samples (figure 2.9). Two partially fused silicic xenoliths from Surtsey lavas have $^{87}\text{Sr}/^{86}\text{Sr} = 0.70370$ and 0.70432 (acid leached). These samples were not analyzed for bulk chemistry due to their small size (<5 cm) and macroscopic heterogeneity.

No comparable range is observed in $^{143}\text{Nd}/^{144}\text{Nd}$. All samples fall within analytic precision of 0.51305 over a greater than 3-fold increase in Nd concentration. The Sr and Nd isotope ratios of acid-leached Vestmannaeyjar samples overlap with the transitional Hekla and tholeiitic Veidivotn lavas (figure 2.10a; Park et al, in prep). Each volcanic system shows minor heterogeneity and most samples plot outside the field of north Atlantic MOR basalts (excluding 43-45°N). The three EVZ volcanic centers have a less depleted isotopic signature than that of Reykjanes picrites and tholeiites (Stecher et al., 1986).

In contrast to the overlapping Sr and Nd isotopic fields (figure 2.10a), basalts from Vestmannaeyjar and Veidivotn have distinct and internally homogeneous Pb isotopic signatures (figure 2.10b). All samples fall outside the field defined by recent basalts from the Reykjanes Ridge and Peninsula but within the range of samples from

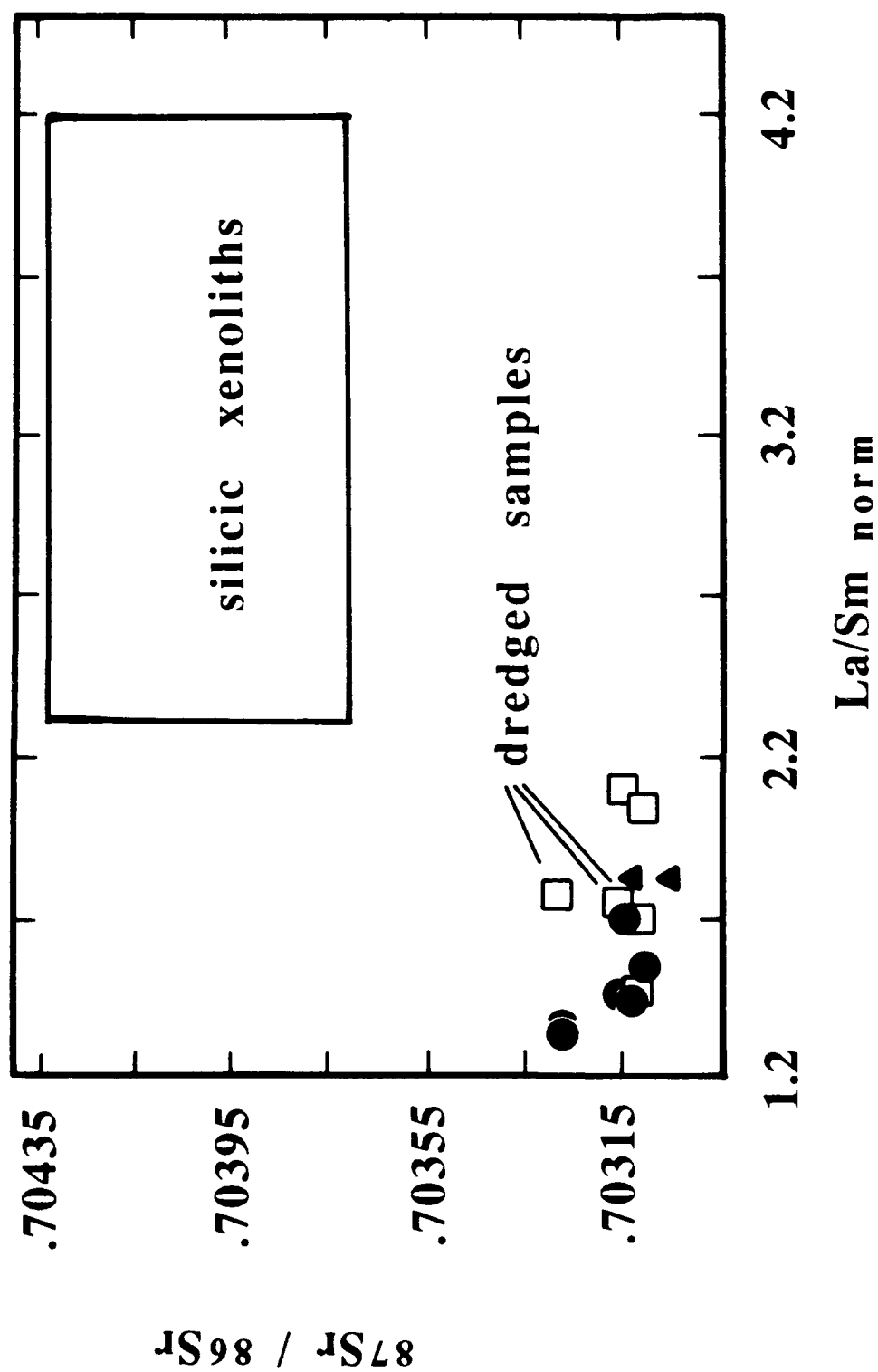


Figure 2.9 Radiogenic Sr of leached subaerial Surtsey samples (filled circles) show a slight inverse correlation with normalized La/Sm. Samples from the remainder of the archipelago fall off this apparent trend. Symbols as in figure 2.5.

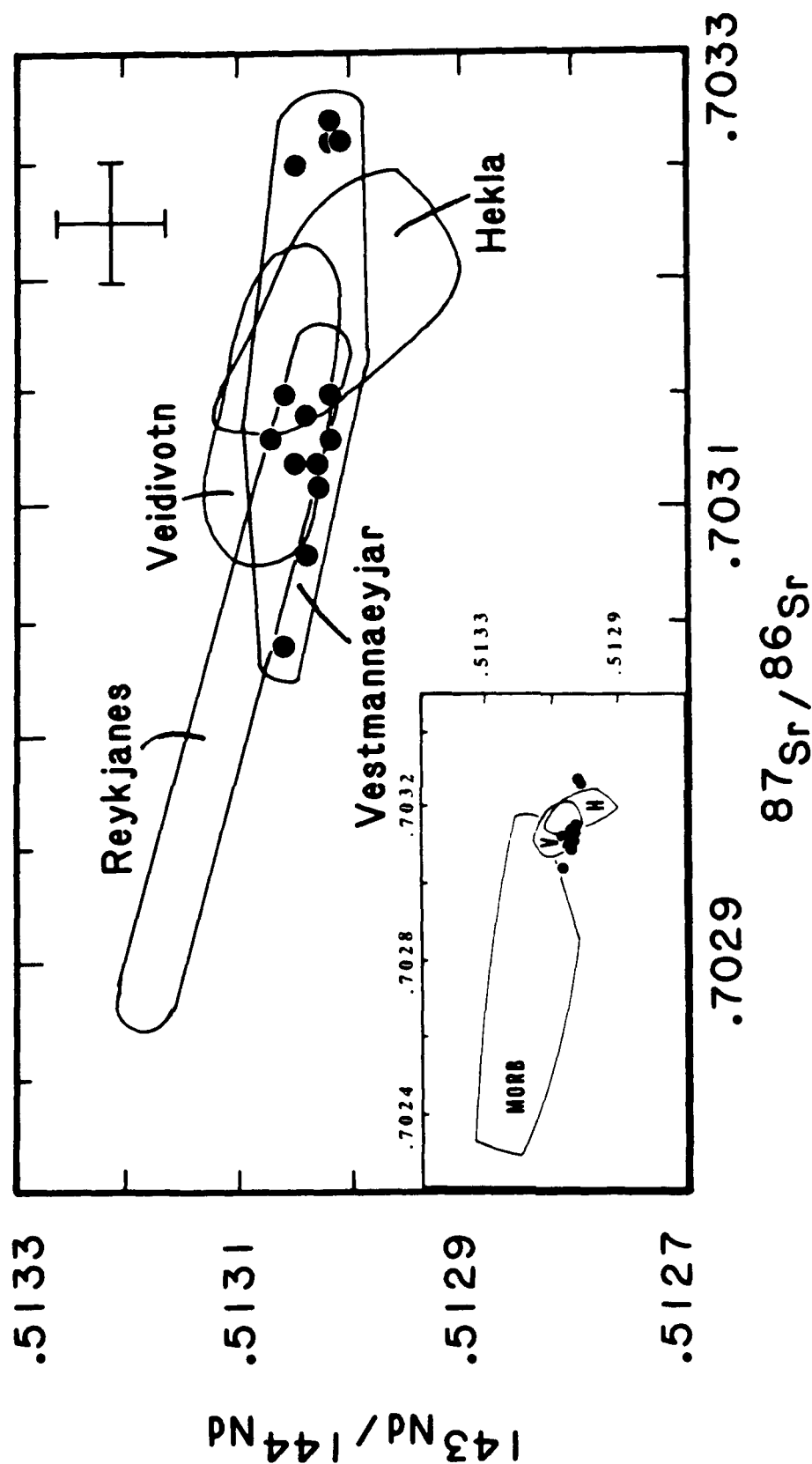
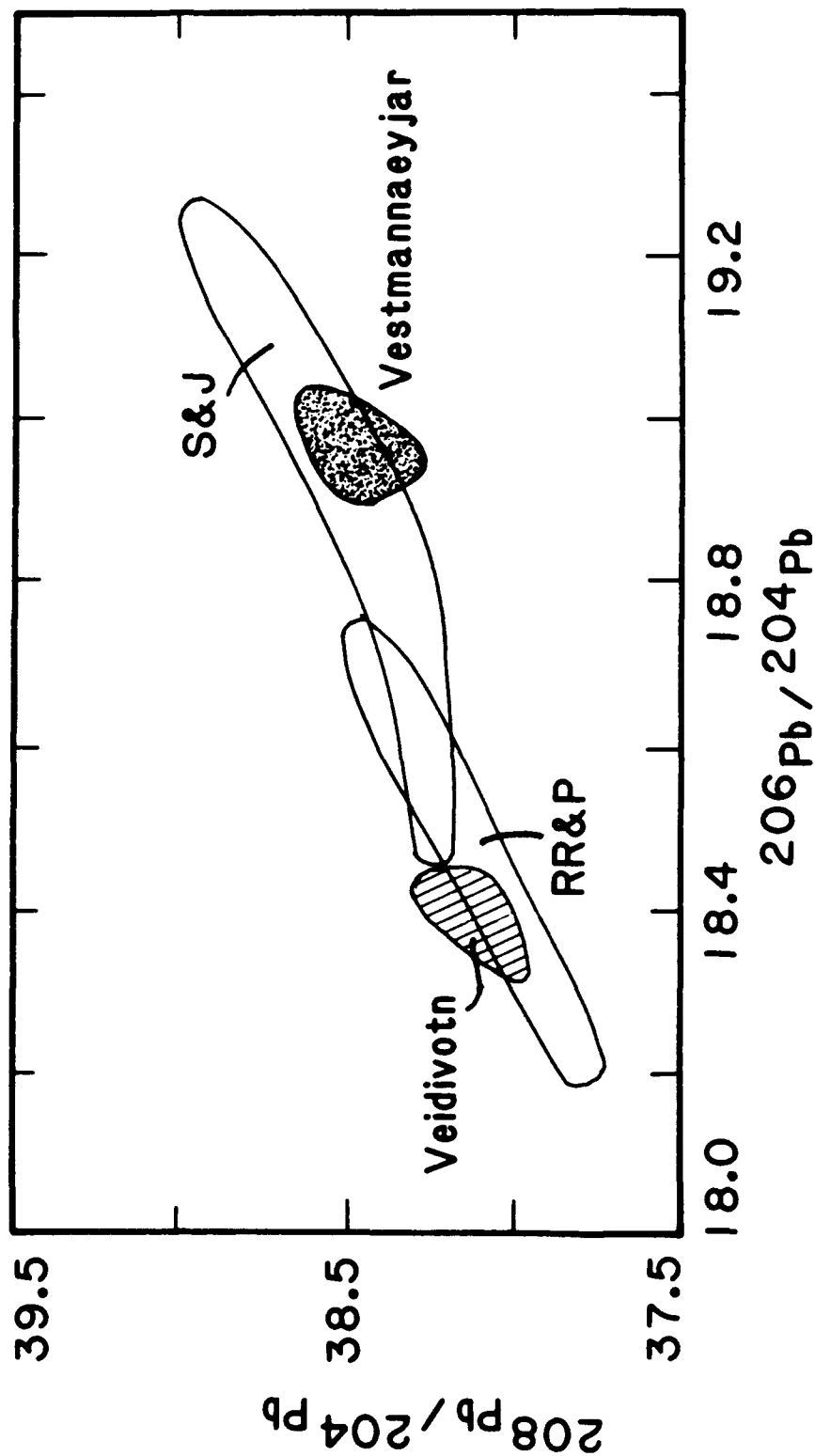


Figure 2.10

(a) The range of Sr- and Nd-isotopic ratios of Vestmannaeyjar basalts (all samples acid-leached) overlaps those of transitional Hekla (7 samples) and tholeiitic Veidivotn basalts (6 samples; Park et al., in prep). Tholeiitic lavas from the Reykjanes Peninsula are also isotopically similar, while Reykjanes picrites have a more depleted signature (range of values on acid-leached samples from Stecher et al., 1986). All samples from Vestmannaeyjar and Veidivotn fall within the field of normal MORB from the north Atlantic (28 samples; White & Hofmann, 1982; Zindler et al., 1982; Ito et al., 1987).



(b) Lavas from Vestmannaeyjar (alkalic) and Veidivotn (tholeiitic) have $^{208}\text{Pb}/^{204}\text{Pb}$ and $^{206}\text{Pb}/^{204}\text{Pb}$ within the field defined by Icelandic samples of Sun & Jahn (1975; 10 samples, field labeled S&J) and Reykjanes Ridge and Peninsula samples of Sun et al (1975; 20 samples, field labeled RR&P, samples are less radiogenic with increasing distance away from Iceland). The two neovolcanic centers each define a homogeneous cluster, suggesting local mantle source homogeneity in Pb isotopic composition.

the remainder of Iceland (Sun et al., 1975; Sun & Jahn, 1975; Park et al., in prep). These data suggest a decoupling of the Pb system from Sr and Nd in the neovolcanic centers, as observed in Tertiary lavas from eastern and western Iceland (Hanan & Schilling, 1986, 1987). The two silicic xenoliths from Surtsey plot within the field of Vestmannaeyjar lavas. In summary, radiogenic isotope ratios in Vestmannaeyjar lavas range slightly beyond analytical precision (thereby providing evidence for a heterogeneous mantle source or open system behavior during fractionation), but their distinctive grouping (e.g., figure 2.10b) suggests that Vestmannaeyjar lavas share a common petrogenesis.

2.3.3 Oxygen Isotope Systematics

Oxygen isotopic ratios have been determined for eleven historic and prehistoric Vestmannaeyjar lavas (Muehlenbachs & Jakobsson, 1973; Muehlenbachs et al., 1974); no additional data were obtained in this study. All samples have $\delta^{18}\text{O}$ between +5.5 and +5.7 per mil relative to SMOW (figure 2.11).

2.4 Discussion

2.4.1 Quantitative Approach to Modelling

The time-stratigraphic sample suites from Eldfell and Surtsey provide a detailed record of these two magmatic events. In both eruptions, the initial lavas were the most evolved (figure 2.3). This eruptive style is commonly attributed to tapping of a stably density-stratified magma chamber (e.g., Hildreth, 1983; Bacon, 1986). Although the radiogenic isotopic evidence suggests either minor heterogeneity in the mantle beneath Vestmannaeyjar or open system behavior during magma ascent, continuous eruptive activity indicates that the lavas are genetically related. A simple initial model for relating compositionally variable lavas from a single eruption is closed-system fractional crystallization. We used mineral and whole rock compositions and experimental phase

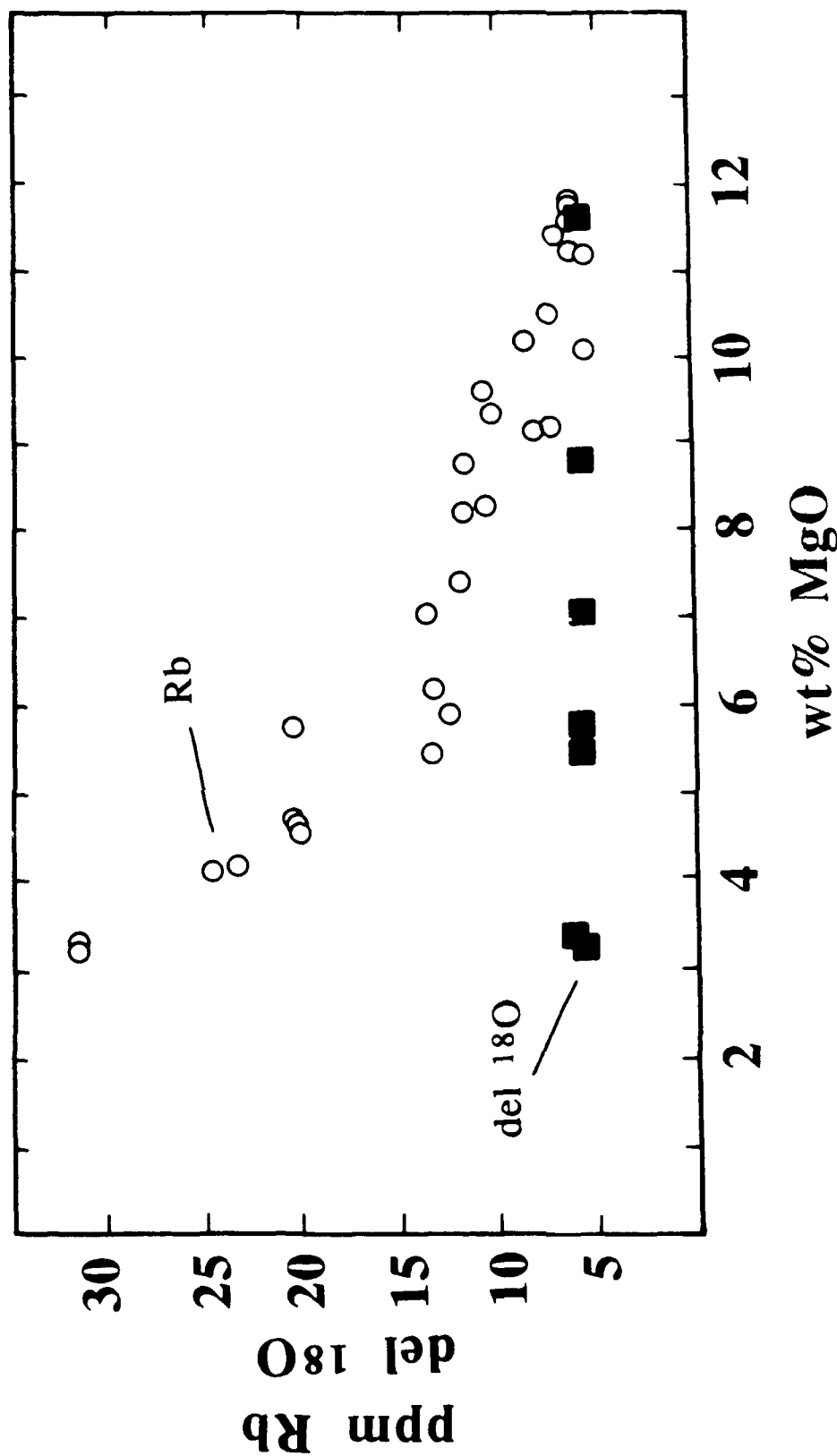


Figure 2.11

Samples from throughout Vestmannaeyjar have oxygen isotope ratios between 5.5 and 5.7 per mil, suggesting they have not interacted with meteoric water. In contrast, the Rb contents of these samples increase systematically with decreasing MgO content. Rb is highly mobile in aqueous fluids so an increase in Rb content due to alteration or hydrothermal interaction would be accompanied by a depletion in oxygen isotopic signature.

equilibria data to test this model for Vestmannaeyjar lavas. Our approach is to evaluate this simple model. If it is unsatisfactory we consider more complex models such as open system fractional crystallization and crustal melting (Oskarsson et al., 1982; Steinthorsson et al., 1985).

One atmosphere anhydrous phase relations have been determined for one Eldfell hawaiite (4.1 wt% MgO - Steinthorsson et al., 1985), and two Surtsey basalts (9.0 wt% MgO - Tilley et al., 1964; 8.1 wt% MgO - Steinthorsson et al., 1985). These experiments show that the phenocrysts in Vestmannaeyjar lavas (olivine + plagioclase + magnetite) are consistent with small degrees of low pressure crystallization. The Eldfell hawaiite has spinel (magnetite?) as the liquidus phase at 1178°C, followed by plagioclase (1167°C) and olivine (1137°C), whereas the Surtsey basalts have olivine on the liquidus (1210°C) followed by plagioclase (1180°C) and clinopyroxene (1160°C).

Previous attempts to model compositional trends within the Eldfell and Surtsey suites using observed and experimentally determined (1 atm) equilibrium phenocryst assemblages have been unsuccessful (Jakobsson, 1979; Thy, 1983). Thy (1983) proposed that Vestmannaeyjar lavas underwent fractionation at moderate pressure, then rose quickly to near-surface conditions where the observed phenocrysts grew immediately prior to eruption. We evaluated this hypothesis for lavas from the Eldfell and Surtsey eruptions. We have not attempted to relate the Eldfell series directly to the Surtsey lavas through fractionation processes, primarily because of the considerable compositional gap between the two suites (from 7.0 to 4.7 wt% MgO). The occurrence of lava compositions intermediate to these two extremes within the remainder of the archipelago (figure 2.5) suggests that a continuum exists between these series.

Crystal fractionation within each lava suite was investigated quantitatively in two ways. We refer to the first method as an inverse model (T. Juster, pers. commun., 1988). This method uses a polynomial fit of order 1 to 4 to describe major element oxide variations as a function of MgO content for a given series of liquid compositions.

These "best-fit" curves are divided into 10 segments within which a standard multiple polynomial regression determines phase proportions. Phase compositions were calculated to be in equilibrium with the residual liquid, using experimentally determined exchange distribution coefficients (Kds) for minerals and melt (see table 2.3 for Kds and sources of experimental data). This method treats the samples as a group, which defines a curved liquid line of descent approximated by short linear segments. The degree of fractionation is constrained by fitting all major element oxides, inasmuch as incompatible major elements (K, P) are not weighted in calculation.

The fractionating phase assemblages were also calculated independently using the major element forward modeling technique of Grove & Baker (1984). This calculation involves incremental subtraction of solid phases (in this case, 2 wt% increments) from a selected parental liquid composition. The residual liquid is renormalized to 100 wt% prior to each increment of phase subtraction. Microprobe data on the actual phenocryst phases (Thy, 1983; Jakobsson et al., in prep) were used to constrain olivine and plagioclase compositions. Phase proportions are estimated from experimental data and published phase diagrams (Grove & Bryan, 1983; Grove & Baker, 1984; Mahood & Baker, 1986; Sack et al., 1987; Tormey et al., 1987); repeated iteration establishes the effects of changing modal proportions. Abundances of incompatible major or trace elements (e.g., K, P, Rb, Ba, La, Ta, Th) may be used to constrain the degree of fractionation, i.e., the number of incremental iterations. This method assumes perfect Rayleigh fractionation such that $C_1/C_0 = F^{D-1}$, where $D = 0$ for these incompatible elements. Estimates of F calculated at Eldfell are consistent for incompatible major and trace elements: K, Ba, Rb, Th suggest $F = 0.65-0.68$ and P, La, Zr, Hf, Ta suggest $F = 0.69-0.71$. The two modeling techniques produce comparable results in the case of the Eldfell lavas; systematic differences encountered in modeling Surtsey lavas will be discussed separately.

Table 2.3 Calculation of Mineral Compositions

Olivine (Mg, Fe)₂SiO₄
 Pyroxenes (Ca, Mg, Fe, Al, Na, Ti)₂(Si, Al)₂O₆
 Plagioclase (Ca, Na)(Al, Si)₄O₈

$$K_D^{ol} = \left(\frac{X_{Fe}}{X_{Mg}} \right)_{oliv} \left(\frac{X_{Mg}}{X_{Fe}} \right)_{liq} = 0.30 - 0.33 \quad (1, 6, 7)$$

$$K_D^{cpx} = \left(\frac{X_{Fe}}{X_{Mg}} \right)_{cpx} \left(\frac{X_{Mg}}{X_{Fe}} \right)_{liq} = 0.23 - 0.25 \quad (2, 3, 4, 5)$$

$$K_D^{opx} = \left(\frac{X_{Fe}}{X_{Mg}} \right)_{opx} \left(\frac{X_{Mg}}{X_{Fe}} \right)_{liq} = 0.28 - 0.29 \quad (6, 7)$$

$$K_D^{plag} = \left(\frac{X_{Ca}}{X_{Na}} \right)_{plag} \left(\frac{X_{Na}}{X_{Ca}} \right)_{liq} = 0.85 - 1.57 \quad (2, 3, 4, 8)$$

$$K_{Al}^{cpx} = \frac{(Al_2O_3)_{cpx}}{(Al_2O_3)_{liq}} = \text{pressure- and composition-dependent} \quad (5, 6, 7, 9)$$

$$K_{Na}^{cpx} = \frac{(Na_2O)_{cpx}}{(Na_2O)_{liq}} = 0.1 - 0.2 \quad (2, 4, 5, 6, 7)$$

$$K_{Ti}^{cpx} = \frac{(TiO_2)_{cpx}}{(TiO_2)_{liq}} = \text{pressure- and composition-dependent} \quad (2, 4, 5, 6, 7)$$

$$K_{Al}^{opx} = \frac{(Al_2O_3)_{opx}}{(Al_2O_3)_{liq}} = 0.21 - 0.36 \quad (6, 7, 9)$$

$$K_{Na}^{opx} = \frac{(Na_2O)_{opx}}{(Na_2O)_{liq}} = 0.04 \quad (6, 7)$$

$$K_{Ti}^{opx} = \frac{(TiO_2)_{opx}}{(TiO_2)_{liq}} = \text{strongly pressure-dependent} \quad (6, 7)$$

- Sources of data:
- 1 Roeder & Emslie, 1970
 - 2 Walker et al., 1979
 - 3 Fisk et al., 1980
 - 4 Grove & Bryan, 1983
 - 5 Mahood & Baker, 1986
 - 6 Takahashi, 1980
 - 7 Takahashi & Kushiro, 1972
 - 8 Thy, 1983
 - 9 Presnall et al., 1979

2.4.2 Evolution of the Eldfell Lava Series

At Eldfell, sample VE-144 was chosen as the parental composition. It has higher MgO and lower incompatible element abundances than other Eldfell samples (table 2.2), and this composition comprises over 80% of the eruption (Jakobsson et al., 1973). If the eruptive episode reflects withdrawal from a single chamber, numerical models of magma extraction (Spera et al., 1986) indicate that this composition (i.e., hawaiite) was dominant within the magma body. We then determined if the relatively evolved Eldfell sample VE-110 could be produced by closed system fractional crystallization of VE-144.

In modeling crystallization of Eldfell liquids, MgO and Al_2O_3 contents are controlled largely by olivine and plagioclase fractionation, respectively. Crystallization of oxide phases depletes residual liquid in FeO^* and TiO_2 while enriching it in SiO_2 . We concur with Jakobsson (1979) and Thy (1983) that it is not possible to explain the compositional trends during the Eldfell eruption by fractionating the 1 atm phenocryst assemblage (olivine + plagioclase + oxides; Jakobsson, 1979). If the inferred F (melt fraction based on incompatible element enrichment) and MgO content are matched, the 1 atm model fails to explain CaO and Al_2O_3 contents; these oxides are sensitive to clinopyroxene fractionation. As indicated in figure 2.12 a clinopyroxene-free fractionating assemblage which matches F and MgO constraints cannot generate the decreases in CaO or $\text{CaO}/\text{Al}_2\text{O}_3$ ratio observed in the Eldfell lava series. An increased proportion of plagioclase in the fractionating assemblage would reduce CaO mismatch but increase the discrepancy in $\text{CaO}/\text{Al}_2\text{O}_3$ ratio.

We can reproduce the Eldfell trends with a fractionation model which utilizes olivine, plagioclase, clinopyroxene and Fe-Ti oxides (table 2.4). Ilmenite precipitation is inferred for samples more evolved than VE-114 because of the abrupt decrease in TiO_2 at this MgO concentration (4.1 wt, figure 2.5). The total amount of crystallization required is 34% (by weight) of parental liquid VE-144.

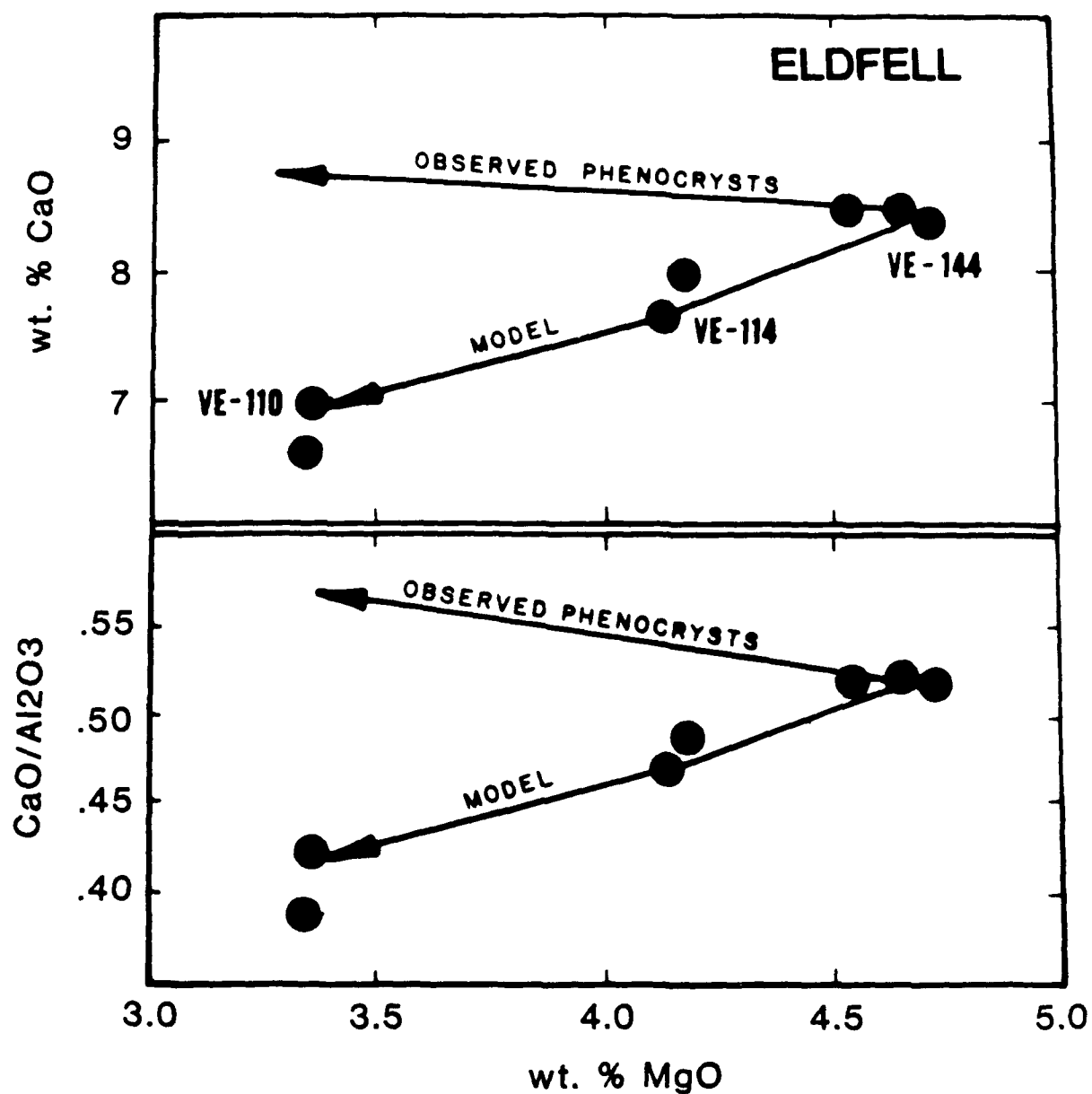


Figure 2.12 Fractional crystallization models for the Eldfell suite which use the observed phenocrysts (olivine + plagioclase +/- oxides) cannot reproduce chemical trends of the samples. A fractionating assemblage which involves clinopyroxene is able to fit the data successfully (see table 2.4 for phase proportions).

Table 2.4 Fractionation of Lavas from 1973 Eldfell Eruption

	Liquid Composition										Mode of Fractionating Solid				F, %
	SiO ₂	TiO ₂	Al ₂ O ₃	FeO*	MgO	MnO	CaO	K ₂ O	Na ₂ O	P ₂ O ₅	olv	plg	aug	tmt	ilm
VE-144	47.52	3.14	16.18	13.64	4.70	0.24	8.49	1.01	4.57	0.51	12.0	43.0	27.7	17.4	-
	47.54	3.16	16.12	13.56	4.70	0.24	8.43	1.00	4.54	0.51	11.6	44.0	26.1	18.3	-
	47.79	3.13	16.16	13.47	4.54	0.24	8.25	1.04	4.62	0.53	11.3	44.9	24.8	19.0	-
	48.06	3.09	16.20	13.36	4.39	0.24	8.08	1.08	4.70	0.55	11.0	45.7	23.6	19.7	-
	48.35	3.03	16.24	13.24	4.24	0.24	7.91	1.13	4.78	0.57	11.0	46.7	22.4	19.5	0.4
	48.66	2.97	16.28	13.11	4.09	0.24	7.74	1.18	4.87	0.59	11.0	47.7	21.3	19.0	1.0
	48.99	2.88	16.32	12.97	3.94	0.25	7.57	1.24	4.96	0.62	11.1	48.6	20.3	18.6	1.5
	49.33	2.79	16.35	12.82	3.79	0.25	7.41	1.30	5.06	0.64	11.1	49.4	19.3	18.1	2.0
	49.69	2.68	16.38	12.66	3.63	0.25	7.25	1.37	5.16	0.67	11.2	50.2	18.5	17.7	2.4
	50.06	2.55	16.41	12.49	3.48	0.26	7.10	1.44	5.26	0.69	sum residuals squared = 0.01				
VE-110	50.12	2.55	16.47	12.53	3.50	0.26	7.13	1.44	5.28	0.70					

Total fractionation interval = 34 wt% crystallization.

Mineral compositions calculated as in table 3 using the following parameters:

olv: Fe/Mg Kd = 0.30 Fo 67-62

plg: An/Ab Kd = 1.45 An 59-51

aug: Fe/Mg Kd = 0.23 Wo = 47.0

tmt: usp = 22.89

ilm: ilm = 50.56

We evaluate our major element model with constraints provided by the trace element data. Assuming perfect Rayleigh fractionation and using the partition coefficients given in the appendix we calculate bulk distribution coefficients (bulk D s) for the model fractionating assemblage (table 2.5). Observed bulk D s are extremely sensitive to the F used in modeling. We used the maximum F (i.e., minimum degree of crystallization) which results in non-negative bulk D s for highly incompatible elements such as Ba, Rb and La. The required bulk D s for the REE are consistent with a crystallizing assemblage dominated by clinopyroxene (figure 2.13); a satisfactory fit to the data uses set B distribution coefficients (see Appendix). The highly compatible behavior of scandium (table 2.5) reflects large clinopyroxene/melt K d's for this element in hawaiitic liquids (Lemarchand et al., 1987). Observed bulk D s for the other transition metals (V, Co) indicate substantial magnetite fractionation, while the increased compatibility of Nb in step II corresponds to precipitation of ilmenite (Green & Pearson, 1987). The importance of plagioclase fractionation is apparent from the large bulk D for Sr and the slight positive Eu anomaly in figure 2.13.

The near-constant proportions of olivine, plagioclase and clinopyroxene crystallizing throughout the fractionation interval (table 2.4) suggest evolution along a multiply saturated cotectic. Moderate pressure (8 kbar) experiments by Mahood & Baker (1986) on a mildly alkalic basalt from Pantelleria showed that liquidus clinopyroxene was followed within 25°C by the 3-phase assemblage olivine + clinopyroxene + plagioclase. The cotectic assemblage inferred at Pantelleria is richer in pyroxene than that at Eldfell and lacks Fe-Ti oxides (cpx 61: plag 30: oliv 9; Mahood & Baker, 1986). These differences may be related to two factors: (1) the Pantelleria starting composition is more magnesian (~7 wt% MgO) than VE-144 and (2) the experiments were conducted under reducing conditions (graphite buffer) where Fe-Ti oxide precipitation is inhibited. In contrast, magnetite-ilmenite pairs from Eldfell lavas indicate an oxygen fugacity near the QFM buffer (Jakobsson et al., 1973).

Table 2.5 Evaluation of Eldfell Model with Trace Elements

Element	C_l/C_0	Bulk D_{obs}	Bulk D_{calc}
Ba	1.48	0.06	0.03-0.30
Sr	0.98	1.05	0.65-1.67
Sc	0.71	1.82	0.47-1.54
V	0.29	3.80	4.83-12.42
Co	0.93	1.17	1.12-2.78
Zr	1.42	0.16	0.12-0.22
Hf	1.40	0.19	0.12-0.22
Nb	1.35	0.28	0.15-0.18
Ta	1.44	0.12	~0.19-0.25
La	1.43	0.14	0.06-0.22
Ce	1.44	0.12	0.06-0.22
Nd	1.35	0.28	0.08-0.27
Sm	1.30	0.37	0.11-0.34
Eu	1.26	0.44	0.19-0.44
Tb	1.29	0.39	0.11-0.39
Yb	1.28	0.41	0.13-0.40
Lu	1.31	0.35	0.13-0.39

Bulk D not calculated for Cr and Ni because samples VE-114 and VE-110 have Cr abundances below detection limit and our Ni are imprecise at these low abundances.

Observed bulk Ds are calculated assuming Rayleigh fractionation, i.e.,

$$C_l/C_0 = F^{D-1}$$

where C_l = concentration of an element in the daughter liquid VE-110

C_0 = concentration of an element in the parent liquid VE-144

F = degree of crystallization calculated from major element modeling (see table 4).

Calculated bulk Ds represent a weighted sum of individual Ds from the Appendix with the model fractionating assemblage.

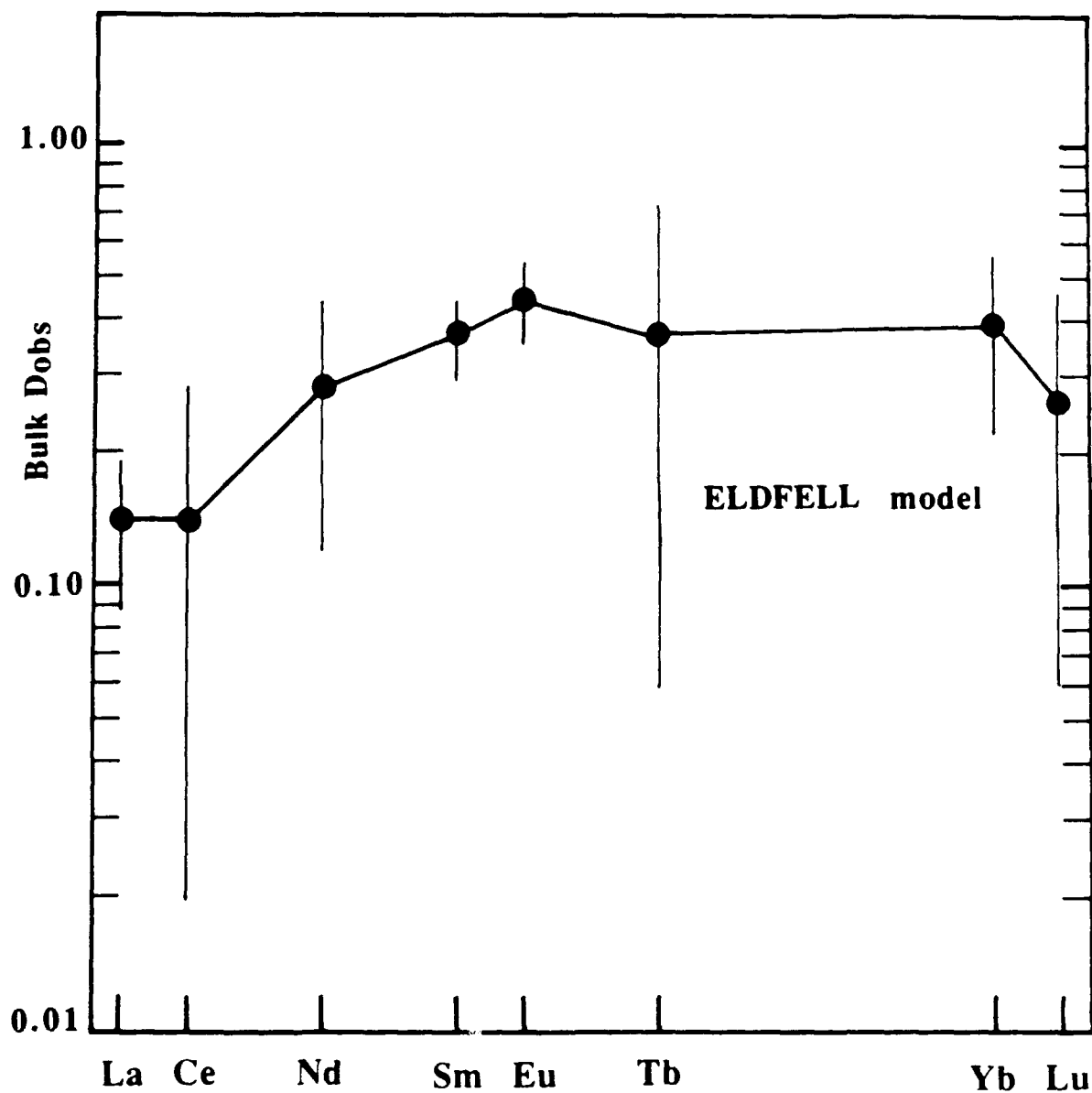
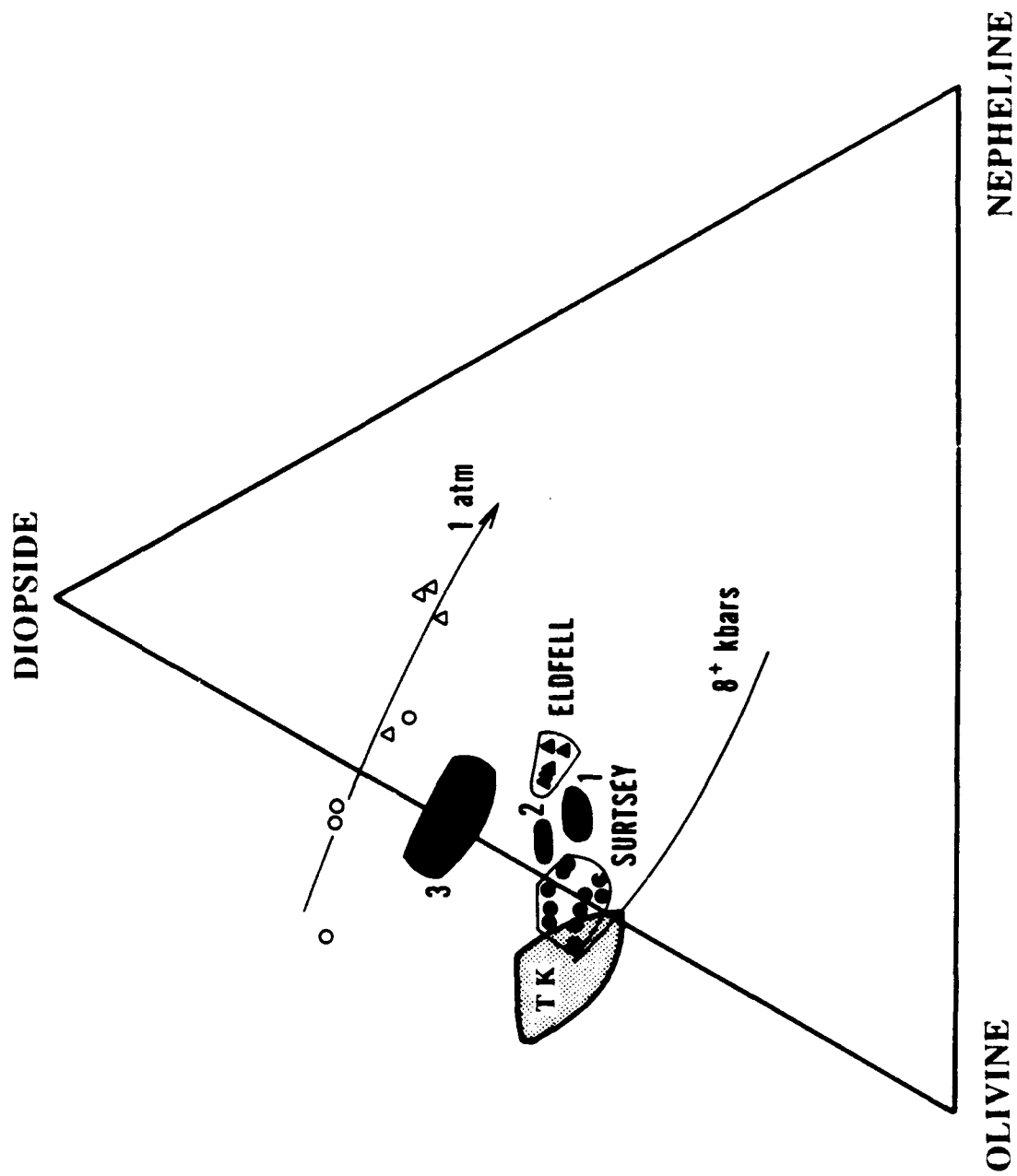


Figure 2.13 Observed bulk distribution coefficients for REE at Eldfell, calculated from element abundances in parent (VE-114) and daughter (VE-110) liquids, using the F determined by major element modeling (table 2.4). Observed bulk D s are very sensitive both to F and to the analyzed concentration of an individual element (see table 2.5 for calculation of bulk D). Note the concave downwards shape indicative of clinopyroxene fractionation and the slightly positive Eu anomaly which is consistent with 43-50% plagioclase in the segregating solid. Data points indicate average values based on replicate analyses of parent and daughter samples; the error bars indicate actual analytic precision.

Strong support for moderate pressure evolution of Vestmannaeyjar lavas is seen in the pseudoquaternary molar projection scheme developed for alkaline rocks (Sack et al., 1987). Figure 2.14 shows the experimentally determined multiply saturated cotectic (olivine + plagioclase + clinopyroxene +/- Fe-Ti oxide) based on 1 atmosphere phase relations of natural and synthetic alkaline compositions. The indicated higher pressure liquid compositions are from the peridotite - basalt melt experiments of Takahashi & Kushiro (1983) and Fujii & Scarfe (1985), and they represent liquids multiply saturated with olivine + clinopyroxene + orthopyroxene + spinel. On the basis of this projection it is clear that the Vestmannaeyjar lavas are not the result of crystallization at 1 atmosphere pressure (figure 2.14). The appropriateness of this projection scheme to Vestmannaeyjar is indicated by basanitic segregation veins in lavas from Eldfell and Surtsey which lie along the 1 atm cotectic. A late-stage low pressure origin is inferred for these veins as they commonly fill cracks and pockets within individual lava flows. They represent evolved alkaline liquids and contain phenocrysts of alkali feldspar, nepheline, aegerine and aenigmatite (Jakobsson, 1979; Sigmarsson et al., in prep.)

We recognize that a moderate pressure fractionation model is not a unique solution for evolution of the Eldfell series, but it is internally consistent and geologically reasonable. The Eldfell eruption was preceded and accompanied by intense seismic activity which decreased as the extrusion rate waned. Earthquake hypocenters were located directly beneath the volcano at 15-25 km depth (Einarsson, 1986; figure 2.15). The seismicity is clearly related to magma movement and suggests that magma was stored prior to eruption in a chamber at 15-25 km, that is, pressures of 5-8 kbars. The Eldfell area is seismically inactive today (P. Einarsson, pers. commun., 1987). The fractionation environment inferred from our petrogenetic model corresponds to the depth range of magma storage suggested from seismic evidence, thus supporting the hypothesis that moderate pressure processes control evolution of Eldfell lavas.

Figure 2.14 Locations of experimentally determined 1 atm and moderate pressure (8-10 kbar) multiple saturation surfaces for alkaline rock series are projected from plagioclase in the plagioclase-olivine-diopside-nepheline tetrahedron using the projection components and data of Sack et al (1987; and references therein). The field labeled TK represents 8-10 kbar liquids of Takahashi & Kushiro (1983). Surtsey whole-rock samples (filled circles) cluster near the 8+ kbar olivine + orthopyroxene saturation surface and show gradual evolution towards higher nepheline component and lower pressure. Shaded fields labeled 1, 2 and 3 enclose glass analyses from the first (December 1963), second (February 1964) and subsequent phases of explosive activity (Jakobsson et al., in prep). Note that the earliest and most evolved Surtsey whole-rock lies within the field of coeval glass analyses. Eldfell lavas (filled triangles) lie at a pressure intermediate to the 1 atm and 8+ kbar saturation surfaces. The most evolved Eldfell samples have higher normative nepheline component. Late-stage segregation veins from both suites (circles = Surtsey, triangles = Eldfell) lie along the experimentally determined 1 atm curve.



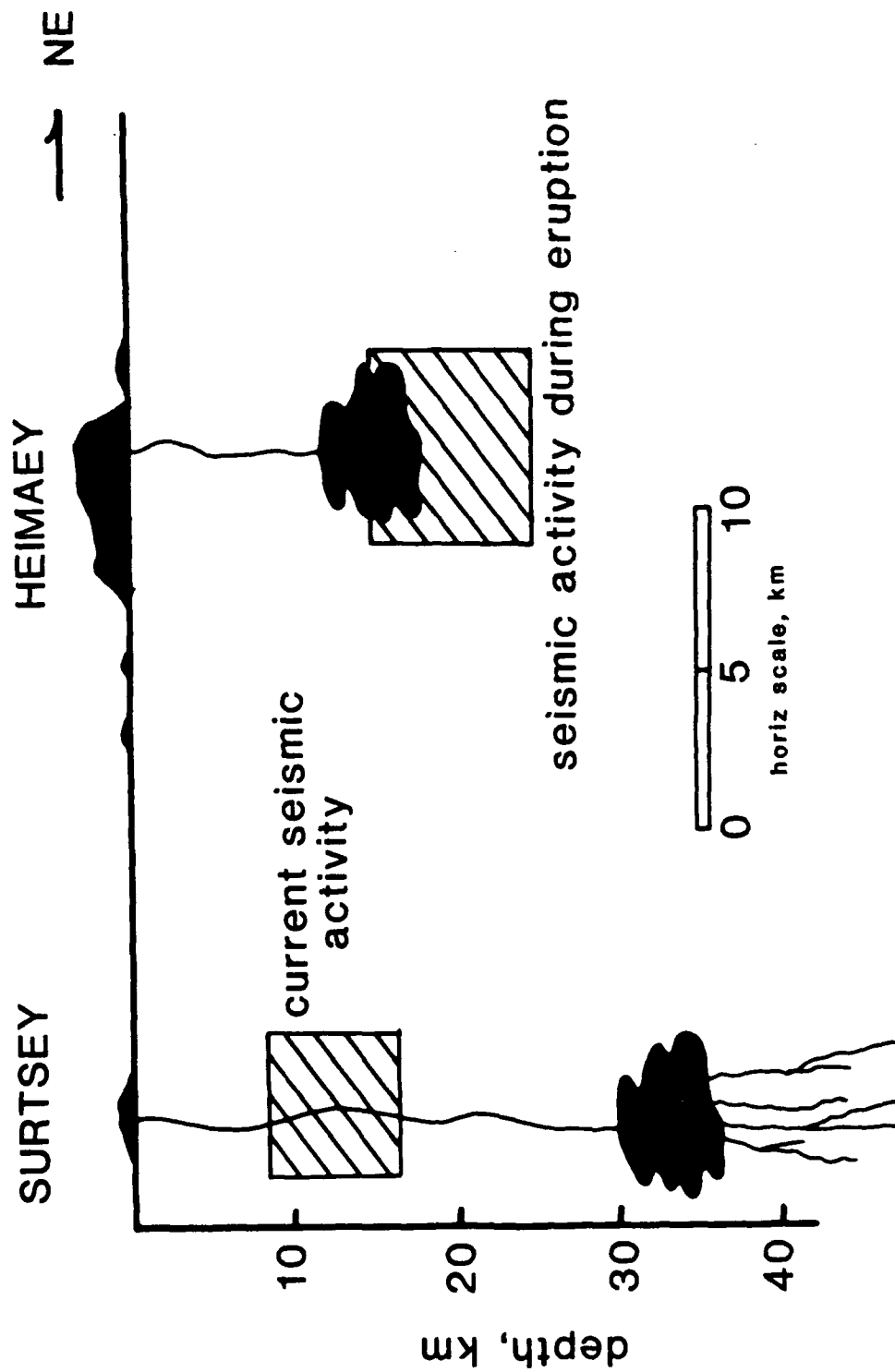


Figure 2.15

Schematic cross section of the Vestmannaeyjar region. Shaded magma chambers are drawn at depths inferred from phase equilibrium studies. Hatched regions are areas of earthquake activity during the 1973 Eldfell eruption (beneath Heimaey) and at present (beneath Surtsey). Melt segregation within the upper mantle is indicated schematically beneath Surtsey.

2.4.3 Evolution of the Surtsey Lava Series

The eruption of Surtsey (1963-1967) was longer-lived and more complex than that of Eldfell. Lavas of comparable composition were erupted through several closely-spaced vents (figures 2.2, 2.3), suggesting repeated influx of material to the system. Lavas from the main vent show a small range in $^{87}\text{Sr}/^{86}\text{Sr}$ (0.70308-0.70326) and they form a distinct field in Pb isotopic ratios (figure 2.10b). Major and trace element trends among Surtsey lavas are systematic (figures 2.5, 2.6, 2.7, 2.8, 2.9). We therefore evaluate a simple model of closed system fractional crystallization to explain the major element compositional trends because the small isotopic heterogeneity may not be manifest in the major elements. We subsequently evaluate this hypothesis using the trace element data. The modeling involves samples from the Surtsey vent plus the initial and most evolved lava of the eruptive sequence, sample 4638 from the submarine vent Surtla (figure 2.2).

The chosen parent is sample 9850, a hypersthene-normative alkali basalt with Mg# 63.8. Although this sample contains 11.7 wt% MgO, we believe it represents a liquid because it is sparsely phyrlic and has Ni, Sc, Co, and Cr abundances comparable to those of primitive ocean floor basalts (BVSP, 1981). Glass and whole rock analyses from the first two tephra - lava eruptive cycles (12/63 and 2/64) overlap (figure 2.14), suggesting that the bulk analyses record acceptable liquid compositions. In contrast, lavas erupted after February 1964 do not have compositional equivalents among glasses analyzed from associated tephtras (figure 2.14). We infer that the later lavas, which do not appear accumulative based on petrographic criteria, also record liquid compositions and that the late tephtras represent material purged from the conduit during eruption. We therefore rely upon the bulk lavas to record the conditions of fractionation within magma bodies beneath Vestmannaeyjar.

As with the Eldfell series, major element models using the observed phenocryst phases (olivine + plagioclase +/- oxides) fail to reproduce the compositional trends of the

basalts. Unlike the Eldfell case, the addition of clinopyroxene alone to the phenocryst assemblage does not yield satisfactory models. Specifically, this assemblage fails not only to fit CaO and Al_2O_3 but there are also large discrepancies in abundances of FeO^* and SiO_2 . In order to estimate a geologically reasonable fractionating phase assemblage, we projected the Surtsey data within the reduced natural pseudoquaternary system CaO-MgO- Al_2O_3 - SiO_2 (CMAS). There are two important observations (figure 2.16). First, the lavas plot in a region described by experimentally determined moderate pressure (>10 kbar) phase boundaries, not those of 1 atm phase equilibria. This is consistent with inferences from figure 2.14. The positions of both moderate and low pressure cotectics are composition dependent (Mahood & Baker, 1986; Sack et al., 1987); the range of 10 kbar melts (Takahashi & Kushiro, 1983; Fujii & Scarfe, 1985; shaded region in figures 2.16a and 2.16b) suggests the magnitude of this effect.

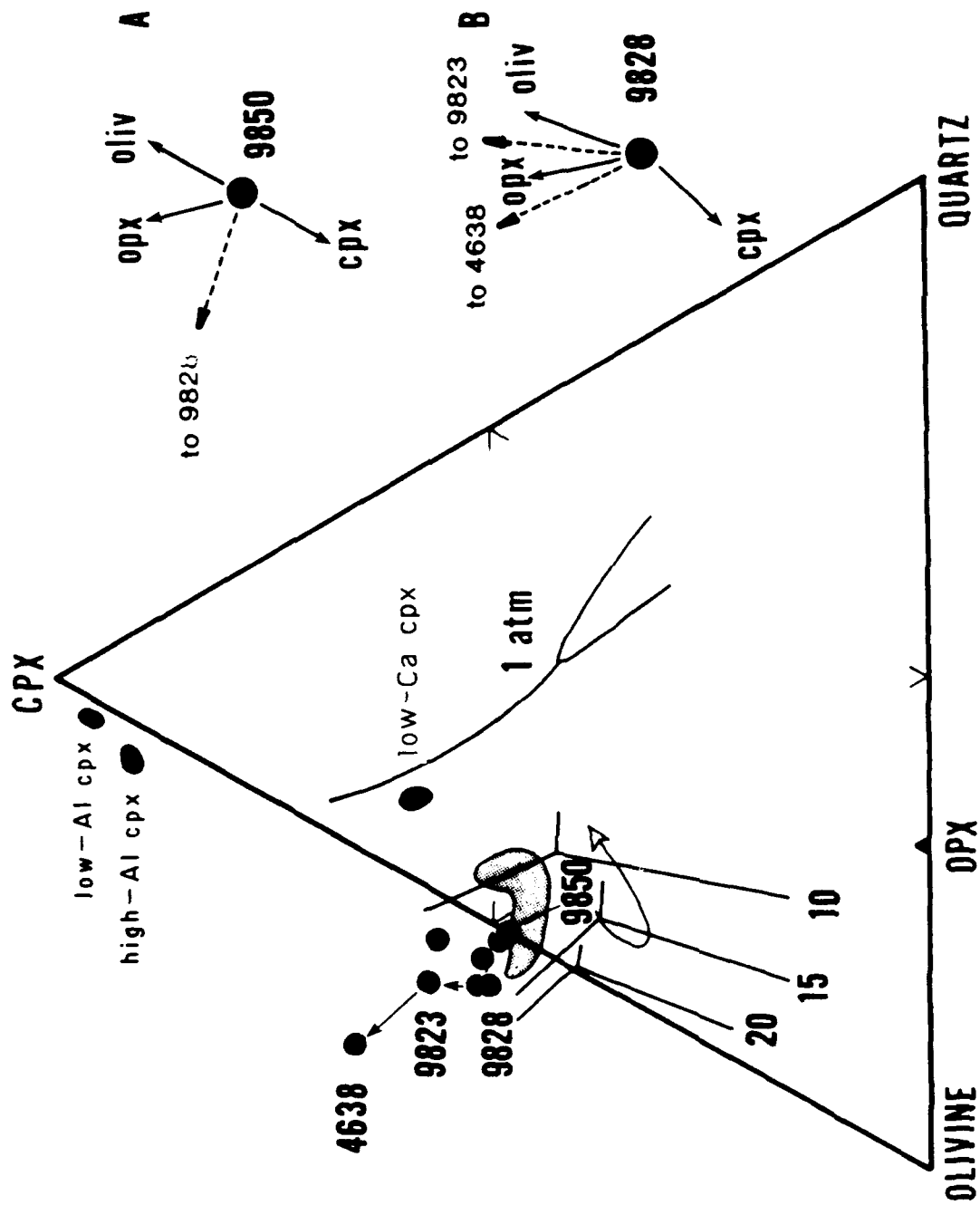
A second important observation is that the more evolved Surtsey samples plot progressively further from the olivine-diopside join away from the quartz apex (figure 2.16a). Surtla sample 4638 which was erupted in December 1963, slightly before sample 9823 (February 1964), is the most evolved and most highly silica-undersaturated lava erupted from the Surtsey volcanic system. No combination of olivine, plagioclase and clinopyroxene (calcic or sub-calcic) crystallization can drive a liquid of 9850 composition along the observed evolutionary path. Extensive Fe-Ti oxide fractionation results in greater silica saturation, the reverse of the observed trend. The trend from 9850 to 9828 requires segregation of a SiO_2 -rich phase such as orthopyroxene. Figure 2.16b shows the major element compositions projected from the diopside apex onto the plane olivine-plagioclase-quartz; orthopyroxene control on fractionation from 9850 to 9828 is apparent here as well.

Qualitatively, evolution from liquid 9850 to 9828 is matched with a crystallizing assemblage which includes orthopyroxene + clinopyroxene. Liquids more evolved than 9828 require a different fractionating assemblage, specifically one involving olivine

Figure 2.16

(a) Projection from plagioclase in the CMAS pseudoquaternary system plagioclase-olivine-clinopyroxene-quartz (projection components of Presnall et al., 1978). We use the CMAS system to facilitate comparison with literature data when $\text{Fe}^{+2}/\text{Fe}^{+3}$, K_2O , P_2O_5 or other components are not reported. The qualitative arguments which we make on the basis of the projected diagrams are not altered by using other projection schemes. For clarity, only samples from the Surtla and Surtsey vents are shown. Phase boundaries at 1 atm are from Grove et al (1982); 10, 15 and 20 kbar phase boundaries are those of Stolper (1980). The shaded region encloses 10 kbar peridotite melts of Takahashi & Kushiro (1983) and Fujii & Scarfe (1985). Parental Surtsey lava 9850 lies on the olivine-clinopyroxene join within the clinopyroxene primary phase volume. This composition falls within the region bounded by olivine, orthopyroxene and calculated equilibrium high-Al clinopyroxene. The calculated composition of equilibrium low-Ca clinopyroxene (Wo 32) is also indicated. Fractionation vectors for these three phases (inset A) indicate that orthopyroxene + clinopyroxene control the observed (dashed) trend from 9850 to 9828. Similar vectors drawn for sample 9828 (inset B) suggest that olivine participates in later stages of evolution of Surtsey lavas. The curved arrow indicates schematically the movement of the pseudoinvariant point at pressures greater than ~15 kbars as suggested by O'Hara (1968).

(b) The same data shown projected from clinopyroxene. Crystallization of an olivine-dominated (and plagioclase-free) assemblage would drive liquids directly towards the plagioclase apex. The deflection of the evolution path of Surtsey liquids away from this apex requires that plagioclase be involved in the fractionating assemblage.



A

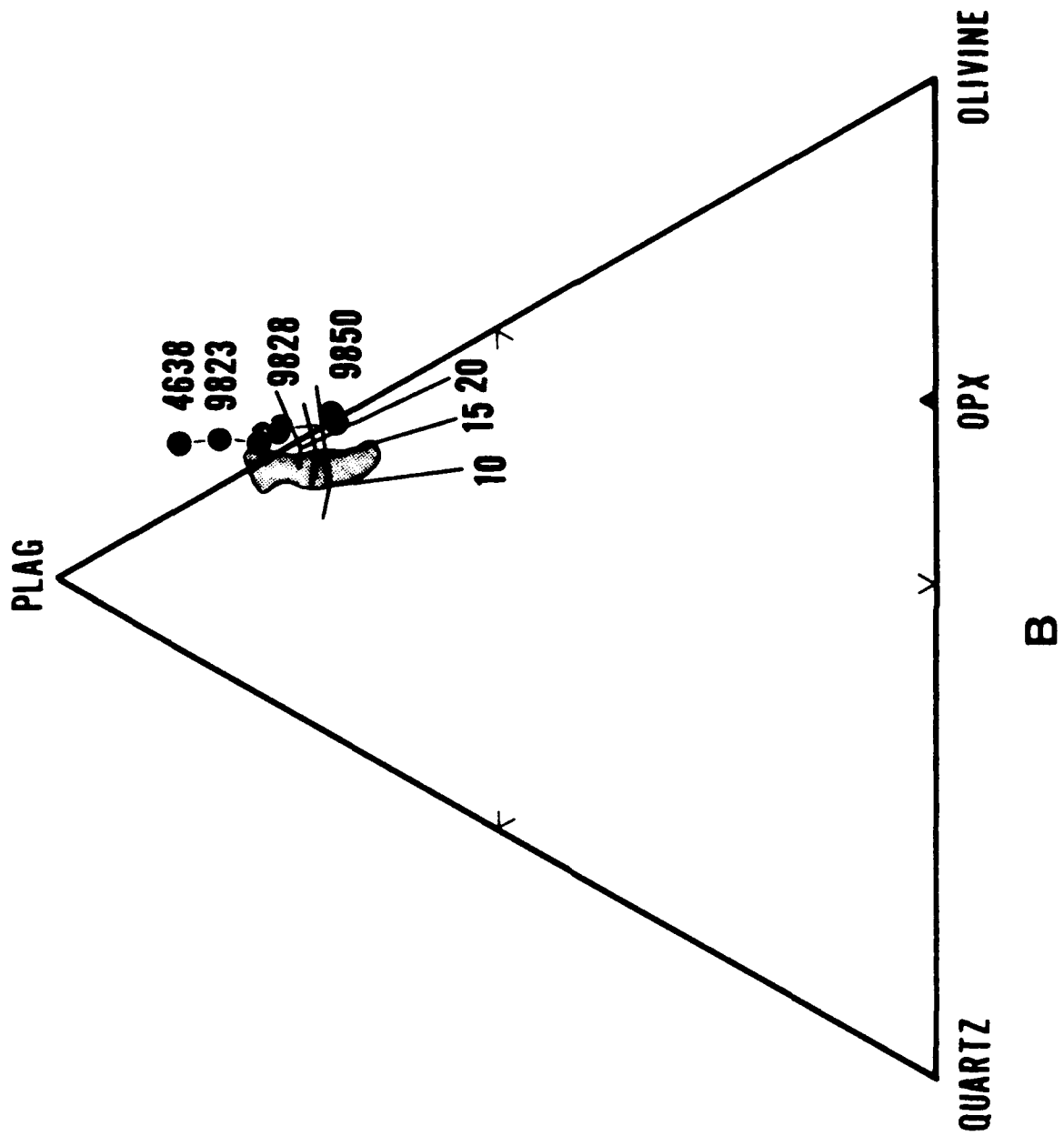


(figure 2.16a, inset B). The geometry of this fractionation path when projected from clinopyroxene (figure 2.16b) requires plagioclase precipitation as well, inasmuch as no combination of mafic phases alone can produce a fractionation path which deviates away from the plagioclase apex. These inferences are qualitative, but a plausible model is that the more evolved liquids formed within the plagioclase stability field at pressures of 8-10 kbars. The inferred depth of 30-35 km corresponds to the base of the lithosphere in the Vestmannaeyjar region (Palmason, 1971; Gebrande et al., 1980).

We applied the same major element modeling techniques used for the Eldfell lavas to constrain the nature and proportions of crystallizing phases. Pyroxene compositions were calculated as indicated in table 2.3 but considered only experiments using mildly alkaline basalt KRB (Mg# 65) as the starting composition because it is similar in composition to Surtsey basalts; compositions of coexisting olivine + orthopyroxene + clinopyroxene + liquid for this basalt are reported at 8, 14 and 20 kbars (Takahashi, 1980; Takahashi & Kushiro, 1983). Partitioning of MgO, FeO and Al_2O_3 between crystals and liquid observed in these experiments is consistent with that seen by Presnall et al (1979) in CMAS at 9 kbar. Using this major element partitioning data (table 2.3), the clinopyroxene in Surtsey xenolith 10172 (e.g., 7.8 wt% Al_2O_3 ; Jakobsson et al., in prep) could be a cogenetic cumulus phase in equilibrium with liquid 9823 (8.2 wt% MgO; table 2.2). Similar aluminous clinopyroxenes were found in high pressure (>8 kbar) experiments by Presnall et al (1978) and Mahood & Baker (1986).

An inverse model using the assemblage clinopyroxene + orthopyroxene with subordinate plagioclase + Fe-Ti oxide reproduces the major element trends for samples with greater than ~10.5 wt% MgO (table 2.6). The 5-phase assemblage inferred for more evolved basalts may reflect crystallization within two 4-phase stability fields (cpx + opx + plag + Fe-Ti oxide; cpx + oliv + plag + Fe-Ti oxide), not a single multiple saturation surface. Our calculated fractionating assemblages are not unique. For example, the relative proportions of aluminous clinopyroxene and plagioclase are

Table 2.6 Fractionation of Lavas from 1963-1967 Surtsey Eruption: Inverse Model

	Liquid Composition					Mode of Fractionating Solid					F, %					
	SiO2	TiO2	Al2O3	FeO*	MgO	CaO	K2O	Na2O	P2O5	olv		plg	aug	opx	tmt	
9850	47.22	2.02	13.63	11.85	11.77	10.56	0.33	2.44	0.20	-	4.2	34.5	51.8	9.5	.96	
	47.31	2.04	13.55	11.77	11.71	10.50	0.36	2.44	0.19	-	9.2	32.2	49.8	8.8	.91	
	47.34	2.05	13.96	11.74	11.19	10.47	0.39	2.55	0.20	-	14.0	30.0	47.8	8.2	.87	
	47.24	2.03	14.42	11.81	10.72	10.49	0.41	2.67	0.21	-	26.4	24.9	31.5	10.0	7.1	.83
	47.18	2.08	14.78	11.81	10.20	10.43	0.45	2.80	0.22	26.7	29.2	29.7	7.8	6.6	.78	
	47.21	2.13	15.09	11.74	9.69	10.35	0.49	2.94	0.24	26.8	33.1	28.1	5.9	6.1	.74	
	47.24	2.18	15.39	11.76	9.18	10.17	0.53	3.09	0.26	26.8	36.7	26.6	4.4	5.6	.69	
	47.27	2.25	15.66	11.80	8.66	10.18	0.56	3.23	0.28	26.5	40.0	25.2	3.2	5.2	.64	
	47.31	2.33	15.90	11.87	8.13	10.08	0.59	3.39	0.31	26.0	43.0	24.1	2.3	4.7	.59	
	47.35	2.42	16.10	11.98	7.61	9.96	0.63	3.55	0.34	sum residuals squared < 0.01						
4638	47.40	2.40	16.12	12.03	7.60	9.96	0.63	3.53	0.33							

Total fractionation interval = 41 wt% crystallization.

Mineral compositions calculated as in table 3 using the following parameters:

olv: Fe/Mg Kd = 0.30 Fo 83-76

plg: An/Ab Kd = 1.45 An 77-68

aug: Fe/Mg Kd = 0.23 Wo = 47.0

opx: Fe/Mg Kd = 0.28 Wo = 4.0

tmt: usp = 22.89

interdependent, as are those of olivine and orthopyroxene. Within each mineral pair, proportions may be varied by up to 10 wt% without seriously affecting the fit of the major element model (expressed as $\sum r^2$). The model assemblage of table 2.6 is consistent with experimentally determined phase equilibria and is geologically reasonable. Sigurdsson (1970) suggested a similar petrogenetic scenario to account for primitive alkali basalts in Snaefellsnes, western Iceland. It has been demonstrated experimentally that clinopyroxene may replace olivine as a liquidus phase above ~10 kbar, with orthopyroxene the second crystallizing phase (Kushiro & Thompson, 1972; Bender et al., 1978; Green et al., 1979; Fujii & Bougault, 1983; Gust & Perfit, 1987). We calculate an increased role for olivine and plagioclase at the expense of orthopyroxene and aluminous clinopyroxene, respectively, during the fractionation sequence. Both of these trends are qualitatively consistent with geometric constraints from figures 2.14 and 2.16 and thus provide an internally consistent framework for investigating evolution of Surtsey liquids.

Clinopyroxenes produced experimentally in both tholeiitic and alkalic systems at moderate pressures are typically sub-calcic relative to equilibrium low-pressure clinopyroxenes (e.g., Takahashi & Kushiro, 1983; Mahood & Baker, 1986; Grove et al., 1988 and unpublished data; Thy, pers. commun., 1989). Major element trends within the Surtsey lavas can also be modeled successfully with a phase assemblage which includes low-Ca pyroxene rather than calcic augite + orthopyroxene. However, the geometric constraints on liquid evolution suggested by figure 2.16 favor an orthopyroxene-bearing assemblage. Crystallization of a single low-Ca pyroxene cannot drive primitive Surtsey liquids towards increased silica undersaturation. For this reason we modeled the Surtsey lava series using stoichiometric calcic augite and orthopyroxene. Subcalcic clinopyroxene is essentially a linear combination of these endmembers; incorporating this phase would reduce but could not eliminate the proportion of orthopyroxene.

We evaluate the results of our major element modeling for Surtsey using trace element data and the partition coefficients in the Appendix. Observed bulk distribution coefficients for Co, Cr, Ni and the HREE (table 2.7) are consistent with those calculated using the mineral proportions in table 2.6. The calculated bulk D_s for several incompatible elements are negative, thus the degree of crystallization based on major element calculations (41 wt%) is insufficient to generate the observed enrichments of highly incompatible elements, which require at least 46 wt% crystallization (table 2.7). Two explanations are possible: 1) the major element model overestimates F , or 2) the major element model is correct and incompatible elements are overenriched because the fractionation process is more complex than closed system fractionation; for example, boundary layer crystallization within a magma chamber beneath Surtsey (Langmuir, in prep).

By considering the Surtsey suite in three segments, defined by samples 9850, 9828, 9823 and 4638 (tables 2.8, 2.9), progressive changes in element partitioning masked by the inverse model provide insight into the genesis of the Surtsey suite. Table 2.8 shows the results of three forward models based on these Surtsey liquids; phase assemblages used in forward modeling are broadly consistent with those determined by inverse modeling. The total crystallization interval inferred is 46 wt%, sufficiently large to ensure non-negative bulk D_s for all incompatible elements. The required bulk D_s for the REE in step I are inconsistent with clinopyroxene partition coefficient sets A and B (see Appendix), because this portion of the liquid evolution trend is characterized by MREE depletion greater than that of LREE or HREE (table 2.9, figure 2.17). This nearly-symmetric concave down REE pattern is observed in some experimental clinopyroxenes at pressures of 20-30 kbar (Shimizu, 1980; Green & Pearson, 1985) and calculated bulk D_s using partition coefficient set C are qualitatively consistent with those observed (table 2.7). Similarly, a reasonable fit for Sr partitioning uses the 20-30 kbar clinopyroxene/melt data of Shimizu (1980). Lack of a positive Eu anomaly in this

Table 2.7 Evaluation of Surtsey Inverse Model with Trace Elements

Element	C_l/C_o	Bulk D_{obs}	Bulk D_{calc}
Ba	2.26	*	0.01-0.19
Sr	1.39	0.34	0.36-0.94
Sc	0.87	1.28	0.57-1.66
V	0.94	1.12	1.92-4.86
Co	0.71	1.68	1.21-2.60
Cr	0.24	3.84	2.54-4.98
Ni	0.37	2.98	2.05-3.25
Zr	1.76	*	0.12-0.20
Hf	1.50	0.19	0.11-0.22
Nb	1.95	*	0.05-0.07
Ta	1.82	*	> 0.10
La	1.91	*	0.03-0.11
Ce	1.88	*	0.03-0.13
Nd	1.64	0.02	0.05-0.19
Sm	1.48	0.22	0.07-0.29 (0.44)
Eu	1.44	0.27	0.12-0.35
Tb	1.25	0.56	0.08-0.36 (0.48)
Yb	1.51	0.18	0.10-0.39
Lu	1.50	0.19	0.10-0.39 (0.37)

Observed bulk D_s are calculated assuming Rayleigh fractionation, i.e.,

$$C_l/C_o = F^{D-1}$$

where C_l = concentration of element in daughter liquid 4638

C_o = concentration of element in parent liquid 9850

F = degree of crystallization calculated from major element modeling

Calculated bulk D_s represent a weighted sum of individual K_d s from the Appendix

* indicates elements for which Bulk $D_{obs} < 0$ (see text for discussion)

Values in parentheses are calculated using partition coefficient set C (high pressure) for clinopyroxene

Table 2.8 Fractionation of Lavas from 1963-1967 Surtsey Eruption: Forward Model

Parental lava	9850
Intermediate I	9828
Intermediate II	9826
Daughter lava	4638

	SiO ₂	Al ₂ O ₃	TiO ₂	FeO*	MgO	CaO	Na ₂ O	K ₂ O	P ₂ O ₅	wt% in Cumulate
--	------------------	--------------------------------	------------------	------	-----	-----	-------------------	------------------	-------------------------------	-----------------

I. 9850 to 9828

21% crystallization

Starting liquid ⁽¹⁾	47.26	13.59	2.03	11.08	11.74	10.56	2.41	0.33	0.19	
Orthopyroxene ⁽²⁾	53.77	4.08	0.40	8.90	30.32	2.41	0.13	0.0	0.0	35
Clinopyroxene ⁽²⁾	50.19	5.52	0.80	4.50	17.79	20.95	0.24	0.0	0.0	43
Plagioclase ⁽²⁾	48.60	33.07	0.0	0.0	0.0	15.89	2.50	0.0	0.0	12
Magnetite ⁽³⁾	0.0	3.80	24.40	67.60	4.20	0.0	0.0	0.0	0.0	10
Calculated liquid	47.44	15.02	1.93	11.70	10.11	10.28	2.89	0.41	0.24	
Target liquid	47.22	15.20	1.93	11.68	10.21	10.19	2.91	0.43	0.22	sum $r^2 = 0.10$

II. 9828 to 9826

17% crystallization

Starting liquid	47.22	15.20	1.93	11.68	10.21	10.19	2.91	0.43	0.22	
Orthopyroxene	53.54	4.06	0.40	9.83	29.64	2.40	0.13	0.0	0.0	30
Clinopyroxene	50.08	5.51	0.80	5.00	17.47	20.91	0.24	0.0	0.0	22
Plagioclase	49.62	32.32	0.0	0.0	0.0	15.09	2.97	0.0	0.0	35
Olivine	39.82	0.0	0.0	15.38	44.81	0.0	0.0	0.0	0.0	5
Magnetite	0.0	3.80	24.40	67.60	4.20	0.0	0.0	0.0	0.0	8
Calculated liquid	47.33	15.47	1.95	11.86	9.24	10.12	3.26	0.52	0.26	
Target liquid	47.24	15.47	2.12	11.80	9.38	10.14	3.05	0.53	0.26	sum $r^2 = 0.10$

III. 9826 to 4638

30% crystallization

Starting liquid	47.24	15.47	2.12	11.80	9.38	10.14	3.05	0.53	0.26	
Orthopyroxene	55.26	1.49	0.21	11.27	30.94	0.82	0.0	0.0	0.0	10
Clinopyroxene	52.57	2.09	0.37	5.14	16.36	23.10	0.38	0.0	0.0	24
Plagioclase	50.79	31.53	0.0	0.0	0.0	14.17	3.51	0.0	0.0	40
Olivine	39.52	0.0	0.0	16.96	43.52	0.0	0.0	0.0	0.0	20
Magnetite	0.0	3.80	24.40	67.60	4.20	0.0	0.0	0.0	0.0	6
Calculated liquid	47.57	16.43	2.45	12.27	6.80	9.72	3.64	0.76	0.37	
Target liquid	47.45	16.38	2.40	12.12	7.07	9.78	3.75	0.69	0.36	sum $r^2 = 0.13$

¹ All liquid compositions are renormalized to 100% on an anhydrous basis and without MnO.² Only initial equilibrium phase compositions are tabulated; see table 4.³ Magnetite composition based on gabbroic xenolith from Eldfell eruption (Jakobsson et al., 1973)

Table 2.9 Evaluation of Surtsey Forward Model with Trace Elements

Element	Step I		Step II		Step III	
	Bulk D _{Obs}	Bulk D _{Calc}	Bulk D _{Obs}	Bulk D _{Calc}	Bulk D _{Obs}	Bulk D _{Calc}
Ba	< 0	.01 - .05	< 0	.02 - .23	.46	.02 - .26
Sr	.70	.21 - .59	.63	.47 - 1.20	.70	.52 - 1.34
Sc	1.07	.86 - 2.19	.98	.62 - 1.48	1.38	.40 - 1.31
V	.93	2.77 - 7.02	1.15	2.14 - 7.39	1.13	1.65 - 4.19
Co	1.47	1.34 - 2.48	1.37	1.14 - 2.13	1.45	1.00 - 2.35
Cr	3.10	3.74 - 12.55	1.43	2.17 - 9.00	3.37	2.04 - 6.79
Ni	2.27	2.12 - 3.98	2.34	1.52 - 2.80	2.27	1.92 - 2.78
Zr	.41	.16 - .22	.34	.10 - .18	.14	.10 - .20
Hf	.18	.15 - .30	.15	.09 - .19	.28	.09 - .20
Nb ^a	.02	.07	.52	.06	.27	.04
La	.31 (.23 - .37)	.03 - .12	.21 (.11 - .30)	.03 - .13	.55 (.52 - .63)	.03 - .13
Ce	.44 (.26 - .62)	.04 - .15	.25 (.11 - .39)	.04 - .16	.57 (.49 - .58)	.03 - .14
Nd	.77 (.64 - .92)	.06 - .24	.36 (.20 - .39)	.05 - .18	.66 (.61 - .71)	.05 - .18
Sm	.80 (.53 - 1.10)	.10 - .40 (.68)	.52 (.30 - .64)	.07 - .26 (.40)	.71 (.66 - .76)	.07 - .26 (.40)
Eu	.80 (.74 - .82)	.12 - .43	.54 (.30 - .58)	.13 - .33	.71 (.64 - .73)	.14 - .35
Tb ^b	-	.12 - .51 (.69)	-	.07 - .31 (.40)	-	.06 - .31 (.41)
Yb	.41 (.23 - .86)	.14 - .56	.56 (.30 - .88)	.09 - .35	.81 (.70 - .94)	.08 - .33
Lu	.25 (.16 - .30)	.14 - .70 (.53)	.51 (.39 - .54)	.09 - .35 (.34)	.80 (.68 - 1.05)	.08 - .33 (.31)

Observed bulk Ds are calculated as in previous tables; the range in observed REE distribution coefficients reflects duplicate analyses of parent and daughter samples (see table 1), with the indicated value plotted in figure 16.

Calculated bulk Ds represent a weighted sum of individual Kds from the Appendix; values in parentheses use set C coefficients for clinopyroxene.

a The high bulk D observed for Nb in steps II and III suggests fractionation of a Ti-rich phase; we did not incorporate this phase in major element modeling.

b Tb is an element for which we have poor precision and it has been omitted from tabulation.

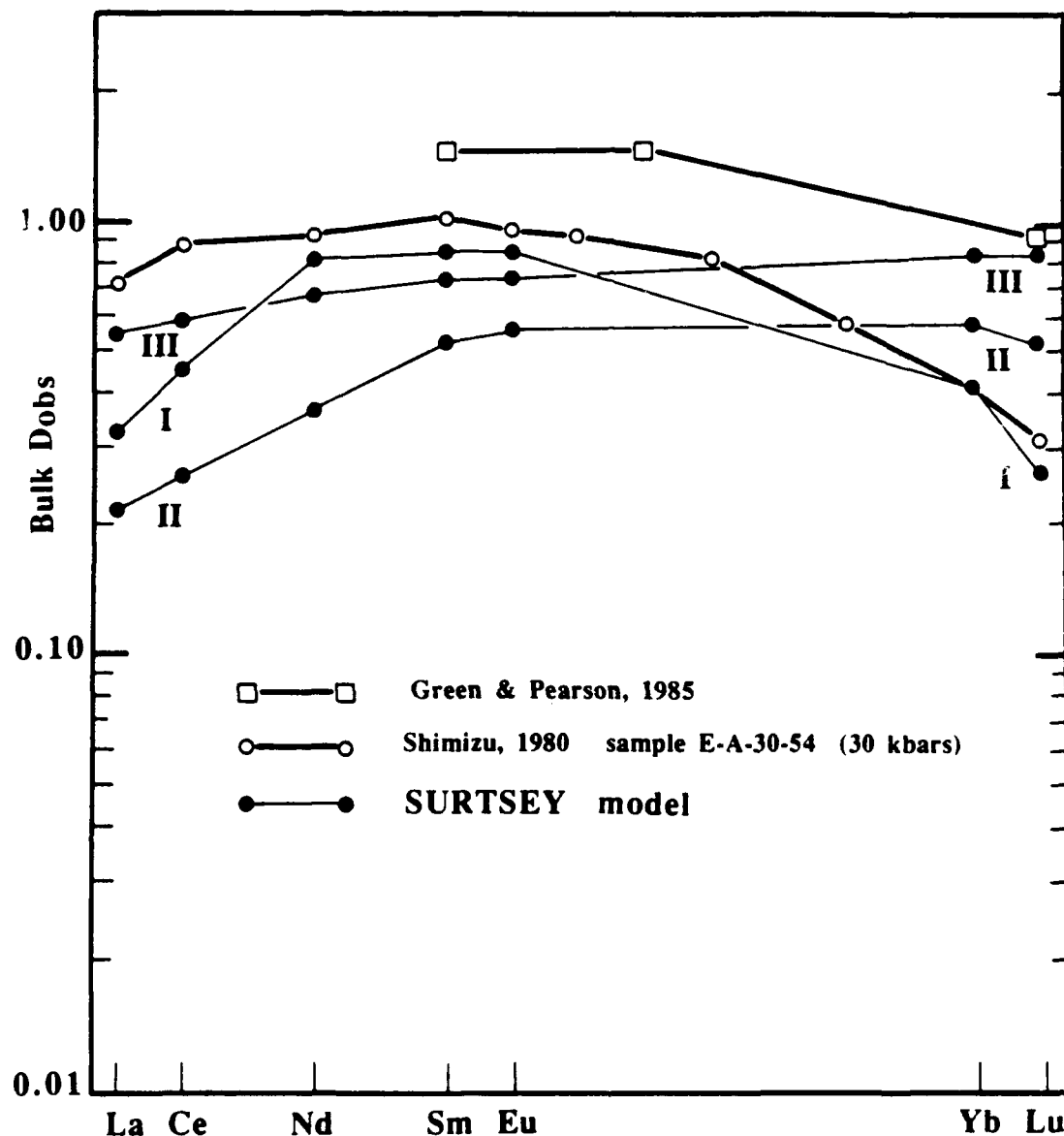


Figure 2.17 Observed bulk distribution coefficients for REE at Surtsey (see text for discussion). Tb has been omitted because we have poor analytic precision for this element at the observed concentrations. The labels I, II and III refer to the three fractionation steps in table 2.8. Open triangles are partition coefficients for clinopyroxene coexisting with garnet in an alkali olivine basalt at 30 kbar (Shimizu, 1980). Open circles are partition coefficients for clinopyroxene at 20 kbar and 1050°C (Green & Pearson, 1985). Note the symmetric downward concavity of these REE partitioning patterns, similar to that observed among the most mafic Surtsey samples (I).

fractionation step is consistent with a limited role (~12%) for plagioclase. The observed partitioning of Sc (bulk $D \sim 1$) is consistent with the high temperature ($T = 1300^{\circ}\text{C}$) clinopyroxene/melt K_d s of Ray et al (1983). Our calculated bulk D s overestimate observed values for V, Co and Cr in step I. By analogy to Sc and Ti (Ray et al., 1983) these metals probably also become less compatible in clinopyroxene at high temperatures. Clinopyroxene in Surtsey xenolith 10712 (Jakobsson et al., in prep) contains <0.5 wt% Cr_2O_3 , indicating a K_d of ~1.6 which is significantly lower than the range noted in the Appendix (7-10; Sun et al., 1979; Hervig & Smith, 1982). The trace element data thus support a model whereby early evolution of primitive Surtsey basalts occurred at elevated pressure and temperature.

Trace element partitioning in steps II and III is consistent with fractionation under conditions of decreasing pressure and temperature. The symmetric concavity of REE partitioning observed in step I is replaced by depletion of the LREE with respect to MREE and HREE similar to that seen at Eldfell (figure 2.17). This change can be modeled by using high pressure (20-30 kbars) partition coefficients for REE in clinopyroxene (Shimizu, 1980; Green & Pearson, 1985) in step I, and more typical upper mantle values (Frey et al., 1978) in subsequent fractionation intervals (see Appendix). Similarly, the nearly constant bulk Sr partition coefficient (~0.7) throughout the lava series despite inferred changes in phase proportions is consistent with the experimentally determined pressure dependency of D_{Sr} in plagioclase (Shimizu, 1980). We infer that increased plagioclase fractionation from steps I to III (leading to higher bulk D s) is offset by decreased partitioning of Sr into clinopyroxene at pressures less than 20 kbar (see Appendix for individual K_d s). The higher bulk D s for Zr and Hf in step I may also be the result of higher pressure fractionation, although this inference is somewhat speculative. Increased compatibility of Sc in steps II and III despite a reduction in clinopyroxene fractionation may reflect a temperature decrease (e.g., 1300° to 1150°C ; Ray et al., 1983); V and Co are also more compatible in these later fractionation steps.

The near-constant values for Nb/Ta (16.4-18.8) and Zr/Hf (42.2-45.7) throughout the compositional range supports our hypothesis that these lavas are cogenetic and that differences in major and minor element chemistry result from crystal fractionation.

Polybaric fractionation of Surtsey liquids is suggested by the change in REE patterns and transition metal partitioning between primitive and evolved samples. The inferred changes in bulk partitioning are consistent with experimental data on appropriate natural systems, and are geologically reasonable based on major element evidence (e.g., figure 2.14). We suggest that primitive Surtsey liquids record a maximum pressure of 20-30 kbars, while more evolved compositions suggest crystallization at ~10 kbars. Seismic activity was not monitored during the Surtsey eruption. Since 1973 frequent tremors have been recorded at 8-16 km depth beneath Surtsey (P. Einarsson, pers. commun., 1987; figure 2.15). These data do not provide additional constraints on magmatism in 1963-1967 but are consistent with moderate pressure magmatic processes at Surtsey. Glass compositions from tephra associated with initial explosive activity during each phase of the Surtsey eruption also record a moderate pressure history (figure 2.14). This observation indicates that the Surtsey liquids ascended directly to the surface without re-equilibrating in a shallow reservoir.

2.4.4 Crustal Origin of Alkali Basalts?

Oskarsson and co-workers (1982, 1985; Steinthorsson et al., 1985; Hemond et al., 1987) proposed that all Icelandic basalts are derived from a single parental olivine tholeiite similar to that erupted along the Reykjanes Peninsula. In this model, the compositional diversity of erupted compositions results from contamination of the parental tholeiite by partial melts of altered lavas buried at different depths within the crust. Anatexis at shallow levels will produce a silicic fluid (ostensible required to form quartz-normative basalts), while subsequent melting of the Si-depleted crust at deeper levels (conditions of amphibolite grade metamorphism) releases a nepheline-normative

component during amphibole breakdown. In this scenario, liquids with greater normative nepheline (e.g., Eldfell mugearite) have assimilated a larger proportion of this latter crustal component. At Vestmannaeyjar, the presence of partially fused silicic xenoliths (Sigurdsson, 1968) and embayed andesine plagioclase (Jakobsson, 1979) provide evidence for some component of open system behavior. We therefore investigate the apparent effects of crustal contamination in the Surtsey and Eldfell lavas.

Despite their obvious alteration and, in some cases, incipient dissolution the silicic xenoliths do not appear to contribute significantly to the geochemical character of the Vestmannaeyjar lavas. Most importantly, the lavas are all silica-undersaturated, and the sample with the highest absolute SiO_2 content (Eldfell mugearite VE-110) has the most highly nepheline-normative composition. It is unrealistic to postulate that the alkalic nature of the Vestmannaeyjar suite derives from contamination of the observed fused granitic and granophyric xenoliths. The isotopic character of the silicic xenoliths provides further evidence against their assimilation in to the Vestmannaeyjar system. Assuming that the xenoliths resemble Icelandic silicic rocks (e.g., Oskarsson et al., 1982), their La/Sm_n could range from ~2.3 to ~4.2 (Furman, unpub. data; Gunnarsson, 1988). Assimilation of this high- $^{87}\text{Sr}/^{86}\text{Sr}$ (.70370-.70432), high-La/Sm component would produce a trend opposite to that observed among subaerial lavas in figure 2.9. The Pb isotopes of the xenoliths are equivalent to those of Vestmannaeyjar basalts (figure 2.10b), suggesting a cogenetic link between these materials. We suggest that the radiogenic Sr signature of the xenoliths reflects circulation of seawater at shallow levels near Vestmannaeyjar. Elderfield & Greaves (1981) report $^{87}\text{Sr}/^{86}\text{Sr}$ ratios between 0.7037 and 0.7042 in hydrothermally altered rocks from boreholes at the Svartsengi geothermal field (Reykjanes peninsula). There is no high temperature geothermal field in Vestmannaeyjar; however, seawater alteration can occur in the shallow crust without surface expression.

If the alkalic nature of Vestmannaeyjar basalts results from melting and dehydration of amphibolite-grade lavas within the crust, we should be able to identify a unique geochemical signature of this process. In particular, lavas from Eldfell are expected to record a greater degree of contamination than the Surtsey basalts because of their more highly silica-undersaturated nature. Reykjanes Ridge basalts form the 10 million year old oceanic crust through which Vestmannaeyjar lavas erupt. Tholeiites from the Reykjanes Peninsula have restricted ranges in $^{87}\text{Sr}/^{86}\text{Sr}$ and $^{143}\text{Nd}/^{144}\text{Nd}$ (0.70289 to 0.70320 and 0.51299 to 0.51318 respectively; Zindler et al., 1979, Stecher et al., 1986), which overlaps the Vestmannaeyjar range for acid leached samples (0.70304 to 0.70327 and 0.51301 to 0.51307; figure 2.10a). However, the apparent trend of decreasing $^{87}\text{Sr}/^{86}\text{Sr}$ with increasing differentiation at Vestmannaeyjar is not consistent with assimilation of altered submarine lavas. Furthermore, the range in Nd isotopes observed at Vestmannaeyjar cannot be explained by progressive contamination via melts of Reykjanes basalts because the Eldfell samples do not lie on mixing lines between Surtsey and Reykjanes isotopic compositions (figure 2.18). In addition, the Pb isotopic signatures of Vestmannaeyjar lavas are nearly uniform and define a field distinct from that of Reykjanes samples (figure 2.10b). All available radiogenic isotopic evidence therefore suggests the Vestmannaeyjar lavas are not contaminated by an identifiable crustal component.

The $^3\text{He}/^4\text{He}$ ratios of two Vestmannaeyjar basalts are 11.0 and 15 Ra, similar to basalts from Krafla and Reykjanes (12-15 Ra; Poreda et al., 1984; Kurz et al., 1985). Crustal contamination can only lower this ratio by addition of radiogenic ^4He to primordial ^3He . The similarity of helium isotope ratios in these areas suggests derivation from a comparable mantle source. Again there is no evidence that alkalic basalts contain components from crustal melts.

Oxygen isotope ratios of all Vestmannaeyjar lavas are +5.5 to +5.7 per mil regardless of their bulk geochemical composition (figure 2.12; Muehlenbachs &

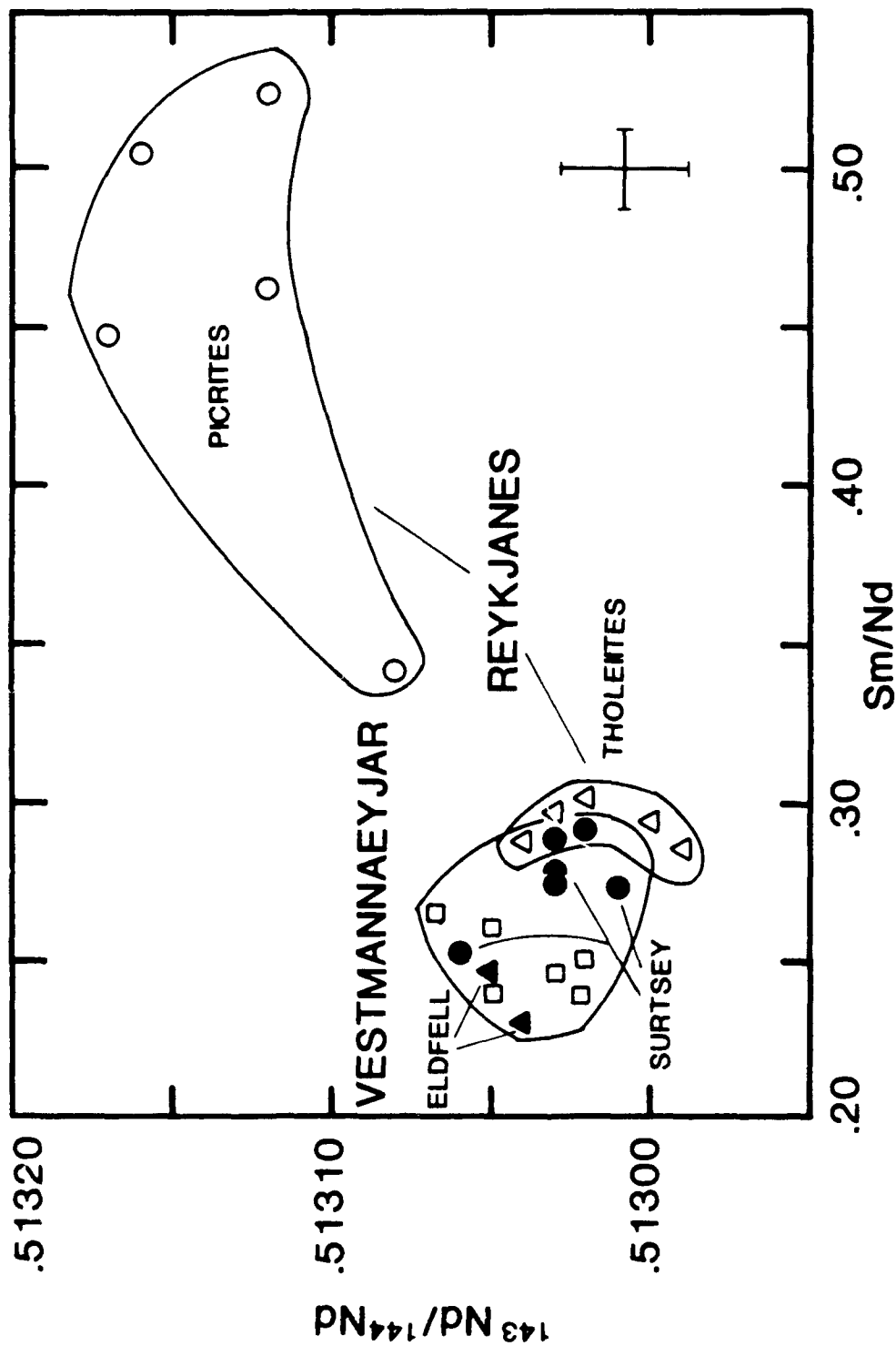


Figure 2.18 Basalts from Reykjanes and Vestmannaeyjar are derived from a source depleted in LREE with respect to Bulk Earth (assumed chondritic, $\text{Sm}/\text{Nd} = 1$). The range in Nd isotopes of Vestmannaeyjar lavas suggests that the alkaline nature of these basalts is not due to contamination of Surtsey basalts with partial melts of Reykjanes tholeiites or picrites, because evolved Eldfell samples (alkalic) are offset away from the Reykjanes fields. Note that all samples fall within the array of north Atlantic MORB (not shown, see figure 2.10).

Jakobsson, 1973; Condomines et al., 1983; Muehlenbachs et al., 1984). In contrast hydrothermally and diagenetically altered Icelandic basalts range between +4.6 and -10.0 per mil (Hattori & Muehlenbachs, 1981; Muehlenbachs et al., 1982), indicative of interaction with meteoric water. Thus, oxygen isotopic ratios of Vestmannaeyjar lavas do not reflect incorporation of hydrothermally altered crust. Significantly, the most evolved Eldfell mugearite and the most primitive Surtsey basalts have identical oxygen isotopic ratios. In summary, none of the isotopic data support an origin involving crustal assimilation. We favor a mantle origin for Vestmannaeyjar alkali basalts.

2.4.5 Melting and Melt Extraction at Depth

Previously the compositional diversity in the EVZ (Meyer et al., 1985) and the Galapagos 95°W area (Christie & Sinton, 1981, 1986; Sinton et al., 1983) were attributed to systematic variations in depth and degree of mantle melting as well as in extent of fractionation of mantle-derived liquids in an immature rift environment. The uniform and primitive nature of lavas from the rift tip in both areas indicates that they have undergone only minor post-melting modification. Behind the rift tip crystal fractionation effects increase dramatically over a distance of <10 (Galapagos) to ~30 km (Iceland's EVZ). In the discussion below we infer: 1) the depth of mantle melting, 2) the extent of melting, and 3) the mineralogy and composition of the mantle source.

Parental Surtsey basalt 9850 (Mg# 64) is in equilibrium with olivine of Fo₈₆ (Jakobsson et al., in prep). Assuming a mantle source with Fo₉₀ olivine, 9850 is a fractionated basalt. Picrites from the Reykjanes Peninsula contain Fo₉₀ olivine (Jakobsson et al., 1978; Hardardottir, 1986) indicating that mantle of this major element composition exists beneath southern Iceland, although it is isotopically depleted relative to the source of Vestmannaeyjar lavas (Zindler et al., 1979; Stecher et al., 1986). In Vestfirðir (NW Iceland), Fo₈₉ olivine has been found in a tholeiite and a picrite which

are LREE-enriched, and may thus represent mantle more analogous to the source of Vestmannaeyjar lavas (Meyer, 1984).

We estimate the amount of crystallization undergone by sample 9850 following the method of Hanson & Langmuir (1978) as outlined in figure 2.19. The compositions of lavas 9850, 8066, 9839 and 9828 are also plotted in figure 2.19. They lie significantly below the "0% melting" contour, confirming that these liquids are not primary mantle melts of this assumed source. Semi-quantitative bounds on the degree of crystallization are found by tracking backwards along the light curved lines, where each increment represents crystallization of 5 mole% olivine. If we consider the 1 atm melting volume as a limit, the liquids have undergone a minimum of 12 mole% olivine crystallization during cooling from 1375-1300°C. At the 30 kbar extreme, the liquids crystallized at least 20 mole% olivine between 1625-1450°C. These are minimum estimates because they address only the limiting case of 0% melting.

A more rigorous approach to determining the early history of sample 9850 utilizes the moderate pressure phase boundaries determined by Stolper (1980), the mantle melting curves of Takahashi & Kushiro (1983) and the approach of Christie & Sinton (1986). In brief, equilibrium mafic phenocrysts are added incrementally to the liquid in question to locate the intersection, if any, of a reasonable primary liquid composition with a univariant mantle melting curve in the oliv-diop-plag-qtz pseudoquaternary (figure 2.20). At most one such intersection is possible for each liquid path. This intersection represents the minimum depth of separation from a lherzolite (ol + opx + cpx) source. The univariant melting curves (Takahashi & Kushiro, 1983) are not strictly compatible with Stolper's phase boundaries, which reflect invariant liquids equilibrated with mantle minerals. As each pressure, however, Stolper's liquids plot within or adjacent to the Takahashi & Kushiro curves, and the sense and amount of curve displacement with increasing pressure is consistent for the two data sets. In our analysis we focus primarily on the Takahashi & Kushiro melting curves given recent

Figure 2.19 Fields of mantle melts and residues at 1 atm (open) and 30 kbars (shaded), redrawn from Hanson & Langmuir (1978). This diagram indicates the compositions of a mantle source and equilibrium olivine, and the fields for mantle melts and residues which are contoured for varying degrees of batch melting. The open field represents melting at 1 atm, while the stippled field corresponds to 30 kbar. The Fe-Mg exchange coefficients of Roeder & Emslie (1970) are used for the olivine-melt system. Temperatures (in degrees C) are indicated for both pressure regimes. Melting percentages are shown for 1 atm only as these values represent a minimum bound on the mantle system. The contoured curved lines indicate 5 mol% intervals of olivine crystallization. Surtsey basalts lie below the fields of primary mantle melts and have therefore undergone a finite amount of olivine crystallization since segregation from their source.

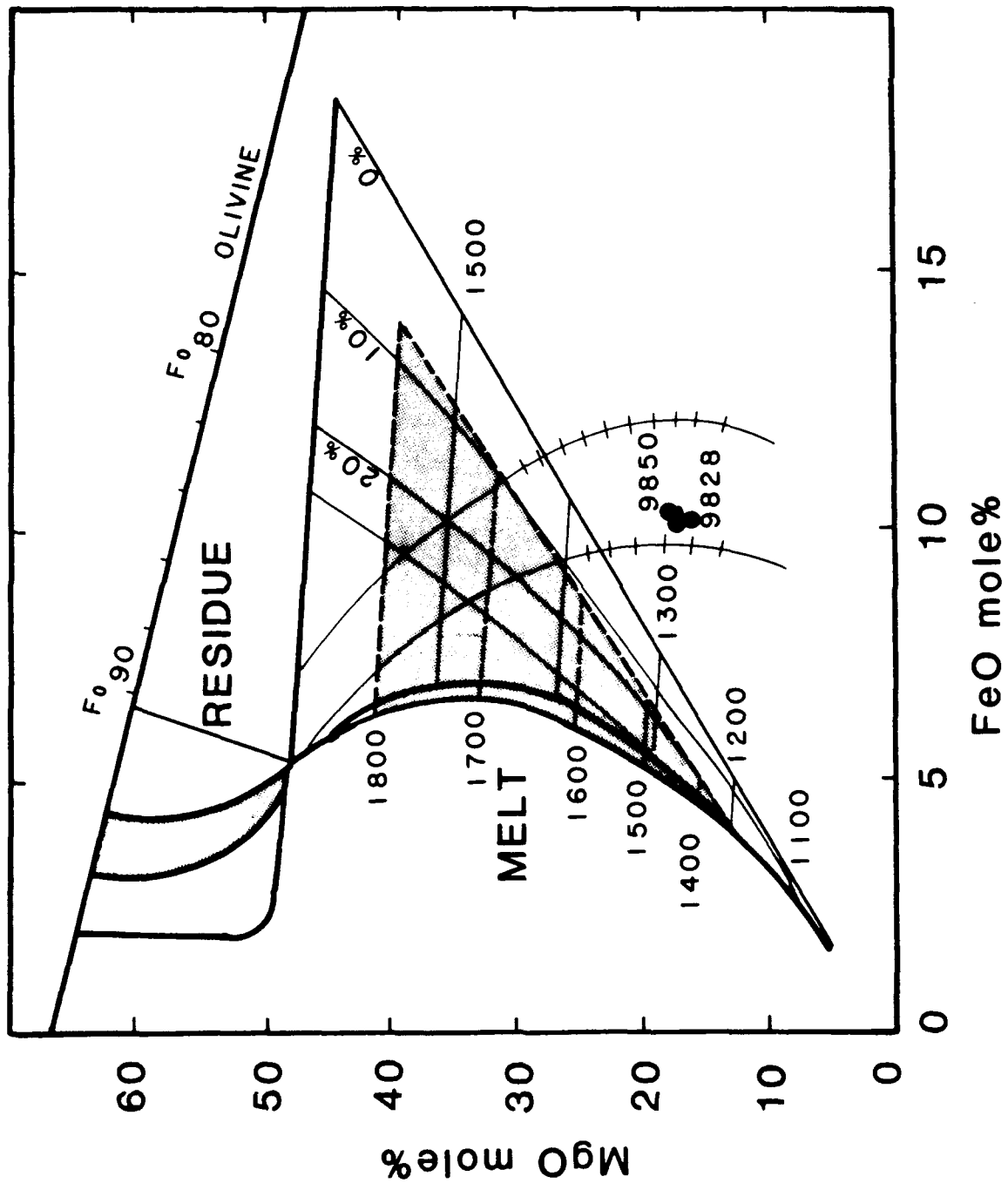
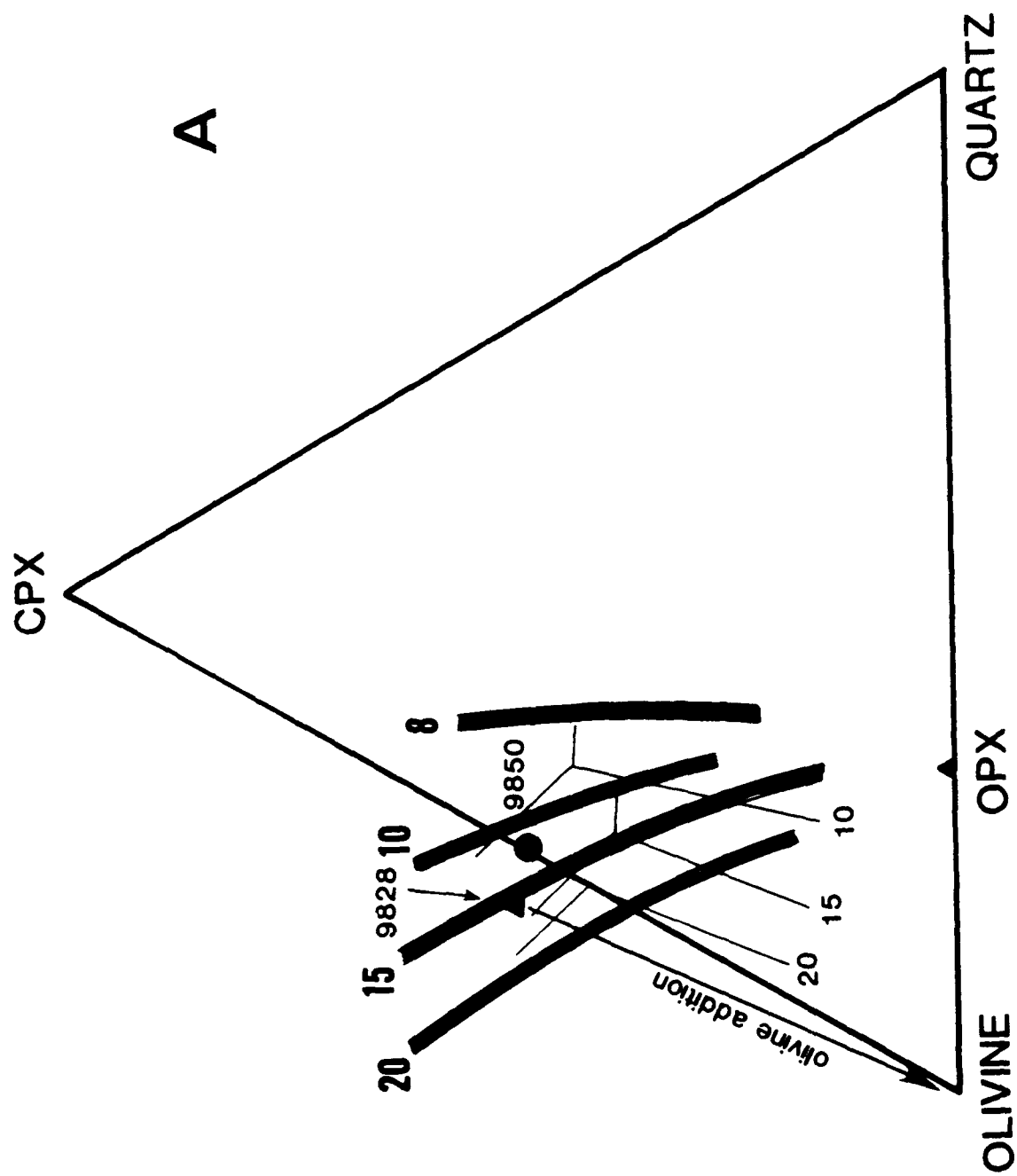
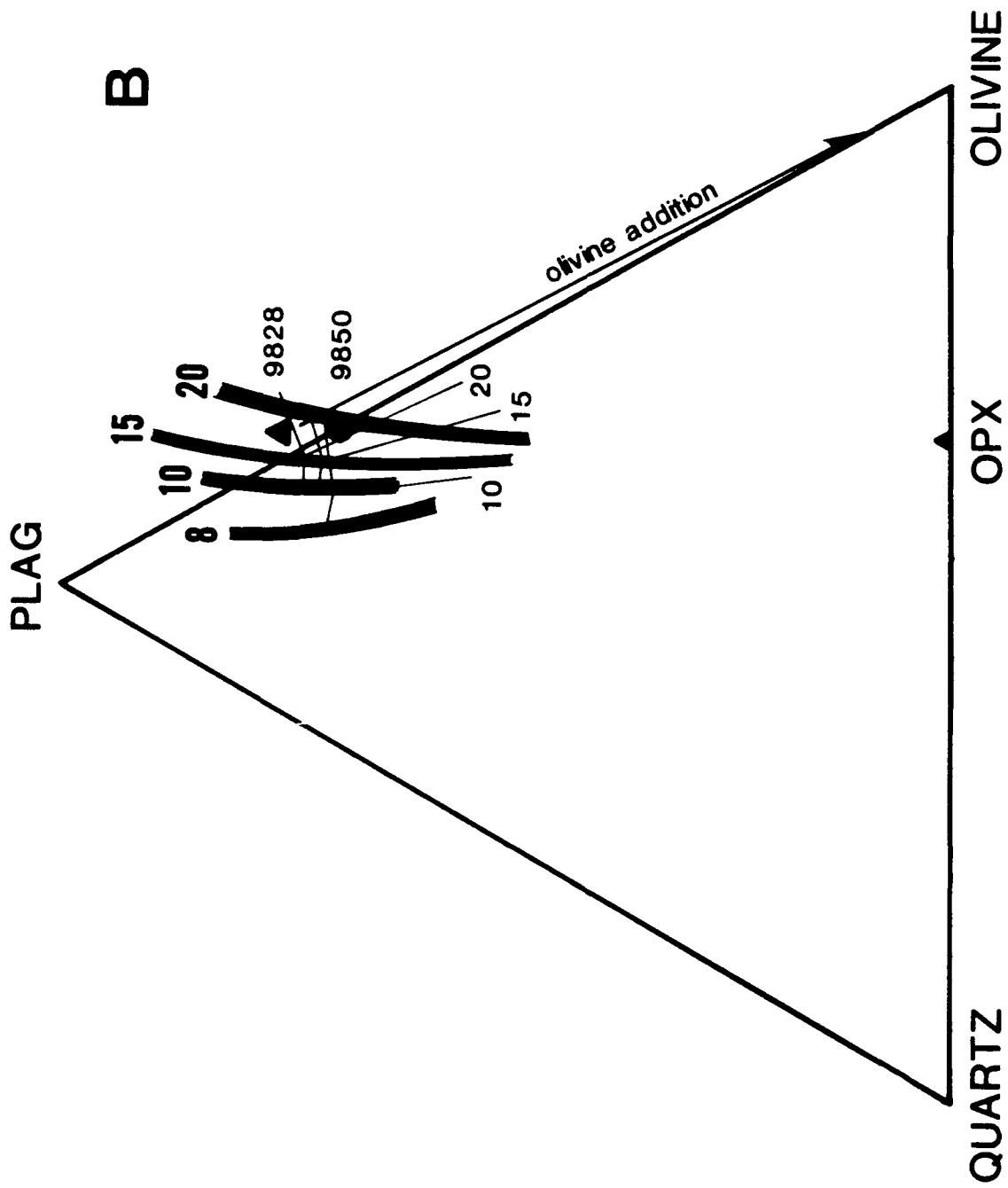


Figure 2.20 (a) Surtsey lavas 9828 and 9850 are shown in the same projection as figure 2.15a, with the moderate pressure phase boundaries of Stolper (1980) for reference. The broad shaded curves indicate the loci of univariant peridotite melt compositions at 8-20 kbars (Takahashi & Kushiro, 1983). Olivine addition vectors are drawn for both liquids, and the Mg-numbers of resulting liquids have been calculated incrementally (not shown). At the intersection of (1) a phase boundary, (2) a melting curve and (3) a calculated liquid trajectory (at a given pressure), the Mg-number of the liquid is calculated. If the liquid is found to be in equilibrium with mantle olivine, then the chosen pressure may correspond to conditions of melt segregation from the mantle. In this projection it is clear that sample 9828 (triangles) cannot have been derived by mono-mineralic fractionation of a primary mantle melt. See text for further discussion.

(b) The same information is shown here projected as in figure 2.15b. Any scenario of melting and crystallization must be consistent with this representation scheme as well.





experimental data supporting univariant, rather than invariant, mantle melting (Takahashi & Kushiro, 1983; Fujii & Scarfe, 1985). The exact locations of the high pressure phase boundaries and melting curves are not well-known, and we assume an error of ± 2 kbar in all of our estimates.

Primitive Surtsey liquids lie within the clinopyroxene primary phase volume at pressures greater than ~ 10 kbars (figure 2.16). Figure 2.20 displays graphically the results of olivine addition to liquids 9850 and 9828. The latter sample is included to investigate the possibility that the MgO-rich Surtsey liquids represent differing degrees of mantle melting rather than crystal fractionation from a common parent. Calculated equilibrium olivine was added to each liquid in 1 wt% increments. Mineral addition vectors are shown in figure 2.20. The liquid path of 9850 intersects the 20 kbar univariant melting curve at Mg# 71 (corresponding to olivine of Fo₈₉) in figure 2.20a and Mg# 66 in figure 2.20b. Similar discrepancies at high pressure were encountered by Christie & Sinton (1986) and probably reflect uncertainties in the melting curves and phase boundaries. The interval of crystallization is roughly 14 wt%. The liquid path of sample 9828 intersects the 20 kbar univariant melting curves at the atypical mantle values of 64 on both projections. We infer that liquid 9850 segregated at a pressure of about 20 kbar (65 km) and that 9828 was not derived in a similar manner. Liquid 9828 could be derived by melting of a more iron-rich source than 9850, but this source difference is unlikely given the similarities in trace elements and isotopes between these two samples. One implication of this interpretation is that only those Surtsey liquids with Mg# close to 64 are derived by mantle melting and subsequent olivine fractionation during ascent. Liquids such as 9828 (Mg# 61) do not originate by this process.

The inferred early history of proto-liquid 9850 is not consistent with the moderate pressure phase boundaries of Stolper (1980) in which the olivine primary phase field shrinks with increasing pressure from 10 to 20 kbars (figure 2.16). O'Hara (1968, 1970) suggested that, at pressures above ~ 15 kbars, the olivine volume expands as the

olivine + clinopyroxene + orthopyroxene pseudoinvariant point moves towards greater silica saturation (figure 2.16). A similar, though less dramatic, shift in phase boundaries was inferred from the 20 kbar experiments of Presnall et al (1979) in the reduced pseudoquaternary system CMAS. Using O'Hara's phase boundaries, a primary liquid that is olivine saturated at ~20 kbars could indeed crystallize ortho- and clinopyroxene at lower pressure (~15 kbars). This geometry is therefore consistent with the proposed fractionation history of primary mantle-derived melts at Surtsey.

2.4.6 Estimating the Degree of Mantle Melting

Unless the source composition is known, the degree of partial melting must be estimated by indirect means. The $\text{CaO}/\text{Al}_2\text{O}_3$ ratio of partial melts can be an indicator of residual mineralogy because clinopyroxene and garnet control the abundances of both of these oxides. If clinopyroxene and garnet are consumed at the same rate, the $\text{CaO}/\text{Al}_2\text{O}_3$ of the melt will remain close to that of the source because the minerals contain roughly inverse proportions of the two oxides. If garnet is exhausted first, the melt ratio will be less than the source ratio for a finite melting interval. For the case of melting spinel lherzolite, the $\text{CaO}/\text{Al}_2\text{O}_3$ of the melt will be less than that of the residue at low melt percentages (i.e., clinopyroxene in the residue). At larger degrees of melting (i.e., clinopyroxene completely melted) the ratio in the melt will be slightly higher than that of the residue because all available CaO will be effectively in the liquid while significant Al_2O_3 will be retained by orthopyroxene (Klein & Langmuir, 1987). The $\text{CaO}/\text{Al}_2\text{O}_3$ of liquids 9850 and 9854 is 0.78; the highest is 0.81 (sample 4693). These values are comparable to that of the primitive upper mantle of Zindler & Hart (1987) which is 0.805. The ratios CaO/TiO_2 and $\text{Al}_2\text{O}_3/\text{TiO}_2$ are significantly lower in Vestmannaeyjar basalts than values inferred for the primitive upper mantle (~18.2, ~22.6; Zindler & Hart, 1987), which is also consistent with melting in the presence of residual clinopyroxene and/or garnet. Major element evidence therefore suggests a low

degree of melting, with minor clinopyroxene and/or garnet present in the residue after melting and segregation. It is not known at what melt percentage these phases are completely removed from the residue. A maximum value of 25% is inferred from the pyrolite melting study of Jaques & Green (1980) while lower values are predicted from estimates of modal clinopyroxene in the mantle (e.g., 15% by Meyer et al, 1985; 21% by Hart & Zindler, 1987). A low degree of melting is also consistent with low La/Nb of Vestmannaeyjar lavas relative to chondrites and normal MORB. This ratio is expected to decrease at low melt percentages because Nb is the more highly incompatible element during fusion of lherzolite (Sun & McDonough, in press).

The isotopic and REE signature of primitive Surtsey basalts place a tighter constraint on the degree of mantle melting beneath Vestmannaeyjar. The $^{143}\text{Nd}/^{144}\text{Nd}$ of these liquids indicate derivation from a source with a time-integrated depletion in LREE (figure 2.18) similar to that of MORB. By considering the partial melting of an assumed MORB source (Sun & Nesbitt, 1977; Wood et al., 1979) to produce sample 9850, we estimated by mass balance ($C_1/C_0 = 1/(F+D-DF)$; Shaw, 1970) the maximum degree of melting consistent with reasonable mantle bulk distribution coefficients for the REE (Frey & Roden, 1987). With this combination of parameters we find a maximum F of 3.2%. Lower degrees of melting are also permissible: a 1% partial melt requires solid/melt bulk Ds of 0.02-0.19. It is not possible to determine uniquely if garnet was present in the source on the basis of this calculation, although the estimated pressure (~20 kbar) of mantle melting is within the garnet stability field (Green & Ringwood, 1967).

To summarize, we estimate that parental Surtsey basalt 9850 is derived by melting of a garnet lherzolite source with olivine of Fo₉₀ at approximately 20 kbar (65 km) depth. This liquid fractionated olivine during its ascent until it ponded in the uppermost mantle (30-35 km) beneath Vestmannaeyjar. At this depth it underwent fractionation of orthopyroxene + clinopyroxene + spinel and, subsequently, olivine +

plagioclase + clinopyroxene + spinel. Eruption was triggered by an influx of 9850-type liquid; repeated influx occurred during the four years of eruptive activity. The abundance of lavas with Mg# 62-64 and the complete absence of lavas more mafic than this composition throughout the archipelago suggests that the primary melt signature (i.e., Mg# 71-73) is lost during an early, deep crystallization event. In other words, primary melts are not available for eruption because all liquids undergo at least some degree of crystallization prior to ponding.

2.5 Summary and Conclusions

Volcanism in Vestmannaeyjar is characterized by small eruptions which emanate from isolated magma pockets. The compositional evolution of recent eruptives from Surtsey and Eldfell can not be modeled by simple low pressure crystal fractionation. In both cases the fractionating assemblage required to fit major and trace element trends is not the low pressure phenocryst assemblage. Rather, magmatic evolution occurred at conditions of moderate pressure, approximately 6 kbars (18-20 km) beneath Eldfell and at least 10 kbars (30-35 km) beneath Surtsey. At Surtsey this depth corresponds to the base of the thickened Icelandic lithosphere. Projections of liquid compositions within the pseudoquaternary systems oliv-plag-diop-qtz and oliv-plag-diop-neph confirm the importance of moderate pressure crystallization processes, and constrain the model fractionating assemblages. At Eldfell, lavas have undergone about 30 wt% crystallization of olivine + plagioclase + clinopyroxene + Fe-Ti oxides from a parental hawaiiite. We suggest these liquids evolved along a cotectic surface. The most mafic Surtsey liquids appear to have fractionated orthopyroxene, clinopyroxene and Fe-Ti oxides. Subsequent fractionation involved olivine, plagioclase, clinopyroxene and oxides. The maximum degree of crystallization observed at Surtsey is ~50% of the parental basalt. Increased normative nepheline within Vestmannaeyjar lavas results from segregation of moderate pressure phases, and not from assimilation of a crustal melt.

Primitive Surtsey basalts (Mg# 64) are parental compositions for lavas within the Vestmannaeyjar archipelago but they are not primary mantle melts of a Fo_{90} source. The inferred primary magma beneath Vestmannaeyjar results from low degrees of partial melting of a lherzolite source at a pressure of approximately 20 kbars (60-65 km). It is likely that this primary melt fractionated 10-15 wt% olivine en route to ponding in a chamber at the base of the lithosphere at roughly 10 kbar (30-35 km). Further compositional evolution occurred within the thickened crustal section beneath the archipelago. The widespread occurrence of the parental lava composition throughout Vestmannaeyjar suggests that mantle melting and transport phenomena operate in a uniform way in this region. In contrast, the diversity of the more evolved lavas reflects variations in fractionation history of individual magma batches. Geochemical data for lavas from the archipelago are consistent with a propagating rift tip tectonic environment.

Appendix: Partition Coefficients Used in Trace Element Modeling of Vestmannaeyjar Lavas

Element	Clinopyroxene			Orthopyroxene		Olivine		Plagioclase		Magnetite		Ilmenite	
	A	B	C ¹	A	B	A	W	D	E	F	G	H	I
La	.02	.08	-	.0005	.0021	.0005	.017	.03	.16	2	.7	.007	.02
Ce	.04	.17	-	.0009	.004	.0008	-	.03	.15	2	(.6)	.007	-
Nd	.09	.38	-	.0019	.0083	.0013	-	.04	.14	2	(.6)	.009	-
Sm	.14	.74	1.4	.0028	.0147	.0019	-	.04	.12	3	(.6)	.01	.08
Eu	.16	.75	-	.0036	.0171	.0019	.027	.20	.32	3	.6	-	-
Tb	.19	.97	1.4	.0059	.0303	.0019	.04	.02	.08	3	.7	-	-
Yb	.20	1.01	-	.0286	.1443	.0040	-	.02	.07	4	(.7)	.06	.6
Lu	.19	.98	.9	.038	.19	.0048	-	.02	.07	4	(.7)	.09	.7
Ba	.01	-.1	(N)	.01	(N)	.01	(N)	.05	.59 (N)	.001	-.01 (S)	.01	(S)
Sr	.06	-.3	(J,N,X) ²	.01	-.016 (J,N)	.01	-.016 (J,N)	1.2	- 3 (E,N) ⁵	4	- 1.0 (G)	-	-
Sc	.8	-4.05	(K,L,W) ³	1.1	(J)	.10	- 25 (W,J)	.02	(K)	1.3	- 3.0 (R)	-	-
V	.7	-1.5	(J,K)	2	- 3 (J)	.09	(J)	.01	(S)	24	- 63 (R)	-	-
Cr	7	-10	(K,Q)	3	(K)	1	(K)	.02	(K)	2.7	- 6.7 (G)	-	-
Co	.76	-1.55	(J,W)	1.3	- 7.0 (Q) ⁴	.28	- 1 (Q)	-	-	27	- 58 (R)	-	-
Ni	2	-4	(J)	2	(J)	2	- 5.4 (J,W)	.1	(K)	3	- 11 (D,G,R)	-	-
Zr	.3	(M,W)		3	- 5 (J)	(T)		.06	(K)	2	- 5 (G)	-	-
Hf	.3	- .5	(D,M,W)	.01	(F)	.01	- .12 (H,W)	.04	- .14 (W)	2	- .7 (G)	.33	- 2.0 (F,H)
Nb	.001	-.01	(S)	.01	(F)	.01	- .05 (H,W)	.01	- .07 (D,W)	2	- .7 (G)	.42	- 1.0 (F,H)
Ta	.08	- .23	(W)	.005	-.08 (S)	.005	-.01 (S)	.001	-.01 (S)	.7	(V)	2.3	- 4.6 (V)
Th	.02	- .10	(W)	-	-	.01	- .03 (W)	<.06	(W)	.8	(V)	2.7	- 6.6 (V)
				-	-	.01	- .03 (W)	.02	- .08 (W)	<.21	(W)	-	-

Notes:

Partition coefficients selected from the literature to represent a reasonable range of values and consistent REE patterns. Phenocryst/matrix data from mildly alkaline basalt series are reported where available. Numbers in parentheses are interpolated values. Specific notes:

- 1 The data of Green & Pearson (1985) are from 20 kbar, 1050°C: DREE between cpx and liquid increase with pressure and these values represent the maximum DMREE/DHREE and most uniform DMREE observed (Tb interpolated from Ho).
- 2 DSr in cpx at 20-30 kbar was determined experimentally to be 0.3 (Shimizu, 1980).
- 3 Ray et al (1983) found DSc cpx/liquid to be strongly temperature dependent, becoming less than unity at T = 1300°C. Lemarchand et al (1987) report cpx/liquid DSc = 2.1 - 3.5 in alkali basalts and DSc = 4.05 in mugearite (assumed near-surface conditions).
- 4 The data of Hervig & Smith (1982) apply only to coexisting olivine, opx and cpx at T = 1200-1300°C.
- 5 The lower DSr for plagioclase corresponds to the T = 1300°C data of Drake & Weill (1975).

Sources of Data for Partition Coefficients

A	Frey et al., 1978, Table A-1, set 1	L	Ray et al., 1983
B	Frey et al., 1978, Table A-1, set 2	M	Watson & Ryerson, 1986
C	Green & Pearson, 1985	N	Schnetzler & Philpotts, 1970
D	Dostal et al., 1983	Q	Hervig & Smith, 1982
E	Drake & Weill, 1975	R	Ewart et al., 1983
F	McKay et al., 1986	S	Gerlach, 1985, Table 8
G	Villemant et al., 1981	T	Hart & Davis, 1978
H	Fujimaki et al., 1984	V	Green & Pearson, 1987
J	Frey et al., 1978, Table A-2	W	Lemarchand et al., 1987
K	Sun et al., 1979	X	Shimizu, 1980

CHAPTER 3

MAGMATIC EVOLUTION OF THE AUSTURHORN CENTRAL VOLCANO

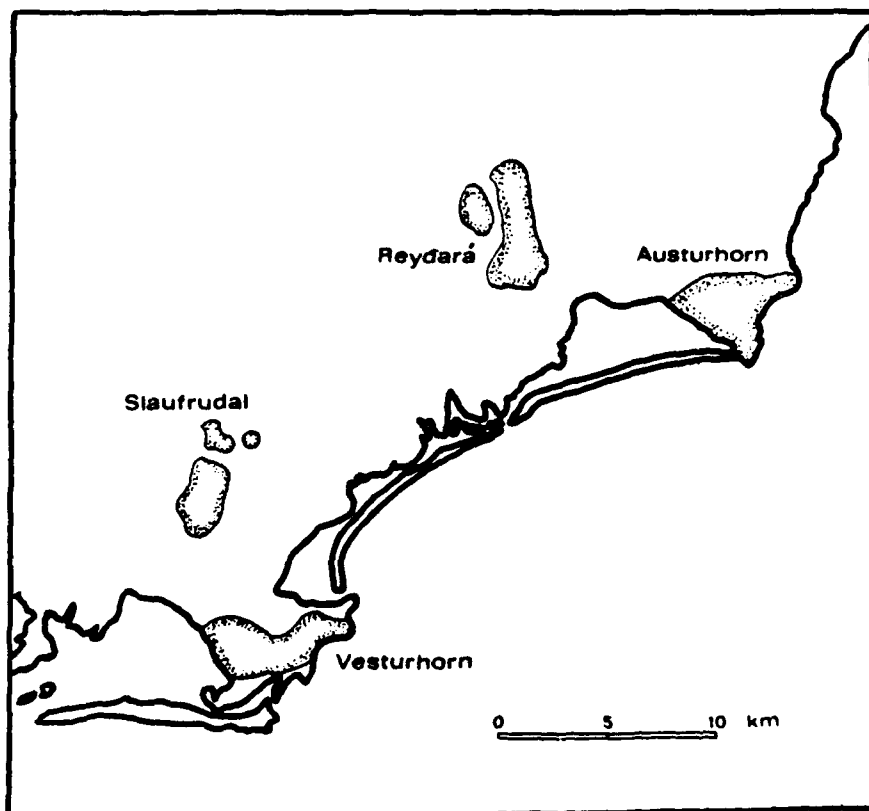
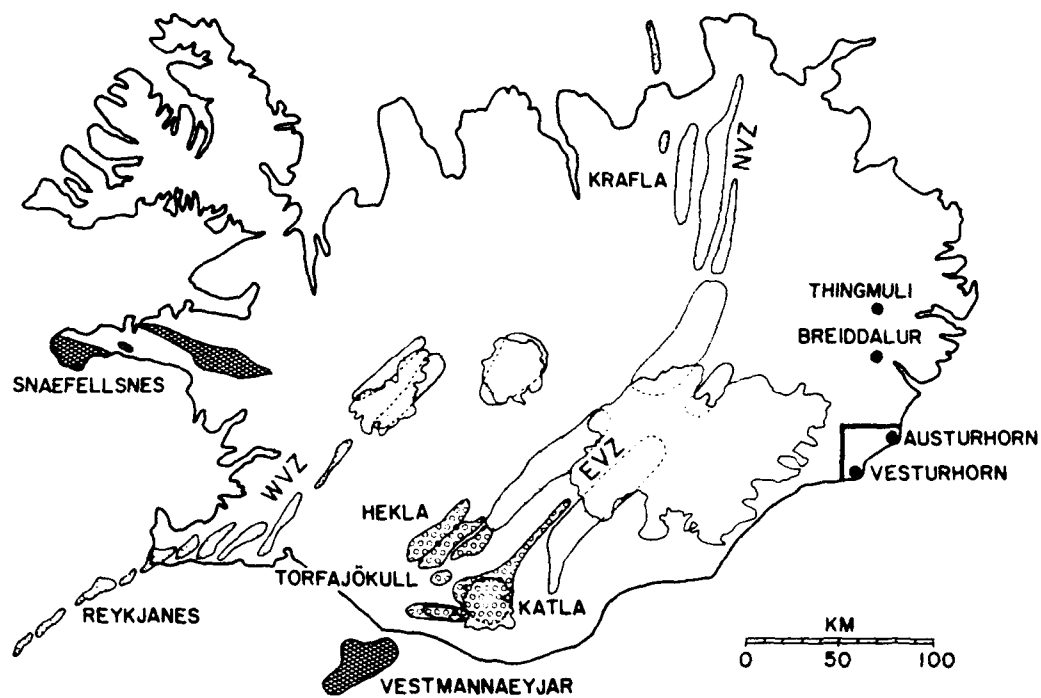
INTRODUCTION

Understanding the magmatic evolution of individual volcanoes is vital to predicting eruptive behavior (e.g., Blake, 1984a; Houghton et al., 1987) as well as to deciphering geochemical features of extrusive sequences (Bailey & Macdonald, 1987; Ho & Garcia, 1988). Seismic and geophysical monitoring of active volcanic systems (Einarsson, 1978; Sanders, 1984; Tryggvasson, 1986; Mortensen & Hopkins, 1987; Wright & Swanson, 1987) enhances our understanding of subsurface processes, yet many fundamental questions remain. In brief, we do not know how magma chambers first develop, nor how they change with time.

My approach to this problem is to study the cumulate and intrusive products of the Austurhorn intrusion, an exhumed Tertiary complex in southeastern Iceland (figure 3.1). Austurhorn is comparable in dimension, and in diversity and abundance of observed rock types to both modern and Tertiary Icelandic central volcanoes. This dissected hypabyssal intrusion preserves the critical interface between volcanic and plutonic environments and is well suited to direct observation of magmatic phenomena.

The focus of this study is to use field relationships to understand evolution of the Austurhorn central volcano, a magmatic system which erupted diverse basaltic and silicic liquids. I use geological evidence from this hypabyssal complex to evaluate aspects of magmatic evolution which have been inferred from petrographic and geochemical investigation of Icelandic lavas and tephra (e.g., Sigvaldason, 1974; Sigurdsson & Sparks, 1978, 1981). Specifically, I demonstrate that a shallow magma chamber did exist at Austurhorn, and document changes in chamber structure throughout the life of the volcanic system. Open-system behavior, including chamber replenishment by dense basaltic and buoyant felsic magmas (Huppert & Sparks, 1980; Sparks et al., 1984; Huppert et al., 1986), is indicated by field evidence for commingling and mixing of basaltic and granitic magmas. Finally, I infer that Austurhorn developed in an immature rift environment analogous to the modern Eastern Volcanic Zone (EVZ;

Figure 3.1 The Austurhorn intrusion in southeast Iceland is the northernmost of four coeval hypabyssal complexes, each with abundant silicic units. The four intrusions define a rift segment parallel to the modern spreading axes, the western and eastern neovolcanic zones [WVZ, EVZ]. Within the active eruptive areas, individual volcanic centers are taken from Jakobsson (1979). Cross-hatched pattern indicates alkaline volcanism (Vestmannaeyjar and Snaefellsnes), open circles are transitional and FeTi enriched centers (Hekla, Katla, Torfajokull), and stippled areas are tholeiitic. The SE Iceland intrusions are 6-7 million years old and represent the exhumed magma chambers of evolved volcanoes with transitional and FeTi-rich chemical affinity. Thingmuli and Breiddalur were tholeiitic central volcanoes between 9-11 Ma.



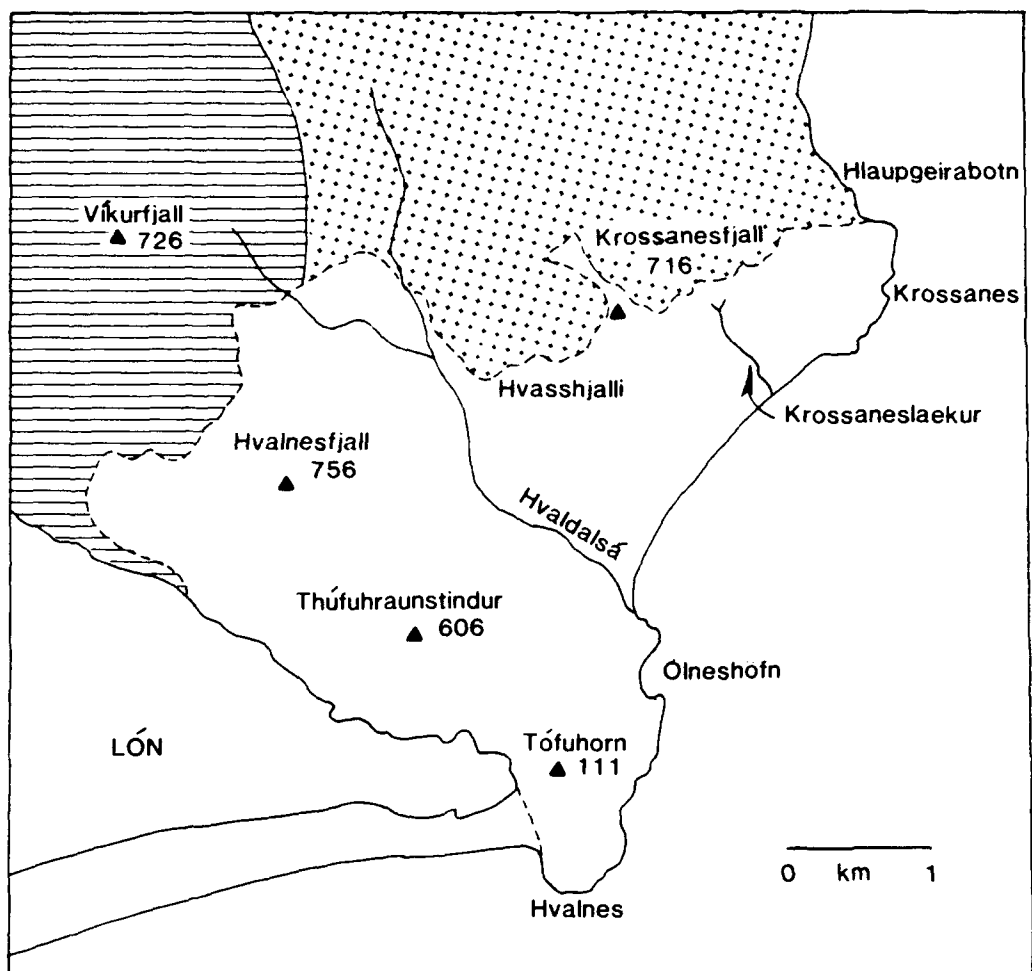
Jakobsson, 1979; Oskarsson et al., 1982; Meyer et al., 1985). This interpretation provides new constraints on the position of active rift segments at the time of a major plate reorganization at ~7 Ma (Jancin et al., 1985). The geochemical evolution of Austurhorn is discussed separately in chapter 4.

3.1 Tectonic and Geologic Setting

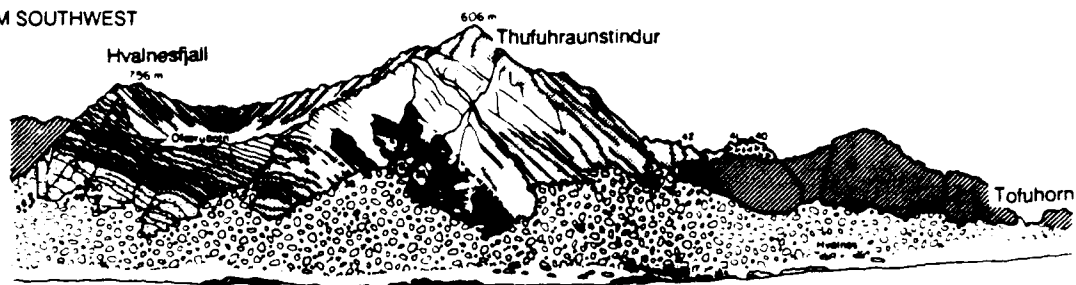
The Austurhorn intrusive complex outcrops over ~15 km² at the northeastern end of Lonsfjordur in eastern Iceland. It comprises the mountains Hvalnesfjall (756 m) and Krossanesfjall (716 m) and the surrounding lowlands (figure 3.2). The exposed portion of the intrusion includes roof and wall contacts in several locations. Sidewall contacts are steep, roof surfaces are subhorizontal and junctions between them are typically angular, with a general absence of warping or stoping features. The overall step-like appearance of the intrusion margins indicates that magma ascent was controlled locally by competent layers in the earlier Tertiary lava pile. A similar intrusive mechanism has been proposed by Gudmundsson (1986) for the neighboring Slafrudalur intrusion.

Products of the Alftafjordur and Lon central volcanoes comprise the host rock for the Austurhorn complex (figure 3.2; Blake, 1964, 1970). They consist of basic, intermediate and acid lavas as well as pyroclastic deposits. Early propylitic alteration of these units has been overprinted by both regional burial metamorphism and contact alteration associated with the Austurhorn complex (Blake, 1970). Outside the Austurhorn aureole, regional laumontite-zone metamorphism suggests the complex was emplaced at a depth of roughly 2000 meters (Walker, 1964; Blake, 1966). The contact aureole is typically hornfels, but localized channels of fossil hydrothermal circulation contain prehnite, epidote, platy calcite and garnet, indicating temperatures above 350°C (O. Sigmarsson, pers. commun., 1983). Blake (1970) estimated the Alftafjordur and Lon volcanics were 9-11 my based on correlations with dated units from Breiddalur. More recent K-Ar dating in eastern Iceland (Ross & Mussett, 1976) indicates an age of ~12

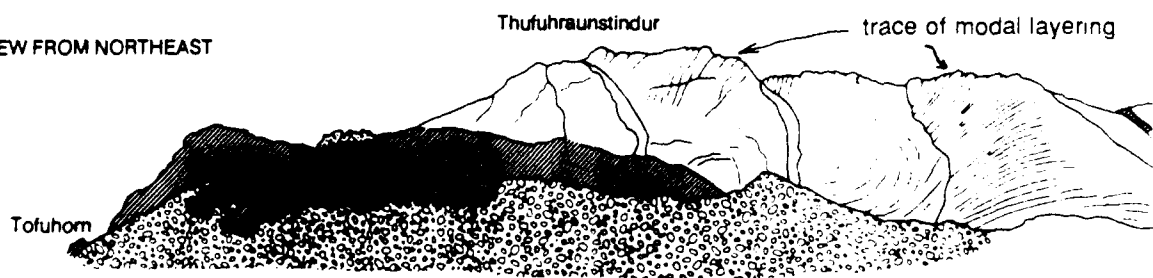
Figure 3.2 Physical geology of the Austurhorn region, indicating areas and mountain names referred to in the text. The surrounding country rock comprises products of the Lon (ruled) and Alftafjordur (patterned) central volcanoes (Blake, 1970). The cross-sections, from Gunnarsson & Sigurdsson (1982), are drawn through the crest of the Hvalnesfjall-Tofuhorn ridge and indicate schematically the relationship between gabbro (white or stippled), granophyre (diagonally ruled) and talus (cobble pattern).



VIEW FROM SOUTHWEST



VIEW FROM NORTHEAST



my. The structural level exposed at Austurhorn is lower than those of Breiddalur and Thingmuli, where lavas and occasional rhyolitic plugs are exposed (Walker, 1963; Carmichael, 1964). The extrusive units of these volcanic centers have intrusive equivalents at Austurhorn, including the unique xenolith-rich agglomerate of the Breiddalur summit group (Walker, 1963).

Several independent observations suggest that Austurhorn developed within a short-lived rift segment. The Austurhorn and neighboring Reydara, Slafrudalur and Vesturhorn intrusions (figure 3.1) are coeval (6-7 Ma; Gale et al., 1966; Moorbath et al., 1968) and define a line segment parallel to both the southern and eastern neovolcanic zones which reflect the modern spreading direction in this portion of the Mid-Atlantic Ridge. The inferred Tertiary rift segment joining the four intrusive complexes does not appear to continue north of Austurhorn. Basalts from Austurhorn and Vesturhorn are generally evolved transitional tholeiites (<7.8 wt% MgO; Mattson et al., 1986; see chapter 4) and all four intrusions are dominated by silicic compositions. By analogy to Iceland's eastern neovolcanic zone, this chemical signature indicates an immature axial rift environment (Meyer et al., 1985). For example, volcanic centers in the EVZ with transitional basaltic chemistry and/or copious silicic volcanism include Torfajökull (Gunnarsson, 1988; Ivarsson et al., in prep.) and Eyjafjallajökull (Arney, 1978; Jakobsson, 1979) (figure 3.1).

Studies of the Pb isotopic systematics of Tertiary plateau basalts in eastern Iceland indicate a pulse in plume activity at approximately 7 Ma (Hanan & Schilling, 1986, 1987). This timing is coincident with a peak in La/Sm of eastern Iceland basalts at 7-8 Ma (Schilling, 1973; Schilling et al., 1982; Meyer, 1984) and a maximum in lava production rate at ~7.5 Ma (Vogt, 1974; Watkins & Walker, 1977). These factors suggest that a plume-related rift segment was active in eastern Iceland at that time, with both Austurhorn and Vesturhorn as axial volcanoes. This scenario is analogous to that proposed by Meyer and co-workers for initiation and propagation of the EVZ at 2.5 Ma

(Kurz et al., 1985; Meyer et al., 1985). Structural studies have shown that ridge relocations were common in the Tertiary (Aronsson & Saemundsson, 1975; Johannesson, 1980; Helgason, 1984), but the position and longevity of active rift segments is poorly constrained. Integrated field, geochemical and isotopic evidence from individual Tertiary volcanoes can be used to determine the link between plume activity and paleo-rift zone movement. Study of the Austurhorn complex thus provides insight into the history of the Iceland mantle plume in addition to the crustal processes attendant to magmagenesis and evolution in an axial rift zone.

3.2 Field Observations: Major Intrusive Units

3.2.1 Previous Work

The juxtaposition of gabbro and granophyre at Austurhorn was first described by Thoroddsen (1896). Cargill et al (1928) interpreted the complex as an irregular composite stock. Blake (1964, 1966) reported the distribution of major rock types within the complex and proposed a mechanism for their near-contemporaneous emplacement. The Hvalnesfjall gabbro was mapped by the National Energy Authority of Iceland during a regional investigation of titanium resources (Gunnarsson & Sigurdsson, 1982), although no mining has taken place. Mattson et al (1986) investigated localized mixing between basaltic and granitic magmas within the coastal net-veined complex. I have incorporated existing field and geochemical data in this integrated tectonomagmatic investigation of the Austurhorn complex.

Remapping of the Austurhorn complex (figure 3.3) included a study of the coastal net veined complex (NVC) at a scale of 1:2400 (figure 3.4). Intrusive units and contacts are well-exposed along the coast and at elevations over ~300 m. Intermediate elevations, including the Hvaldalsa river valley (figure 3.2), are typically covered with skree.

Figure 3.3 Geology of the Austurhorn intrusion. The base map of Blake (1964) has been modified by Furman (this study). Key to major units is as follows: gabbro - open stipple; granophyre - black; net veined complex - pebble pattern; Krossanes felsite (NE margin of intrusion) - cross-hatching; Tertiary volcanics - vertical rule. Pegmatoidal gabbro outcrops in three locations indicated by "p." Dips of modal layering are indicated in Hvalnesfjall gabbro. Margins of the intrusion are dashed where inferred; contacts between gabbro and granophyre are dotted where inferred. Cross-sections A-A' and B-B' are drawn through Hvalnesfjall and indicate the intrusive relations between major rock units and the direction of layer dips in the gabbro (no vertical exaggeration).

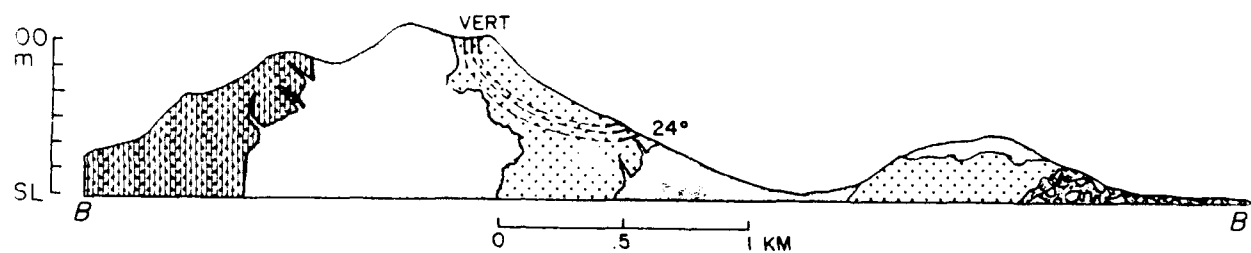
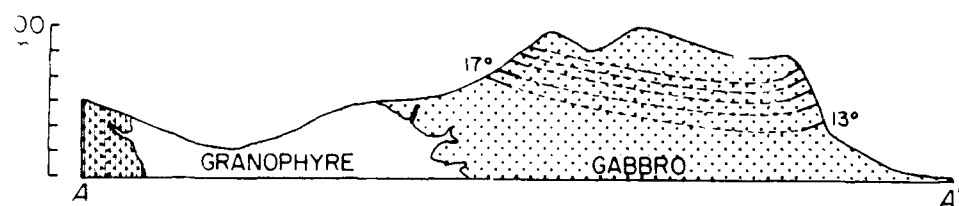
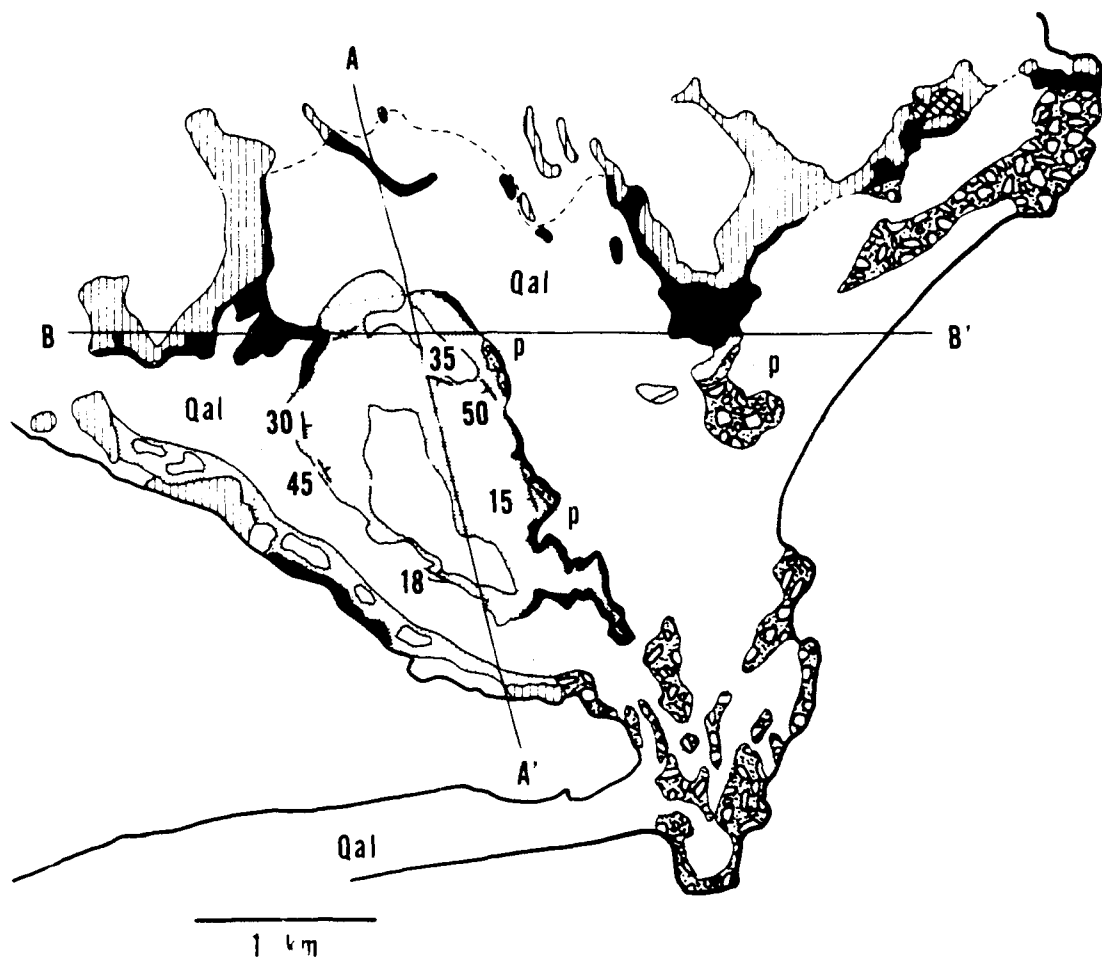
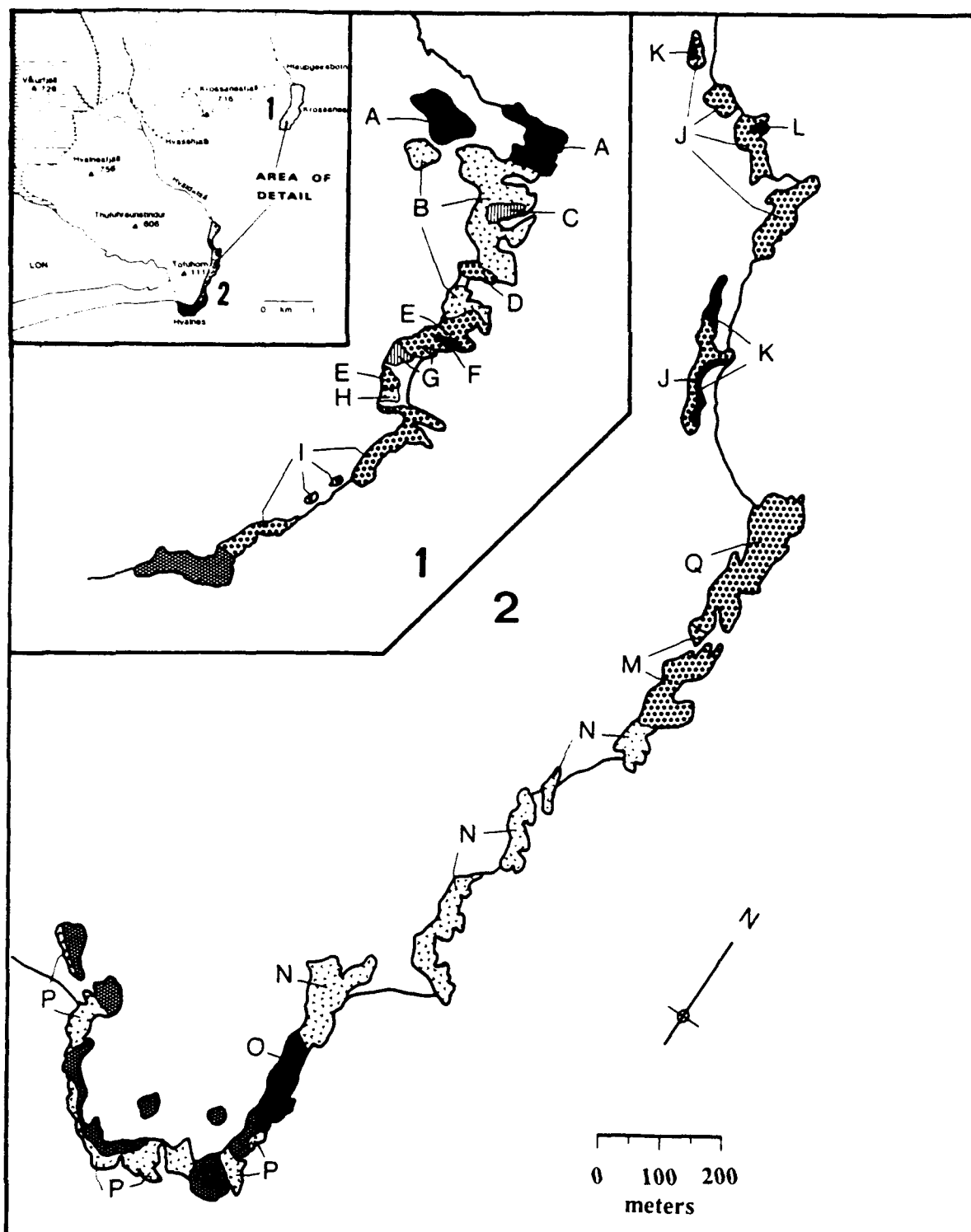


Figure 3.4 Outcrop map of the coastal net veined complex, mapped at the scale of 1:2400. Patterns indicate types of felsic rock; basalts are omitted for clarity and to emphasize contact relations among the granophyres. **Shaded** units [A, F, K, L, O] are Type 1 granophyres, **random-V** pattern [B, H, N, P] indicates Type 2 granophyres, **dot pattern** [D, E, I, J, M Q] indicates type 3 granophyres, **vertical stripes** [C, G] are finegrained granodiorites. **Cross-hatched** regions are gabbro; substantial outcrops of gabbro (unlabeled) also occur in regions occupied by units N and I.



3.2.2 Hvalnesfjall Gabbro

This mafic body forms Hvalnesfjall proper and also outcrops along strike across the valley at Hvasshjalli (figure 3.2). It forms steep cliffs underlain by talus slopes. Average color index (CI) of the gabbro is 35-40, with equant interlocking crystals of plagioclase and clinopyroxene (2-5 mm) comprising over 80 vol% of most samples (figure 3.5). Plagioclase and clinopyroxene have restricted compositional ranges within individual samples, although bimodal plagioclase populations (typically An_{60-65} and $An_{>75}$) are observed in some cases (figure 3.6, table 3.1). Plagioclase are often zoned by up to 30 mol% An to more sodic compositions at crystal margins. Gabbroic clinopyroxenes define an evolutionary trend similar to that observed in the mildly alkaline Kiglapait intrusion (figure 3.6, table 3.2; Morse, 1969, 1980). Cumulate and intercumulus ilmenite and titanomagnetite are locally abundant, with concentrations over 20 vol% in some places (Gunnarsson & Sigurdsson, 1982). Layers with highly concentrated oxides tend to occur in, but are not restricted to, structurally lower regions of the gabbro. Individual layers with ~20 vol% olivine are found in the northwestern portion of Hvalnesfjall and at Hvasshjalli (figures 3.2, 3.3). Within olivine-rich units olivine core compositions vary by up to 10 mol% Fo content (Fo_{76} to Fo_{66} ; table 3.3), whereas samples with sparse olivine have crystals of constant composition. Olivine and hypersthene (typically <5 vol%) are locally pseudomorphed by mixed-layer silicates. A highly leucocratic gabbro (CI <10) outcrops on Hvalnes peninsula and near the Hvaldalsá river (figure 3.3). This unit contains >70 vol% tabular plagioclase (3-5 mm; An_{50-35} , table 3.1) with subordinate volumes of augite, magnetite and apatite. Hydrothermal alteration is generally restricted to a network of fractures <1 cm thick. Accessory and alteration minerals include apatite, calcite, chlorite, epidote and serpentine.

Many cumulates sampled at Hvalnesfjall have modal abundances unlike those predicted for 1 atm crystallization of Austurhorn basalts (figure 3.7; see chapter 4). Certain Hvalnesfjall gabbros are enriched in plagioclase relative to calculated low

Table 3.1 Representative Plagioclase Analyses

	gb-23 (a)	gb-23 (b)	gb-29 (a)	gb-29 (b)	gb-31	gb-41	gb-83	p-62a (a)	p-62a (b)	p-62b
SiO ₂	50.37	52.40	48.71	57.66	46.29	58.55	56.16	52.02	54.04	52.50
Al ₂ O ₃	31.60	30.03	32.80	27.24	33.60	26.36	27.55	29.68	28.68	29.60
FeO	0.47	0.49	0.55	0.37	0.50	0.19	0.36	0.74	1.00	0.80
MgO	0.07	0.08	0.02	0.01	0.05	0.01	0.03	0.12	0.05	0.04
CaO	14.39	12.76	15.39	9.03	16.88	7.77	9.75	13.45	11.81	12.84
Na ₂ O	3.06	4.06	2.56	6.10	1.62	6.73	5.89	3.91	4.74	4.14
K ₂ O	0.18	0.30	0.11	0.36	0.06	0.45	0.26	0.13	0.18	0.17
total	100.14	100.12	100.14	100.77	99.00	100.06	100.00	100.05	100.49	100.09
% An	71.5	62.4	76.3	44.1	84.9	38.0	47.1	65.0	57.3	62.5

Cations on the basis of 8 oxygens

	2.295	2.379	2.227	2.568	2.151	2.617	2.528	2.370	2.442	2.387
Si	1.697	1.607	1.768	1.430	1.840	1.388	1.461	1.594	1.527	1.586
Al	0.018	0.018	0.021	0.014	0.019	0.007	0.013	0.028	0.038	0.031
Fe	0.005	0.005	0.001	0.001	0.003	0.001	0.002	0.008	0.003	0.002
Mg	0.702	0.621	0.754	0.431	0.840	0.372	0.470	0.656	0.572	0.626
Ca	0.270	0.357	0.227	0.527	0.146	0.583	0.514	0.345	0.415	0.365
Na	0.001	0.017	0.006	0.020	0.003	0.026	0.015	0.008	0.010	0.010
K	4.998	5.004	5.004	4.991	5.002	4.994	5.003	5.009	5.007	5.007
sum										

Table 3.1 Continued

	g-62	g-42	g-65 (a)	g-65 (b)	g-64	d-43 (a)	d-43 (b)	d-5 (a)	d-5 (b)	d-5 (c)
SiO ₂	59.54	57.69	63.88	65.61	67.03	47.70	51.15	48.90	51.58	52.85
Al ₂ O ₃	25.62	26.73	22.75	18.46	19.66	33.17	30.74	32.02	29.77	29.06
FeO	0.26	0.39	0.29	0.00	0.00	0.07	0.08	0.83	0.73	0.66
MgO	0.02	0.00	0.02	0.00	0.00	0.07	0.08	0.11	0.14	0.14
CaO	7.39	8.69	4.13	0.03	0.99	16.48	13.65	16.06	13.64	12.57
Na ₂ O	7.21	6.54	8.95	0.42	8.80	2.04	3.60	2.44	3.73	4.26
K ₂ O	0.26	0.28	0.62	16.30	3.52	0.08	0.21	0.09	0.15	0.19
total	100.30	100.32	100.64	100.85	100.20	100.30	100.23	100.45	99.74	99.73
% An	35.6	41.7	19.6	0	4.7	81.3	66.9	78.0	66.3	61.3

Cations on the basis of 8 oxygens

Si	2.651	2.581	2.812	3.005	2.966	2.187	2.329	2.237	2.359	2.408
Al	1.344	1.409	1.180	0.996	1.025	1.793	1.650	1.726	1.604	1.561
Fe	0.010	0.014	0.011	0.000	0.007	0.029	0.030	0.032	0.028	0.025
Mg	0.001	0.000	0.001	0.000	0.000	0.005	0.005	0.008	0.009	0.009
Ca	0.353	0.417	0.195	0.001	0.047	0.810	0.666	0.787	0.668	0.614
Na	0.622	0.566	0.763	0.037	0.755	0.182	0.317	0.217	0.331	0.377
K	0.015	0.016	0.035	0.953	0.199	0.005	0.012	0.005	0.009	0.011
sum	4.996	5.003	4.997	4.992	4.999	5.011	5.009	5.012	5.008	5.005

Table 3.2 Representative Clinopyroxene Analyses

	gb-23	gb-29	gb-31 (a)	gb-31 (b)	gb-41	gb-83	p-62a	p-62b
SiO ₂	50.70	53.38	50.77	50.92	50.27	52.07	52.85	53.17
TiO ₂	1.16	0.14	1.04	0.74	0.55	0.36	0.23	0.06
Al ₂ O ₃	3.39	0.96	2.91	1.93	1.28	0.93	1.12	0.32
FeO	8.24	7.92	7.75	9.77	16.62	12.06	8.71	9.19
MnO	0.20	0.30	0.26	0.29	0.55	0.50	0.29	0.21
MgO	15.31	15.21	16.45	14.92	10.61	13.52	14.35	13.86
CaO	20.69	21.84	20.36	21.00	19.44	20.18	22.93	23.00
Na ₂ O	0.24	0.30	0.29	0.30	0.33	0.38	0.23	0.22
Cr ₂ O ₃	0.26	0.04	0.21	0.07	0.07	0.00	0.00	0.02
total	100.19	100.09	100.04	99.94	99.72	100.00	100.71	100.04
Wo	42.7	44.4	41.3	42.5	41.2	41.7	46.1	46.5
En	44.0	43.0	46.4	42.0	31.3	38.9	40.2	29.0
Fs	13.3	12.6	12.3	15.4	27.5	19.4	13.7	14.5

Cations on the basis of 6 oxygens

Si	1.881	1.978	1.882	1.911	1.945	1.965	1.961	1.989
Ti	0.032	0.004	0.029	0.021	0.016	0.010	0.006	0.002
Al	0.148	0.042	0.127	0.085	0.058	0.041	0.049	0.014
Fe	0.255	0.245	0.240	0.306	0.538	0.380	0.270	0.287
Mn	0.006	0.009	0.008	0.009	0.018	0.016	0.009	0.006
Mg	0.847	0.840	0.909	0.835	0.612	0.761	0.794	0.773
Ca	0.822	0.867	0.809	0.844	0.805	0.816	0.911	0.922
Na	0.017	0.021	0.021	0.022	0.025	0.027	0.016	0.016
Cr	0.008	0.001	0.006	0.002	0.002	0.000	0.000	0.001
sum	4.016	4.007	4.031	4.034	4.019	4.016	4.016	4.010

Table 3.2 Continued

	g-23 (a)	g-23 (b)	g-62 (a)	g-62 (b)	d-5	d-43	d-81
SiO ₂	47.45	47.21	47.85	48.43	51.40	51.43	51.70
TiO ₂	0.72	0.46	0.81	0.47	1.08	0.66	0.67
Al ₂ O ₃	1.18	0.49	1.61	0.75	2.59	1.65	1.26
FeO	26.95	30.15	24.97	26.64	8.81	11.16	14.50
MnO	0.97	1.13	0.80	0.92	0.23	0.37	0.65
MgO	3.38	0.75	4.39	2.58	15.56	14.21	14.41
CaO	19.00	19.26	18.92	19.70	20.33	19.91	17.27
Na ₂ O	0.21	0.27	0.29	0.29	0.35	0.33	0.22
Cr ₂ O ₃	0.00	0.00	0.03	0.04	0.02	0.00	0.01
total	99.86	99.72	99.67	99.82	100.37	99.72	100.69
Wo	42.5	43.9	42.5	44.7	41.6	41.1	35.5
En	10.5	2.4	13.7	8.2	44.3	40.9	41.2
Fs	47.0	53.7	43.8	47.2	14.1	18.0	23.3

Cations on the basis of 6 oxygens

Si	1.936	1.965	1.934	1.973	1.905	1.938	1.945
Ti	0.022	0.014	0.025	0.015	0.030	0.019	0.019
Al	0.057	0.024	0.077	0.036	0.113	0.073	0.056
Fe	0.920	1.049	0.844	0.908	0.273	0.351	0.456
Mn	0.034	0.040	0.027	0.032	0.007	0.012	0.021
Mg	0.205	0.047	0.264	0.157	0.860	0.798	0.808
Ca	0.831	0.859	0.819	0.860	0.807	0.803	0.696
Na	0.016	0.022	0.022	0.023	0.025	0.024	0.016
Cr	0.000	0.000	0.001	0.001	0.001	0.000	0.000
sum	4.021	4.020	4.013	4.005	4.021	4.018	4.017

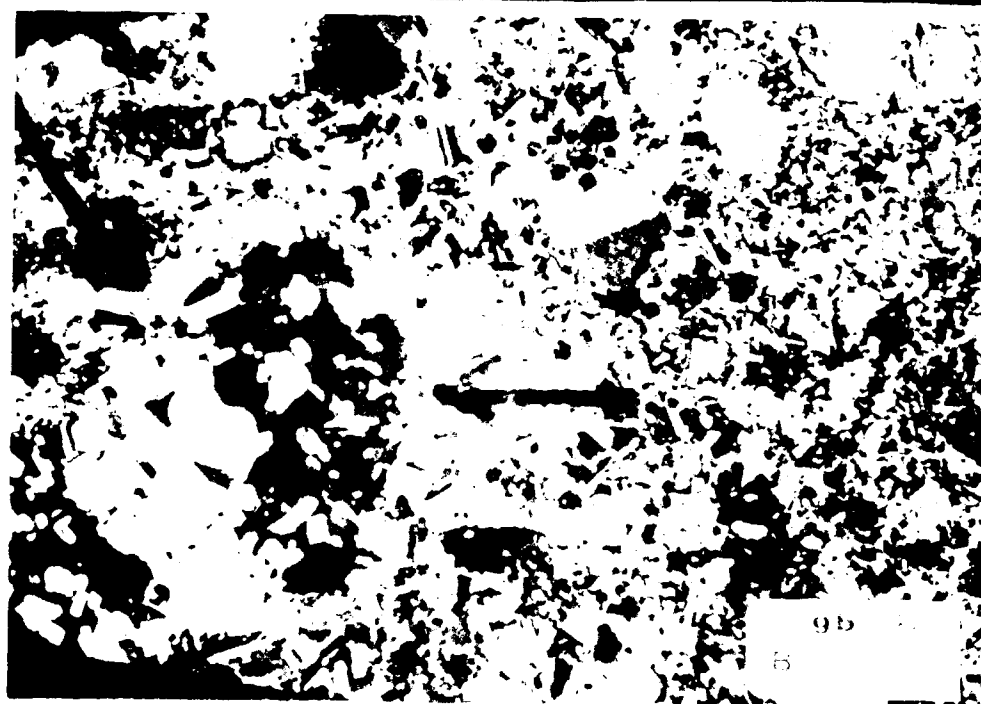
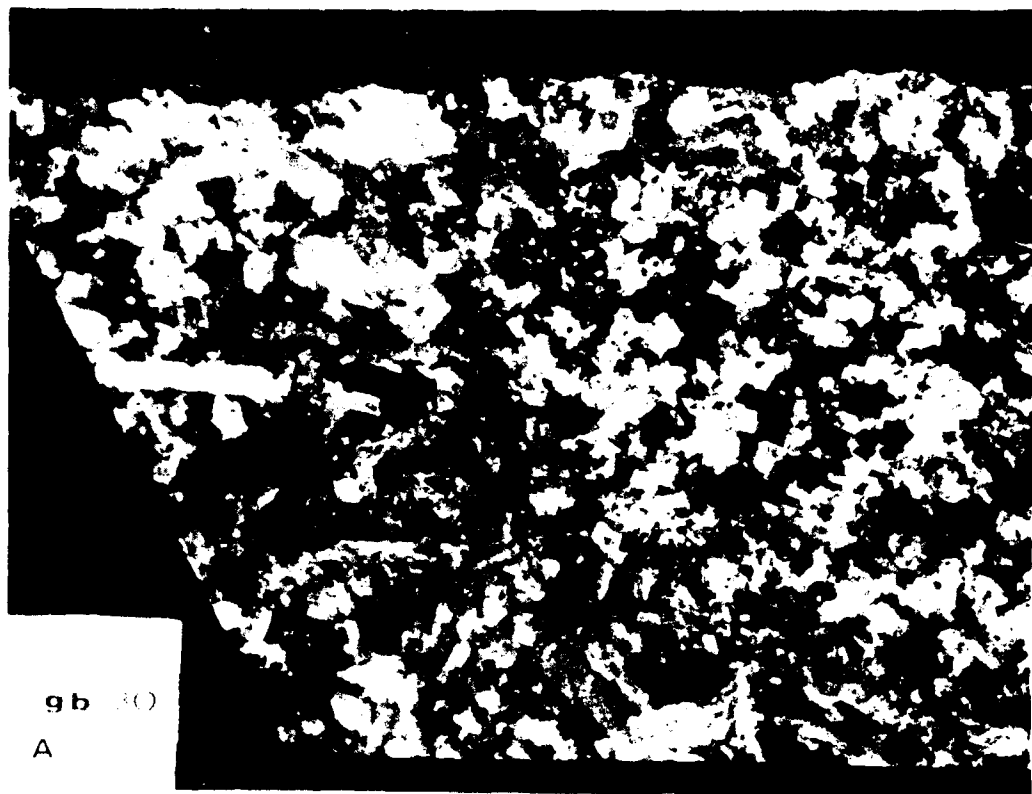
Table 3.3 Representative Olivine Analyses

	gb-32 (a)	gb-32 (b)	gb-42 (a)	gb-42 (b)	g-23
SiO ₂	37.21	37.00	38.06	36.56	30.21
TiO ₂	0.03	0.00	0.00	0.03	0.11
Al ₂ O ₃	0.02	0.02	0.03	0.09	0.05
FeO	27.06	30.06	22.33	31.69	65.65
MnO	0.46	0.44	0.32	0.61	3.23
MgO	34.79	32.52	39.12	31.46	0.88
CaO	0.00	0.04	0.28	0.22	0.38
NiO	0.03	0.03	0.09	0.02	0.11
total	99.60	100.11	100.23	100.68	100.62
Fo	70.7	65.8	75.7	63.8	2.3

Cations on the basis of 4 oxygens

Si	0.996	0.999	0.989	0.991	1.006
Ti	0.001	0.000	0.000	0.001	0.003
Al	0.000	0.001	0.001	0.003	0.002
Fe	0.606	0.679	0.485	0.718	1.828
Mn	0.010	0.010	0.007	0.014	0.091
Mg	1.388	1.309	1.516	1.272	0.044
Ca	0.000	0.001	0.008	0.006	0.014
Ni	0.001	0.001	0.002	0.000	0.003
sum	3.002	3.000	3.008	3.005	2.991

Figure 3.5 Features of the Hvalnesfjall gabbro. (a) Handsample of moderately melanocratic gb-30 showing plagioclase, clinopyroxene and abundant FeTi oxides. (b) Photomicrograph of melanocratic gabbro gb-42. Arrows indicate Fo-rich olivine overgrown by clinopyroxene, while smaller isolated olivines are up to 10 mole% less forsteritic. Field of view approximately 6 cm. (c) Backscattered electron (BSE) image of ilmenite lamellae in magnetite crystal in sample gb-30 used for assessment of temperature and oxygen fugacity. Scale bar is 1 mm. (d) BSE image of adjacent ilmenite and magnetite domains in sample gb-34 used for temperature - oxygen fugacity evaluation. Scale bar is 1 mm.



C D



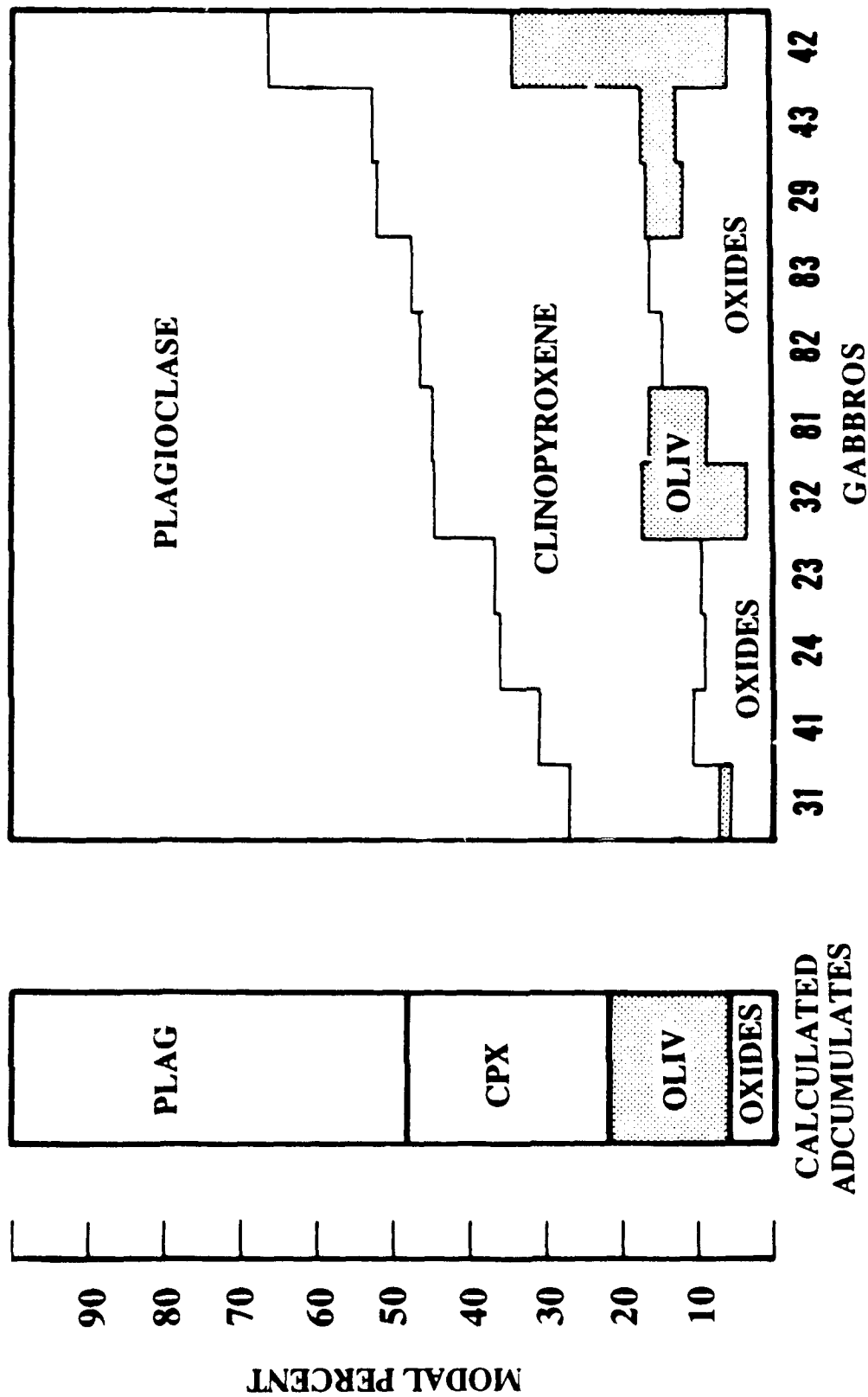


Figure 3.7 Comparison of calculated adcumulates generated during differentiation of Austurhorn pillow basalts (see chapter 4) and modal assemblages of Hvalnesfjall gabbro (calculated by mass balance using bulk rock analyses and microprobe data on observed mineral phases). The olivine field is shaded for clarity. Plagioclase field includes K-feldspar and quartz in leucocratic samples (gb-41, 82, 83). See text for further discussion.

pressure adcumulates; these samples typically contain oscillatory zoned plagioclase (e.g., gb-23, gb-24, gb-31). Bimodal plagioclase populations in mafic dikes and gabbros (figure 3.6, table 3.1) suggest that local plagioclase accumulation is common in this magmatic environment. Similarly, the most melanocratic gabbros have olivines with diverse Fo contents (e.g., gb-42), again suggesting local mineral accumulations.

Modal layering (apparently rhythmic) defined by varying proportions of clinopyroxene and plagioclase is well-developed throughout most of the unit (figure 3.8). Layers are generally 1-3 meters thick and dip inward towards the center of the mountain. Dips range from 10-30° NE on the southern face of Hvalnesfjall to 30-50° SW on the northern face to vertical at the NW corner of the body (figure 3.3). Individual layers can be traced for several hundred meters as they change in orientation from subhorizontal to subvertical. Layering is strictly sub-horizontal at Hvasshjalli. Where rhythmic modal layering is best developed, (NE Hvalnesfjall) clinopyroxene-rich basal mafic units of CI 65-70 and grain size 2-3 mm comprise roughly one-third of each layer. Isolated dark (CI >70) coarse (3-4 mm) pyroxene-rich bands 5-10 cm thick occur sporadically within the associated overlying leucocratic (CI <30) units. Contacts within and between layers are sharp on a scale of 1-5 cm and can be traced laterally as exposure permits.

Mafic sills 10-30 cm thick occur locally between modally layered units. They are typically plagioclase phyric and often display a flow texture defined by plagioclase laths up to 2 mm. Some sills are diabasic and are distinguished from the host gabbro by their uniform grain size and mineral abundances. Less frequently, irregular patches of diabase are evident within moderately leucocratic units, where they appear to represent partially digested or incorporated comagmatic mafic dikes.

The structurally lowest zone of the gabbro is not modally layered, but contains abundant irregularly shaped pegmatoidal patches (figure 3.9). They comprise up to 30 vol% of individual outcrops on Hvasshjalli and Hvalnes. Pegmatoids range in size from

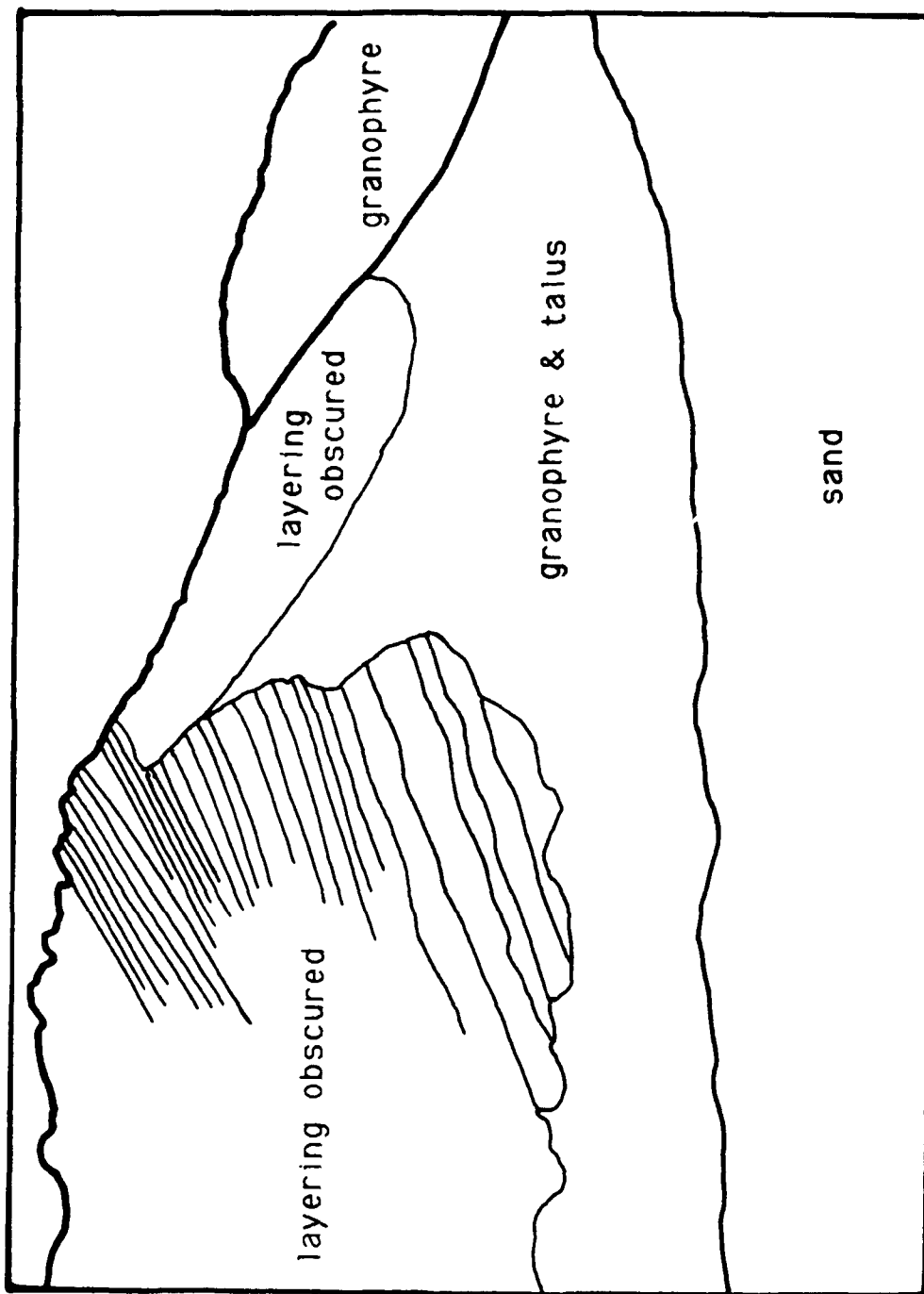


Figure 3.8 Modal layering of Hvalnesfjall gabbro viewed from Krossanesfjall (3 km away), looking south. Tracing in this figure was made from photograph on following page.



Figure 3.9 (a) Photo of pegmatoidal pocket in gabbro from Hvalnes peninsula. In this figure the curved margins of an irregularly shaped pocket are visible; note that the average grain size in the felsic pocket is much greater than that of the host gabbro.





(b) This tracing of a photomicrograph indicates that compositions of plagioclase (unpatterned) and clinopyroxene (parallel dashes) from a pegmatoidal sample show no systematic variations with distance away from the pocket (right hand margin of figure). The large tabular plagioclase is more sodic than cores of common gabbroic plagioclase but is of comparable composition to their outer rims (An₅₃₋₄₉). Filled circles indicate plagioclase analyses, with numbers corresponding to anorthite content. Filled triangles represent clinopyroxene analyses, and numbers indicate molar Mg/(Mg+Fe) ratios. Minor quartz (Q) and apatite (A) are present at the pocket margin; FeTi oxides (shaded) are abundant throughout the sample.

10 cm to 1 m and contain crystals up to 10 cm long. The large tabular plagioclase and clinopyroxene which protrude into the pegmatoids are generally unzoned (figure 3.9). Coarse altered olivine (1-3 cm) is common in pegmatoids even when the adjacent host gabbro is olivine-free. Ubiquitous in the interstices between these phases is a fine equigranular intergrowth of plagioclase + quartz + K-feldspar with abundant apatite and magnetite.

3.2.3 Hvasshjalli Granophyre

Metaluminous to mildly peralkaline felsic rocks (64-75% SiO_2 ; see chapter 4) form a composite body which occupies fully half of the Austurhorn complex. In keeping with previous work, I refer to these units collectively as granophyres, although quartz-feldspar intergrowths are not present in every sample. Felsic magmas were emplaced into gabbro at Hvalnesfjall and Hvasshjalli (figure 3.10), but intruded Tertiary country rock in all other areas. The granophyres are not resistant to weathering and form large skree and talus slopes. Fresh and sea-washed surfaces are grey while exposed surfaces weather to a salmon color.

Most of the felsic bodies consist of tabular plagioclase crystals (2-5 mm, 5-30 vol%; figure 3.6) within an equigranular (0.5-1 mm) matrix of plagioclase, K-feldspar and quartz (figure 3.11). Where granophyric texture is not well-developed, dusty K-feldspar mantles each large plagioclase crystal (figure 3.11). Mafic phases comprise <10 vol% of the rock and include FeTi oxides, ferrohedenbergite, amphibole, fayalite and biotite (figure 3.6). Amphibole (<0.2 mm, after clinopyroxene) is typically euhedral in units with <66 wt% SiO_2 but anhedral in more silicic samples. Acicular and rosetta pyroxenes up to 7 cm long (figure 3.11) occur locally within 2-5 meters of contacts between granophyre and Hvalnesfjall gabbro. Accessory phases include apatite, zircon and monazite. Pegmatites and aplites are extremely rare, but most granophyres contain abundant miarolitic cavities with euhedral quartz and albite (cleavelandite). Although

Figure 3.10 View of Hvasshjalli, looking north. The sequence of rock units is that drawn on cross-section B-B' (figure 3.3). From sea level these are: 1) net veined complex, 2) pegmatoidal gabbro, 3) layered gabbro, 4) granophyre, and 5) Hvasshjalli tholeiitic sill. Tertiary volcanic country rock (6) is visible in the background.



Table 3.4 Representative Amphibole Analyses

	g-43	g-65
SiO ₂	45.53	44.10
TiO ₂	1.74	1.91
Al ₂ O ₃	5.89	7.07
FeO	21.04	21.02
MnO	0.48	0.38
MgO	10.17	9.55
CaO	9.68	10.20
Na ₂ O	2.39	2.15
K ₂ O	0.73	0.91
Cr ₂ O ₃	0.05	0.00
total	97.70	97.29
Wo	24.1	25.6
En	35.2	33.3
Fs	40.8	41.1

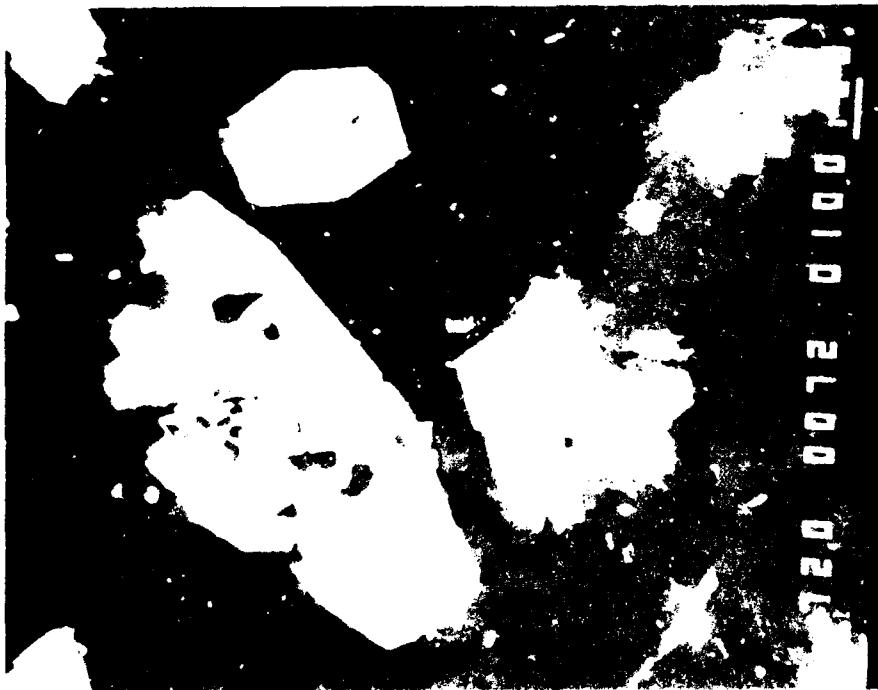
Cations on the basis of 23 oxygens

Si	6.961	6.793
Ti	0.200	0.221
Al	1.061	1.284
Fe	2.689	2.708
Mn	0.062	0.050
Mg	2.317	2.192
Ca	1.586	1.684
Na	0.707	0.642
K	0.142	0.178
Cr	0.006	0.000
sum	15.631	15.752

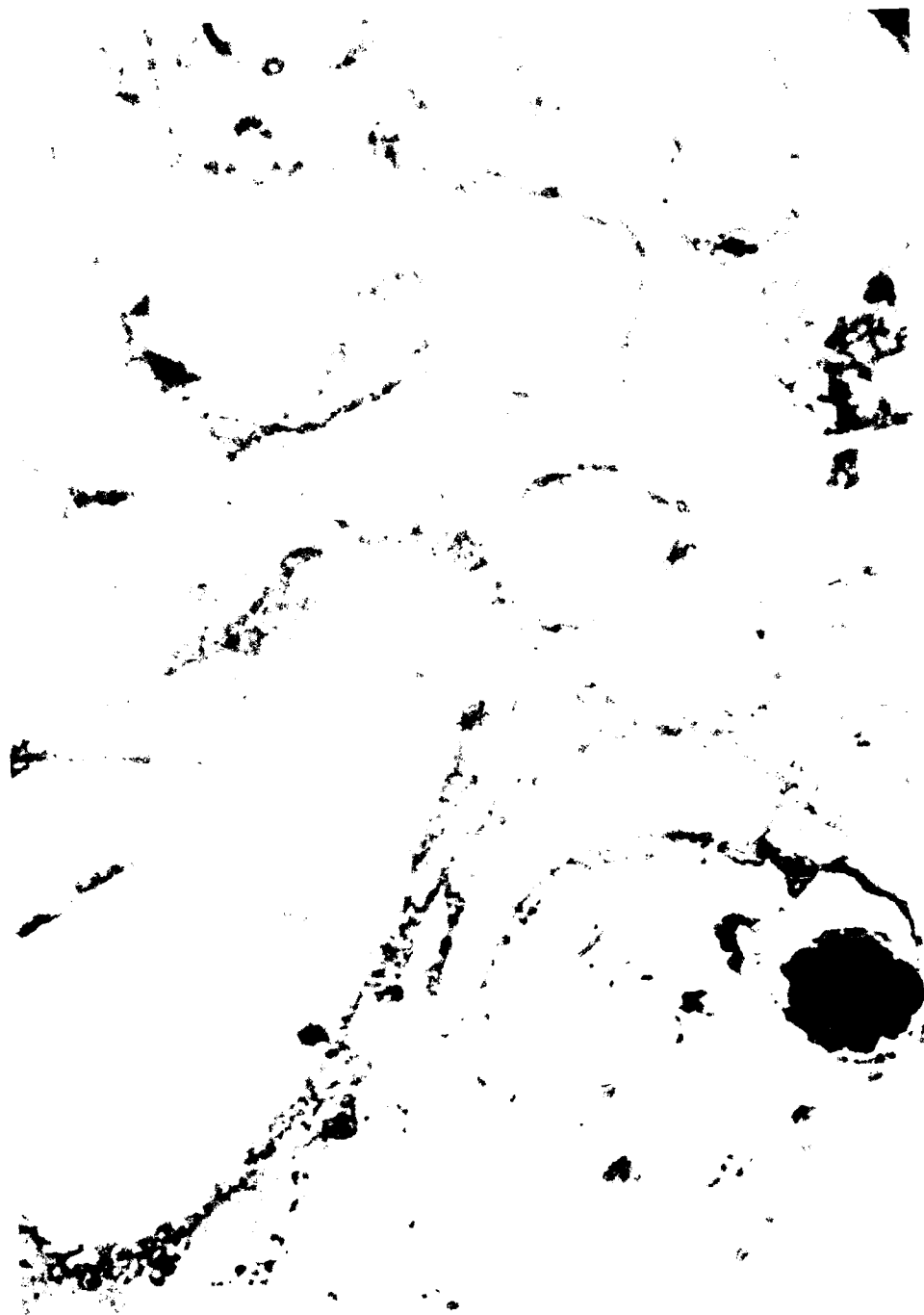
Figure 3.11 Petrographic features of Austurhorn felsic rocks. (a) Rosetta clinopyroxene intergrown with plagioclase in sample g-23 (scale bar in lower left is 1 mm). (b) Euhedral amphiboles (after clinopyroxene?) in granodiorite g-65 (scale bar is 1 mm). (c) Partial melt texture in glassy rhyolite f-61 showing resorbed quartz (clear) and feldspar (cloudy).



A



B



the granophyre has undergone significant hydrothermal alteration, marked by the presence of haematite, calcite, epidote and zoisite, analyses consistently indicate less than 1 wt% H₂O (usually <0.2 wt%).

With few exceptions, Austurhorn granophyres contain numerous small (1-10 mm) inclusions of fine grained mafic material. These tiny mafic inclusions have several distinct textural populations which aid in distinguishing felsic units in the field. The most abundant inclusions (typically 2-7 vol%) are composed of finely crystalline (<0.1 mm) equigranular plagioclase + oxides + chlorite (after clinopyroxene). Comparable volumes of glassy or holocrystalline mafic inclusions have been found in most Icelandic rhyolites and granites. Well-studied examples include the Skessa tuff (Walker, 1963), Thorsmork ignimbrite (Jorgensen, 1980) and some Torfajokull rhyolites (Gunnarsson, 1988; McGarvie, 1984).

3.2.4 Felsic Dikes and Sills

The Krossanesfjall felsite (~73 wt% SiO₂) forms the highest exposures in the eastern half of the Austurhorn intrusion. It contains ~5 vol% plagioclase crystals with sparse plagioclase + clinopyroxene glomerocrysts up to 3 mm long (figure 3.11). The felsite bears numerous angular clasts of hornfelsed basic volcanics, suggesting that it represents a near- or in-vent deposit. Thin veins of felsite (1-7 cm) cut the adjacent granophyre and typically have aphanitic margins. This unit was previously interpreted by Blake (1970) as a phase of acid activity associated with the Alftafjordur central volcano, whose lavas predate Austurhorn by several million years; the cross-cutting relationships documented here are inconsistent with this interpretation.

Three populations of felsic dikes are found at Austurhorn. The most abundant dikes are equigranular (<0.5 mm) and can be traced laterally or downward to the composite granophyre. A second group similar to the Krossanesfjall felsite is found sporadically throughout the complex and cannot be traced to larger granitic bodies. The

third population is variably porphyritic (5-20 vol% phenocrysts, 2-5 mm), typically within a microcrystalline groundmass at lower elevations and a glassy matrix at higher elevations. Felsic dikes average 5-15 cm thick, although those derived from larger felsic units widen significantly towards their source. One glassy rhyolite (sample f-61) shows textural evidence for partial melting (figure 3.11). Phenocryst phases in this sample include quartz, anorthoclase, sodic plagioclase and FeTiMn oxides, suggesting the melt was derived locally or from a comparably evolved substrate. The geochemistry and significance of this sample are discussed in chapter 4.

3.2.5 Basaltic Dikes and Sills

The regional dike density in southeastern Iceland is approximately 10% (H. Torfason, unpub. data), but is higher near central volcanoes like Austurhorn. Dikes within and immediately adjacent to the Austurhorn complex show no preferred structural orientation (figure 3.12) except on Hvalnes peninsula where the latest brittle phase has a general northeast strike and southeast dip (figure 3.12). Away from the Austurhorn intrusion, dikes in the Alftafjörður region strike to the northeast (Blake, 1970). Many Austurhorn dikes are comagmatic with their gabbroic or felsic hosts; others clearly postdate these two major intrusive episodes.

Austurhorn mafic liquids are generally evolved: all contain <7.8 wt% MgO (figure 3.13). Mafic dikes range from 10-200 cm thick and are highly porphyritic (10-25 vol% phenocrysts) or uniformly microcrystalline (<5 vol% phenocrysts). Porphyritic dikes contain compositionally heterogeneous (table 3.1) blocky plagioclase and, occasionally, clinopyroxene (<15 mm); crystals tend to be concentrated in the center of dikes >100 cm thick but are distributed evenly throughout smaller dikes. In sparsely phytic dikes, plagioclase + clinopyroxene glomerocrysts (<2 mm) or groundmass plagioclase laths (<0.5 mm) often define a weak flow texture. Groundmass plagioclase, clinopyroxene and FeTi oxides are generally equigranular, and fresh or devitrified glass

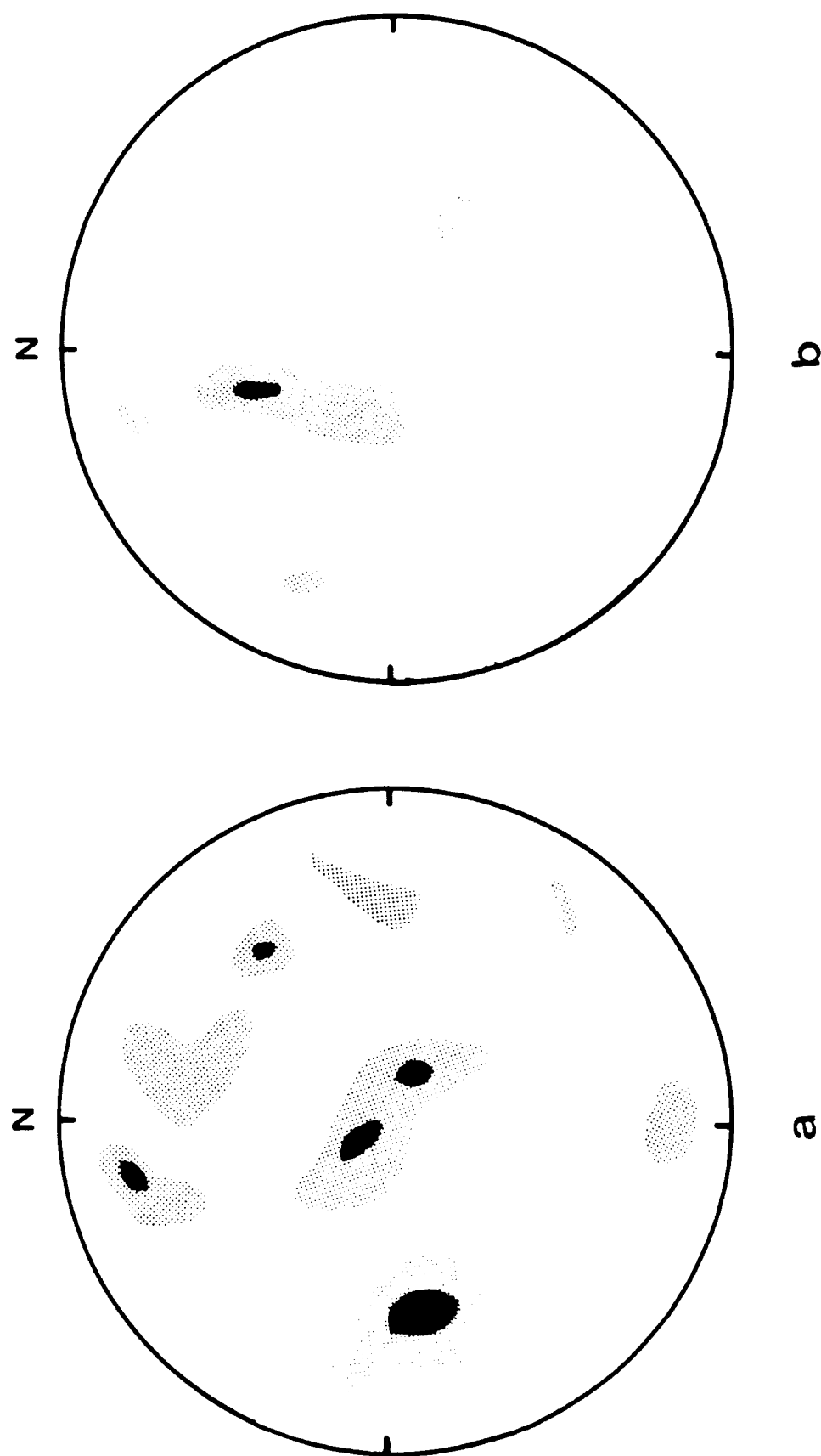


Figure 3.12 Poles to dike orientations from throughout the Austurhorn complex (figure 3.12a) have no preferred orientation (71 dikes measured), whereas those from Hvalnes peninsula (figure 3.12b) have a general NE trend (15 dikes measured; statistically insignificant but optically apparent). The Hvalnes dikes represent the final stage of intrusive activity in this area, as they crosscut granohpyre in a brittle fashion. Their trend is parallel to the current spreading axes as well as to spreading axes inferred for the late Tertiary. Both figures are southern hemisphere projections.

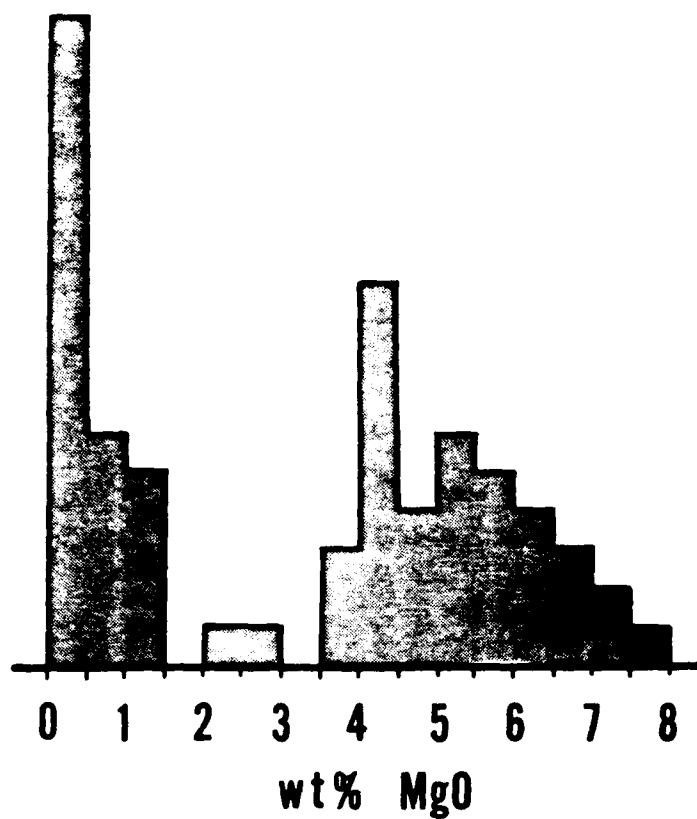


Figure 3.13 Histogram indicating bimodal distribution of liquid compositions from Austurhorn based on bulk rock analyses of basaltic dikes and pillows, granophyres and felsic dikes (see chapter 4).

is never observed. Olivine phenocrysts (~5 vol%, 1 mm) were found in only one dike (sample d-1; see Appendix I).

Composite and multiply-intruded dikes are common both within and outside the Austurhorn complex. Xenoliths are generally absent, but one dike on Vikurfjall contains over 30 vol% gabbroic fragments which span the lithologic range of Hvalnesfjall gabbro. Amygdaloidal basalt dikes occur near Olleshofn. Many dikes are hornfelsed and/or hydrothermally altered; they are typically rust stained and finely fractured and contain sulphides along joint faces and fractures.

Mafic sills over 10 m thick occupy the highest structural level of the intrusion in two locations - Hvasshjalli and SE Vikurfjall (figures 3.2, 3.9). Both sills intrude Tertiary volcanics and are not extensively altered, indicating their association with the Austurhorn complex. The Hvasshjalli sill is intruded by granophyre and is thus loosely contemporaneous with Hvalnesfjall gabbro (which also predates granophyre). It represents the most primitive liquid of the Austurhorn system (figure 3.13). Extreme enrichment in iron and incompatible elements (19 wt% FeO*, 1.6 wt% P₂O₅) is found in a dike which crosscuts this body. The Vikurfjall sill is also enriched in iron and titanium relative to more primitive Austurhorn basalts. The relative intrusive age of the Vikurfjall sill could not be determined from field relations. Basalt and diabase sills 20-30 cm wide occur between and within modally layered units of Hvalnesfjall gabbro. The diabase sills are finer grained than host gabbro but have locally indistinct margins, suggesting a low thermal contrast at the time of emplacement.

3.2.6 The Net Veined Complex

This composite unit occupies the lowest structural levels exposed from Hvalnes north to Hlaupgeirabotn, where it intrudes Tertiary volcanics (figures 3.2, 3.4). The best exposures are restricted to coastal areas but some characteristic features may also be observed above Krossaneslaekur and along Tofuhorn (figure 3.2). The term "net veined"

has been applied to contemporaneous mafic-felsic intrusive complexes throughout the Brito-Arctic Tertiary province, and is intended as a descriptive term devoid of implications for intrusive mechanism.

Several distinctive rock types comprise the NVC. These are: granite, diabase, basalt and irregular intermediate hybrids. The overall appearance of the complex is that of a large composite granite which contains clasts, pillows and tabular masses of diabasic and basaltic rock. Felsic magmas of the net veined complex are locally continuous with the Hvasshjalli granophyre. I define the margins of the NVC to be where a felsic host rock bearing mafic blocks >5 cm in dimension is in contact with Hvalnesfjall gabbro or Tertiary volcanics, or where the mafic blocks disappear abruptly without apparent change in the felsic matrix itself.

i. Felsic rocks of the Net Veined Complex

Excellent coastal exposures enable detailed description of the Austurhorn NVC felsic magmas and their style of emplacement. Within the coastal complex, intrusive contacts separate sixteen individual felsic units, commonly sills of up to 500 m lateral exposure (figure 3.4). Timing of relative emplacement is usually clearly indicated by brittle or ductile deformation. Contacts are sharp although 2-15 cm wide zones of fluidal interaction are common. One exception is the M-N contact NE of Hvalnes which is gradational over ~80 meters (figure 3.4).

The units have similar mineralogy but can be distinguished in the field because textural differences between units are markedly greater than internal heterogeneities (table 3.5; Appendix I). Each felsic unit contains 5-25 vol% tabular or blocky plagioclase (2-4 mm) in a subhedral matrix (<1.2 mm) of plagioclase, quartz and K-feldspar. The large plagioclase crystals may be more albitic (g-65) or anorthitic (g-42) than matrix phases, and all are concentrically zoned (table 3.1). FeTi oxides (1-3 vol%) are ubiquitous, and amphibole, clinopyroxene and/or olivine are variably abundant (up

to 10 vol%). Zircon, apatite and monazite are found in trace amounts; alteration minerals include calcite, epidote, zoisite, biotite and haematite. Granophyric texture is often well-developed adjacent to mafic pillows but is otherwise lacking from the coastal complex. I retain the term "granophyre" for these units to emphasize the physical and geochemical continuity between the NVC and the rest of the Austurhorn complex.

Four felsic rock types are identified on the bases of grain size, color index and relative abundance and size distribution of angular mafic clasts (table 3.5). Clast-free granophyre (type 1; units A, F, K, L, O in figure 3.4) occurs only in small pockets. It is distinguished by $CI < 5$ and contains abundant quartz-bearing vugs. Type 2 clast-bearing granophyres (units B, H, N, P in figure 3.4) contain up to 40 vol% angular to subrounded mafic clasts (5–50 cm) within a felsic matrix which itself consists of 7–10% fine-grained mafic clasts (figure 3.14). Individual outcrops display crude internal stratification between two textural types, one dominated by 2–4 mm tabular plagioclase and the other nearly equigranular (1 mm). Type 3 granophyres (units D, E, I, J, M, Q in figure 3.4) are heterogeneous on all scales. They are mottled and streaky, with rounded clasts that have reacted with the host material. The fourth felsic rock type (units C, G in figure 3.4) is fine-grained granodiorite. These units contain up to 10 vol% euhedral or acicular hornblende, often cored by clinopyroxene. They are locally weakly foliated and lack clasts. Granodiorites crosscut, and are often chilled against, clast-bearing granites.

In the northern NVC the emplacement sequence is grossly linked to lithology, with clast-free granophyres (type 1) and granodiorites (type 4) intruding clast-bearing units. Between Hvalnes and Olleshofn in the southern NVC clast-free units are subordinate in volume and the final intrusive unit (Q) is the most heterogeneous of the Austurhorn complex.

ii. Mafic rocks of the Net Veined Complex

Table 3.5 Felsic Units of the Austurhorn Net Veined Complex

TYPE	MAP UNITS	CLASTS OVER 5 mm		MATRIX CLASTS---		OVERALL	SIO ₂
		VOL%	SIZE*	SHAPE DISTRIBUTION	VOL% DISTRIBUTION	APPEARANCE	
1	A,F,K,L,O	-	-	-	<1	homogeneous	>72 wt%
2	B,H,N,P	10-40	5-50	angular heterogeneous	7-10	homogeneous	variable
3	D,E,I,J,M,Q	10-50	5-50	rounded heterogeneous	>20	heterogeneous	variable
4	C,G	-	-	-	-	homogeneous	<66 wt%

* average dimension, in centimeters

INTRUSIVE SEQUENCE (OLDEST --> YOUNGEST)

NORTHERN NVC (gabbro) -> I -> H -> E -> G
-> B -> A, C, D, F

SOUTHERN NVC (gabbro) -> P -> O (?) N -> M -> Q
J -> K

Figure 3.14 Photograph of a type 2 granophyre showing small, randomly oriented clasts. Note the textural and size variations among clasts.



Mafic bodies in the coastal complex have four distinct morphologies: 1) pillows, 2) dikes, 3) angular clasts and 4) tabular bodies. The examples below highlight differences between morphologic types which may be found together in a single outcrop.

a) Pillows and Dikes

Pillows of mafic magma within granite have been documented clearly at Austurhorn and other localities (Wager & Bailey, 1953; Blake et al., 1965; Blake, 1966; Mattson et al., 1986). They form when small amounts of hot, low viscosity basic magma solidify rapidly after intruding larger bodies of cooler felsic magma (Wager & Bailey, 1953; Blake et al., 1965). Austurhorn pillows are lobate bodies, usually <1 meter in dimension with sharp crenulate contacts concave towards the mafic member (figure 3.15). Pillow margins are aphanitic, while interiors contain 1-2 mm crystals. Plagioclase crystals with swallowtail morphology occur 0.5-2.0 cm from pillow margins (figure 3.16), and are irregularly mantled by highly sodic compositions. Stubby (<1 mm) sector-zoned augite is generally fresh and occurs in subophitic intergrowths with plagioclase toward pillow centers. Representative analyses of plagioclase and clinopyroxene phenocrysts are found in tables 3.1 and 3.2. Acicular oxide phases in pillow margins have grown radially away from augite and quench plagioclase; titanomagnetite phenocrysts occur in pillow interiors (figure 3.16). Sparse olivine phenocrysts are typically altered to serpentine + magnetite. Hydrothermal alteration is often extreme along pillow margins (<1 cm) but does not penetrate to the interior. Granophyric intergrowths and euhedral honey-colored amphiboles are commonly found in granite immediately adjacent to mafic pillows.

Coherent mafic dikes are rare in the NVC. They commonly change along strike from planar-sided to elongate "blobs" and finally to smaller lobate pillows. Where such dikes intrude clast-laden granophyre they do not crosscut angular fragments but weave irregularly between them to retain an approximate strike direction. That is, the dikes

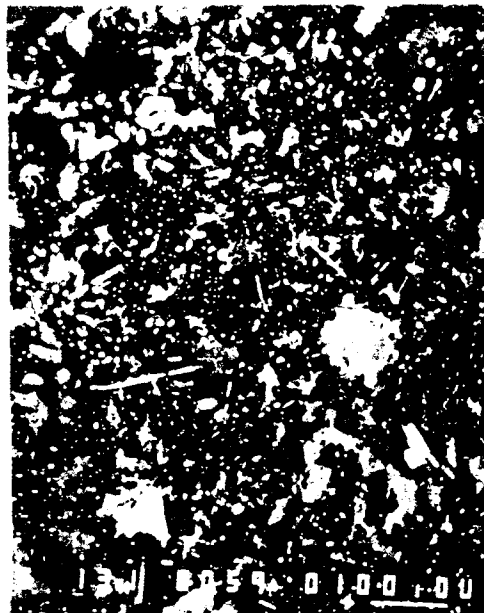
Figure 3.15 Photograph of a mafic pillow from the coastal net veined complex.



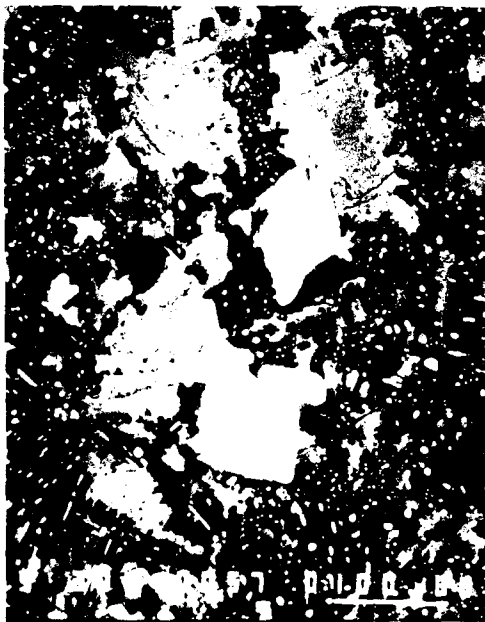
Figure 3.16 Petrographic features of mafic pillows, as revealed in backscattered electron images. (a) Plagioclase with quench morphology near pillow margin indicates rapid cooling (sample p-65, 300x). (b) Acicular oxides appear as bright lines in the groundmass of sample p-66 (130x). (c) FeTi oxides also occur as phenocrysts in some mafic pillows (sample p-66, 130x). (d) This plagioclase with swallowtail morphology (sample p-67) has acicular FeTi oxides growing radially away from the crystal surface.



A



B



C



D

postdate entrainment of angular fragments. These dikes often cut across granophyre-granophyre contacts.

The Austurhorn mafic pillows are transitional tholeiitic (mildly alkalic; see chapter 4), and contain calcic augites similar to those observed in the alkaline Kiglapait intrusion (figure 3.6; Morse, 1969, 1980) and undersaturated volcanic series (Carmichael et al., 1974). In contrast, some Austurhorn dikes are tholeiitic, as evidenced by their clinopyroxene compositions (figure 3.6). The petrogenetic evolution of these suites is discussed in chapter 4.

b) Angular Fragments

Angular to subrounded mafic clasts range from <10 cm to >1 m, with a median size of 10-35 cm (figure 3.17). Some clasts have sharp, angular contacts with the felsic host, while others have one or more diffuse margin suggesting prolonged physical and chemical interaction. Most are basaltic to diabasic (<3 mm), although gabbroic blocks are abundant in some type 2 granites and on Hvalnes peninsula. The clasts typically contain plagioclase and clinopyroxene, variably altered to sericite, epidote, amphibole and FeTi oxides. In contrast to dikes and pillows, clasts show no indication of having chilled against surrounding granophyre. They do not contain swallowtail plagioclase, and granophyric intergrowths and euhedral hornblende are never observed in adjacent host material.

It is important to note that these fragments are not derived from the Tertiary volcanics which host the Austurhorn intrusive complex. Clast lithologies do not include pyroclastic breccias, zeolitized basalts or silicic compositions, all of which are abundant in the country rock (Blake, 1970). Diagnostic alteration minerals of the Austurhorn aureole (e.g., platy calcite, garnet, prehnite) have not been observed in the mafic fragments. I interpret the clasts as fragments of hypabyssal basaltic magmas associated with the Austurhorn system itself. Basalt and diabase readily undergo thermal fracture

Figure 3.17 Photograph of clasts in granophyre. In contrast to the pillows, they are diabasic and show no change in grain size adjacent to contacts with the granophyre.



if intruded by felsic magma (Marsh, 1982); alternatively, mafic pillows can fracture if their host continues to flow after the mafic magma is below its solidus. The field evidence indicates both of these physical situations existed at Austurhorn.

c) Tabular Bodies and "Mega-Pillows"

Mafic bodies 1-10 meters in dimension are abundant in two associations with felsic magma. In the first, mafic units resemble pillows up to 10 m (horizontal) by 1 m (diameter). Up to 30 cm of granophyre (often clast-bearing) surrounds each mafic body with contacts that are always sharp and often crenulate or cusped. The texture of the mafic material changes from aphanitic (with occasional swallowtail plagioclase) at the borders to subophitic cumulus (2-4 mm) in the interiors.

The second association appears as large outcrops of diabase cut by parallel felsic veins. The regular spacing and planarity of the felsic veins is striking (figure 3.18). Spacing of both horizontal and high-angle veins is consistent within an area, but differs from place to place within the intrusion. Two sets of typical vein spacings are: (1) 150-200 cm (high-angle) and 60-80 cm (horizontal) and (2) 8-10 m (high-angle) and 170-200 cm (horizontal). Horizontal vein spacing is always less than that of the near-vertical veins. Vein surfaces are asymmetric: lower margins are sharp whereas upper contacts are locally wispy and indistinct. Crenulations on the lower surfaces are commonly lined by tabular plagioclase and hornblende (after clinopyroxene) which project into the felsic material, resembling the gabbroic pegmatoids at a much smaller scale. In contrast, upper margins of veins are often indistinct: felsic magma appears to have penetrated *as a fluid* into overlying mafic material. On horizontal felsic veins the migration direction is uniformly upwards, while on high-angle veins it shows minor variation (figure 3.18). The upward projections have a constant spacing periodicity in each area.

3.2.7 Intermediate, Hybrid and Commingled Rocks

Figure 3.18 Photo of felsic veins in outcrop, showing upwards wispy protrusions of felsic material (light shape in center of photo). A planar felsic vein is also visible approximately 50 cm above the wispy vein. Hammer in lower part of photo for scale.



Homogeneous intermediate rocks are not found at Austurhorn. No dikes have been sampled which contain 54-63% SiO_2 , and plutonic rocks in this compositional range are always grossly heterogeneous. In this and subsequent discussion, I adopt the terminology of Sparks & Marshall (1986) regarding the physical mixing of magmas. Mixed magmas which are macroscopically homogeneous are termed hybrids. In this case the bulk liquid is uniform although disequilibrium phenocrysts from each endmember may be found. Where macroscopic heterogeneities are preserved, the term commingled is applied. The distinction between hybridization and commingling is often one of scale. Hybridization is observed locally along the margins of individual clasts in felsic magmas, and commingling on outcrop scale where the progressive dissolution of mafic clasts is recorded. The resultant mixtures (type 3 granites) lack angular clasts and are of irregular, blotchy and streaky appearance. They are further generally characterized by tabular (2 mm) plagioclase readily distinguishable within a patchy dark matrix. Most Austurhorn granophyres show evidence of commingling. Within the NVC, intermediate magmas are clearly the result of mechanical interaction between magmas. Mixing calculations (Mattson et al., 1986) indicate that local areas of intermediate composition (52-63 wt% SiO_2) between disrupted mafic clasts and granitic host may represent physical mixtures of the observed starting materials. Complete homogenization is observed on a scale of up to tens of centimeters in such cases.

3.3 Evolution of the Austurhorn Magmatic System

3.3.1 Summary of Intrusive Activity

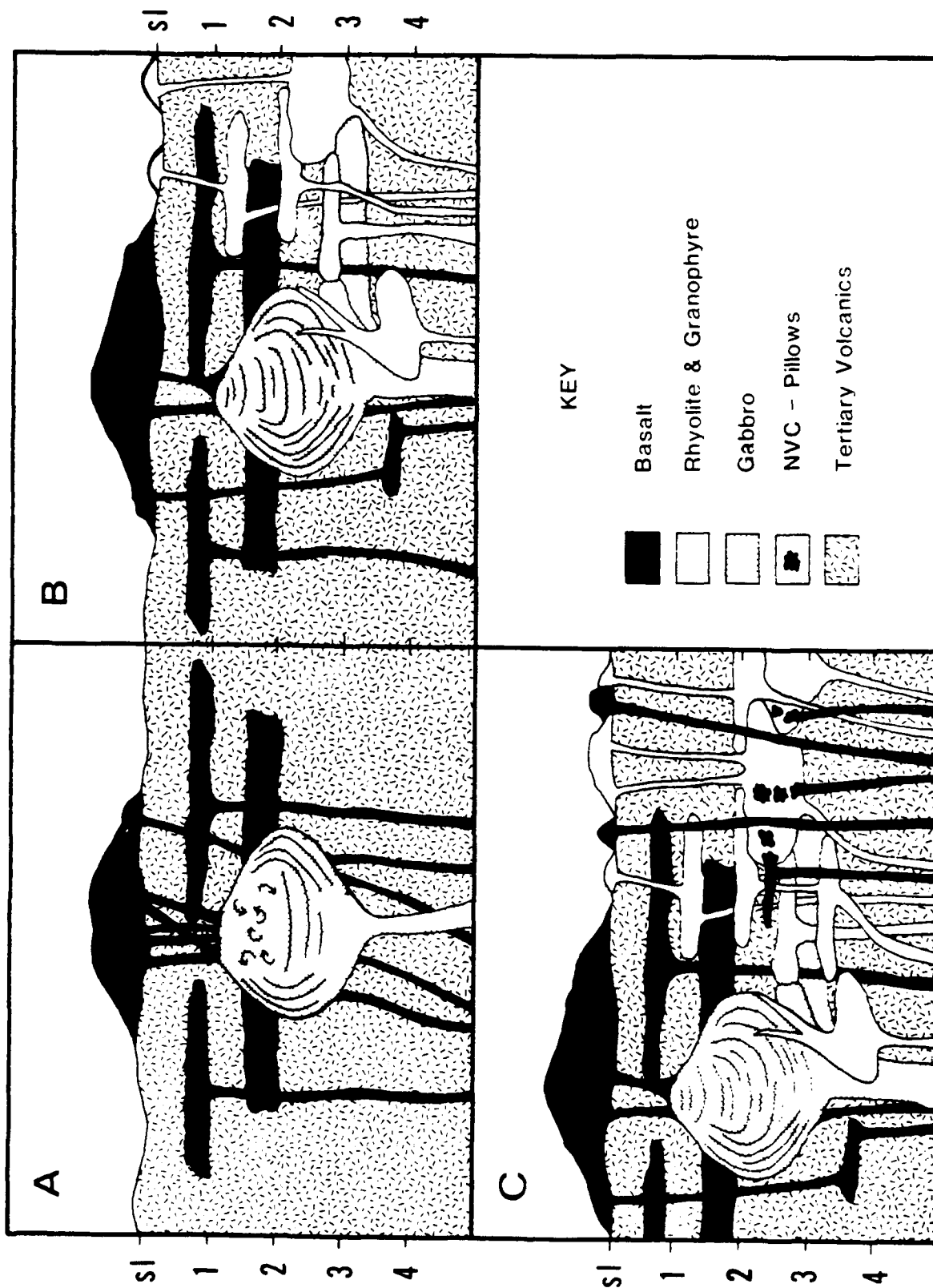
There is no direct evidence of volcanism at Austurhorn, presumably because overlying lavas were eroded by glaciation. However, the following geologic considerations suggest Austurhorn was an active volcano in latest Tertiary time:

1. Abundant vertical dikes within the complex indicate upward transport of magma.
2. Icelandic rhyolites are invariably associated with central volcanoes (Walker, 1974; Jakobsson, 1972, 1979).
3. The high-temperature geothermal activity recorded by the Austurhorn aureole ($T > 350^{\circ}\text{C}$) is today found only in areas of active volcanism (H. Torfason, pers. commun., 1982; Fridleifsson, 1983).
4. Current volcanism at Krafla emanates from a magma volume at 3-7 km depth (Einarsson, 1978; Tryggvasson, 1986), comparable to the emplacement depth inferred at Austurhorn (> 2 km; Blake, 1966).

Evolution of the magma chamber involved two distinct stages (figure 3.19). Initial basaltic activity was concentrated in the SW portion of the intrusion. The bowl-shaped modally layered Hvalnesfjall gabbro reflects a small stable magma chamber which formed during this earliest phase of sustained magmatism. Rhythmic layering on NE Hvalnesfjall suggests the chamber grew through repeated injection of mafic magma. Additional evidence for this interpretation comes from co-magmatic mafic dikes and sills throughout the gabbro body. The bowl-shaped layering indicates simultaneous crystallization along horizontal and vertical surfaces.

A second stage of development is indicated by the multiple granophyres and the net veined complex. Field relations indicate that before the gabbro solidified completely it was invaded from below by several pulses of granophyre (64-73% SiO_2) which stopped through the S and NE gabbro margins. Although the multiply-injected nature of the granophyre makes it difficult to constrain the exact timing of emplacement, this unit clearly postdates the gabbro, consistently filling fractures and joints within it. On the northwestern and northeastern faces of Hvalnesfjall there is evidence for contemporaneous magmatism: a zone of irregularly hybridized material extends tens of meters along the contact between the two units. The resultant hybrid contact trend is at

Figure 3.19 Evolution of the Austurhorn magma system. All views are from the SE portion of the intrusive complex, looking towards the northwest. (A) The Stage I magma chamber grew through repeated diking, as a central conduit stabilized. A polygenetic volcanic edifice at the surface was linked to a stable replenished chamber of fractionating basalt in the shallow crust. Cumulate layering is shown schematically by solid lines; the convecting liquid in the top of the chamber was likely stably stratified from ferrobalt to dacite or rhyolite (Sigurdsson & Sparks, 1981). (B) As fresh basalt replenishment decreased and the thickness of cumulates within the chamber grew, fresh basalt magma ponded in the crust at the base of the chamber. These "failed replenishments" cooled slowly in the warm crust, forming the pegmatoidal gabbro. (C) The Stage II system, as magmatism migrated away from the original conduit. New replenishments to this crustal level were predominantly silicic, and ascended through the warm crust rather than the gabbro body. Silicic bodies were typically sill-like. The late stage NE-trending mafic dike swarm both cross-cut silicic units and formed comagmatic pillows within them.



an angle to that of modal layering in the gabbro. This magmatic period was further characterized by episodic influx of diverse liquids through several conduits (figure 3.19). The net-veined complex preserves the abundance and diversity of resulting co-magmatic interactions. Mafic pillows in the NVC represent the final phase of igneous activity at Austurhorn (figure 3.19). They originated from a NE-trending dike swarm which entered the system before the granophyre was completely solidified.

The inferred chamber development is consistent with volcanic evidence suggesting that a period of basaltic fissure eruption preceeds development of an evolved central volcano (Walker, 1963; 1974). One important implication of the field data is that the shallow Austurhorn edifice was not a closed magmatic system. This chamber received input from both mafic and felsic magmas throughout and perhaps beyond its active eruptive history. These replenishments must have come from magma bodies located at deeper crustal levels. That these chambers may communicate with one another is indicated by the high degree of magma mixing observed, in particular the abundant mafic clots in granophyre. The "cedar tree" structure inferred for the shallow crust by Walker (1963) thus probably extends to significant depth beneath an active magma chamber as well (figure 3.20). In the following discussion I use field and mineralogic data from the gabbro, basalts and granophyres to elucidate geochemical and physical aspects of the basalt-to-rhyolite transition in an evolving central volcano.

3.3.2 Stage 1: Basaltic Differentiation in the Shallow Crust

The association of coeval transitional tholeiitic liquids and cumulates at Austurhorn can be used to constrain models of shallow crustal magmatism. Compositions of plagioclase and clinopyroxene in Hvalnesfjall gabbro are analogous to those found in Austurhorn pillow basalts (figure 3.6), suggesting the cumulates and liquids record analogous fractionation processes. Plagioclase and clinopyroxene compositions co-vary

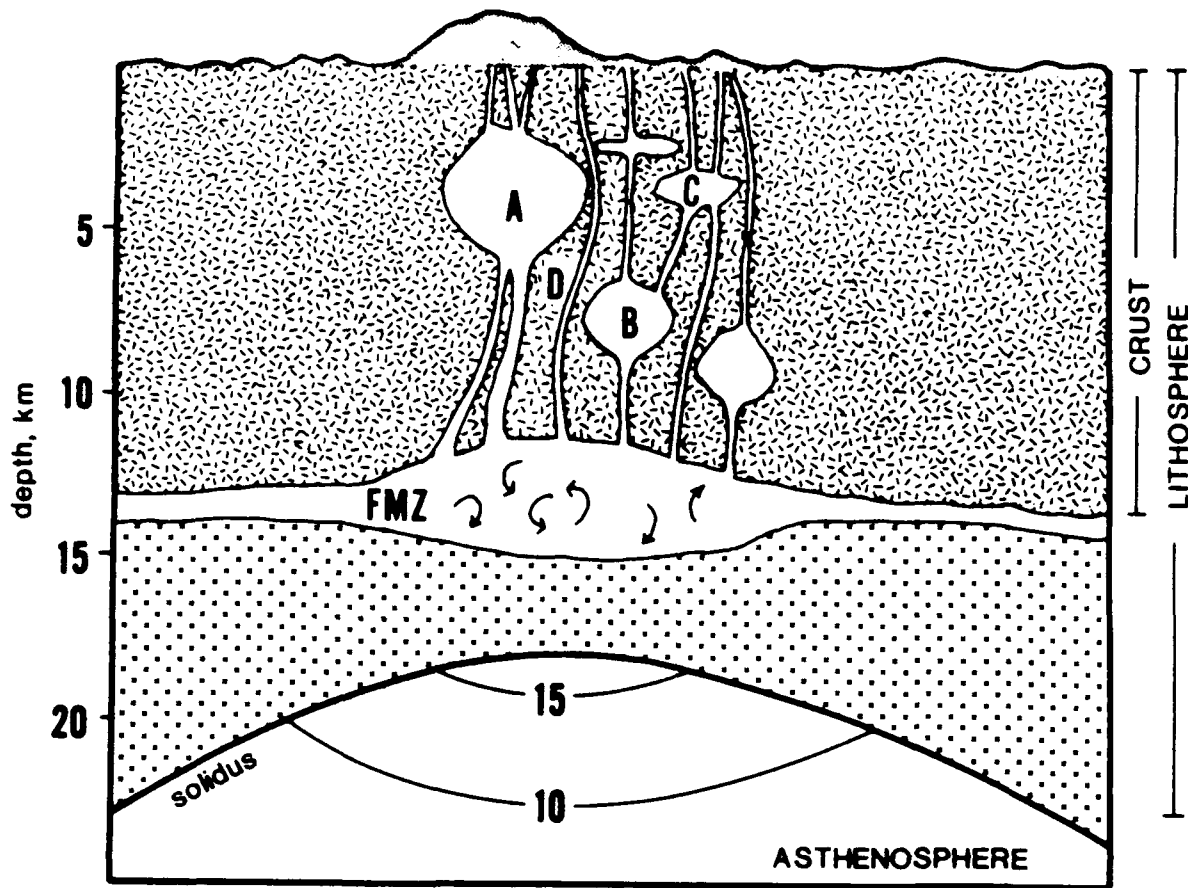


Figure 3.20 Proposed crustal structure beneath Austurhorn, and by analogy beneath modern immature rift zones as well. Mantle derived melts pond at the base of the crust rather than ascending directly to the surface. The resulting molten zone extends beneath the entire rift axis but is of variable thickness and melt composition depending on the local depth and degree of melting, here represented by 10 and 15% melt isopleths in the upwelling asthenosphere. In regions of low magma supply and high cooling rates, liquid compositions are controlled by fractionation and mixing in this subcrustal zone (FMZ). Erupted liquids are unlikely to include primary mantle melts, which cannot penetrate the melt layer effectively. Pathways to the surface usually involve further modification in shallow crustal chambers at various depths (A, B, C) although dikes may tap the FMZ directly (D). The Stage 1 chamber at Austurhorn is represented by chamber A, with Stage 2 silicic differentiates generated in magma pockets such as B and C.

systematically from $An_{85}, Mg\#78 (Wo_{42}En_{46}Fs_{12})$ to $An_{39}, Mg\#51 (Wo_{41}En_{29}Fs_{30})$ and define an apparent differentiation sequence (figure 3.21).

The Austurhorn suite is noteworthy in that magnetite forms about 10% of the fractionating assemblage in mafic liquids with up to ~7 wt% MgO (see chapter 4). As a result, successive differentiated liquids vary dramatically in both silica content and density; that is, FeTi oxide removal enriches the liquid in silica while forming dense Fe-rich cumulates. It is reasonable to expect that the relative densities of cumulates and liquids will influence magma chamber evolution in this iron-rich system. Unlike MORB suites which fractionate through a density minimum at ~9 wt% MgO (Sparks et al., 1980), the Austurhorn pillow liquids evolved with continually decreasing density. In addition, all mafic pillow liquids are less dense than their associated calculated cumulates (figure 3.22), and progressive differentiation of parental basalt results in stably stratified cumulates and liquids.

To first order, the proposed Stage 1 chamber represented by Hvalnesfjall gabbro is analogous to that inferred by Sigurdsson & Sparks (1981) beneath Askja prior to the 1875 caldera-forming eruption (figure 3.19a). In their model, dense ferrobasaltic melt occupies the lower portion of a shallow magma chamber, overlain by icelandite and compositionally zoned silicic liquids in stable density stratification. Sidewall crystallization is also probably important in the Stage 1 chamber, as it is physically unlikely that vertical layering forms strictly through basal crystallization. The thick rhythmically layered sequence on Hvalnesfjall may indicate episodic chamber replenishment. Huppert et al (1982) and Sparks et al (1984) demonstrated that repeated influx of relatively hot, light fluid at the base of a high-density cumulate pile could produce cumulates with cyclic layering. Rapid replenishment is accompanied by turbulence and convective mixing of the new fluid with liquids above the cumulate pile; slower magma influx may involve essentially laminar percolation of the more primitive fluid through a crystal network. At Austurhorn, fresh mafic pillow magma would be

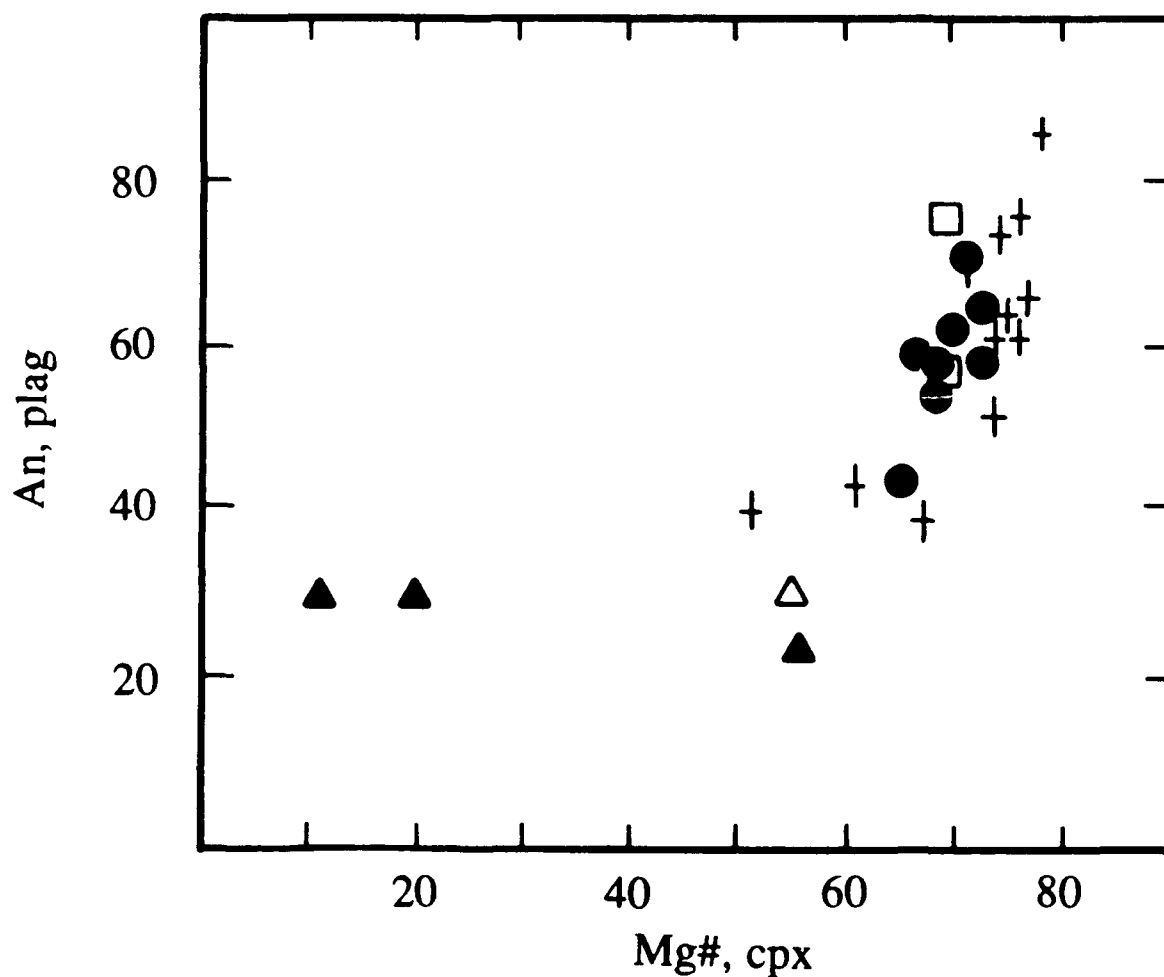


Figure 3.21 Co-variations in plagioclase and clinopyroxene compositions from Austurhorn define a consistent differentiation trend. Key to symbols: **filled circles** =mafic pillows, **plus signs** = Hvalnesfjall gabbro, **open square** = mafic dike, **open triangle** = felsic dike, **solid triangles** = granophyres.

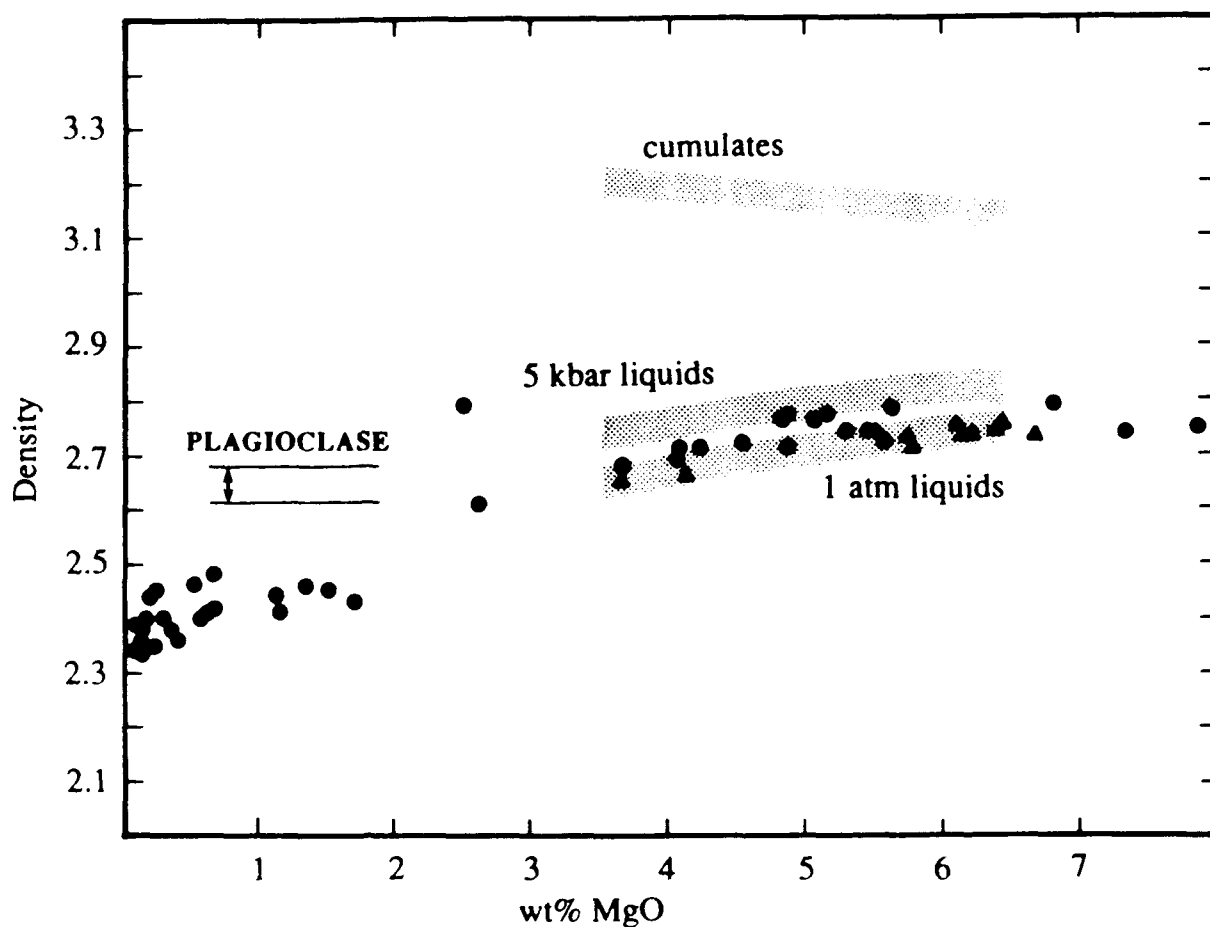


Figure 3.22 Early precipitation of FeTi oxides causes the density of Austurhorn liquids to decrease with progressive differentiation, ensuring that evolved liquids are lighter than primitive compositions, and all liquids are lighter than their associated cumulates. In this diagram, the data points represent liquid densities calculated using the methods of Bottinga & Weill (1972) and Luhr and Carmichael (1987) at 1 atm pressure (circles = dikes and granophyre bodies, triangles = pillows). The lone dense liquid at ~2.5 wt% MgO contains >19 wt% total Fe. Shaded liquid fields represent model compositions used to evaluate fractional crystallization of the Austurhorn suite, calculated using the method of Luhr & Carmichael at 1 atm and 5 kbars. Note that the plagioclase field reflects only density, not MgO content.

less dense than the oxide-rich cumulates and would pond above the growing crystal pile (figure 3.22).

3.3.3 Chamber Isolation: Transitional Stage

This stable configuration can break down if the cumulate pile becomes a barrier to magma influx. I believe this process is observed at Austurhorn and, as described below, marks an essential stage of magma chamber evolution. Basaltic replenishment is retarded if either (1) individual crystallizing units (i.e., crystals plus intercumulus liquid) are less dense than incoming mafic liquids or (2) crystallization of intercumulus material produces floor cumulates with negligible porosity which provide an effective barrier to magma and, consequently, heat (Campbell, 1978; McBirney & Noyes, 1979). Geologic evidence from the Hvalnesfjall gabbro indicates the latter transformation took place at Austurhorn. Because the Austurhorn pillow basalts differentiate with continually decreasing density (figure 3.7) the evolved intercumulus liquid should be able to percolate upwards through the growing cumulate pile. However, preliminary mass balance calculations based on incompatible element abundances indicate Hvalnesfjall gabbro is typically orthocumulate, with up to 50% trapped liquid (table 3.6). Campbell (1987) demonstrated that the distribution of intercumulus material within a cumulate body is controlled primarily by the local thermal regime, rather than compositional or rheological parameters of crystals and associated liquids. Specifically, orthocumulates represent regions of high thermal gradients (i.e., rapid cooling) whereas adcumulates require efficient removal of intercumulus material in a more insulated environment. The Hvalnesfjall gabbro is a small mafic body located in the shallow crust, where rapid cooling and solidification are expected, as evidenced by abundant orthocumulates.

When basaltic liquids are unable to ascend above the cumulate pile, the shallow crustal chamber is effectively isolated from fresh mafic input. Liquids within the chamber will cool and may differentiate rapidly to highly silicic compositions. Isolation

Table 3.6 Estimates of Intercumulus Liquid in Gabbro Samples

Gabbro	Calculated percent intercumulus liquid (p-61a) Estimates based on:				Calculated percent intercumulus liquid (p-41b) Estimates based on:			
	P2O5	Zr	La	best guess	P2O5	Zr	La	best guess
gb-23	48.3	46.6	49.9	45 - 50	18.2	16.2	20.3	~20
gb-24	51.7	65.2	71.5	~60	19.5	12.8	29.2	~20
gb-29	44.8	55.6	64.9	~50	16.9	19.4	26.4	~20
gb-30	6.9	19.1	16.7	10 - 15	2.6	6.6	6.8	<7
gb-31	44.8	39.9	51.5	~45	16.9	13.9	21.0	~15
gb-32	20.7	32.6	133	25 - 30	7.8	11.4	54.2	~10
gb-34	69.0	48.3	73.3	50 - 60	26.0	16.8	29.9	20 - 25
gb-41	317	163	231	*	119	56.7	94.3	*
gb-42	58.6	56.2	61.8	~60	22.1	19.6	25.2	~20
gb-83	307	95.5	42.2	*	116	33.3	17.2	*

Percentages of parental (p-61a) and evolved (p-41b) mafic pillow liquids present as intercumulus material are calculated by mass balance, assuming that all of the incompatible element (P, Zr or La) resides in the melt phase. That is,

$$INC_g = (INC_b)(X_b) + (INC_{cm})(X_{cm}),$$

where INC is the absolute abundance of an incompatible element in gabbro (g), basalt (b) or cumulus minerals (cm), X_i is the weight fraction of intercumulus basalt (X_b) or cumulate minerals (X_{cm} , assumed to equal zero). Bulk geochemical data from table 4.1. Estimates based on different elements do not always agree (e.g., gb-32) but the "best guess" value is likely to suffice for the present purpose. The selected basalts represent the range of mafic pillows at Austurhorn, but need not indicate the complete spectrum of liquids available during solidification of the gabbro. Leucocratic samples designated by asterisks have higher incompatible element abundances than the basalts and cannot be represented accurately by this scheme.

of the Stage I chamber is recorded in the Hvalnesfjall gabbro where thin sills between modally layered units suggest that replenishing liquids could not ascend through the cumulate pile by percolation, but rather caused fractures between competent cyclic units. The pegmatoidal gabbro further documents this new magmatic environment. I suggest the Austurhorn pegmatoidal pockets contain evolved intercumulus melt (derived from closed-system differentiation of basalt sills) which became concentrated when vertical percolation was not possible (figure 3.19). Macroscopically similar gabbroic pegmatites have been reported in the Skaergaard (McBirney & Noyes, 1979) and Duke Island (Irvine, 1974) layered complexes, where they have also been interpreted as local accumulations of intercumulus material. Several lines of evidence indicate the pegmatoidal material is derived from local fractionation rather than external contamination. The pockets are physically isolated from nearby granophyres and do not contain evolved xenocrysts. Most importantly, pegmatoidal gabbro was intruded by granophyre, resulting in brittle failure of the gabbro without formation of pegmatoidal structures along contacts. For comparison, highly differentiated veinlets observed in Kilauea Iki lava lake samples where felsic contaminants are unavailable are also interpreted as local segregations of evolved liquid (Helz, 1987).

3.3.4 Stage 2: Abundant Silicic Magmatism

The second phase of activity at Austurhorn is characterized by copious silicic magmatism and formation of a net veined complex (figure 3.19b). Whereas the Stage 1 chamber is characterized by localized influx of hot primitive fluids, Stage 2 involves emplacement of relatively cool, viscous felsic magmas into a laterally extensive warm mafic chamber. Experiments with aqueous solutions suggest that buoyant felsic magma will rise as a plume (turbulent or laminar, depending on the ascent velocity) until reaching its maximum stratigraphic height, determined by relative densities of the magmas involved (Sparks et al., 1980; Campbell et al., 1983). The fluid will not rise

beyond its stable height, but will spread out laterally to form a sill at that elevation. This model is compatible with observations from the Austurhorn NVC. The random orientation of most mafic clasts indicates they were suspended in a turbulent fluid. Less commonly, groups of clasts may be pieced back together in jig-saw puzzle fashion, suggesting local thermal fracture but no turbulent transport. The felsic units themselves always have subhorizontal surfaces, whether in contact with other granitoids, mafic magmas or Tertiary country rocks. This configuration is strongly suggestive of density-driven stratification. Some felsic magmas were at least slightly superheated, as evidenced by their low crystallinity and ability to form extremely narrow dikes (<20 cm). In contrast, most granophyres contain abundant 2-4 mm phenocrysts and do not appear to have ascended under superliquidus conditions.

The origin of the silicic magmas cannot be addressed through field relations alone (see chapter 4). However, field relations constrain the crustal structure beneath a stage 2 volcano regardless of how the silicic magma was derived. The structural model in figure 3.19 is consistent with two fundamental features of the Austurhorn granophyres. First, felsic magmas clearly intrude both NVC basalt and Hvalnesfjall gabbro from below, therefore they were not generated in the presently exposed shallow storage chamber. Evolved liquids associated with the Stage I chamber would presently be located above the current erosional surface. A second consideration is that no central conduit has been identified; each felsic body was emplaced independently of the others. Crystallization of numerous isolated pockets of basaltic magma at depth provides an explanation for the variety and exposures of felsic rocks at the surface (figure 3.19). Detailed trace element and oxygen-strontium isotope analysis of individual silicic flows from the Torfajokull area support this hypothesis. For example, Gunnarsson (1988) found that rhyolites erupted along adjacent fissures less than 1 km apart have distinct trace element and isotopic signatures. This observation suggests that each eruption site is fed by a separate magma body where fractionation, mixing and crustal melting may

occur in different proportions. These field and geochemical data are clearly not consistent with development of large homogeneous convecting silicic chambers in the shallow Icelandic crust.

3.3.5 Development of the Net Veined Complex

Marshall & Sparks (1984) recently proposed that the net veined complexes of St. Kilda and Ardnamurchan formed through cauldron subsidence associated with magma mixing and explosive volcanism. Evidence from Austurhorn suggests, however, that interaction of diverse magmas is a fundamental part of chamber evolution and not strictly related to caldera formation (figure 3.19c). The summit agglomerate of Breiddalur, consisting of angular fragments of gabbro, diabase and granophyre in a tuffaceous matrix (Walker, 1963), is the closest volcanic analog to the hypabyssal Icelandic net veined complexes. Its stratigraphic position, vesicular nature and association with pyroclastics may indicate emplacement during caldera collapse. However, most Icelandic pyroclastics are quite unlike the Breiddalur agglomerate. Inclusions of mafic melt in silicic units is common (e.g., Sigurdsson & Sparks, 1981; Mork, 1984), as are small isolated silicic or gabbroic xenoliths, but holocrystalline angular mafic fragments have not been reported in the well-documented pyroclastic sequences (Blake, 1970; Jorgensen, 1980; Sigurdsson & Sparks, 1981). More importantly, there is no evidence for calderas associated with the net veined complexes in SE Iceland. Ring fractures have not been identified at Austurhorn or Vesturhorn. Steeply dipping (55° SW) Alftafjordur lavas NNE of the Austurhorn complex reflect caldera collapse of the Alftafjordur volcano and are not associated with activity at Austurhorn (Blake, 1970; Torfason, 1979).

The net veined complex at Austurhorn formed essentially in situ through prolonged diverse interaction of mafic and felsic magmas. Angular mafic clasts in granophyre require the NVC to postdate emplacement and solidification of a mafic

magma at shallow crustal levels. The overall uniform fine grain size and lack of plastic deformation suggests that the clasts result from stoping of felsic magma into a near-solidus basaltic host. Clast-bearing granophyres have not been observed above ~300 m, whereas clast-free granophyres extend to the intrusion roof. The clasts themselves show no evidence of internal gravitational stratification. This relationship is also observed at Vesturhorn (Roobol, 1974; Mattson et al., 1986) but differs from that at Slafrudalur where basalt clasts are restricted to lower portions of felsic sills (Carmody & Marsh, 1988). I infer that the NVC material is not far-travelled, and that the angular mafic component is present near its original structural level.

Blake (1964, 1966) concluded that the tabular mafic bodies and "mega-pillows" form from sequential intrusion of mafic sills into a felsic body. I disagree, however, because repeated injections of basalt could not produce the distinctive parallelism of the mafic bodies. No mafic unit is crosscut or disrupted by an adjacent body as would be expected during multiple intrusive events. The uniform volume of felsic material between mafic units is also difficult to reconcile with repeated basalt intrusion. I interpret the "mega-pillows" as evidence for intrusion of felsic magma into a cooling mafic sill. Under low confining pressure, tensile forces generated during crystallization and cooling of basalt are sufficient to cause brittle failure prior to complete solidification. This phenomenon produces both columnar joints and tension gashes in lava flows and hypabyssal intrusions. At Austurhorn, intrusion of felsic magma would expedite this process and/or induce thermal fracture of the basalt (Marsh, 1982). "Mega-pillows" result when both mafic and felsic magmas are abundant and the volume of silicic magma is sufficient to form chilled margins on the mafic units. In contrast, when a subordinate volume of silicic magma is available, it forms narrow planar veins but does not chill the adjacent basalt on contact. The planarity of felsic veins and tabular mafic bodies over large outcrop area suggests they result from brittle fracture of the mafic magma during cooling. The wisp-like protrusions of felsic material in

overlying mafic bodies (figure 3.18) result from the density-controlled upwards migration of this silicic material after the fracture event. Contact with warm basalt would cause the felsic magma to become superheated locally, reducing its viscosity and allowing silicic melt to flow easily through small fractures. A similar interpretation was made independently by Marshall & Sparks (1984) for portions of the Mullach Sgar complex of St. Kilda, Scotland.

One remaining question is whether the planar felsic veins, like gabbroic pegmatoids, contain silicic magma derived locally during crystallization of basalt. Wickham (1987) applied the physical model and equations of McKenzie (1984) to segregation of low melt-fraction silicic melts from more refractory matrices under conditions of both passive compaction and catastrophic matrix failure using parameters appropriate for leucogranite melt from the Trois Seigneurs Massif (Pyrenees) (700-750°C, 7-8 wt% H₂O, viscosity 10⁴-10⁵ Pa-s). Wickham's calculated compaction times for passive segregation are on the order of 8x10⁴ years, indicating that the planar felsic veins could not originate from 10 m thick basalt sills in this manner. In contrast, Wickham calculated that a 20% melt fraction of hydrous leucogranite could migrate 2 m/yr under a stress gradient of grad P = 10 MPa/m. While this analysis considers regional metamorphic pressure gradients (Etheridge et al., 1984), the values are also appropriate for thermal stress gradients during comagmatic interaction (Marsh, 1982). Crystallization of pooled wet granite melts involves a positive volume change which may catalyze tensional failure. This mechanism provides an alternative to gas filterpressing (Anderson et al., 1984) which may be more appropriate for melt segregation in plutonic bodies.

In summary, I infer that the thin planar felsic veins at Austurhorn result from tensional failure during cooling of basalt sills and contain at least some locally-derived felsic material. Thicker felsic veins and dikes undoubtedly contain intrusive silicic magmas, as evidenced by the presence of mafic clasts. Field relations at Austurhorn

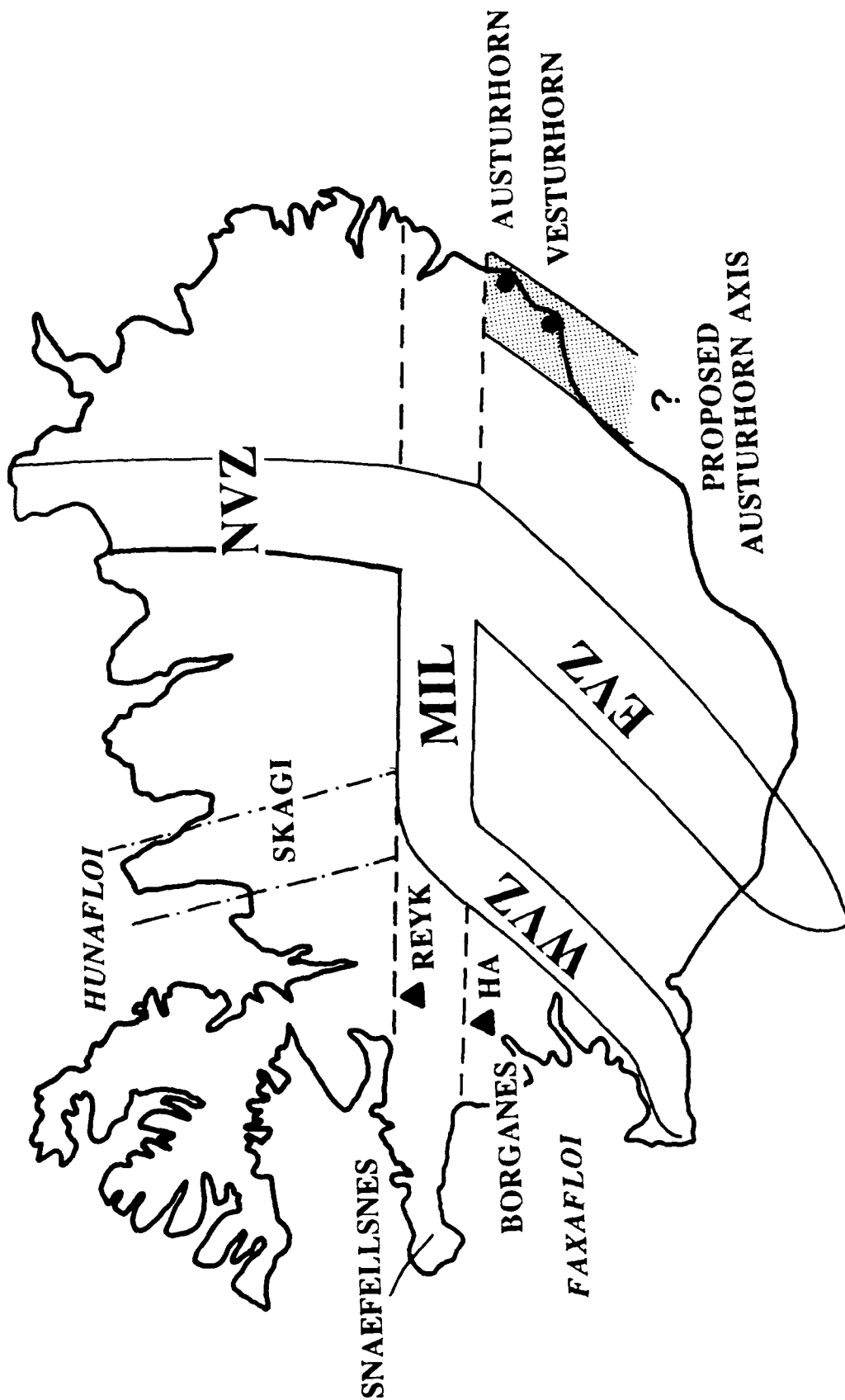
indicate a characteristic length scale for release of thermal stresses within the cooling mafic material. That this length scale is uniform within an outcrop area yet different in disparate parts of the chamber reflects variations in thermal regime from one area to the next.

3.4 Implications for Tertiary Rift Zone Systematics

The preponderance of transitional tholeiitic basalts and silicic intrusives in southeastern Iceland is evidence that Austurhorn and its coeval neighbors occupied an environment similar to that of the modern EVZ some 6-7 million years ago. A late Tertiary spreading axis has not been recognized previously in southeastern Iceland, although Torfason (1979) noted the colinearity of the Austurhorn, Reydara, Slafrudalur and Vesturhorn intrusions (figure 3.1) and interpreted them as volcanic edifices. The inception of rifting in SE Iceland is coincident with that documented in ridge segments from throughout Iceland, and supports the conclusion of Jancin et al (1985) that relocation of several ridge segments occurred at ~7 Ma. *In the following discussion I cite examples of late Tertiary ridge relocations taken from the literature, and speculate on the comparative stability of Tertiary and neo-volcanic spreading axes.*

1. Northern Iceland. K/Ar ages of lavas from the core of the Hunafloi-Skagi syncline (figure 3.23) indicate that volcanism ceased in this area ~6.7 Ma (Cotman, 1979; cited in Jancin et al., 1985). Volcanic activity resumed in Skagi between 2.5-0.5 Ma (Sigurdsson et al., 1978), but the northern volcanic zone (NVZ, figure 3.23) which became active in the late Tertiary has existed in its present configuration for over 6.0 My (Jancin et al., 1985). The oldest lavas associated with this rifting episode are at least 6.2-5.8 Ma and overlie unconformably a sequence of >9.5 Ma flood basalts (dates based on magnetostratigraphy and K/Ar whole-rock ages; Jancin et al., 1985). The inferred ridge jump from Skagi to the NVZ is ~100 km eastward.

Figure 3.23 Proposed evolution of Icelandic rift zones from ~7 Ma to present. The mid-Iceland belt [MIL, dashed where inferred] connects the single spreading axis in northern Iceland [NVZ] with parallel rift zones [WVZ, EVZ] in the south. The NVZ has been stable for ~7 Ma (Jancin et al., 1985). The ephemeral Skagi rift zone was active for less than 2 million years ~2.8 Ma (Sigurdsson et al., 1978) and represents the only other known spreading axis in northern Iceland. South of the MIL, contemporaneous central volcanoes Reykjadalur (REYK) and Hallarmuli (HA) were part of a volcanic belt trending parallel to the EVZ and WVZ which passed through Borganes offshore into Faxafloi (Johannesson, 1980). This rift zone was active ~6-7 Ma and is coeval with the proposed Austurhorn axis located in southeastern Iceland. The positions of the Borganes and Austurhorn axes, after correcting for subsequent crustal accretion, are roughly equivalent to those of the neovolcanic zones in southern Iceland, suggesting that this parallel rift configuration has occurred previously in Iceland's evolution.



2. Southwest Iceland. One analysis reported by Moorbath et al (1968) from the core of the Snaefellsnes syncline (figure 3.23) is 6.9 Ma (recalculated with an updated decay constant), suggesting an approximate bound for the end of volcanism in northern Snaefellsnes (Jancin et al., 1985). Roughly 50 km to the southeast, the Reykjadalur and Hallarmuli central volcanoes became active between 6.7-6.0 Ma (Johannesson, 1975). A sedimentary sequence, the Hredavatn unconformity, separates products of these volcanoes from underlying ~12-13 Ma Tertiary lavas. Dates cited are based on regional magnetostratigraphic and K/Ar analysis (Johannesson, 1975, 1980). It must be noted that volcanism in southwestern Snaefellsnes did not cease entirely until ~900 AD.

3. Eastern Iceland. Watkins & Walker (1977) report a continuous sequence of Tertiary lavas from 13-2 Ma from Iceland's eastern fjords, with an apparent maximum in volcanic activity 7.3-6.4 Ma. Structural analysis of dike trends within this sequence led Helgason (1983, 1985) to conclude that the anomalously copious volcanism may represent a period of frequent ridge jumps of limited displacement (10-40 km). The results of the present study indicate a single significant unconformity (i.e., superposition of 6-7 Ma volcanics upon 9-11 Ma volcanics) within the southeastern sequence that is not observed in the northeast.

There are three important implications of the proposed Austurhorn rift segment. The first is a confirmation that reorganization of the plate boundaries at ~7 Ma occurred throughout Iceland. Jancin et al (1985) demonstrated the contemporaneity of ridge relocations in northern and southwestern Iceland, and this study extends the event to include the southeastern region as well. A second point is that the "transform" which runs across central Iceland (the MIL, or Mid-Iceland Belt of Oskarsson et al., 1982; figure 3.23) must have been a structural feature during the Tertiary as well. Activity along the Austurhorn rift segment is contemporaneous with that of the Borganes-Faxafloi area (figure 3.23), which also dies out in central Iceland. Neither of these axes can be traced across the MIL. Steinthorsson (1981) noted that central volcanoes of all

ages are more abundant along and south of the MIL than to its north. The exact significance of the MIL remains unknown, but is apparently a long-lived feature. Finally, this study provides further evidence that the present configuration of parallel rift zones existed throughout Iceland's geologic record. Helgason (1983) reported that lava isochrons from eastern and western Iceland are not parallel and that closing of known rift segments under present spreading conditions cannot account for the distribution of Tertiary lavas. He concluded that two active spreading ridges located 100-200 km apart are required to produce the current structural configuration. The present analysis indicates that near-parallel ridges are not unique to the modern Icelandic landscape. The long term stability of individual dual-ridge systems is beyond the scope of this work, but this style of spreading appears to have been the norm for over 10 million years.

3.5 Conclusions

The Austurhorn intrusion is a hypabyssal complex in southeastern Iceland which represents the exhumed remains of an evolved Tertiary central volcano. Field relations at Austurhorn provide convincing evidence for the existence of shallow Icelandic magma chambers, and allow documentation of the physical processes which accompany volcanic evolution. The chamber itself was evidently not a closed system; it had a complex history of replenishment by small, often highly differentiated magma batches.

Volcanism at Austurhorn was strongly bimodal: early localized basaltic activity gave way to a later episode of sustained silicic magmatism. The transitional tholeiitic geochemistry and highly silicic character of the complex indicate an immature rift zone environment analogous to the eastern neovolcanic zone. Magmatic activity at Austurhorn may be summarized as follows:

1. Early centralized magmatic activity established a shallow basaltic chamber roughly 5 km in diameter. The parental basalt (~7.8 wt% MgO) differentiated by precipitating

olivine, plagioclase, clinopyroxene, magnetite and ilmenite. Repeated influx of parental basalt (less dense than FeTi oxide-rich cumulates) sustained chamber activity by supplying both magma and heat.

2. Crystallization of low-density plagioclase-rich gabbros isolated the shallow chamber from replenishment by mafic liquids. Subsequent "failed replenishments" ponded in the crust near the base of the chamber.

3. Felsic magmas were emplaced from below into the cooling gabbro and smaller adjacent mafic sills. Intrusion of felsic magmas into basalts of varying degrees of solidification produced an extensive net veined complex. Several individual felsic units are identified in the field; they generally form small (< 500 m extent) sills. Felsic replenishment was infrequent enough that a single large convecting felsic body did not develop.

4. Renewed basaltic activity in the form of a NE-trending dike swarm postdates emplacement of some granophyres, and is contemporaneous with others. Mafic pillows result from this interaction and are common in the net veined complex.

The distinctive basalt chemistry (transitional tholeiitic, MgO <8 wt%; see chapter 4) and abundance of silicic rocks at Austurhorn are controlled by the crustal structure of an immature rift. The major reorganization of ridge segments inferred at ~7 Ma (Jancin et al., 1985) may correspond to centralization of certain rift systems (in particular the western volcanic zone) which matured sufficiently to erupt mafic liquids more similar to MORB than those which characterized Icelandic volcanism in the Tertiary period (Schilling et al., 1982, 1983; Zindler et al., 1979).

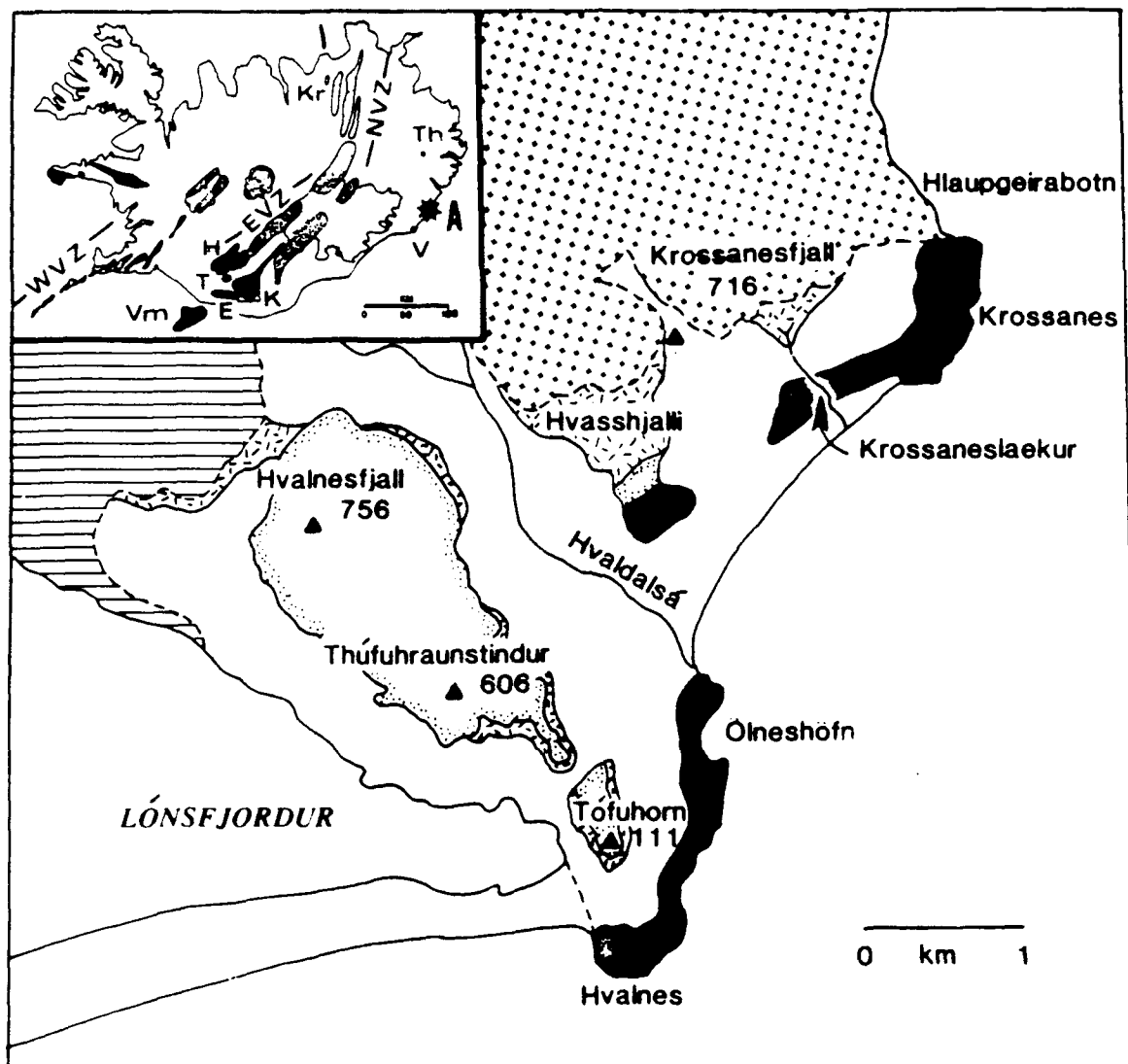
CHAPTER 4
PETROGENESIS OF EVOLVED BASALTS AND SILICIC MAGMAS
AT AUSTURHORN, SOUTH-EAST ICELAND

INTRODUCTION

Modern Icelandic basalts show significant regional variations in petrology and major element geochemistry (e.g., Jakobsson, 1972, 1979). Tholeiitic basalts are erupted in the Northern and Western Volcanic Zones [NVZ and WVZ] where the mid-Atlantic Ridge crosses Iceland in a configuration which has remained stable for over 7 million years (Steinthorsson, 1981; Jancin et al., 1985). Basalts of the Eastern Volcanic Zone (EVZ) change systematically from dominantly tholeiitic in central Iceland to transitional tholeiitic and FeTi-enriched near Hekla and Katla to alkalic off the southern coast in Vestmannaeyjar (figure 4.1; Jakobsson, 1979). Metaluminous to peralkaline rhyolites are common in transitional tholeiitic central volcanoes but are rare in the NVZ and absent along the Reykjanes Peninsula. Rifting and volcanism in the EVZ began ~2.5 Ma, triggered perhaps by a pulse in plume activity (Kurz et al., 1984; Meyer et al., 1985). The EVZ is interpreted as an immature rift axis propagating southward from central Iceland with its tip now located at Surtsey, the southernmost island of the Vestmannaeyjar archipelago (Meyer et al., 1985; Einarsson, 1988).

Most workers agree that the geochemical gradients observed along the EVZ reflect systematic changes in mantle and crustal processes in a young rifting environment. Meyer et al (1985) proposed that the major and trace element signatures of EVZ basalts record variable conditions of mantle melting and subsequent fractionation in crustal magma chambers. In this model evolved (including some silicic) compositions common to FeTi and transitional centers reflect extensive fractionation in isolated magma bodies. Alkalic lavas from Vestmannaeyjar are interpreted as unfractionated low-degree partial melts of spinel or garnet lherzolite (Meyer et al., 1985; Furman et al., 1988). In contrast, Oskarsson and co-workers (1982, 1985; Steinthorsson et al., 1985; Hemond et al., 1988) suggested a single mantle-derived (MORB-like) olivine tholeiite is parental to all Icelandic volcanics, with compositional diversity resulting from variable contamination of this basalt with crustally derived liquids. In this model, evolved

Figure 4.1 Simplified geological map of the Austurhorn intrusive complex showing key topographical and geographic features as well as rock units. The host rocks to the intrusion are lavas of the Alftafjordur (x-pattern) and Lon (striped) central volcanoes. Within the intrusion, **gabbro** is outlined by stipple, **granophyre** has a random dash pattern, and **net-veined complex** areas are lightly shaded. The inset map of Iceland shows location of the **Austurhorn** (asterisk labeled A) and **Vesturhorn** (V) intrusions, plus the neo-volcanic rift zones (WVZ, EVZ, NVZ). Labeled volcanoes are: **Krafla** (Kr, tholeiitic), **Hekla** (H, transitional), **Katla** (K, transitional), **Torfajokull** (T, transitional with abundant silicics), and **Vestmannaeyjar** (V, alkalic). The Tertiary volcano **Thingmuli** (Th, tholeiitic) is located in eastern Iceland.



(quartz-normative and FeTi) basalts represent mixtures of olivine tholeiite and subalkaline rhyolite, the latter generated by melting of hydrated crust near the rift axis. Alkaline magmas are thought to be produced during extensive lower crustal melting; this liquid mixes with parental olivine tholeiite to form transitional and mildly nepheline-normative basalts.

The Austurhorn intrusion, an exhumed Tertiary volcanic center in southeastern Iceland (figure 4.1; Blake, 1966; see chapter 3) was a transitional tholeiitic center with copious silicic magmatism, similar to the Torfajökull complex in the modern EVZ (figure 4.1; Ivarsson et al., in press, Gunnarsson, 1988). In this chapter an integrated field, petrologic and geochemical study is used to determine the origin of evolved basalts and silicic magmas. My approach uses incompatible trace element contents (e.g., Ba, La, Nb) and Pb isotopic ratios to infer the scale of heterogeneity within the sub-Icelandic mantle, and compatible trace elements to constrain the conditions of mantle melting and subsequent crystal fractionation. Geochemical and mineralogic data from basalts, granophyres and the cogenetic cumulate Hvalnesfjall gabbro are used to evaluate models of closed system crystallization. Analysis of comagmatic basaltic and felsic liquids from the extensive net veined complex (Blake, 1966; Mattson et al., 1986; chapter 3) enables quantitative assessment of assimilative processes in the shallow crust.

Major conclusions are that fractionation of parental basalt at crustal levels under conditions of variable oxygen fugacity can generate the observed range of liquid compositions:

1. Evolved quartz normative basalts can be derived by closed system fractionation of transitional tholeiitic (hypersthene- to mildly nepheline normative) basalts at near-surface conditions and high f_{O_2} (approx. Ni-NiO buffer [NNO]) by removal of olivine, plagioclase, augite, titanomagnetite and ilmenite.

2. Contemporaneous tholeiitic and transitional tholeiitic mafic liquids which differentiated at lower f_{O_2} (locally <QFM) did not undergo comparable silica enrichment.

3. The cumulus mineralogy of the gabbro indicates the evolved (quartz-normative) basalts precipitated plagioclase, augite, FeTi oxides and apatite while evolving to dacitic residual liquids.

4. Exposed felsic units evolved at $P > 1$ kbar, where fractionation of plagioclase, clinopyroxene, oxides and K-feldspar from dacite (granodiorite) produced fayalite-bearing rhyolites. This conclusion is supported by field evidence which indicates that Austurhorn silicic magmas intrude the shallow chamber from below and therefore must be generated at > 2 km depth. Mineralogic and geochemical considerations suggest the Austurhorn felsic magmas originated through extreme differentiation of mildly alkalic (transitional tholeiitic) basalts and are not extensively contaminated by crustal melts.

4.1 Geologic Background

The Austurhorn intrusion is exposed over ~ 15 km² at the northeastern end of Lonsfjordur, SE Iceland (figure 4.1). The complex includes a layered gabbro body and a large composite granitic/-granophyric stock, multiply intruded by basaltic and rhyolitic dikes and sills (Blake, 1966; chapter 3). K-Ar dating of biotites indicates an intrusive age of 6.6 ± 0.4 Ma (Moorbath et al., 1968). The intrusion was emplaced at a depth of ~ 2000 meters into 12 million year old basalts, rhyolites and pyroclastics, products of the Alftafjordur and Lon central volcanoes (Blake, 1970; Ross & Mussett, 1976). Repeated glaciation has dissected the complex and surrounding country rocks, thus exposing internal igneous structures.

In chapter 3 I interpreted the intrusive complex as the exhumed magma chamber of a mature central volcano. Austurhorn basalts are compositionally diverse and include nepheline normative, quartz-normative, and FeTi-rich liquids. Silicic magmas range

from granodiorites to metaluminous and mildly peralkaline granites and rhyolites. These geochemical features are characteristic of an immature axial rift environment, viz the modern EVZ. An inferred short-lived rift segment connected Austurhorn and the nearby Vesturhorn volcanoes in latest Tertiary time. The two intrusions are coeval and exhibit comparable histories of magmatic evolution (Roobol, 1974; Mattson et al., 1986; Furman, unpub. data). Basalts from Austurhorn and Vesturhorn are enriched in radiogenic Pb relative to both older and younger plateau basalts from eastern Iceland (Hanan, unpub. data; Hanan & Schilling, 1986, 1987). This isotopic signature is interpreted as that of the Iceland mantle plume and suggests that spreading along the Austurhorn-Vesturhorn rift segment was triggered by a pulse in plume activity (Hanan & Schilling, 1986, 1987). The Austurhorn complex therefore developed in a tectonic environment analogous to that of Torfajökull (EVZ; figure 4.1), where transitional tholeiitic basalts and metaluminous to peralkaline rhyolites dominate.

Early basaltic activity at Austurhorn was localized in the southwestern third of the complex where it formed a shallow magma body, now preserved as the modally layered Hvalnesfjall gabbro (figure 4.1). A thick rhythmic(?) layered sequence on Hvalnesfjall suggests the chamber underwent frequent replenishment. As the gabbro body cooled it was intruded from below by several pulses of granophyre. Felsic magmas stopped through the gabbro body margins to form a composite stock which comprises the majority of the Austurhorn complex (figure 4.1). Intrusive contacts are preserved between individual felsic units of distinctive petrology and geochemical character, indicating that a single convecting silicic chamber never developed. During ascent the felsic magmas interacted with both solid and semi-molten mafic units, forming a large net veined complex (Blake, 1966). The final magmatic phase at Austurhorn was basaltic, forming brittle dikes at high structural elevations and "pillows" in granitic magma within the coastal net veined complex. Specific field relations are discussed in detail in chapter 3.

4.2 Analytic Techniques

Weathered surfaces were removed and samples were cut into ~1 cm thick slabs, which were polished with alumina grit to remove saw marks and surface contamination. Slabs were washed with distilled water in an ultrasonic cleaner and oven dried at 100°C prior to crushing. Most samples were crushed to <0.5 cm fragments using a porcelain jaw crusher; others were crushed by hammer between sheets of polyethelene. All fragments were then powdered in an agate disc mill. Over 500 grams of powder was prepared whenever possible.

Major element analyses of all samples were obtained by x-ray fluorescence (XRF) on fused discs and the trace elements Ba, Rb, Ga, Nb, Ni, Pb, Sr, V, Y, Zn, Zr were analyzed by XRF on pressed powder pellets, both at the University of Massachusetts (Amherst). Instrumental neutron activation analyses for the rare earth elements (REE), Co, Cr, Hf, Na, Sc, Ta and Th were done at M.I.T. Water content (H_2O^+) was determined for selected samples with an HCN analyzer at Woods Hole Oceanographic Institution. Major, minor and trace element data are given in table 4.1. Estimates of precision and accuracy are given in Appendix II.

Electron microprobe analyses of individual minerals were done on the JEOL 733 Superprobe at M.I.T., using an operating current of 10 nanoamperes and an accelerating potential of 15 kV. Spot analyses were performed with a beam diameter of 1 micron except for sodic plagioclase ($<An_{20}$) and rhyolite glass which were analyzed with a 10 micron beam to reduce sodium loss by volatilization. On-line data reduction and matrix correction procedures of Bence and Albee (1968; modified by Albee & Ray, 1970) were used. All analyses reported in Appendix III represent an average of at least three spot analyses.

A subset of the Austurhorn samples has been analyzed for radiogenic Pb isotopes by B. Hanan at the University of Rhode Island. Rock chips, rather than powders, were

Table 4.1 Major and Trace Element Data for Austurhorn Samples

AUSTURHORN MAFIC DIKES

Sample	d-1 A-2	d-7 A-17	d-25 A-18	d-62 T-4	d-43 T-17	d-45 T-21	d-29 T-47	d-81 T-50	d-23 T-58	d-63 K-4	d-42 K-30	d-41 K-31a	d-44 K-43a	d-82 HN-18	d-46 F-11
SiO ₂	45.84	47.49	50.34	47.53	46.74	48.96	50.25	50.16	49.81	47.13	49.48	53.81	45.24	49.76	48.68
TiO ₂	2.84	3.79	2.98	4.14	2.74	2.12	3.78	3.27	3.60	3.71	3.48	2.15	3.28	2.86	2.10
Al ₂ O ₃	16.07	14.78	13.96	13.03	16.80	14.75	13.17	12.57	13.40	14.00	13.65	13.13	17.40	14.48	14.16
Fe ₂ O ₃	15.22	15.69	13.19	15.78	12.91	13.73	15.68	14.05	14.61	15.63	15.79	12.27	21.26	13.10	13.02
MnO	.22	.27	.19	.29	.19	.20	.38	.22	.28	.22	.29	.36	.22	.20	.26
MgO	6.70	4.96	5.49	4.74	5.37	7.75	4.76	3.97	4.01	5.53	5.06	2.55	2.05	4.80	7.24
CaO	9.94	8.31	9.81	9.46	11.44	9.77	9.22	7.84	7.63	10.29	9.86	5.84	3.49	9.70	11.26
Na ₂ O	2.41	3.26	3.01	3.15	2.86	2.50	2.28	5.27	3.59	2.67	2.03	6.44	3.91	3.64	3.04
K ₂ O	.55	.87	.95	.95	.72	.15	.51	1.56	2.66	.56	.07	1.99	2.56	1.12	.26
P ₂ O ₅	.34	.70	.33	1.05	.28	.20	.49	.99	.59	.37	.39	1.00	1.60	.33	.20
total	100.13	100.11	100.25	100.12	100.05	100.13	100.52	99.90	100.18	100.11	100.10	99.54	101.01	99.99	100.22
Mg#	46.6	38.5	45.2	37.3	45.2	52.8	37.6	35.9	35.2	41.2	38.8	29.2	16.7	42.1	52.4
Cs	.6	1.2	0.4	.6	1.2	0.6	0.8	1.4	3.2	0.1	.8	1.5	0.7	0.7	0.4
Rb	326	16.1	23.1	14.5	22.7	3.7	16.9	53.4	396	371	247	371	289	343	308
Sr	326	393	332	281	405	267	292	395	308	157	51	302	635	176	87
Ba	141	251	141	256	125	62	131	268	308	35.1	37.9	21.9	33.5	31.8	40.9
Sc	29.2	27.7	36.2	29.1	29.9	40.5	35.4	24.6	26.9	378	423	46	144	323	324
V	324	192	297	248	330	329	380	205	223	29.4	21.1	3	5	59.3	168
Cr	45.6	6	31.1	2	45.1	163	31.3	7	4	51.2	44.4	10.4	28.4	39.1	50.7
Co	53.4	36.0	46.5	33.2	43.1	52.3	41.6	27.0	33.4	53	33	17	21	48	59
Ni	92	18	58	8	68	79	37	22	10	117	157	311	234	180	209
Zn	113	141	70	211	163	158	170	117	403	117	33	17	21	180	209
Ga	22.2	24.1	24.0	23.9	22.7	20.8	25.0	22.5	-	23.4	24.5	27.8	31.4	23.6	20.4
Y	29.7	48.9	34.9	47.9	26.1	27.0	50.6	51.6	-	33.6	46.9	60.9	103	35.3	32.9
Zr	184	328	187	246	150	114	302	273	301	195	223	373	483	240	116
Nb	18.8	36.3	15.7	27.0	14.9	10.9	27.0	25.5	28.2	17.7	22.6	29.3	48.0	19.1	10.5
Hf	4.2	7.5	5.5	5.8	3.5	3.0	7.4	6.5	7.0	4.9	6.3	8.5	11.3	6.2	3.0
Ta	1.05	2.32	1.09	1.70	.94	.78	1.79	1.60	1.64	1.15	1.40	1.83	2.76	1.25	.70
Th	1.0	1.9	1.5	1.4	.7	.5	2.2	1.6	2.2	1.2	1.8	2.5	3.7	2.4	.6
La	15.98	29.12	18.28	25.79	12.34	9.44	24.03	28.20	25.9	16.26	18.21	36.90	50.20	19.40	10.47
Ce	39.9	76.6	47.0	68.8	32.4	25.9	62.6	73.7	65.6	43.8	52.8	95.1	131.0	49.9	27.0
Nd	23.6	44.3	27.9	45.9	20.1	16.5	38.0	48.0	41.7	26.8	32.3	58.4	87.2	28.6	17.9
Sm	6.16	11.02	7.37	11.31	5.43	4.78	9.89	12.39	10.97	6.86	8.05	14.30	21.24	7.18	5.12
Eu	2.08	3.54	2.33	4.10	1.83	1.57	3.02	4.36	3.55	2.67	2.75	6.19	7.36	2.28	1.81
Tb	.9	1.5	1.4	2.0	.9	.8	1.5	2.0	1.6	1.4	1.5	2.2	3.8	1.2	1.0
Yb	2.49	4.19	2.92	3.62	2.21	2.47	4.47	3.98	4.11	2.93	4.10	5.01	7.98	3.01	2.91
Lu	.37	.66	.43	.55	.32	.37	.71	.60	.60	.41	.61	.71	1.12	.44	.42

MAFIC PILLOWS

Sample	p-61a rim C-2a	p-61b core C-2b	p-62a rim C-6a	p-62b core C-6b	p-41a rim KF-14a	p-41b core KF-14b	p-65 CC-1	p-67 CC-15	p-66 CC-23	p-63a rim VS-10a	p-63b core VS-10b	p-64 VS-19
SiO ₂	48.00	48.28	47.69	50.02	50.03	53.46	48.99	47.84	53.32	47.96	48.04	48.05
TiO ₂	2.32	2.66	2.74	2.53	2.61	2.83	3.00	2.94	2.72	2.66	2.69	3.02
Al ₂ O ₃	16.76	15.48	15.26	15.32	14.77	13.78	14.30	14.48	14.36	15.53	15.56	14.57
Fe ₂ O ₃	12.04	12.79	13.16	12.21	12.52	12.56	14.16	13.73	12.49	12.94	13.05	13.90
MnO	.19	.23	.21	.19	.18	.25	.21	.21	.20	.21	.21	.24
MgO	6.61	5.62	6.27	5.65	5.67	3.57	5.42	6.00	4.06	6.07	6.15	6.38
CaO	10.78	10.30	10.50	10.12	9.61	6.82	9.60	10.46	7.98	10.42	10.41	10.51
Na ₂ O	2.72	2.76	2.90	3.00	3.13	3.84	3.31	3.40	4.02	3.66	3.52	3.19
K ₂ O	.68	1.10	.79	.73	.87	1.55	.75	.67	.54	.59	.67	.57
P ₂ O ₅	.29	.37	.34	.36	.33	.77	.37	.36	.39	.35	.36	.37
total	100.39	99.59	99.86	100.13	99.72	99.43	100.11	100.09	100.08	100.39	100.66	100.80
Mg#	52.1	46.5	48.5	47.8	47.3	36.0	43.2	46.5	39.2	48.1	48.2	47.6
CS	-	0.3	0.3	0.1	0.2	0.3	0.8	0.3	0.2	-	-	-
Rb	11.4	19.6	14.8	12.0	16.3	26.4	17.9	10.4	9.2	-	-	-
Sr	419	345	381	409	367	354	329	393	303	-	-	-
Ba	150	234	186	183	183	385	196	164	165	-	-	-
Sc	30.6	30.0	33.3	31.8	30.6	23.8	31.8	34.6	27.1	-	-	-
V	242	265	273	239	260	145	345	327	269	-	-	-
Cr	174	115	138	140	115	9.3	76	111	16	-	-	-
Co	46.5	40.1	45.9	40.9	42.0	26.3	44.0	46.2	35.0	-	-	-
Ni	80	56	68	56	64	24	76	59	42	-	-	-
Zn	188	144	123	149	87	147	140	205	144	-	-	-
Ga	21.1	22.0	22.2	22.5	23.9	26.0	23.3	21.8	24.3	-	-	-
Y	26.9	35.6	32.2	35.4	36.6	64.2	41.0	33.4	51.8	-	-	-
Zr	180	263	207	200	193	495	233	195	320	-	-	-
Nb	15.2	20.3	16.8	19.9	18.6	35.6	23.2	18.6	31.6	-	-	-
Hf	4.3	6.1	4.9	5.6	5.3	11.5	5.8	4.8	8.2	-	-	-
Ta	1.01	1.20	1.05	1.28	1.30	2.37	1.43	1.11	2.00	-	-	-
Th	.9	1.5	1.0	1.8	1.6	2.5	1.8	1.2	3.6	-	-	-
La	14.72	19.96	17.2	19.86	22.77	36.11	22.31	17.96	31.20	-	-	-
Ce	35.3	50.7	43.2	50.8	56.3	95.2	56.1	45.4	79.4	-	-	-
Nd	22.4	29.3	26.0	28.9	32.0	57.6	33.3	27.0	40.8	-	-	-
Sm	5.73	7.62	6.61	7.15	7.68	13.41	7.93	6.93	10.32	-	-	-
Eu	2.01	2.60	2.47	2.57	2.44	4.55	2.53	2.36	2.77	-	-	-
Tb	1.0	1.3	1.2	1.2	1.1	2.0	1.3	1.1	1.6	-	-	-
Yb	2.18	3.09	2.52	2.80	3.08	5.38	3.51	2.87	4.57	-	-	-
Lu	.33	.44	.36	.45	.48	.81	.54	.40	.70	-	-	-

GRANOPIRYRES, GRANODIORITES AND GRANITES

Sample	g-65 VS-15	g-43 KF-49	g-63 VS-21	g-62 K-40	g-23 R-40	B-1	g-21 ET-3	g-22 G-2	g-41 KF-37	g-83 HN-6	g-42 KF-31	g-61 G-1	g-81 C-26	g-64 VS-33	g-82 HN-21
SiO ₂	62.47	64.10	65.65	66.78	68.19	67.88	68.61	69.01	70.93	71.20	71.54	72.44	73.32	75.17	75.16
TiO ₂	1.12	1.03	.90	.50	.42	.67	.57	.67	.30	.31	.22	.26	.20	.21	.19
Al ₂ O ₃	15.84	15.01	15.33	13.46	13.46	14.18	14.11	14.04	13.44	13.72	13.32	12.25	13.33	12.96	12.43
Fe ₂ O ₃	6.47	6.31	5.39	7.87	6.90	5.30	4.78	4.66	4.58	3.81	4.69	3.35	2.62	2.10	2.73
MnO	.13	.14	.11	.22	.24	.15	.09	.14	.17	.06	.16	.11	.07	.02	.04
MgO	1.44	1.34	1.13	.24	.19	.66	.61	.58	.17	.36	.14	.12	.23	.14	.05
CaO	3.59	3.17	2.82	2.99	2.76	2.13	2.02	1.79	1.28	1.29	1.25	.82	.78	.25	.14
Na ₂ O	5.32	5.12	5.47	5.01	4.85	5.16	4.80	4.95	5.66	4.95	5.39	5.38	4.42	4.12	4.85
K ₂ O	2.68	3.05	3.32	2.63	2.70	3.24	3.73	3.30	3.20	3.66	3.53	3.85	4.43	4.46	3.99
P ₂ O ₅	.32	.28	.24	.09	.08	.15	.10	.13	.02	.06	.02	.02	.03	.02	.01
total	99.38	99.55	100.36	99.79	99.79	99.52	99.42	99.27	99.63	99.42	100.26	98.60	99.43	99.45	99.59
Mg#	30.6	29.5	29.3	5.7	5.2	19.8	20.4	19.8	2.1	15.6	5.6	6.6	14.8	11.6	3.5
CS	0.3	0.2	-	0.6	0.8	0.5	-	0.4	0.2	0.3	0.4	0.6	0.4	0.3	0.6
Rb	52.0	51.4	-	70.6	62.3	69.5	-	70.4	-	64.6	71.2	78.9	90.1	100	-
Sr	241	220	-	262	254	186	-	162	110	122	100	56.5	58.5	31.2	34.6
Ba	698	624	-	460	559	565	-	625	818	567	804	683	533	375	588
Sc	10.3	9.5	-	14.2	10.2	9.4	-	8.2	2.1	5.9	1.4	1.4	2.2	1.3	0.5
V	34	34	-	0	0	7	-	4	2	5	1	2	1	7	3
Cr	5	5	-	3	3	4	-	3	4	4	5	4	4	4	5
Co	10	9	-	1	1	3	-	3	0	2	0	1	2	1	1
Ni	2	1	-	5	4	4	-	0	4	1	3	5	7	2	8
Zn	101	111	-	183	241	121	-	94	159	64	188	161	101	78	105
Ga	24.7	24.9	-	28.9	28.0	23.7	-	23.3	-	23.5	31.2	30.4	26.2	27.8	-
Y	65.2	74.4	-	88.0	82.8	81.1	-	78.9	-	70.4	135	97.2	92.4	101	-
Zr	1156	1067	-	880	939	679	-	731	932	595	908	674	466	401	592
Nb	48.1	57.0	-	59.0	50.2	59.7	-	61.5	62.0	47.0	128.8	77.7	70.3	79.6	82.8
Hf	23.2	22.2	-	19.4	22.3	17.1	-	18.0	21.8	16.7	25.2	19.3	14.4	14.4	19.0
Ta	2.90	3.54	-	3.76	3.25	3.65	-	3.80	3.59	3.29	8.46	4.76	4.71	5.57	5.65
Th	5.7	5.5	-	5.6	5.9	8.0	-	8.3	6.8	8.0	10.6	8.3	10.0	10.4	9.4
U	-	1.6	-	-	-	2.2	-	2.1	-	-	2.1	2.5	3.0	2.0	-
La	51.0	50.3	-	53.5	54.4	58.1	-	60.7	77.8	58.1	89.2	71.3	72.7	71.4	81.5
Ce	123.3	127.6	-	133.0	133.1	135.9	-	143.8	178.0	132.9	208.7	166.6	167.4	161.7	205
Nd	64.5	65.5	-	72.2	71.9	69.7	-	72.4	91.0	66.5	107.9	84.5	80.3	77.3	107.0
Sm	13.96	14.82	-	16.85	16.80	15.92	-	15.75	28.60	14.47	24.55	19.71	18.42	16.75	24.86
Eu	4.18	3.99	-	5.27	5.20	3.80	-	3.82	5.48	2.94	5.88	3.83	2.39	1.84	3.42
Tb	2.1	2.3	-	2.8	2.8	2.6	-	2.5	3.0	2.3	4.3	3.3	3.0	2.9	4.1
Yb	6.48	6.93	-	8.45	8.85	7.97	-	8.24	10.78	7.75	13.61	10.64	9.55	9.68	11.59
Lu	1.00	1.04	-	1.19	1.23	1.11	-	1.12	1.57	1.07	1.90	1.54	1.27	1.32	1.59

AUSTURHORN FELSIC DIKES

Sample	f-62 8335-C	f-61 T-8	f-45 KF-20	f-44 KF-23	f-43 KF-28	f-1 A-14	f-23 T-31	f-24 T-59	f-22 H-12b	f-41 KF-15a	f-42 KF-51	f-21 GN-3	f-81 ON-4
SiO ₂	71.37	75.50	72.52	72.78	72.88	69.85	65.23	66.48	64.31	69.80	80.49	73.24	68.07
TiO ₂	.40	.13	.26	.22	.25	.62	.74	.73	1.10	.41	.13	.48	.51
Al ₂ O ₃	12.88	13.13	13.01	12.98	12.66	14.41	13.90	13.10	14.54	13.76	11.39	13.16	15.49
Fe ₂ O ₃	5.04	1.54	4.18	3.85	3.81	4.12	8.73	8.51	7.84	5.01	.35	2.61	3.79
MnO	.09	.03	.03	.13	.13	.08	.26	.27	.13	.17	.01	.02	.03
MgO	.17	.14	.04	.09	.06	1.15	.67	.52	1.31	.30	.09	.41	.56
CaO	1.80	.71	.71	1.60	.79	2.42	3.28	2.60	3.48	1.62	1.42	1.32	2.15
Na ₂ O	3.13	4.11	4.77	4.27	4.96	3.16	4.07	5.85	4.44	5.58	4.45	3.22	4.78
K ₂ O	4.24	4.68	3.78	3.66	3.62	3.73	3.22	1.45	2.37	3.44	1.55	4.86	4.46
P ₂ O ₅	.06	.02	.01	.01	.02	.12	.16	.16	.34	.06	.01	.08	.11
total	99.18	99.99	99.31	99.59	99.18	99.66	100.26	99.67	99.86	100.15	99.88	99.40	99.95
Mg#	6.2	15.2	1.8	4.4	3.0	35.6	13.1	10.8	24.8	10.6	33.4	23.6	22.5
Cs	0.1	0.8	-	-	0.2	-	-	-	-	-	-	-	0.3
Rb	64.9	102.6	-	74.2	71.2	-	-	-	-	-	-	-	-
Sr	274	47	-	62	70	-	-	-	-	-	-	-	264
Ba	720	467	-	626	667	-	-	-	-	-	-	-	689
Sc	8.3	2.2	-	-	1.1	-	-	-	-	-	-	-	5.2
V	1	5	-	4	2	-	-	-	-	-	-	-	25
Cr	3	4	-	-	4	-	-	-	-	-	-	-	3
Co	3	1	-	-	0	-	-	-	-	-	-	-	7
Ni	11	8	-	1	1	-	-	-	-	-	-	-	6
Zn	93	34	-	130	233	-	-	-	-	-	-	-	38
Ga	24.3	20.4	-	27.5	30.0	-	-	-	-	-	-	-	-
Y	96.4	46.1	-	119	113	-	-	-	-	-	-	-	-
Zr	802	213	-	850	946	-	-	-	-	-	-	-	694
Nb	64.6	27.9	-	89.2	86.3	-	-	-	-	-	-	-	43.4
Hf	19.2	7.7	-	-	22.6	-	-	-	-	-	-	-	18.5
Ta	3.99	2.41	-	-	5.27	-	-	-	-	-	-	-	2.52
Th	7.5	11.7	-	-	8.6	-	-	-	-	-	-	-	7.9
U	-	2.8	-	-	.8	-	-	-	-	-	-	-	-
La	62.9	48.4	-	-	75.7	-	-	-	-	-	-	-	54.1
Ce	151.2	100.7	-	-	184	-	-	-	-	-	-	-	122.1
Nd	72.9	42.9	-	-	98.0	-	-	-	-	-	-	-	54.7
Sm	19.15	8.48	-	-	21.2	-	-	-	-	-	-	-	12.18
Eu	4.57	1.03	-	-	4.65	-	-	-	-	-	-	-	3.33
Tb	3.2	1.4	-	-	3.6	-	-	-	-	-	-	-	1.8
Yb	9.64	5.15	-	-	11.04	-	-	-	-	-	-	-	6.51
Lu	1.31	.77	-	-	1.56	-	-	-	-	-	-	-	1.00

HIVALENEFJALL GABBRO

Sample	gb-30 8502-A3	gb-34 H-18B	gb-24 D-15	gb-23 D-16	gb-29 D-27	gb-32 D-55	gb-31 D-73	gb-28 A-20	gb-83 HN-13	gb-41 F-10	gb-42 F-16	gb-36 F-62
SiO ₂	42.22	47.32	48.44	46.85	47.42	48.13	48.77	48.68	47.13	54.81	45.89	48.54
TiO ₂	4.11	2.34	2.55	2.36	3.00	.93	1.40	2.10	4.23	2.03	2.38	2.74
Al ₂ O ₃	13.49	20.03	18.80	19.58	13.72	17.76	22.63	22.07	13.01	14.38	9.99	13.67
Fe ₂ O ₃	18.45	10.84	10.63	10.57	13.68	9.15	7.00	9.10	16.41	12.90	16.02	14.21
MnO	.19	.14	.15	.14	.19	.13	.09	.11	.27	.29	.26	.23
MgO	6.68	3.89	4.07	4.25	7.02	8.80	3.60	2.93	4.93	2.40	14.52	7.22
CaO	13.37	12.54	12.05	12.91	12.32	13.06	13.38	12.15	8.91	6.16	9.37	10.05
Na ₂ O	1.72	2.75	2.66	2.28	2.26	2.10	2.55	2.93	3.16	4.62	1.03	2.78
K ₂ O	.18	.42	.57	.32	.50	.27	.45	.43	.87	1.72	.69	.85
P ₂ O ₅	.02	.20	.15	.14	.13	.06	.13	.18	.89	.92	.17	.32
total	100.43	100.47	100.07	99.40	100.24	100.39	100.00	100.68	99.81	100.23	100.32	100.61
Mg#	41.9	41.5	43.1	44.3	50.4	65.5	50.4	38.9	37.3	26.9	64.2	50.1
Cs	-	-	-	-	0.2	0.7	-	0.1	0.2	0.4	0.9	1.3
Rb	3.6	6.4	10.5	4.2	11.4	19.9	9.1	7.6	5.0	45.5	-	-
Sr	404	466	471	466	343	351	482	497	424	320	228	334
Ba	45	113	118	82	96	169	92	109	73	320	89	165
Sc	49.9	27.2	27.9	28.3	44.9	27.8	20.5	22.2	35.1	20.7	35.2	35.6
V	617	354	252	303	360	259	117	121	134	18	191	299
Cr	14.1	22.8	51.3	55.2	157.2	4	54.9	5	270	4	304	84.3
Co	72.4	44.8	33.6	35.2	52.0	34.3	26.8	33.1	52.0	10.6	82.7	54.3
Ni	39	37	32	53	47	164	36	37	20	0	327	106
Zn	74.8	68.8	72.7	60.5	83.9	60	40.9	51	146	126	136	159
Ga	23.1	23.0	23.9	24.2	21.2	19.0	23.8	25.4	23.7	27.4	-	-
Y	11.6	20.9	23.1	19.2	24.7	46.2	12.8	17.3	11.4	56.4	-	-
Zr	34	86	116	83	99	170	71	75	58	290	100	185
Nb	2.3	10.9	8.8	9.4	9.4	21.0	5.7	7.2	3.8	28.5	10.1	18.8
Hf	1.2	3.0	3.0	2.4	3.1	4.1	2.0	2.2	1.8	8.6	2.7	5.0
Ta	.20	.81	.72	.68	.79	1.24	.44	.59	.29	1.88	.64	1.18
Th	.2	1.0	.9	.5	.8	1.2	.8	.6	.4	3.5	.4	1.2
La	2.46	10.8	10.53	7.34	9.55	19.56	7.58	8.82	6.21	34.05	9.10	17.9
Ce	7.2	26.5	26.1	18.2	25.9	52.9	17.0	22.5	15.2	89.6	24.0	46.0
Nd	5.9	15.2	16.0	12.0	16.8	35.0	10.0	13.3	9.2	54.6	16.2	28.0
Sm	2.01	4.16	4.28	3.31	4.58	8.73	2.61	3.36	2.59	12.96	4.02	7.21
Eu	.97	1.66	1.76	1.43	1.52	3.32	1.30	1.52	1.04	4.63	1.58	2.40
Tb	.4	.7	.8	.6	.9	1.5	.5	.6	.4	1.9	.7	1.13
Yb	.95	1.66	1.82	1.42	1.92	3.11	1.17	1.40	1.11	4.69	1.74	2.98
Lu	.14	.24	.26	.22	.30	.45	.16	.21	.16	.65	.28	.44

HVALNESFJALL GABBRO, continued

Sample	gb-22 D-12	gb-26 D-13	gb-27 A-22	gb-25 A-28	gb-21 A-36	gb-43 T-13	gb-82 T-57	gb-37 T-60	gb-35 T-63	gb-81 HN-22	gb-38 H-52	gb-39 821-A	gb-33 AU-5
SiO ₂	45.86	48.70	47.07	45.48	49.94	46.20	47.49	50.16	48.25	47.40	50.35	49.35	50.24
TiO ₂	2.78	2.34	2.57	3.14	1.54	3.05	3.66	2.20	2.93	2.44	2.22	2.17	1.31
Al ₂ O ₃	17.27	18.98	18.63	16.74	22.87	14.35	13.28	18.00	13.57	16.39	17.89	17.38	20.55
Fe ₂ O ₃	13.09	10.92	10.74	14.62	6.71	15.36	15.40	10.28	14.39	12.33	10.84	11.27	7.56
MnO	.16	.15	.14	.17	.10	.19	.26	.18	.23	.10	.16	.19	.11
MgO	5.35	3.72	3.48	4.84	3.39	6.69	4.69	4.04	6.71	6.59	4.28	5.31	4.94
CaO	13.60	11.86	12.91	12.28	13.07	11.70	9.28	10.61	10.58	10.91	10.79	11.71	12.59
Na ₂ O	2.16	3.37	2.17	2.25	2.43	2.43	3.62	3.52	2.54	2.80	2.90	2.41	2.23
K ₂ O	.25	.69	.30	.46	.53	.52	.97	1.05	.72	.89	.77	.43	.57
P ₂ O ₅	.09	.27	.04	.10	.14	.21	1.00	.29	.28	.26	.29	.21	.09
total	100.61	101.00	100.05	100.08	100.72	100.70	99.65	100.33	100.20	100.20	100.49	100.43	100.19
Mg#	44.7	40.2	50.2	39.6	50.0	46.3	37.6	43.7	48.0	51.4	43.9	48.2	56.4

AUSTURHORN MAFIC DIKES, continued

Sample	d-47 K-29	d-5 A-11	d-48 T-46	d-22 H-28	d-6 A-16	db-21 D-63b	d-2 A-5	d-3 A-7	d-21 T-23
SiO ₂	50.51	49.12	50.95	39.96	51.78	50.98	49.41	46.54	47.96
TiO ₂	3.24	3.00	3.22	5.11	1.84	2.34	2.68	2.95	3.22
Al ₂ O ₃	13.42	15.91	13.41	14.16	18.32	17.47	15.61	16.47	14.46
Fe ₂ O ₃	14.76	13.93	14.57	23.30	9.48	10.85	14.25	16.47	14.62
MnO	.28	.21	.27	.22	.14	.16	.29	14.44	14.62
MgO	4.14	4.46	4.02	4.37	4.28	4.04	4.26	.19	.26
CaO	8.06	9.18	8.36	10.13	10.23	10.47	8.03	7.24	5.20
Na ₂ O	3.52	3.01	3.02	2.67	2.69	2.88	3.36	9.27	9.07
K ₂ O	1.36	.92	1.33	.13	.70	.80	1.02	2.33	3.99
P ₂ O ₅	.73	.38	.74	.25	.25	.26	1.39	.58	1.02
total	100.02	100.12	99.89	100.30	99.71	100.25	100.33	100.34	100.12
Mg#	35.7	38.8	35.3	27.1	47.2	42.5	37.2	49.8	41.3

ALFATAFIJORDUR LAVA						PEGMATOIDAL POCKETS		
Sample	db-41 K-50a	db-42 K-35	db-61 K-8	Sample	peg-1 HN-2	peg-2 HN-4	peg-3 A-33	
KY-1	48.17	47.43	51.41	SiO ₂	53.66	53.22	46.05	
	2.57	2.78	3.20	TiO ₂	2.34	3.94	2.03	
	15.43	15.06	14.27	Al ₂ O ₃	14.10	13.75	18.98	
	14.80	13.48	13.51	Fe ₂ O ₃	12.93	12.01	11.41	
	.25	.20	.21	MnO	.20	.24	.14	
	5.50	5.73	4.14	MgO	3.08	3.56	5.64	
	9.66	10.19	8.34	CaO	6.59	6.75	13.87	
	3.00	2.44	3.67	Na ₂ O	4.95	3.98	2.12	
	.54	.60	.97	K ₂ O	1.02	2.28	.20	
	.27	.32	.47	P ₂ O ₅	1.31	.47	.05	
total	100.19	100.10	100.14	total	100.18	100.20	100.49	
Mg#	42.4	49.6	37.8	Mg#	32.0	37.0	49.4	
Cs	-	0.4	-	Cs	1.4	0.3	-	
Rb	8.4	27.9	20.0	Rb	23.2	41.1	3.1	
Sr	330	372	352	Sr	473	379	443	
Ba	173	-	252	Ba	273	497	63	
Sc	36.0	35.0	-	Sc	17.6	24.0	35.7	
V	394	-	306	V	48	155	371	
Cr	41.4	149.0	-	Cr	3	4	189	
Co	49.2	49.0	-	Co	23.9	31.0	48.7	
Ni	40	-	-	Ni	12	15	76	
Zn	125	-	129	Zn	126	79	59	
Ga	22.5	21.1	25.2	Ga	25.1	25.1	23.0	
Y	30.5	28.9	44.3	Y	48.9	52.2	11.5	
Zr	154	-	203	Zr	344	122	38	
Nb	16.5	-	26.7	Nb	15.7	48.5	3.2	
Hf	3.6	4.0	-	Hf	10.3	4.9	1.1	
Ta	.93	1.03	-	Ta	1.29	3.02	.18	
Th	1.2	.9	-	Th	3.6	3.1	.2	
La	15.14	14.44	-	La	28.4	34.8	4.0	
Ce	40.2	40.7	-	Ce	78.3	86.0	10.0	
Nd	22.6	24.4	-	Nd	50.1	48.9	8.3	
Sm	6.14	6.22	-	Sm	7.63	11.90	2.18	
Eu	2.07	2.15	-	Eu	4.97	3.10	1.14	
Tb	1.1	1.0	-	Tb	1.8	1.8	.4	
Yb	2.57	2.37	-	Yb	3.80	4.34	.94	
Lu	.40	.35	-	Lu	.54	.64	.14	

dissolved for isotopic analysis. These data (table 4.2) will be discussed in detail in Hanan et al (in preparation).

4.3 Mineral Chemistry

Representative minerals were analyzed by electron microprobe in several samples from each major rock type. Samples were selected from throughout the complex (figure 4.2) and cover the observed range in bulk chemistry (table 4.1). Mineral data are given in Appendix III and discussed by rock type below. Reported Kds are mineral/whole rock and thus may not reflect true crystal-liquid partitioning. All calculated exchange coefficients assume total iron as FeO. Additional sampling and petrographic details are found in chapter 3.

4.3.1 Olivine

Groundmass and sparse olivine phenocrysts (<2 vol%, <1 mm) are found in most mafic pillows, but are generally pseudomorphed by calcite, clays and opaques. A fresh olivine phenocryst in sample p-63a is zoned from Fo₇₅ to Fo₅₇ at its outermost margin; the core analysis indicates a crystal/bulk rock Fe-Mg exchange coefficient of 0.30, suggesting equilibrium partitioning of these elements (Roedder & Emslie, 1970). One dike (sample d-1) contains ~5 vol% olivine phenocrysts that have been replaced by alteration minerals.

Several layers within Hvalnesfjall gabbro contain abundant olivine, but most crystals are altered to iddingsite. Two samples, gb-32 and gb-42, have fresh olivine phenocrysts up to 5 mm across enclosed by augite oikocrysts. Individual olivines are unzoned, and range from Fo₆₄₋₇₆ in gb-42 and Fo₆₆₋₇₆ in gb-32 (figure 4.3a). Olivines within each sample have uniform CaO contents, but the two samples have distinct CaO ranges (gb-42 = 0.04-0.06; gb-32 = 0.11-0.25). Low calcium in the gb-42

Table 4.2 Pb Isotopes in Austurhorn Samples

Sample	$^{206}\text{Pb}/^{204}\text{Pb}$	$^{207}\text{Pb}/^{204}\text{Pb}$	$^{208}\text{Pb}/^{204}\text{Pb}$
f-61	18.61	15.51	38.26
g-83	18.49	15.50	38.21
"	18.51	15.51	38.26
gb-34	18.41	15.48	38.13
d-81	18.45	15.49	38.13
p-65	18.37	15.47	38.02

(B. Hanan, personal communication, 1988)

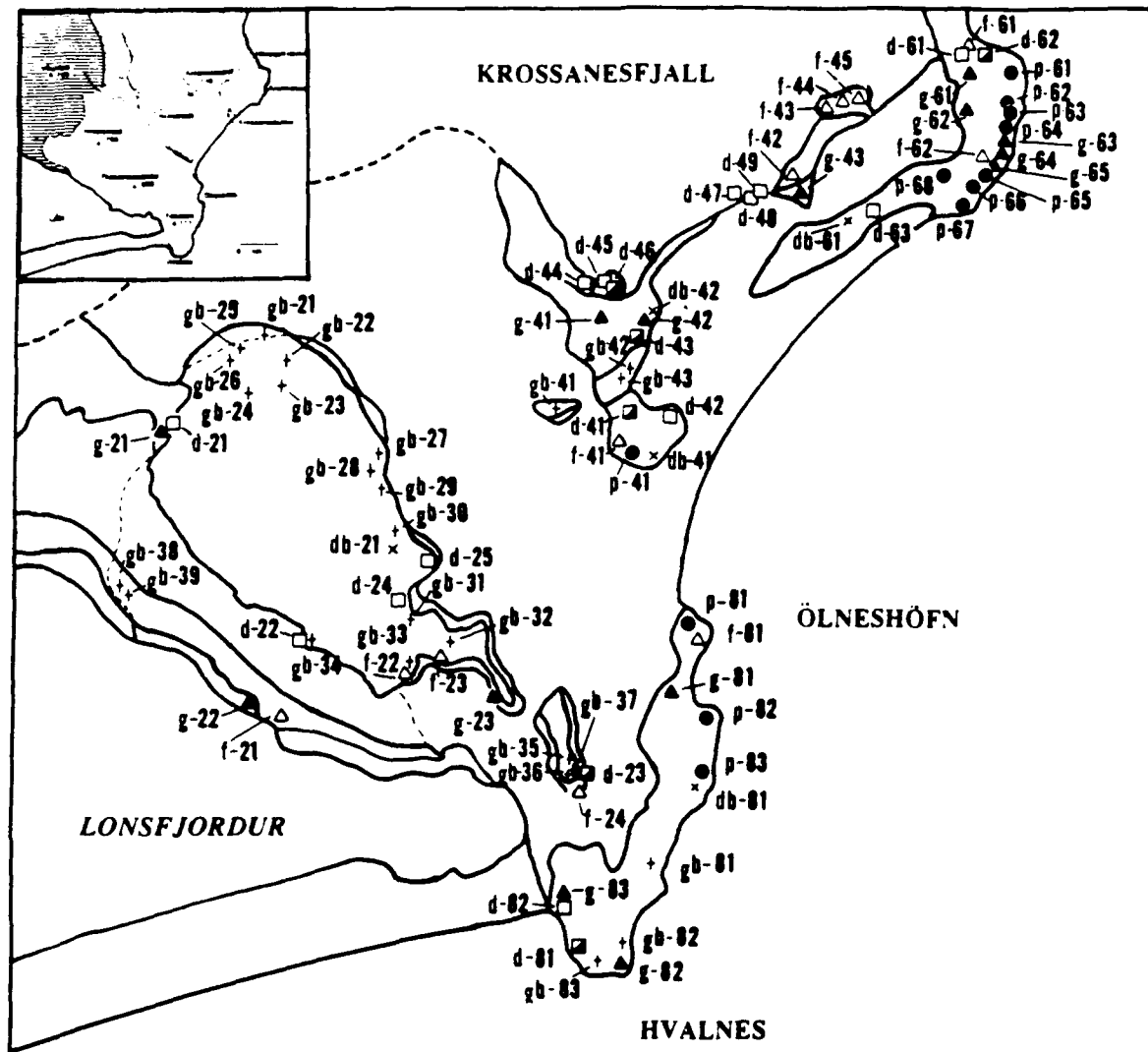


Figure 4.2 Sample locality map for rocks referred to in this text. Heavy lines denote borders of geologic units as shown in previous figure. Samples are **lettered** and **symboled** by rock type and **numbered** by area. Thus granophyre **g-83** is located near gabbro **gb-82**. Symbols on this map are used throughout the paper: cross with **gb** prefix = gabbro; solid triangle with **g** prefix = granophyre; open triangle with **f** prefix = felsic dike; solid circle with **p** prefix = pillow; open square with **d** prefix = mafic dike; half-filled square with **d** prefix (if shown) = alkalic dike; x with **db** prefix = diabase. Sample numbers with single digits (d-1 through d-7, f-1, g-1) were sampled along Vikurfjall to the northwest of the region of this figure and are not indicated.

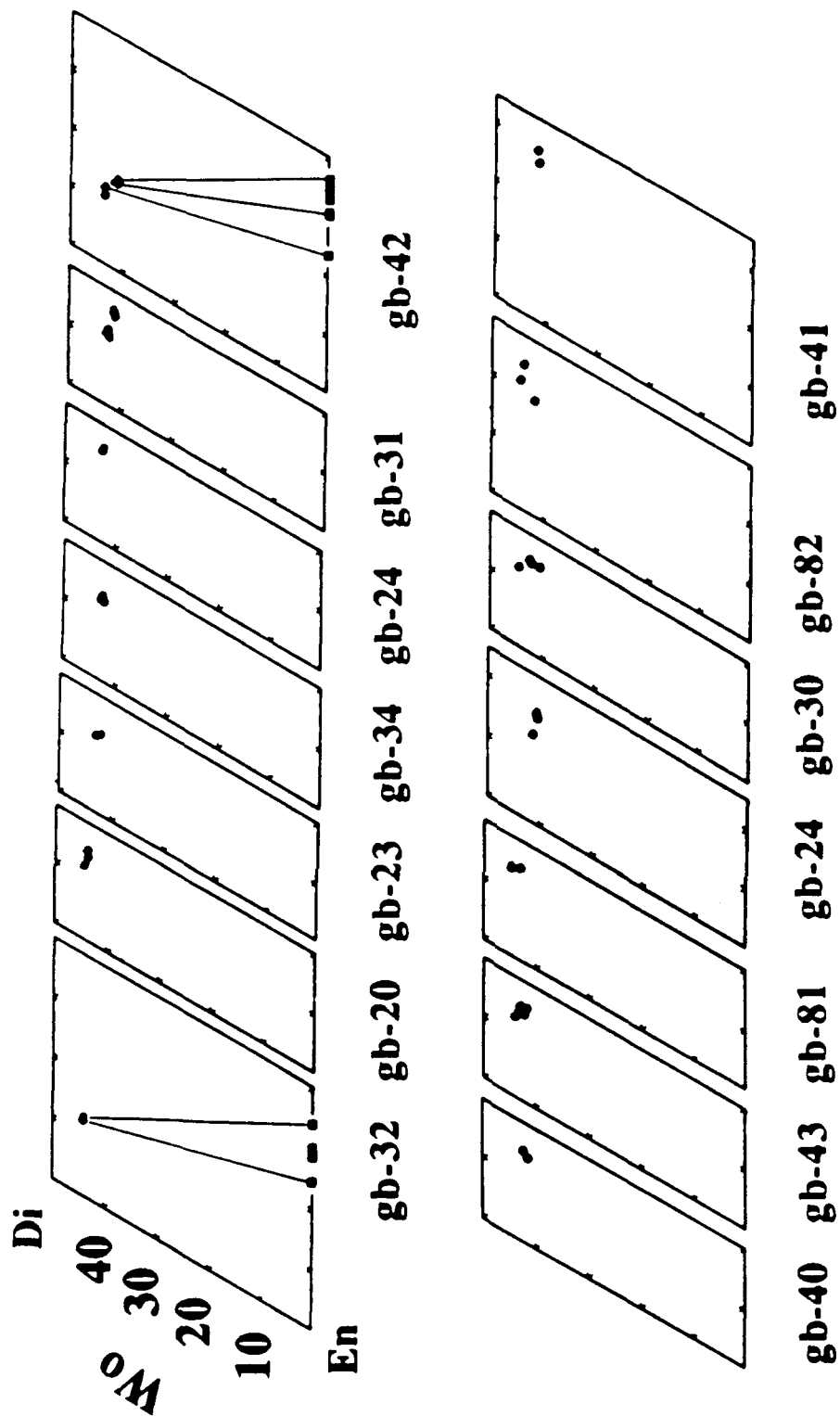


Figure 4.3a Clinopyroxene and olivine compositions for Austurhorn gabbro samples

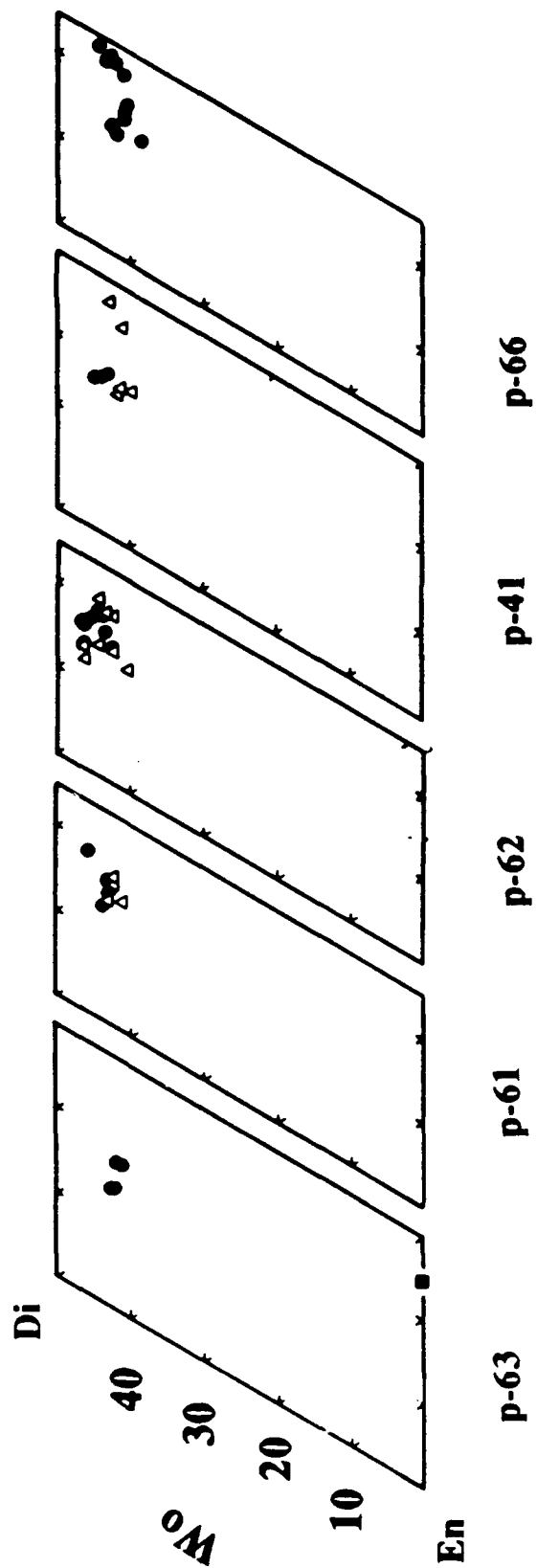


Figure 4.3b Clinopyroxene and olivine compositions for Austurhorn mafic pillow samples. Where two samples are plotted together, filled circles represent analyses from pillow margins, open triangles represent analyses from pillow interiors.

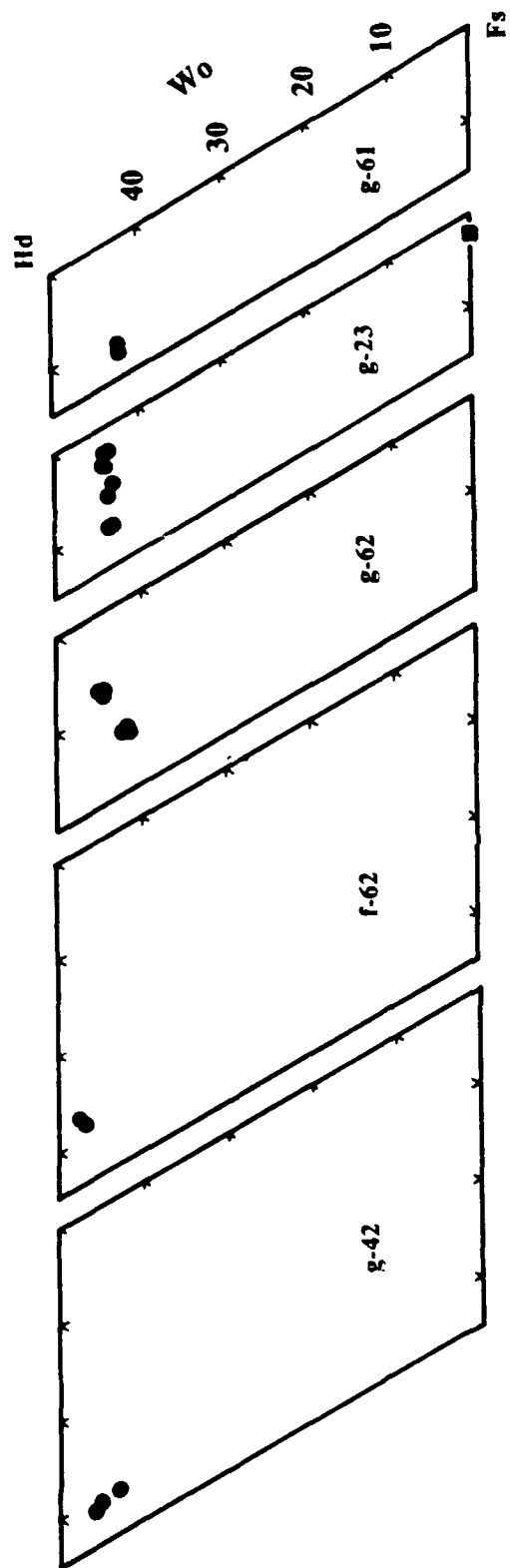


Figure 4.3c Clinopyroxene and olivine compositions for Austurhorn felsic samples.

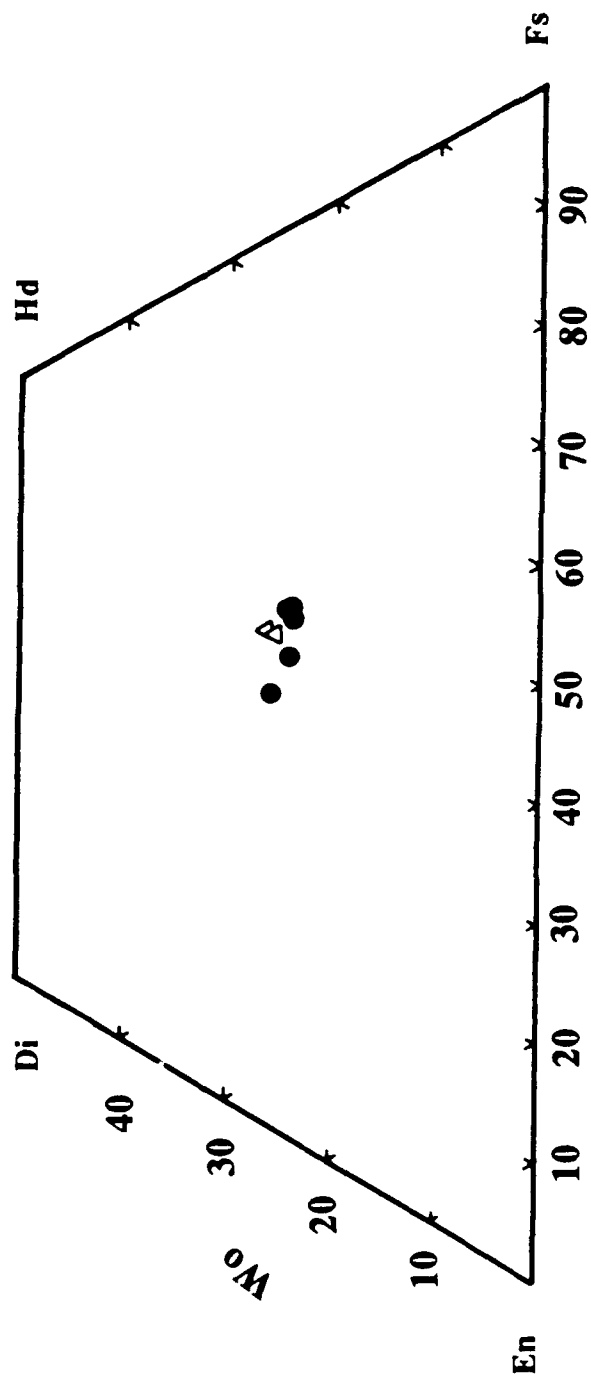


Figure 4.3d Amphibole compositions in lieu of clinopyroxene in Austurhorn granodiorites. Filled circles are from sample g-43, open triangles from g-65.

olivines probably reflects subsolidus re-equilibration within this sample (Jurewicz & Watson, 1988).

Only one felsic sample (iron-rich granophyre g-23) contains fresh olivine (Fo_{20}). Magnetite (usp 32.80) and quartz occur in the same thin section, suggesting crystallization at oxygen fugacity near the QFM buffer. The Fe-Mg exchange coefficient for this sample is 2.4 ± 0.3 , based on replicate analyses of bulk sample and crystal. The olivine is MnO-rich (3.2 wt%) and yields a combined Fe-(Mg+Mn) exchange coefficient of 1.3 ± 0.3 . Comparable combined exchange coefficients are found for fayalitic olivines ($\text{Fo}_{<3}$) in comendites from Torfajökull ($K_d = 0.9\text{--}1.0$; MnO in olivine = 3.4–4.0; Ivarsson et al., in press) and rhyolites from Sierra la Primavera, Mexico ($K_d = 1.2\text{--}1.3$; MnO in olivine = 3.5–3.7; Mahood, 1981). These data suggest that divalent manganese is an essential structural component of olivine in highly evolved iron-rich systems. Ferric iron was not determined in the Austurhorn fayalite or whole rock, so its effect on the calculated K_d cannot be assessed directly. However, Mossbauer spectroscopic analyses of "Fe-deficient" fayalite (nomenclature of Mahood, 1981) from Sierra la Primavera (Mexico), Pantelleria and St. Peter's Dome (Colorado) indicate abundant ferric iron (Schaefer, 1983), suggesting the Austurhorn sample may also be ferrifayalitic. No other olivines more iron-rich than Fo_{57} were analyzed at Austurhorn.

4.3.2 Clinopyroxene

With the exception of augites in dikes d-29 and d-81, the Austurhorn clinopyroxenes define an alkaline trend at constant Wo content (figure 4.4) similar to that of the Kiglapait intrusion (Morse, 1969, 1979). In this important respect Austurhorn is clearly different from the tholeiitic Thingmuli suite despite gross similarities in their bulk chemical makeup (figure 4.4).

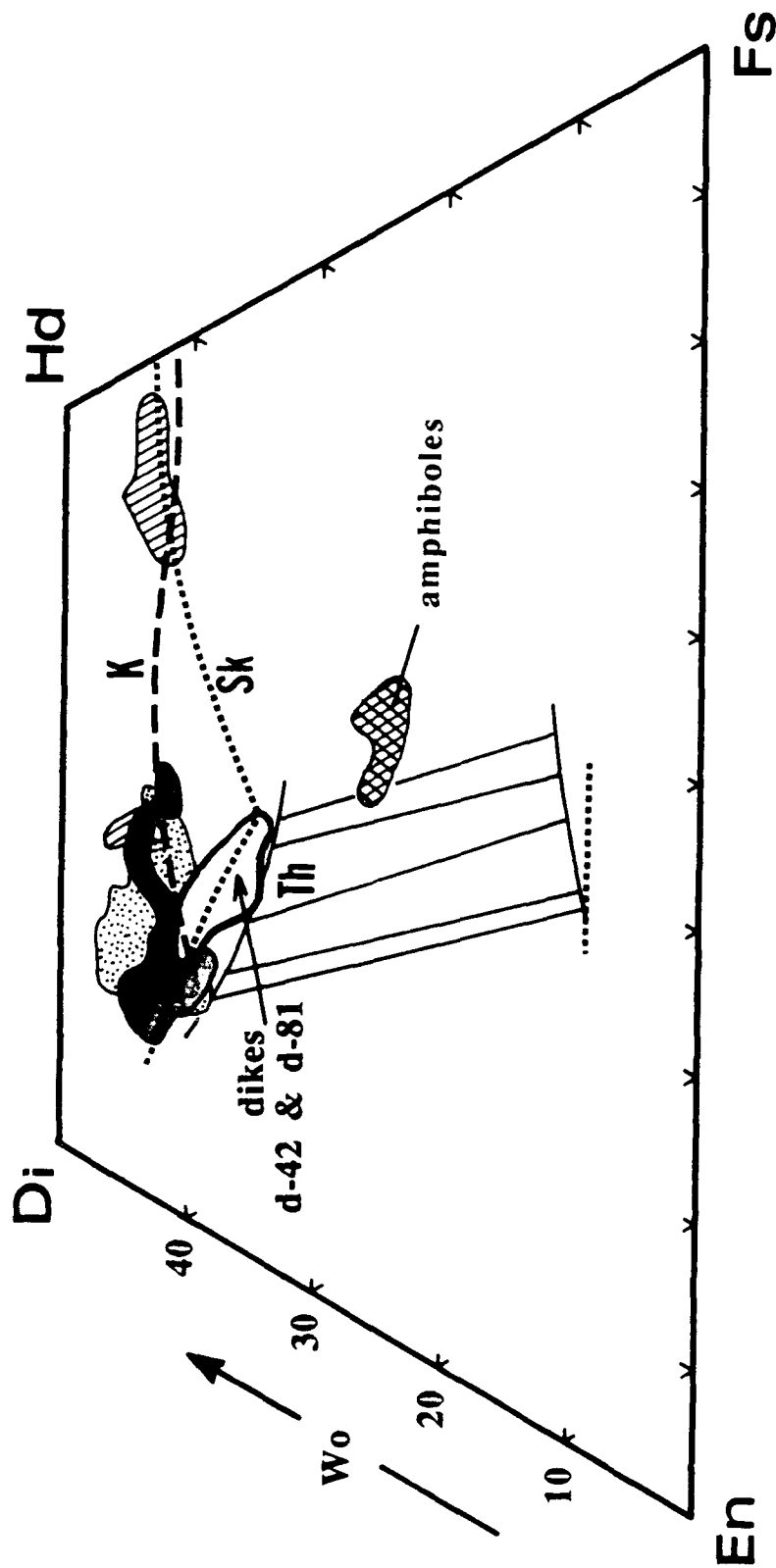


Figure 4.4 Composite diagram of Austurhorn clinopyroxene data. Stippled region indicates mafic pillow samples, shaded region is gabbro samples, and diagonally striped area is felsic samples. Open field is data from dikes d-81 and d-42. Also shown for comparison are the trends of Skaergaard clinopyroxenes and pigeonites (dotted curves labeled Sk; Wager & Brown, 1968), Thingmuli augites and pigeonites (solid curves labeled Th, with tie-lines connecting analyses from the same sample; Carmichael, 1967), and clinopyroxenes from the mildly alkaline Kiglapait intrusion (K; Morse, 1980). Note that the Austurhorn gabbro and pillow samples define a trend similar to that of the Kiglapait intrusion, while the two dikes are more similar to the tholeiitic Skaergaard suite. The ruled field in the center of the quadrilateral encompasses amphibole analyses from Austurhorn granodiorites.

Augite occurs as both a phenocryst and a groundmass phase in the mafic pillows, although groundmass augites are commonly altered to amphibole. Glomerocrysts of augite + plagioclase +/- FeTi oxide are found in most mafic pillows. In the mafic dikes, phenocryst augite is usually restricted to glomerocrysts with plagioclase. Augite in mafic pillows is often sector zoned and sometimes normally zoned to more iron-rich rims as well. The total compositional range observed in the pillows is $Wo_{39}En_{45}Fs_{16}$ - $Wo_{43}En_{30}Fs_{27}$ (figures 4.3b, 4.4). Cores of augite in mafic pillow interiors yield crystal/whole rock Fe-Mg exchange coefficients of $K_d = 0.22$ - 0.29 , comparable to those determined experimentally at 1 atm in normal MORB (0.23-0.25; Grove & Bryan, 1983; Tormey et al., 1987). Calculated crystal/whole rock K_d s for augites in the pillow margins are significantly higher (0.35-0.51), suggesting growth under disequilibrium conditions.

Gabbroic augites are typically unzoned and have a compositional range comparable to that observed in the pillows ($Wo_{42}En_{46}Fs_{12}$ - $Wo_{41}En_{29}Fs_{30}$), but within-sample variability is far lower (figure 4.3). Abundances of Al_2O_3 and TiO_2 are typically lower in gabbroic pyroxenes than in either sector of pillow pyroxenes (at comparable clinopyroxene Mg#; Appendix III). In samples with heterogeneous augite populations (gb-24, gb-82) the more magnesian grains have higher concentrations of Al_2O_3 and TiO_2 .

Phenocryst and groundmass clinopyroxenes in two evolved mafic dikes (d-29 and d-81) are strikingly dissimilar to augites analyzed in mafic pillows and gabbros: they are of tholeiitic affinity (figure 4.4). Calculated Fe-Mg K_d s for groundmass augites in these dikes are comparable to those of other Austurhorn samples (0.23-0.29), whereas phenocrysts in dike d-81 are complexly zoned between $Wo_{39}En_{38}Fs_{23}$ - $Wo_{33}En_{46}Fs_{21}$ and yield higher K_d s (0.32-0.34). The tholeiitic character of d-81 augites is particularly significant because this dike has elevated bulk alkali contents relative to most Austurhorn transitional tholeiites.

The iron-rich granodiorites have primary clinopyroxene with rosetta morphology (up to 8 mm). These crystals are zoned at their margins to more Fe-rich compositions similar to those of groundmass pyroxenes ($\text{Wo}_{42}\text{En}_{14}\text{Fs}_{44}$ - $\text{Wo}_{44}\text{En}_3\text{Fs}_{53}$; figure 4.3c). They are slightly lower in Na_2O and significantly higher in MnO than either gabbroic or pillow pyroxenes. Calculated Fe-Mg exchange coefficients between these pyroxenes and their host rock are $K_d = 0.19$ - 0.23 . These values are consistent with Fe-Mg exchange coefficients determined by Juster & Grove (1988) in silicic liquids (~65 wt% SiO_2) derived experimentally by crystallization of Galapagos basalts at 1 atm. Crecraft et al (1981) also observed Fe-Mg exchange coefficients of 0.24-0.26 in natural rhyolites (71 wt% SiO_2) from Twin Peaks, Utah. Clinopyroxenes in highly evolved samples (f-62, g-42; 71-72 wt% SiO_2) may not be primary igneous minerals, as they appear far too magnesian to record equilibrium Fe-Mg partitioning ($K_d \sim 0.05$); however, they are not embayed as expected of xenocrysts. These clinopyroxenes are almost always in contact with euhedral iron oxides and they are also low in TiO_2 , suggesting late-stage subsolidus re-equilibration. An anomalously low Fe-Mg exchange coefficient (0.08) is also found for clinopyroxene in a rhyolite (76 wt% SiO_2) from Twin Peaks, Utah (Crecraft et al., 1981). No petrographic details were presented for this sample. It is interesting to note that Fe-Mg K_d s for augite are slightly lower in evolved samples relative to basalts, whereas Fe-Mg K_d s for olivine are significantly higher. This difference may indicate the incorporation of ferric iron into evolved olivines (i.e., ferrifayalite; see chapter 3) but not into evolved clinopyroxenes.

4.3.3 Low-Ca Pyroxene

Fresh orthopyroxene has not been observed at Austurhorn. Sparse chlorite + clay pseudomorphs are tentatively identified as hypersthene in Hvalnesfjall gabbro (Blake, 1966; chapter 3), although intercumulus hypersthene is abundant in the rhythmically layered gabbro at Vesturhorn (Roobol, 1974). Neither pigeonite nor orthopyroxene are

observed in the mafic dikes or pillows. A similar mineralogy occurs in the mildly alkaline Kiglapait intrusion, where hypersthene is present in only minor amounts and a continuum of olivine and augite compositions are observed (Morse, 1969, 1979). These data suggest that olivine + augite remain the stable crystallizing phases in silica-undersaturated systems, rather than yielding to low-Ca pyroxene as observed in tholeiitic suites (e.g., Skaergaard, figure 4.4) (Morse, 1980). Definitive petrologic support for this hypothesis is lacking at Austurhorn, where a complete spectrum of olivine and augite have not been analyzed. However, the similarity in augite evolution trends for Austurhorn and Kiglapait indicates that the absence of low-Ca pyroxene at Austurhorn is real, and results from the alkaline nature of the crystallizing liquids.

4.3.4 Amphibole

Hornblende often occurs as patchy intergrowths with phenocryst augite in mafic pillows, where it records high temperature hydration. Anhedral and locally ophitic hornblende is also found in the groundmass of primitive and evolved mafic pillows. I suggest these hornblendes reflect addition of water to the basaltic liquids during cooling, followed by recrystallization of hydrated groundmass augite. Amphibole is not more prevalent in evolved pillows or pillow interiors, as would be expected if water were concentrated during differentiation like other incompatible elements. Icelandic basalts (*sensu lato*), including those from Austurhorn, typically contain anhydrous phenocryst phases indicative of low magmatic water contents.

Austurhorn granodiorites contain honey-colored hornblende (<1 mm) as the only ferromagnesian silicate phase (figure 4.3d). Individual crystals are generally euhedral and occasionally have cores of patchy altered clinopyroxene, suggesting that amphibole replaced primary igneous augite during cooling. Euhedral amphiboles also occur in granophyric magmas adjacent to some mafic pillows, where the crystals grow radially away from the co-magmatic interface. This association was observed experimentally

upon heating juxtaposed polished wafers of basalt and rhyolite under hydrous conditions at 2 kbars (T. Sisson, pers. commun.) and must be considered a result of commingling. In the case of the Austurhorn granodiorites, however, amphibole growth does not appear to reflect co-magmatic interaction. The crystals are not preferentially aligned or concentrated, and these felsic magmas are entirely free of mafic inclusions and dikes. Minor subhedral amphibole is present in roughly half of the granophyres. It is frequently associated with euhedral FeTi oxides and may replace clinopyroxene.

4.3.5 Plagioclase Feldspar

Mafic pillows and dikes typically contain <5 vol% blocky crystals up to 1 cm across that are >10 mol% more anorthitic than associated groundmass (swallowtail) plagioclase (figures 4.5, 4.6). The compositional range of large phenocrysts is An_{84-87} , whereas that of quench crystals is An_{54-69} . Large grains are usually zoned to groundmass compositions at their extreme rims and are not embayed. The quench swallowtail plagioclase record crystal/liquid coupled NaSi-CaAl exchange coefficients of 0.85-1.10, similar to those observed and produced experimentally at 1 atm among FeTi-rich Galapagos basalts (Juster & Grove, 1988).

The granophyres contain primarily tabular plagioclase <3 mm long that are normally zoned over their outer 0.2 mm. A continuum of plagioclase compositions is found between An_{37} and An_{16} ; samples with greater than ~70 wt% SiO_2 contain phenocrysts of anorthoclase (figures 4.5b, 4.6). Plagioclase core compositions are usually homogeneous within a sample, although granodiorite g-65 contains ~10 vol% "megacrysts" (10-15 mm) that are more albitic than the abundant phenocrysts (An_{18} vs. An_{25}) and high-silica granophyre g-42 contains sparse anorthitic megacrysts (An_{40} vs. An_{18-26} ; figure 4.5b). Plagioclase/whole rock Kds (coupled NaSi-CaAl exchange) generally increase with increasing silica content, ranging from ~0.9 in granodiorites to >2.0 in highly differentiated samples.

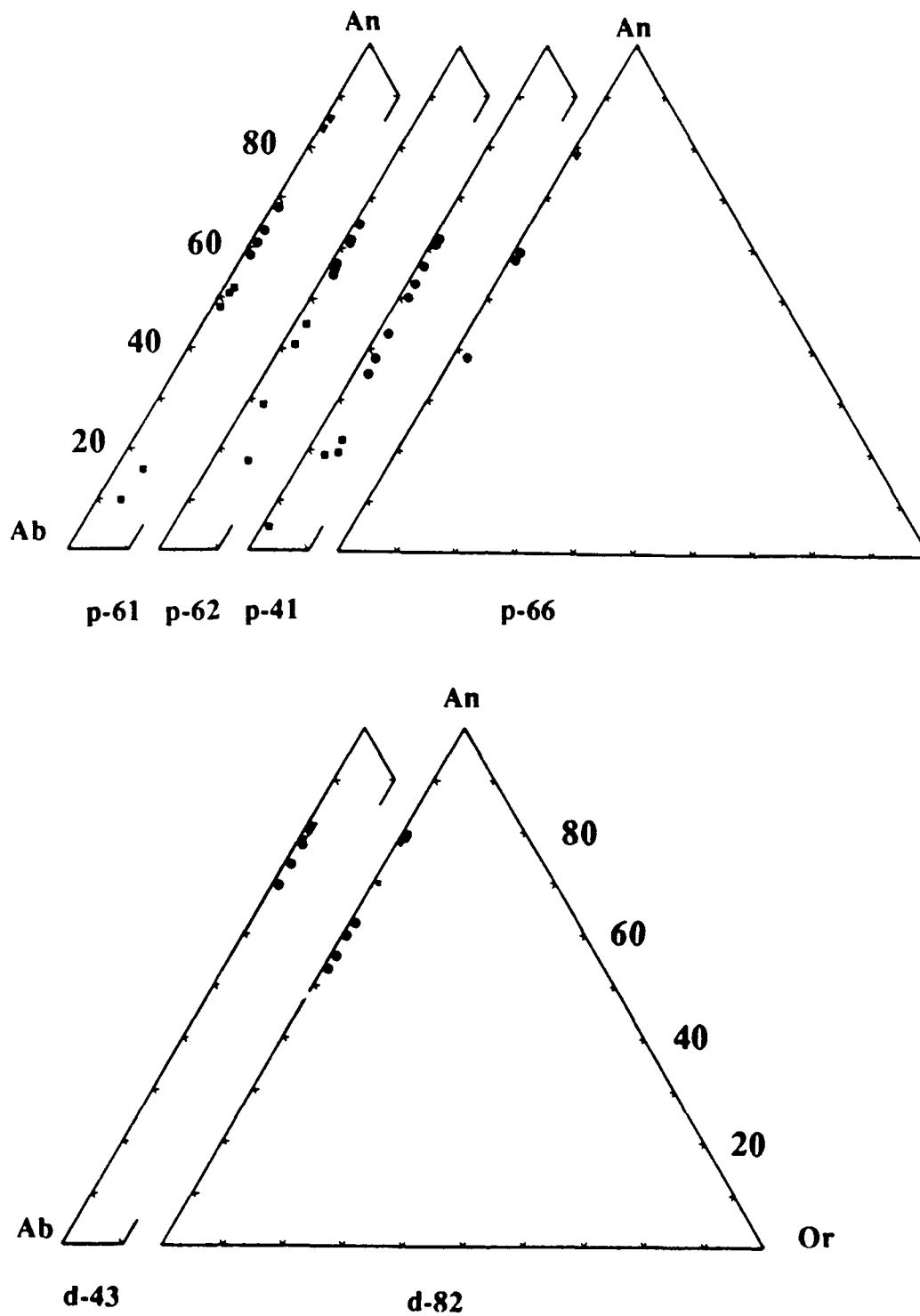


Figure 4.5a Plagioclase in Austurhorn mafic pillows and dikes. Downward-pointing triangles (An₇₅₋₈₇) are large tabular crystals, circles are quench (swallowtail morphology) crystals, and squares indicate zoning.

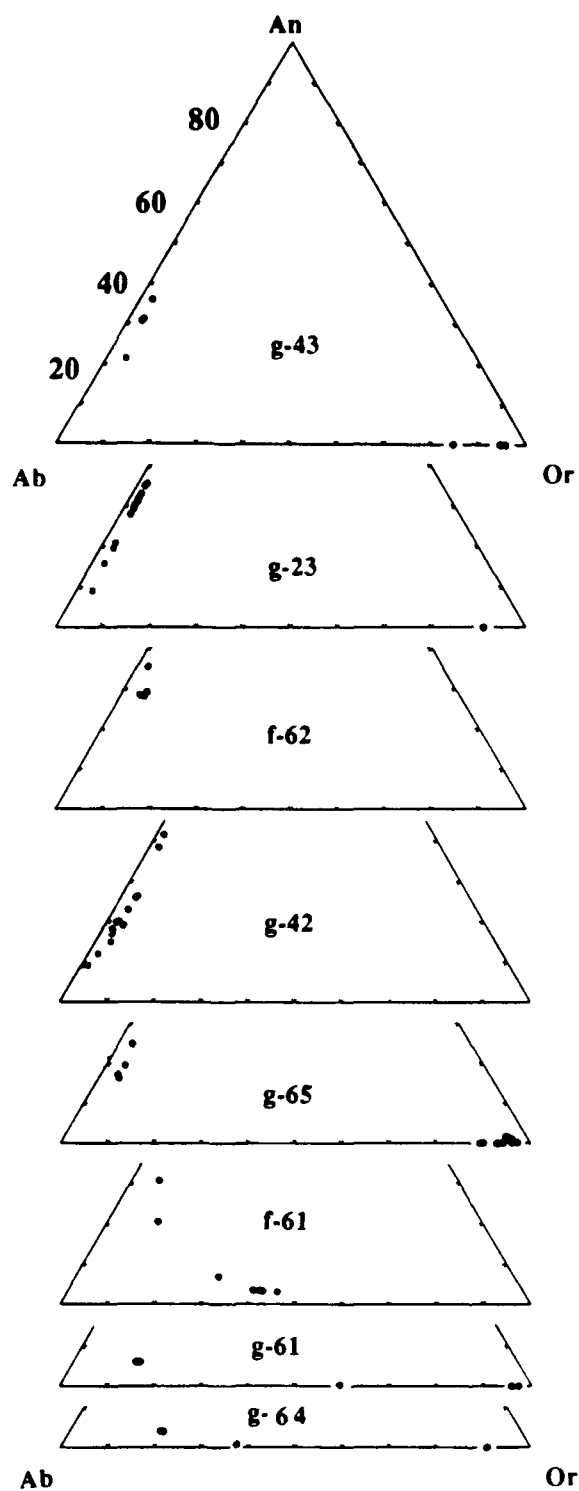


Figure 4.5b Feldspars in Austurhorn felsic samples. Circles are tabular crystals, and squares illustrate the extent of zoning.

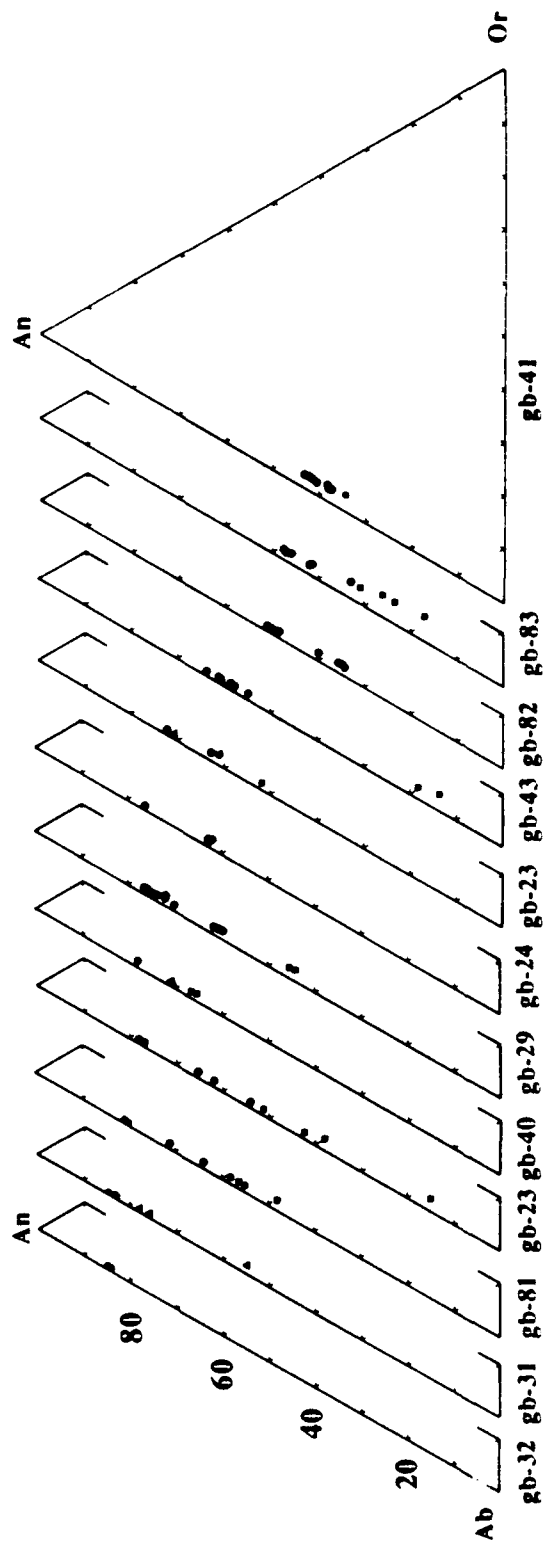


Figure 4.5c Plagioclase in Austurhorn gabbros. Filled circles are blocky and tabular phenocrysts (see figure 4.6b), triangles are inclusions in clinopyroxene, and squares illustrate the extent of zoning.

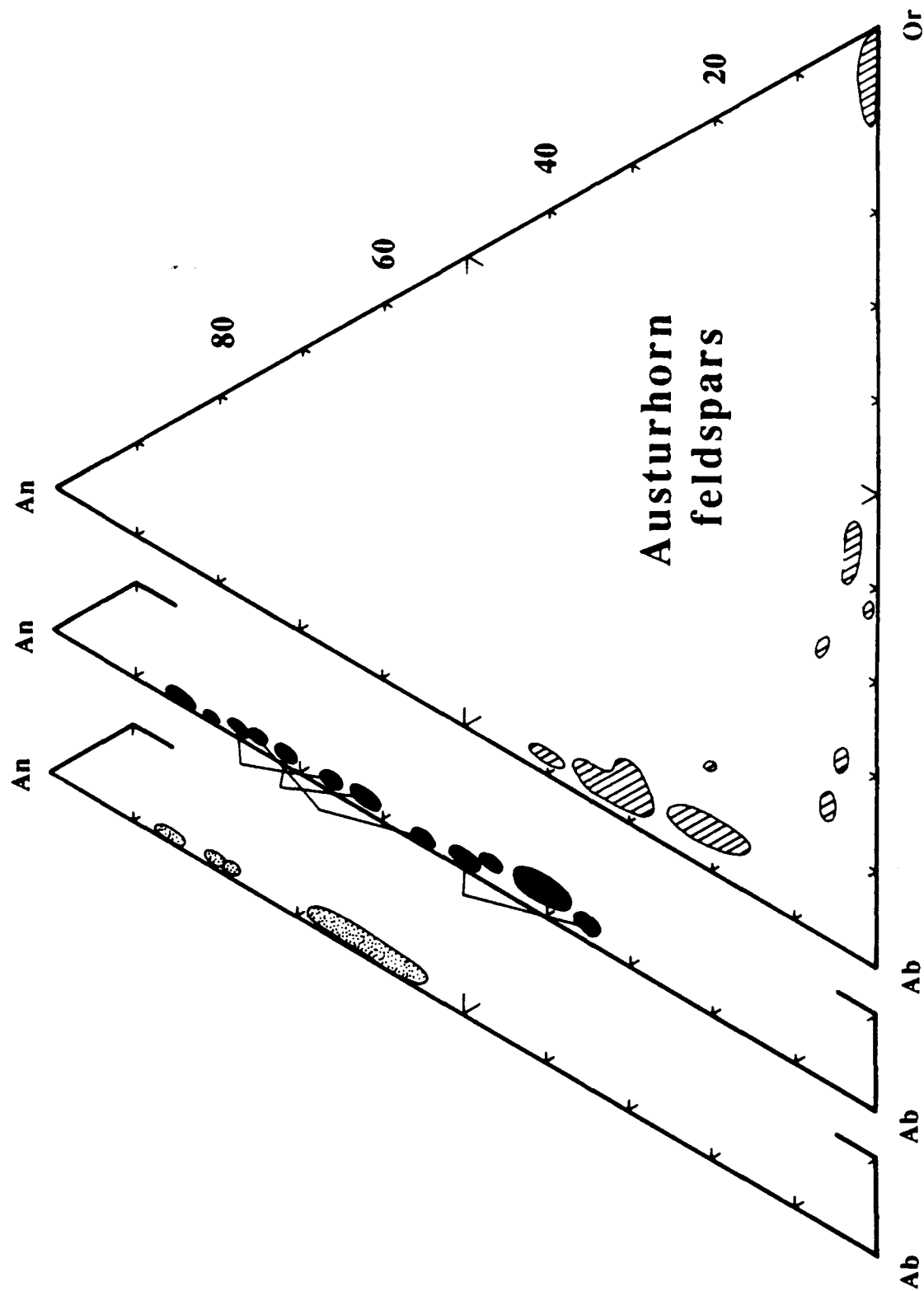


Figure 4.6a Composite diagram of Austurhorn feldspar data. Stippled area is mafic pillow samples (all samples with An >75 have bimodal populations), black regions are gabbro samples, with bimodal populations connected, and diagonally ruled areas are for felsic samples.

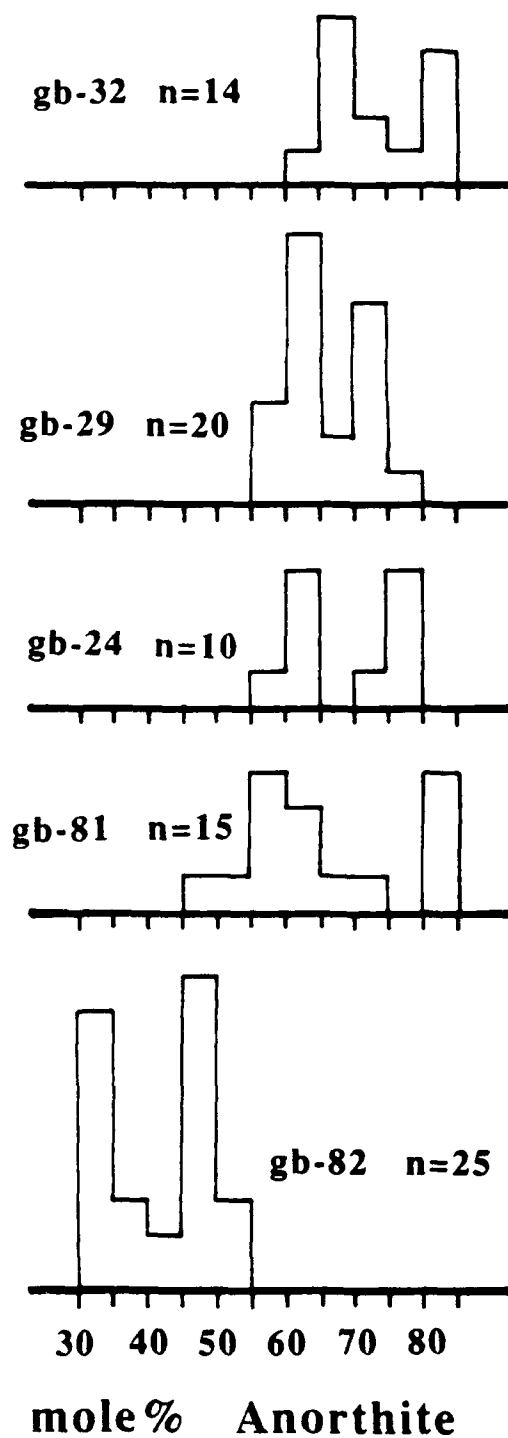


Figure 4.6b Histogram showing bimodal distributions of plagioclase in selected Austurhorn gabbro samples. In each case, the crystals with higher anorthite content are morphologically distinct from those with lower anorthite content, although both groups are zoned to more sodic compositions at their margins.

Gabbros often contain bimodal plagioclase populations (figure 4.5c,d), with blocky calcic crystals and abundant tabular evolved plagioclase. Zoning to highly albitic compositions is restricted to the outermost rims of both populations. Complex oscillatory zoning was observed in samples gb-23, gb-24 and gb-29 but is not widespread in the intrusion as a whole. Gabbroic plagioclases cover the compositional range from An_{66-34} , thus forming a continuum between the mafic liquids and felsic magmas (figure 4.6).

4.3.6 Potassium Feldspar

Austurhorn granophyres contain orthoclase + quartz intergrowths ranging in size from ~1-100 microns. In the NVC, granophyric texture occurs only within 10 cm of co-magmatic interfaces, while in the remainder of the intrusion it is ubiquitous in clast-free units. Many felsic units contain tabular crystals of orthoclase (Or_{89-99}) which are not of primary igneous origin (Stormer, 1975). Primary anorthoclase was analyzed in granophyres g-61 and g-64 and rhyolite f-61 (figure 4.6). Anorthoclase is not found in the tholeiitic suites of eastern Iceland (Carmichael, 1963), but has been reported in mildly alkaline rhyolites from Snaefellsnes, Oraefajokull and the EVZ (Sigurdsson, 1971).

4.3.7 Fe-Ti Oxides

Magnetite (usp 26.6-31.4) and ilmenite (ilm 92.1-92.3) occur as phenocrysts and groundmass phases in the mafic pillows, but are generally restricted to the groundmass of mafic dikes. They appear as both cumulus and intercumulus minerals in the gabbros, where they comprise >20 vol% of individual layers. Manganese-rich ilmenite is common in felsic samples, but the elevated MnO contents (up to 11 wt%) are not primary (Bacon & Hirschmann, 1988).

4.4 Major & Trace Element Geochemistry

4.4.1 Sample Selection and Nomenclature

I analyzed 40 basalts (sparsely phyrlic dikes and pillow margins) and diabases from the Austurhorn complex for major element compositions (see figure 4.2 for sample localities); a subset of 30 was analyzed for trace element abundances. All mafic pillows and most mafic dikes are of transitional tholeiitic affinity. That is, they are richer in alkalis than Reykjanes tholeiites of comparable SiO_2 content and generally plot near the alkalic-tholeiitic division line of Macdonald & Katsura (1964; figure 4.7). Most contain normative olivine + hypersthene, and some have up to 4% normative nepheline (table 4.3). Four samples labeled on figure 4.7 (d-23, d-41, d-44, d-81) have $\text{Na}_2\text{O} + \text{K}_2\text{O} > 6$ wt% and are classified as "alkali-rich" dikes. The distinctive geochemical characteristics of these dikes will be discussed in detail in a subsequent section. In the following discussion, the term "basalt" is used for all samples containing less than 54 wt% SiO_2 and thus includes both hawaiitic and basaltic andesitic compositions. Most basalt dikes have < 2 or > 20 vol% plagioclase crystals. Samples from the latter group are assumed to contain accumulated plagioclase and are not treated as liquids (e.g., samples d-4, d-5, d-61; table 4.1; Appendix III).

From a suite of 28 felsic samples analyzed for major element compositions we selected 12 granophyres and 3 fresh felsic dikes for trace element analysis (table 4.1). Granophyric intergrowths occur in most samples regardless of bulk composition, and we use this term when referring collectively to the felsic units. Three samples are termed granodiorites (g-43, g-63, g-65); they contain 63-66 wt% SiO_2 and 1.0-1.5 wt% MgO. The remaining felsic rocks are granitic or rhyolitic, with up to 76 wt% SiO_2 and < 0.7 wt% MgO. All felsic units contain small fragments of basalt. Mafic inclusions over 5 mm were removed during sample crushing, but smaller fragments may have been missed.

Most Austurhorn felsic rocks are metaluminous (PI 0.74-0.94; peralkalinity index defined as molar $(\text{Na} + \text{K})/\text{Al}$), but four samples are mildly peralkaline (PI 0.99-1.03). Austurhorn felsic magmas have a higher peralkalinity index than those from Hekla (avg. PI 0.63; Sigvaldason, 1974) but are not as alkali-rich as the pantellerites and comendites

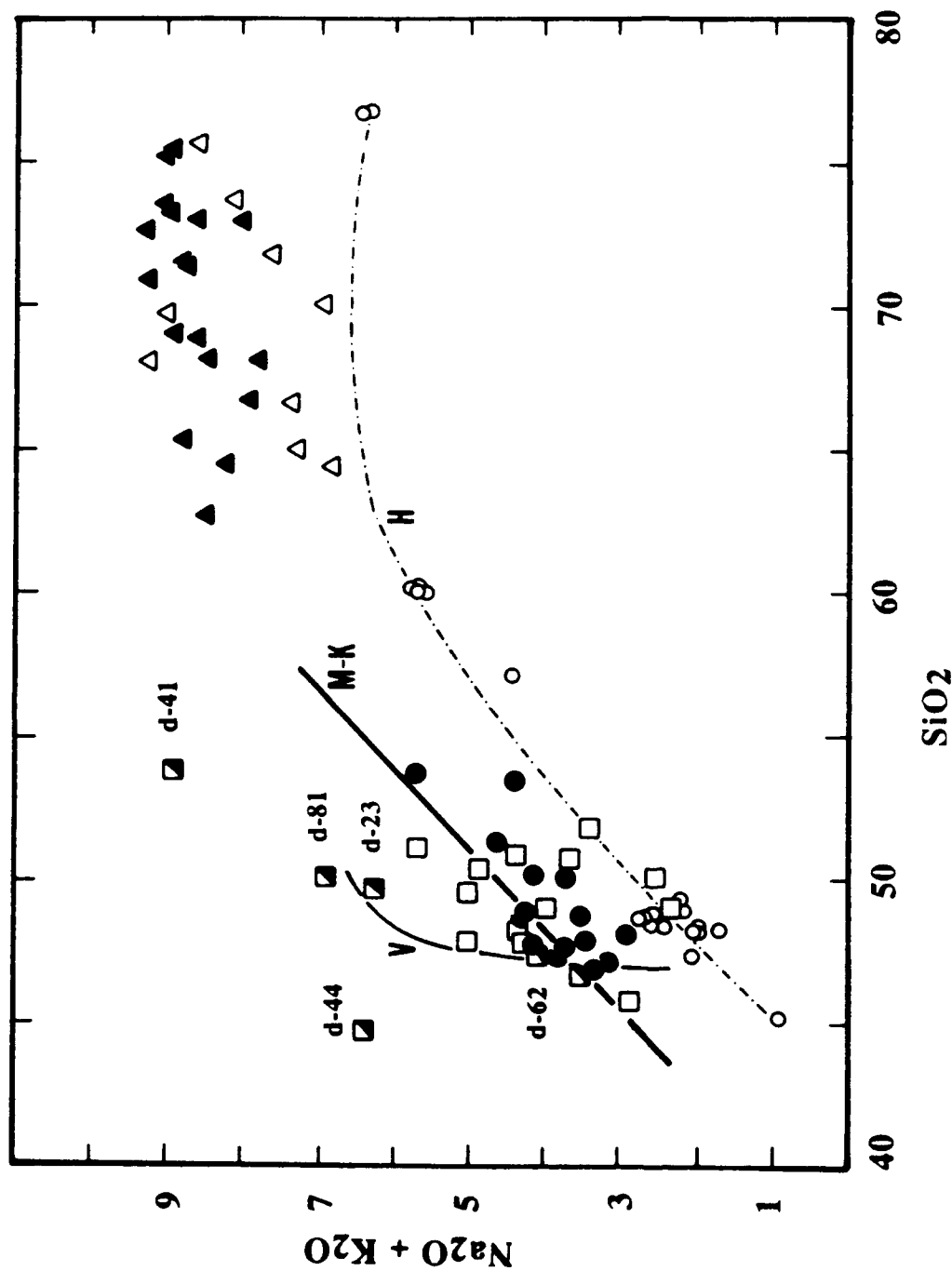


Figure 4.7 Total alkalis vs. silica, with the Macdonald-Katsura (1964) division line for Hawaiian lavas shown as M-K. The trend labeled V is for 22 samples from Vestmannaeyjar (Furman et al., 1988), including alkali basalts through hawaiitic and mugearitic liquids. The trend labeled H connecting open circles is a tholeiitic trend from the Hengill central volcano from the WVZ (Hardardottir, 1983). Symbols for Austurhorn samples: filled circles = mafic pillows, open squares = mafic dikes, filled triangles = granophyres, open triangles = felsic dikes. The half-shaded squares indicate five liquids designated as alkalic on the basis of $(\text{Na}_2\text{O} + \text{K}_2\text{O})$ [samples d-23, d-41, d-44, d-81] and/or $\text{P}_2\text{O}_5/\text{Hf}$ ratios [i.e., sample d-62].

Table 4.3 Normative Mineralogy of Austurhorn Mafic Dikes and Pillows

Sample	Q	Or	Ab	An	Ne	Di	He	En	Fs	Fo	Fa	Il	Ap
d-1	-	3.31	19.63	32.46	-	6.12	6.69	3.44	4.31	7.47	10.32	5.47	0.79
d-2	-	6.09	28.77	24.78	-	2.03	3.28	8.06	14.90	1.21	2.47	5.15	3.28
d-3	-	3.49	19.97	33.09	-	4.81	4.50	5.95	6.39	7.04	8.33	5.66	0.77
d-5	-	5.50	25.81	27.55	-	5.54	8.02	5.47	9.10	2.26	4.13	5.77	0.88
d-6	2.93	4.20	23.02	36.31	-	5.45	5.75	8.26	9.98	-	-	3.53	0.58
d-7	-	5.20	27.08	23.99	-	4.59	6.54	4.74	7.75	3.98	7.17	7.31	1.65
d-21	-	6.09	26.89	18.83	3.95	8.99	11.71	-	-	6.28	10.34	6.19	0.74
d-22	-	0.77	12.33	26.82	5.83	5.67	13.82	-	-	5.94	18.32	9.91	0.60
d-23	-	15.90	28.83	12.70	1.11	6.97	11.40	-	-	4.82	9.97	6.93	1.39
d-24	-	6.50	39.18	15.12	-	5.95	10.46	1.53	3.08	3.30	7.32	5.77	1.81
d-25	-	5.67	25.72	22.02	-	9.95	10.92	6.52	8.20	1.89	2.62	5.72	0.77
d-29	5.41	3.07	17.60	25.53	-	5.91	8.87	9.27	15.94	-	-	7.27	1.16
d-41*	-	11.94	43.99	-	7.14	5.73	13.70	-	-	2.64	7.99	4.14	2.35
d-42	3.73	0.41	18.53	27.73	-	6.61	9.56	9.71	16.10	-	-	6.70	0.93
d-43	-	4.31	21.71	32.63	0.25	9.12	10.22	-	-	6.55	9.28	5.28	0.65
d-44+	-	15.31	33.25	6.93	-	-	-	0.92	5.44	2.97	19.35	6.31	3.77
d-45	-	0.89	18.19	30.81	-	7.53	6.66	14.01	14.21	1.49	1.66	4.08	0.46
d-46	-	1.54	25.98	24.53	-	13.38	11.98	0.26	0.27	8.25	9.33	4.03	0.46
d-47	-	8.16	30.21	17.06	-	5.95	9.85	5.66	10.75	1.44	3.01	6.25	1.72
d-48	1.51	7.98	25.98	19.40	-	5.62	9.45	7.56	14.57	-	-	6.21	1.74
d-62	-	5.67	26.49	19.21	-	7.34	10.74	4.36	7.33	2.95	5.47	7.98	2.49
d-63	-	3.37	22.17	25.36	-	8.85	11.27	4.56	6.66	3.74	6.02	7.16	0.88
d-81	-	9.34	34.57	5.84	6.07	8.78	14.12	-	-	4.18	8.50	6.31	2.32
d-82	-	6.68	29.81	18.97	1.87	10.18	12.86	-	-	5.16	8.24	5.49	0.77
p-41a	-	5.20	27.92	23.46	-	9.29	9.59	4.48	5.31	3.88	5.06	5.03	0.79
p-41b	1.39	9.28	35.37	14.80	-	4.67	7.57	6.88	12.80	-	-	5.45	1.81
p-61a	-	6.56	24.93	24.71	1.58	9.89	10.57	-	-	6.72	9.08	5.11	0.88
p-61b	-	4.08	19.21	34.10	-	8.01	6.97	6.47	6.46	4.56	5.01	4.46	0.70
p-62a	-	4.73	22.76	27.91	-	9.49	9.33	2.83	3.19	6.07	7.55	5.30	0.86
p-62b	-	4.37	25.47	26.57	-	9.06	9.19	6.45	7.52	2.50	3.21	4.86	0.81
p-63a	-	3.55	25.30	24.42	3.21	10.55	10.59	-	-	7.27	9.23	5.09	0.81
p-63b	-	3.96	25.16	24.86	2.59	10.31	10.28	-	-	7.46	9.40	5.15	0.84
p-64	-	3.37	26.50	23.91	0.36	10.79	10.92	-	-	7.70	9.85	5.77	0.86
p-65	-	4.49	30.21	21.19	-	9.24	11.26	0.56	0.78	6.17	9.50	5.75	0.88
p-66	2.85	3.25	33.17	20.48	-	5.91	8.43	7.50	12.27	-	-	5.24	0.93
p-67	-	4.02	24.46	20.96	4.03	11.73	12.48	-	-	6.77	9.10	5.64	0.84

* sample d-41 has 0.42 NS

+ sample d-44 has 5.79 C

CIPW norms calculated with total iron as Fe⁺²

of the Jokulgil group at Torfajokull (PI 1.15-1.46; Ivarsson et al., in press). The variation in alkalinity is among contemporaneous units.

Major element analyses of 25 gabbro samples indicate the chemical diversity of this unit; twelve samples which span the compositional range were further analyzed for trace element abundances (table 4.1). Austurhorn gabbros are medium- to coarse-grained (>2 mm) cumulates and therefore are generally not interpreted as liquids. Evolution of the Hvalnesfjall gabbro is discussed in chapter 3.

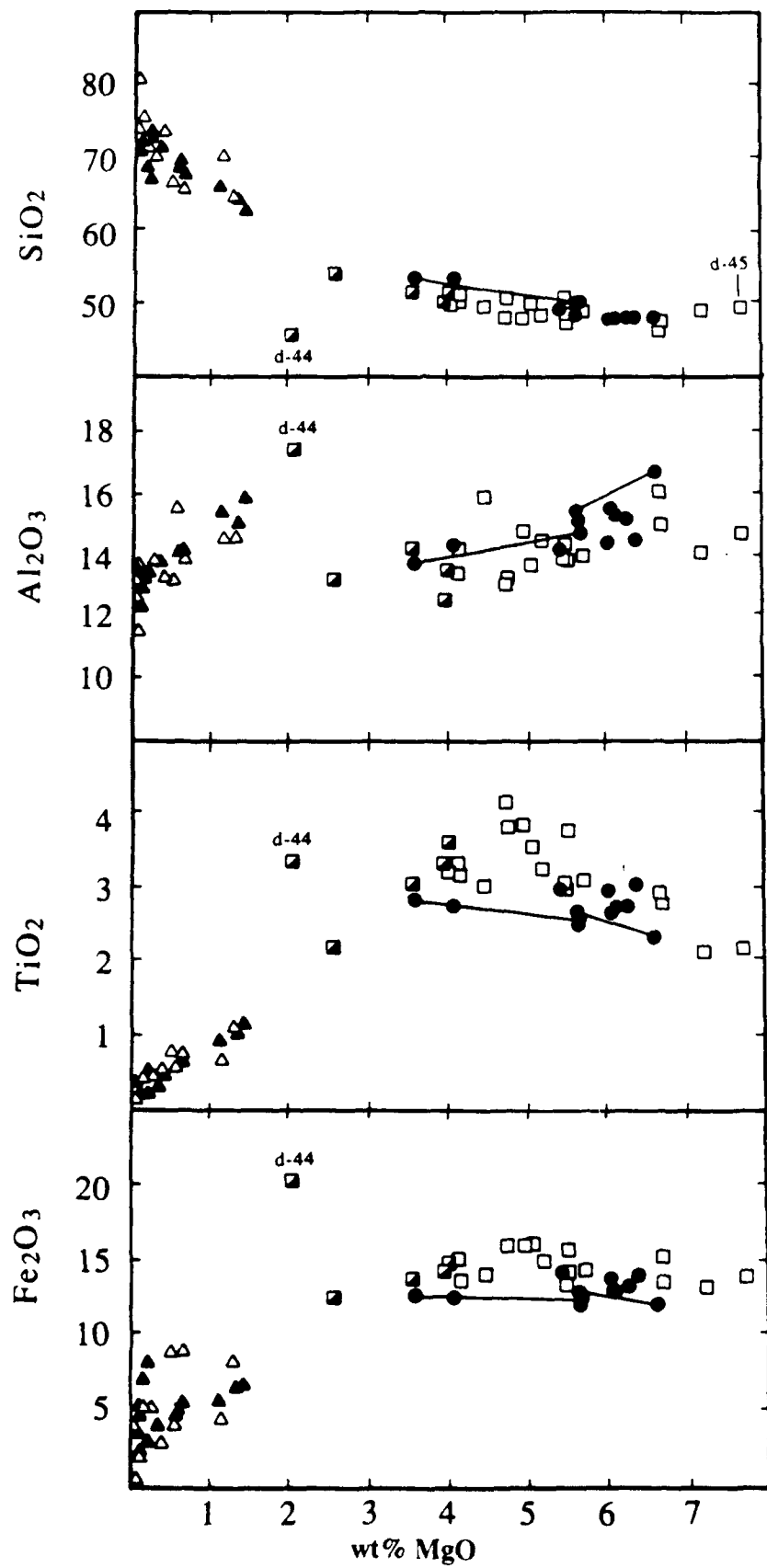
4.4.2 Major Element Geochemistry

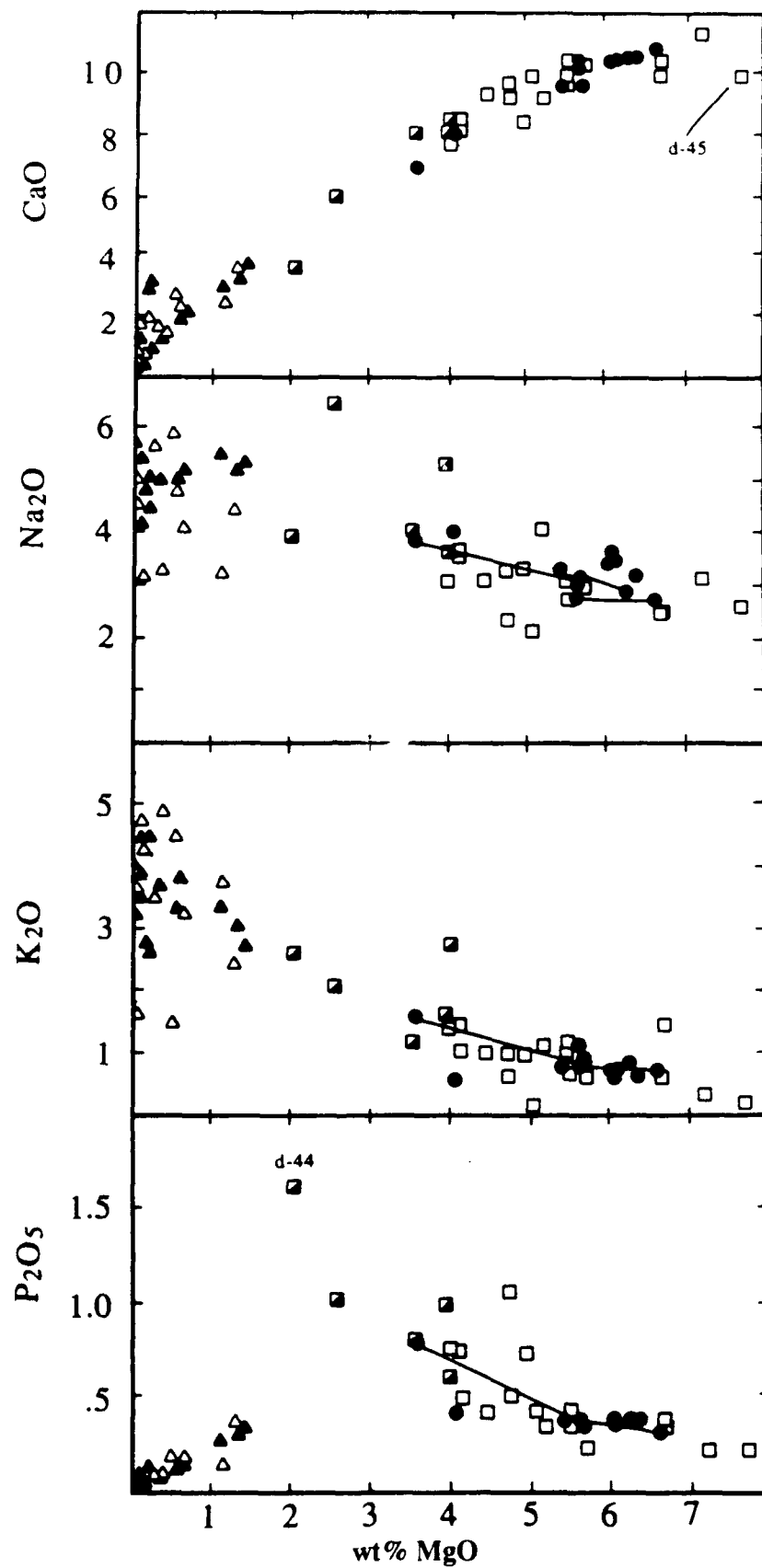
The Austurhorn samples show broadly coherent curvilinear trends among major and incompatible trace elements (figures 4.8, 4.9), suggesting that fractionation (rather than mixing) governs magmatic evolution in this suite. Gabbro samples were omitted from figures 4.8 and 4.9 because they do not represent liquid compositions. Silica content increases with decreasing MgO throughout the series, except for sample d-44 which has unusually low SiO₂ and high Al₂O₃, TiO₂, Fe₂O₃ and P₂O₅ (figure 4.8). This sample is considered "mafic" by virtue of its low SiO₂ content (45.2 wt%). One dike (f-42) contains over 80 wt% SiO₂, however, this sample is severely kaolinitized and does not represent a magmatic liquid composition.

Within both the mafic (SiO₂ <54 wt%) and felsic (SiO₂ >63 wt%) suites Al₂O₃ and CaO decrease with decreasing MgO, whereas Na₂O and K₂O show broad increases accompanied by scatter. In general the felsic dikes have lower alkali contents than the granophyres (at comparable silica content; figure 4.8), suggesting either a compositional distinction or alkali loss by alteration. We favor the latter hypothesis because dikes are heavily fractured and commonly show incipient propylitization along fracture surfaces.

Mafic dikes exhibit a sharp maximum in TiO₂ (4.1 wt%) at 4.7 wt% MgO, whereas mafic pillows have more uniform TiO₂ (2.3-3.0 wt%) which does not correlate systematically with MgO. Similarly, mafic dikes have a broad maximum in total iron

Figure 4.8 Major element oxide variations in Austurhorn samples as a function of MgO content. All data are renormalized to 100% anhydrous using INAA Na_2O data where possible. Open squares are mafic dikes, half-filled squares are "alkali-rich" dikes (see text), filled circles are mafic pillows, open triangles are felsic dikes and filled triangles are granophyres. Lines between pillow samples connect rim and interior of the same large pillow; for visual clarity these lines are not indicated in all cases.





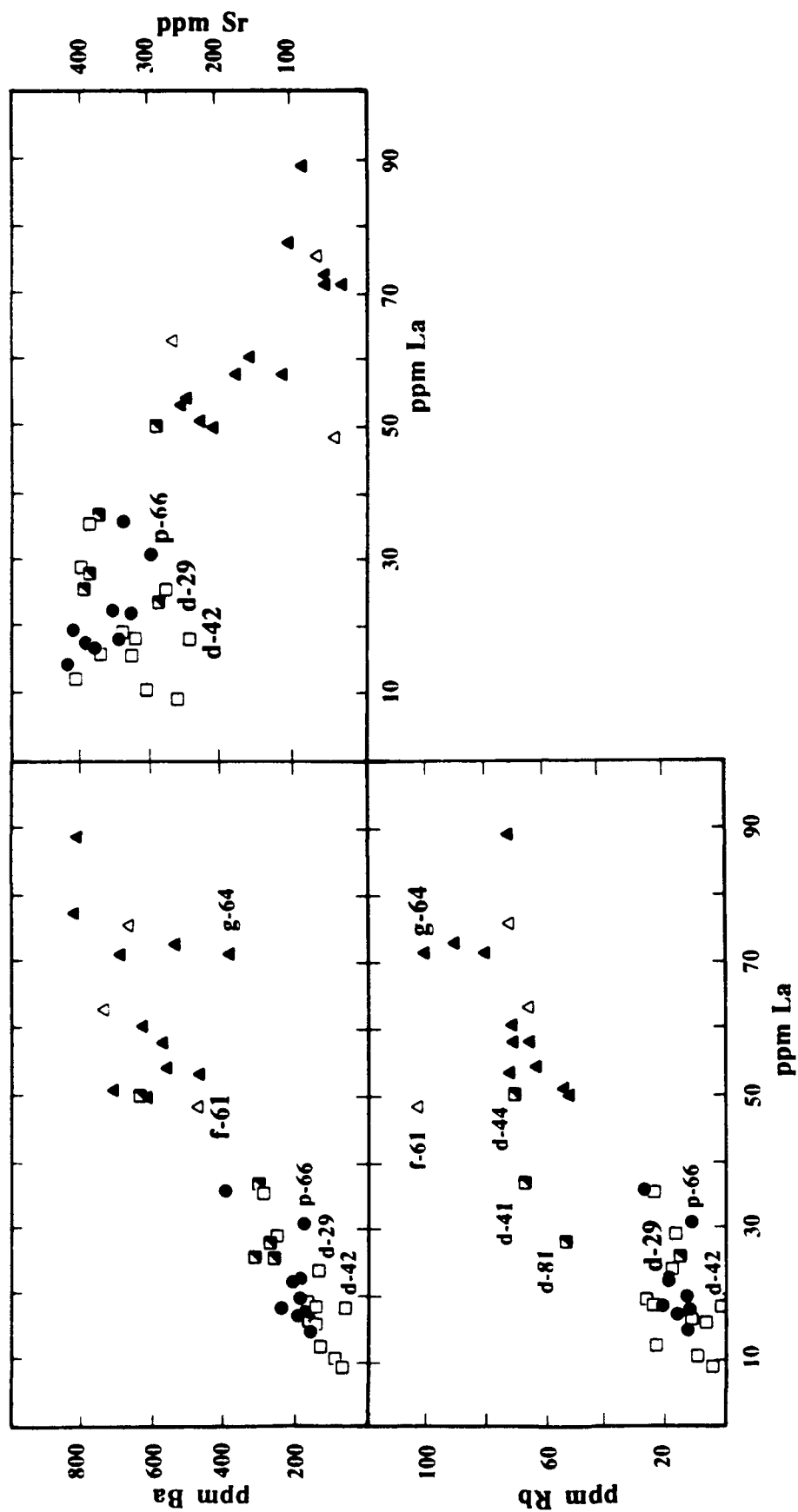


Figure 4.9a Variations in alkali and alkaline-earth element abundances at Austurhorn. Note that : 1) several samples are enriched in Rb relative to the majority; 2) four samples are depleted in Ba. See text for further discussion.

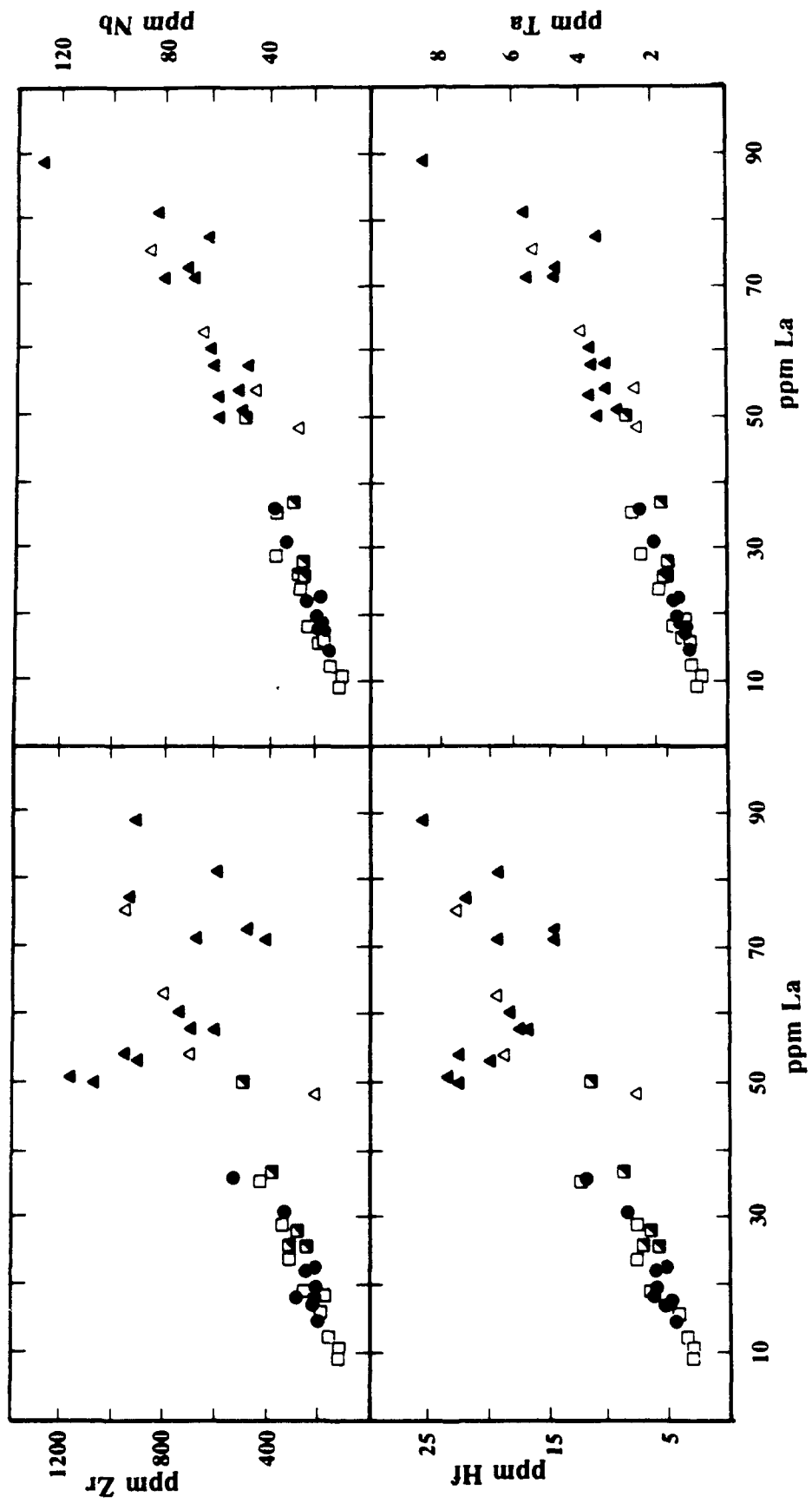


Figure 4.9b Variations in high field strength elements at Austurhorn.

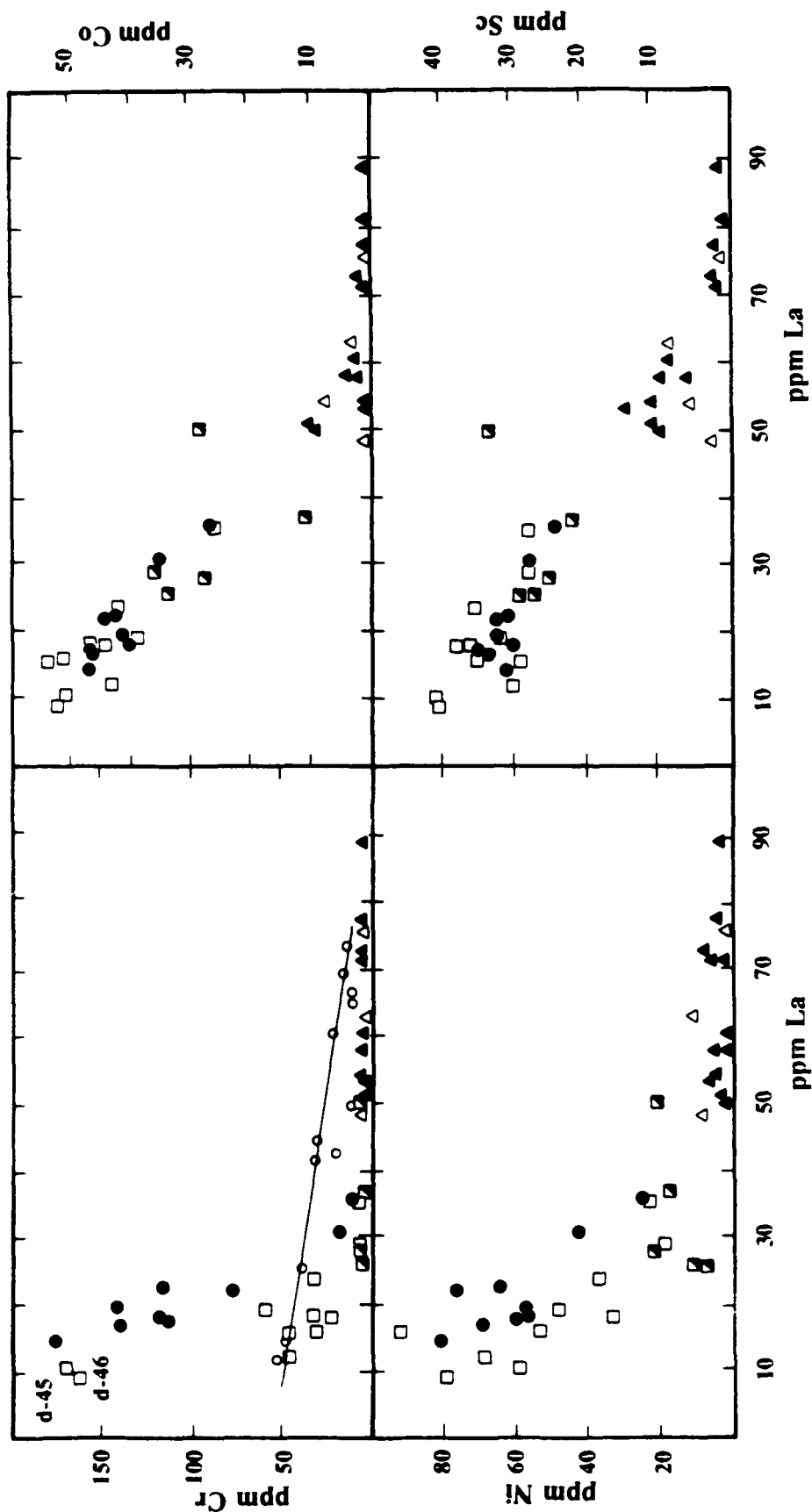


Figure 4.9c Compatible trace element variations in Austurhorn samples. Symbols as before, with filled circles for mafic pillows, open squares for mafic dikes, filled triangles for granophyres, and open triangles for mafic dikes. Note two features of the Cr vs. La plot: 1) pillows and dikes (excluding d-45, d-46) define distinct groups at comparable La contents, with the exception that dikes with >7.3 wt% MgO are similar to pillows. 2) I have included the data of Mattson et al (1986) as open circles because they define a straight line trend suggestive of mixing, whereas my samples define a curved trend suggestive of fractionation.

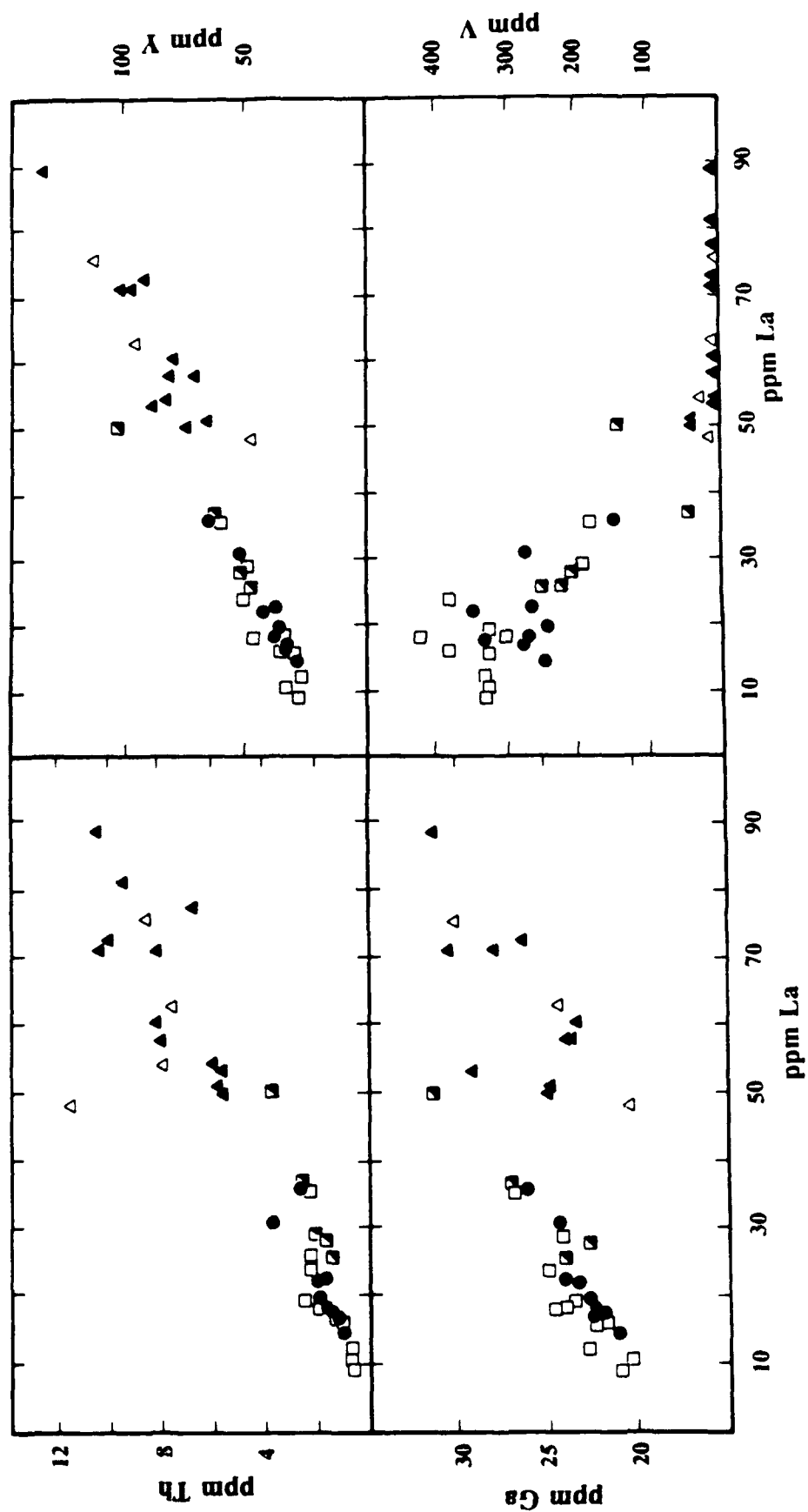


Figure 4.9d Variations in Th, Ga, Y and V.

(15.7 wt% Fe_2O_3) at ~5 wt% MgO, while mafic pillows contain 12.0-14.2 wt% Fe_2O_3 . Iron content of the felsic rocks is highly variable (up to 8 wt% Fe_2O_3) and Mg#s ($100 \times \text{Mg}/(\text{Mg}+\text{Fe})$ with total Fe recalculated as Fe^{+2} ; table 4.1) range from 2 to 30.

Mafic dikes have a maximum of 1.6 wt% P_2O_5 at 2.0 wt% MgO (sample d-44), and three samples between 2.6-4.7 wt% MgO contain ~1 wt% P_2O_5 . The mafic pillows exhibit increasing P_2O_5 with decreasing MgO to a maximum of 0.77 wt% P_2O_5 ; felsic samples contain <0.32 wt% P_2O_5 .

4.4.3 Rare Earth Element Geochemistry

All Austurhorn basalts have higher LREE/HREE than Reykjanes tholeiites. LREE abundances range from 30-162x chondrites, and HREE abundances from 10-38x chondrites (figure 4.10). The Austurhorn basalts have moderate ranges in LREE/MREE ($\text{La}/\text{Sm}_n = 1.2-1.9$) and LREE/HREE ($\text{Ce}/\text{Yb}_n = 2.5-4.9$). Both ratios are higher among basalts with low MgO contents. These features are typical of modern transitional tholeiitic volcanoes which have unexpectedly higher and more variable Ce/Yb_n than the alkaline lavas of Vestmannaeyjar (Meyer et al., 1985; Furman et al., 1988; figure 4.11). Modern tholeiitic centers (e.g., Reykjanes, Langjokull) have larger ranges in Ce/Yb_n than Austurhorn or neovolcanic transitional tholeiitic volcanoes (Zindler et al., 1979; Meyer et al., 1985).

Austurhorn granophyres and rhyolites are enriched in all REE relative to Austurhorn basalts, with LREE between 155-290x chondritic and HREE 32-60x chondritic (figure 4.12). Felsic samples have LREE/MREE greater than that of the basalts ($\text{La}/\text{Sm}_n = 2.0-2.7$, with one sample = 3.6), but LREE/HREE of the two groups overlap (felsic $\text{Ce}/\text{Yb}_n = 3.9-5.1$; figure 4.11). Granodiorites have higher Ce/Yb than more evolved felsic samples. Austurhorn liquids show a regular decrease in Eu/Eu^* with decreasing Sr content throughout the differentiation sequence from basalt ($\text{Eu}/\text{Eu}^* \sim 1.0$) to rhyolite ($\text{Eu}/\text{Eu}^* = 0.35$; figure 4.13). Eu/Eu^* has a broad negative correlation

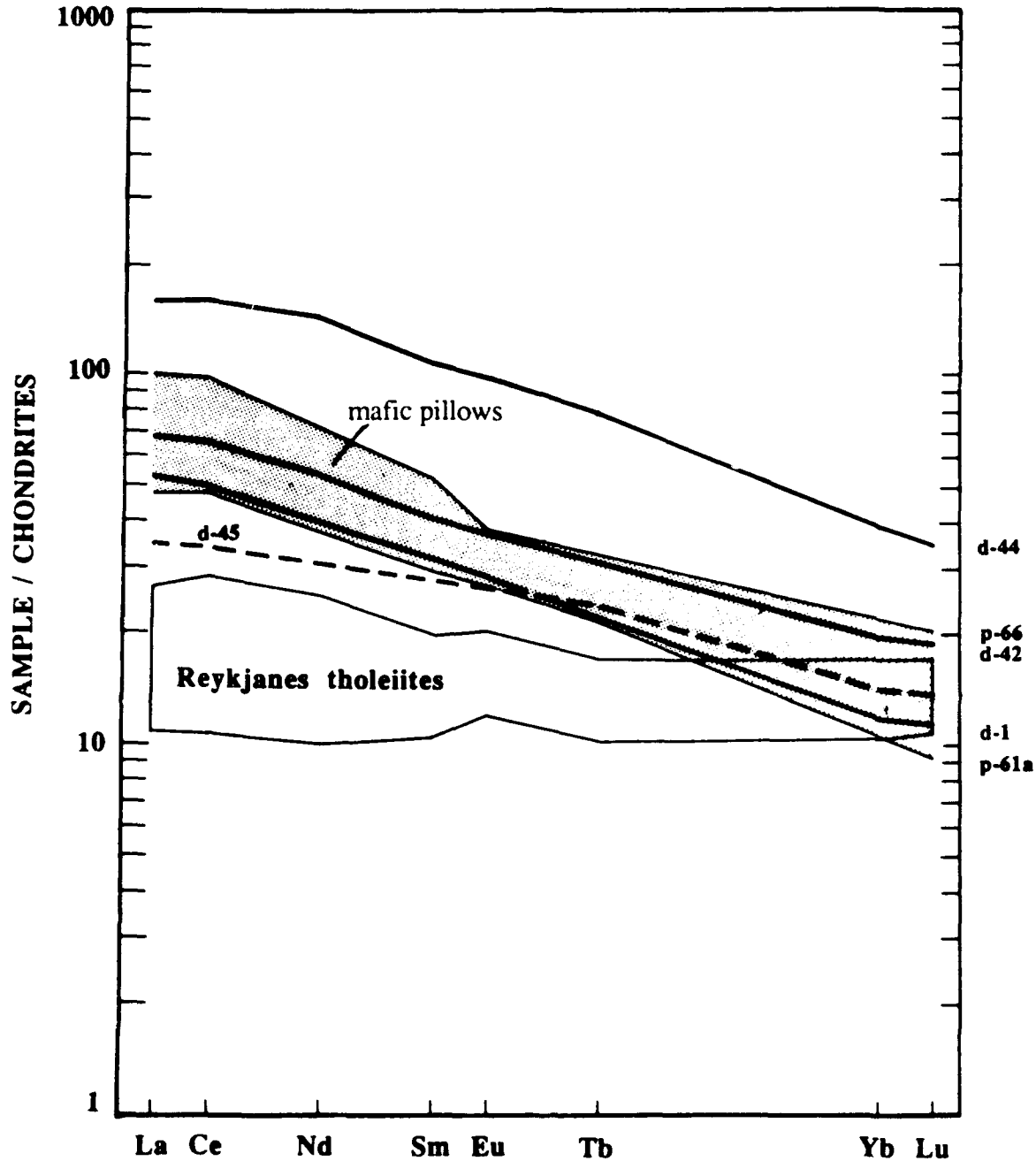
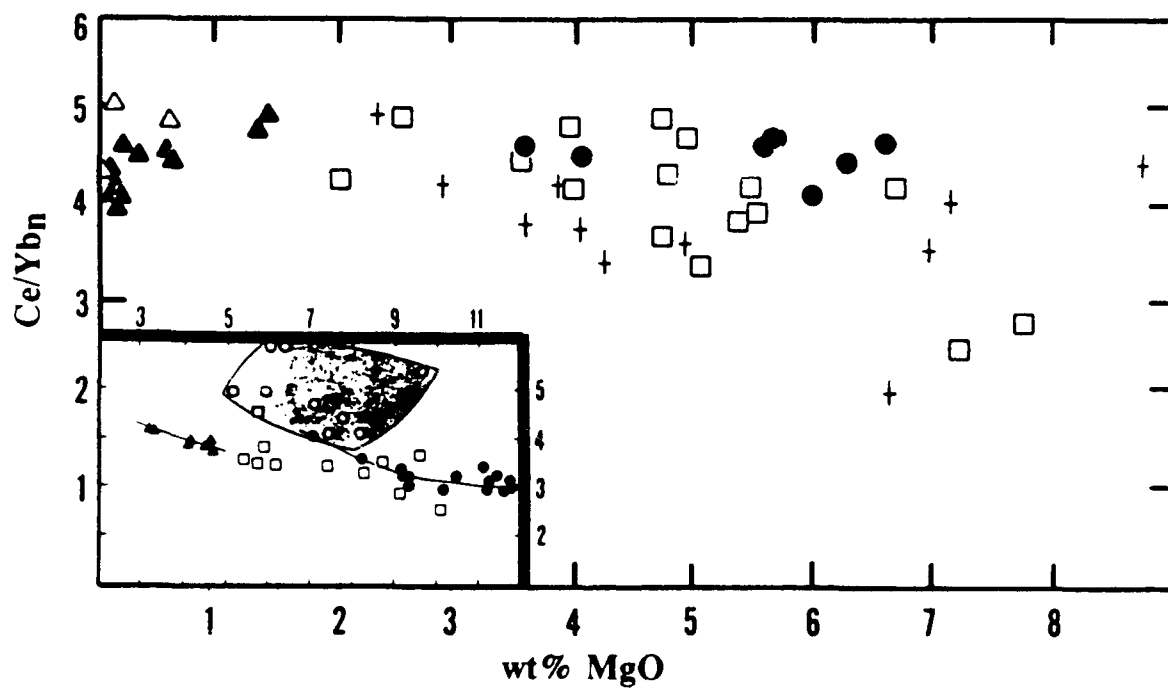
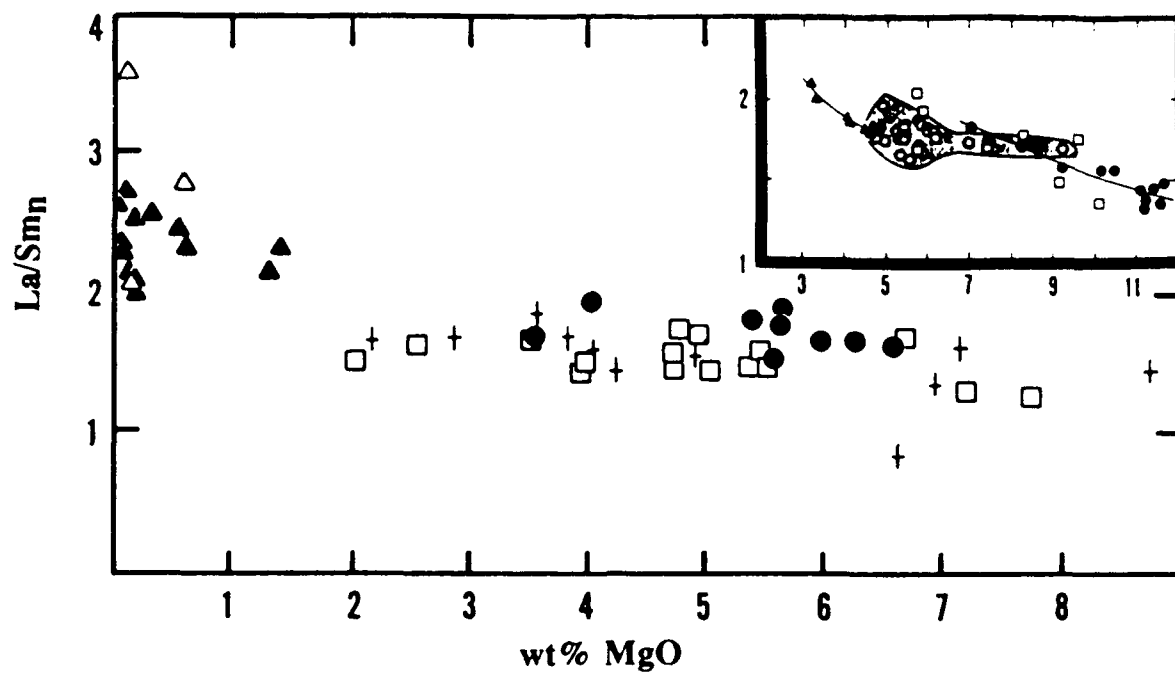


Figure 4.10 Austurhorn basalts are enriched in LREE relative to Reykjanes tholeiites and olivine tholeiites (data from Zindler et al., 1979). Most samples have nearly parallel patterns, but those of dike d-45 (7.75 wt% MgO) and d-46 (7.25 wt% MgO, not shown) have lower La/Sm and La/Yb and cross-cut other patterns. The field of mafic pillows (9 samples) is shaded. Data have been normalized using the chondritic values of Boynton (1966).

Figure 4.11 La/Sm and Ce/Yb (chondrite normalized) for **Austurhorn** samples, with inset comparisons to **Vestmannaeyjar** (solid circles = Surtsey, triangles = Eldfell; squares = additional samples; Furman et al., 1988) and transitional tholeiitic basalts from the **EVZ** (shaded region; Meyer et al., 1985). Note that transitional tholeiitic basalts from Austurhorn and the EVZ have more variable La/Sm and Ce/Yb ratios than those of Vestmannaeyjar. At Austurhorn there is a general increase in Ce/Yb with differentiation, but the scatter is greater than analytic uncertainty.



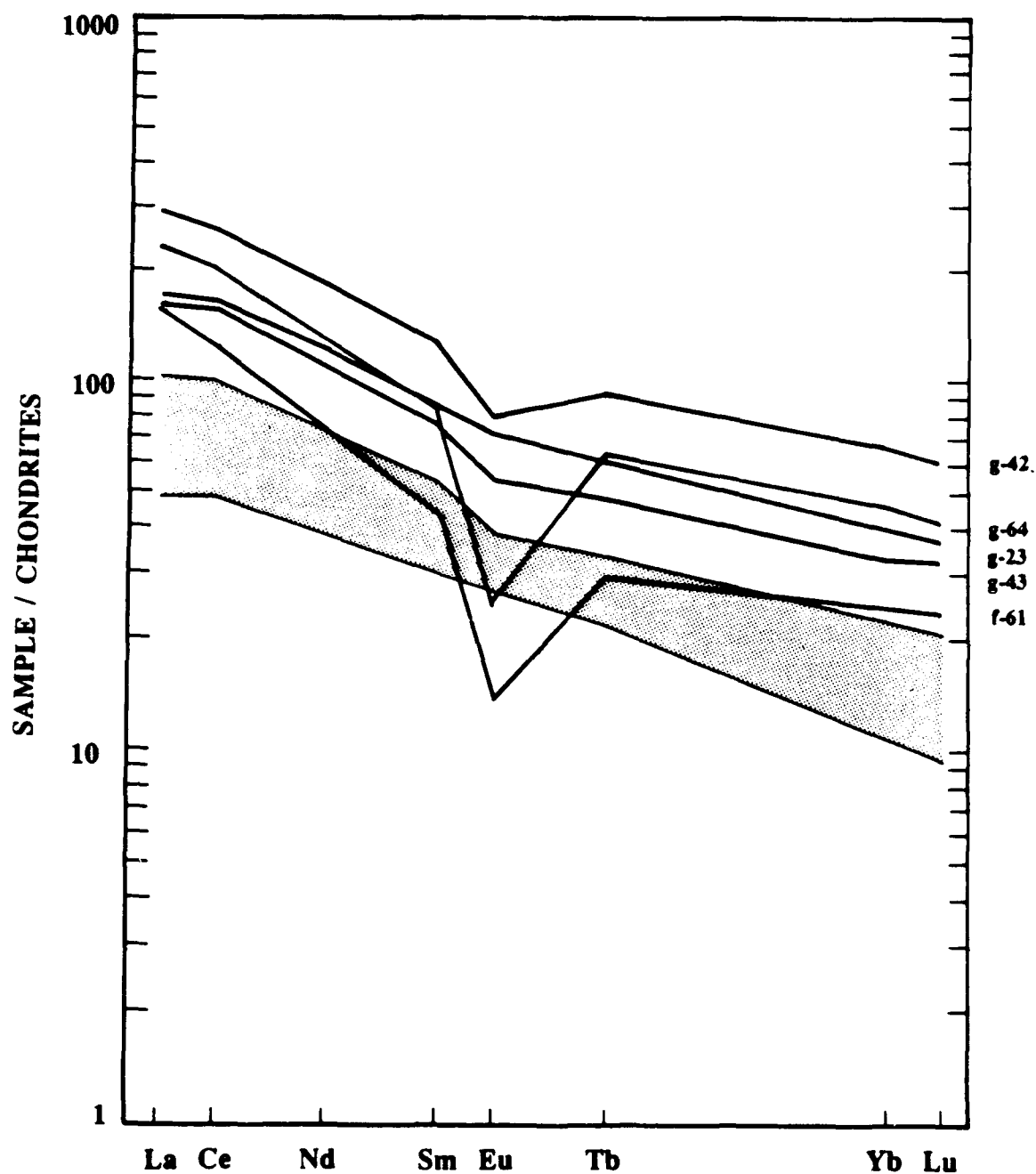


Figure 4.12 REE patterns of selected Austurhorn felsic magmas, with field of mafic pillows (shaded) for comparison. Negative europium anomalies are not marked in granodiorites (e.g., g-43) or Fe-rich granophyres (e.g., g-23) and are variably developed in rocks of higher silica content.

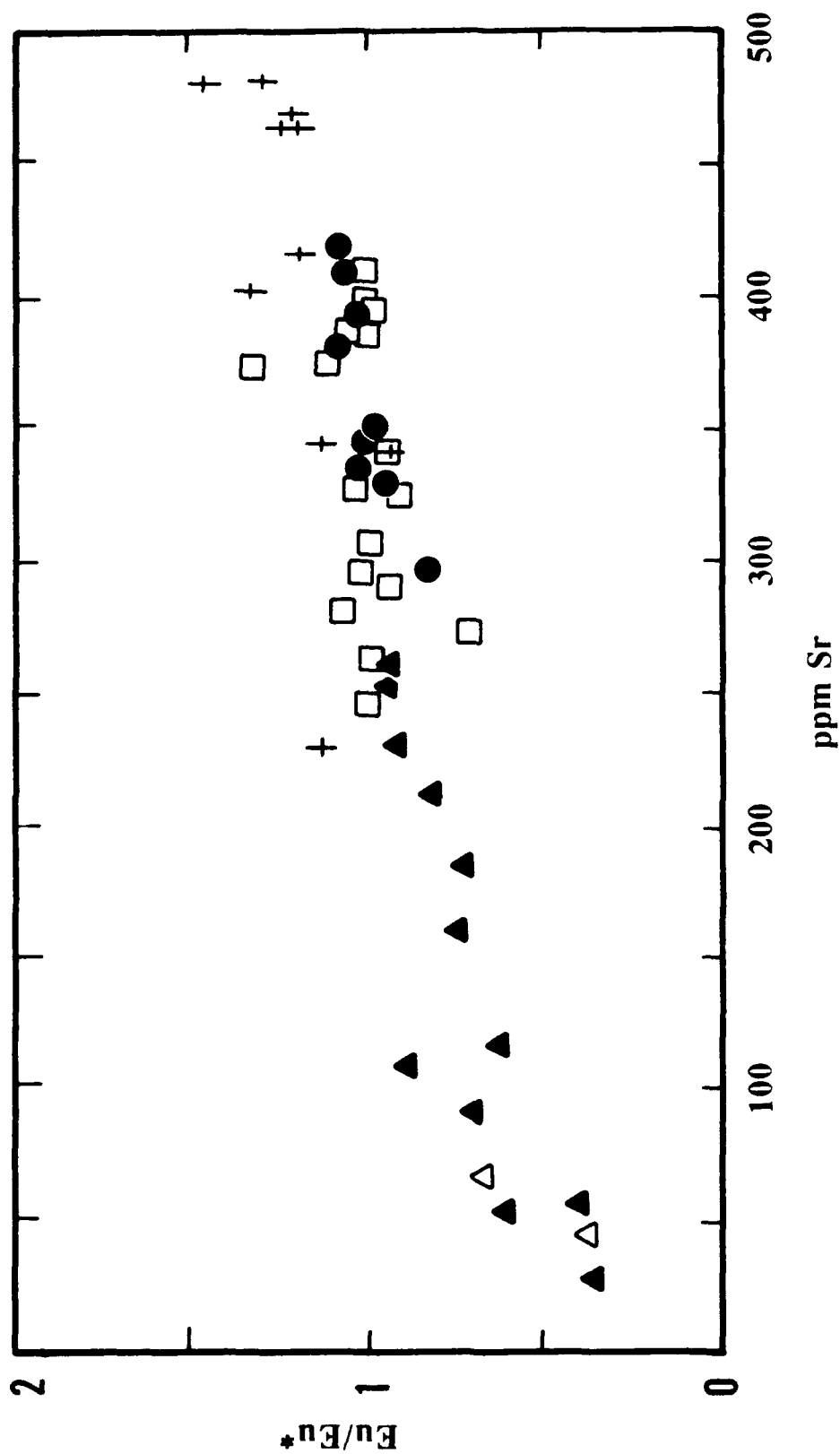


Figure 4.13 Austurhorn samples display increasingly negative europium anomalies (Eu/Eu^*) with decreasing Sr abundances, indicating that plagioclase is important in this fractionation sequence. Notice the gabbros with >450 ppm Sr and positive Eu anomalies - they contain over 70 vol% plagioclase, presumably accumulative (see table 4.4). Symbols: filled circles = mafic pillows, open squares = mafic dikes, filled triangles = granophyres, open triangles = felsic dikes, plus signs = gabbros.

with La abundances. Post-glacial rhyolites from the Torfajökull complex have a comparable range in Eu/Eu^* with a strong negative correlation with La content (Gunnarsson, 1988). P_2O_5 correlates negatively with La (figure 4.14), except in sample f-61 which has anomalously low concentrations of these elements (see section 4.4.8). This relationship requires that either La or P_2O_5 is not incompatible; I infer that apatite crystallization controls P_2O_5 abundances in the felsic samples. The correlation between La and P_2O_5 plus the observed constant La/Sm among felsic samples (figure 4.14) indicates that the LREE are moderately incompatible despite crystallization of apatite. For this reason, La is a viable indicator of fractionation progress among felsic samples as well as mafic.

Bulk rock REE analyses indicate two gabbro types: "liquid analogs" with REE patterns similar to those of basalts and cumulates with REE patterns reflecting modal mineralogy (figure 4.15). All gabbros are enriched in LREE/HREE with respect to chondrites, although most are depleted in LREE compared to Austurhorn basalts. LREE/HREE and LREE/MREE of the gabbros are somewhat more variable than those of basalts and felsic rocks ($\text{Ce}/\text{Yb}_n = 1.96\text{--}5.40$, $\text{La}/\text{Sm}_n = 0.78\text{--}1.82$; figure 4.11). Cumulate gabbros typically have positive Eu anomalies ($\text{Eu}/\text{Eu}^* 0.93\text{--}1.45$) indicating accumulated plagioclase; Eu/Eu^* is positively correlated with bulk Sr content (figure 4.13).

4.4.4 Trace Element Geochemistry

Abundances of Th, Rb, Ba, Zr, Hf, REE, Nb, Ta, Y and Ga are positively correlated in the transitional tholeiitic Austurhorn basalts ($\text{SiO}_2 < 54 \text{ wt\%}$), with the abundance ranges of Th (7.2), Rb (7.1) and Ba (6.2) exceeding those of other elements (4.5–3.4, but 2.4 for Y and 1.3 for Ga). Samples d-42 and d-29 show depletions in Ba, Rb and Sr and sample p-66 is depleted in Ba and Rb (figure 4.9a). Alkali mobility is presumably due to alteration; however these samples do not contain abundant alteration

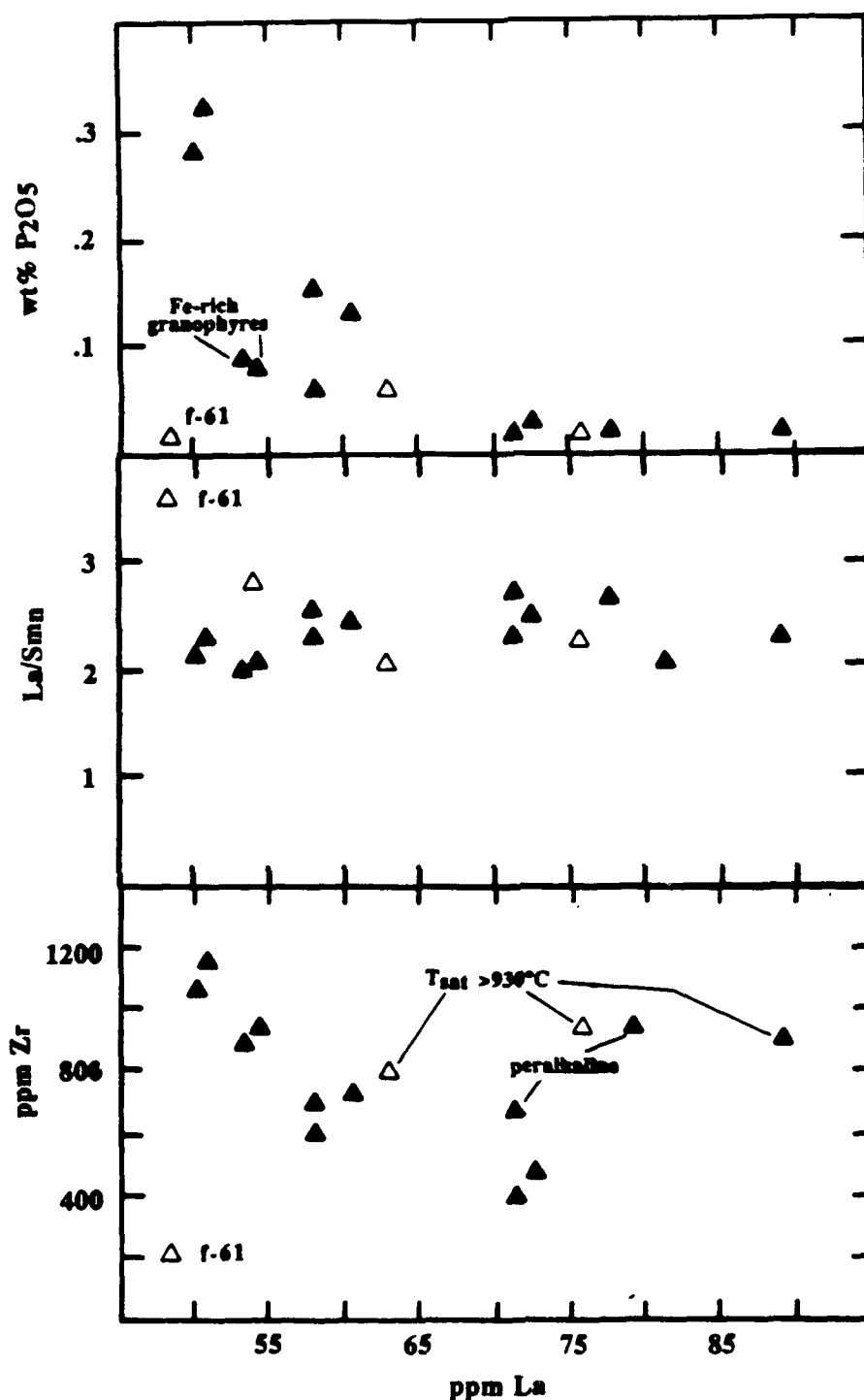


Figure 4.14 Detailed geochemical features of felsic magmas as discussed in text. Notice the following: 1) Felsic dike f-61 has lower P2O5 and La concentrations than other felsic magmas. 2) La/Sm does not change with differentiation. 3) Zirconium abundances decrease with fractionation except for samples which are peralkaline or have high calculated temperatures of zircon saturation. See text for discussion.

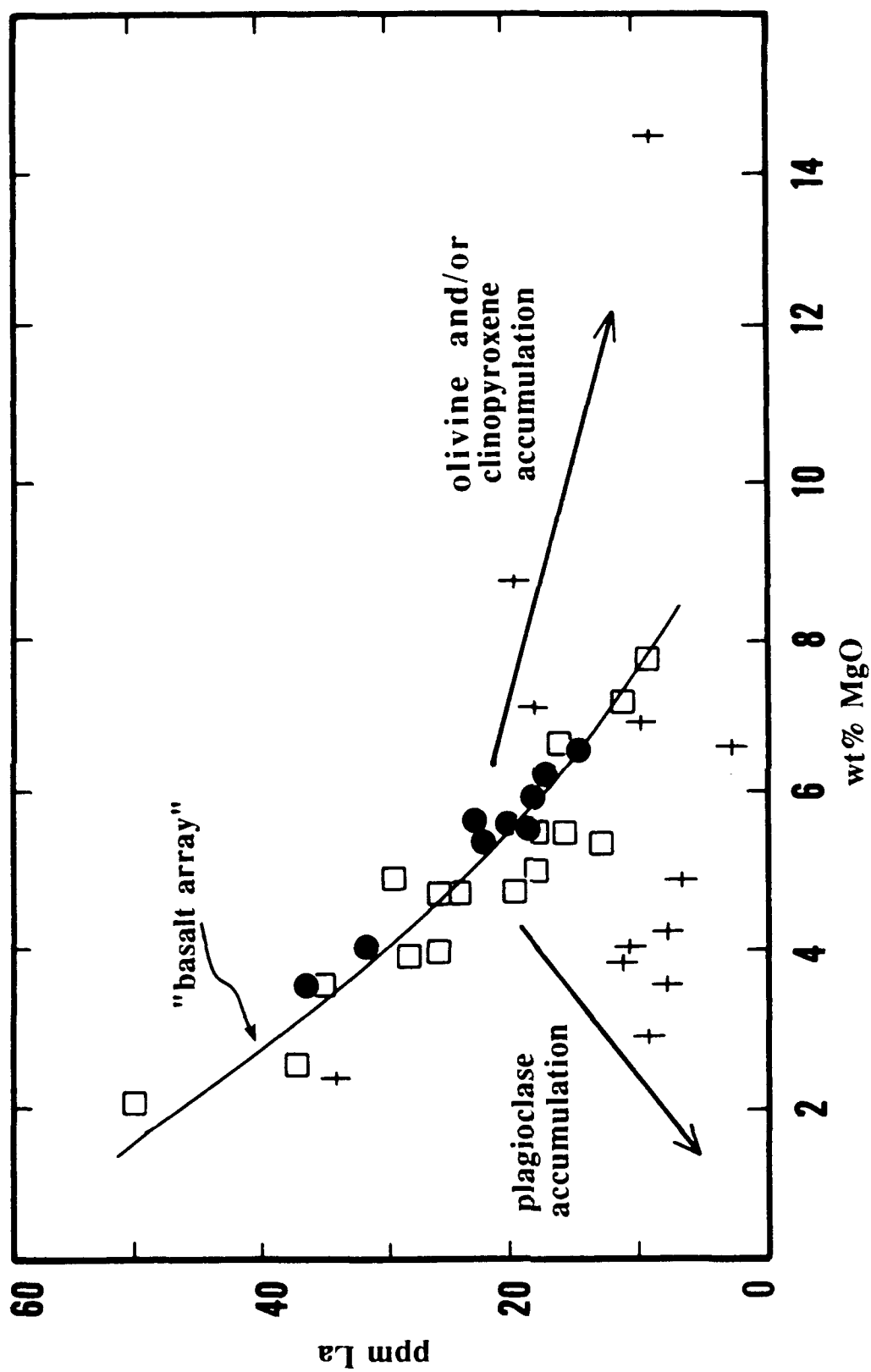


Figure 4.15a This plot of La (a highly incompatible element) vs MgO (a differentiation indicator) shows that a few Austurhorn gabbros ("plus" symbols) resemble liquids, but most are cumulates with low incompatible element abundances. The effects of plagioclase and clinopyroxene accumulation are indicated by arrows. Symbols as in figure 4.13.

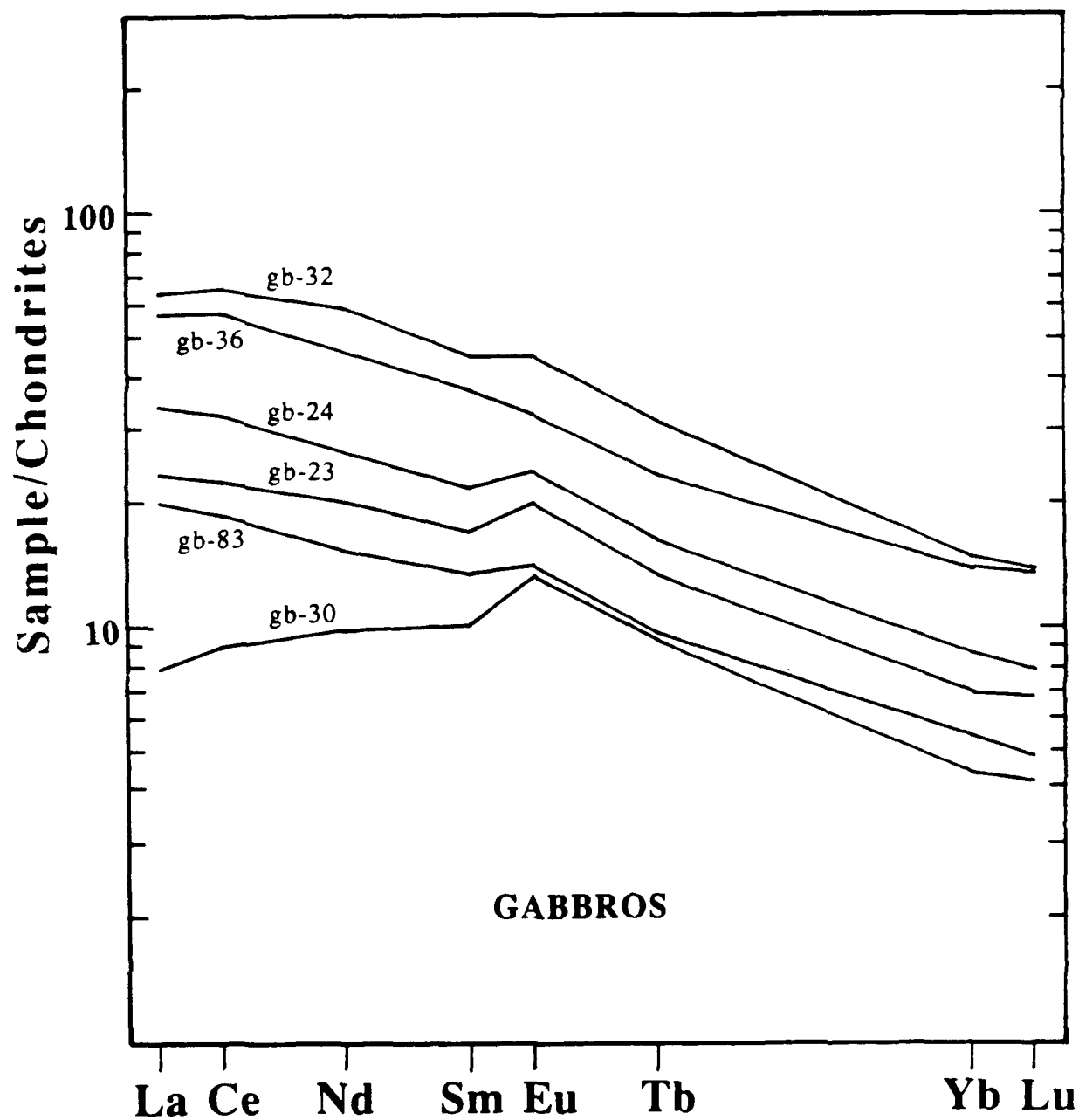


Figure 4.15b Selected rare earth element patterns of Austurhorn gabbros indicate their compositional range. The effects of plagioclase accumulation are indicated by positive Eu anomalies, and clinopyroxene accumulation results in a concave-down pattern.

phases (e.g., epidote, hornblende, zeolites, clays). There are, in general, excellent correlations between Ba, La and Y in most of the Austurhorn basalts. The alkali-rich basalts have higher abundances of all incompatible elements than the transitional tholeiitic samples. Abundance ranges of Rb (18.9) and Ba (10.2; relative to the least evolved basalt d-45) are significantly higher than those of Austurhorn transitional tholeiites, but observed enrichments in Th (7.4) and other elements (5.3-3.8, but 1.5 for Ga) are roughly comparable between suites.

Among felsic samples Th, Nb, Ta, REE and Y are positively correlated, with enrichment of Th (21.1, relative to the least evolved basalt d-45) greater than that of other elements (9.5-11.8, but 5.0 for Y). Abundances of Ba and Rb show a weak positive correlation with La, with total enrichments of 13.0 and 19.2, respectively. Exceptions to these general trends include two samples with elevated Rb contents and low Ba (f-61, g-64; figure 4.9a). In general, the Rb-La trend is not coherent, presumably because of alteration effects. The greater compatibility of Ba relative to Rb, plus the correlation between Eu anomaly and Sr content (figure 4.13), suggests that plagioclase exerts a major control on differentiation of the Austurhorn felsic magmas.

Zr and Hf co-vary uniformly but their behavior with respect to La or other differentiation indices is not simple (figure 4.9b). A negative correlation with La is observed among most zircon-bearing granophyres (figure 4.14). An important role for zircon fractionation is inferred among the felsic samples. Calculated zircon-saturation temperatures for these samples range between 860-900°C (Harrison & Watson, 1983; Watson & Harrison, 1983). The two mildly peralkaline granophyres (samples g-41 and g-61, which have atypically high Ba and low Rb) have higher Zr contents for a given La, consistent with the observation that high Zr contents are necessary to saturate zircon in these highly polymerized melts (Watson & Harrison, 1983; Harrison & Watson, 1983). Additional evidence for the role of zircon in controlling Zr and Hf abundances is the monotonic increase in Nb and Ta with increasing La (figure 4.9b). Sample f-61 has

anomalously low abundances of Zr, La and other incompatible trace elements (see section 4.4.8).

The elements Sc, Ni, Cr and Co exhibit broad negative correlations with La (figure 4.9c). Cr and Ni contents of felsic samples are scattered near their detection limits (5 and 10 ppm, respectively). V correlates negatively with La among samples with <7 wt% MgO.

Hvalnesfjall gabbro samples have positively correlated abundances of the incompatible elements Ba, Rb, Ta, Th, Zr, Hf, Nb and Y (figure 4.16). Within this group, Th, La, Rb and Nb vary by factors of 14.0-12.4, Ta, Zr, Hf and Ba by factors of 9.4-7.1, and Y by 4.9. Compatible trace elements (Sr, Sc, V, Co, Cr, Ni) do not correlate with La or other incompatible elements but reflect modal mineralogy of individual samples (table 4.4). For example, all samples with >450 ppm Sr contain >70 vol% plagioclase. Gabbros with >100 ppm Ni (gb-32, gb-36, gb-42) have abundant olivine, whereas samples with the highest concentrations of Sc, V and Co have high proportions of clinopyroxene and FeTi oxides but no olivine. All gabbros with >80 ppm Cr (gb-29, gb-36, gb-42, gb-83) have high percentages of all mafic phases (table 4.4).

Cumulate and "liquid analog" gabbros are clearly distinguished in an MgO vs. La diagram (figure 4.15) when compared to the liquid line of descent defined by Austurhorn basalts. Since La is highly incompatible in the cumulus phases, the abundance of La in cumulate gabbros is directly proportional to the amount of intercumulus material. Preliminary calculations based on La concentration indicate many Hvalnesfjall gabbros are orthocumulates with greater than 25% trapped liquid (see chapter 3).

4.4.5 The Ratios Ba/La, La/Nb and P/Ce

The elements Ba, Nb, La, Ce and P are not readily fractionated from one another by melting and crystallization (in the absence of apatite or oxide) and their ratios in

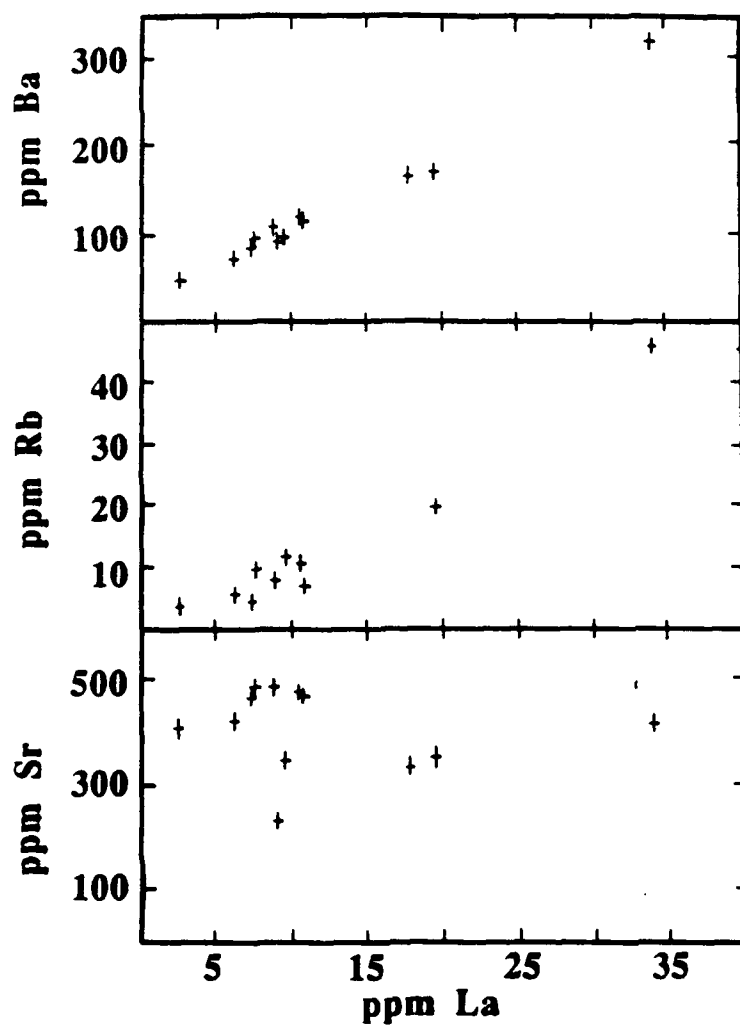


Figure 4.16a The incompatible elements Ba and Rb are positively correlated with La in Austurhorn gabbros, while Sr abundances reflect plagioclase contents of the samples.

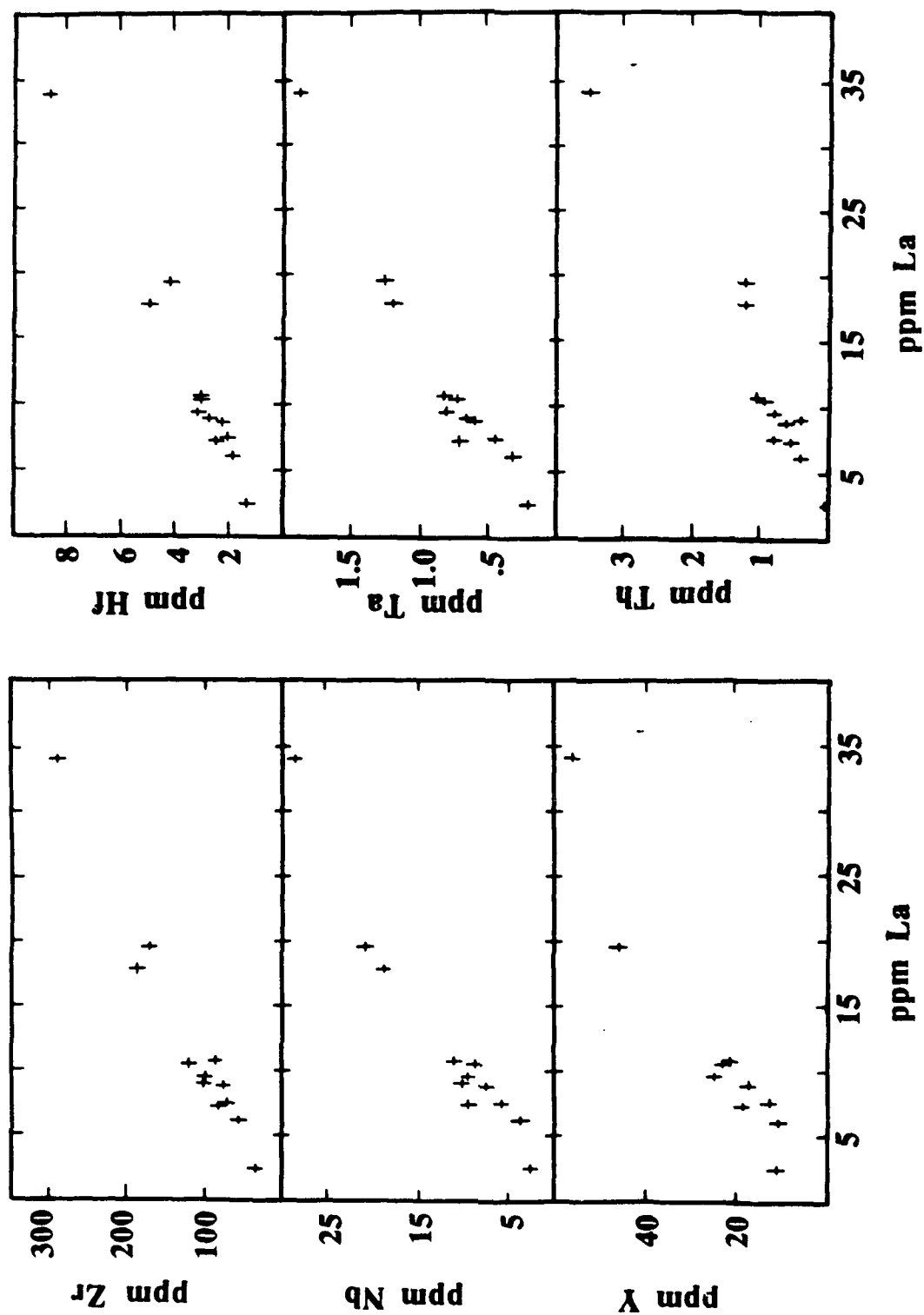


Figure 4.16b These high field strength and incompatible elements are positively correlated with La in the Austurhorn gabbros.

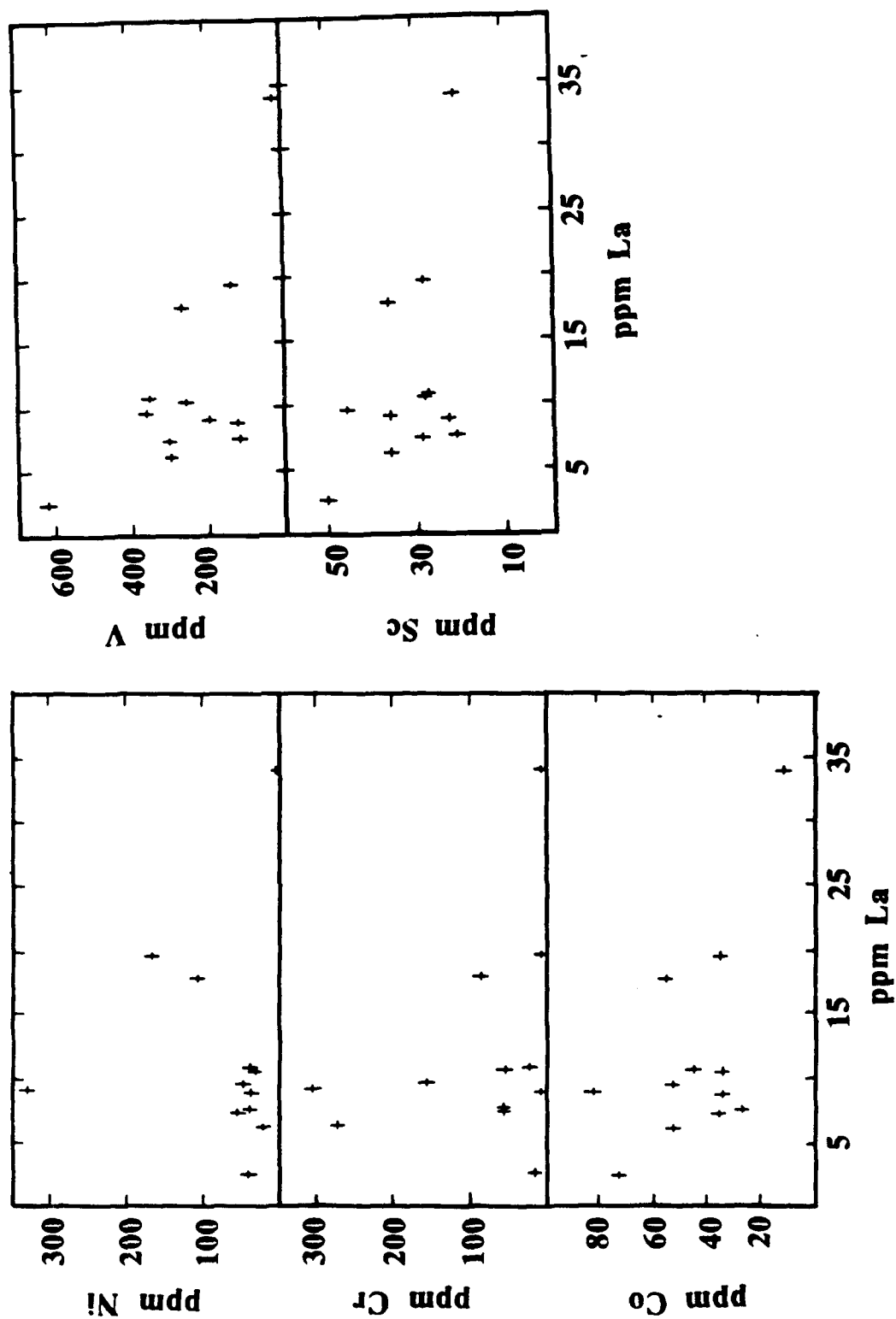


Figure 4.16c Variations in compatible elements among gabbro samples indicate the effects of accumulated mafic phases.
See text for discussion.

Table 4.4 Modal Analyses of Representative Samples

A. Felsic Samples

Sample	Glass	Ca-Na Feldspar	K-feldspar	Quartz	FeTi Oxide	Mafic Phases
f-61	72.6	16.8 (Anor)	-	6.3	0.7	-
g-43	-	49.5 (Plag)	17.4	17.6	4.3	10.9 (Amph)
g-65	-	53.9 (Plag)	15.0	14.5	4.2	12.3 (Amph)
g-23	-	63.4 (Plag)	1.0	25.2	1.4	8.0 (Oliv)
g-62	-	48.3 (Plag)	14.0	26.6	6.7	3.6 (Cpx)
g-42	-	43.4 (Plag)	19.5	31.9	4.3	-
g-64	-	46.9 (Anor)	20.1	31.3	2.1	-

B. Mafic Pillows

Sample	Plagioclase	Clinopyroxene	FeTi Oxide	Olivine
p-61a	50.2	39.6	10.2	tr
p-61b	53.0	33.9	13.1	-
p-62a	60.6	31.2	8.2	-

C. Gabbro Samples (Calculated Volume% - see below)

Sample	Plagioclase	Clinopyroxene	FeTi Oxide	Olivine	Quartz	K-Feldspar
gb-23	70.2	24.2	5.5	-	-	-
gb-24	70.5	24.3	5.2	-	-	-
gb-29	55.0	33.3	6.9	4.8	-	-
gb-31	78.2	17.7	3.0	1.0	-	-
gb-32	61.6	24.1	2.0	12.3	-	-
gb-42	43.6	33.6	3.9	30.5	-	-
gb-43	54.8	33.4	7.8	4.0	-	-
gb-81	61.5	26.2	5.1	7.2	-	-
gb-83	59.8	30.5	9.8	-	-	-
gb-41	59.3	18.0	6.1	-	5.9	9.1
gb-82	55.8	29.7	8.7	-	-	5.8

D. Gabbro Samples (Calculated Weight Percents)

Sample	Plag-1	Plag-2	Clinopyroxene	Olivine	Magnetite	Ilmenite	K-spar	Quartz
gb-23	51.4 (64.8)	12.1 (39.2)	27.3 (76.7)	-	6.3	3.1	-	-
gb-24	32.4 (68.1)	31.7 (39.2)	27.2 (70.9)	-	5.4	3.4	-	-
gb-29	19.2 (63.1)	28.8 (39.2)	35.8 (74.9)	5.2 (70.4)	5.9	5.4	-	-
gb-31	48.2 (75.1)	25.1 (39.2)	20.4 (75.8)	1.2 (70.4)	3.3	1.9	-	-
gb-32	37.0 (75.1)	18.3 (39.2)	26.7 (77.7)	13.6 (70.4)	2.2	1.2	-	-
gb-42	10.0 (63.7)	23.9 (39.2)	32.1 (75.9)	29.2 (67.8)	1.7	4.0	-	-
gb-43	17.6 (60.3)	30.0 (39.2)	35.7 (73.9)	4.3 (70.4)	7.9	4.6	-	-
gb-81	7.5 (61.0)	47.3 (43.0)	28.7 (72.9)	7.9 (67.8)	4.9	3.5	-	-
gb-83	27.5 (38.6)	25.1 (22.1)	33.0 (67.2)	-	8.8	7.2	-	-
gb-41	54.2 (22.1)	-	20.3 (51.3)	-	7.7	2.8	-	5.9
gb-82	24.5 (43.0)	24.0 (22.1)	31.8 (60.8)	-	7.2	7.0	5.0	-

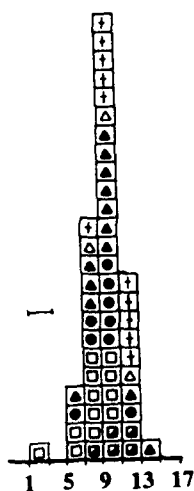
Notes: Modes of felsic samples and mafic pillows were obtained by point counting (1000 points) on standard thin sections. However, a multiple linear regression (based on bulk sample and microprobe data) was used to verify quartz and K-feldspar proportions in the felsic samples. The gabbros were not point counted, and all data in this table represent multiple linear regression analyses based on bulk sample and microprobe data. Only samples for which all major phases were analyzed are reported. Average mineral compositions were used (ignoring zoning in plagioclase and clinopyroxene), and a second (more sodic) plagioclase incorporated to account for zoning. Modes reported in volume percent (section C) are based on the weight percent modes tabulated in section D. Numbers in parentheses refer to the anorthite content of plagioclase, and the Mg#s $[100 \cdot \text{Mg}/(\text{Mg} + \text{Fe})]$ of clinopyroxene and olivine.

basaltic liquids may reflect those of the mantle source. Figure 4.17 shows the range of Ba/La, La/Nb and P/Ce in Austurhorn liquids and cumulates compared to those from Vestmannaeyjar in southern Iceland, where uniform Pb isotopic ratios in primitive basalts indicate a homogeneous mantle source (Furman et al., 1988; Park et al., in prep). Both volcanic systems have mean Ba/La within analytic error of the primitive mantle ratio for these elements (9.9; Sun & McDonough, in press); no Vestmannaeyjar samples fall outside this narrow range. Low Ba/La in some Austurhorn liquids (e.g., Ba/La of sample d-42 is 2.8) may reflect alkali loss through alteration (figure 4.9a) whereas the extremely high ratio in gabbro gb-30 (Ba/La >18) is not a reasonable primary magmatic feature. Even allowing for these caveats, the variation in Ba/La among Austurhorn samples exceeds that of analytic error.

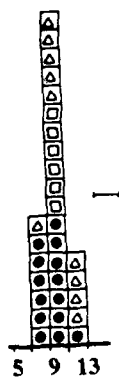
At Vestmannaeyjar, lavas from the Eldfell and Surtsey eruptions have identical average La/Nb (0.776), while a few samples from the remainder of the archipelago are beyond analytic error of this value (figure 4.17). The La/Nb of Vestmannaeyjar is significantly lower than that estimated for a primitive mantle composition (0.99; Sun & McDonough, in press) and may reflect the low degree of mantle melting inferred for this region (<~3%; Furman et al., 1988), assuming that La is more compatible than Nb in residual phases. Austurhorn samples show variable La/Nb beyond analytic error, but form a Gaussian distribution around a prominent mean of ~1.0. Variable Ba/La and La/Nb within the Austurhorn suite does not correspond to compositional differences of the liquids (i.e., mafic vs. felsic) and may therefore record some component of source heterogeneity.

The P/Ce ratio does show a relationship to major element composition (figure 4.17). Mafic liquids and cumulates have P/Ce ratios distributed about a mean value of ~34, only slightly lower than that of the Vestmannaeyjar system. The Austurhorn "alkali-rich" dikes tend to higher P/Ce than other samples from either area. Almost all basalts from Austurhorn and Vestmannaeyjar have lower P/Ce than normal MORB (75

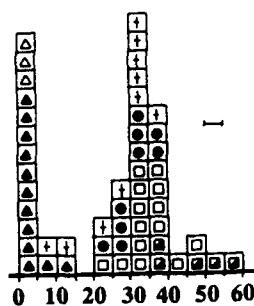
Figure 4.17 Histograms of incompatible element ratios facilitate comparison of source heterogeneities between Austurhorn and Vestmannaeyjar. In general, samples from Vestmannaeyjar (circles = Surtsey, squares = Eldfell, triangles = archipelago; Furman et al., 1988) show significantly less variation than those from Austurhorn (symbols as in previous figures) although both regions have Gaussian distributions about a prominent mean. Both Austurhorn and Vestmannaeyjar have mean Ba/La similar to that of the primitive mantle (~9.9; Sun & McDonough, in press); Austurhorn La/Nb is also comparable to mantle estimates (~0.99; Sun & McDonough, in press) whereas Vestmannaeyjar La/Nb is somewhat lower. Basalts from both areas have P/Ce ~35, and felsic rocks from Austurhorn have lower P/Ce as a result of apatite fractionation. Error bars indicate 1-sigma variation based on replicate analyses.



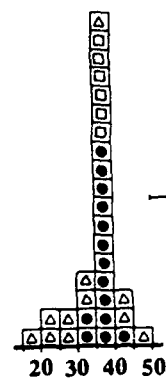
Austurhorn
n = 52
Ba/La



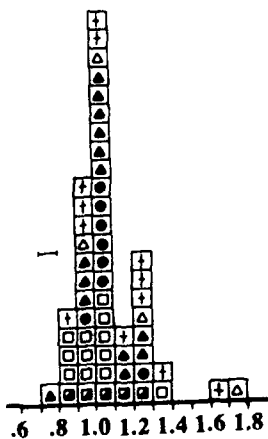
Vestmannaeyjar
n = 30
Ba/La



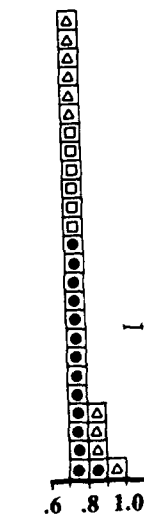
Austurhorn
n = 53
P/Ce



Vestmannaeyjar
n = 30
P/Ce



Austurhorn
n = 51
La/Nb



Vestmannaeyjar
n = 30
La/Nb

+/- 15; Sun & Hanson, 1975). Among felsic samples, crystallization of apatite results in P/Ce ratios much lower than those observed in Austurhorn basalts. Two gabbro samples with low P/Ce (samples gb-30, gb-32) have low abundances of all incompatible elements; I infer that P_2O_5 is more incompatible than Ce in the cumulus phases. The leucocratic gabbros (gb-41 and gb-83) have high P/Ce, consistent with petrographic evidence for apatite crystals.

4.4.6 The Ratios Zr/Y and Zr/Hf

Elemental ratios involving high field strength elements (Zr/Y, Zr/Hf) show variability beyond that of analytic error (figure 4.18). Among basalts, Zr/Y increases with progressive differentiation. This relationship holds at Vestmannaeyjar also, where Eldfell hawaiites have consistently higher Zr/Y than do primitive Surtsey basalts. Evolved basalts at Austurhorn and Vestmannaeyjar have Zr/Hf comparable to those of coexisting MgO-rich liquids. Zr/Y and Zr/Hf are lower in Hvalnesfjall gabbros than in the basalts although there is some overlap between the two groups (figure 4.18). These ratios do not correlate with MgO content of the gabbros but do reflect modal clinopyroxene contents and also have a broad inverse correlation with the modal proportion of FeTi oxides (table 4.4). Austurhorn basalts and gabbros do not contain zircon, hence variable Zr/Y and Zr/Hf may indicate crystallization of a phase in which these elements have different degrees of compatibility (e.g., clinopyroxene; Lemarchand et al., 1987). The negative correlation between Zr/Y and Sc among Austurhorn basalts and gabbros (figure 4.19) suggests that Y is somewhat more compatible than Zr in clinopyroxene.

Among the felsic rocks, Zr/Y and Zr/Hf are controlled primarily by zircon precipitation; these ratios decrease progressively from granodiorite to iron-rich granitoids to granophyres and rhyolites. High Zr/Y in the granodiorites reflects the greater compatibility of Y relative to Zr in the FeTi oxide- and clinopyroxene-rich crystallizing

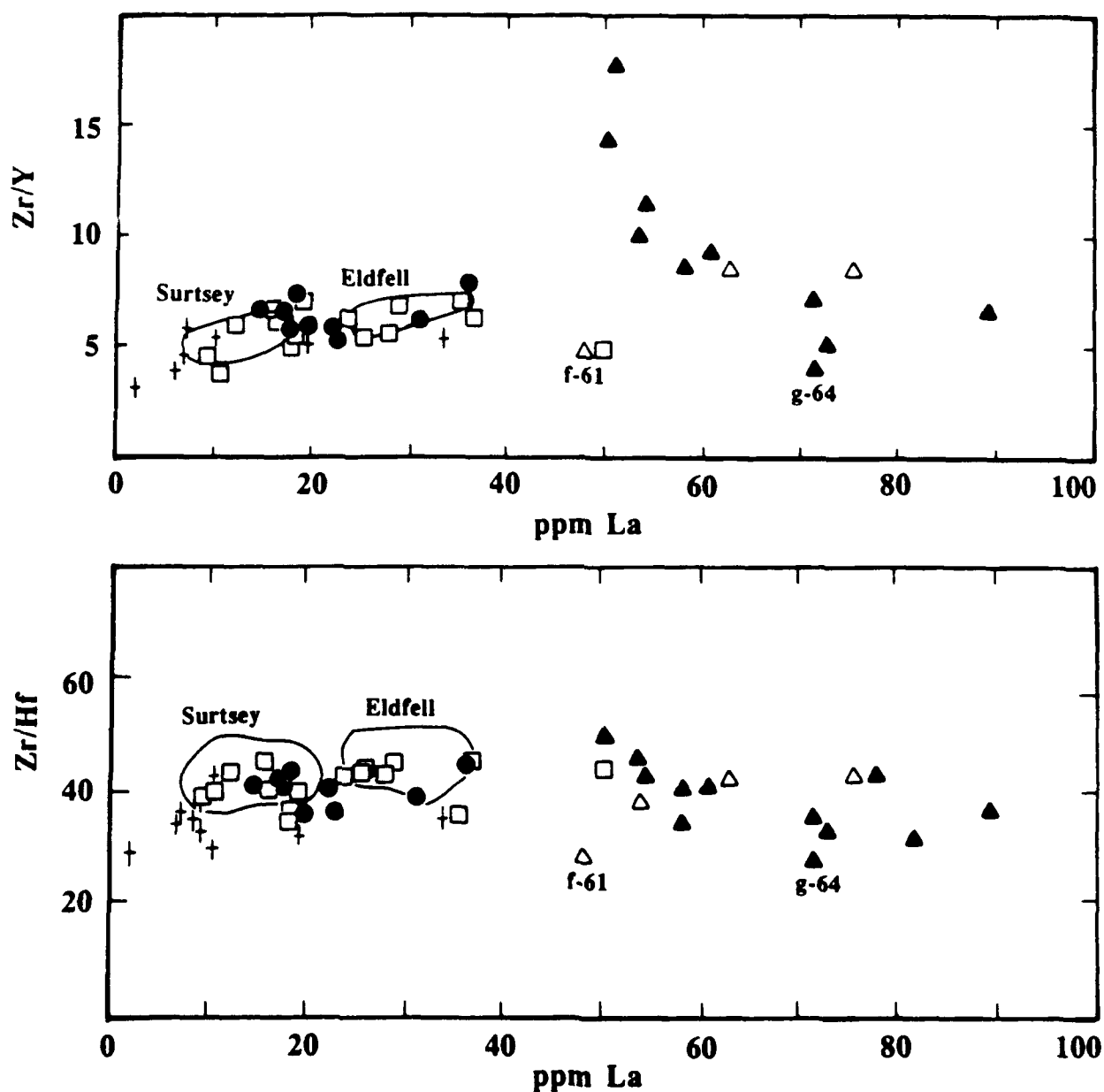


Figure 4.18 Ratios of high field strength elements are comparable for basalts from Austurhorn and Vestmannaeyjar. Among basalts Zr/Y increases gradually with differentiation (see figure 4.19). Both Zr/Y and Zr/Hf decrease among evolved samples due to zircon fractionation. High Zr/Y in granodiorites reflects the greater compatibility of Y relative to Zr in FeTi oxides and/or clinopyroxene throughout the fractionation sequence.

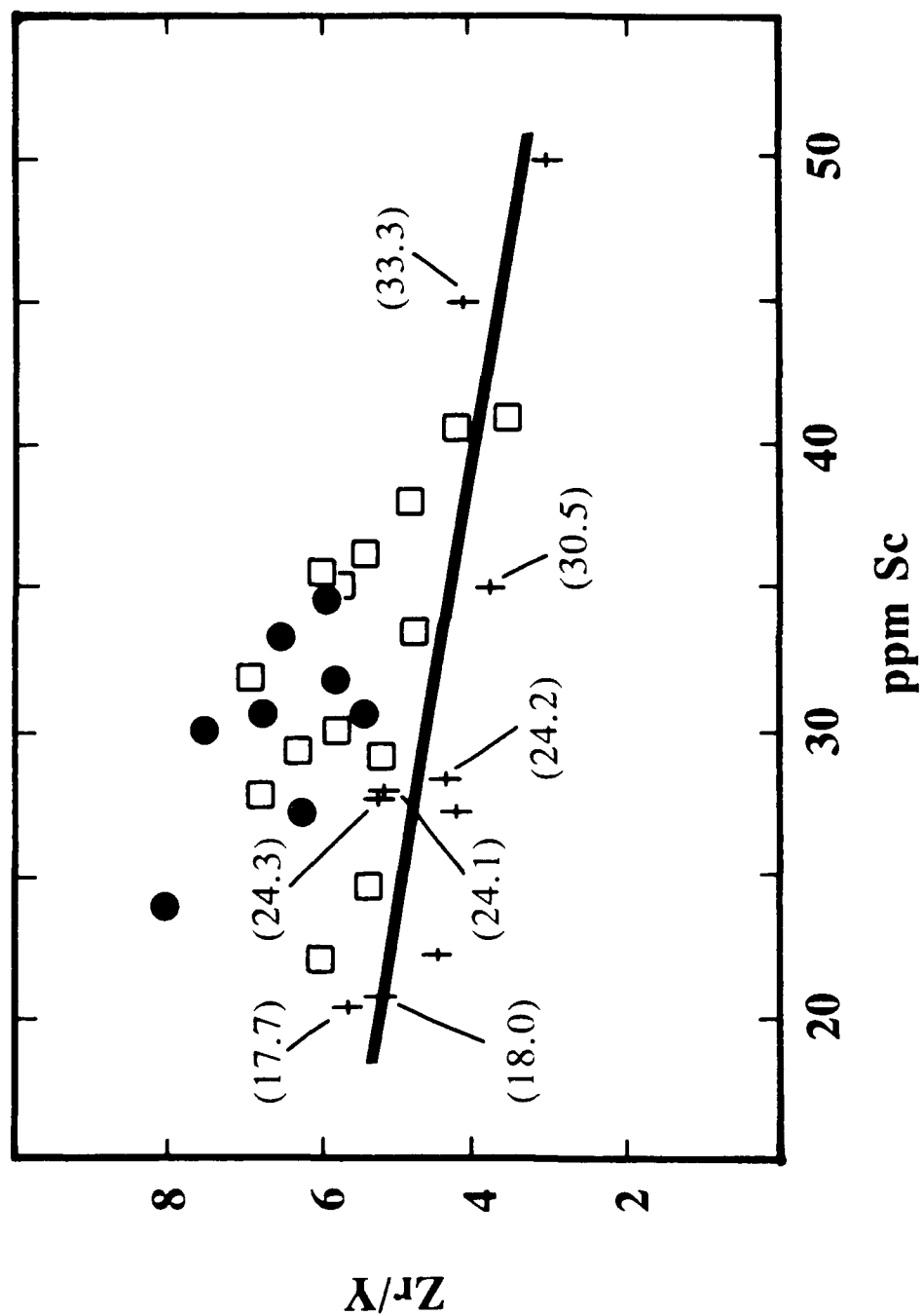


Figure 4.19 A negative correlation between Zr/Y and Sc, particularly among Austurhorn gabbros, suggests that clinopyroxene incorporates Y in slight preference to Zr. Gabbro samples with >40 ppm Sc are interpreted as clinopyroxene accumulates (see figure 4.15). Trend shown is for gabbro samples only; numbers in parentheses indicate calculated modal percentages of clinopyroxene (table 4.4). Symbols as in figure 4.13.

assemblage inferred for the basalt-dacite fractionation interval (see chapter 3). Samples f-61 and g-64 have anomalously low Zr/Y and Zr/Hf although bulk Zr of the latter granophyre is not unusually low (figure 4.14).

4.4.7 Radiogenic Isotopic Data

There are well documented secular and geographic variations in the trace elemental (La/Sm) and Sr isotopic character of Tertiary and recent Icelandic basalts which indicate a component of spatial and/or temporal source variability in the sub-Icelandic mantle (O'Nions & Pankhurst, 1973; Schilling et al., 1982; O'Nions et al., 1976). Austurhorn basalts have La/Sm and $^{87}\text{Sr}/^{86}\text{Sr}$ comparable to those of coeval samples from eastern Iceland (figure 4.20). The range of La/Sm at Austurhorn is less than that observed within the Tertiary sequence as a whole, suggesting that the secular trends are real, rather than an artifact of limited sampling. Neovolcanic basalts show a wider range in $^{87}\text{Sr}/^{86}\text{Sr}$ than their Tertiary counterparts, although individual centers yield nearly constant $^{87}\text{Sr}/^{86}\text{Sr}$ and $^{143}\text{Nd}/^{144}\text{Nd}$. Silicic lavas from central volcanoes tend towards higher $^{87}\text{Sr}/^{86}\text{Sr}$ than coexisting basalts, although complete overlap is often observed (O'Nions & Pankhurst, 1973; O'Nions & Gronvold, 1973; O'Nions et al., 1973, 1976; Sun & Jahn, 1975; Zindler et al., 1979; Wood et al., 1979; Condomines et al., 1983; Stecher et al., 1986; Gunnarsson, 1988; Park et al., in prep.). At Austurhorn, Sr isotope data on four samples of gabbro and granophyre are within analytical precision, suggesting derivation from a common and uniform source (initial $^{87}\text{Sr}/^{86}\text{Sr} = 0.70350\text{--}0.70354$; O'Nions & Pankhurst, 1973).

Tertiary basalts from eastern and western Iceland exhibit temporal changes in Pb isotope systematics which are decoupled from secular trends in REE and radiogenic Sr (Schilling et al., 1982; Hanan & Schilling, 1986, 1987). Austurhorn samples have radiogenic Pb signatures comparable to, or less radiogenic than, those of coeval samples analyzed previously from eastern Iceland (figure 4.21; Hanan & Schilling, 1986, 1987).

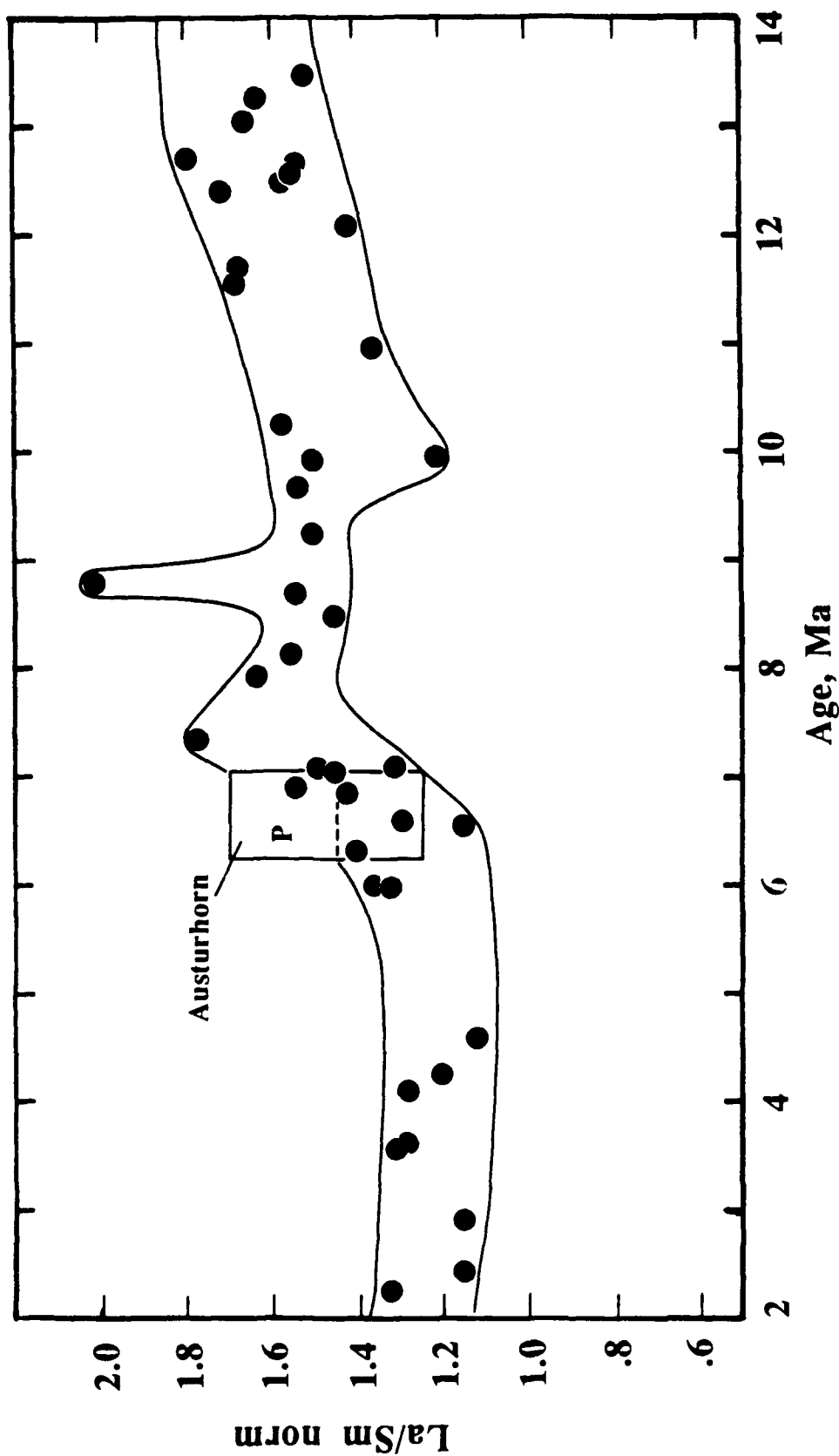


Figure 4.20a

Secular variations in La/Sm and $^{87}\text{Sr}/^{86}\text{Sr}$ in basalts from eastern Iceland.

Mafic dikes and pillow basalts from Austurhorn have La/Sm comparable to that of coeval basalts from northeastern Iceland (data from Meyer, 1984 and Meyer et al., 1985). Austurhorn dike samples plot within the boxed region, with pillow basalts restricted to the portion labeled "P." The shape of the secular trend is not changed by using data of Wood (1978), although the latter data show a greater absolute range in La/Sm .

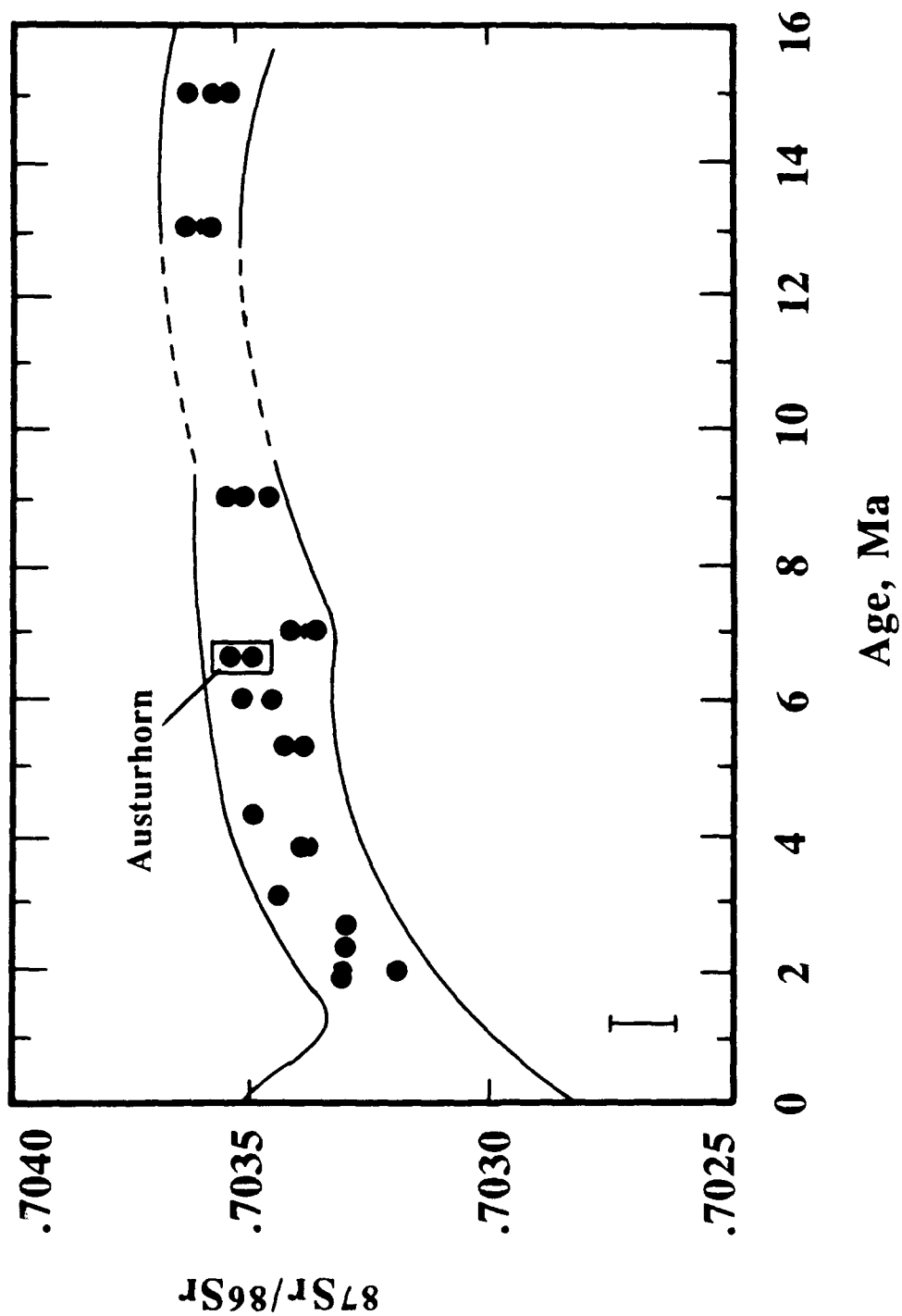


Figure 4.20b Austurhorn gabbro and granophyre have indistinguishable $^{87}\text{Sr}/^{86}\text{Sr}$ which fall within a consistent secular trend of gradually decreasing radiogenic Sr from ~15 - 2 Ma (O'Nions et al., 1976). Neovolcanic samples from the EVZ show much greater variability (individual data points not shown; Park et al., in preparation).

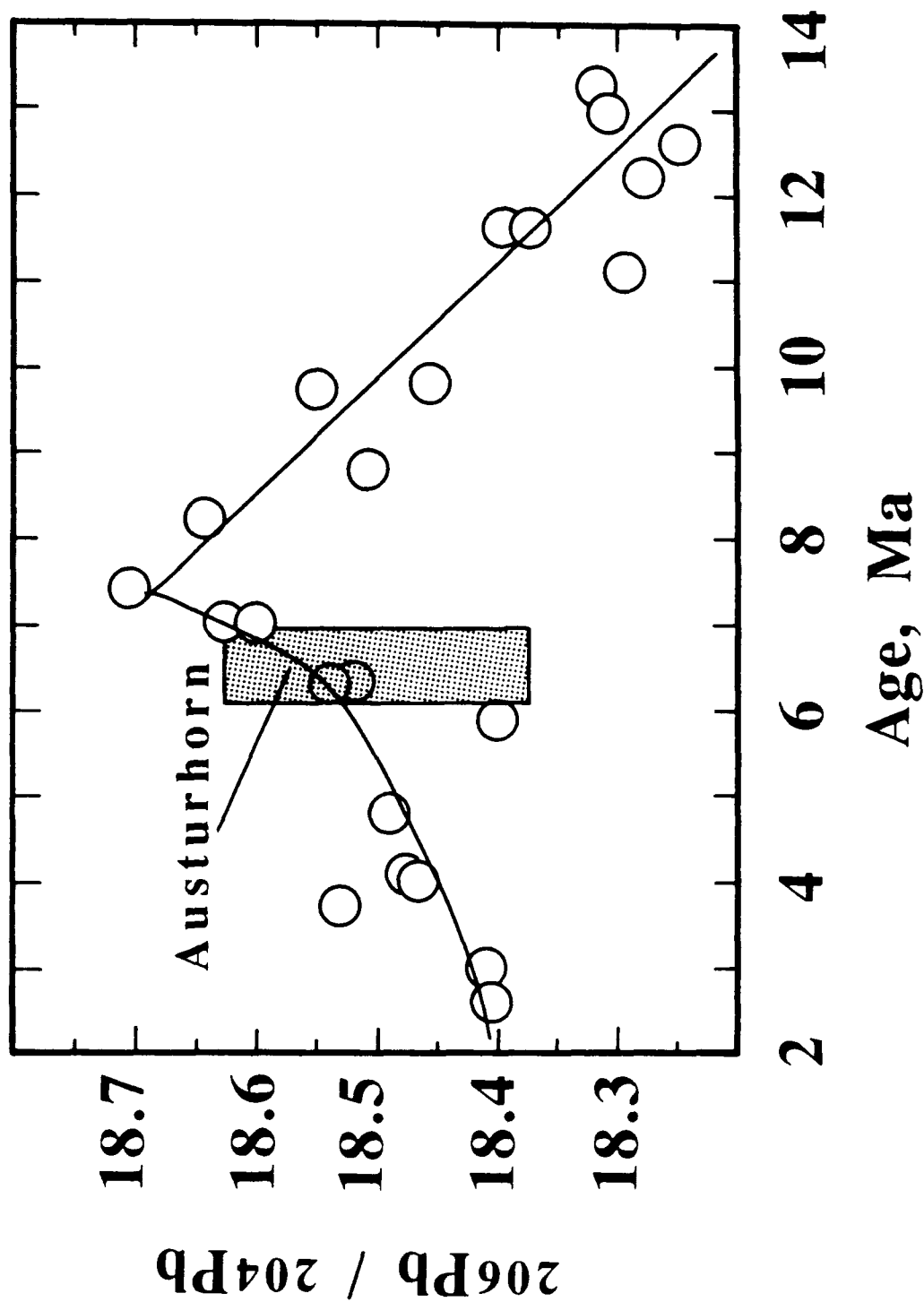


Figure 4.21 Secular variation in radiogenic Pb, based on basalts from eastern Iceland. The shaded field encompasses Austurhorn samples (B. Hanan, pers. comun. 1988).

The range of Pb isotopes observed among basalts, gabbros and granophyres at Austurhorn exceeds those of the neovolcanic basalt centers Vestmannaeyjar and Veidivotn (figure 4.22; Park et al in preparation). These latter basaltic systems have Pb isotopic signatures that are homogeneous within each suite but do not overlap despite comparable ranges in $^{87}\text{Sr}/^{86}\text{Sr}$ and $^{143}\text{Nd}/^{144}\text{Nd}$ (Park et al., in preparation). Austurhorn rhyolite f-61 is enriched in ^{206}Pb relative to the other samples (figure 4.22; section 4.4.8). With the exception of this single sample, mafic and felsic rocks from Austurhorn have overlapping radiogenic isotopic characteristics and may be considered to derive from a common mantle source.

4.4.8 Geochemistry of Rhyolite f-61

One felsic sample (glassy rhyolite f-61) is petrographically and geochemically distinct from the remainder of the Austurhorn suite. This dike is comprised of ~27 vol% crystals of anorthoclase and quartz with minor FeTiMn oxides (see table 4.4) in a matrix of fresh glass in which a gentle flow texture is preserved locally. The crystals are typically fractured and infilled by glass (see chapter 3), and I interpret the textures as indicative of partial melting.

This sample has anomalously low abundances of most incompatible elements (REE, Zr, Hf, Y, Nb, Ta, Th, Cs; figures 4.9, 4.14) but has Sr, Ba and Rb concentrations comparable to granophyres of similar silica content (figure 4.9a). The REE pattern of sample f-61 is different from other Austurhorn felsic rocks: it has unusually high La/Sm (figure 4.14) and a large negative Eu anomaly (figure 4.16). Finally, this sample is enriched in ^{206}Pb relative to both mafic and felsic samples at Austurhorn (figure 4.22). The textural and geochemical evidence suggest this rhyolite had a different petrogenetic evolution than the majority of Austurhorn samples (see section 4.9.3).

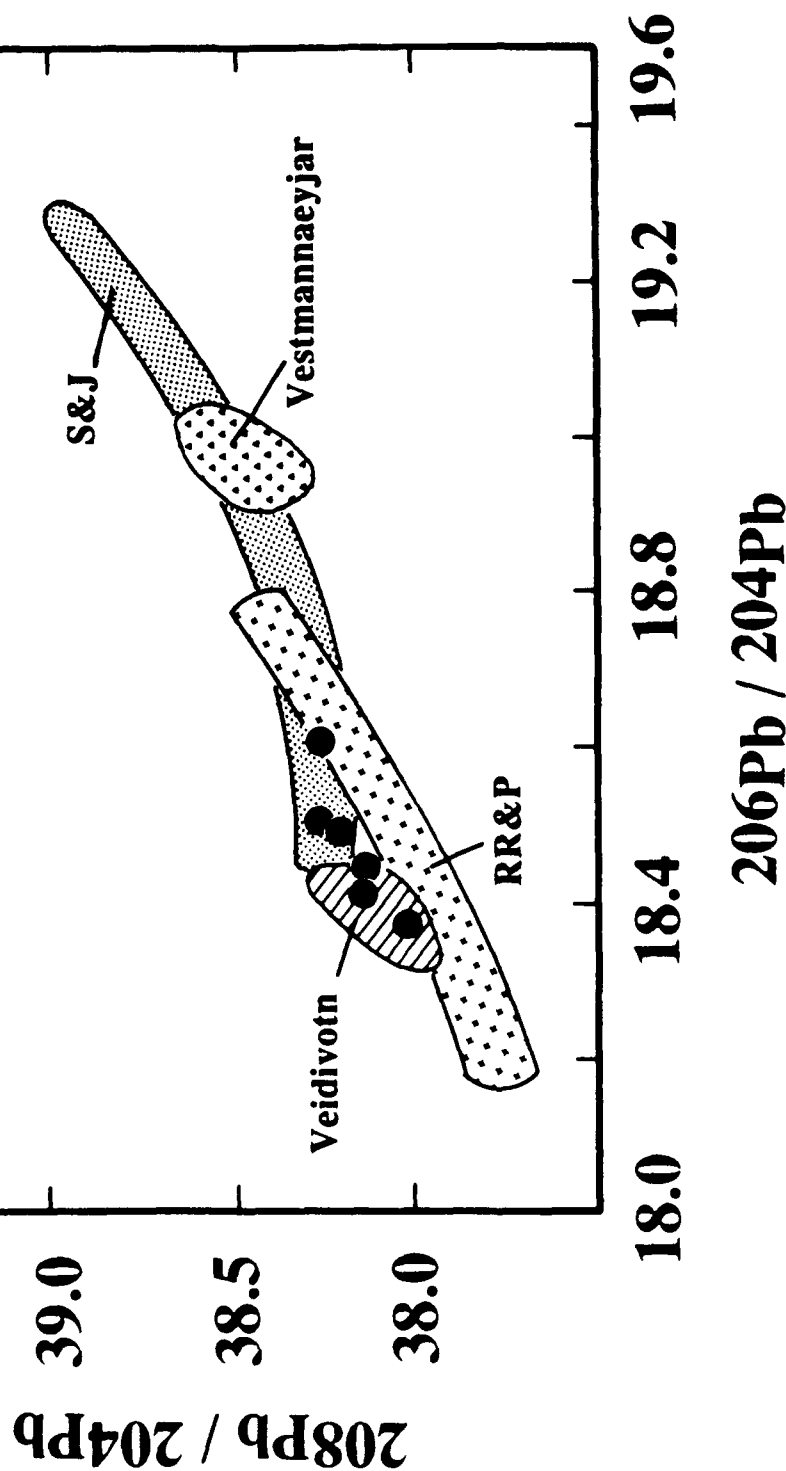
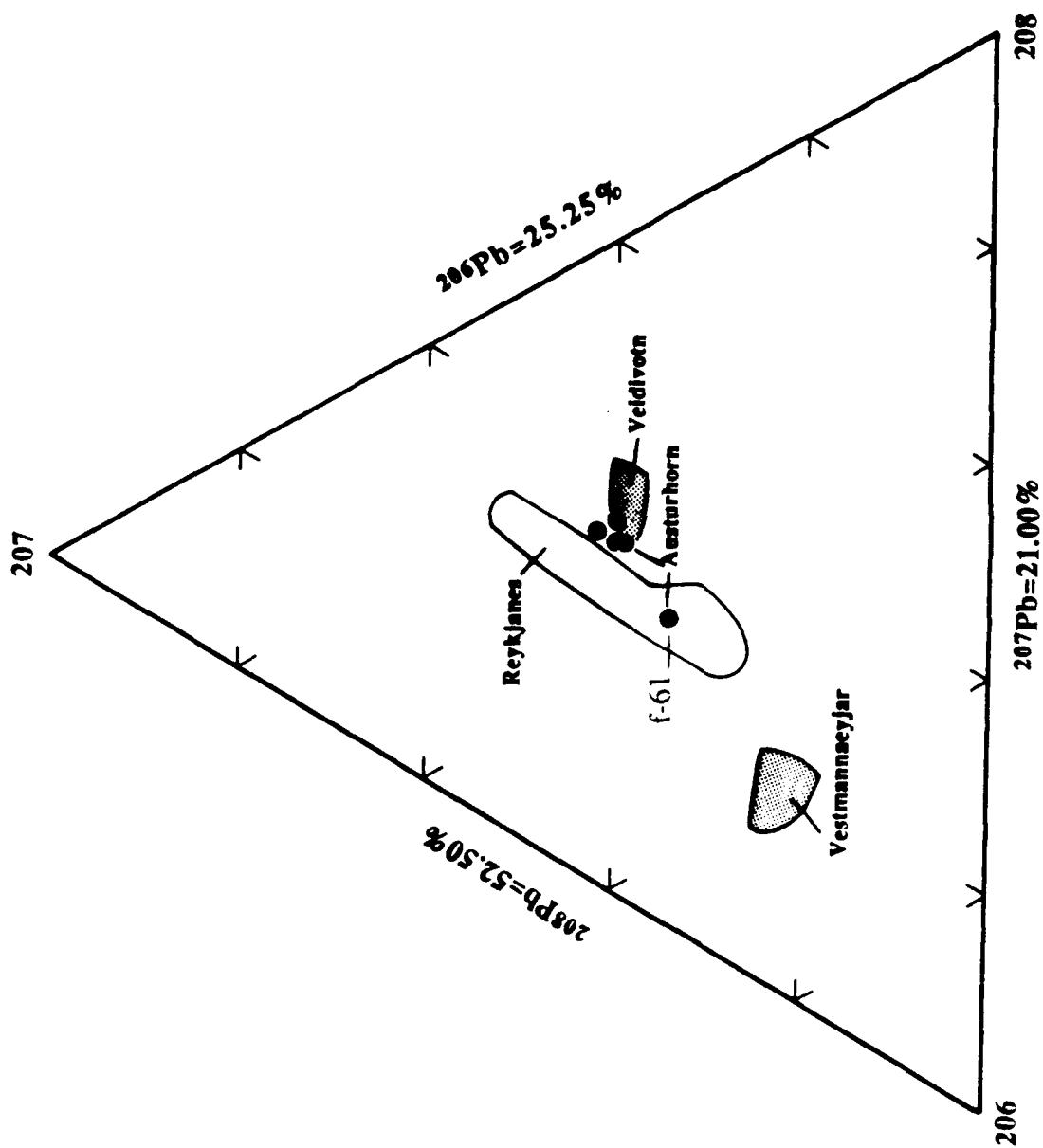


Figure 4.22a

Pb isotopic composition of Austurhorn samples (Hanan et al., in preparation).

Samples from Austurhorn have more variable radiogenic Pb isotopes than neovolcanic tholeiites from Veidivotn or alkali basalts from Vestmannaeyjar (Park et al., in preparation). This observation corroborates evidence from incompatible trace elements (figure 4.17) suggesting a component of source heterogeneity beneath the Austurhorn system. No apparent correlation exists between bulk chemistry and isotopic composition of the Austurhorn suite. Fields labels RR&P (data from Sun et al., 1975) and S&J (Sun & Jahn, 1979) indicate the total variation in Pb isotopes observed along the Reykjanes Ridge and Peninsula and in the neovolcanic basalt systems, respectively.

Figure 4.22b The relative percentages of each Pb isotope [$^{206}\text{Pb}/^{204}\text{Pb}$, $^{207}\text{Pb}/^{204}\text{Pb}$, $^{208}\text{Pb}/^{204}\text{Pb}$; see Hanan & Schilling, 1987 for discussion] are comparable for Austurhorn basalts and granophyres, but felsic dike f-61 is enriched in ^{206}Pb , suggesting a different source component for this sample. This evidence is consistent with petrographic and trace element indications that f-61 derived by crustal melting rather than fractionation of basalt.



4.5 Distinctive Basic Compositional Groups

Three groups of basaltic liquids are identified on the basis of field relationships, petrography and/or major and trace element characteristics. These groups are: transitional tholeiitic mafic pillows, alkaline dikes and tholeiitic or transitional tholeiitic dikes. I first examine geochemical variations within each of these suites, then explore relationships between the groups. None of the Austurhorn basalts represents a primary melt of peridotite with olivine of $Fo_{>88}$. They have $Mg\# < 53$ (calculated with total iron as Fe^{+2}) and contain less than 100 ppm Ni and 175 ppm Cr. These values are typical for Tertiary basalts from eastern and western Iceland (Carmichael et al., 1973; Wood, 1978; Meyer, 1984) and indicate a greater degree of evolution than that observed along the Reykjanes Ridge and the MAR (Jakobsson et al., 1978; Zindler et al., 1979; Sigurdsson, 1981). Rare lavas with phenocrysts of Fo_{88-89} olivine from the Tertiary Vestfirðir region (NW Iceland; Meyer, 1984 and pers. commun., 1988) indicate that the predominance of iron-rich liquids may not require an iron-rich mantle source in the Tertiary. Rather, the lack of erupted and hypabyssal primitive compositions in the Tertiary centers suggests significant fractionation of mantle-derived liquids at crustal levels.

4.5.1 Mafic Pillows

Discussion of the mafic pillows as a group is warranted by their coherent field appearance and petrology (see chapter 3). Pillows contain < 3 vol% tabular plagioclase crystals in a matrix of plagioclase + augite + FeTi oxides +/- olivine. Rapid cooling is indicated by sector-zoned augite, sheaflike and swallowtail plagioclase and acicular oxides (e.g., Lofgren, 1983), and I interpret pillow margins as liquid compositions (see discussion of pillow formation in chapter 3). Mineralogic and geochemical evidence indicates that pillow interiors, although more slowly cooled, also represent liquids. They have a diabasic texture (< 2 mm crystals) with subophitic intergrowth of plagioclase +

augite + FeTi oxides. Silicate phenocrysts are zoned from cores indistinguishable from those observed near pillow margins to more evolved compositions (figures 4.3, 4.5; see Appendix III). Backscattered electron imaging indicates that crystal cores were not rounded or embayed prior to overgrowth formation. For pillows >1 meter surface dimension, the interiors are more evolved than associated margins and may contain interstitial quartz, albite and K-feldspar. However, all sampled interiors fall within the compositional range defined by margins of pillows <1 meter in dimension (figure 4.8, table 4.1).

The pillow-forming basalts evolve towards silica-oversaturated normative compositions: sample p-41 records progressive differentiation from a magnesian chilled margin (p-41a, Mg# 47.3) to a quartz-normative coarse grained interior (p-41b, Mg# 36.0) (see figure 4.23). Whole rock compositions define an apparent olivine + clinopyroxene + plagioclase cotectic similar to that of Thingmuli lavas (Carmichael, 1964) although mafic Austurhorn liquids extend to nepheline-normative compositions (figure 4.23). The phase boundaries of both Icelandic systems are similar to that determined in anhydrous 1 atm experiments on other basalt systems (e.g., Grove et al., 1982; figure 4.23). However, clinopyroxene phenocrysts in the mafic Austurhorn samples project outside the pseudoquaternary system (figure 4.23) while those in calc-alkaline and normal MOR basalts plot within the reduced tetrahedron.

The majority of pillows sampled in this study (all but two) are more primitive than those analyzed by Mattson et al (1986) which have maximum MgO content of 5.3 wt%. In addition, several of their samples fall within the Daly gap defined by our samples (54-63 wt% SiO₂; figure 4.8). This difference is primarily one of classification: we restrict use of the term "pillow" to mafic bodies which exhibit a pronounced change in grain size between margin and interior, with quench morphologies present in crystals adjacent to the pillow margin. Based on field descriptions (Mattson, unpublished ms) the "unchilled" and "gradational" pillows of Mattson et al (1986) are the "angular mafic

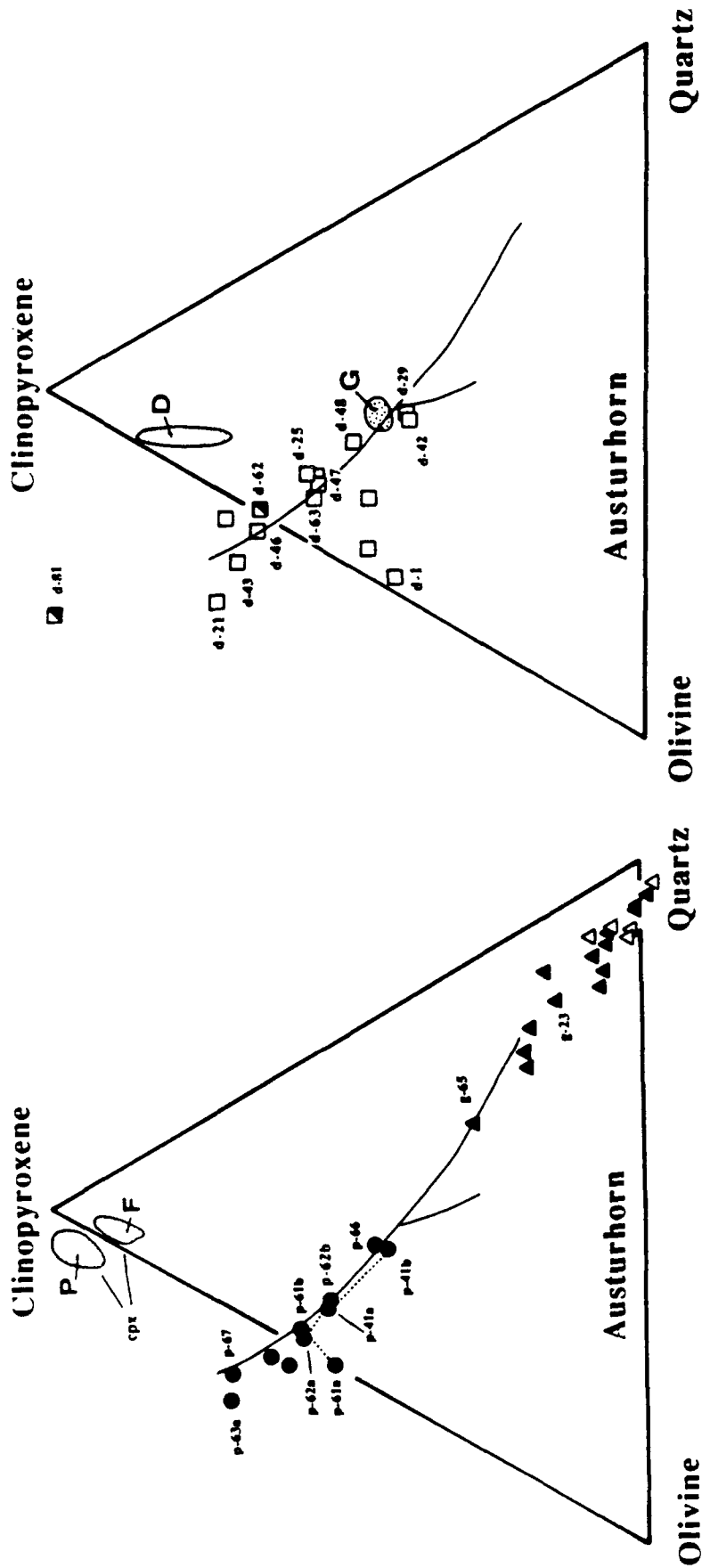


Figure 4.23a Pseudoternary diagrams in the pseudoquaternary system plagioclase-olivine-clinopyroxene-quartz, projected from plagioclase. All compositions were plotted using oxygen units and projecting through ilmenite, with total iron as Fe+2. The 1 atm trend is based on that of Grove et al (1982).
Left: Mafic pillows and felsic samples. Fields labeled P and F indicate microprobe analyses of Austurhorn clinopyroxenes in pillows and felsic samples, respectively. Dashed lines connect pillow rim and interior for p-41, p-61 and p-62 (a=rim, b=interior).
Right: Mafic dikes. The field labeled D encompasses clinopyroxene analyses from dikes d-81 and d-42. The stippled field labeled G is the locus of pigeonite saturation in Galapagos basalts at 1 atm (Juster & Grove, 1988).

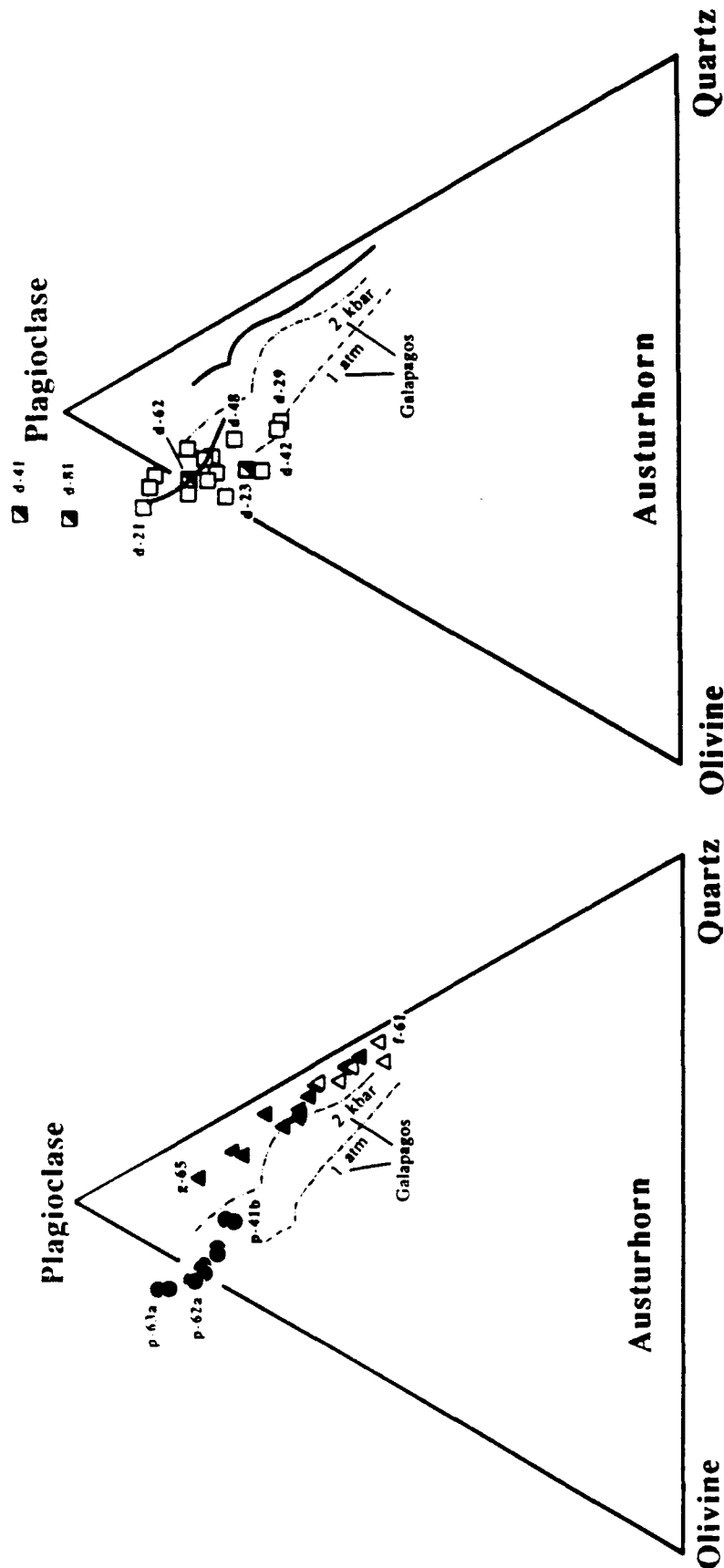


Figure 4.23b

The same data, projected from clinopyroxene. In both panels the dash-dot line indicates 1 atm evolution of Galapagos liquids (Juster & Grove, 1988) and the dash-double dot line is data from Spulber & Rutherford (1983) from cooling rate experiments on a primitive Galapagos basalt at 2 kbars (fluid pressure ~0.66 total pressure).

Left: Mafic pillows and felsic samples. Down-temperature evolution among the pillows proceeds from sample p-63a to p-41b, and from g-65 to f-61 among the felsic samples. Notice that felsic liquids in the Austurhorn data set resembles this higher pressure trend more closely than the 1 atm trends.

Right: Mafic dikes. The solid trends are those of pillows and felsic samples. The alkalic dikes (half-shaded) become more evolved with increasing distance away from the ternary; samples d-41 and d-81 contain 6 and 7% normative nepheline, respectively.

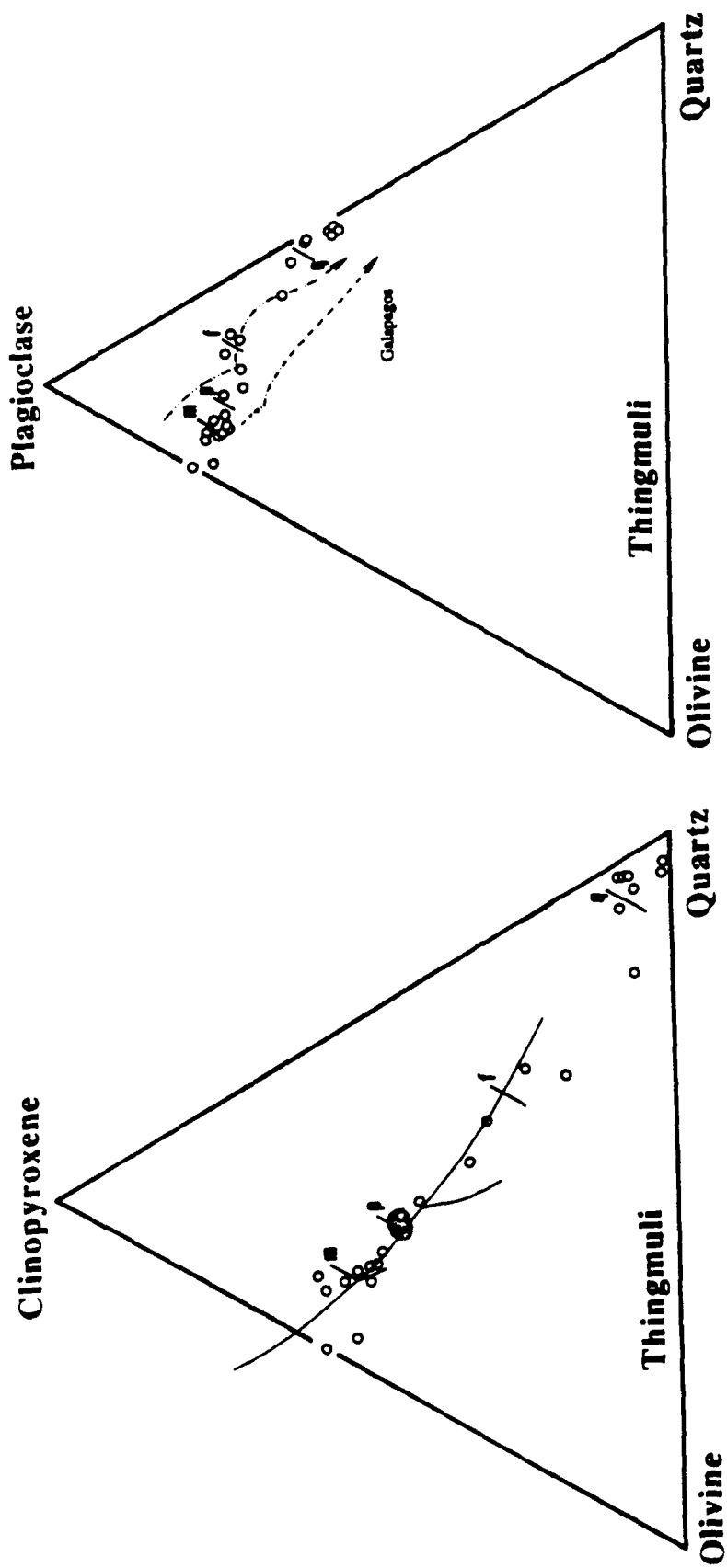


Figure 4.23c Bulk rock analyses from the Thingmuli central volcano in eastern Iceland (Carmichael, 1964) show trends similar to those of Austurhorn samples, but no samples plot outside of the pseudoquaternary tetrahedron.

fragments" and "heterogeneous mixed rocks" discussed in chapter 3. These rock types are not considered in the present analysis. Linear least squares calculations indicate that major element variations in "gradational pillows" can be explained by mixing of mafic and felsic magmas (Mattson et al., 1986). The mixed samples show a linear relationship between compatible and incompatible elements distinct from the curvilinear trends of our samples (e.g., Cr vs. La, figure 4.9c). No samples in the current study provide clear indication of mixing.

4.5.2 Alkaline dikes

One group of dikes is geochemically distinct from the mafic pillows and remaining dikes. Most notably, they are enriched in Rb, K_2O and P_2O_5 relative to the transitional tholeiitic pillows. The dikes are termed "alkaline" because their Na_2O+K_2O contents are greater than those of tholeiites or transitional tholeiites at comparable SiO_2 (figure 4.7). However, the classification of "alkaline" dikes vs. transitional tholeiitic pillows is based on several criteria and does not simply reflect Na_2O+K_2O abundance. Alkaline dikes are characterized by comparatively low Ba/Rb and K/Rb, and high K/Nb and K/La (table 4.5; figure 4.24). They also have elevated P_2O_5 contents which are manifest in high P/Ce and P_2O_5/Hf relative to the mafic pillows (figures 4.17, 4.24; table 4.5). Sample d-62 is included in this category by virtue of its high P_2O_5 content; this sample does not have unusual alkali abundances (table 4.5). Previous studies sampled no alkali-rich liquids at Austurhorn (Blake, 1964, 1966; Mattson et al., 1986); their volume is clearly subordinate to that of the transitional tholeiites.

The dikes are sparsely phyrlic and contain groundmass plagioclase + augite + FeTi oxides. Alkaline dikes were emplaced into Austurhorn's most primitive mafic sill (d-44 into d-46) as well as both molten (d-81) and solidified granophyre (d-23, d-41, d-62). They range from hypersthene normative (d-62, Mg# 37.3) to silica-undersaturated: samples d-81 and d-41 contain 6 and 7% normative nepheline at Mg#s 35.9 and 29.2,

Table 4.5 Geochemical Characteristics of Selected Icelandic Basalts

	MgO	K/Nb	K/La	K/Rb	Ba/Rb	P/Ce	P2O5/Hf	Zr/Hf
Alkalic Dikes								
d-23	4.01	783	853	nd	nd	39.2	.08	43.0
d-41	2.55	564	448	256	4.6	45.9	.12	43.9
d-43	5.37	401	484	263	5.5	37.5	.08	42.9
d-44	2.05	443	423	304	9.1	53.3	.14	42.7
d-81	3.97	508	459	242	5.0	58.1	.15	42.0
d-62(+)	4.74	2.92	3.06	5.44	17.7	66.6	.18	42.4
Mafic Pilows								
p-41a	5.67	388	317	443	11.2	25.6	.06	36.4
p-41b	3.57	361	356	487	14.6	35.4	.07	44.4
p-61a	6.61	371	384	495	13.2	33.3	.06	41.4
p-61b	5.62	450	497	466	11.9	33.3	.07	43.1
p-62a	6.27	390	381	443	12.6	36.5	.07	42.2
p-62b	5.65	305	305	505	15.2	29.2	.06	35.7
p-65	5.42	268	279	348	18.4	28.8	.06	40.2
p-67	6.00	299	310	535	15.8	34.4	.07	40.6
Granophyres								
(12)	0.05	228	328	309	3.7	0.2	<.01	27.8
	1.44	646	523	470	13.4	5.7	<.01	49.8
Eldfell								
(6)	3.32	242	334	398	11.2	35.6	.08	44.3
	4.70	273	346	430	12.6	36.8	.09	48.1
Surtsey								
(11)	7.01	229	307	418	11.3	34.4	.06	40.3
	11.82	279	363	573	14.3	37.4	.08	45.7
Torfajokull								
(2)	3.48	200	nd	814	nd	nd	.03*	40*
	5.95	215	nd	841	nd	nd	.33*	44*
Snaefellsnes								
(10)	5.40	nd	nd	278	13.2	nd	nd	nd
	7.20	nd	nd	739	52.1	nd	nd	nd

Sources of data: Eldfell, Surtsey Furman et al., 1988
Torfajokull Ivarsson et al., in press
Snaefellsnes Oskarsson et al., 1982; Steinthorsson et al., 1985

Numbers in parentheses indicate the number of samples reported for each group. Data for these groups reflect minimum and maximum values in each category.

+ Sample d-62 has P/Ce and P2O5/Hf comparable to Austurhorn alkali-rich dikes but is not enriched in monovalent alkali elements.

* Hf abundances for Torfajokull calculated assuming Zr/Hf = 40-44, using given Zr data

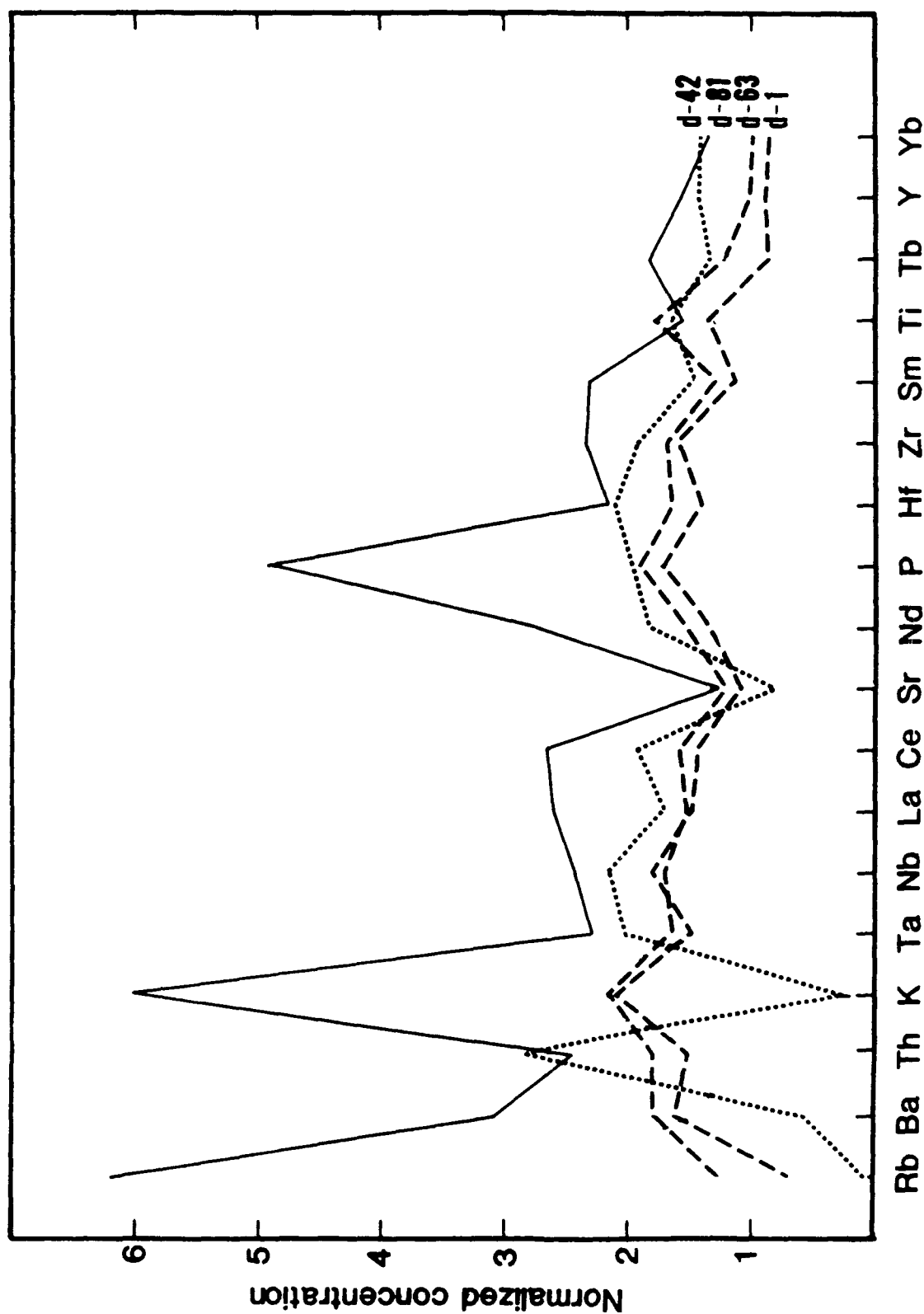


Figure 4.24 Extended Coryell-Masuda diagram for selected Austurhorn samples, normalized to the least evolved Austurhorn basalt [d-45]. The alkalic sample (d-81, solid line) is enriched in Rb, K and P relative to transitional tholeiites (long-dashed lines). The dotted line is a visibly altered dike (sample d-42) - notice that alteration causes linked depletions in K, Rb and Ba, not selective enrichments as observed in the alkalic dike.

respectively. Sample d-44 (Mg# 16.7) contains normative corundum and is extremely enriched in total Fe (21.3 wt%) and P_2O_5 (1.6 wt%). Note that the P_2O_5 content of this sample is significantly lower than those observed in late stage immiscible liquids (>6 wt%, Dixon & Rutherford, 1979) but corresponds well to an origin by extensive crystallization at low f_{O_2} .

Austurhorn alkali basalt compositions project outside the olivine-clinopyroxene-plagioclase-quartz tetrahedron (figure 4.23). In the nepheline saturated pseudoquaternary system of Sack et al (1987) samples d-41 and d-81 lie adjacent to the experimentally determined 1 atm cotectic for alkalic basalts (Sack et al., 1987) suggesting they have experienced low pressure fractionation (figure 4.25). Samples d-23 and d-62 project slightly outside the nepheline-bearing pseudoquaternary (figure 4.25) whereas the unusual composition of sample d-44 becomes distorted in projection and is not shown. The small number of samples makes a rigorous treatment of differentiation impractical.

4.6 Estimates of Intensive Parameters

Ambient oxygen fugacity plays an important role in determining the fractionation history of magma series, because it controls FeTi oxide precipitation. Removal of magnetite and ilmenite from a basalt enriches the residual liquid in silica and depletes it in total iron, whereas limited FeTi oxide precipitation results in iron enrichment at roughly constant silica content (e.g., Carmichael et al., 1974). The Austurhorn suite includes samples with a large range in both silica and iron content; for this reason I investigated the apparent oxygen fugacity under which individual rock types crystallized.

Sandwich lamellae of magnetite and ilmenite with demonstrated Mg/Mn equilibrium in sample p-67 indicate temperatures of 708-748°C at $\log f_{O_2}$ between -15.1 and -15.7, i.e., along the Ni-NiO buffer (figures 4.26, 4.27; Andersen & Lindsley, 1988; Bacon & Hirschmann, 1988). These results can not be extrapolated unambiguously to magmatic conditions but do suggest oxidizing conditions during cooling of the pillow

magmas. Magnetite and ilmenite lamellae in individual oxide grains from Hvalnesfjall gabbro also indicate cooling near the NNO buffer at magmatic temperatures (897-1158°C; figure 4.26). Adjacent magnetite and ilmenite domains in glassy rhyolite f-61 record oxygen fugacity slightly above the NNO buffer at 955°C (figures 4.26, 4.27). The calculated oxygen fugacities are higher than those inferred for basalts at Vestmannaeyjar, Jan Mayen and Vestfirðir, but are comparable to f_{O_2} calculated for icelandite and rhyolite from the 1875 Askja eruption (figure 4.26).

Coexisting magnetite and ilmenite in Austurhorn mafic dikes do not record Mg/Mn equilibrium and are therefore unsuitable for estimating oxygen fugacity during crystallization (Bacon & Hirschmann, 1988). However, comparison of iron and titanium concentrations between the mafic dikes and pillows suggests that most dikes evolved under lower oxygen partial pressures than those inferred from pillow and gabbro samples. In general, the mafic dikes have maximum FeO* and TiO₂ that are higher and occur at lower MgO content than peaks observed in the pillow suite (figure 4.28). One extreme example is alkali-rich dike d-44 which is highly enriched in both iron and titanium at low MgO (figure 4.28). The shifts in magnitude and MgO content of peak iron and titanium abundances indicate earlier saturation of magnetite and ilmenite in pillows relative to most dikes, and imply variable conditions of oxygen fugacity in the magma system as a whole.

This inference is supported by experimental determinations of the 1 atm liquid line of descent of an FeTi-rich Galapagos basalt at oxygen fugacities between QFM and NNO⁺² (2 log units above NNO; Juster & Grove, 1988). Under oxidizing conditions (i.e., NNO⁺²) enhanced growth of magnetite and, subsequently, ilmenite results in rapid silica enrichment and early FeO depletion relative to crystallization at QFM (figure 4.28). Qualitative comparison of the natural and experimental data suggest that the Austurhorn pillows evolve along a path similar to that of the NNO⁺² Galapagos experiments, and unlike those observed at QFM or more reducing oxygen buffers (figure 4.28). Sample

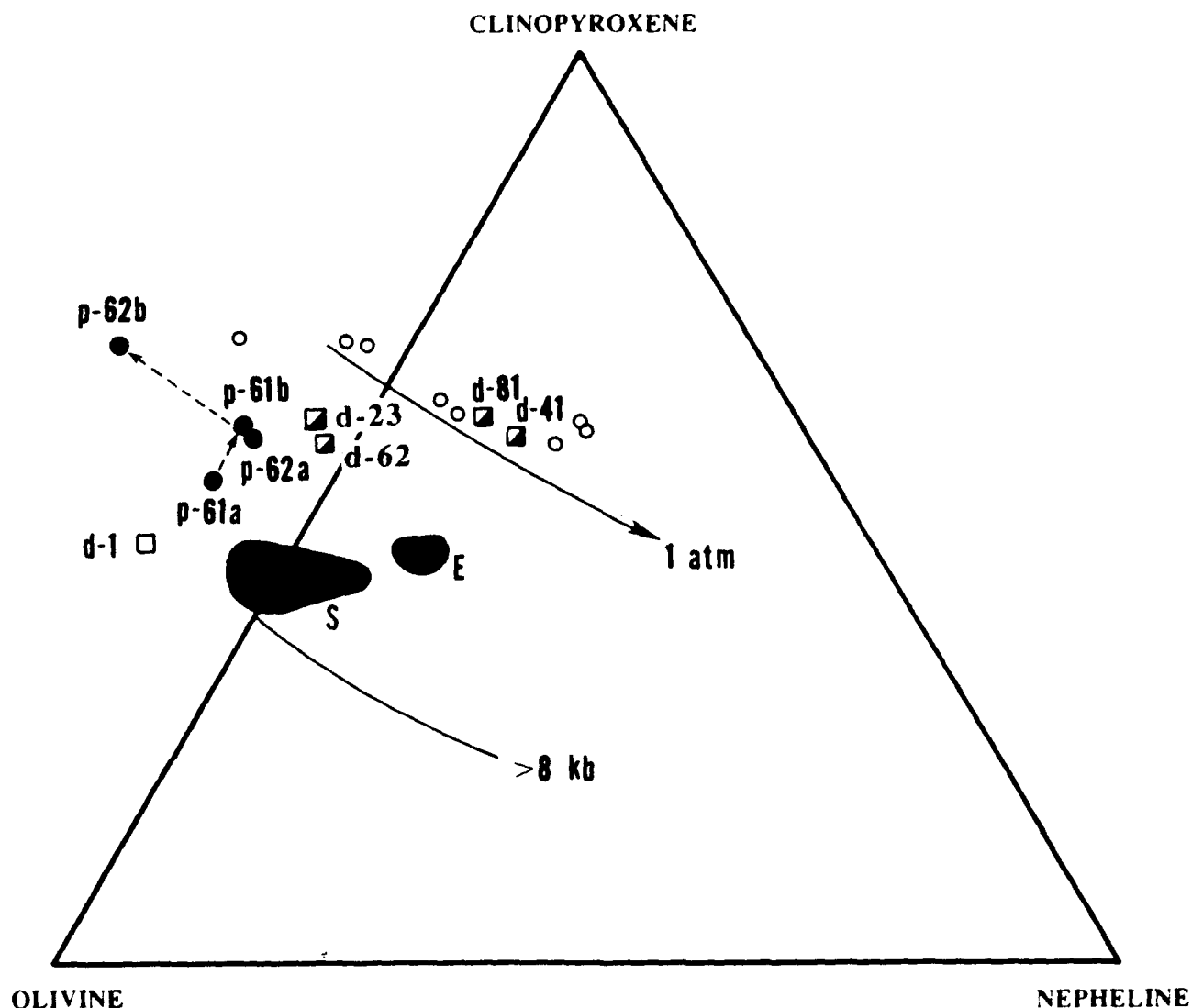
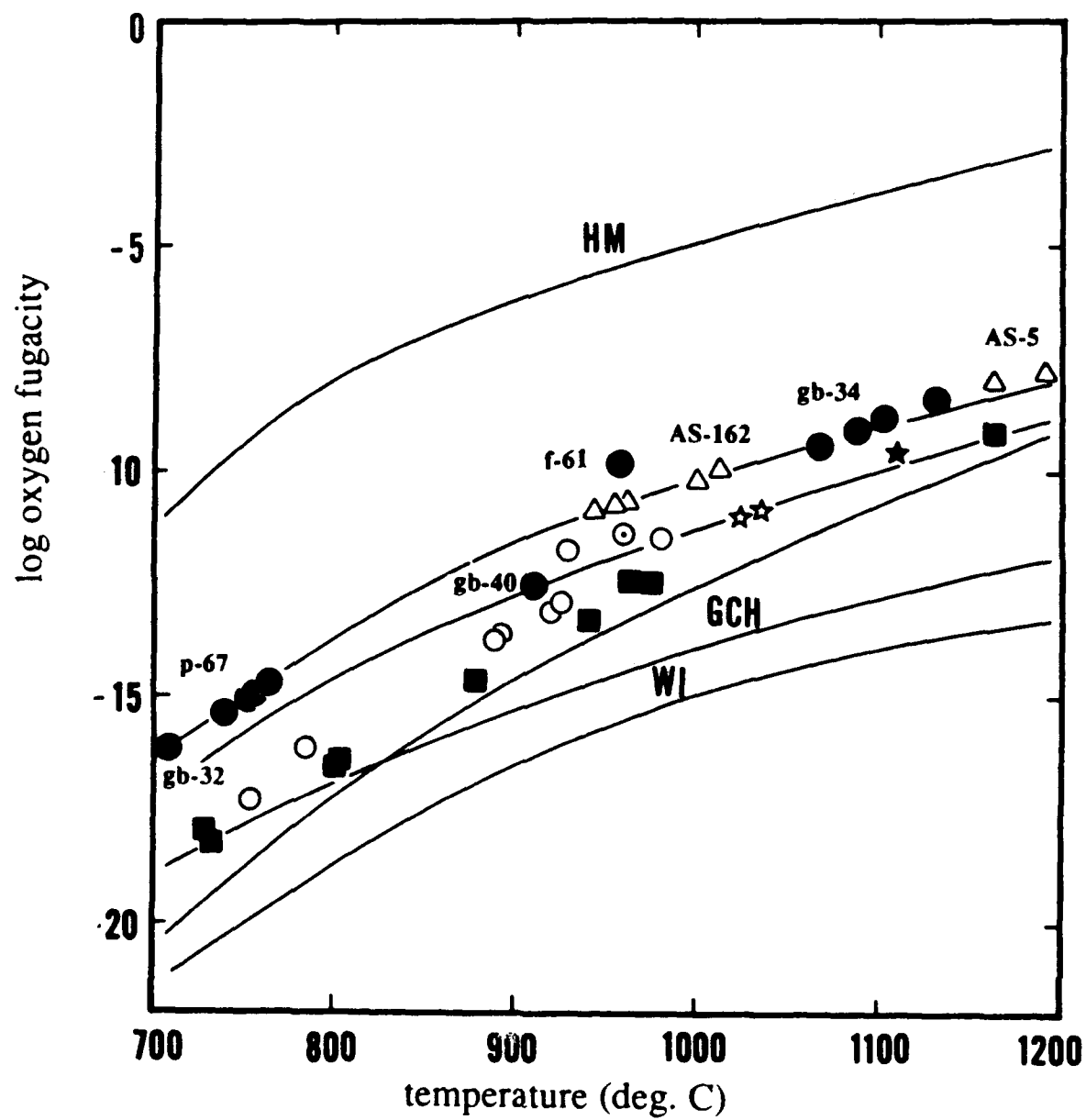


Figure 4.25 Selected samples plotted in the nepheline-saturated pseudoquaternary using the projection scheme of Sack et al (1987). Two alkalic dikes appear to have evolved at low pressures, because they project adjacent to the experimentally determined 1 atm saturation surface for alkalic liquids. For comparison, note the open symbols which are evolved late-stage segregation veins within alkalic lavas from Vestmannaeyjar (field evidence is consistent with their projected position near the 1 atm cotectic). Samples from Eldfell (E) and Surtsey (S) record higher pressure fractionation environments. Austurhorn pillows p-61a,b and p-62a,b are not critically silica undersaturated and evolve away from the nepheline-bearing system.

Figure 4.26a Relationship between temperature and oxygen fugacity determined by coexisting oxide geothermometry. All data have been recalculated assuming stoichiometric distribution of ferric and ferrous iron, and ilmenite/ulvospinel components calculated following Andersen & Lindsley (1988). Filled circles are Austurhorn samples as labeled. Open triangles are icelandite (AS-5) and rhyolite (AS-162) from the 1875 Askja eruption (Sigurdsson & Sparks, 1981). Filled star is a gabbro xenolith (VE-119) from the Eldfell eruption in Vestmannaeyjar, and open stars are from hawaiite (VE-111) erupted in the same episode (Jakobsson et al., 1973). Open circles are data from Jan Mayen (Imsland, 1984). Filled squares are tholeiitic basalt dikes from Vestfirðir (NW Iceland; Meyer, 1978). Data from Jan Mayen are on coexisting grains with the exception of the dotted circle which is from sandwich lamellae in a single grain. Data from Eldfell, Vestfirðir and Askja are from coexisting groundmass crystals. Data from Austurhorn are generally from sandwich lamellae, except for two of the four high-temperature points which are from coexisting crystals in a single thin section (sample gb-34). The other two high-temperature points are from sandwich lamellae from single grains within that same sample. These data suggest that the Askja and Austurhorn samples crystallized and cooled at higher oxygen fugacity than the alkalic Vestmannaeyjar, transitional tholeiitic Jan Mayen and tholeiitic Vestfirðir suites. Oxygen buffers from Spulber & Rutherford (1983). Data are tabulated in Appendix IV.



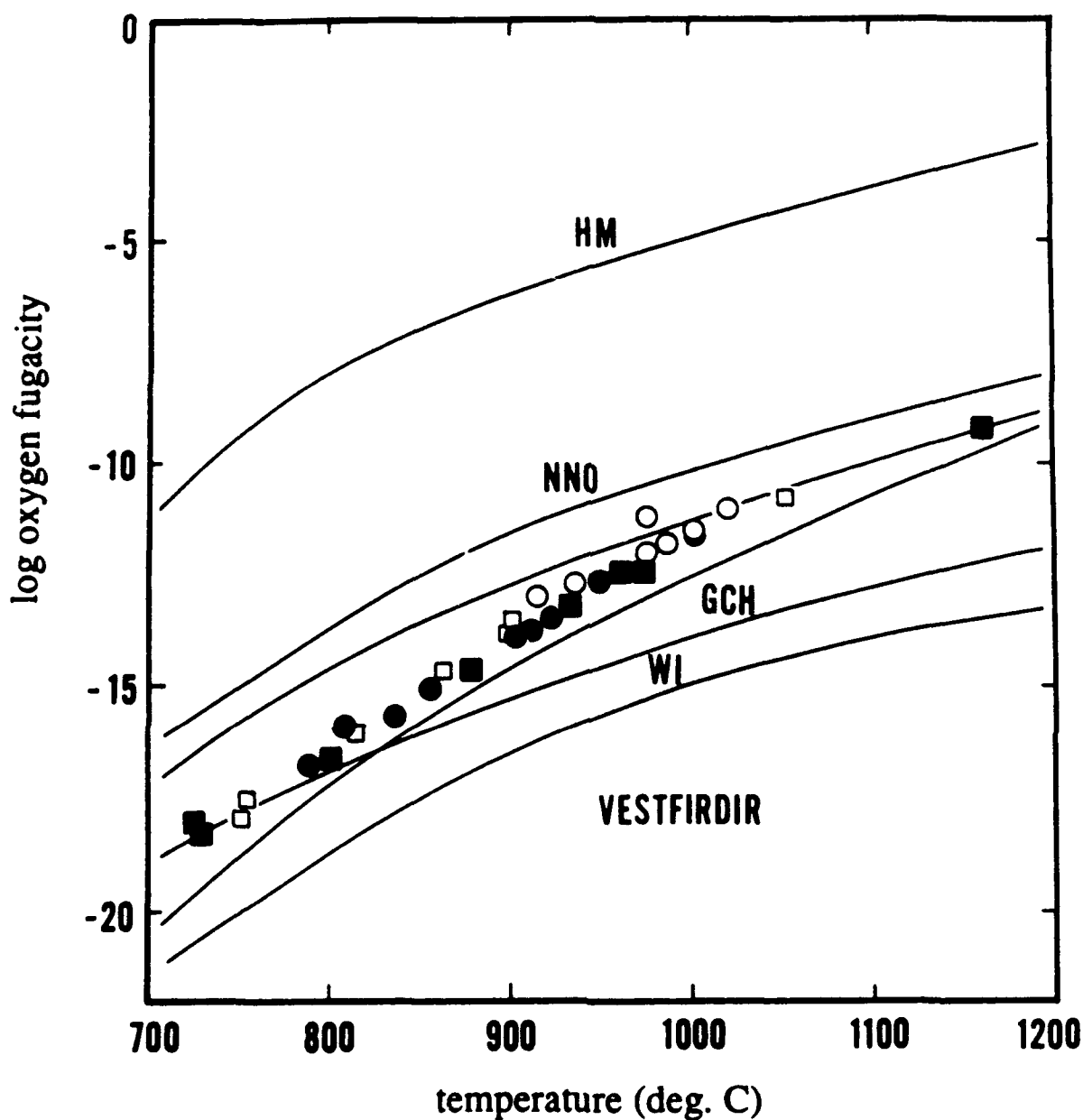


Figure 4.26b The absolute temperatures and oxygen fugacities calculated from microprobe analyses of oxide phases depend upon algorithms used for cation distribution. For example, all data sets shown here use a single set of analyses from Meyer (1978). All circles represent ferric-ferrous redistribution after Carmichael (1967), whereas squares indicate stoichiometric calculations after Sack et al (1980). Open symbols were calculated using the experimental curves of Buddington & Lindsley (1964), and filled symbols use data of Andersen & Lindsley (1988). The **filled squares** are shown in figure 4.26a and were used for comparison with other data sets. Note that all data points lie along a single buffer, although absolute values are not consistent between data sets. Data are tabulated in Appendix IV.

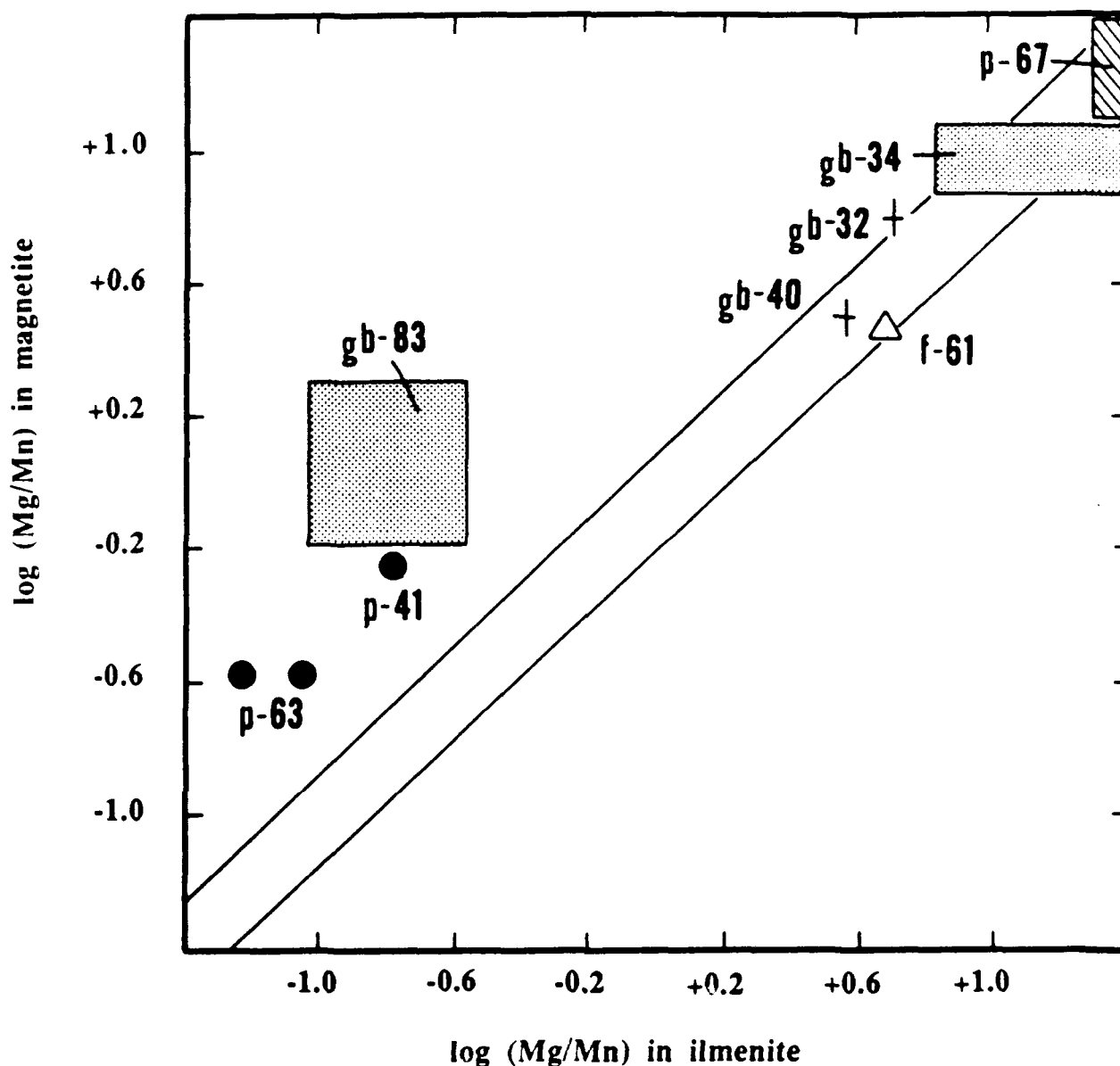
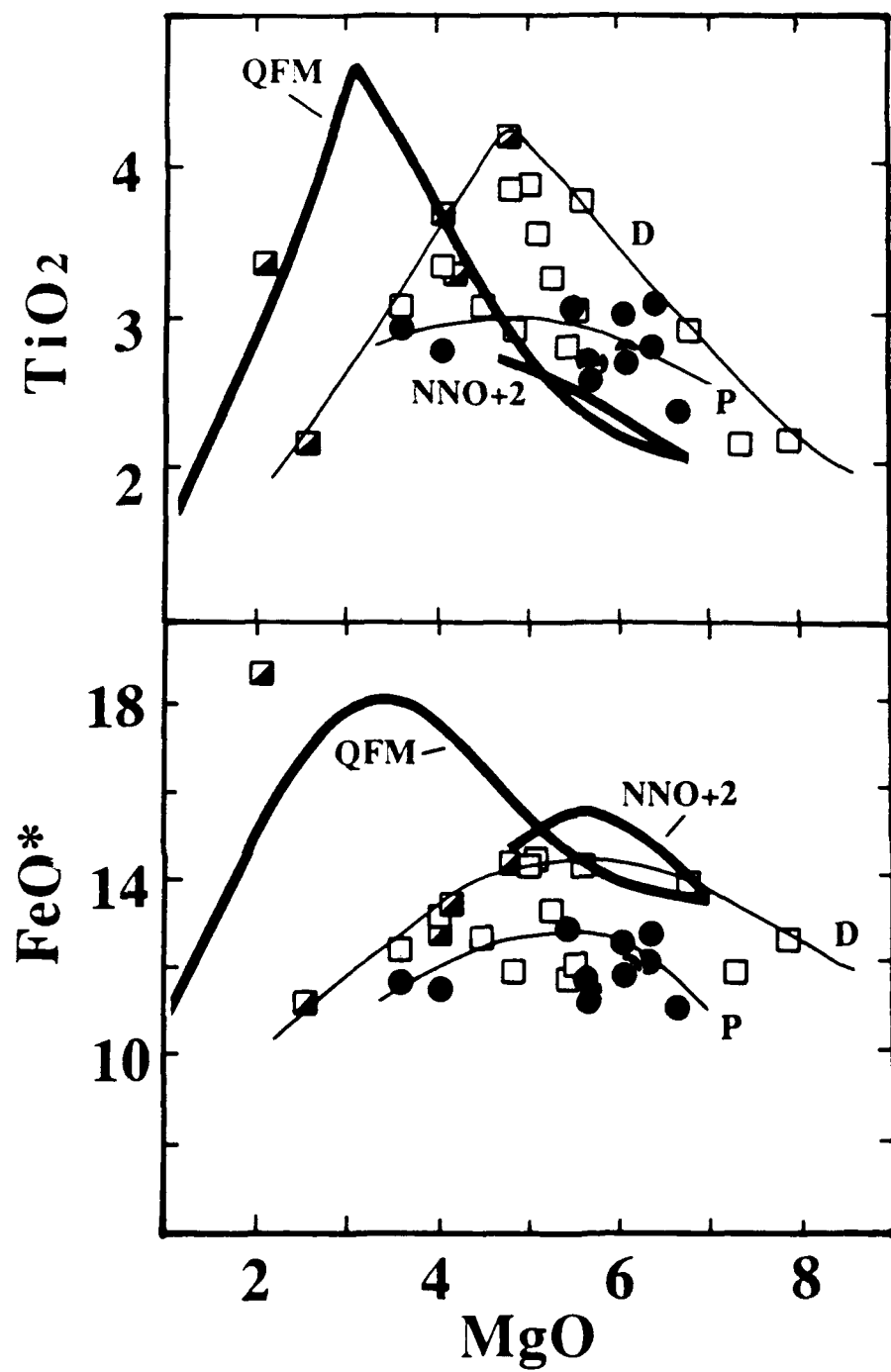


Figure 4.27 Manganese and magnesium can readily become redistributed between coexisting FeTi oxide phases. Bacon & Hirschmann (1988) demonstrated this phenomenon and proposed a quantitative test for Mg/Mn equilibrium. From their compilation of natural and experimental data, the field between the diagonal lines appears to be "acceptable" and allow for reasonable analytic uncertainty. The data for Austurhorn samples are plotted for evaluation. Data from samples p-67, gb-34, gb-32, gb-40 and f-61 have been used in estimating intensive parameters for the Austurhorn intrusion. Data for these samples is shown in figure 4.26.

Figure 4.28 These two panels illustrate the effect of oxygen fugacity on the behavior of Fe and Ti during crystallization. Data points are samples from Austurhorn (symbols as before). Curves labeled **P** and **D** are drawn through pillow and dike samples, respectively. Curves labeled **QFM** and **NNO** indicate data from Juster & Grove (1988) on crystallization of Galapagos FeTi basalt at 1 atm. Notice that the Austurhorn pillows have a lower maximum FeO* than the dikes, and reach this maximum value at higher MgO. When considering TiO₂ notice that the mafic pillows seem to mimic NNO experimental data, whereas some mafic dikes are relatively enriched in TiO₂ and trend more parallel to QFM than to NNO. In summary, we see that the Austurhorn pillows seem to record oxygen fugacity higher than dikes.



d-44 records locally reducing conditions; its composition is similar to those produced experimentally during progressive crystallization of primitive Galapagos basalt at 1 atm and low oxygen fugacity (GCH) (Dixon & Rutherford, 1979). Although these estimates are not quantitative they indicate a significant range in oxygen fugacity during crystallization of individual magma batches at Austurhorn.

4.7 Approach to Petrogenetic Modeling

The Austurhorn liquids are closely related both spatially and temporally, and there is no evidence to suggest that they derive from a mantle source grossly heterogeneous in major element or isotopic composition. For this reason I evaluate the relative importance of crystal fractionation, magma mixing and contamination by crustal melting in controlling basalt and rhyolite compositions. Field relations at Austurhorn indicate that the shallow crustal magma chamber was open to input of diverse basaltic and silicic magmas (Blake, 1966; chapter 3). At the same time, however, large-scale homogenization of coexisting liquids is not observed; heterogeneous commingling is restricted to portions of the net veined complex (Mattson et al., 1986; chapter 3). Although open-system processes occurred, their chemical impact and volumetric significance in central volcanic evolution is unclear. I investigated geochemical features of the Austurhorn complex to address this question further.

First, I evaluate the ability of closed-system fractionation to explain the observed compositional trends (Carmichael, 1964; Sigurdsson & Sparks, 1981). The Austurhorn volcano is considered analogous to Thingmuli and other Tertiary centers in eastern Iceland where fractionation of observed phenocryst phases can explain major element variations in the lavas (Carmichael, 1964; Wood, 1978; Flower et al., 1982; chapter 3). The closest oceanic analog to these Fe-rich Icelandic systems is found near the Galapagos spreading center, where FeTi-rich tholeiitic basalts and evolved silicic liquids occur (Byerly et al., 1976; Christie & Sinton, 1981; Perfit et al., 1983). Cooling rate

experiments were performed on a primitive Galapagos basalt (Mg# 65) at pressures between 1 atm and 2.5 kbars under varying conditions of f_{O_2} and $P_{(H_2O)}$ (Dixon & Rutherford, 1979; Spulber & Rutherford, 1983). More recently, Juster & Grove (1988) investigated differentiation of evolved Galapagos basalts (Mg# 46) at oxygen fugacities between QFM and NNO^{+2} . The combined natural and experimental data thus permit a reasonable assessment of fractionation processes at Austurhorn. Where fractionation is proven incapable of reproducing the documented geochemical variations, we investigate more complex scenarios of wholesale or selective crustal assimilation (Oskarsson et al., 1982, 1985; Macdonald et al., 1987).

Crystal fractionation was investigated quantitatively using both a stepwise **inverse** technique (T. Juster, pers. commun., 1988) and the major element **forward** modeling technique of Grove & Baker (1984). These techniques are preferable to single step linear least squares calculations (which are commonly employed to model fractionation of individual parent-daughter liquid pairs) in that they treat a given fractionation interval as a sequence of smaller increments, thereby reducing misfits to curved surfaces. The **inverse modeling technique** fits first- to fourth-order polynomials to variations in each major element oxide expressed as a function of MgO content. The entire fractionation interval is then evaluated in ten incremental steps, using a multiple polynomial regression of liquid compositions and calculated equilibrium phenocrysts to model all oxides simultaneously. In **forward** modeling, equilibrium phenocrysts are subtracted incrementally from a designated parental liquid until the desired evolved daughter composition is reached. The extent of fractionation is constrained by the degree of enrichment of highly incompatible major and trace elements (e.g., K_2O , P_2O_5 , Ba, La) in the calculated residual differentiate. In both methods, minerals are assumed to be stoichiometric and their compositions are varied using mineral-melt partition coefficients for major and minor components obtained by microprobe analysis of Austurhorn samples (table 4.6). The availability of a wide spectrum of gabbroic cumulates allows direct

Table 4.6 Calculation of Mineral Compositions

Olivine (Mg, Fe)₂SiO₄
 Pyroxenes (Ca, Mg, Fe, Al, Na, Ti)₂(Si, Al)₂O₆
 Plagioclase (Ca, Na)(Al, Si)₄O₈

$$K_D^{ol} = \left(\frac{X_{Fe}}{X_{Mg}} \right)_{oliv} \left(\frac{X_{Mg}}{X_{Fe}} \right)_{liq} = 0.30 - 0.33 \quad (1, 6, 7)$$

$$K_D^{cpx} = \left(\frac{X_{Fe}}{X_{Mg}} \right)_{cpx} \left(\frac{X_{Mg}}{X_{Fe}} \right)_{liq} = 0.23 - 0.25 \quad (2, 3, 4, 5)$$

$$K_D^{opx} = \left(\frac{X_{Fe}}{X_{Mg}} \right)_{opx} \left(\frac{X_{Mg}}{X_{Fe}} \right)_{liq} = 0.28 - 0.29 \quad (6, 7)$$

$$K_D^{plag} = \left(\frac{X_{Ca}}{X_{Na}} \right)_{plag} \left(\frac{X_{Na}}{X_{Ca}} \right)_{liq} = 0.85 - 1.57 \quad (2, 3, 4, 8)$$

$$K_{Al}^{cpx} = \frac{(Al_2O_3)_{cpx}}{(Al_2O_3)_{liq}} = \text{pressure- and composition-dependent} \quad (5, 6, 7, 9)$$

$$K_{Na}^{cpx} = \frac{(Na_2O)_{cpx}}{(Na_2O)_{liq}} = 0.1 - 0.2 \quad (2, 4, 5, 6, 7)$$

$$K_{Ti}^{cpx} = \frac{(TiO_2)_{cpx}}{(TiO_2)_{liq}} = \text{pressure- and composition-dependent} \quad (2, 4, 5, 6, 7)$$

$$K_{Al}^{opx} = \frac{(Al_2O_3)_{opx}}{(Al_2O_3)_{liq}} = 0.21 - 0.36 \quad (6, 7, 9)$$

$$K_{Na}^{opx} = \frac{(Na_2O)_{opx}}{(Na_2O)_{liq}} = 0.04 \quad (6, 7)$$

$$K_{Ti}^{opx} = \frac{(TiO_2)_{opx}}{(TiO_2)_{liq}} = \text{strongly pressure-dependent} \quad (6, 7)$$

- Sources of data: 1 Roeder & Emslie, 1970
 2 Walker et al., 1979
 3 Fisk et al., 1980
 4 Grove & Bryan, 1983
 5 Mahood & Baker, 1986
 6 Takahashi, 1980
 7 Takahashi & Kushiro, 1972
 8 Thy, 1983
 9 Presnall et al., 1979

comparison between calculated and observed crystalline products and residual liquids.

Tables 4.7, 4.11 and 4.12 report results based on **inverse** model calculations.

4.8 Petrogenesis of Austurhorn Basalts

The diversity in major element bulk rock compositions of Austurhorn basalts (e.g., $K_2O/P_2O_5 = 1.88 \pm 0.81$) is greater than that observed among Reykjanes tholeiites ($K_2O/P_2O_5 = 1.10 \pm 0.12$; Jakobsson et al., 1978) or Vestmannaeyjar alkali basalts ($K_2O/P_2O_5 = 1.93 \pm 0.53$; Jakobsson, 1979; Furman et al., 1988). Comparable diversity is found among the Tertiary sequence of eastern Iceland and the modern eastern volcanic zone, where samples from several volcanic centers have been grouped together (Wood, 1978; Gibson et al., 1982; Meyer et al., 1985). At Torfajökull coexisting tholeiitic and mildly alkaline basalts are generally interpreted as the result of lateral injection of tholeiite from the nearby Veidivötn fissure swarm (Mork, 1984; Blake, 1984b; McGarvie, 1984), although both rock types were intrinsic to the system during its early history (Ivarsson et al., in press; K. Saemundsson, pers. commun., 1988). Excellent field control at Austurhorn removes the question of inter-system heterogeneity: all of these liquids are part of a single magmatic center. At Austurhorn alkaline and tholeiitic dikes are contemporaneous and in this section we investigate their petrogeneses.

4.8.1 Mafic Pillows

Geochemical trends within the pillow suite (figures 4.8, 4.9) suggest a common basaltic parent. Pillow margins and interiors are unequivocally cogenetic and are taken to represent liquid compositions. In modeling evolution of the Austurhorn pillows I selected sample p-61a as the parental liquid because it has lower abundances of incompatible elements and a higher MgO content than other pillows (table 4.1). This sample is the only pillow composition which appears to project within the olivine primary phase volume rather than along the three-phase (olivine + plagioclase +

clinopyroxene) cotectic defined by remaining pillow samples (figure 4.23). Pillow interior p-41b was chosen as the daughter composition because it has higher abundances of incompatible elements and a lower MgO content than all other sampled pillows (table 4.1). The remaining pillow analyses were also incorporated in modeling; these compositions constrain curvature of the liquid line of descent between parent and daughter.

Major element trends among the pillow suite can be modeled by five-phase crystallization in the proportions olivine (12 → 4%); plagioclase (56 → 51%); clinopyroxene (23 → 33%); magnetite (~8%); ilmenite (~2%) (table 4.7). The changing phase proportions correspond to down-temperature evolution along the "pillow cotectic" in figure 4.23. Both magnetite and ilmenite were used in the calculation even though their compositions in these samples do not record magmatic temperatures because their relative abundances could not reliably be estimated petrographically. Relative proportions of mafic phases differ from those of MORB at 1 atm (Grove & Bryan, 1983; Grove & Baker, 1984; table 4.8) where magnetite is not observed and olivine forms a larger portion of the fractionating assemblage. The calculated phase assemblage is comparable to that observed most frequently in Hvalnesfjall gabbro (table 4.4). Compositional overlap of plagioclase and clinopyroxene between pillows and gabbroic cumulates (figures 4.4, 4.6) support this model of shallow level fractionation. Note, however, that the bimodal plagioclase populations in both pillow and gabbro samples suggests an earlier stage of crystal growth at greater depth.

I evaluated this major element model using our trace element data and published phenocryst/matrix partition coefficients (table 4.9). In this discussion of trace element behavior, "observed" bulk distribution coefficients are calculated by assuming Rayleigh fractionation ($C_l/C_o = F^{D-1}$) and letting F , the amount of liquid remaining, equal the value calculated by major element modeling (table 4.8). "Calculated" bulk D s represent a

Table 4.7 Fractionation Model for Austurhorn Mafic Pillow Liquids

Liquid Composition						Calculated Cumulate Mode						Fo, An		
SiO2	TiO2	Al2O3	FeO*	MgO	CaO	K2O	Na2O	P2O5	olv	plg	aug	tmt	ilm	
initial	48.47	2.59	16.12	11.68	6.74	10.95	0.54	0.34	11.1	56.2	23.7	8.1	0.8	76, 64
	48.29	2.59	16.02	11.68	6.76	11.01	0.55	0.27	10.0	55.2	25.6	8.4	0.9	75, 62
	48.57	2.66	15.54	11.78	6.38	10.70	0.67	0.29	9.0	54.2	27.4	8.5	1.0	74, 59
	49.22	2.74	15.21	11.91	6.03	10.41	0.79	0.31	8.0	53.1	29.3	8.6	1.1	73, 56
	49.80	2.80	14.88	11.96	5.67	10.04	0.91	0.35	7.1	52.0	31.1	8.7	1.2	71, 54
	50.46	2.85	14.61	11.97	5.32	9.62	1.03	0.39	6.2	50.9	32.8	8.8	1.4	70, 52
	51.19	2.89	14.39	11.95	4.97	9.15	1.13	0.45	5.3	49.9	34.4	8.8	1.6	69, 50
	51.99	2.90	14.22	11.89	4.62	8.64	1.24	0.52	4.4	49.3	35.7	8.8	1.9	67, 48
	52.88	2.91	14.12	11.79	4.28	8.09	1.33	0.60	3.6	48.9	36.5	8.7	2.2	65, 46
	53.85	2.89	14.06	11.67	3.93	7.48	1.41	0.68	sum residuals squared = 0.04-0.21					
target	53.49	2.89	14.10	11.66	3.89	7.59	1.49	0.67						

Initial and final target liquid compositions correspond to pillow samples p-61a (rim) and p-41b (interior), respectively.

Total fractionation interval = 74 wt% crystallization.

Mineral compositions calculated as follows (see table 4.6):

olv: Fe/Mg Kd = 0.30

plg: An/Ab Kd = 0.90

aug: Fe/Mg Kd = 0.23

tmt: usp = 17.83

ilm: ilm = 49.44

Wo = 42.0

Table 4.8 Experimental and Calculated Phase Assemblages

I. Clinopyroxene-saturated Cotectic Proportions

Sample Suite	wt% MgO in liquid	oliv	plag	aug	tmt	ilm
MORB -- 43°N (Grove & Bryan, 1983)	8.13	36	57	7	-	-
	7.80	20	52	28	-	-
	6.92	18	52	29	-	-
	6.23	14	53	33	-	-
MORB -- FAMOUS (Grove & Bryan, 1983)	7.47	32	59	9	-	-
	6.61	23	55	21*	-	-
MORB -- 23°N (Grove & Bryan, 1983)	6.81	14	77	9	-	-
	6.16	13	66	21	-	-
Austurhorn mafic pillows (table 4.7)	6.76	11	56	24	8	1
	6.03	9	54	27	9	1
	3.93	4	49	36	9	2
Austurhorn mafic dikes (table 4.11)	8.04	25	58	13	4	-
	5.95	19	55	20	6	-
	3.88	15	52	25	8	-

Experimental data: In each suite, the first row records phase proportions and MgO content of coexisting liquid at first occurrence of clinopyroxene phenocrysts. Phase proportions for selected liquids of lower MgO are shown to facilitate comparison with Austurhorn calculated phase assemblages. Asterisk indicates this value includes both orthopyroxene and clinopyroxene.

Austurhorn data: Selected phase assemblages are given for mafic suites, including initial and final increments.

II. REACTION BOUNDARIES

olivine + liquid --> plagioclase + augite + pigeonite +/- magnetite

Sample suite	oliv	plag	aug	pig	tmt
MORB					
(Grove & Baker, 1984)	-18	37	23	58	-
Galapagos					
(Juster & Grove, 1988)	-18	44	19	54	-
Austurhorn mafic dike (d-42)	-18	40	10	36	13
Austurhorn mafic pillow (p-41b)	-44	49	-12	93	12

Notes: All results report calculated reaction coefficients for pseudo-univariant equilibria at the reaction boundary. The experiments of Juster & Grove (1988) are olivine-seeded and were run at QFM. Magnetite is not part of the assemblage at the reaction boundary but is prominent in experimental charges a few degrees below the reaction temperature. Results for Austurhorn liquids are calculated using observed liquid compositions and calculated equilibrium phases (see table 6) using pigeonite data from Carmichael (1964). Results based on pillow p-41b are included for comparison to indicate that the calculated proportions do not resemble those observed experimentally, suggesting that this reaction does not occur in evolved pillow liquids.

Table 4.9 Partition Coefficients Used in Trace Element Modeling of Austurhorn Basalts

Element	Clinopyroxene		Olivine		Plagioclase		Magnetite		Ilmenite		Amphibole	
	A	B	A	C	D	E	F	G	H	G	J (ex. La)	I
La	.02	.08	.0005	.017	.03	.16	2	.7	.007	.02	.10 - 1.4 (C)	-
Ce	.04	.17	.0008	(.022)	.03	.15	2	(.6)	.007	-	.12 - 25	-
Nd	.09	.38	.0013	(.024)	.04	.14	2	(.6)	.009	-	.16 - 40	-
Sm	.14	.74	.0019	(.027)	.04	.12	3	(.6)	.01	.08	.22 - 55	.7
Eu	.16	.75	.0019	.027	.20	.32	3	.6	-	-	.25 - 63	.4
Tb	.19	.97	.0019	.04	.02	.08	3	.7	-	-	-	(1.0)
Yb	.20	1.01	.0040	(.05)	.02	.07	4	(.7)	.06	.6	.22 - 30	(1.0)
Lu	.19	.98	.0048	(.05)	.02	.07	4	(.7)	.09	.7	.44	.9
Ba	.01 - .1 (J)		.01 (J)		.05 - .59 (J)		(.001 - .01)		-		.42 - .73 (T)	
Sr	.06 - .51 (J)		.01 - .016 (J,L)		1.2 - 3 (E,J)		4 - 1.0 (G)		-		.55 - .64 (T)	
Sc	1.2 - 2.8 (C,K)		.10 - .25 (C,L)		.02 (K)		1.3 - 3.0 (R)		-		-	
V	.7 - 1.5 (K,L)		.09 - .3 (L)		(.01)		24 - 63 (R)		-		-	
Cr	7 - 10 (K)		1 (K)		.02 (K)		2.7 - 6.7 (G)		-		-	
Co	.76 - 1.55 (C,L)		2 - 5.4 (C,L)		.1 (K)		27 - 58 (R)		-		-	
Ni	2 - 4 (L)		(P)		.06 (K)		3 - 11 (D,G,R)		-		-	
Zr	.3 (C,M)		.01 - .12 (C,H)		.04 - .14 (C)		2 - 5 (G)		-		-	
Hf	.3 - .5 (C,D,M)		.01 - .05 (C,H)		.01 - .07 (C,D)		2 - .7 (G)		.33 - 2.0 (F,H)		.32 - .49 (C)	
Nb	.1 (N)		.01 (N)		.05 (N)		2 - .7 (G)		.42 - 1.0 (F,H)		.38 - .55 (C)	
Ta	.08 - .23 (C)		.01 - .03 (C)		<.06 (C)		.07 - 2.0 (N,S)		2.3 - 4.6 (S)		.11 - .24 (C)	
Th	.02 - .10 (C)		.01 - .03 (C)		.02 - .08 (C)		.05 - 1.4 (N,S)		2.7 - 6.6 (S)		.03 - .09 (C)	
A	Frey et al., 1978, Table A-1, set 1				J		Schnetzer & Philpotts, 1970					
B	Frey et al., 1978, Table A-1, set 2				K		Sun et al., 1979					
C	Lemarchand et al., 1987				L		Frey et al., 1978, Table A-2					
D	Dostal et al., 1983				M		Watson & Ryerson, 1986					
E	Drake & Weill, 1975				N		Pearce & Norry, 1979					
F	McKay et al., 1986				P		Hart & Davis, 1978					
G	Villemant et al., 1981				R		Ewart et al., 1983					
H	Fujimaki et al., 1984				S		Green & Pearson, 1987					
I	Green & Pearson, 1987				T		Philpotts & Schnetzler, 1970					

weighted sum of individual mineral/melt distribution coefficients, using the calculated phase assemblage (table 4.8) and the Kds in table 4.9.

Observed and calculated bulk distribution coefficients generally compare quite well (table 4.10), suggesting that the model fractionating phase assemblage is reasonable. Most observed bulk Ds fall near the high end of the calculated range; a change in F of 0.02 (from 0.26 to 0.24) could reduce the calculated distribution coefficients to within the predicted range. Two elements are not satisfied by the model: La and V. The misfit of La is ameliorated by noting that observed bulk Ds of the remaining REE define a smooth concave-downward trend with a slightly elevated bulk D for Eu, indicative of substantial clinopyroxene and plagioclase fractionation. However, the La misfit could be significant. The observed bulk D for V ($D_V = 1.38$) is lower than predicted, but V is clearly compatible in the crystallizing assemblage. Both Nb and Ta are somewhat more compatible than predicted ($D_{\text{obs Nb,Ta}} = 0.37, 0.35$; table 4.10), which probably reflects the evolved nature of the basalts (Green & Pearson, 1987). Their similar behavior and moderate incompatibility are consistent with extensive FeTi oxide precipitation (table 4.7). The elements Zr and Hf are partitioned similarly ($D_{\text{obs Zr,Hf}} = 0.25, 0.25$), and are less compatible than Nb and Ta. Th has the lowest observed bulk D ($D_{\text{obs Th}} = 0.16$) although this value is slightly larger than the calculated bulk D_{Th}.

Among compatible elements, the observed bulk distribution coefficient for Sr (bulk $D_{\text{Sr}} = 1.13$) is consistent with a phase assemblage containing ~50 wt% plagioclase. Compatible behavior of Sc (bulk $D_{\text{Sc}} = 1.18$) reflects the high proportion of clinopyroxene, while variable amounts of clinopyroxene, olivine and FeTi oxides produce the high bulk Ds of Cr, Ni, Co and V.

Fractionation of the calculated modal assemblage from designated parental liquid p-61a therefore provides an internally consistent mechanism for generating the observed trace element variations among the pillow suite. Actuar' orrelations between abundances

Table 4.10 Evaluation of Basalt Fractionation Model with Trace Elements

Element	C_l/C_o	Bulk D_{obs}	Bulk D_{calc}
La	2.45	0.33	0.04-0.17
Ce	2.70	0.26	0.05-0.18
Nd	2.57	0.31	0.07-0.24
Sm	2.34	0.37	0.09-0.34
Eu	2.26	0.39	0.18-0.45
Yb	2.50	0.33	0.11-0.42
Lu	2.49	0.33	0.11-0.41
Ba	2.57	0.30	0.03-0.31
Sr	0.84	1.13	0.68-2.71
Sc	0.78	1.18	0.51-1.18
V	0.60	1.38	2.60-6.72
Cr	0.05	3.22	2.50-3.82
Co	0.57	1.42	0.73-2.00
Ni	0.30	1.89	1.63-2.54
Zr	2.75	0.25	0.13-0.26
Hf	2.67	0.25	0.12-0.25
Nb	2.34	0.37	0.09-0.27
Ta	2.47	0.33	0.16-0.26
Th	3.12	0.16	0.04-0.10

Observed bulk D_s are calculated assuming Rayleigh fractionation, i.e.,

$$C_l/C_o = F^{D-1}$$

where C_l = concentration of element in daughter p-41b

C_o = concentration of element in parent p-61a

F = degree of crystallization calculated from major element modeling.

Calculated bulk D_s represent a weighted sum of individual K_d s from Table 4.9, using average modes calculated in major element modeling.

of compatible (e.g., Ni, Sc) and highly incompatible elements (e.g., La, figure 4.9c) show scatter beyond that of analytic uncertainty. This slight, but real, variability suggests intrusion of multiple magma batches rather than differentiation of a single homogeneous magma. The pillow suite thus represents, not a continuous differentiation spectrum from a single large pulse of basalt, but rather repeated modification of a plentiful basalt type.

Major and trace element trends of three margin/interior pairs indicate apparent intra-pillow fractionation (figures 4.8, 4.23), with pillow interiors more evolved than associated margins. This comparison indicates that chilling of pillow margins forms an effective barrier to bulk chemical interaction with host granophyre (e.g., Wager & Bailey, 1953; Wiebe, 1973). Each pillow sampled in this way was >1 meter in dimension; smaller pillows and mafic dikes (generally <50 cm) were not examined for internal geochemical variations. It is important to recall that pillow margins and interiors show complete compositional overlap (for example compare p-62a with p-61b, and p-62b with p-41a in figures 4.8, 4.9, 4.23). Intra-pillow variations may indicate prolonged magma flow through individual conduits, with magmatic differentiation occurring prior to or during emplacement. The conclusion that intra- and interpillow differences result from fractionation of a single parental basalt type differs from that of Mattson et al (1986), who called upon mixing of silicic and mafic magmas to explain variations in P_2O_5 and TiO_2 contents among the pillows. As indicated earlier, I feel this difference stems from the different sampling and nomenclature of the two studies, which are complementary rather than contradictory in approach and conclusions.

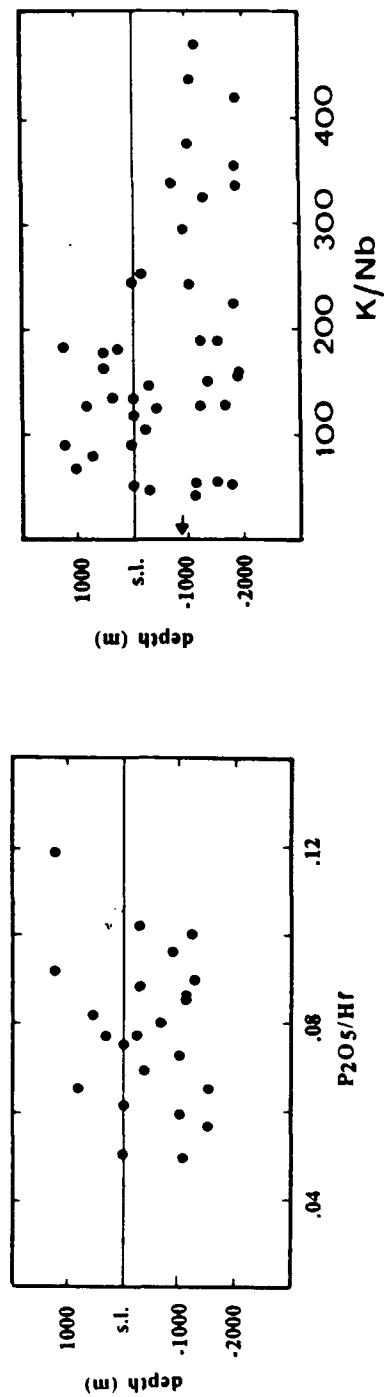
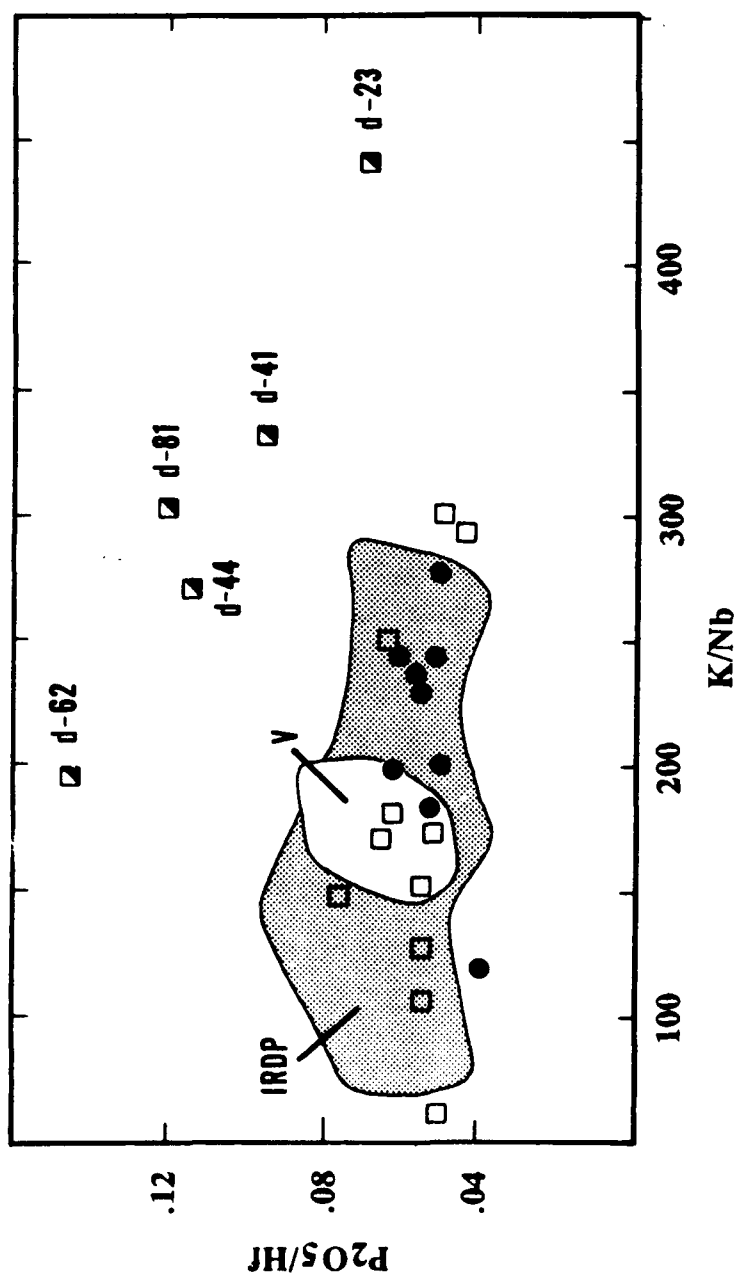
Investigation of the Austurhorn pillows demonstrates that quartz-normative compositions (i.e., p-41b; see table 4.7) can indeed be generated by closed system fractionation of transitional tholeiitic basalt. This suggestion has been rejected by Oskarsson et al (1982, 1985), who proposed instead that quartz tholeiites result from mixing of parental olivine tholeiite with ~15% silicic liquid derived by crustal melting.

These authors further contend that transitional tholeiitic basalts (e.g., pillows at Austurhorn) require admixtures of "nepheline basalt (~15%, also produced by crustal melting)" plus olivine tholeiite. Although mixing at depth between melts of different compositions cannot be ruled out, I suggest that a simpler alternative exists. In my preferred model (table 4.7), silica-enrichment results directly from precipitation of iron-titanium oxides during fractionation. I suggest that the Austurhorn series (in particular, the mafic pillows) differentiated under conditions of higher oxygen fugacity than has been recognized previously, leading to Fe-Ti oxide saturation in basalts with ~6 wt% MgO. Coexisting oxide geothermometry (figure 4.26) suggests that Austurhorn pillows and gabbros cooled at oxygen fugacity near the NNO buffer, that is, conditions more oxidizing than those determined for Vestmannaeyjar alkali basalts or Vestfirðir tholeiites (figure 4.26). Similarly, total iron abundances among the Austurhorn suite are consistent with those determined for FeTi-rich Galapagos basalts under conditions more oxidizing than QFM (figure 4.28). The lack of iron enrichment among Austurhorn pillows is consistent with precipitation of FeTi oxides during fractionation. The high ilmenite and magnetite modes of Hvalnesfjall gabbro provide further support for this proposed scenario (table 4.4). This analysis indicates that a continuous evolutionary spectrum can exist from ne- to hy- to qtz-normative basalts, and that all these types can be related by progressive closed-system fractionation in shallow magma chambers. It is worth noting that the transitional tholeiites at Austurhorn are only mildly nepheline-normative (table 4.3); I do not suggest that alkali basalts *sensu stricto* (e.g., Vestmannaeyjar) would differentiate to quartz-tholeiites under elevated oxygen fugacity.

4.8.2 Alkaline Dikes

Four Austurhorn dikes are characterized by elevated abundances of K, Rb and P_2O_5 (figure 4.29; the fifth sample indicated in this figure, d-62, has anomalous P_2O_5 but normal K, Rb). These dikes have relative alkali contents unlike those observed in

Figure 4.29 Austurhorn alkalic dikes are distinct in their elevated P_2O_5/Hf and K/Nb ratios, reflecting unusually high P_2O_5 and K_2O contents (K_2O content has been normalized to Nb to account for differentiation). By comparison, alkali basalts from Vestmannaeyjar (field labeled **V**) are not enriched in either oxide relative to transitional tholeiitic Austurhorn samples (pillows & mafic dikes shown as data points). The range in K/Nb of Austurhorn samples is similar to that observed among dikes and lavas from the IRDP drill core in eastern Iceland (field labeled **IRDP**). The lower panels indicate that K_2O variations may result from alteration, because K/Nb increases with greater depth in the core samples (the arrow indicates inception of prehnite-pumpellyite facies metamorphism); however, P_2O_5 variations do not result from alteration.



other Icelandic alkaline liquids. Compared to the Austurhorn pillows, the Austurhorn alkaline dikes are enriched in $Rb > K \gg Ba$, lavas from Torfajokull and Snaefellsnes are enriched in Ba and $K > Rb$, and Vestmannaeyjar basalts show no differential alkali enrichments (table 5). The Vestmannaeyjar basalts and Austurhorn pillows have Ba/Rb comparable to the global average of MORB and OIB (~ 12 ; Hofmann & White, 1982); therefore the Austurhorn alkaline dikes are anomalous. Compositional differences between Vestmannaeyjar and other alkalic regions may imply that Austurhorn, Snaefellsnes and Torfajokull alkali basalts are indeed contaminated. The source and mechanism of contamination are not readily identified, however.

The most convincing evidence for a contamination scenario is the tholeiitic character of augites in sample d-81 (figure 4.4). If the high alkali content of d-81 were a primary feature, one would expect crystallization of alkalic (i.e., high-Wo) clinopyroxenes. However, phenocryst and groundmass augites analyzed from d-81 define a trend similar to that of augites from the tholeiitic Skaergaard intrusion (Wager & Brown, 1968; figure 4.4).

Comparison between the Austurhorn alkali-rich dikes and altered basalts from the IRDP drill core from eastern Iceland suggests that burial-related metamorphism alone cannot produce the geochemical characteristics observed at Austurhorn. At IRDP, samples with $K/Nb > 250$ are found at depths below 980 meters, corresponding to alteration within the prehnite-pumpellyite facies (figure 4.29; Viereck et al, 1982). Elevated K/Nb reflects K_2O enrichment (relative to that of Nb, another incompatible element); no comparable relationship exists between depth and P_2O_5 content (figure 4.29). In addition the Austurhorn samples are not enriched in all highly incompatible elements as might be expected if they had interacted with crustally-derived fluids. For example, they do not contain anomalously high Th concentrations (figure 4.9d), but rather have Rb/Th of 19-33, much higher than the Rb/Th of 8-12 observed in

remaining Austurhorn samples and Vestmannaeyjar alkali basalts (table 4.5; Furman et al., 1988).

Several authors have suggested that alkalic liquids at Snaefellsnes and Torfajökull derive by amphibole breakdown during extensive melting of hydrated crust (Oskarsson et al., 1982, 1985; Steinthorsson et al., 1985; Ivarsson et al., in press). Liquids in equilibrium with an amphibole-bearing residue should be depleted in MREE (because amphibole has high MREE/LREE and MREE/HREE partition coefficients; table 4.9). This geochemical signature is not present in the Austurhorn alkaline dikes, which have slightly higher Sm/Yb_n (2.85-3.34) than those of Austurhorn transitional tholeiites and granophyres (1.85-2.85).

Juxtaposition of sub-liquidus basalt and molten rhyolite has been demonstrated experimentally to result in rapid K_2O enrichment in the basalt (Watson, 1982; Watson & Jurewicz, 1984; Johnston & Wyllie, 1988). In these experiments, monovalent cations (e.g., K, Rb) diffuse more rapidly than divalent species, providing a possible explanation for the lack of Ba enrichment in the Austurhorn dikes. Recall that, in contrast, the mafic pillow margins do not have elevated contents of K_2O or Rb. The anomalously high P_2O_5 contents of the alkaline dikes also remain enigmatic, inasmuch as experimental partitioning studies (Watson, 1976; Ryerson & Hess, 1978) suggest K_2O and P_2O_5 are unlikely to behave similarly. Furthermore, the low P_2O_5 contents of Austurhorn granophyres (0.01-0.32 wt%) would require extremely effective uphill diffusion to produce the levels observed in the alkaline dikes (up to 1.6 wt%). Green & Watson (1982) found that K-rich basalts saturate apatite at higher P_2O_5 concentrations than low-K basalts of comparable MgO and SiO_2 . It is possible that selective assimilation of K_2O by basalt early in its crystallization history changes the subsequent fractionation path to postpone apatite fractionation.

In summary, the geochemical signatures of the Austurhorn alkalic liquids are not simply explained by crystal accumulation, alteration, assimilation or bulk mixing of

transitional tholeiite and granophyre at the current level of exposure. I suggest that the Austurhorn alkalic liquids were created by selective contamination of basalt by rhyolite below the current level of exposure. Elevated P_2O_5 abundances can be reconciled with this scenario if the changed bulk chemistry of the mafic magma affects timing of apatite saturation.

4.8.3 Transitional Tholeiitic Dikes

The Austurhorn mafic dikes define a different liquid line of descent than the mafic pillows although the dikes do not form a homogeneous group. I interpret these compositions as liquids because they are sparsely phyrlic, containing less than 5 vol% phenocrysts. In the following discussion I focus first on consistent differences between dikes and pillows, then address heterogeneities within the dike suite.

The projected compositions of 7 dike samples (d-21, d-25, d-46, d-47, d-48, d-62, d-63) plot along the pillow cotectic in figure 4.23. Major element variations among these samples can be modeled using phase proportions broadly similar to those used for the pillows (olivine (25 → 1%): plagioclase (58 → 43%): augite (13 → 42%): magnetite (8 → 14%); table 4.11). This model is qualitatively valuable in understanding the fractionation histories of these liquids. The high proportion of plagioclase suggests differentiation at $P \sim 1$ atm, and the absence of ilmenite indicates a major difference between the dikes and pillows. The most differentiated mafic dikes have >3.5 wt% TiO_2 (figures 4.8, 4.26), indicating a delay of oxide saturation relative to that observed among the mafic pillows. These dikes also have lower silica contents than the evolved mafic pillows (<51 vs. >53 wt% SiO_2) corroborating a reduced role for FeTi oxide fractionation.

Another important difference between dikes and pillows is the calculated appearance of low-Ca pyroxene in basalts with <5 wt% MgO. Dikes d-42 and d-29 project near the liquid + olivine → pigeonite + augite + plagioclase reaction boundary

Table 4.11 Fractionation Model for Austurhorn Mafic Dikes

Liquid Composition		SiO ₂	TiO ₂	Al ₂ O ₃	FeO*	MgO	MnO	CaO	K ₂ O	Na ₂ O	P ₂ O ₅	Calculated Cumulate Mode			
		SiO ₂	TiO ₂	Al ₂ O ₃	FeO*	MgO	MnO	CaO	K ₂ O	Na ₂ O	P ₂ O ₅	olv	plg	aug	tmt
initial	48.32	2.13	15.57	12.13	7.98	0.22	10.59	0.18	2.67	0.23	0.23	24.6	58.3	13.4	3.8
	48.12	2.14	15.56	12.29	8.04	0.20	10.59	0.28	2.59	0.20		22.7	57.2	15.5	4.6
	48.07	2.40	15.26	12.78	7.52	0.21	10.59	0.39	2.59	0.21		21.2	56.2	17.3	5.3
	48.11	2.69	14.96	13.17	6.99	0.21	10.50	0.50	2.63	0.23		19.9	55.4	18.8	5.9
	48.26	2.97	14.67	13.46	6.47	0.22	10.32	0.62	2.73	0.27		18.8	54.7	20.1	6.4
	48.55	3.23	14.39	13.66	5.95	0.23	10.07	0.73	2.87	0.33		17.8	54.1	21.3	6.8
	49.98	3.41	14.12	13.75	5.43	0.24	9.74	0.86	3.06	0.40		16.9	53.4	22.5	7.2
	49.58	3.49	13.89	13.76	4.91	0.25	9.35	0.99	3.30	0.50		15.9	52.8	23.6	7.7
	50.34	3.41	13.70	13.68	4.39	0.27	8.90	1.12	3.59	0.61		15.0	52.2	24.8	8.1
	51.28	3.12	13.57	13.53	3.88	0.28	8.40	1.26	3.94	0.74		sum residuals squared = 0.05-0.34			
target	51.02	3.43	13.79	13.31	4.12	0.28	8.30	1.29	3.78	0.70					

Initial and final target liquid compositions correspond to samples d-45 and d-47, respectively.

Total fractionation interval = 74 wt% crystallization

Mineral compositions calculated as follows (see table 4.6):

ol: Fe/Mg Kd = 0.30

plg: An/Ab Kd = 0.90

aug: Fe/Mg Kd = 0.23 Wo = 42.0

determined for Galapagos FeTi basalts at 1 atm (Juster & Grove, 1988; figure 23). A linear least squares mass balance calculation was employed to solve for reaction coefficients in the equation: liquid + olivine = pigeonite + augite + plagioclase using observed liquid and crystals (see table 6) and Thingmuli pigeonite (Carmichael, 1964). Solution of this equation for samples d-42 and d-29 suggests the reaction liquid + 0.18 olivine \rightarrow 0.40 plagioclase + 0.10 augite + 0.36 pigeonite + 0.13 magnetite (table 4.8). These proportions are comparable to those observed experimentally in Galapagos basalts (liq + 0.18 oliv \rightarrow 0.44 plag + 0.19 aug + 0.54 pig; Juster & Grove, 1988; table 4.8). Pigeonite is not observed in the Austurhorn samples (groundmass pyroxenes are variably altered to amphibole) but the similarity in calculated phase proportions to those determined for Galapagos samples suggests the reaction may occur. In contrast, a similar calculation for the evolved mafic pillows yields both olivine and augite as reactants (table 4.8).

The remaining mafic dikes do not define a single cotectic surface analogous to that of the pillows (figure 4.23). One sample (d-1) plots within the olivine primary phase volume and must fractionate olivine + plagioclase +/- magnetite to reach the olivine-plagioclase-augite boundary. All liquids more primitive than d-1 appear to be multiply-saturated; therefore sample d-1 cannot be derived from them by fractionation. The most primitive sill (d-46; 7.8 wt% MgO) is near the olivine:clinopyroxene and olivine:plagioclase joins, whereas samples with 5-6 wt% MgO are located both within (e.g., d-25) and outside (e.g., d-43) the pseudoquaternary tetrahedron. Differences in projected positions of these dikes exceed analytic or projection errors and reflect variations in bulk chemistry of the individual dikes (figure 4.8). This variability in major element composition suggests that the dikes represent several differentiation events rather than a single liquid line of descent.

In addition, variable REE patterns among the dikes indicate multiple parental magmas were present at depth. The mafic dikes range in Ce/Yb_n between 2.7 and 4.9

(figure 4.11); this variation is comparable to that of Tertiary basalts sampled subaerially and in the IRDP drill core (Wood, 1978; Flower et al, 1982). Specifically, the two most magnesian basalts (samples d-45, d-46) have lower Ce/Yb than other Austurhorn samples and their REE patterns cross those of pillows and remaining dikes (figure 4.10). In the absence of mantle source heterogeneity, variable REE patterns may be attributed to either crystal fractionation or source melting processes. Closed system fractionation of the cotectic assemblage inferred for the mafic pillows leads to little if any change in Ce/Yb (figure 4.30). Open system behavior, specifically that of a replenished, tapped and fractionating chamber as described by O'Hara & Matthews (1981), can lead to the observed enrichments in Ce/Yb once the system has attained steady state. However, using the bulk distribution coefficients calculated for our cotectic phase assemblage ($D_{\text{Ce}} = 0.26$, $D_{\text{Yb}} = 0.33$), a nearly two-fold increase in Ce/Yb should be accompanied by a ten-fold increase in Ce concentration which is not observed. A similar discrepancy was encountered by Meyer et al (1985) in their study of geochemical variations in basalts from Iceland's eastern neovolcanic zone. Most importantly, fractionation processes among basalts are generally not capable of generating lower HREE abundances in successively evolved liquids.

The most effective way to fractionate Ce and Yb (in the absence of a HREE-bearing phase such as garnet) is through a dynamic partial melting process (Langmuir et al., 1977; Wood, 1979) in which successive melts are derived from a single mantle source that becomes progressively depleted in incompatible elements. Wood et al (1979) invoked this process to explain a 5-fold variation in Ce/Yb among Icelandic lavas of constant $^{87}\text{Sr}/^{86}\text{Sr}$. No temporal change in Ce/Yb may be discerned among the Austurhorn mafic dikes because they are essentially contemporaneous. In light of the limited variations in Ba/La, La/Nb, Zr/Hf, P/Ce and Pb isotopic ratios among Austurhorn basalts, I suggest that the lower Ce/Yb of samples d-45 and d-46 records a complex melting process rather than a grossly heterogeneous mantle source.

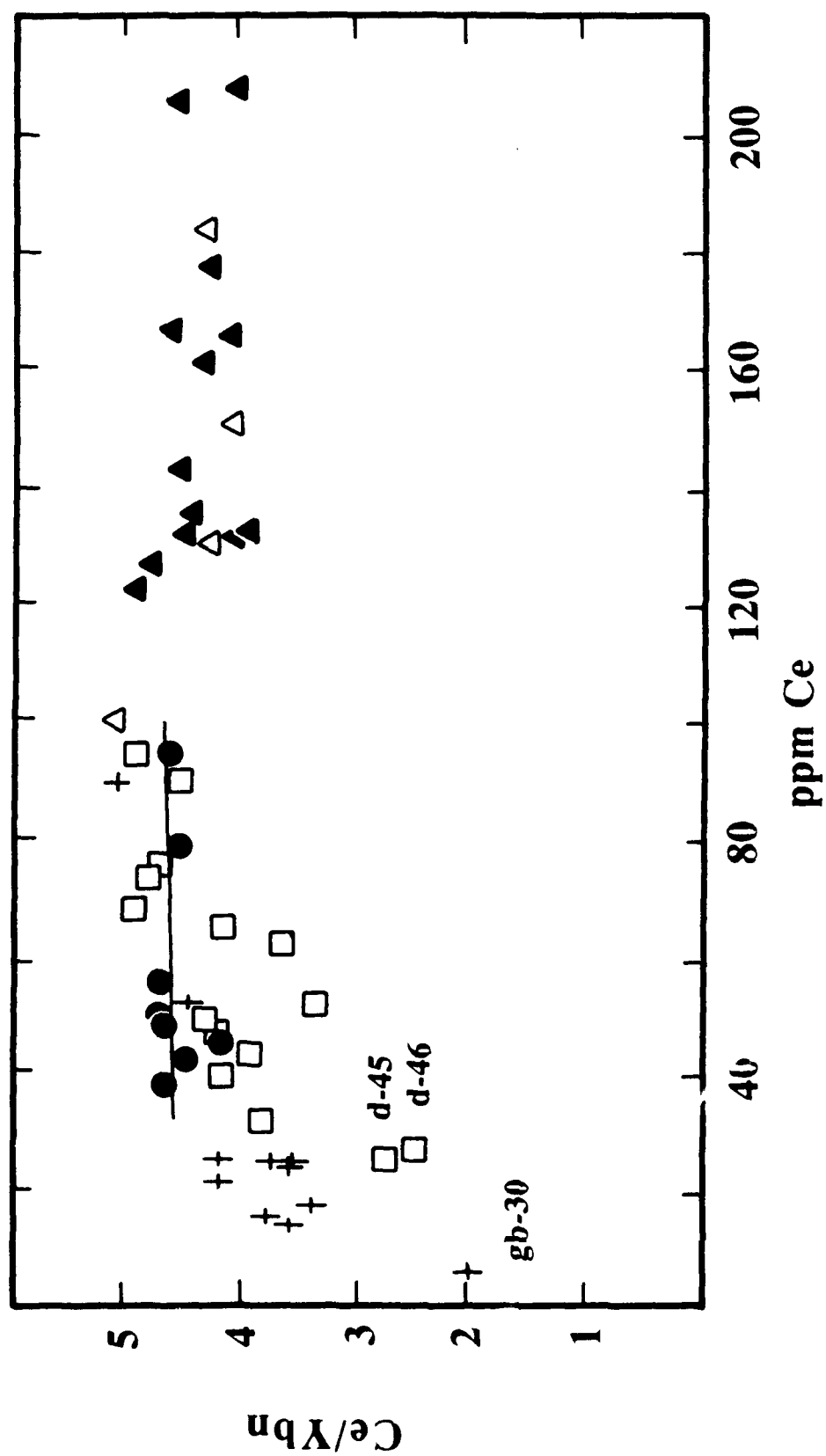


Figure 4.30 The ratio Ce/Yb should not change much with differentiation, witness the near-constant values in mafic pillow samples. Austurhorn mafic dikes show more variation, which probably reflects different degrees of mantle melting. The solid line indicates modeled variations in Ce/Yb during closed system fractional crystallization of mafic pillow samples.

In summary, Austurhorn mafic dikes record variable conditions of both melting and crystallization. Differences in major element geochemistry between the dikes and pillows as groups reflect different fractionation histories. The two differentiation sequences are most clearly manifest in TiO_2 and total Fe abundances and appear to indicate a heterogeneous fractionation environment (i.e., pillows record higher oxygen fugacity). Variability of major and minor elements within the dike suite (e.g., TiO_2 , P_2O_5 ; figure 4.8) supports a physical scenario of multiple differentiation events similar to that proposed for the mafic pillows. In addition, however, low Ce/Yb of dikes with >7 wt% MgO (leading to crossing REE patterns between primitive and evolved dikes) supports the existence of several parental magmas generated by variable melting of a mantle source. Although source heterogeneities cannot be ignored altogether at Austurhorn (e.g., figures 4.17, 4.22) they appear small in comparison to the subsequent effects of fractionation.

4.9 Petrogenesis of Austurhorn Felsic Liquids

The occurrence of silicic eruptives in Iceland is generally attributed to either extreme fractionation of a basaltic parent (Carmichael, 1964; Wood, 1978; Sigurdsson & Sparks, 1981) or partial melting of hydrated, metamorphosed basaltic crust (O'Nions & Gronvold, 1973; Oskarsson et al., 1982, 1985; Gunnarsson & Marsh, 1988). Partial melting of extant rhyolites and plagiogranites (Sigurdsson, 1977; Gunnarsson & Marsh, 1988) provides a secondary mechanism for neo-volcanic rhyolite genesis. Crystal fractionation and crustal melting need not be mutually exclusive processes in any given volcanic system. For example, in the 1875 Askja eruption some silicic xenoliths appear to represent crustally contaminated melts while others are consistent with a fractionation origin (Macdonald et al., 1987). A successful model of rhyolite petrogenesis at Austurhorn must be consistent with several geochemical and mineralogical features of the felsic magmas as a group:

1. The projected compositions of Austurhorn granophyres and rhyolites define a tight linear array analogous to that of Thingmuli liquids within the olivine-plagioclase-clinopyroxene-quartz pseudoquaternary system (figure 4.23).

2. Felsic samples define a curved array which trends towards the experimentally determined granitic minimum in the composition plane Q-Ab-Or (figure 4.31).

3. Eu/Eu^* correlates negatively with SiO_2 (figure 4.32) and positively with Sr (figure 4.13).

4. Most incompatible (REE, Nb, Ta, Y) trace elements correlate well among the felsic suite and between basalts and silicic samples (figure 4.9). The elements Sr, Zr, Hf, Ba, Rb, Th and Ga show more variation, particularly among the highly evolved samples while the compatible elements (Co, Cr, Ni, Sc, V) have uniformly low abundances in the felsic rocks (figure 4.9).

5. Plagioclase/whole rock NaSi-CaAl exchange coefficients vary from ~ 0.9 to >2.0 and gradually increase from granodiorite to high-silica granite.

6. Granodiorites contain plagioclase and K-feldspar phenocrysts, whereas the more evolved samples contain plagioclase and anorthoclase.

7. Samples with >66 wt% SiO_2 contain only anhydrous phases.

4.9.1 Models Involving Fractional Crystallization

Field evidence precludes the Austurhorn felsic magmas from recording a single differentiation sequence, because granodiorites intrude and therefore post-date more evolved magmas at the current exposure level (see chapter 3). With this caveat in mind, I investigated whether the most differentiated felsic magmas could be derived from a dacitic (granodioritic) liquid by fractionation of observed mineral phases. A possible genetic relationship between mafic and felsic magmas at Austurhorn is discussed in section 4.9.4. Clinopyroxene was used in modeling because the observed amphiboles do not appear to be magmatic. Average magnetite and ilmenite compositions determined by

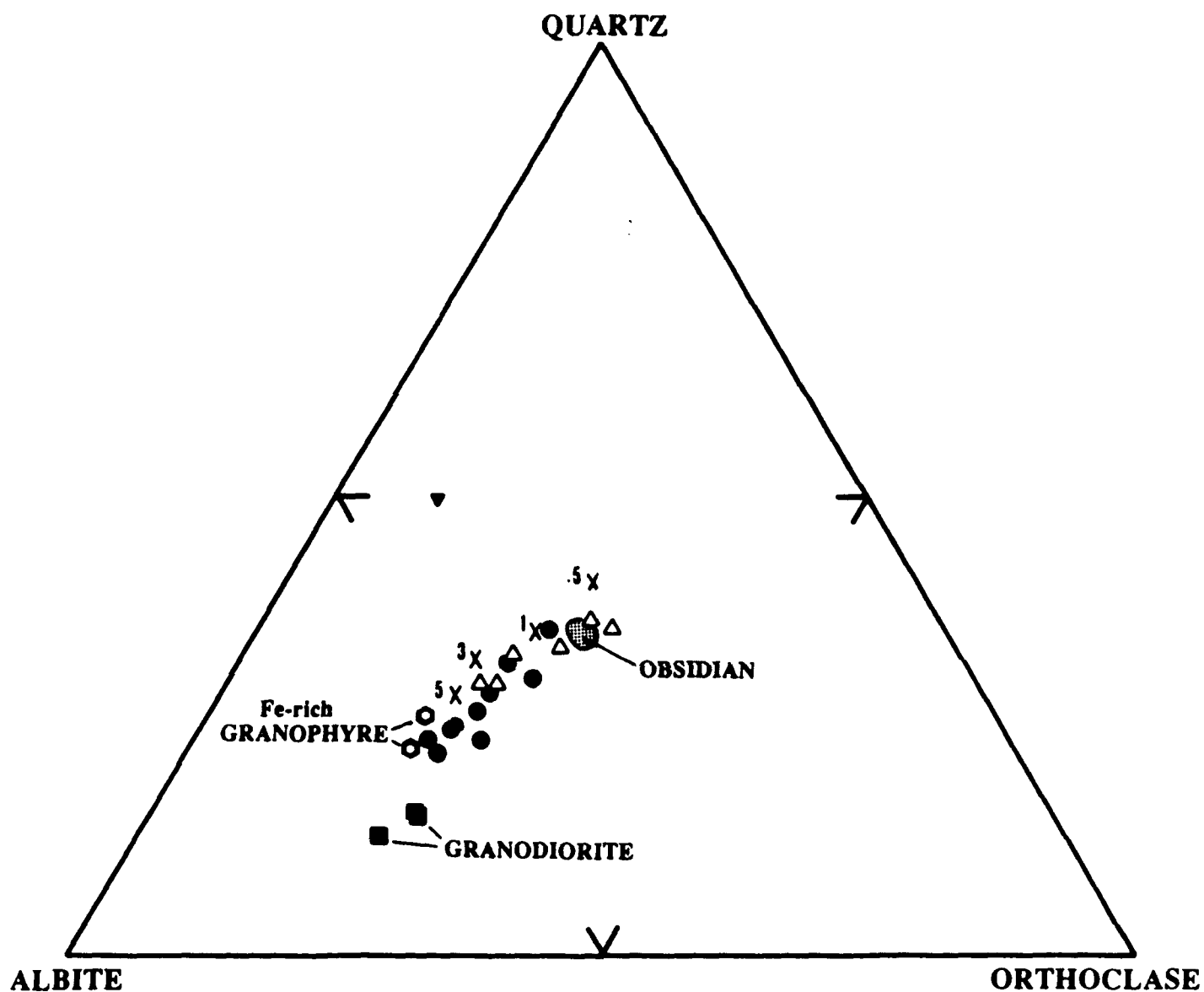


Figure 4.31 Projection of Austurhorn felsic samples within the ternary system quartz-albite-orthoclase is reasonable because these 3 components make up over 85% of the normative components of each analysis. Notice that the samples trend towards the ternary minimum and lie on the orthoclase side of the albite-orthoclase join, which is indicated by X's with the pressure in kbars next to each one. The filled triangle that plots near the Q-Ab join is an extensively altered dike.

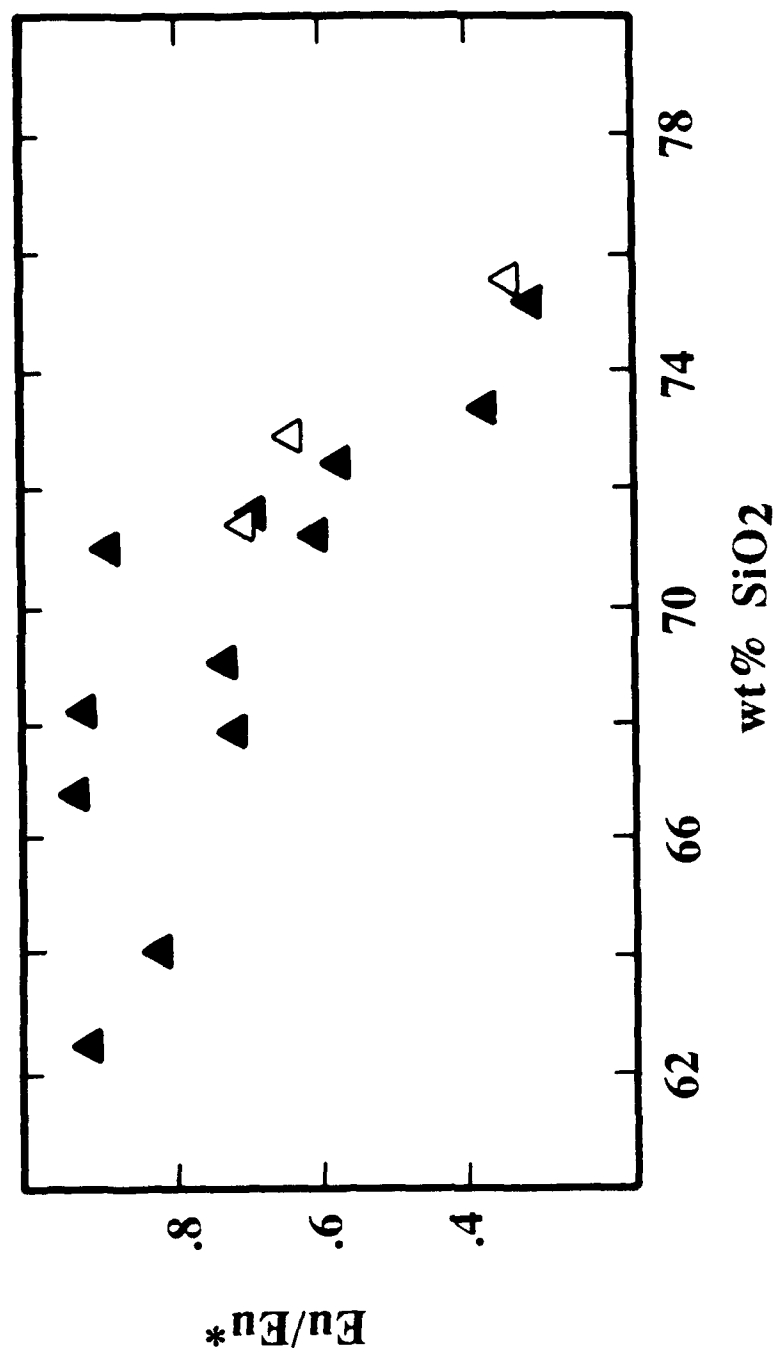


Figure 4.32 Among the felsic samples, Eu anomaly correlates with silica enrichment, suggesting a significant role of feldspar crystallization during progressive evolution.

microprobe were used although all have undergone post-magmatic redistribution of cation species (Bacon & Hirschmann, 1988). I used the analyzed compositions because post-magmatic re-equilibration does not violate our initial assumption of closed system behavior, and because experimental constraints on more appropriate phase compositions are lacking. The calculated phase assemblage which best reproduces observed liquid trends involves plagioclase (56%) + K-feldspar (10 -> 16%) + clinopyroxene (~24%), with minor amounts of magnetite (<5%), ilmenite (~3%) and apatite (~1%) (table 4.12). Fractionation of alkali feldspar is consistent with the position of the Austurhorn samples to the orthoclase side of the Ab-Or binary minimum in the system Q-Ab-Or (figure 4.31). To match petrographic observations, anorthoclase substitutes for the two-feldspar assemblage at ~71 wt% SiO₂. An equally acceptable fit is obtained using olivine in place of magnetite; however, olivine is observed only in an extremely iron-rich granophyre which is not representative of the majority of Austurhorn felsic magmas. The calculated crystallization interval is 53.5% (by weight) which is comparable to that estimated from Ta concentrations assuming Rayleigh fractionation and bulk $D_{Ta} = 0$ (58.2% crystallization).

Modal feldspar proportions (69-73%) and compositions ($An_{<37}$) are consistent with those observed petrographically (table 4.4). The correlation between Eu anomaly (Eu/Eu^*) and Sr also supports a major role for plagioclase in evolution of the felsic magmas (figure 4.17). Fractionation of K-feldspar is suggested by less incompatible behavior of Ba in the evolved samples (figure 4.9). Rubidium is also not uniformly enriched in the evolved rocks; however it is highly susceptible to alteration and interpretations based on Rb abundance alone must be evaluated with caution.

Abundances of certain trace elements are controlled by accessory phases not incorporated into the model fractionating assemblage. For example, thorium and LREE are readily partitioned into allanite and monazite (Mahood & Hildreth, 1983; Mittlefehldt & Miller, 1983) which occur in Austurhorn granophyres. Zr, Hf and HREE abundances

Table 4.12 Fractionation Model for Austurhorn Felsic Liquids

Liquid Composition				Calculated Cumulate Mode												
SiO2	TiO2	Al2O3	FeO*	MgO	MnO	CaO	K2O	Na2O	P2O5	plg	cpx	apa	tmt	ilm	fsp(+)	
initial	63.92	1.08	15.77	5.87	0.13	3.92	2.83	4.73	0.27							
	64.24	1.06	15.57	5.84	0.14	3.96	2.83	4.70	0.26	56.1	24.0	1.0	5.2	3.6	10.6	
	65.35	0.96	15.31	5.53	0.13	3.59	2.93	4.71	0.23	56.2	23.2	1.0	4.8	3.5	11.3	
	66.46	0.86	15.04	5.23	0.12	3.22	3.02	4.73	0.20	56.3	22.5	1.0	4.6	3.2	12.5	
	67.58	0.77	14.78	4.92	0.11	2.84	3.12	4.75	0.17	56.2	21.9	1.0	4.2	3.2	13.6	
	68.71	0.68	14.50	4.62	0.10	2.47	3.21	4.77	0.15	56.1	21.7	0.8	3.7	3.0	14.8	
	69.85	0.58	14.22	4.31	0.09	2.09	3.31	4.79	0.12	55.8	21.8	0.8	3.0	2.8	15.8	
	71.03	0.49	13.85	4.01	0.09	1.68	3.38	4.87	0.10	-	25.8	0.9	1.5	2.5	69.2	
	72.20	0.40	13.58	3.70	0.08	1.33	3.47	4.87	0.06	-	27.5	0.9	0.1	2.5	68.9	
	73.39	0.31	13.33	3.42	0.07	0.94	3.57	4.87	0.04	-	27.3	1.1	0	2.8	68.8	
target	73.25	0.30	13.52	3.38	0.06	0.89	3.57	4.77	0.04	sum residuals squared = 0.04-0.18						

Initial and final target liquid compositions correspond most closely to samples g-43 and g-81, respectively.

Total fractionation interval = 55 wt% crystallization

Mineral compositions calculated as follows (see table 4.6):

plg: An/Ab Kd = 1.45

aug: Fe/Mg Kd = 0.23 Wo = 43.7

+ note that plagioclase and K-feldspar are used in the first 6 steps, whereas anorthoclase is used in the final 3 steps.

are affected by zircon saturation, which is controlled in part by peralkalinity of the host magma (Watson & Harrison, 1983; Harrison & Watson, 1983; see earlier discussion). Geochemical features of the Austurhorn suite can thus be reconciled by fractionation of observed and calculated or accessory mineral phases.

Field evidence constrains Austurhorn felsic liquids to be derived at >2 km depth. Two petrologic lines of evidence support this hypothesis and provide additional insight into felsic magmagenesis. First, the higher plagioclase/whole rock Kds in felsic magmas relative to the basalts suggests fractionation under conditions of greater $P_{(H_2O)}$ (Kushiro, 1972). Spulber & Rutherford (1983) observed plagioclase/liquid Kd ~2.5 in experiments conducted on Galapagos basalt D08 at 2 kbars ($P_{fluid} \sim 0.66 P_{total}$), while anhydrous experiments at 1 atm on the same composition yielded Kd ~1.1. Ironically, the pyroxene-bearing felsic samples have Kds higher than those of the amphibole-bearing granodiorites. Juster & Grove (1988) noted similarly elevated Kds in evolved liquids from the Galapagos spreading center, and suggested that increased silica content of the melt will also raise plagioclase/liquid Kds. Secondly, the bulk compositions projected in the pseudoquaternary system (olivine-plagioclase-clinopyroxene-quartz) plot at significantly higher plagioclase component than Galapagos and MORB liquids produced experimentally at 1 atm (figure 4.23). The trend of Austurhorn samples is similar to that of Galapagos basalt D0-8 crystallized at 2 kbars ($P_{fluid} \sim 0.66 P_{total}$; Spulber & Rutherford, 1983). Expansion of the olivine primary phase volume occurs at higher water pressure, presumably because changes in the melt structure inhibit crystallization of plagioclase. Alternatively, the projected positions may reflect a compositional difference between Austurhorn liquids and MORB (Grove & Juster, in press).

Geochemical and field considerations are fully consistent with a differentiation scenario analogous to that proposed for the basalts: many small magma batches rather than a single large chamber. The important difference between mafic and felsic

fractionation schemes is that the latter occurs at pressures greater than the former. Juster & Grove (1988) reached a similar conclusion in their experimental investigation of evolved liquids from the Galapagos.

4.9.2 The Case Against Crustal Anatexis

I concur with Sigurdsson (1977) that hydrothermal anatexis is an unlikely mechanism for generation of Icelandic felsic magmas, which are often erupted nearly dry and typically contain only anhydrous mafic phases. For example, the Austurhorn granophyres do have miarolytic cavities, indicating water saturation during final solidification, but all contain primary pyroxene rather than amphibole or biotite. However, I explore this question in quantitative detail because recent studies infer a substantial role for melting of hydrated crust in Iceland (Oskarsson et al., 1982, 1985; Hemond et al., 1987; Gunnarsson, 1988; Gunnarsson et al., 1988). Helz (1973, 1978) conducted melting experiments on tholeiitic and alkalic basalts at 5 kbars ($P_{\text{fluid}} = P_{\text{total}}$) and oxygen fugacities buffered at QFM and HM. The experimental results are essentially independent of basaltic starting composition and may therefore be applied to the Austurhorn system to constrain melt percentages and compositions as well as residual phase assemblages present during hydrothermal melting of basalt in the shallow crust.

Experimental anatectic melts coexisting with residual hornblende have distinctive geochemical characteristics that are not matched by the Austurhorn felsic magmas. All melts analyzed by Helz (1978) are peraluminous (most contain normative corundum); this feature was noted also by Green & Ringwood (1968) and Holloway & Burnham (1972) for liquids coexisting with hornblende. In contrast, most Austurhorn magmas are metaluminous and some are mildly peralkaline.

More importantly, the trace element systematics of the Austurhorn samples are not those expected of melts equilibrated with residual hornblende. In addressing this question I first use major element compositions of the experimental melts to place

approximate limits on the degree of melting represented by a given felsic unit. From figure 4.33 I infer: 1) liquids with >75 wt% SiO₂ record <10 vol% melting; 2) liquids with 70-75 wt% SiO₂ record 10-25 vol% melting (all but one sample are <20 vol% melts); and 3) K₂O/Na₂O of felsic melts is significantly higher than that of initial basalts for samples with <20 vol% melt. Applying these estimates to the Austurhorn suite, I expect samples f-61, g-64 and g-82 to reflect <10 vol% melting and samples f-21, f-43, f-44, f-45, f-62, g-41, g-42, g-61, g-81 and g-83 to reflect 10-25 vol% partial melting. Although these percentages are estimates, it is reasonable to assume that the highly silicic Austurhorn units do not record >25 vol% melting of associated basalts.

This analysis compares observed trace element signatures (Zr, La and Sr) of Austurhorn felsic units with those calculated for equilibrium modal melts of a hydrated basaltic source containing 60% amphibole, 35% plagioclase and 5% Fe-Ti oxides (shaded fields in figure 4.34). These percentages are consistent with those reported by Helz (1978) for melt volumes less than 25%. The fundamental conclusions are not highly dependent upon the residual phase proportions, as indicated in figure 4.34 using a second source comprised of 40% amphibole and 60% plagioclase (open fields in figure 4.34). Two basalt compositions that cover the range observed at Austurhorn (d-45 and d-81) were used for modeling abundances of Sr, Zr and REE in anatectic melts. Of these, d-45 is the most primitive composition observed (7.8 wt% MgO) and is likely to be a common constituent at depth in the Austurhorn system, whereas d-81 is an evolved alkali-rich basalt (4 wt% MgO) which may be present in smaller volumes at all crustal levels. Trace element abundances in anatectic melts were calculated using the batch melting equation of Shaw (1970) [i.e., $C_l/C_o = 1/(F+D-DF)$] and the range of partition coefficients given in table 4.9. Nash & Crecraft (1985) report plagioclase/liquid D_{Sr} of 6-13 for crystals with 30-35 mol% An; this may be a reasonable residual plagioclase composition and calculations include a maximum D_{Sr} of 10 for plagioclase.

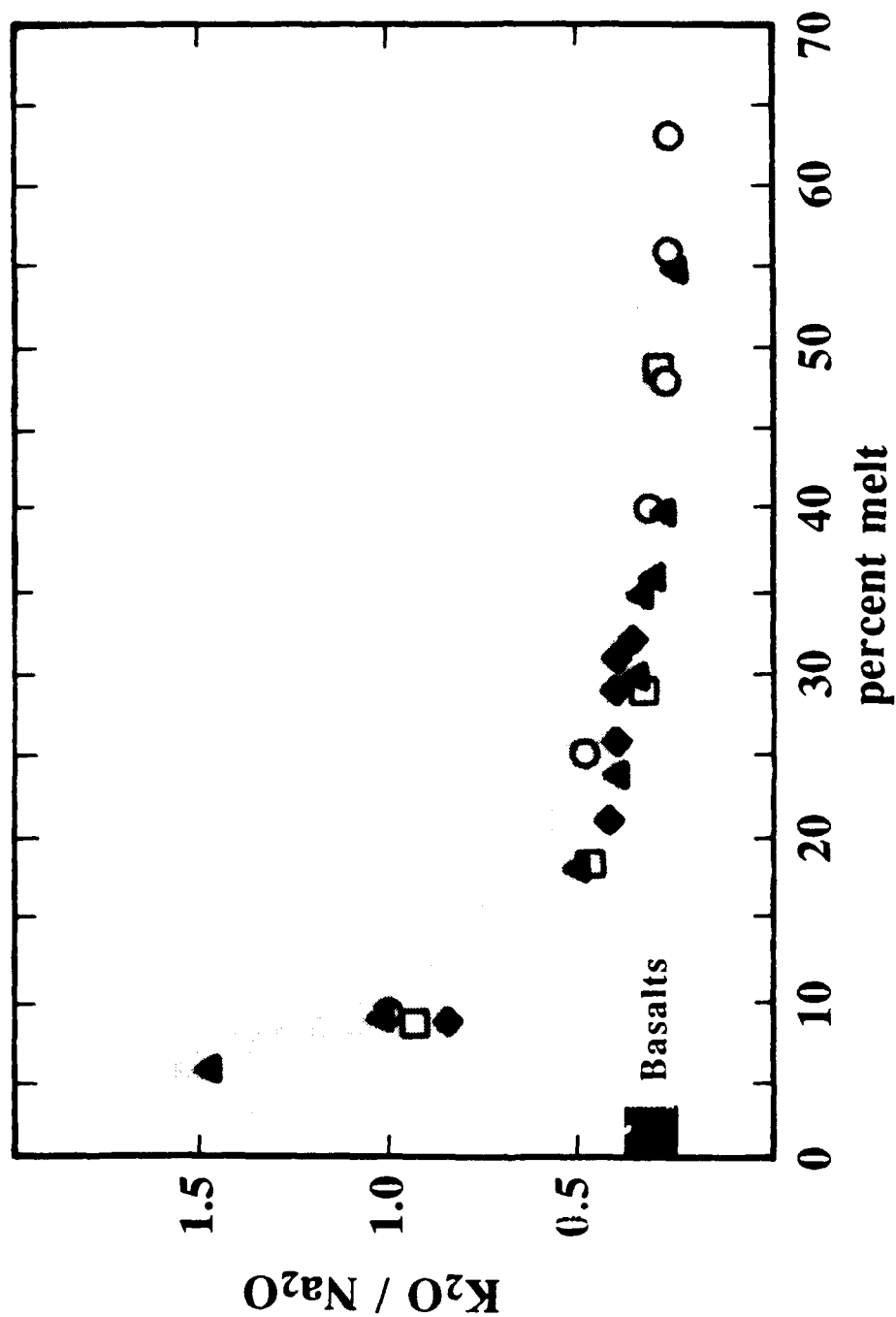


Figure 4.33a The experimental data of Helz (1978) on melts produced by hydrothermal anatexis of basalt at $P=5$ kbars are used to estimate melt percentages represented by the Austurhorn felsic liquids. Experimental liquids with $K_2O/Na_2O > 0.5$ uniformly indicate melt volumes less than 20%; liquids generated by greater degrees of melting have K_2O/Na_2O similar to that of starting basalts.

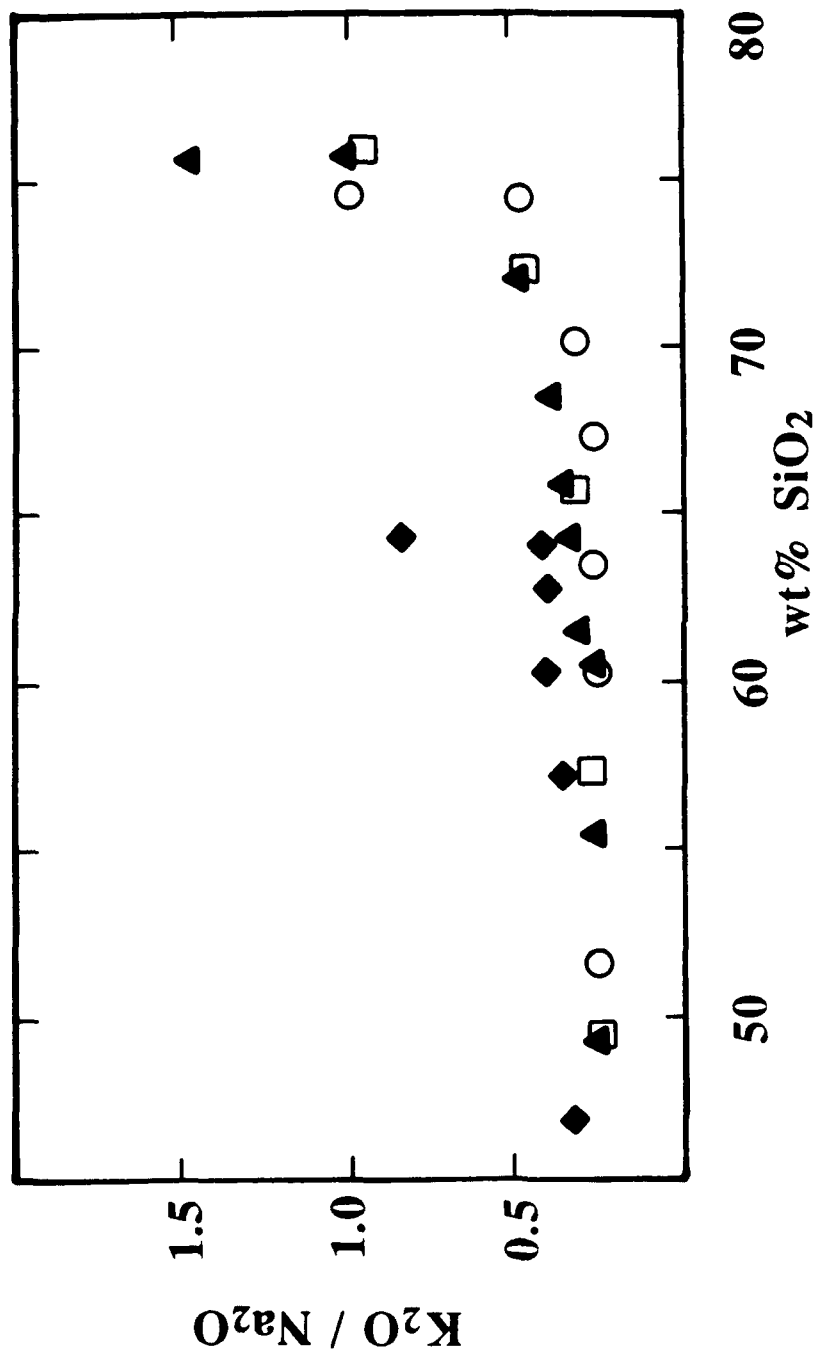


Figure 4.33b Silica content of anatectic melts depends on initial basalt composition, but low melt percentages show the greatest degree of silica enrichment and highest K_2O/Na_2O . Symbols for starting basalts: diamonds = 1801 Hualalai alkali basalt, circles = Picture Gorge tholeiite, triangles = 1921 Kilauea tholeiite, squares = 1921 Kilauea tholeiite at high oxygen fugacity (HIM; other experiments conducted at QFM; Helz, 1978). Same data points as in figure 4.33a.

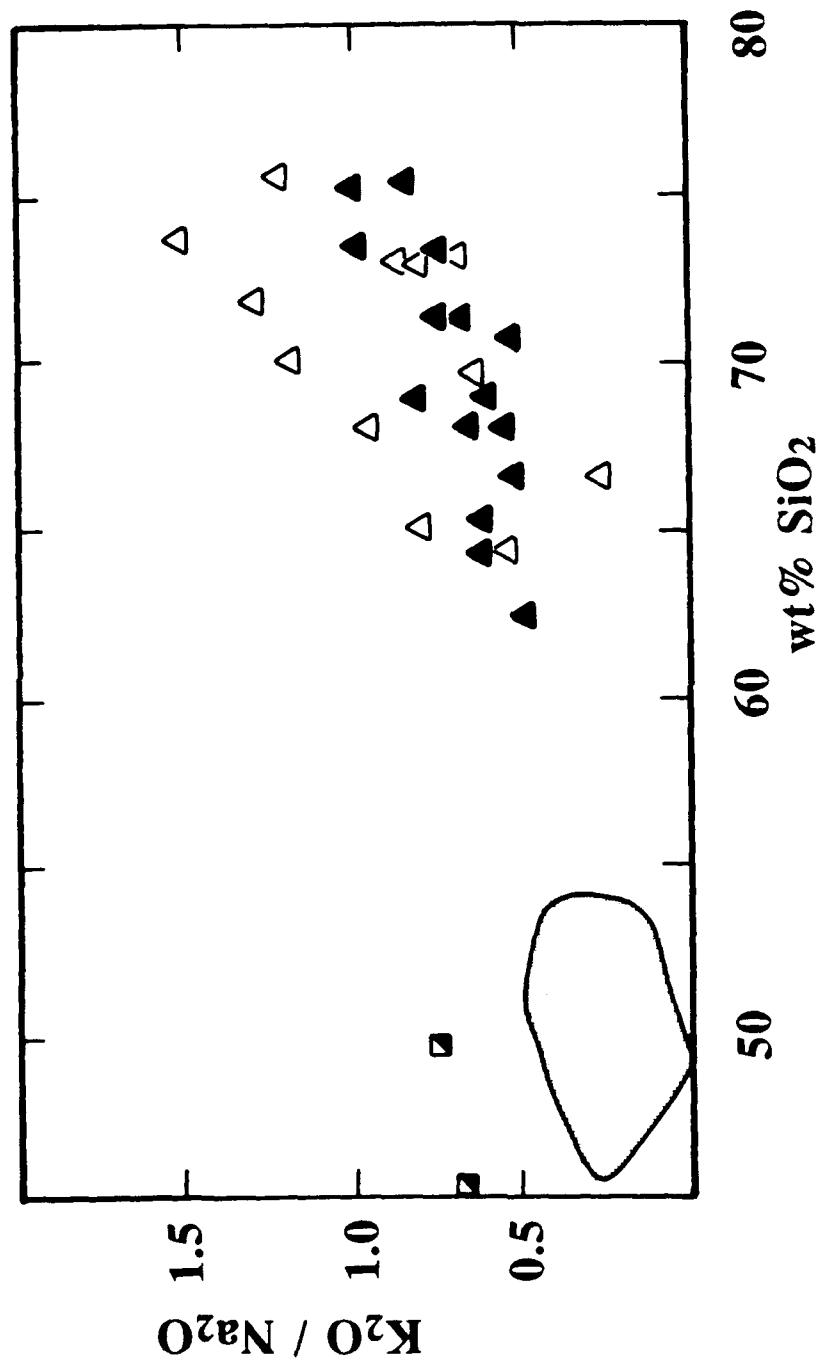


Figure 4.33c Austurhorn felsic samples are generally enriched in K_2O/Na_2O relative to associated basalts (shaded field plus two alkali-rich dikes indicate range of basalts). By analogy to the data of Helz (1978), all samples with >70 $wt\% SiO_2$ could represent < 20 vol% melting of hydrothermally altered basalt. See text for further discussion.

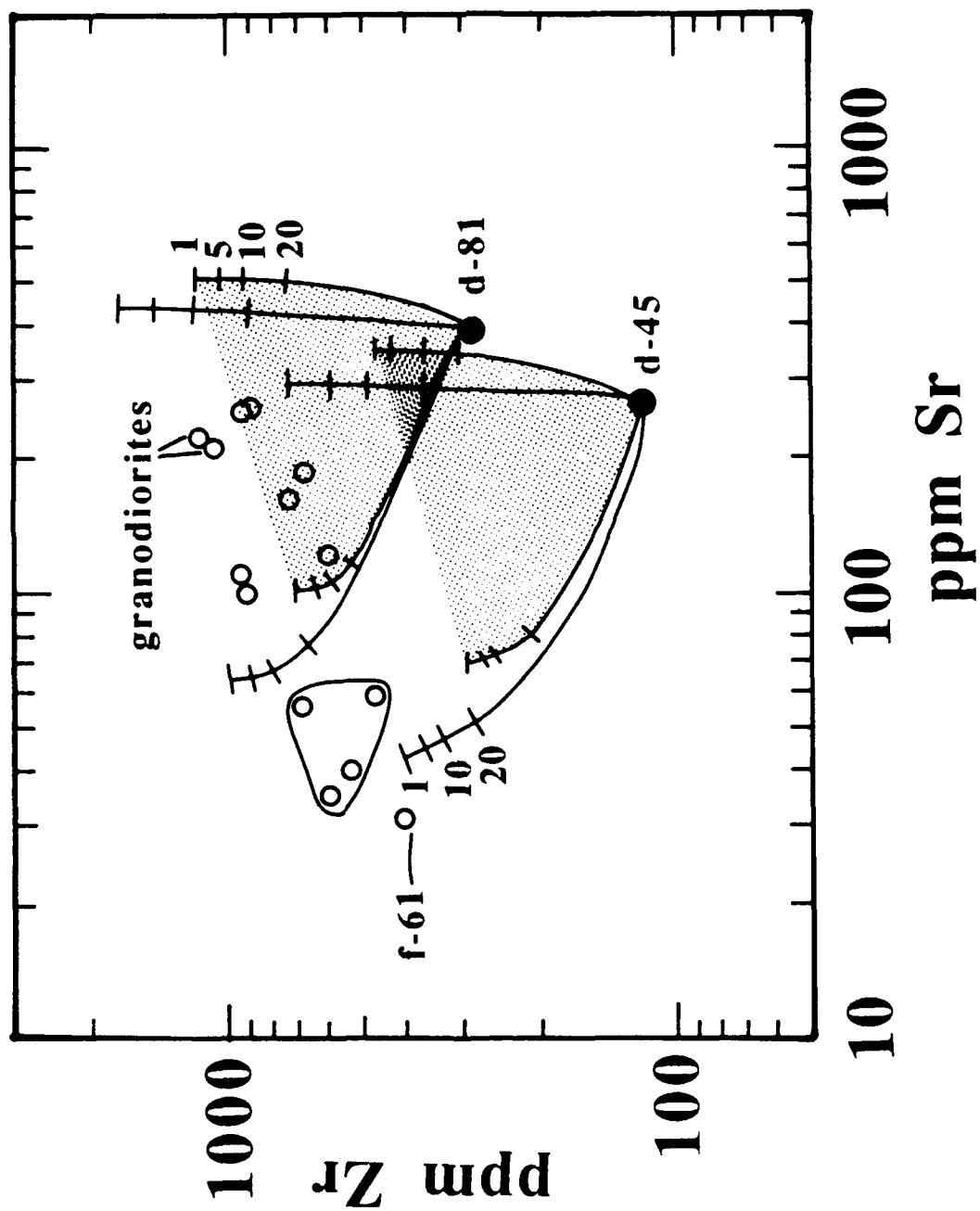
Most Austurhorn granophyres have Zr and Sr abundances consistent with those predicted for low percentage melts (<20%) of the assumed source (figure 4.34a). The required plagioclase/liquid D_{Sr} is between 3-10; the implied plagioclase composition is not unrealistic for an evolved residuum but is more sodic than plagioclase phenocrysts in mafic Austurhorn samples (An_{57} ; figure 4.6). The measured Sr contents of Austurhorn samples are maxima for true melts, because the granophyres contain abundant 2-5 mm plagioclase phenocrysts. The phenocrysts are not embayed or resorbed and are zoned concentrically from euhedral tabular cores to sodic margins with granophyric overgrowths. This petrographic evidence suggests the Austurhorn magmas crystallized without significant loss of plagioclase.

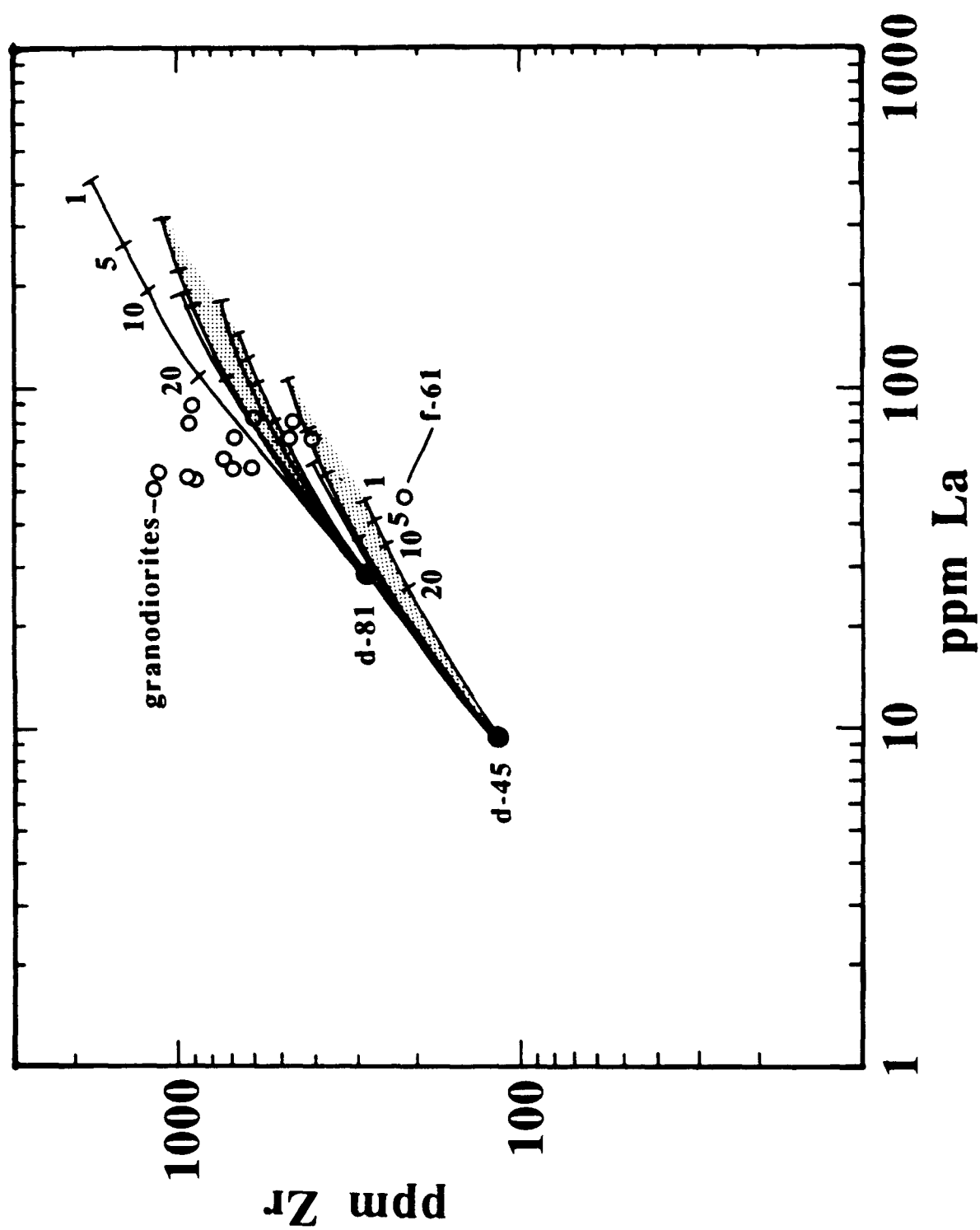
Five samples with $SiO_2 > 71$ wt% (granophyres g-61, g-64, g-81, g-82 [circled in figure 4.34a] and glassy rhyolite f-61) have Zr-Sr concentrations outside the range of melts produced from a source with 35% plagioclase; samples with less than 45 ppm Sr fall outside the predicted ranges for melts of a 60% plagioclase source (figure 4.34a). The extremely low Sr abundances in these feldspar-bearing samples suggest they do not originate by partial melting of hydrated basalt.

In contrast, only these same high-silica granites (g-61, g-64, g-81 and g-82) have Zr-La contents within the predicted range (figure 4.34b). The high Zr contents of granodiorites (g-43, g-65) and other felsic samples cannot be achieved through any realistic melting model. This scenario is inconsistent with that inferred from Zr-Sr abundances, which indicated that high-silica granites were not anatectic melts but granodiorites could be.

In summary, the partial melting hypothesis fails to explain geochemical features of the felsic magmas. In particular, the high Zr contents of low-silica granodiorites appear to require a differentiation event. As discussed earlier, the Zr-La-Sr systematics of the entire Austurhorn felsic suite are consistent with an origin by progressive

Figure 4.34 Trace element abundances in anatectic melts of hydrothermally altered Austurhorn basalts are not consistent with those observed in the granophyres. Fields of element abundances in the calculated melts use the ranges in partition coefficient for plagioclase, amphibole and Fe-Ti oxide given in table 4.9, assuming batch melting of basalt with initial Sr, Zr and La contents of samples d-45 (7.8 wt% MgO) and d-81 (4.0 wt% MgO). In each figure, the **shaded** field shows range of compositions calculated assuming a source with 60% amphibole, 35% plagioclase and 5% oxide and the **open** field indicates a source with 40% amphibole and 60% plagioclase. See text for discussion of modal proportions. Numbered tic-marks indicate the percent of melting (1, 5, 10, 20%). The important feature apparent in comparison of the two panels is that the granodiorites have Zr-La concentrations inconsistent with the melting calculations, whereas the high-silica samples have Sr-La concentrations which cannot be reproduced by the models. Implications of the model are discussed in detail in the text.





fractionation. The single exception to this differentiation model is rhyolite f-61; the petrogenesis of this sample is discussed below.

4.9.3 Petrogenesis of Rhyolite f-61

The geochemical and, more importantly, Pb isotopic characteristics of this sample are distinct from the remainder of the Austurhorn suite. Low abundances of incompatible elements (e.g., La, Ta) are inconsistent with an origin by progressive fractionation from a basaltic parent, and anomalously low concentrations of Sr and Zr indicate the sample is not an anatectic melt of hydrated basalt. The textural evidence for partial melting in rhyolite f-61 is striking. Phenocrysts invaded by the rhyolite glass are predominantly anorthoclase and quartz, and I interpret the sample as recording melting of an *evolved* (i.e., silicic) substrate. In this scenario, most incompatible elements would be contained in minor phases (e.g., zircon, apatite, allanite, monazite) which are likely to be stable during initial melting (Watson & Harrison, 1983; Harrison & Watson, 1984). It is not obvious why this sample should be enriched in ^{206}Pb , but this difference indicates rhyolite f-61 is unusual among Austurhorn samples.

4.9.4 Bridging the Daly Gap

To this point I have explored petrogenetic relationships among basaltic and rhyolitic suites, and determined that intra-group variations are generally consistent with a history dominated by fractional crystallization processes. In this section, geochemical and mineralogical data are used to address the possible genetic link between isotopically equivalent mafic and felsic samples. Two scenarios are plausible: 1) the samples represent a continuous differentiation sequence, or 2) the suites are not related.

Limited isotopic, and abundant trace element, evidence suggests that mafic and felsic magmas at Austurhorn were derived from a common source. O'Nions & Pankhurst (1973) report Sr isotopes of 4 mafic and felsic samples from Austurhorn that are within

analytic error of one another. These samples were not acid-leached, however, so it is possible that new analyses would reveal heterogeneities in radiogenic Sr. Pb isotopic analyses of 5 compositionally diverse samples (p-65, d-81, gb-34, g-83 and f-61) reveal a small amount of internal variability (figure 4.22). With the exception of sample f-61, the isotopic variations at Austurhorn are comparable to those at Vestmannaeyjar and Veidivotn, two neovolcanic basalt centers with roughly homogeneous but different Pb signatures (figure 4.22). The observation that scatter in Pb isotopes is not enhanced by the greater compositional (bulk chemical) range at Austurhorn strengthens arguments for a common - if slightly heterogeneous - source for both mafic and felsic magmas. As discussed previously, ratios of highly incompatible (La, Nb, Ba, P, Ce) and high field strength (Zr, Hf) elements among Austurhorn samples show limited variability. These variations support the idea of minor source heterogeneity, but do not indicate a separate source for mafic and felsic magmas.

Assuming the two groups are related by crystallization, it is relatively straightforward to determine both the fractionation interval and the mineral phases involved. However, the most evolved mafic pillow (p-41b) is separated from the least evolved granodiorite (g-65) by significant gaps in most major elements (9 wt% SiO₂, 1.7 wt% TiO₂, 6 wt% total Fe, 2 wt% MgO, 3.2 wt% CaO, ~0.5 wt% P₂O₅; table 4.1, figure 4.8). CaO/Al₂O₃ of the felsic magma is 0.23, whereas that of the basalt is 0.49. Incompatible trace elements Th and Hf are enriched in g-65 over p-41b by factors of 2.3 and 2.0, respectively, while other elements have lower enrichment factors. The compositional gap is also manifest in a break in plagioclase phenocryst compositions between An₅₃ and An₃₇ (figure 4.6). To first order, the major element data suggest that to bridge the gap the fractionating assemblage is clinopyroxene (to lower CaO/Al₂O₃), plagioclase (An₅₃₋₃₇), FeTi oxides (to remove total Fe, TiO₂ and enrich SiO₂), and apatite (to remove P₂O₅). Trace element abundances suggest a crystallization

interval of ~50%, assuming Rayleigh fractionation with Th and Hf excluded from precipitating phases.

The leucocratic gabbro which outcrops on Hvalnes peninsula and lower Hvasshjalli contains mineral assemblages consistent with these predictions (table 4.4). In both locations, the leucogabbro grades laterally into more melanocratic gabbro and is intruded by granophyre. Plagioclase in three leucogabbro samples (gb-41, gb-82, gb-83) has core compositions ranging between An_{50} and An_{30} (figure 4.5). The samples also contain subequal volumes of cumulus clinopyroxene and FeTi oxides plus apatite. The presence of these cumulate rocks demonstrates that the crystallization step required to generate dacite at Austurhorn did indeed occur in some areas, and strengthens arguments for a fractionation origin for the rhyolitic liquids.

Grove & Donnelly-Nolan (1986) suggested that the andesite-rhyolite compositional gap in calc-alkaline series results from a flattening of the solidus curve in temperature-composition (T-X) space. In practical terms, large changes in liquid composition (e.g., silica content) occur during extensive crystallization over a narrow temperature interval. Experimental studies of crystallization in natural systems (Spulber & Rutherford, 1983; Rutherford et al., 1985) suggest that the solidus slope changes when olivine is replaced by low-Ca pyroxene or amphibole in the fractionating assemblage. At Austurhorn we see no direct petrographic evidence for this specific change in crystallizing assemblage; however, solidus curvature in T-X space results from the shape of the free energy surface of the liquid and does not therefore depend on the actual solid phases precipitating (Grove & Donnelly-Nolan, 1986). I suggest that the compositional gap among sampled Austurhorn liquids reflects this phenomenon, and that the bimodality of liquid compositions is consistent with an origin by fractionation.

4.10 Conclusions

This investigation of mineralogic and geochemical trends among compositionally diverse liquids from the Austurhorn intrusive complex provides new insight into genesis of evolved basalts and rhyolites at Icelandic central volcanoes. The Austurhorn suite is strongly bimodal, with a maximum MgO content of 7.8 wt% and a well defined "Daly gap" between 3.5-1.5 wt% MgO. Austurhorn basalts are dominantly transitional tholeiitic, and the associated felsic rocks are metaluminous to mildly peralkaline. Mafic and felsic samples have comparable ranges in incompatible trace element ratios (Ba/La, La/Nb) as well as Sr- and Pb-isotopes (O'Nions & Pankhurst, 1973; B. Hanan, pers. commun., 1988), suggesting derivation from a common mantle source. The principal finding of this study is that major and trace element systematics within Austurhorn basaltic and silicic sequences are consistent with progressive fractional crystallization of the observed minerals. One felsic dike with petrographic evidence of in situ anatexis is geochemically distinct, with anomalous trace element abundances and an unusually high proportion of ^{206}Pb .

At Austurhorn, quartz normative basalts (3.6 wt% MgO) can be derived from a mildly nepheline normative parental liquid (6.6 wt% MgO) by extensive low pressure fractional crystallization. The inferred crystallizing assemblage of olivine, augite, plagioclase, magnetite and ilmenite is consistent with modal mineralogy of the Hvalnesfjall gabbro. Plagioclase and clinopyroxene compositions from basalts and gabbro samples show complete overlap, suggesting that the shallow level fractional crystallization scenario is geologically reasonable.

Silica enrichment and iron depletion among basaltic pillow samples indicate extensive fractionation of FeTi oxides which, in turn, suggests crystallization under oxidizing conditions. Oxygen fugacities calculated from coexisting magnetite and ilmenite in both basalt pillows and gabbro samples support this hypothesis, and record cooling along the nickel-nickel oxide buffer. I conclude that this enhanced role of

magnetite and ilmenite precipitation drives silica enrichment in Icelandic transitional tholeiitic systems.

Several basalt dikes evolved under conditions of lower oxygen fugacity, as evidenced by enrichment in iron rather than silica. In one extreme case, a dike with ~19 wt% iron and ~2 wt% MgO, efficient magnetite suppression requires oxygen fugacity well below that of the quartz-fayalite-magnetite buffer. These data indicate a range in ambient oxygen fugacity existed within the Austurhorn magmatic system. The cause of such large variations in local f_{O_2} is not apparent, but is of primary importance in determining the evolutionary paths taken by individual magma batches.

Differences in bulk geochemistry between contemporaneous mafic dikes reflect additional heterogeneities within the Austurhorn system. Tholeiitic to transitional tholeiitic mafic dikes (7.8-4.0 wt% MgO) at Austurhorn have Ce/Yb ratios that vary from 2.5-4.7, indicating they were not derived by fractionation of a single parental liquid but probably represent separate mantle melting events. Tholeiitic clinopyroxene phenocrysts were analyzed in two dikes but were not observed among the gabbroic cumulates. Finally, subordinate alkali-rich basalts appear to originate through contamination of transitional tholeiitic basalt by molten granophyre at depths below the current level of exposure.

The cumulus mineralogy of leucocratic gabbros gives important evidence for fractionation processes in a compositional interval not represented by dikes and sills. Differentiation from quartz normative basalt to dacite may be modeled by precipitation of plagioclase, augite, FeTi oxides and apatite. Leucocratic gabbros with this assemblage grade laterally into more melanocratic units, suggesting that the evolutionary process from mafic to silicic compositions is continuous, although sampling of these liquids by eruption or shallow emplacement is not.

Field evidence indicates the felsic magmas evolved at deeper crustal levels than the basaltic suite ($P > 1$ kbar). Major and trace element trends among most felsic samples

can be modeled by fractionation of the observed mineral phases: plagioclase, K-feldspar, clinopyroxene, magnetite, ilmenite and apatite (samples with >73 wt% SiO₂ contain anorthoclase). It is possible that crustal melting augments fractional crystallization in producing Icelandic rhyolites, particularly within the thick crust beneath the EVZ. However, most Austurhorn felsic samples are unlike liquids derived experimentally by progressive melting of hydrated basalts (Helz, 1978). Specifically, the Zr, Sr and La systematics of the felsic rocks are inconsistent with an origin by melting a plagioclase- and amphibole-rich source. The unusual felsic dike with anomalous Pb isotopes and a partially melted texture has low incompatible element abundances and fractured crystals of anorthoclase and quartz, suggesting anatexis of an existing felsic unit.

In summary, geochemical heterogeneity of the Austurhorn liquid suite provides evidence for progressive crystallization of small magma batches at various crustal levels. By analogy to the Hvalnesfjall gabbro, these bodies are likely to be 2-5 km in diameter. These small magma body volumes undergo extensive crystallization during cooling and their liquids do not record significant crustal melting or assimilation.

CHAPTER 5
MATURE VOLCANOES, IMMATURE RIFTS

In this thesis I have sought to document and interpret the magmatic evolution of individual volcanic centers as manifest in the geochemistry and petrology of their eruptive and intrusive products. To this end I have presented mineralogic and geochemical data from the Vestmannaeyjar volcanic and Austurhorn intrusive complexes. Geochemical differences between these two areas imply fundamentally different magmatic environments, yet evidence from the eastern neovolcanic zone [EVZ] indicates comparable diversity on a scale of ~150 km (Jakobsson, 1972, 1979; Meyer et al., 1985). The results of the present study thus afford insight into models of modern rift zone evolution as well as the petrogenetic development of individual volcanic centers.

Variations in major elements, REE and radiogenic isotopes (He, Sr, Nd, Pb) indicate that significant heterogeneity exists among Iceland's neovolcanic basalts (e.g., Schilling, 1973; Hart et al., 1973; Sun et al., 1975; O'Nions et al., 1976; Langmuir et al., 1978; Wood et al., 1979; Jakobsson, 1979; Zindler et al., 1979; Kurz et al., 1985; Stecher et al., 1986; Park et al., in preparation). Concurrent oxygen isotope studies (Muehlenbachs, 1973; Muehlenbachs & Jakobsson, 1973; Muehlenbachs et al., 1974; Gunnarsson et al., 1988) and coupled O-Sr and Th-O-Sr variations (Condomines et al., 1983; Hemond et al., 1988) demonstrated convincingly that crustal contamination (*sensu lato*) occurs in modern Icelandic central volcanoes. The variations are not random, however, indicating that an integrated picture of crustal and mantle processes is required. Recent syntheses of petrologic and geochemical data by Schilling et al (1982) and Meyer et al (1985) provide a comprehensive model of Icelandic rift zone evolution by incorporating secular variations in mantle sources (O'Nions & Pankhurst, 1973), some crustal assimilation (particularly in the EVZ) and mixing and fractionation in replenished magma chambers (O'Hara & Matthews, 1981). In contrast, Oskarsson et al (1982, 1985) and Hemond et al (1988) proposed that the sub-Icelandic mantle is geochemically homogeneous, and that observed chemical and isotopic variations result almost entirely from assimilation of crustal melts by a homogeneous olivine tholeiite.

The question of chemical, mineralogic and isotopic heterogeneity in the mantle source therefore remains unresolved. This issue bears on geochemical constraints for models of rift zone evolution (particularly in defining isotopic characteristics of potential assimilants) and consequently on models for the dynamics of hotspot-mantle interactions. In the following discussion I explore stable and radiogenic isotope evidence for heterogeneity within Iceland's neovolcanic zones. The goal is to determine which isotopic systems appear decoupled, and to infer whether variability arises in the crust, the mantle or both. Finally, I integrate the concomitant evolution of rifting and magmatism inferred from observations at Vestmannaeyjar and Austurhorn with models of crustal and mantle evolution beneath Iceland's active rift zones (e.g., Oskarsson et al., 1982, 1985; Meyer et al., 1985). This work builds upon previous studies by incorporating four additional aspects of Icelandic petrology and geochemistry: 1) oxygen isotope signatures of axial and flank rift zones, 2) the paucity of basalts with >8 wt% MgO at mature central volcanoes, 3) geochemical diversity among basalts from transitional tholeiitic volcanic systems, and 4) localized copious silicic magmatism. An explicit premise of this discussion is that the Austurhorn complex developed in a tectonic and magmatic environment analogous to that of geochemically similar volcanic centers in the EVZ (e.g., Eyjafjallajökull, see chapter 4). Some of the inferences drawn below are necessarily speculative but can be tested by further investigations of appropriate magmatic systems.

5.1 Mantle Heterogeneity Beneath Iceland: Fact or Artifact?

Combinations of six isotopic systems (Sr, Nd, Pb, Th, He, O) have been measured in neovolcanic Icelandic basalts, although a complete data set does not exist for any single sample. In assessing the variability of, and possible relationships between, the different isotopic systems I consider only recent lavas and glasses, thereby omitting questions of secular heterogeneity (O'Nions & Pankhurst, 1973; Schilling et al., 1982;

Hanan & Schilling, 1986, 1987). I also restrict discussion initially to lavas with <54 wt% SiO₂.

5.1.1 Oxygen Isotope Ratios of Neovolcanic Basalts

The single stable isotopic system, oxygen, shows the least global variability among basaltic lavas and glasses, which are typically enriched in ¹⁸O by +5.5 to +6.5 per mil relative to standard mean ocean water [SMOW] (e.g., Anderson et al., 1971; Ito et al., 1987). Icelandic groundwater is depleted in ¹⁸O relative to SMOW (typically -8 to -13.5 per mil; Arnason, 1976; Bjornsson & Kristmansdottir, 1984). Interaction with hydrothermal fluids or altered crust is expected to lower the ¹⁸O of mantle-derived magmas relative to source values. Altered silicic xenoliths (Muehlenbachs et al., 1974; Macdonald et al., 1987) and samples from deep boreholes (Hattori & Muehlenbachs, 1982) attest to this process, with delta ¹⁸O values as low as -10 per mil.

Glass and whole rock oxygen isotope data (table 5.1) exhibit compositional dependency. Most significantly, alkali basalts and picrites record unambiguous mantle oxygen signatures. The alkali basalts from Vestmannaeyjar, Snaefellsnes and Jan Mayen (figure 5.1) have a narrow range of near-mantle values (+5.1 to +5.7 per mil; Muehlenbachs et al., 1974; Muehlenbachs & Jakobsson, 1979; Condomines et al., 1983) as do hawaiitic and mugearitic lavas from Vestmannaeyjar (+5.5 to +5.7 per mil; Muehlenbachs & Jakobsson, 1973), indicating they have not experienced significant interaction with crustal melts or groundwater.

Similarly, picrites from throughout Iceland have near-mantle ratios, with one exception from central Iceland that is somewhat depleted (+4.72 per mil; Hemond et al., 1988). Undepleted signatures (delta ¹⁸O = 5.45-5.7; see table 5.1) are also found among olivine-normative basalts (Muehlenbachs et al., 1974; Hemond et al., 1988) and transitional tholeiitic glasses from Hekla and Torfajokull (Gunnarsson et al., 1988), although both groups range to ~+4 per mil. Quartz-normative basalts are variably

Table 5.1 Oxygen and Helium Isotope Ratios

Area	Sample Type	Delta ^{18}O	$^3\text{He}/^4\text{He}$ ($\text{R}/\text{R}_\text{A}$)	References
N. Atlantic	MORB glasses (52)	5.52 - 5.84	6.5 - 11	1
Reykjanes	picrite (1)	6.25	-	2
	ol. tholeiites (8)	4.8 - 5.7	13.4 - 14.0 (6)	2, 3
WVZ	ol. tholeiites (8)	4.0 - 5.2	8.7 - 15.9 (7)	2, 3
	glasses (4)	4.6 - 4.8	-	3
MIL	picrites (2)	4.72 - 5.75	-	2
	ol. tholeiites (5)	4.02 - 5.30	19.7 - 22.2 (6)	2
	qtz. tholeiites (3)	3.1 - 3.90	-	2, 3
NVZ	picrite (1)	5.75	-	2
	ol. tholeiite (1)	5.45	5.1 - 11.0 (5)	2
	qtz. tholeiites (4)	4.70 - 5.20	-	2
	lavas* (17)	3.0 - 5.3	-	3
EVZ	trans. tholeiites (5)	3.9 - 4.9	13.9 - 26.2 (7)	3
	andesites (9)	4.2 - 5.0	-	4
	glasses**	5.3 - 5.6	-	5
Vestman.	alk. basalts (7)	5.5 - 5.7	11.0 - 15.1 (3)	3, 6, 8, 9
	hawaiite, mugearite (4)	5.5 - 5.7	-	6
Snaef.	alk. basalts (6)	5.2 - 5.6	-	3
	glasses**	5.1 - 5.6	-	5
Jan Mayen	alk. basalts (2)	5.4 - 5.6	-	3

Notes: Numbers in parentheses indicate number of analyses quoted.

* indicates composition not given

** indicates unspecified number of analyses

- References:
- 1 Ito et al., 1987
 - 2 Hemond et al., 1988
 - 3 Muehlenbachs et al., 1974
 - 4 Muehlenbachs, 1973
 - 5 Gunnarsson et al., 1988
 - 6 Muehlenbachs & Jakobsson, 1973
 - 7 Condomines et al., 1983
 - 8 Kurz et al., 1985
 - 9 Poreda et al., 1986

depleted in ^{18}O , with a maximum value of +5.3 per mil (table 5.1; Muehlenbachs, 1973, Muehlenbachs et al., 1974; Hemond et al., 1988).

These data are consistent with a petrogenetic model which predicts a mantle origin for alkali basalts and picrites and permits (but does not require) variable amounts of crustal interaction in volcanic centers with transitional tholeiitic and evolved liquids (e.g., Schilling et al., 1982; Meyer et al., 1985). They are not, however, consistent with the suggestion of Oskarsson et al (1982, 1985) and Steinthorsson et al (1985) that all Icelandic alkali basalts originate through melting of hydrothermally altered crust. In subsequent sections I rely upon the assumption that lavas (or glasses) which have $\delta^{18}\text{O}$ greater than +5.5 per mil have not interacted to any significant degree with crustal melts or fluids, but rather record the isotopic characteristics of their source.

5.1.2 Oxygen-Helium Relationships

Global MORB have strikingly uniform He isotopic ratios ($^3\text{He}/^4\text{He} \sim 8.4 R_A$ [R_A = atmospheric ratio of 1.384×10^{-6}] Kurz, 1982), whereas hot spot or plume related basalts with high $^3\text{He}/^4\text{He}$ ratios sample a comparatively less degassed mantle source (e.g., Loihi seamount; Kurz et al., 1983). Crustal contamination (incorporation of radiogenic ^4He produced by U and Th decay) can only lower $^3\text{He}/^4\text{He}$ ratios, which are therefore interpreted as providing a minimum value of the helium isotope ratio of the local mantle source. Helium isotope ratios may thus provide unquestionable evidence for variations in mantle helium isotopic composition.

Icelandic basalts (Condomines et al., 1983) and subglacial glasses (Kurz et al., 1985) as well as submarine basalts dredged from the Reykjanes Ridge and Iceland plateau (Poreda et al., 1980, 1985) have $^3\text{He}/^4\text{He}$ ratios higher than normal MORB, with a maximum value of $26.2 R_A$ reported in central Iceland (table 5.1; Kurz et al., 1985). Kurz et al (1985) noted a trimodal distribution of helium isotopic ratios within Iceland's neovolcanic zones, with ratios of 12-16 R_A in the WVZ and Reykjanes, 8-11 R_A in the

NVZ and 18-26.2 R_A in the EVZ and MIL (table 5.1; figure 5.1). The data of Condomines et al (1983; table 5.1) are consistent with this interpretation with one exception of 23 R_A in a Reykjanes basalt. Icelandic geothermal waters also have higher $^3\text{He}/^4\text{He}$ ratios than normal MORB, with higher ratios measured in wells on the Reykjanes Peninsula (10.7-12.7x atmospheric) than in wells from the NVZ (7.9-9.0x atmospheric; Torgersen & Jenkins, 1982).

Helium isotopes may be decoupled from oxygen isotopes, because the helium content of meteoric water is significantly lower than that of basalt, so fluid-rock interactions which remove ^{18}O are unlikely to alter the basaltic $^3\text{He}/^4\text{He}$ ratio. However, assimilation of isotopically distinct crustal melts can change magmatic helium isotope ratios. Paired He and O isotopic measurements are available for several neovolcanic tholeiites (table 5.1; Condomines et al., 1983); these data are shown as points in figure 5.2 with regional fields drawn on the basis of data in table 5.1. Note that no paired analyses have been made of picrites or of samples from the EVZ or Vestmannaeyjar.

The most important features of figure 5.2 are: (1) separate groupings of $^3\text{He}/^4\text{He}$ for samples with mantle oxygen isotope signatures from Reykjanes, the EVZ and Vestmannaeyjar; (2) all three groups have high $^3\text{He}/^4\text{He}$ with respect to normal MORB; (3) the lack of correlation between $^3\text{He}/^4\text{He}$ and $\delta^{18}\text{O}$ when "altered" samples are included. Fields of data for Reykjanes and the NVZ are elongate in the direction of their respective geothermal fluids (Torgersen & Jenkins, 1982; figure 5.2). A final important observation is that although both olivine- and quartz-normative tholeiites from the MIL (central Iceland; figure 5.1) are depleted in ^{18}O , their He-O signatures can not result from simple alteration of Reykjanes, Vestmannaeyjar or MORB mantle products. This diagram therefore confirms the existence of regional helium isotopic heterogeneity among pristine mantle-derived Icelandic basalts (Kurz et al., 1985)

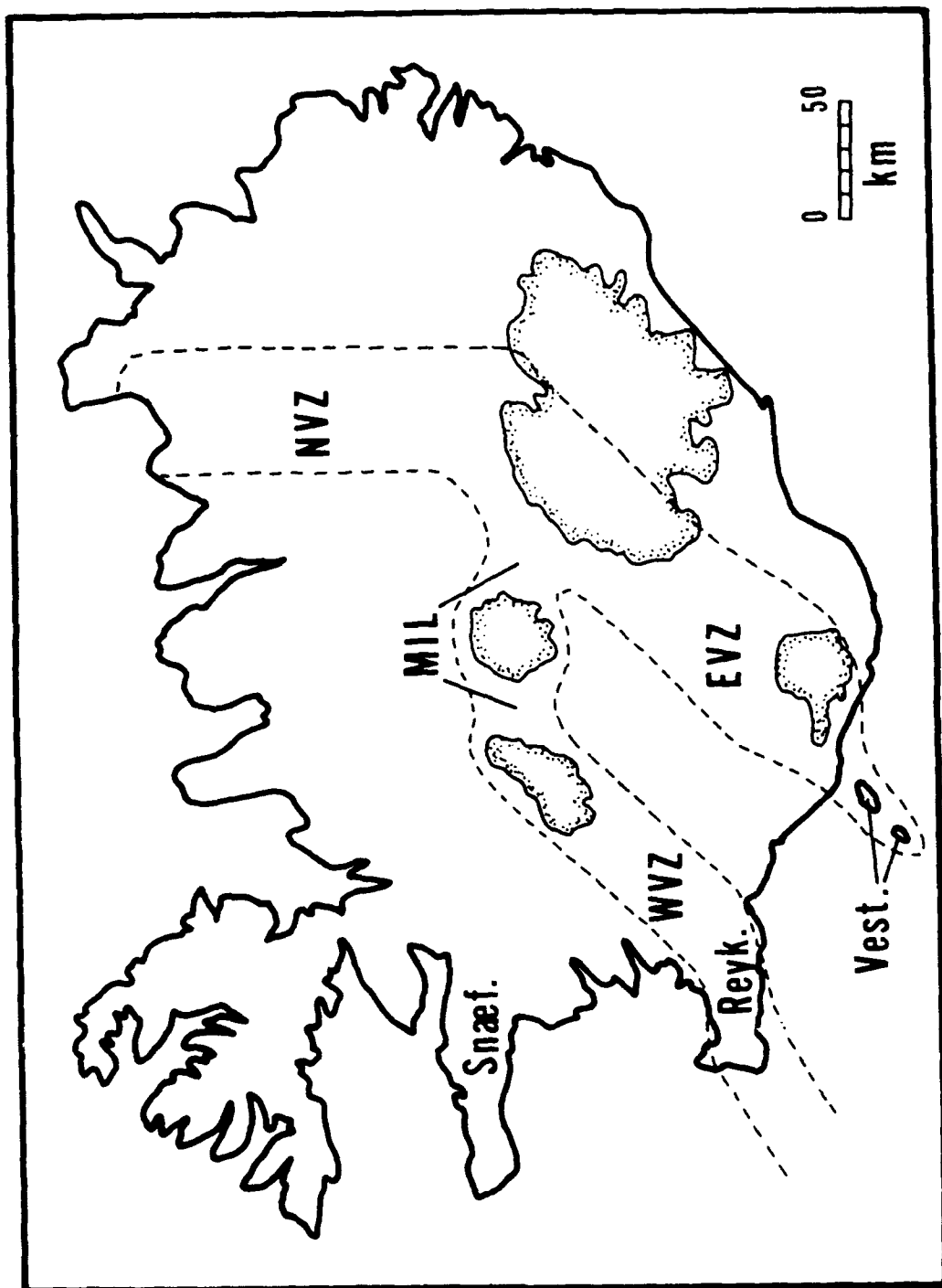


Figure 5.1a Map of Iceland showing geographic distribution of samples with oxygen isotopic data reported in table 5.1. The neovolcanic zones are located within the dashed lines. Reykjanes and Vestmannaeyjar are treated separately in table 5.1 although they comprise portions of the western [WVZ] and eastern [EVZ] volcanic zones, respectively.

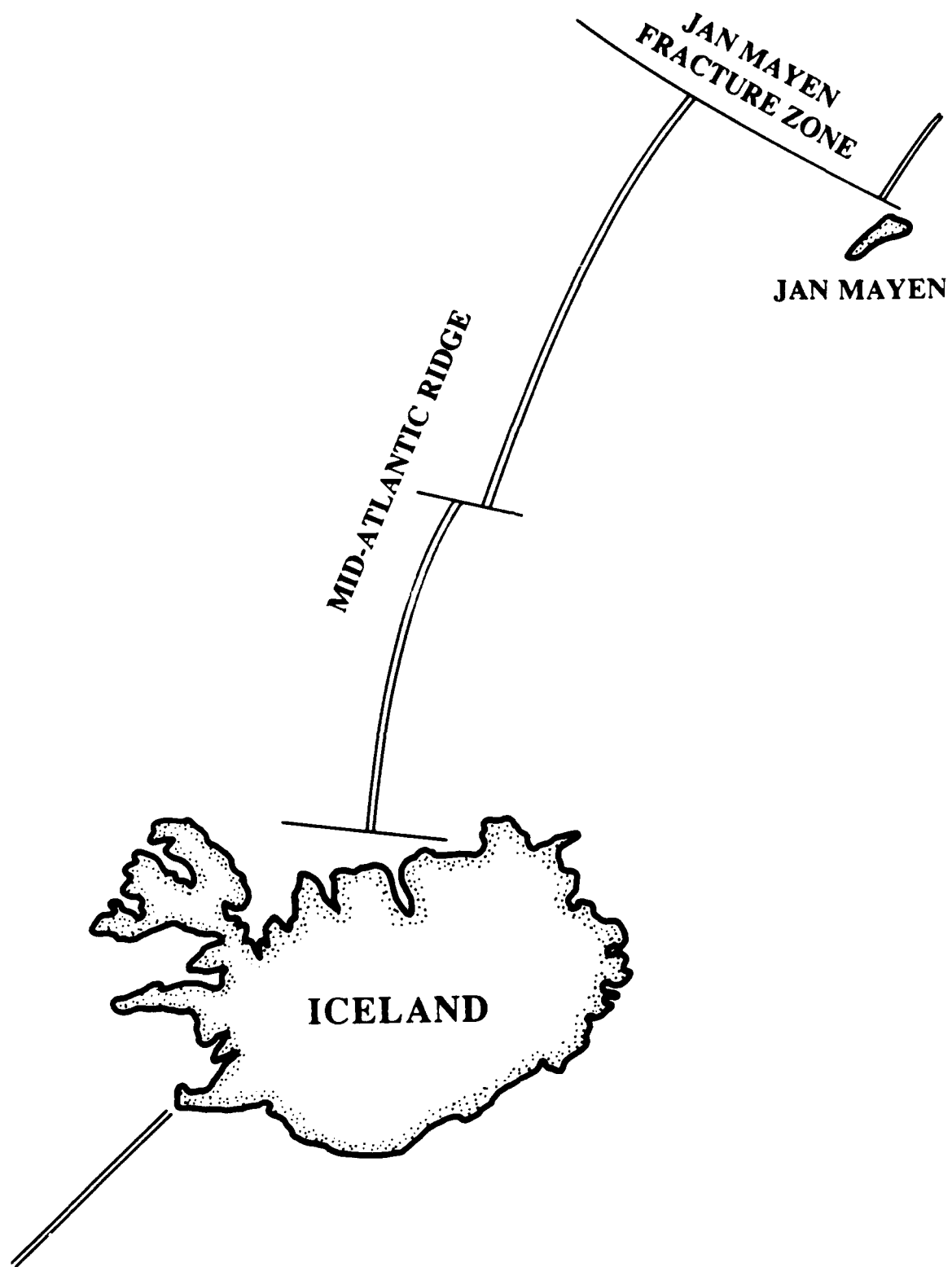


Figure 5.1b Location of Jan Mayen with respect to Iceland and other prominent features of the north Atlantic.

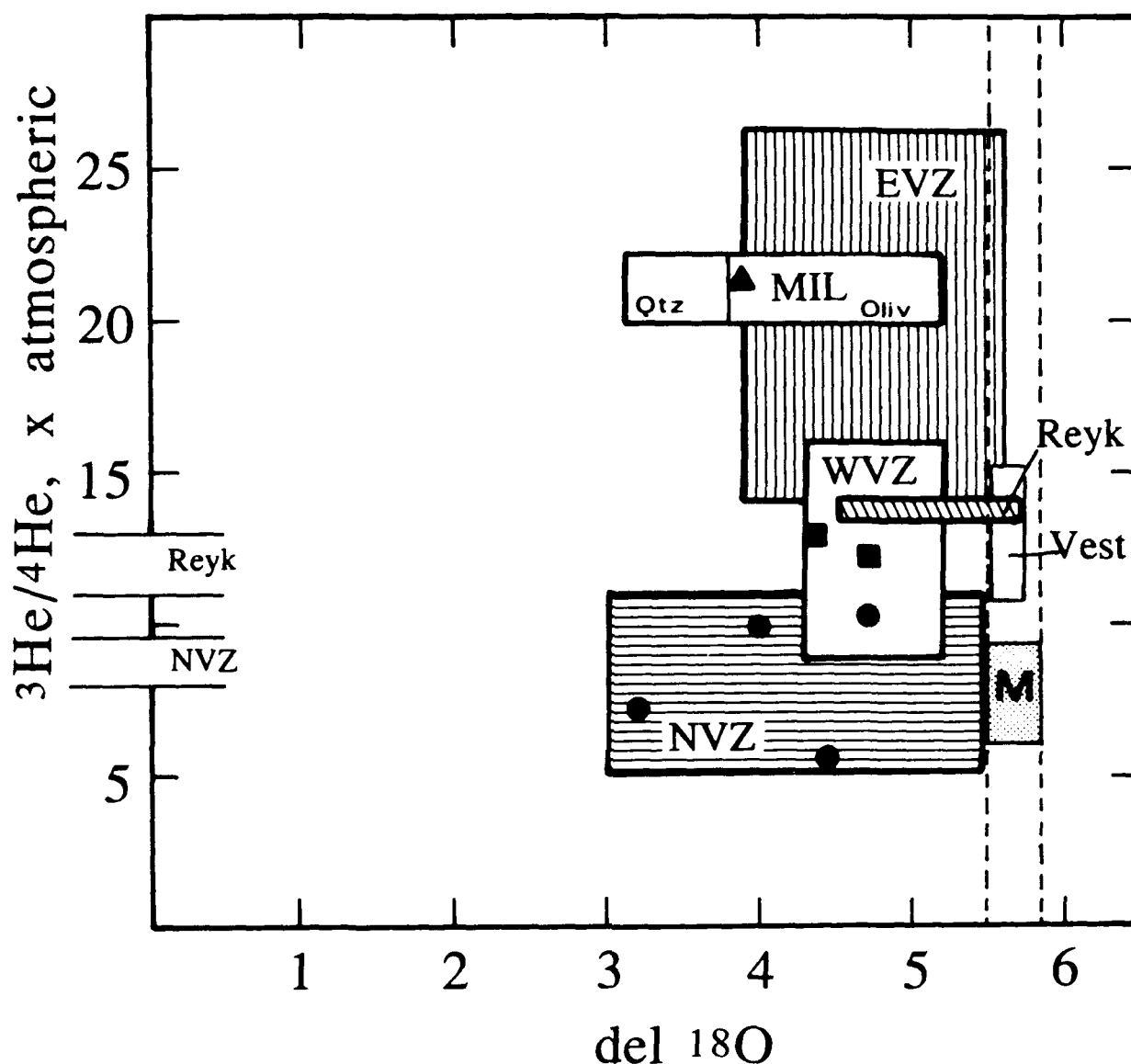


Figure 5.2 Paired analyses of oxygen and helium isotopes in neovolcanic Icelandic basalts define distinct ranges for the geographic provinces labeled in figure 5.1a. Symbols: circles = NVZ, squares = WVZ, triangle = MIL olivine tholeiite; ranges defined by data in table 5.1 and references therein. Three paired analyses from Reykjanes are not indicated specifically. Field labeled M encompasses MORB data, with dashed extension indicating the acceptable range for unaltered oxygen isotope data. Open areas labeled Reyk and NVZ indicate the range in helium isotopes of geothermal waters from these areas (Torgersen & Jenkins, 1982) but do not indicate their oxygen signatures.

and indicates that isotopic variations among neovolcanic basalts do not result entirely from simple alteration of homogeneous basalt magma.

5.1.3 Sr-Nd-Pb Relationships

Several studies of Sr, Nd and Pb isotopes also indicate a heterogeneous source for Icelandic magmas (e.g., Hart et al., 1973; Sun et al., 1975; Sun & Jahn, 1975; O'Nions et al., 1976; Zindler et al., 1979; Condomines et al., 1983; Stecher et al., 1986).

Neovolcanic basalts from the EVZ show limited variations in $^{87}\text{Sr}/^{86}\text{Sr}$ and $^{143}\text{Nd}/^{144}\text{Nd}$ which do not correlate with either bulk geochemistry or geographic occurrence (figure 5.3; Park et al., in preparation). As discussed in chapters 2 and 4, each volcanic system displays Sr-Nd isotopic variability beyond analytic error. The important feature of figure 5.3a, however, is the relative homogeneity within the EVZ basalts. However, new Pb isotopic data from the EVZ require heterogeneity in the sub-Icelandic mantle (Park et al., in prep.; B. Hanan, unpublished data). The strength of these new data is the demonstration that volcanic centers with overlapping ranges in Sr and Nd isotopes have distinctly different Pb isotopic signatures (figure 5.3b). Unlike variations in radiogenic Sr which may be relegated to the effects of seawater, rainwater or magmatic assimilation, the observed range in radiogenic Pb is most readily attributed to the mantle source. In particular, the low U and Th contents of Icelandic lavas (<1 and <4 ppm, respectively for basalts and <3, <11 ppm for silicic rocks; see chapter 4) require unreasonably long times to produce the observed diversity within the crust and then apply it selectively to neovolcanic magmas.

Condomines et al (1983) noted an apparent decoupling between He and Sr-Nd isotopic systems in silicic and differentiated tholeiitic rocks. No additional paired analyses are available to address this question, but recent He and Sr data do support this suggestion. Hemond et al (1988) noted no geographic variation in $^{87}\text{Sr}/^{86}\text{Sr}$ across the

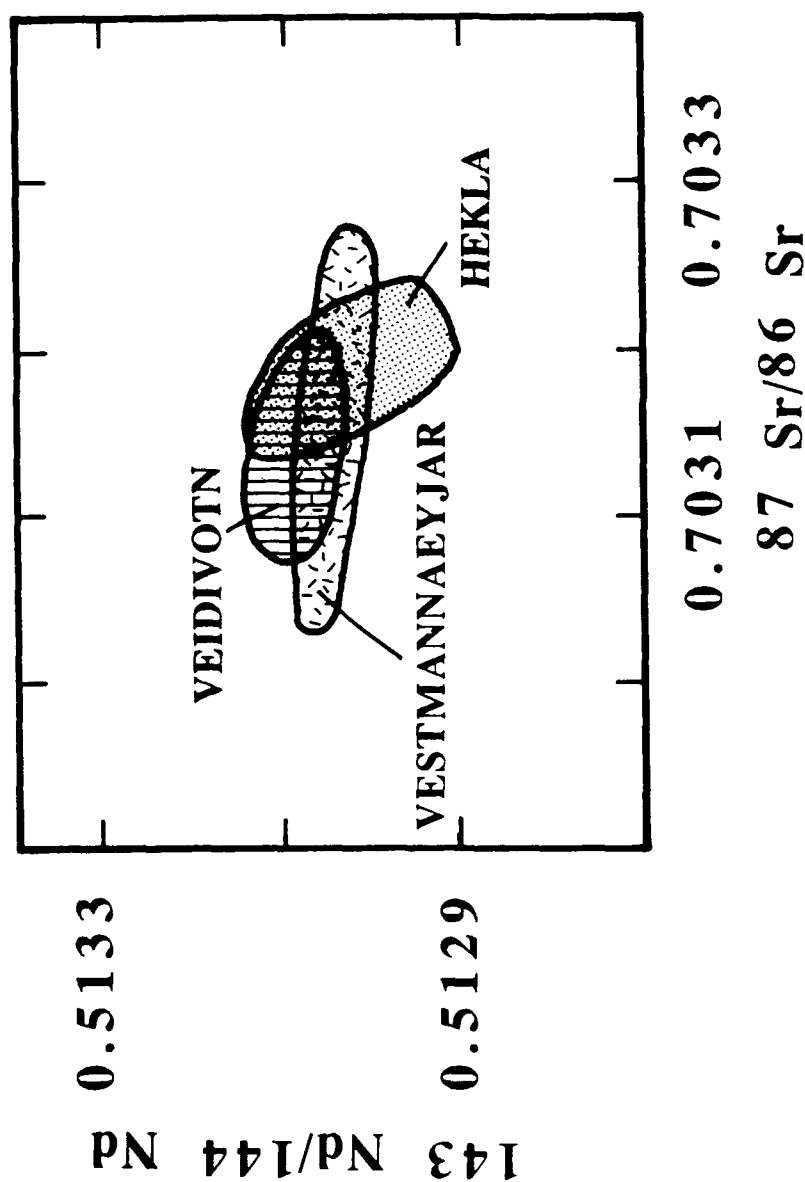


Figure 5.3a Lavas from these three neovolcanic centers have overlapping Sr and Nd isotopes (K-H. Park, unpublished data). The Austurhorn samples (not shown for lack of Nd data) have more highly radiogenic Sr than the modern lavas, a difference that O'Nions & Pankhurst (1973) attribute to secular variations in the geochemistry of the Iceland mantle plume.

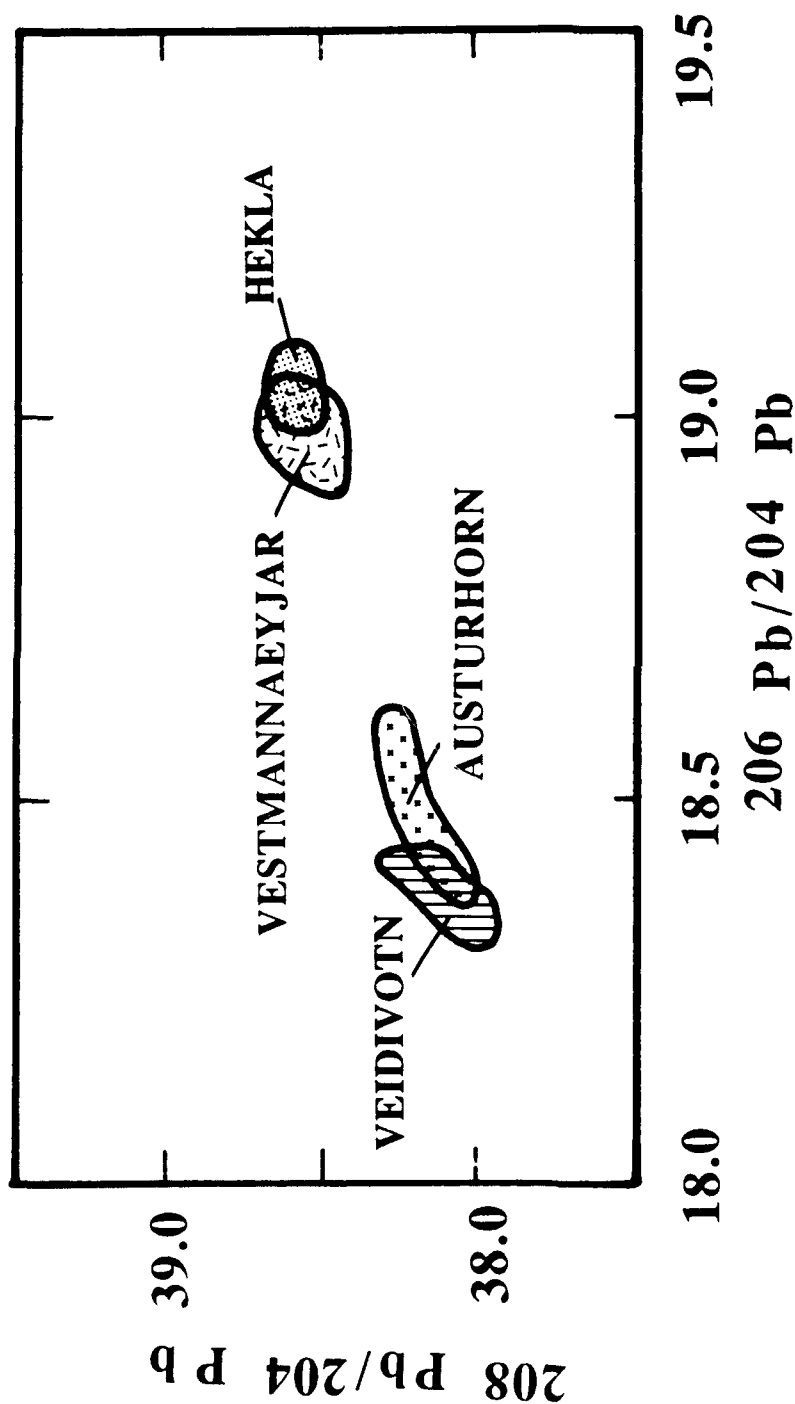


Figure 5.3b Individual Icelandic volcanic systems show little variation in Pb, Sr and Nd isotopes. However, consistent differences in Pb isotopic ratios between contemporaneous volcanoes from the eastern volcanic zone (Hekla, Vestmannaeyjar, Veidivotn) require a heterogeneous mantle source (K-H. Park and B. Hanan, unpublished data).

tholeiitic neovolcanic zones, whereas the He data of Kurz et al (1985) indicated significant regional heterogeneity within the tholeiitic volcanics.

5.1.4 Summary of Observations

I concur with the philosophical approach of Oskarsson et al (1985) that "only when the capability of crustal processes accounting for the observations has been tested to the full is it permissible to refer the residual variation to the properties of the mantle source." Indeed, the major and trace element variations reported in this thesis are interpreted as resulting primarily from processes acting within the crust and lithosphere. However, the overwhelming bulk of isotopic evidence does not support the existence of a single parental tholeiitic magma beneath all Icelandic volcanic systems. On the contrary, regional differences in neovolcanic parental basalt geochemistry (as exemplified by variations within the EVZ) are consistent with models inferring an isotopically non-uniform source (e.g., Schilling, 1973; Hart et al., 1973; O'Nions et al., 1976; Kurz et al., 1985).

5.2 Crustal Contamination and Overprinting

Two lines of evidence indicate that many Icelandic basalts are contaminated (*sensu lato*) prior to eruption. First, many fresh lavas and glasses are depleted in ^{18}O relative to normal MORB (table 5.1; references therein). Evolved (quartz-normative) basalts are often more depleted than olivine tholeiites, suggesting either direct assimilation of, or oxygen exchange with, hydrothermally altered wall rocks (e.g., Hattori & Muehlenbachs, 1982; Condomines et al., 1983). Secondly, individual basalts are often enriched in K, Rb, Th and U relative to contemporaneous lavas (Hemond et al., 1988; chapter 4). Abundances of these elements in excess of those predicted by crystal fractionation models are interpreted as indicative of contamination by silicic magmas generated within the crust (Hemond et al., 1988; chapter 4). Depletions in ^{18}O coupled

with enrichments in radiogenic Sr among neovolcanic tholeiites (Hemond et al., 1988) are consistent with assimilation of an altered evolved silicic component.

I concur with Oskarsson and co-workers (1982, 1985; Hemond et al., 1988) that crustal contamination is an important agent in Icelandic magma systems. Three aspects of this process must be clarified, however:

- (1) Are all silicic magmas the result of crustal melting?
- (2) Are quartz tholeiites generated by mixing of basaltic and silicic magmas?
- (3) Does contamination occur by bulk mixing or selective assimilation?

Each of these questions is one of degree, and it is unlikely that a unique answer exists for all Icelandic volcanoes. An affirmative answer to the first question is supported by enrichments in radiogenic Sr in some neovolcanic felsic rocks relative to associated basalts (e.g., O'Nions & Gronvold, 1973; Wood et al., 1979). Similarly, Hemond et al (1988) demonstrated that the isotopic (Sr-O-Th) features of quartz tholeiites could be produced by bulk mixing of mantle derived tholeiite and silicic melts of hydrothermally altered rocks.

The results of the present study at Austurhorn help constrain this model of crustal assimilation. If the depleted oxygen isotopic ratios of quartz-normative basalts (table 5.1) are due to assimilation of low- ^{18}O crustal melts (e.g., Hemond et al., 1988) it is possible to calculate the relative volumes of "mantle" and "crustal" materials involved. As an example, a quartz tholeiite with $\delta^{18}\text{O} = +3.1$ per mil would require addition of 17% silicic melt with $\delta^{18}\text{O} = -10$ per mil to transitional or olivine tholeiite with $\delta^{18}\text{O} = +5.6$ per mil. This assimilant volume is a minimum because of the assumed extreme depletion (Muehlenbachs et al., 1974). A quantitative evaluation of bulk mixing between mafic and felsic compositions (table 5.2) indicates that this process cannot reproduce the geochemical trends observed at Austurhorn.

The "parent" and "daughter" basalts used in this calculation are the same as those selected for modeling fractional crystallization in chapter 4 (samples p-61a, p-41b). The

Table 5.2 Bulk Assimilation Calculation

Element	Basalt p-61a	Granophyre g-64	Result*	Basalt p-41b
SiO ₂	48.00	75.12	52.62	53.46
TiO ₂	2.32	.21	1.96	2.83
Al ₂ O ₃	6.76	12.96	16.11	13.78
Fe ₂ O ₃	12.04	6.76	16.11	13.76
MgO	6.61	.14	5.51	3.57
CaO	10.78	.25	8.99	6.82
Na ₂ O	2.72	4.12	2.96	3.84
K ₂ O	.68	4.46	1.32	1.55
P ₂ O ₅	.29	.02	.24	.77
Rb	11.4	100	26.5	26.4
Sr	419	311	353	354
Ba	150	375	188	385
V	242	7	202	145
Co	46.5	1	38.8	26.3
Y	26.9	101	34.5	64.2
Zr	180	401	216	495
Hf	43	14.4	6.0	11.5
Ta	1.01	5.57	1.79	2.37
Th	.9	10.4	2.52	2.5
La	14.72	71.4	24.36	36.11
Sm	5.73	16.75	7.60	13.41
Yb	2.15	9.68	3.43	5.38

* Result = 83% Basalt (p-61a) + 17% Granophyre (g-64)

felsic endmember (sample g-64) was selected because it provides a good fit to targeted abundances of SiO_2 , Rb, Sr and Th (table 5.2). While these particular elements are crucial to bulk contamination models for the origin of quartz tholeiites, I stress that no other elements are fit successfully. Specifically, bulk endmember mixing (in the proportions 83% basalt + 17% rhyolite) can not reproduce the high concentrations of TiO_2 , Fe_2O_3 , P_2O_5 and Zr observed in the quartz-normative basalt. The model also underestimates abundances of the incompatible elements Y, Ta and REE; combined assimilation-fractional crystallization models that could reproduce these observed data would overestimate abundances of Rb, Sr and Th in the evolved basalt.

In summary I conclude that not all quartz-normative basalts are highly contaminated by silicic melts (and that all silicic magmas are not crustally derived, as discussed in chapter 4). I infer that the assimilation process leading to Th, U, K and Rb enrichment in evolved basalts probably involves selective incorporation of incompatible elements rather than wholesale mixing. As an example, the alkali-rich basalts at Austurhorn do not have anomalous abundances of Ba, Ta or other incompatible elements which would be incorporated by bulk mixing. Longer crustal residence times required to produce evolved liquids in flank zones permit depletion in ^{18}O via assimilation or direct exchange of oxygen with surrounding country rocks and circulating fluids. I concur with Hattori & Muehlenbachs (1982) that oxygen exchange between magma and wall rocks during storage and fractionation can produce the observed range of oxygen isotopic ratios of Icelandic basalts, and that this process may operate independent of other contamination phenomena. Finally, I emphasize that each magmatic system is unique, and that the relative contributions of assimilation, mixing and fractional crystallization may vary widely even within a single volcanic center (e.g., chapter 4).

5.3 Speculations: Crustal Controls on Basalt Geochemistry

5.3.1 Major Element Evidence

The presence of a subcrustal ponded melt volume which is not in direct or continuous contact with upwelling asthenosphere (figure 5.4) virtually ensures that no primary mantle melts are tapped by eruption of flank zone volcanoes. In Vestmannaeyjar the limited degree and depth of mantle melting dictates a narrow range of ponded compositions. Behind the rift tip less restrictive melting conditions should provide a greater diversity of parental liquids. However, the most mafic liquid observed at Austurhorn contains 7.8 wt% MgO. Similar MgO contents are characteristic of the Tertiary sequence in eastern Iceland (Carmichael, 1964; Wood, 1978; Gibson et al., 1982) and are comparable to inferred parental liquids from transitional tholeiitic central volcanoes in the EVZ (Jakobsson, 1979; Meyer et al., 1985) and at Askja (Sigurdsson & Sparks, 1981). At Krafla, evolved basalts occur within the caldera area, while magmas with up to 7.8 wt% MgO are found along fissures several kilometers away (Saemundsson, 1988).

In contrast, primitive Reykjanes tholeiites typically contain 8-10 wt% MgO (Jakobsson et al., 1978) and are similar to common parental MORBS (e.g., Grove & Bryan, 1983, 1986). The absence of lavas with >7.8 wt% MgO in Icelandic central volcanoes suggests that more primitive liquids cannot be tapped during rifting episodes. Sparks et al (1980) and Stolper & Walker (1980) noted that MORB liquids fractionate through a density minimum at Mg# 60-65 (MgO <9 wt%), and suggested that this composition is therefore preferentially sampled by eruption. Similarly, I propose that the thickened Icelandic lithosphere serves as a density filter in the transitional tholeiitic systems. The subcrustal ponded melt zone is likely to be a region of substantial residence time, located at a depth where lithostatic pressure is approximately equal to buoyancy of the 7.8 wt% MgO basalts (Ryan, 1987). The assumption of neutral buoyancy does not require a density minimum for the erupted liquids, but indicates a local balance between magma release (i.e., depth of rifting) and magma storage (i.e., fractionation). This physical scenario could explain why the 7.8 wt% MgO parental

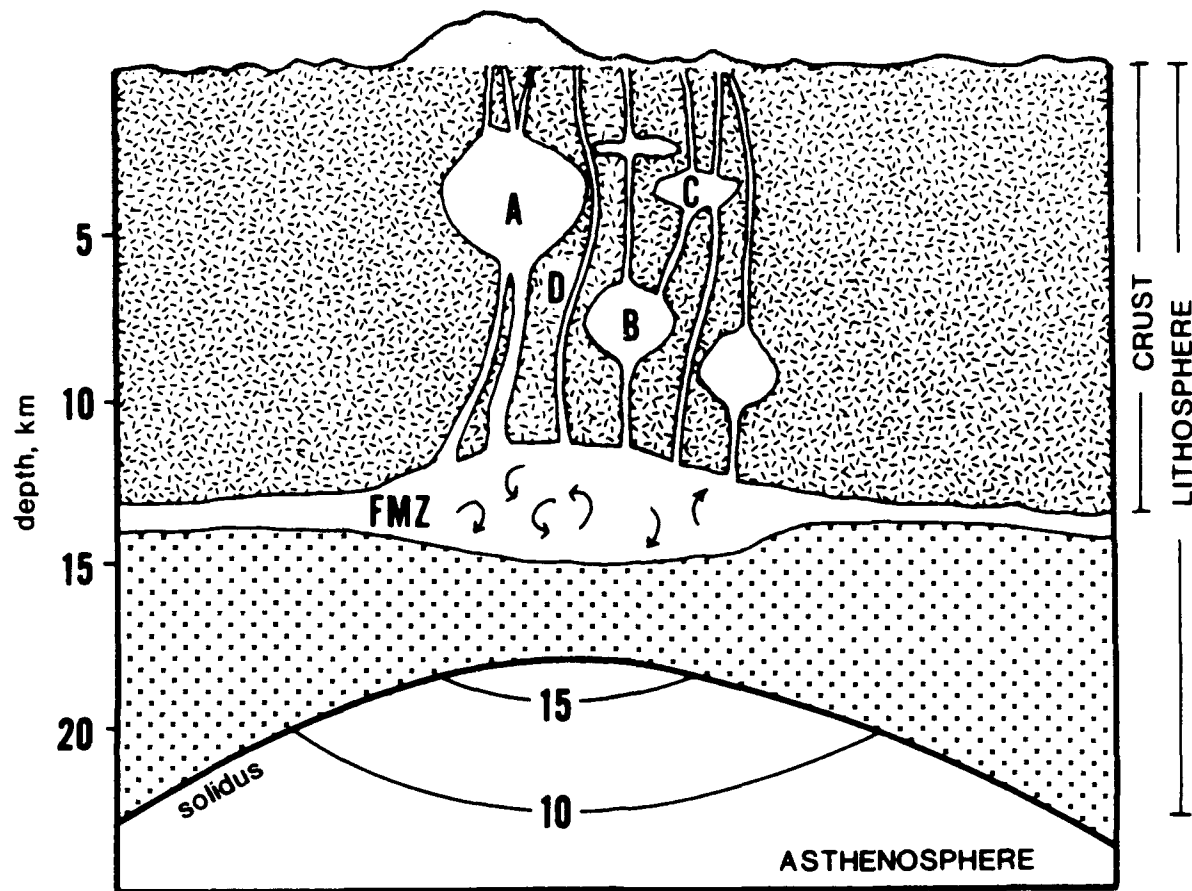


Figure 5.4 Schematic crustal cross-section drawn through an immature rift axis (a.k.a. flank zone). Upwelling asthenosphere undergoes partial melting (approximate melt percentages indicated by contours) beneath the thick lithosphere; these melts crystallize olivine (+/- plagioclase, clinopyroxene) during ascent to the base of the crust and do not retain their primary major element signatures. A continuous (?) ponded subcrustal melt region is represented here as a zone of fractionation and mixing (FMZ), in which mantle-derived liquids undergo further evolution before fracture-assisted emplacement into the shallow crust. I hypothesize that the average liquid contained in the FMZ has ~7.8 wt% MgO (see text). Individual magma bodies located within the crust (A, B, C) allow liquids to mix and differentiate further before eruption or solidification as dikes and sills. Sampling of magmas directly from the FMZ (conduit D) is rare in mature central volcanoes.

liquid composition is sampled either during the early stages of magmatism (e.g., the Hvasshjalli sill at Austurhorn) or outside main sub-chamber conduits (e.g., at Krafla), where it does not undergo further differentiation in shallow magma bodies.

5.3.2 Trace Element Effects

Major and trace element characteristics of Austurhorn basalts with <6 wt% MgO indicate a high degree of intra-system heterogeneity not apparent from the work of Carmichael (1964) or Meyer et al (1985). Several observations are important in this regard (see chapter 4): (1) Aphyric mafic dike compositions projected within the olivine-plagioclase-clinopyroxene-quartz pseudoquaternary define a surface of multiple saturation, but not a true liquid line of descent. That is, relative position along the "pillow cotectic" does not correlate absolutely with MgO content. (2) Dikes with comparable major element characteristics have variable trace element contents. (3) Certain Austurhorn basalts have elevated monovalent alkali contents, apparently resulting from contamination by silicic material at an early stage. These observations can be explained by invoking variable melting and crystallization histories for individual melts, and can be reconciled with a magmatic plumbing system in which several isolated crustal chambers feed a single volcanic center (e.g., Walker, 1963; Christie & Sinton, 1986; figure 5.4). As Meyer et al (1985) point out, low magma supply rates within the immature rift environment lead to infrequently replenished magma chambers. This phenomenon is not observed at the rift tip in Vestmannaeyjar, where magmas are erupted directly from the ponded melt zone. I suggest that differentiation of transitional tholeiitic liquids within isolated shallow magma bodies produced the major and trace element inhomogeneities of Austurhorn liquids, and that the more regional approach of Meyer et al (1985) masked the variations exhibited by individual volcanic centers of the EVZ.

5.4 Silicic Magmatism

In chapter 4 I demonstrated that fractional crystallization is a viable mechanism for producing silicic magmas in flank zone volcanoes. I further suggest that in short-lived (probably <1.5 My) Icelandic transitional tholeiitic systems, silicic liquids are generated by differentiation as the rule, not the exception. The most important factor in this interpretation is that measured thermal gradients for flank zones (Palmason, 1971; Palmason et al., 1979) indicate a low rate of basalt supply relative to that inferred for axial rift segments.

The relatively low abundance of basalt in immature rift zones influences production of silicic magmas. Infrequently replenished crustal magma bodies rapidly become thermally isolated and differentiate to evolved compositions due to the large thermal contrast with surrounding wall rocks ($T_{\text{magma}} \sim 1050^{\circ}\text{C}$, $T_{\text{wall}} < 200^{\circ}\text{C}$). These isolated magma pockets may melt the surrounding country rocks, but are unlikely to be extensively contaminated because the diffusivity of heat ($10^{-2} \text{ cm}^2/\text{sec}$) is far greater than that of chemical species in silicate melts (10^{-8} to $10^{-11} \text{ cm}^2/\text{sec}$). That is, the initial magmas will be extensively cooled and crystallized before they can erupt as contaminated liquids. As Grove et al (1988) demonstrate, only subsequent basalt pulses are likely to entrain crustal melts as contaminants. Similarly, only extensive basalt dikeing can cause sufficient local melting to generate eruptable silicic liquids. At Austurhorn, only a small number of dikes are demonstrably contaminated by interaction with crustal melts. This observation suggests that individual conduits were not developed or maintained sufficiently to effect extensive melting at crustal levels below that of the shallow magma chamber now observed.

As magma supply rates increase, or if rifting is sustained, well-developed chambers or conduits will focus heat and magma in selected areas. This physical scenario can lead to melting along conduit walls and chamber surfaces. Gunnarsson (1988) concluded that silicic lavas in the Torfajökull area, where magmatism has

persisted for ~2.5 Ma, contain a substantial component of crustally derived melt. In this sense the Torfajökull complex differs from Austurhorn and other Tertiary central volcanoes, most of which developed along rift segments that were active for less than 2 My (Helgason, 1984).

A final, and more speculative, control on the development of evolved magmas is the normal differentiation sequence of the parental liquid. Icelandic volcanoes with abundant silicic material are always populated by transitional tholeiitic basalts (Jakobsson, 1979); this composition is characteristic of flank zone segments such as the EVZ and the Skagi region in north-central Iceland (Sigurdsson et al., 1978). These basalts are not primary mantle melts, but their slight alkaline affinity suggests they, like Vestmannaeyjar alkali basalts, derive from fairly low degrees of melting beneath the thick Icelandic lithosphere. Mildly alkaline mafic liquids are likely parents for rhyolite, because they do not undergo the peritectic reaction olivine + liquid \rightarrow pigeonite + augite + plagioclase (Morse, 1980). This behavior is unlike that observed in tholeiitic systems, where peritectic reaction may consume significant volumes of liquid without producing silicic differentiates (Grove & Baker, 1984; Juster & Grove, 1988). Silica enrichment is further enhanced by the extensive removal of FeTi oxides during differentiation. Certainly the common occurrence of both ilmenite-rich gabbros (Danielsson et al., 1978) and silicic volcanics lends support to this hypothesis.

In summary, the present analysis supports differentiation over crustal melting as the source of rhyolite in central volcanoes located along immature or short-lived rift segments. This conclusion is consistent with the magmato-tectonic scenario proposed by Meyer et al (1985), suggesting that their model is appropriate to understanding evolution of both modern and Tertiary Icelandic volcanic systems.

5.5 Nota Bene

The evolution of silicic magmas in central volcanoes is presently best addressed by oxygen isotopic measurements on cogenetic mafic and felsic units. Analyses of 18 Austurhorn bulk rock samples (mafic pillows, mafic and felsic dikes, gabbro and granophyre) indicate the influence of meteoric water in all units, with measured delta ^{18}O between -3.7 and +3.7 per mil (W. Cornell, unpublished data). Handpicked aliquots of plagioclase, quartz, clinopyroxene and FeTi oxides from selected gabbro and granophyre samples are currently awaiting analysis and may yield illuminating results. The combination of field, geochemical, mineralogic and isotopic data from this single magmatic center makes it particularly valuable in evaluating petrogenetic models of extensional volcanism.

References

- Albee, A.L. & L. Ray, 1970, Correction factors for electron probe microanalysis of silicates, oxides, carbonates, phosphates, and sulphates, *Analyt. Chem.* 42, 1408-1414.
- Andersen, D.J. & D.H. Lindsley, 1988, Internally consistent solution models for Fe-Mg-Mn-Ti oxides: Part 1. Fe-Ti oxides, *Am. Mineral.*, in press.
- Anderson, A.T., Jr., R.N. Clayton & T.K. Mayeda, 1971, Oxygen isotope thermometry of mafic igneous rocks, *J. Geol.*, 79, 715-729.
- Anderson, A.T., Jr., G.H. Swihart, G. Artoli & C.A. Geiger, 1984, Segregation vesicles, gas filterpressing and igneous differentiation, *J. Geol.*, 92, 55-72.
- Arnason, B., 1976, Groundwater system in Iceland, traced by deuterium, *Soc. Scient. Islandica*, 236 pp.
- Arney, B.H., 1978, Geochemistry of Eyjafjoll, a volcano in southern Iceland, MS thesis, Mass. Inst. of Technol., Cambridge, MA.
- Aronsson, J.R. & K. Saemundsson, 1975, Relatively old basalts from structurally high areas in central Iceland, *Earth Planet. Sci. Lett.*, 28, 83-97.
- Bacon, C.R., 1986, Inclusions of mafic magma in intermediate volcanic rocks, *J. Geophys. Res.*, 91, 6091-6112.
- Bacon, C.R. & M.M. Hirschmann, 1988, Mg/Mn partitioning as a test for equilibrium between coexisting Fe-Ti oxides, *Am. Mineral.*, 73, 57-61.
- Bailey, D.K. & R. Macdonald, 1987, Dry peralkaline felsic liquids and carbon dioxide flux through the Kenya rift zone, in Mysen, B. (ed), *Magmatic Processes: Physicochemical Principles*, 91-106.
- Basaltic Volcanism Study Project, 1981, *Basaltic Volcanism on the Terrestrial Planets*, New York: Pergamon, 1286 pp.
- Beblo, M. & A. Bjornsson, 1978, Magnetotelluric investigation of the lower crust and upper mantle beneath Iceland, *J. Geophys. Res.*, 45, 1-16.
- Beblo, M. & A. Bjornsson, 1980, A model of electrical resistivity beneath NE-Iceland, correlation with temperature, *J. Geophys.*, 47, 184-190.
- Bence, A.E. & A.L. Albee, 1967, Empirical correction factors for the electron microanalysis of silicates and oxides, *J. Geol.*, 76, 382-403.
- Bender, J.F., F.N. Hodges & A.E. Bence, 1978, Petrogenesis of basalts from the project FAMOUS area: experimental study from 0 to 15 kbars, *Earth Planet. Sci. Lett.*, 41, 277-302.
- Bjornsson, H. & H. Kristmannsdottir, 1984, The Grimsvotn geothermal area, Vatnajokull, Iceland, *Jokull*, 34, 25-50.

- Blake, D.H., 1964, The volcanic geology of the Austurhorn area, south-eastern Iceland, PhD thesis, Univ. of London.
- Blake, D.H., 1966, The net-veined complex of the Austurhorn intrusion, south-eastern Iceland, *J. Geol.*, 74, 891-907.
- Blake, D.H., 1970, Geology of the Alftafjordur volcano, a Tertiary volcanic centre in south-eastern Iceland, *Sci. Islandica*, 2, 43-63.
- Blake, D.H., R.W.D. Elwell, I.L. Gibson, R.R. Skelhorn & G.P.L. Walker, 1965, Some relationships resulting from intimate association of acid and basic magmas, *Quart. J. Geol. Soc. London*, 121, 31-49.
- Blake, S., 1984a, Volatile oversaturation during the evolution of silicic magma chambers as an eruption trigger, *J. Geophys. Res.*, 89, 8237-8244.
- Blake, S., 1984b, Magma mixing and hybridization at the alkaline, silicic, Torfajokull central volcano triggered by tholeiitic Veidivotn fissuring, south Iceland, *J. Volcan. Geotherm. Res.*, 22, 1-31.
- Bottinga, Y. & D.F. Weill, 1970, Densities of liquid silicate systems calculated from partial molar volumes of oxide components, *Am. Jour. Sci.*, 269, 169-182.
- Bunsen, R., 1851, Ueber die Prozesse der vulkanischen Gesteinsbildungen Islands, *Annalen der Physik*, 83, 197-272.
- Byerley, G.R., W.G. Melson & P.R. Vogt., 1976, Rhyodacites, andesites, ferrobasalts and ocean tholeiites from the Galapagos Spreading Center, *Earth Planet. Sci. Lett.*, 30, 215-221.
- Campbell, I.H., 1978, Some problems with the cumulus theory, *Lithos*, 11, 311-323.
- Campbell, I.H., A.J. Naldrett & S.J. Barnes, 1983, A model for the origin of the platinum-rich sulfide horizons in the Bushveld and Stillwater complexes, *J. Petrol.*, 24, 133-165.
- Carmichael, I.S.E., 1963, The crystallisation of feldspar in volcanic acid liquids, *Quart. J. Geol. Soc. London*, 119, 95-131.
- Carmichael, I.S.E., 1964, The petrology of Thingmuli, a Tertiary volcano in eastern Iceland, *J. Petrol.*, 5, 434-460.
- Carmichael, I.S.E., 1967, The mineralogy of Thingmuli, a Tertiary volcano in eastern Iceland, *Am. Mineral.*, 52, 1815-1841.
- Carmichael, I.S.E., F.J. Turner & J. Verhoogen, 1974, *Igneous Petrology*. New York: McGraw Hill, 739 pp.
- Carmody, R.W., & B.D. Marsh, 1988, Slafrudalur intrusion of SE Iceland: a layered, epizonal silicic magma chamber, *EOS*, 69, 526
- Cargill, H.K., L. Hawkes & J.A. Ledeboer, 1928, The major intrusions of south-eastern Iceland, *Quart. J. Geol. Soc. London*, 84, 505-539.

- Chen, C.-Y. & F.A. Frey, 1985, Trace element and isotopic geochemistry of lavas from Haleakala Volcano, East Maui, Hawaii: Implications for the origin of Hawaiian basalts, *J. Geophys. Res.*, 90, 8743-8768.
- Christie, D.M. & J.M. Sinton, 1981, Evolution of abyssal lavas along propagating segments of the Galapagos spreading center, *Earth Planet. Sci. Lett.*, 56, 321-335.
- Christie, D.M. & J.M. Sinton, 1986, Major element constraints on melting, differentiation and mixing of magmas from the Galapagos 95.5 W propagating rift system, *Contrib. Mineral. Petrol.*, 94, 274-288.
- Clague, D.A. & F.A. Frey, 1982, Petrology and trace element geochemistry of the Honolulu volcanics, Oahu: Implications for the oceanic mantle below Hawaii, *J. Petrol.*, 23, 447-504.
- Condomines, M., K. Gronvold, P.J. Hooker, K. Muehlenbachs, R.K. O'Nions, N. Oskarsson & E.R. Oxburgh, 1983, Helium, oxygen, strontium and neodymium isotopic relationships in Icelandic volcanics, *Earth Planet. Sci. Lett.*, 66, 125-136.
- Cotman, R.M., 1979, Potassium-argon evidence for shifting of the axial rift zone in northern Iceland, MS thesis, Case Western Reserve University, Cleveland, OH.
- Cox, A., 1969, Geomagnetic reversals, *Science*, 163, 237-245.
- Crecraft, H.R., W.P. Nash & S.H. Evans, Jr., 1981, Late Cenozoic volcanism at Twin Peaks, Utah: Geology and petrology, *J. Geophys. Res.*, 86, 10303-10320.
- Danielsson, F., G. Einarsson, A. Hjartarson & F. Sigurdsson, 1978, *Islenskt ilmenit: konnunaraskýrsla 1. Heimildakönnun, Orkustofnun (Jardkonnunadeild) report OS JKD 7802.*
- Dixon, S. & M.J. Rutherford, 1979, Plagiogranites as late-stage immiscible liquids in ophiolite and mid-ocean ridge suites: an experimental study, *Earth Planet. Sci. Lett.*, 45, 45-60.
- Dostal, J., C. Dupuy, J.P. Carron, M. le Guen de Kerneizon & R.C. Maury, 1983, Partition coefficients of trace elements: application to volcanic rocks of St. Vincent, West Indies, *Geochim. Cosmochim. Acta*, 47, 525-533.
- Drake, M.J. & D.F. Weill, 1975, Partition of Sr, Ba, Ca, Y, Eu²⁺, Eu³⁺, and other REE between plagioclase feldspar and magmatic liquid: an experimental study, *Geochim. Cosmochim. Acta*, 39, 689-712.
- Einarsson, P., 1978, S-wave shadows in the Krafla caldera in NE-Iceland: evidence for a magma chamber in the crust, *Bull. Volcan.*, 41, 1-9.
- Einarsson, P., 1986, Seismicity along the eastern margin of the North American plate, in Vogt, P.R. & B.E. Tucholke (eds), *The Geology of North America, Volume M, The Western North Atlantic Region*. Geol. Soc. America, 99-116.

- Einarsson, P., 1988, The South Iceland Seismic Zone: Structure and faulting near a sideways migrating transform, in, Symposium on Geologic and Geochemical Evidence for Segmentation for Continental and Oceanic Rifts, conference held at WHOI, January, 1988.
- Elderfield, H. & M.J. Greaves, 1981, Strontium isotope geochemistry of Icelandic geothermal systems and implications for sea water chemistry, *Geochim. Cosmochim. Acta*, 45, 2201-2212.
- Etheridge, M.A., V.J. Wall & R.H. Vernon, 1984, High fluid pressures during regional metamorphism and deformation: implications for mass transport and deformation mechanisms, *J. Geophys. Res.*, 89, 4344-4358.
- Ewart, A., W.B. Bryan & J.B. Gill, 1973, Mineralogy and geochemistry of the younger volcanic islands of Tonga, S.W. Pacific, *J. Petrol.*, 14, 429-465.
- Eysteinnsson, H. & J.F. Hermance, 1985, Magnetotelluric measurements across the eastern neovolcanic zone in south Iceland, *J. Geophys. Res.*, 90, 10093-10103.
- Feigenson, M.S., A.W. Hofmann & F.J. Spera, 1983, Case studies on the origin of basalt, II, The transition from tholeiitic to alkalic volcanism on Kohala volcano, Hawaii, *Contrib. Mineral. Petrol.*, 84, 390-405.
- Fisk, M.R., J-G. Schilling & H. Sigurdsson, 1980, An experimental investigation of Iceland and Reykjanes ridge tholeiites: I. Phase relations, *Contrib. Mineral. Petrol.*, 74, 361-374.
- Flower, M.F.J., R.G. Pritchard, G. Brem, J.R. Cann, J. Delaney, R. Emmerman, I.L. Gibson, P.J. Oakley, P.T. Robinson & H-U. Schmincke, 1982, Chemical stratigraphy, Iceland Research Drilling Project, Reydarfjordur, eastern Iceland, *J. Geophys. Res.*, 87, 6489-6510.
- Frey, F.A. D.H. Green & S.D. Roy, 1979, Integrated models of basalt petrogenesis: a study of olivine melilitites to quartz tholeiites from southeastern Australia utilizing geochemical and experimental petrological data, *J. Petrol.*, 19, 463-513.
- Frey, F.A. & M.F. Roden, 1987, The mantle source for the Hawaiian Islands: constraints from the lavas and ultramafic inclusions, in *Mantle Metasomatism*. London: Academic Press, 423-463.
- Fridleifsson, G.O., 1983, Mineralogical evolution of a hydrothermal system, *Trans. Geotherm. Res. Council*, 7, 147-152.
- Fujii, T. & H. Bougault, 1983, Melting relations of a magnesian abyssal tholeiite and the origin of MORBs, *Earth Planet. Sci. Lett.*, 62, 283-295.
- Fujii, T. & C.M. Scarfe, 1985, Composition of liquids coexisting with spinel ilherzolite at 10 kbar and the genesis of MORBs, *Contrib. Mineral. Petrol.*, 90, 18-28.
- Fujimaki, H., M. Tatsumoto & K. Aoki, 1984, Partition coefficients of Hf, Zr and REE between phenocrysts and groundmass, *J. Geophys. Res.*, 89, B662-B672.

- Furman, T., F.A. Frey & S.P. Jakobsson, 1988, Petrogenesis of mildly alkaline lavas from Vestmannaeyjar, Iceland: the Eldfell (1973) and Surtsey (1963-1967) eruptions, in preparation.
- Gale, N.H., S. Moorbath, J. Simons & G.P.L. Walker, 1966, K-Ar ages of acid intrusive rocks from Iceland, *Earth Planet. Sci. Lett.*, 1, 284-288.
- Gebrande, H., H. Miller & P. Einarsson, 1980, Seismic structure of Iceland along RRISP profile I, *J. Geophys.*, 47, 239-249.
- Gibson, I.L., R.J. Kirkpatrick, R. Emmerman, H-U. Schmincke, G. Pritchard, P.J. Oakley, R.S. Thorpe & G.F. Marriner, 1982, The trace element composition of the lavas and dikes from a 3-km vertical section through the lava pile of eastern Iceland, *J. Geophys. Res.*, 87, 6532-6546.
- Gibson, I.L. & J.D.A. Piper, 1973, Structure of the Iceland basalt plateau and the process of drift, *Philos. Trans. R. Soc. London*, A271, 141-150.
- Green, T.H. & N.J. Pearson, 1985, Rare earth element partitioning between clinopyroxene and silicate liquid at moderate to high pressure, *Contrib. Mineral. Petrol.*, 91, 24-36.
- Green, D.H., W.O. Hibberson & A.L. Jacques, 1979, Petrogenesis of mid-ocean ridge basalts, in McElhinney, M.W. (ed), *The earth: its origin, structure and evolution*. London: Academic Press, 265-290.
- Green, T.H. & N.J. Pearson, 1985, Experimental determination of REE partition coefficients between amphibole and basaltic to andesitic liquids at high pressure, *Geochim. Cosmochim. Acta*, 49, 1465-1468.
- Green, T.H. & N.J. Pearson, 1987, An experimental study of Nb and Ta partitioning between Ti-rich minerals and silicate liquids at high pressure and temperature, *Geochim. Cosmochim. Acta.*, 51, 55-62.
- Green, T.H. & A.E. Ringwood, 1968, Genesis of the calc-alkaline igneous rock suite, *Contrib. Mineral. Petrol.*, 18, 105-162.
- Green, T.H. & E.B. Watson, 1982, Crystallization of apatite in natural magmas under high pressure, hydrous conditions, with particular reference to 'orogenic' rock series, *Contrib. Mineral. Petrol.*, 79, 96-105.
- Grove, T.L. & M.B. Baker, 1984, Phase equilibrium controls on the tholeiitic versus calc-alkaline differentiation trends, *J. Geophys. Res.*, 89, 3253-3274.
- Grove, T.L. & W.B. Bryan, 1983, Fractionation of pyroxene-phyric MORB at low pressure: an experimental study, *Contrib. Mineral. Petrol.*, 84, 293-309.
- Grove, T.L. & W.B. Bryan, 1986, End members of magma mixing in sites 395 and 396 basalts: constraints from phase equilibrium experiments on "normal" MORB, *EOS*, 67, 1213.
- Grove, T.L. & J.M. Donnelly-Nolan, 1986, The evolution of young silicic lavas at Medicine Lake Volcano, California: Implications for the origin of compositional gaps in calc-alkaline series lavas, *Contrib. Mineral. Petrol.*, 92, 281-302.

- Grove, T.L., D.C. Gerlach & T.W. Sando, 1982, Origin of calc-alkaline series lavas at Medicine Lake volcano by fractionation, assimilation and mixing, *Contrib. Mineral. Petrol.*, 80, 160-182.
- Grove, T.L., R.J. Kinzler, M.B. Baker, J.M. Donnelly-Nolan & C.E. Leshner, 1988, Assimilation of granite by basaltic magma at Burnt Lava flow, Medicine Lake volcano, northern California: Decoupling of heat and mass transfer, *Contrib. Mineral. Petrol.*, 99, 320-343.
- Gudmundsson, A., 1986, Formation of crustal magma chambers in Iceland, *Geology*, 14, 164-166.
- Gunnarsson, B., 1988, PhD thesis
- Gunnarsson, B. & B.D. Marsh, 1988, Generation of Icelandic rhyolites: II. An evolutionary model of central volcano on oceanic crust, *EOS*, 69, 732.
- Gunnarsson, B. & F. Sigurdsson, 1982, Titanrikar steindir i gabbroir ur Hvalnesfjalli i Loni of Medalfelli i Nesjum, Orkustofnun Report OS82094/VOD15.
- Gunnarsson, B., H.P. Tylor & B. Marsh, 1988, Origin of oxygen isotope anomalies in Icelandic lavas: Part I. Flank zone volcanoes, *Geol. Soc. Am. Abst. Programs*, A158-A159.
- Gust, D.A. & M.R. Perfit, 1987, Phase relations of a high-Mg basalt from the Aleutian Island Arc: Implications for primary arc basalts and high-Al basalts, *Contrib. Mineral. Petrol.*, 97, 7- 18.
- Hanan, B.B. & J-G. Schilling, 1986, The source origin of Iceland basalt volcanism: Pb isotopes in the eastern Iceland Tertiary section, *EOS*, 67, 409.
- Hanan, B.B. & J-G. Schilling, 1987, Pb isotope evolution of the Iceland plume, *EOS*, 68, 437.
- Hanson, G.N. & C.H. Langmuir, 1978, Modelling of major elements in mantle-melt systems using trace element approaches, *Geochim. Cosmochim. Acta*, 42, 725-741.
- Hardardottir, V., 1983, The petrology of the Hengill volcanic system, southern Iceland, MS thesis, McGill University, Montreal.
- Harrison, T.M. & E.B. Watson, 1983, Kinetics of zircon dissolution and zirconium diffusion in granitic melts of variable water content, *Contrib. Mineral. Petrol.*, 84, 66-72.
- Harrison, T.M. & E.B. Watson, 1984, The behavior of apatite during crustal anatexis: Equilibrium and kinetic considerations, *Geochim. Cosmochim. Acta*, 48, 1467-1477.
- Hart, S.R. & K.E. Davis, 1978, Nickel partitioning between olivine and silicate melt, *Earth Planet. Sci. Lett.*, 40, 203-219.

- Hart, S.R., J-G. Schilling & J.L. Powell, 1973, Basalts from Iceland and along the Reykjanes Ridge: Sr isotope geochemistry, *Nature Phys. Sci.*, 246, 104-107.
- Hattori, K. & K. Muehlenbachs, 1982, Oxygen isotope ratios of the Icelandic crust, *J. Geophys. Res.*, 87, 6559-6565.
- Helgason, J., 1983, Structural relationships and magnetostratigraphy of the volcanic succession and the Breiddalur dyke swarm in Reydarfjordur, eastern Iceland, PhD thesis, Dalhousie Univ.
- Helgason, J., 1985, Frequent shifts of the volcanic zone in Iceland, *Geology*, 12, 212-216.
- Helz, R.T., 1973, Phase relations of basalts in their melting range at $P_{H_2O} = 5$ kbar as a function of oxygen fugacity. Part I. Mafic phases, *J. Petrol.*, 14, 249-302.
- Helz, R.T., 1978, Phase relations of basalts in their melting ranges at $P_{H_2O} = 5$ kb. Part II. Melt compositions, *J. Petrol.*, 17, 139-193.
- Helz, R.T., 1987, Differentiation behavior of Kilauea Iki lava lake, Kilauea Volcano, Hawaii: An overview of past and current work, in Mysen, B. (ed), *Magmatic Processes: Physicochemical Principles*, 241-258.
- Hemond, Ch., M. Condomines, S. Fourcade, C.J. Allegre, N. Oskarsson & M. Javoy, 1988, Thorium, strontium and oxygen isotopic geochemistry in recent tholeiites from Iceland: crustal influence on mantle-derived magmas, *Earth Planet. Sci. Lett.*, 87, 273-285.
- Hermance, J.F., 1981, Crustal genesis in Iceland: geophysical constraints on crustal thickening with age, *Geophys. Res. Letts.*, 8, 203-206.
- Hervig, R.L., & J.V. Smith, 1982, Temperature-dependent distribution of Cr between olivine and pyroxenes in lherzolite xenoliths, *Contrib. Mineral. Petrol.*, 81, 184-189.
- Hildreth, W., 1983, Gradients in silicic magma chambers: implications for lithospheric magmatism, *J. Geophys. Res.*, 86, 10153-10192.
- Ho, R.A. & M.O. Garcia, 1988, Origin of differentiated lavas at Kilauea Volcano, Hawaii: implications from the 1955 eruption, *Bull. Volcan.*, 50, 35-46.
- Hofmann, A.W. & W.M. White, 1982, Ba, Rb and Cs in the earth's mantle, *Z. Naturforsch.*, 381, 256-266.
- Holloway, J.R. & C.W. Burnham, 1972, Melting relations of basalt with equilibrium water pressure less than total pressure, *J. Petrol.*, 13, 1-30.
- Houghton, B.F., J.H. Latter & W.R. Hackett, 1987, Volcanic hazard assessment for Ruapehu composite volcano, Taupo volcanic zone, New Zealand, *Bull. Volcan.*, 49, 737-751.
- Huppert, H. & R.S.J. Sparks, 1980, The fluid dynamics of a basaltic magma chamber replenished by influx of hot, dense ultrabasic magma, *Contrib. Mineral. Petrol.*, 75, 279-289.

- Huppert, H.E., J.S. Turner & R.S.J. Sparks, 1982, Replenished magma chambers: effects of compositional zonation and input rates, *Earth Planet. Sci. Lett.*, 57, 345-357.
- Huppert, H.E., R.S.J. Sparks, J.R. Wilson & M.A. Hallworth, 1986, Cooling and crystallization along an inclined plane, *Earth Planet. Sci. Lett.*, 79, 319-328.
- Imsland, P., 1984, Petrology, mineralogy and evolution of the Jan Mayen magma system, Visindafelag Islendinga, Reykjavik.
- Irvine, T.N., 1974, Petrology of the Duke Island Ultramafic Complex, southeastern Alaska, *Geol. Soc. Am. Mem.* 138.
- Ito, E., W.M. White & C. Gopel, 1987, The O, Sr, Nd and Pb isotope geochemistry of MORB, *Chem. Geol.*, 62, 157-176.
- Ivarsson, G., K. Saemundsson & S. Arnorsson, 1988, The Torfajokull silicic central volcano, south Iceland: stratigraphy, structural geology and rock chemistry, Jokull, submitted.
- Jakobsson, S.P., 1972, Chemistry and distribution pattern of recent basaltic rocks in Iceland, *Lithos*, 5, 365-386.
- Jakobsson, S.P., 1979, Petrology of recent basalts of the eastern volcanic zone, Iceland, *Acta. Nat. Islandica*, 26, 103 pp.
- Jakobsson, S.P., 1982, *Dredge hauls from Vestmannaeyjargrunn*, Iceland, Surtsey Research Progress Report IX, 142-148.
- Jakobsson, S.P., A.K. Pedersen, J.G. Ronsbo & L.M. Larsen, 1973, Petrology of mugearite-hawaiite: Early extrusives in the 1973 Heimaey eruption, Iceland, *Lithos*, 6, 203-214.
- Jakobsson, S.P., J. Jonsson & F. Shido, 1978, Petrology of the western Reykjanes Peninsula, Iceland, *J. Petrol.*, 19, 669-705.
- Jancin, M., K.D. Young, B. Voight, J.L. Aronson & K. Saemundsson, 1985, Stratigraphy and K/Ar ages across the west flank of the northeast Iceland axial rift zone, in relation to the 7 Ma volcano-tectonic reorganization of Iceland, *J. Geophys. Res.*, 90, 9961-9985.
- Jacques, A.L. & D.H. Green, 1980, Anhydrous melting of peridotite at 0-15 kb pressure and the genesis of tholeiitic basalts, *Contrib. Mineral. Petrol.*, 73, 287-310.
- Johannesson, H., 1975, Structure and petrochemistry of the Reykjadalur central volcano and the surrounding areas, Midwest Iceland, PhD thesis, Univ. of Durham.
- Johannesson, H., 1980, *Jardlagaskipan og throun rekbelta a Vesturlandi*, *Naturufraedingurinn*, 50, 13-31.
- Johnston, A.D. & P.J. Wyllie, 1988, Interaction of granitic and basic magmas: experimental observations on contamination processes at 10 kbar with H₂O, *Contrib. Mineral. Petrol.*, 98, 352-362.

- Jorgensen, K.A., 1980, The eruption of the Thorsmork ignimbrite, south Iceland: the structure of the magma chamber deduced from the eruption products, Nordic Volc. Inst. Report 8103.
- Jurewicz, A.J.G. & E.B. Watson, 1988, Cations in olivine, part I: Calcium partitioning and calcium-magnesium distribution between olivines and coexisting melts, with petrologic applications, *Contrib. Mineral. Petrol.*, 99, 176-185.
- Juster, T.C. & T.L. Grove, 1988, Experimental constraints on the generation of FeTi basalts, andesites and rhyodacites at the Galapagos Spreading Center, 85 W and 95 W, *J. Geophys. Res.*, in press.
- Klein, E.M. & C.H. Langmuir, 1987, Global correlations of ocean ridge basalt chemistry with axial depth and crustal thickness, *J. Geophys. Res.*, 92, 8089-8115.
- Kurz, M.D., W.J. Jenkins, S.R. Hart & D. Clague, 1983, Helium isotopic variations in volcanic rocks from Loihi seamount and the island of Hawaii, *Earth Planet. Sci. Lett.*, 66, 388-406.
- Kurz, M.D., P.S. Meyer & H. Sigurdsson, 1985, Helium isotope systematics within the neovolcanic zones of Iceland, *Earth Planet. Sci. Lett.*, 74, 291-305.
- Kushiro, I., 1972, Effect of water on the composition of magmas formed at high pressure, *J. Petrol.*, 13, 311-334.
- Kushiro, I. & R.N. Thompson, 1972, Origin of some abyssal tholeiites from the Mid-Atlantic Ridge, *Carnegie Inst. Wash. Yearbook*, 71, 403-406.
- Langmuir, C.H., J.F. Bender, A.E. Bence, G.N. Hanson & S.R. Taylor, 1977, Petrogenesis of basalts from the FAMOUS area: Mid-Atlantic Ridge, *Earth Planet. Sci. Lett.*, 36, 133-156.
- Lemarchand, F., B. Villemant & G. Calas, 1987, Trace element distribution coefficients in alkaline series, *Geochim. Cosmochim. Acta.*, 51, 1071-1081.
- Lofgren, G., 1983, Effect of heterogeneous nucleation on basaltic textures: a dynamic crystallization study, *J. Petrol.*, 24, 229-255.
- Macdonald, G.A. & T. Katsura, 1964, Chemical composition of Hawaiian lavas, *J. Petrol.*, 5, 82-133.
- Macdonald, R., R.S.J. Sparks, H. Sigurdsson, D.P. Matney, D.W. McGarvie & R.L. Smith, 1987, The 1875 eruption of Askja volcano, Iceland: combined fractional crystallization and elective contamination in the generation of rhyolitic magma, *Min. Mag.*, 51, 183-202.
- Mahood, G., 1981, A summary of the geology and petrology of the Sierra La Primavera, Jalisco, Mexico, *J. Geophys. Res.*, 86, 10137-10152.
- Mahood, G.A. & D.R. Baker, 1986, Experimental constraints on depths of fractionation of mildly alkalic basalts and associated felsic rocks: Pantelleria, Strait of Sicily, *Contrib. Mineral. Petrol.*, 93, 251-264.

- Mahood, G. & W. Hildreth, 1983, Large partition coefficients for trace elements in high-silica rhyolites, *Geochim. Cosmochim. Acta*, 47, 11-30.
- Marsh, B.D., 1982, On the mechanics of igneous diapirism, stoping and zone melting, *Am. Jour. Sci.*, 282, 808-855.
- Marshall, L.A. & R.S.J. Sparks, 1984, Origin of some mixed-magma and net-veined ring intrusions, *J. Geol. Soc. London*, 141, 171-182.
- Mattson, S.R., T.A. Vogel & J.T. Wilband, 1986, Petrochemistry of the silicic-mafic complexes at Vesturhorn and Austurhorn, Iceland: evidence for zoned/stratified magma, *J. Volcan. Geotherm. Res.*, 28, 197-223.
- McBirney, A.R. & R.M. Noyes, 1979, Crystallization and layering of the Skaergaard Intrusion, *J. Petrol.*, 20, 487-554.
- McGarvie, D.W., 1984, Torfajökull: a volcano dominated by magma mixing, *Geology*, 11, 685-688.
- McKay, G., J. Wagstaff & S-R. Yang, 1986, Zirconium, hafnium and rare earth element partition coefficients for ilmenite and other minerals in high-Ti lunar mare basalts: an experimental study, *J. Geophys. Res.*, 91, D229-D237.
- McKenzie, D.P., 1984, The generation and compaction of partially molten rock, *J. Petrol.*, 25, 713-765.
- Meyer, P.S., 1978, Petrology of basaltic dikes from Vestfirðir: Iceland's Northwest Peninsula, MS thesis, Univ. of Rhode Island, Kingston, unpublished.
- Meyer, P.S., 1984, Petrology of basaltic dikes from Vestfirðir: Iceland's Northwest Peninsula, MS theses, Univ. of Rhode Island, Kingston, RI.
- Meyer, P.S., H. Sigurdsson & J-G. Schilling, 1985, Petrological and geochemical variations along Iceland's neovolcanic zones, *J. Geophys. Res.*, 90, 10043-10072.
- Meyer, P.S., H. Sigurdsson & J-G. Schilling, 1985, Petrological and geochemical variations along Iceland's neovolcanic zones, *J. Geophys. Res.*, 90, 10043-10072.
- Mittlefehldt, D.W. C.F. Miller, 1983, Geochemistry of the Sweetwater Wash pluton, California: implications for "anomalous" trace element behaviors during differentiation of felsic magmas, *Geochim. Cosmochim. Acta*, 47, 109-124.
- Moorbath, S., H. Sigurdsson & R. Goodwin, 1968, K-Ar ages of the oldest exposed rocks in Iceland, *Earth Planet. Sci. Lett.*, 4, 197-205.
- Mork, M.B.E., 1984, Magma mixing in the post-glacial Veidivotn fissure eruption, southeast Iceland: a microprobe study of mineral and glass variations, *Lithos*, 17, 55-75.
- Morse, S.A., 1969, Geology of the Kiglapait layered intrusion, Labrador, *Mem. Geol. Soc. Am.*, 112.
- Morse, S.A., 1979, Kiglapait geochemistry II: Petrography, *J. Petrol.*, 20, 591-624.

- Morse, S.A., 1980, *Basalts and Phase Diagrams*, Springer-Verlag, 493 pp.
- Mortensen, C.E. & D.G. Hopkins, 1987, Tiltmeter measurements in the Long Valley Caldera, California, in Decker, R.W. et al (eds.), *Hawaii Symposium on How Volcanoes Work*, 182.
- Muehlenbachs, K., A.T. Anderson & G. E. Sigvaldason, 1974, Low- O^{18} basalts from Iceland, *Geochim. Cosmochim. Acta.*, 38, 577-588.
- Muehlenbachs, K. & S.P. Jakobsson, 1973, The oxygen isotope composition of the 1973 Heimaey lava, *Carnegi Inst. Wash. Yearbook*, 72, 597-598.
- Nash, W.P. & H.R. Crecraft, 1985, Partition coefficients for trace elements in silicic magmas, *Geochim. Cosmochim. Acta*, 49, 2309-2322.
- O'Hara, M.J., 1968, The bearing of phase equilibria studies on the origin and evolution of basic and ultrabasic rocks, *Earth Sci. Rev.*, 4, 69-133.
- O'Hara, M.J., 1970, Upper mantle composition inferred from laboratory experiments and observation of volcanic products, *Phys. Earth Planet. Interiors*, 3, 236-245.
- O'Hara, M.J. & R.E. Mathews, 1981, Geochemical evolution of an advancing, periodically tapped, continuously fractionated magma chamber, *J. Geol. Soc. London*, 138, 237-277.
- O'Nions, R.K. & K. Gronvold, 1973, Petrogenetic relationships of acid and basic rocks in Iceland: Sr-isotopes and rare-earth elements in late and postglacial volcanics, *Earth Planet. Sci. Lett.*, 19, 397-409.
- O'Nions, R.K. & R.J. Pankhurst, 1973, Secular variation in the Sr-isotope composition of Icelandic volcanic rocks, *Earth Planet. Sci. Letts.*, 21, 13-21.
- O'Nions, R.K., R.J. Pankhurst, I.B. Fridleifsson & S.P. Jakobsson, 1973, Strontium isotopes and rare earth elements in basalts from the Heimaey and Surtsey volcanic eruptions, *Nature*, 243, 213- 214.
- O'Nions, R.K., R.J. Pankhurst & K. Gronvold, 1976, Nature and development of basalt magma sources beneath Iceland and the Reykjanes Ridge, *J. Petrol.*, 17, 315-338.
- Oskarsson, N., G.E. Sigvaldason & S. Steinthorsson, 1982, A dynamic model of rift zone petrogenesis and the regional petrology of Iceland, *J. Petrol.*, 23, 28-74.
- Oskarsson, N., S. Steinthorsson & G.E. Sigvaldason, 1985, Iceland geochemical anomaly: origin, volcanotectonics, chemical fractionation, and isotope evolution of the crust, *J. Geophys. Res.*, 90, 10011-10026.
- Palmason, G., 1971, Crustal structure of Iceland from explosion seismology, *Visindafelag Isl.*, 40, 187 pp.
- Palmason, G., 1973, Kinematics and heat flow in a volcanic rift zone, with application to Iceland, *Geophys. J. Roy. Astron. Soc.*, 33, 451-481.

- Palmason, G., S. Arnorsson, I.B. Feidleifsson, H. Kristmansdottir, K. Saemundsson, V. Stefansson, B. Steingrimsson, J. Tomasson & L. Kristjansson, 1979, The Iceland crust: evidence from drill hole data on structure and processes, in Talwani, M. et al (eds) Deep Drilling Results in the Atlantic Ocean: Ocean Crust, Maurice Ewing Series, 2, Am. Geophys. Union., 43-65.
- Pearce, J.A. & M.J. Norry, 1979, Petrogenetic implications of Ti, Zr, Y, and Nb variations in volcanic rocks, *Contrib. Mineral. Petrol.*, 69, 33-47.
- Perfit, M.R., D.J. Fornari, A. Malahoff & R.W. Embley, 1983, Geochemical studies of abyssal lavas recovered by DSRV Alvin from Eastern Galapagos Rift, Inca Transform, and Ecuador Rift. 3. Trace element abundances and petrogenesis, *J. Geophys. Res.*, 88, 10551-10572.
- Philpotts, J.A. & C.C. Schnetzler, 1970, Phenocryst-matrix partition coefficients for K, Rb, Sr and Ba, with applications to anorthosites and basalt genesis, *Geochim. Cosmochim. Acta*, 34, 307-322.
- Poreda, R., H. Craig & J-G. Schilling, 1980, $^3\text{He}/^4\text{He}$ variations along the Reykjanes Ridge, *EOS*, 16, 1158.
- Poreda, R., J-G. Schilling & H. Craig, 1986, Helium and hydrogen isotopes in ocean-ridge basalts north and south of Iceland, *Earth Planet. Sci. Letts.*, 78, 1-17.
- Poreda, R., J. Welhan & H. Craig, 1984, Helium isotopes and mantle methane in Icelandic geothermal fluids and volcanic rocks, *EOS*, 65, 1152.
- Presnall, D.C., S.A. Dixon, J.R. Dixon, T.H. O'Donnell, N.L. Brenner, R.L. Schrock & D.W. Dycus, 1978, Liquidus phase relations on the join diopside-forsterite-anorthite from 1 atm to 20 kbar: their bearing on the generation and crystallization of basaltic magma, *Contrib. Mineral. Petrol.*, 66, 203-220.
- Presnall, D.C., J.R. Dixon, T.H. O'Donnell & S.A. Dixon, 1979, Generation of mid-ocean ridge tholeiites, *J. Petrol.*, 20, 3-35.
- Prestvik, T., 1980, Petrology of hybrid intermediate and silicic rocks from Oraefajokull, southeast Iceland, *Geol. Foren. Forhand.*, 101, 299-307.
- Ray, G.L., N. Shimizu & S.R. Hart, 1983, An ion microprobe study of the partitioning of trace elements between clinopyroxene and liquid in the system diopside-albite-anorthite, *Geochim. Cosmochim. Acta*, 47, 2131-2140.
- Roden, M.F., F.A. Frey & D.A. Clague, 1984, Geochemistry of tholeiitic and alkalic lavas from the Koolau Range, Oahu, Hawaii: Implications for Hawaiian volcanism, *Earth Planet. Sci. Letts.*, 69, 141-158.
- Roeder, P.L. & R.F. Emslie, 1970, Olivine-liquid equilibrium, *Contrib. Mineral. Petrol.*, 29, 275-289.
- Roobol, M.J., 1974, The geology of Vesturhorn intrusion, south-eastern Iceland, *Geol. Mag.*, 111, 273-368.
- Ross, J.G. & A.E. Musset, 1976, $^{40}\text{Ar}/^{39}\text{Ar}$ dates for spreading rates in eastern Iceland, *Nature*, 259, 36-38.

- Rutherford, M.J., H. Sigurdsson & S. Carey, 1985, The May 18 eruption of Mount St. Helens: 1. Melt composition and experimental phase equilibria, *J. Geophys. Res.*, 90, 2929-2947.
- Ryan, M.P., 1987, Neutral buoyancy and the mechanical evolution of magmatic systems, in Mysen, B. (ed), *Magmatic Processes: Physicochemical Principles*, 259-288.
- Ryerson, F.J. & P.C. Hess, 1980, The role of P_2O_5 in silicate melts, *Geochim. Cosmochim. Acta*, 44, 611-624.
- Sack, R.O., I.S.E. Carmichael, M.L. Rivers & M.S. Ghiorso, 1980, Ferric-ferrous equilibria in natural silicates at 1 bar, *Contrib. Mineral. Petrol.*, 75, 369-376.
- Sack, R.O., D. Walker & I.S.E. Carmichael, 1987, Experimental petrology of alkalic lavas: constraints on cotectics of multiple saturation in natural basaltic liquids, *Contrib. Mineral. Petrol.*, 96, 1-23.
- Saemundsson, K., 1974, Evolution of the axial rifting zone in northern Iceland and the Tjornes fracture zone, *Geol. Soc. Am. Bull.*, 85, 495-504.
- Saemundsson, K., 1978, Fissure swarms and central volcanoes of the neovolcanic zones of Iceland, in Bowes, D.R. & B.E. Leake (eds) *Crustal evolution in northwestern Britain and adjacent regions*. Liverpool: Seel House, 415-432.
- Saemundsson, K., 1988, Structure and evolutionary trends of volcano systems within the neovolcanic zones of Iceland, in, *Symposium on Geologic and Geochemical Evidence for Segmentation for Continental and Oceanic Rifts*, conference held at WHOI, January, 1988.
- Sanders, C.O., 1984, Location and configuration of magma bodies beneath Long Valley, California, determined from anomalous earthquake signals, *J. Geophys. Res.*, 89, 8287-8302.
- Schaefer, M.W., 1983, Crystal chemistry of ferric-rich fayalites, MS thesis, Mass. Inst. Tech., unpublished.
- Schilling, J-G., 1973, Iceland mantle plume, *Nature*, 246, 141-143.
- Schilling, J-G., P.S. Meyer & R.H. Kingsley, 1982, Evolution of the Iceland hotspot, *Nature*, 296, 313-320.
- Schilling, J-G., P.S. Meyer & R.H. Kingsley, 1983, Rare earth geochemistry of Icelandic basalts: spatial and temporal variations, in *Structure and Development of the Greenland-Scotland Ridge: New Methods and Concepts*, NATO Advanced Res. Inst. Series, 319-342.
- Schnetzler, C.C. & J.A. Philpotts, 1970, Partition coefficients of rare-earth elements between igneous matrix material and rock-forming mineral phenocrysts II, *Geochim. Cosmochim. Acta*, 34, 331-340.
- Shaw, D.M., 1970, Trace element fractionation during anatexis, *Geochim. Cosmochim. Acta*, 34, 237-243.

- Shimizu, H., 1980, Experimental study on rare-earth element partitioning in minerals formed at 20 and 30kb for basaltic systems, *Geochem. Jour.*, 14, 185-202.
- Sigurdsson, H., 1968, Petrology of acid xenoliths from Surtsey, *Geol. Mag.*, 105, 440-453.
- Sigurdsson, H., 1970, The petrology and geochemistry of the Setberg volcanic region and intermediate and acid rocks of Iceland, PhD thesis, Univ. of Durham.
- Sigurdsson, H., 1971, Feldspar relations in Icelandic alkalic rhyolites, *Min. Mag.*, 38, 503-510.
- Sigurdsson, H., 1977, Generation of Icelandic rhyolites by melting of plagiogranites in the oceanic layer, *Nature*, 269, 25-28.
- Sigurdsson, H., 1981, First-order major element variation in basalt glasses from the Mid-Atlantic Ridge: 29 N to 73 N, *J. Geophys. Res.*, 86, 9483-9502.
- Sigurdsson, H. & R.S.J. Sparks, 1978, Lateral magma flow within rifted Icelandic crust, *Nature*, 274, 126-130.
- Sigurdsson, H. & R.S.J. Sparks, 1981, Petrology of rhyolitic and mixed-magma ejecta from the 1875 eruption of Askja, Iceland, *J. Petrol.*, 22, 41-84.
- Sigurdsson, H., J-G., Schilling & P.S. Meyer, 1978, Skagi and Langjokull volcanic zones in Iceland: 1. Petrology and structure, *J. Geophys. Res.*, 83, 3971-3982.
- Sigvaldason, G.E., 1974, The petrology of Hekla and origin of silicic rocks in Iceland, in *Visindafelag Islendinga: The Hekla eruption 1947-1948*, 44 pp.
- Sinton, J.M., D.S. Wilson, D.M. Christie, R.N. Hey & J.R. Delaney, 1983, Petrologic consequences of rift propagation on oceanic spreading ridges, *Earth Planet. Sci. Lett.*, 62, 193-207.
- Sparks, R.S.J. & L.A. Marshall, 1986, Thermal and mechanical constraints on mixing between mafic and silicic magmas, *J. Volcan. Geotherm. Res.*, 29, 99-124.
- Sparks, R.S.J., H. Sigurdsson & L. Wilson, 1977, Magma mixing: a mechanism for triggering acid explosive eruptions, *Nature*, 267, 315-318.
- Sparks, R.S.J., P.S. Meyer & H. Sigurdsson, 1980, Density variation amongst mid-ocean ridge basalts: implications for magma mixing and the scarcity of primitive lavas, *Earth Planet. Sci. Lett.*, 46, 419-430.
- Sparks, R.S.J., H.E. Huppert & J.S. Turner, 1984, The fluid dynamics of evolving magma chambers, *Phil. Trans. Roy. Soc. London*, 310, 511-534.
- Sparks, R.S.J., H.E. Huppert, R.C. Kerr, D.P. McKenzie & S.R. Tait, 1985, Postcumulus processes in layered intrusions, *Geol. Mag.*, 122, 555-568.
- Spera, F.J., D.A. Yuen, J.C. Greer & G. Sewell, 1986, Dynamics of magma withdrawal from stratified magma chambers, *Geology*, 14, 723-726.

- Spulber, S.D. & M.J. Rutherford, 1983, The origin of rhyolite and plagiogranite in oceanic crust: an experimental study, *J. Petrol.*, 24, 1-25.
- Stecher, O., R.W. Carlsson & S.B. Shirey, 1986, Sr and Nd isotopes and the petrological evolution of post-glacial lavas from the Reykjanes Peninsula, Iceland, *EOS*, 67, 413.
- Steinthorsson, S., N. Oskarsson & G.E. Sigvaldason, 1985, Origin of alkali basalts in Iceland: a plate tectonic model, *J. Geophys. Res.*, 90, 10027-10042.
- Steinthorsson, S., 1981, Island og flekakenningin, *Natturu Islands*, 2, 29-63.
- Stolper, E. & D. Walker, 1980, Melt density and the average composition of basalt, *Contrib. Mineral. Petrol.*, 74, 7-12.
- Stormer, J.C., 1975, A practical two-feldspar geothermometer, *Am. Mineral.*, 60, 667-674.
- Sun, S-S. & G.N. Hanson, 1975, Origin of Ross Island basanitoids and limitations upon the heterogeneity of mantle sources for alkali basalts and nephelinites, *Contrib. Mineral. Petrol.*, 52, 77-106.
- Sun, S-S. & B. Jahn, 1975, Lead and strontium isotopes in post-glacial basalts from Iceland, *Nature*, 255, 527-530.
- Sun, S-S. & W.F. McDonough, Chemical and isotopic systematics of oceanic basalts: *implications for mantle composition and processes*, in press.
- Sun, S-S. & R.W. Nesbitt, 1977, Chemical heterogeneity of the Archaen mantle, composition of the earth and mantle evolution, *Earth Planet. Sci. Lett.*, 35, 429-448.
- Sun, S-S., R.W. Nesbitt & A. Sharaskin, 1979, Geochemical characteristics of mid-ocean ridge basalts, *Earth Planet. Sci. Lett.*, 44, 119-138.
- Sun, S-S., M. Tatsumoto & J-G. Schilling, 1975, Mantle plume mixing along the Reykjanes Ridge axis: Lead isotopic evidence, *Science*, 190, 243-247.
- Takahashi, E., 1980, Melting relations of an alkali-olivine basalt to 30 kbar and their bearing on the origin of alkali basaltic magmas, *Yb. Carnegie Inst. Wash.*, 79, 271-276.
- Takahashi, E. & I. Kushiro, 1983, Melting of a dry peridotite at high pressures and basalt magma genesis, *Am. Mineral.*, 68, 859-879.
- Thoroddsen, Th., 1896, Fra det sydostlige Island, *Geograf. Tidskrift (Copenhagen)*, 13, 3-37.
- Thy, P., 1983, Phase relations in transitional and alkali basalt glasses from Iceland, *Contrib. Mineral. Petrol.*, 82, 232-251.
- Tilley, C.E., H.S. Yoder & J.F. Schairer, 1964, New relations on melting of basalts, *Yb. Carnegie Inst. Wash.*, 63, 260-269.

- Torfason, H., 1979, Investigations into the structure of south-eastern Iceland, PhD thesis, Univ. of Liverpool.
- Torgersen, T. & W.J. Jenkins, 1982, Helium isotopes in geothermal systems: Iceland, the Geysers, Raft River and Steamboat Springs, *Geochim. Cosmochim. Acta*, 46, 739-748.
- Tormey, D.R., T.L. Grove & W.B. Bryan, 1987, Experimental petrology of normal MORB near the Kane Fracture Zone: 22°-25° N mid-Atlantic ridge, *Contrib. Mineral. Petrol.*, 96, 121-139.
- Tryggvason, E., 1986, Multiple magma reservoirs in a rift zone volcano: ground deformation and magma transport during the September 1984 eruption of Krafla, Iceland, *J. Volcan. Geotherm. Res.*, 28, 1-44.
- Viereck, L.G., B.J. Griffen, H.-U. Schmincke & R.G. Pritchard, 1982, Volcaniclastic rocks of the Reydarfjörður drill hole, eastern Iceland, 2. Alteration, *J. Geophys. Res.*, 87, 6459-6476.
- Villemont, B., H. Jaffrezid, J.-L. Joron & M. Treuil, 1981, Distribution coefficients of major and trace elements; fractional crystallization in the alkali basalt series of Chaîne des Puys (Massif Central, France), *Geochim. Cosmochim. Acta*, 45, 1997-2016.
- Vink, G.E., 1984, A hotspot model for Iceland and the Voring Plateau, *J. Geophys. Res.*, 89, 9949-9959.
- Vogt, P.R., 1974, The Iceland phenomenon: imprints of a hot spot on the ocean crust, and implications for flow below the plates, in Kristjansson, L. (ed) *Geodynamics of Iceland and the North Atlantic area*. Dordrecht: Reidel, 105-126.
- Wager, L.R. & E.B. Bailey, 1953, Basic magma chilled against acid magma, *Nature*, 172, 68-69.
- Wager, L.R. & G.M. Brown, 1968, *Layered Igneous Rocks*. Oliver & Boyd, London, 588 p.
- Walker, D., T. Shibata & S.E. DeLong, 1979, Abyssal tholeiites from the Oceanographer fracture zone. II, Phase equilibria and mixing, *Contrib. Mineral. Petrol.*, 70, 111-125.
- Walker, G.P.L., 1960, Zeolite zones and dyke distribution in relation to the structure of the basalts in eastern Iceland, *J. Geol.*, 68, 515-528.
- Walker, G.P.L., 1963, The Breiddalur central volcano, eastern Iceland, *Quart. Jour. Geol. Soc. London*, 119, 29-63.
- Walker, G.P.L., 1964, Geological investigations in eastern Iceland, *Bull. Volcan.*, 27, 3-15.
- Walker, G.P.L., 1974, The structure of eastern Iceland, in Kristjansson, L. (ed) *Geodynamics of Iceland and the North Atlantic area*. Dordrecht: Reidel.

- Watkins, N.D. & G.P.L. Walker, 1977, Magnetostratigraphy of eastern Iceland, *Am. Jour. Sci.*, 277, 513-584.
- Watson, E.B., 1976, Two-liquid partition coefficients: experimental data and geochemical applications, *Contrib. Mineral. Petrol.*, 56, 119-134.
- Watson, E.B., 1980, Apatite and phosphorus in mantle source regions: an experimental study of apatite/melt equilibria at pressures to 25 kbar, *Earth Planet. Sci. Lett.*, 51, 322-335.
- Watson, E.B., 1982, Basalt contamination by continental crust: some experiments and models, *Contrib. Mineral. Petrol.*, 80, 83-87.
- Watson, E.B. & T.M. Harrison, 1983, Zircon saturation revisited: temperature and composition effects in a variety of crustal magma types, *Earth Planet. Sci. Lett.*, 64, 295-304.
- Watson, E.B. & S.R. Jurewicz, 1984, Behavior of alkalis during diffusive interaction of granitic xenoliths with basaltic magma, *J. Geol.*, 92, 121-131.
- Watson, E.B. & F.J. Ryerson, 1986, Partitioning of zirconium between clinopyroxene and magmatic liquids of intermediate composition, *Geochim. Cosmochim. Acta*, 50, 2523-2526.
- White, W.M. & A.W. Hofmann, 1982, Sr and Nd isotopic geochemistry of oceanic basalts and mantle evolution, *Nature*, 296, 821-825.
- Wickham, S.M., 1987, The segregation and emplacement of granitic magmas, *J. Geol. Soc. London*, 144, 281-297.
- Wiebe, R.A., 1973, Relations between coexisting basaltic and granitic magmas in a composite dike, *Am. Jour. Sci.*, 273, 130-151.
- Wood, D.A., J.L. Joron, M. Treuil, M. Norry & J. Tarney, 1979, Elemental and Sr isotope variations in basic lavas from Iceland and the surrounding ocean floor, *Contrib. Mineral. Petrol.*, 70, 319-339.
- Wright, T.L. & D.A. Swanson, 1987, The significance of observations at active volcanoes: A review and annotated bibliography of studies at Kilauea and Mount St. Helens, in Mysen, B. (ed), *Magmatic Processes: Physicochemical Principles*, 231-240.
- Wood, D.A., 1976, Spatial and temporal variation in the trace element geochemistry of the eastern Iceland flood basalt succession, *J. Geophys. Res.*, 81, 4353-4360.
- Wood, D.A., 1978, Major and trace element variations in the Tertiary lavas of eastern Iceland and their significance with respect to the Iceland geochemical anomaly, *J. Petrol.*, 19, 392-436.
- Wood, D.A., 1979, A variably veined suboceanic upper mantle - Genetic significance for mid-ocean ridge basalts from geochemical evidence, *Geology*, 7, 499-503.

- Wood, D.A., 1981, Partial melting models for the petrogenesis of Reykjanes Peninsula basalts, Iceland: Implications for the use of trace elements and strontium and neodymium isotope ratios to record inhomogeneities in the upper mantle, *Earth Planet. Sci. Letts.*, 52, 183-190.
- Wood, D.A., J.L. Joron, M. Treuil, M. Norry & J. Tarney, 1979, Elemental and Sr isotope variations in basic lavas from Iceland and the surrounding ocean floor, *Contrib. Mineral. Petrol.*, 70, 319-339.
- Zindler, A., S.R. Hart, F.A. Frey & S.P. Jakobsson, 1979, Nd and Sr isotope ratios and rare earth element abundances in the Reykjanes Peninsula basalts: evidence for mantle heterogeneity beneath Iceland, *Earth Planet. Sci. Lett.*, 45, 249-262.
- Zindler, A., E. Jagoutz & S. Goldstein, 1982, Nd, Sr and Pb isotopic systematics in a three-component mantle: a new perspective, *Nature*, 298, 519-523.

APPENDIX I

REPRESENTATIVE MICROPROBE ANALYSES OF AUSTURHORN MINERALS

Notes:

1. All data were collected using the MIT JEOL 733 Superprobe under the operating conditions specified in the text.
2. Cation sums available upon request.
3. Analyses of plagioclase rims are denoted by the suffix "r" and traverses through individual crystals by the prefix "A" followed by the distance from the center of the crystal in millimeters.

Plagioclase Microprobe Analyses

Sample Analysis		SiO ₂	Al ₂ O ₃	FeO	MgO	CaO	Na ₂ O	K ₂ O	An
Dikes:									
d-42	1	53.90	28.29	1.31	0.09	11.96	4.76	0.16	58
d-42	2	57.36	25.85	0.89	0.06	9.02	6.79	0.29	42
d-42	3	55.98	27.26	1.00	0.05	10.33	6.04	0.19	48
d-42	4	54.33	28.28	1.02	0.08	11.65	5.02	0.14	56
d-43	1	50.26	31.06	0.82	0.06	14.12	3.34	0.17	69
d-43	2	48.95	31.78	0.85	0.03	14.97	2.91	0.08	74
d-43	3	47.73	33.14	0.72	0.07	16.56	2.08	0.09	81
d-43	4	48.39	32.53	0.58	0.09	15.78	2.45	0.07	78
d-49	2	53.91	28.33	0.57	0.03	16.36	4.79	0.44	64
d-49	3	54.35	28.07	0.53	0.02	11.34	5.00	0.47	54
d-49	4	55.14	27.68	0.76	0.04	10.91	5.13	0.53	52
d-49	5	54.12	28.08	0.56	0.06	11.47	4.90	0.47	55
d-49	6	59.37	25.00	0.58	0.06	7.88	6.75	0.76	38
d-49	7	55.26	27.39	0.58	0.04	10.48	5.22	0.48	51
d-49	8	55.55	27.24	0.82	0.02	10.50	5.46	0.50	50
d-5	1	52.83	28.99	0.72	0.16	12.56	4.33	0.18	61
d-5	2	50.43	30.52	0.83	0.15	14.49	3.28	0.13	70
d-5	3	52.50	29.24	0.75	0.14	12.91	4.08	0.17	63
d-5	4	48.45	31.90	0.84	0.11	16.21	2.34	0.08	79
d-5	5	55.57	26.64	1.27	0.18	10.34	5.64	0.26	50
d-61	1	49.25	30.99	0.73	0.20	15.23	2.86	0.09	74
d-61	2	49.07	31.20	0.73	0.12	15.55	2.77	0.08	75
d-61	3	53.12	28.72	0.79	0.17	12.54	4.44	0.14	60
d-61	4	53.85	27.89	1.26	0.20	11.83	5.00	0.12	56
d-61	5	53.79	27.74	1.21	0.20	11.66	5.12	0.14	55
d-81	1-r	68.69	20.46	0.05	0.04	1.04	11.57	0.14	5
d-81	2-r	68.44	20.50	0.33	0.00	1.21	11.39	0.19	5.5
d-82	1	53.20	28.84	1.06	0.05	11.79	4.34	0.08	60
d-82	2	53.68	28.83	0.84	0.42	11.52	4.91	0.11	56
d-82	3	54.02	28.20	1.20	0.04	10.98	5.24	0.10	53
d-82	4	51.71	29.50	2.18	0.25	12.71	4.17	0.13	62
f-61	3	63.46	22.74	0.14	0.00	4.31	7.85	1.91	21
f-61	5	60.82	24.68	0.26	0.00	6.47	7.21	0.98	31

f-62	44	61.01	24.31	0.33	0.01	6.26	7.69	0.96	29
f-62	45	60.48	24.09	0.28	0.01	5.84	7.62	0.84	28
f-62	55	60.82	24.48	0.71	0.00	7.22	7.14	0.30	35
f-62	35	61.62	24.15	0.36	0.01	5.99	7.87	0.71	28
f-62	37	62.01	24.10	0.30	0.01	6.01	7.89	0.64	29

Granophyres:

g-23	1	59.31	24.73	0.37	0.01	6.84	7.73	0.48	32
g-23	2	58.93	25.20	0.55	0.00	7.02	7.75	0.43	33
g-23	3	58.82	24.83	0.44	0.00	7.07	7.62	0.48	33
g-23	4	62.24	22.96	0.20	0.00	4.34	9.04	0.70	20
g-42	1	61.63	23.93	0.31	0.03	5.49	8.27	0.50	26
g-42	2	58.33	26.34	0.37	0.07	8.11	6.92	0.33	39
g-42	3	57.64	26.74	0.35	0.00	8.58	6.48	0.29	42
g-42	4-r	63.84	22.68	0.33	0.03	4.02	9.04	0.69	19
g-42	5	62.89	23.40	0.33	0.02	4.89	8.66	0.49	23
g-42	6	64.90	22.13	0.36	0.02	3.23	9.68	0.59	15
g-42	7-r	65.58	21.44	0.25	0.00	2.58	10.19	0.41	12
g-42	9	62.75	23.58	0.30	0.01	4.92	8.74	0.55	23
g-42	10	63.18	23.01	0.26	0.00	4.28	9.12	0.42	20
g-42	11	64.11	22.55	0.28	0.03	3.84	9.49	0.37	18
g-42	12	61.59	24.30	0.37	0.03	5.62	8.27	0.58	26
g-42	13	63.73	23.00	0.26	0.00	4.23	9.20	0.39	20
g-42	14	64.39	22.52	0.28	0.00	3.63	9.56	0.46	17
g-43	1	63.16	23.12	0.25	0.00	4.60	8.74	0.76	22
g-43	2	60.47	24.26	0.35	0.02	6.41	7.65	0.52	31
g-43	3	58.99	25.42	0.46	0.05	7.54	7.12	0.44	36
g-43	5	60.14	24.52	0.41	0.03	6.59	7.49	0.53	32
g-62	1	59.93	25.13	0.37	0.03	7.09	7.26	0.31	34
g-62	2	60.66	24.80	0.32	0.03	6.73	7.52	0.34	32
g-62	3	59.54	25.62	0.26	0.02	7.39	7.21	0.26	36
g-62	5	59.64	25.02	0.25	0.02	6.95	7.45	0.34	33
g-62	6	59.10	25.37	0.25	0.01	7.31	7.10	0.31	36
g-62	7	59.83	25.14	0.29	0.02	6.75	7.49	0.36	33
g-62	8	60.96	24.37	0.25	0.02	5.99	7.90	0.38	29
g-62	9	60.49	24.93	0.24	0.02	6.49	7.66	0.34	31
g-62	10	63.55	22.92	0.28	0.03	4.22	8.55	0.45	21
g-62	11-r	65.03	21.96	0.20	0.02	3.30	9.48	0.47	16
g-62	12	60.96	24.33	0.31	0.03	6.05	7.89	0.38	29
g-62	13	60.49	24.85	0.27	0.00	6.46	7.43	0.30	32
g-62	14	64.70	22.46	0.29	0.02	3.74	8.31	0.45	19
g-62	16	60.70	24.36	0.26	0.01	6.02	8.04	0.40	29
g-62	17	59.49	25.58	0.29	0.02	6.95	7.46	0.32	33
g-62	18	60.69	24.31	0.43	0.02	5.93	8.21	0.39	28
g-62	19	60.28	24.68	0.24	0.02	6.05	8.08	0.34	29

g-64	2-r	67.21	19.06	0.07	0.00	0.25	7.03	6.47	1.2
------	-----	-------	-------	------	------	------	------	------	-----

g-65	1	65.25	22.07	0.15	0.02	3.36	8.97	0.78	16
------	---	-------	-------	------	------	------	------	------	----

g-65	2	64.45	22.44	0.18	0.02	3.72	9.16	0.62	18
------	---	-------	-------	------	------	------	------	------	----

g-65	3	64.31	22.77	0.16	0.02	4.09	8.83	0.71	20
------	---	-------	-------	------	------	------	------	------	----

g-65	4	62.21	23.75	0.17	0.03	5.29	8.35	0.53	25
------	---	-------	-------	------	------	------	------	------	----

Gabbros:

gb-23	1	50.11	31.98	0.41	0.05	14.75	3.03	0.15	72
-------	---	-------	-------	------	------	-------	------	------	----

gb-23	2	52.67	30.07	0.47	0.08	12.71	4.03	0.28	63
-------	---	-------	-------	------	------	-------	------	------	----

gb-23	3	52.76	30.30	0.44	0.05	12.83	4.00	0.27	63
-------	---	-------	-------	------	------	-------	------	------	----

gb-23	4	50.33	31.33	0.56	0.05	14.23	3.10	0.16	71
-------	---	-------	-------	------	------	-------	------	------	----

gb-23	5	50.68	31.66	0.50	0.07	14.27	3.09	0.18	71
-------	---	-------	-------	------	------	-------	------	------	----

gb-23	6	53.44	30.05	0.48	0.04	12.27	4.11	0.31	61
-------	---	-------	-------	------	------	-------	------	------	----

gb-23	7-r	55.63	28.55	0.34	0.03	10.63	5.21	0.20	52
-------	-----	-------	-------	------	------	-------	------	------	----

gb-24	1	49.16	32.51	0.58	0.05	15.56	2.58	0.10	77
-------	---	-------	-------	------	------	-------	------	------	----

gb-24	2	52.85	30.12	0.56	0.04	12.81	4.12	0.19	63
-------	---	-------	-------	------	------	-------	------	------	----

gb-24	3	52.80	30.20	0.50	0.06	12.72	4.05	0.22	63
-------	---	-------	-------	------	------	-------	------	------	----

gb-24	4	50.82	31.58	0.51	0.04	14.16	3.15	0.16	71
-------	---	-------	-------	------	------	-------	------	------	----

gb-29	A0.15	53.20	29.63	0.56	0.02	21.09	4.28	0.26	72
-------	-------	-------	-------	------	------	-------	------	------	----

gb-29	A0.30	52.92	29.92	0.48	0.00	12.24	4.23	0.26	61
-------	-------	-------	-------	------	------	-------	------	------	----

gb-29	A0.45	53.00	29.84	0.45	0.03	12.34	4.07	0.27	62
-------	-------	-------	-------	------	------	-------	------	------	----

gb-29	A0.60	51.61	29.23	2.46	0.02	12.04	4.33	0.25	60
-------	-------	-------	-------	------	------	-------	------	------	----

gb-29	A0.75	49.12	32.19	0.51	0.00	14.92	2.87	0.12	74
-------	-------	-------	-------	------	------	-------	------	------	----

gb-29	A0.90	49.90	32.35	0.42	0.00	14.94	2.73	0.10	75
-------	-------	-------	-------	------	------	-------	------	------	----

gb-29	A1.05	48.71	32.81	0.55	0.02	15.39	2.56	0.11	76
-------	-------	-------	-------	------	------	-------	------	------	----

gb-29	A1.20	52.98	30.09	0.50	0.02	12.61	4.17	0.23	62
-------	-------	-------	-------	------	------	-------	------	------	----

gb-29	A1.35	52.91	29.73	0.44	0.02	12.32	4.21	0.25	61
-------	-------	-------	-------	------	------	-------	------	------	----

gb-29	A1.50	57.66	27.16	0.35	0.00	9.00	5.76	0.32	45
-------	-------	-------	-------	------	------	------	------	------	----

gb-29	A1.65	57.66	27.24	0.37	0.01	9.03	6.10	0.35	44
-------	-------	-------	-------	------	------	------	------	------	----

gb-29	1	53.20	29.63	0.56	0.02	12.09	4.28	0.26	60
-------	---	-------	-------	------	------	-------	------	------	----

gb-29	2	48.71	32.80	0.55	0.02	15.39	2.56	0.11	76
-------	---	-------	-------	------	------	-------	------	------	----

gb-29	3	52.98	30.09	0.50	0.02	12.61	4.17	0.24	62
-------	---	-------	-------	------	------	-------	------	------	----

gb-29	4-r	57.66	27.16	0.35	0.00	9.00	5.76	0.32	45
-------	-----	-------	-------	------	------	------	------	------	----

gb-29	5	52.88	29.82	0.69	0.06	12.08	4.12	0.31	61
-------	---	-------	-------	------	------	-------	------	------	----

gb-29	6	50.91	31.51	0.57	0.00	14.17	3.27	0.17	70
-------	---	-------	-------	------	------	-------	------	------	----

gb-29	7	50.47	31.68	0.45	0.01	14.32	3.02	0.17	72
-------	---	-------	-------	------	------	-------	------	------	----

gb-29	8	53.03	29.96	0.47	0.03	12.27	4.13	0.27	61
-------	---	-------	-------	------	------	-------	------	------	----

gb-31	1	48.42	32.44	0.44	0.05	15.29	2.66	0.13	76
-------	---	-------	-------	------	------	-------	------	------	----

gb-31	2	47.71	32.77	0.53	0.05	15.63	2.33	0.12	78
-------	---	-------	-------	------	------	-------	------	------	----

gb-31	3-r	53.42	28.74	0.47	0.06	11.34	4.95	0.34	55
-------	-----	-------	-------	------	------	-------	------	------	----

gb-31	4	46.32	33.51	0.57	0.06	16.77	1.68	0.07	84
-------	---	-------	-------	------	------	-------	------	------	----

gb-31	5	46.39	33.56	0.51	0.03	16.40	1.79	0.10	83
-------	---	-------	-------	------	------	-------	------	------	----

gb-32	1	44.94	32.38	0.36	0.05	16.05	1.54	0.06	85
-------	---	-------	-------	------	------	-------	------	------	----

gb-40	1	47.00	34.05	0.54	0.03	16.87	1.64	0.07	85
gb-40	2	51.78	30.80	0.51	0.04	13.30	3.70	0.22	66
gb-40	3	48.67	32.77	0.58	0.04	15.62	2.35	0.14	78
gb-40	4	51.76	30.84	0.49	0.03	13.26	3.73	0.23	65
gb-40	5	50.89	31.70	0.52	0.04	14.23	3.18	0.15	71
gb-41	1	60.31	25.40	0.18	0.00	6.86	6.92	0.53	34
gb-41	2	58.55	26.36	0.19	0.01	7.77	6.73	0.45	38
gb-41	3	58.61	26.58	0.23	0.03	8.27	6.43	0.42	41
gb-41	4	59.11	26.06	0.21	0.02	7.68	6.75	0.46	38
gb-41	5	57.70	26.95	0.20	0.01	8.67	6.30	0.45	42
gb-41	6	58.80	26.14	0.20	0.01	7.86	6.65	0.53	38
gb-41	7	57.72	26.96	0.25	0.00	8.78	6.15	0.39	43
gb-41	8	58.93	25.92	0.19	0.01	7.67	6.81	0.50	37
gb-41	9	57.92	26.70	0.24	0.02	8.54	6.32	0.45	42
gb-42	1	51.59	30.41	0.58	0.05	13.36	3.81	0.12	66
gb-42	2	48.89	32.43	0.62	0.08	15.77	2.40	0.08	78
gb-42	3	48.85	32.13	0.67	0.09	15.53	2.54	0.09	77
gb-42	4	48.92	32.53	0.64	0.04	15.76	2.48	0.05	78
gb-42	5	49.24	32.14	0.68	0.12	15.38	2.63	0.09	76
gb-42	6-r	54.67	28.32	0.69	0.12	11.09	5.08	0.21	54
gb-42	7	52.91	29.73	0.57	0.07	12.60	4.22	0.13	62
gb-42	A0.00	57.66	26.97	0.31	0.06	8.92	6.42	0.30	43
gb-42	A0.50	58.86	26.14	0.35	0.01	7.99	6.94	0.35	38
gb-42	A1.00	49.21	32.27	0.58	0.03	15.45	2.69	0.07	76
gb-42	A1.25	49.28	32.02	0.51	0.02	15.40	2.56	0.07	77
gb-42	A1.50	55.08	28.36	0.40	0.06	11.08	5.04	0.16	54
gb-42	A1.75	55.72	28.11	0.51	0.02	10.68	5.53	0.14	51
gb-43	1	54.02	29.08	0.46	0.05	11.29	4.99	0.16	55
gb-43	2	52.27	30.10	0.39	0.04	12.54	4.33	0.09	61
gb-43	3	52.34	29.97	0.57	0.06	12.62	4.28	0.13	62
gb-43	4	53.36	29.26	0.42	0.02	11.83	4.70	0.13	58
gb-43	5	52.97	29.30	0.66	0.06	12.01	4.55	0.14	59
gb-43	6	52.02	30.00	0.62	0.06	12.88	3.97	0.11	64
gb-43	9	51.94	30.37	0.46	0.04	13.14	4.07	0.10	64
gb-81	1	52.19	30.17	0.77	0.14	13.04	3.93	0.17	64
gb-81	2	53.82	29.16	0.57	0.10	11.61	4.80	0.21	57
gb-81	3	56.11	27.78	0.39	0.08	9.81	5.73	0.29	48
gb-81	4	54.15	29.02	0.55	0.11	11.00	4.87	0.21	55
gb-81	5	48.01	33.41	0.53	0.08	16.46	2.06	0.05	81
gb-81	6	48.29	32.97	0.56	0.10	15.84	2.16	0.05	80
gb-81	7	53.69	29.35	0.69	0.12	11.97	4.63	0.18	58
gb-81	8	50.55	31.30	0.61	0.20	14.44	3.20	0.12	71
gb-81	9-r	59.68	25.62	0.28	0.05	7.33	7.08	0.49	35

gb-82	1	55.32	28.06	0.34	0.04	10.28	5.72	0.18	49
gb-82	2	55.18	28.43	0.26	0.00	10.51	5.46	0.17	51
gb-82	3	59.26	25.63	0.35	0.01	7.27	7.41	0.31	35
gb-82	4	58.97	25.81	0.35	0.02	7.46	7.26	0.34	36
gb-82	5	55.64	27.94	0.38	0.03	10.15	5.79	0.22	49
gb-82	6	59.32	25.34	0.31	0.03	7.25	7.32	0.37	35
gb-82	7	54.58	28.39	0.36	0.01	10.37	5.57	0.17	50
gb-82	8	57.83	26.35	0.43	0.10	8.23	6.66	0.26	40

gb-83	1	56.42	27.08	0.37	0.02	9.37	5.83	0.35	46
gb-83	2	62.24	24.31	0.33	0.04	5.58	8.15	0.72	26
gb-83	3	59.97	25.38	0.32	0.02	7.01	7.45	0.52	33
gb-83	5	60.38	24.85	0.27	0.02	6.58	7.71	0.62	31
gb-83	7	56.08	27.81	0.38	0.01	10.02	5.89	0.30	48
gb-83	8	62.66	23.09	0.27	0.00	4.91	8.44	0.68	23
gb-83	9	56.16	27.55	0.36	0.03	9.75	5.89	0.26	47
gb-83	10	55.88	27.62	0.32	0.00	9.81	5.79	0.30	48
gb-83	12	57.72	26.78	0.43	0.02	8.76	6.56	0.34	42
gb-83	13	57.57	26.75	0.42	0.04	8.67	6.44	0.32	42

gb-84	1	54.96	27.93	0.54	0.07	10.05	5.53	0.22	50
gb-84	2	55.35	27.68	0.64	0.06	9.93	5.72	0.24	48
gb-84	3	54.96	28.00	0.58	0.10	10.27	5.44	0.22	50
gb-84	4	55.11	27.91	0.56	0.09	10.17	5.52	0.23	50
gb-84	5	53.26	29.55	0.49	0.06	11.72	4.60	0.18	58

Pillows:

p-41a	1	52.65	30.05	0.38	0.03	12.51	4.30	0.18	61
p-41a	3	54.24	28.53	0.47	0.04	11.10	5.26	0.24	53
p-41a	5	52.64	29.19	0.57	0.03	11.64	4.79	0.21	57
p-41a	7	52.41	29.73	0.87	0.05	12.88	4.29	0.16	62

p-41b	1	56.94	27.08	0.45	0.06	9.19	6.50	0.34	43
p-41b	3	55.42	28.13	0.61	0.05	10.68	5.58	0.28	51
p-41b	4	58.55	26.25	0.42	0.03	8.05	6.94	0.37	38

p-61a	1	46.89	33.32	0.59	0.12	17.01	1.76	0.05	83
p-61a	2-r	54.66	28.08	0.77	0.09	10.89	5.36	0.26	52
p-61a	3	52.89	29.31	0.59	0.14	12.38	4.21	0.21	61
p-61a	4	46.45	33.37	0.61	0.10	17.55	1.54	0.05	86

p-61b	1-r	54.95	27.94	0.46	0.05	10.08	5.84	0.25	48
p-61b	4-r	54.67	28.11	0.54	0.07	10.60	5.46	0.26	51
p-61b	5	50.03	30.62	0.66	0.16	13.88	3.51	0.12	68
p-61b	6	50.80	30.01	0.83	0.14	12.79	3.97	0.15	64
p-61b	7	52.29	29.12	0.70	0.10	11.94	4.59	0.16	58

p-62a	25	57.79	26.67	0.45	0.02	8.74	6.60	0.41	41
p-62a	26	57.00	26.99	0.48	0.03	9.56	6.23	0.36	45
p-62a	28	54.19	28.30	0.65	0.10	11.66	4.93	0.23	56
p-62a	29	52.02	29.68	0.74	0.12	13.45	3.91	0.13	65
p-62a	30	53.90	28.71	0.93	0.06	11.89	4.74	0.19	58
p-62a	31	54.58	28.43	0.63	0.07	11.38	4.99	0.23	55
p-62a	32	54.67	28.14	0.71	0.35	11.18	4.91	0.29	55
p-62b	14	52.68	29.50	0.68	0.04	12.63	4.23	0.18	62
p-62b	15	52.75	29.37	0.78	0.14	12.74	4.27	0.19	62
p-66	1	52.92	29.40	0.77	0.07	12.38	4.55	0.17	60
p-66	2	58.76	25.88	0.86	0.03	8.12	6.96	0.43	38
p-66	3	53.65	28.97	0.86	0.10	12.23	4.82	0.14	58
p-66	4	48.25	32.52	0.74	0.08	16.09	2.38	0.05	79
p-69	16	53.60	28.84	1.13	0.05	11.90	4.57	0.12	59
p-69	17	52.22	29.59	0.96	0.07	12.96	4.07	0.09	63
p-69	32	51.29	30.31	0.85	0.09	14.06	3.48	0.05	69

Clinopyroxene Microprobe Analyses

Sample	Analysis	SiO ₂	TiO ₂	Al ₂ O ₃	FeO	MnO	MgO	CaO	Na ₂ O	Mg#
Dikes:										
d-42	1	51.89	0.83	1.91	11.81	0.48	13.94	19.24	0.28	67.8
d-43	1	51.16	0.64	1.71	11.39	0.35	14.22	19.93	0.32	69.0
d-5	1	50.98	1.06	2.62	8.86	0.16	15.55	20.34	0.35	75.8
d-5	2	50.37	1.19	3.46	8.39	0.14	14.93	21.03	0.36	76.0
d-61	1	50.02	1.23	3.28	9.33	0.21	15.20	19.67	0.44	74.4
d-61	2	50.70	1.05	2.76	8.89	0.21	15.78	19.63	0.33	76.0
d-81	1	50.88	0.93	2.08	14.08	0.57	13.75	17.83	0.32	63.5
d-81	2	50.50	1.16	2.81	12.30	0.39	13.94	19.17	0.40	66.9
d-81	3	50.12	1.14	2.78	13.80	0.54	13.07	18.48	0.39	62.8
d-81	4a	51.58	0.56	1.09	17.95	0.33	12.36	16.50	0.28	55.1
d-81	4b	50.34	1.42	3.16	10.76	0.34	14.72	19.42	0.36	70.9
d-81	5	51.86	0.75	1.37	12.95	0.50	15.78	16.69	0.30	68.5
d-82	1	47.17	2.15	5.50	9.49	0.19	13.38	21.08	0.38	71.5
d-82	2	47.81	1.74	4.91	10.90	0.31	11.72	21.25	0.97	65.7
d-82	6	47.87	2.09	4.69	11.01	0.29	13.83	19.74	0.43	69.1
d-82	7	49.76	1.27	3.37	8.99	0.23	14.97	21.14	0.40	74.8
d-82	8	47.30	2.25	5.21	10.32	0.21	13.22	20.54	0.55	69.5
d-82	9	51.35	0.89	2.19	8.83	0.23	15.41	20.81	0.31	75.7
d-82	12	51.21	0.50	0.87	14.59	0.46	11.47	20.82	0.54	58.3
f-62	57	52.44	0.09	0.44	14.71	1.34	10.05	21.69	0.36	54.9
f-62	20	51.99	0.01	0.27	14.78	1.15	9.66	21.98	0.50	53.8
Granophyres:										
g-23	1	47.11	0.64	1.16	26.66	1.07	3.55	19.31	0.30	19.2
g-23	2	47.49	0.61	1.00	26.50	1.00	3.53	19.40	0.19	19.2
g-23	3	47.21	0.45	0.59	29.80	1.19	1.03	19.39	0.25	5.8
g-23	4	47.24	0.46	0.68	29.47	1.18	1.46	19.37	0.22	8.1
g-23	5	47.09	0.42	0.54	29.44	1.23	1.31	19.44	0.22	7.3
g-23	6	47.10	0.31	0.37	30.29	1.18	0.90	19.20	0.27	5.0
g-23	7	47.32	0.50	0.82	28.07	1.08	2.47	19.36	0.24	13.6
g-23	8	47.15	0.49	0.79	28.74	1.17	2.04	19.03	0.24	11.2
g-42	1	52.05	0.03	0.27	14.53	1.48	10.43	21.16	0.44	56.1
g-42	2	52.06	0.01	0.16	13.83	1.56	10.57	21.59	0.43	57.6
g-42	3	51.78	0.08	0.26	15.83	1.66	10.24	20.17	0.45	53.5
g-61	1	49.30	0.25	0.40	26.49	1.50	3.57	18.62	0.52	19.4
g-61	2	49.40	0.18	0.34	26.35	1.41	3.80	19.05	0.48	20.4

g-62	1	47.95	0.67	1.30	24.97	0.87	4.43	19.02	0.25	24.0
g-62	2	47.84	0.58	0.81	26.77	1.01	2.69	19.87	0.23	15.2
g-62	3	48.00	0.64	1.09	25.54	1.00	4.27	18.87	0.23	22.9
g-62	4	48.08	0.73	1.21	25.96	1.11	4.22	18.67	0.27	22.5
g-62	5	48.03	0.68	1.18	25.57	0.95	4.42	18.74	0.25	23.5
g-62	6	48.13	0.61	1.11	24.89	0.91	4.29	18.82	0.24	23.5
g-62	7	48.43	0.48	0.75	26.64	0.92	2.58	19.70	0.29	14.7
g-62	8	48.09	0.46	0.75	26.51	0.99	2.59	19.96	0.36	14.8

Gabbros:

gb-23	1	50.81	1.20	3.03	8.48	0.22	15.40	20.58	0.30	76.4
gb-23	2	50.61	1.18	3.44	8.13	0.18	15.21	20.80	0.26	76.9
gb-24	1	52.28	0.49	1.31	11.69	0.46	14.32	19.89	0.27	68.6
gb-24	2	51.10	1.28	2.91	9.41	0.26	15.47	20.37	0.32	74.6
gb-24	3	52.20	0.53	1.46	11.49	0.38	14.72	20.12	0.26	69.5
gb-29	1	53.58	0.14	0.96	7.92	0.30	15.21	21.84	0.30	77.4
gb-29	2	53.35	0.12	0.59	9.59	0.37	14.50	22.00	0.24	72.9
gb-29	3	52.57	0.36	1.44	9.02	0.34	14.73	21.67	0.34	74.4
gb-30	19	50.05	1.07	2.63	9.60	0.28	15.22	20.85	0.27	73.9
gb-30	20	49.94	1.06	2.65	10.03	0.28	15.79	20.20	0.32	73.7
gb-30	24	52.27	0.18	0.89	8.69	0.29	15.07	22.43	0.17	75.6
gb-30	35	50.87	1.17	2.73	9.82	0.20	14.61	20.87	0.00	72.6
gb-30	37	50.08	1.31	2.93	9.82	0.32	14.77	20.72	0.32	72.8
gb-31	1	50.92	0.63	1.64	10.24	0.30	14.97	20.37	0.28	72.3
gb-31	2	50.61	0.99	2.93	7.52	0.22	16.47	20.74	0.27	79.6
gb-31	3	50.33	1.06	2.78	8.03	0.20	15.87	20.87	0.30	77.9
gb-31	4	50.69	0.80	1.95	10.30	0.28	15.10	20.25	0.27	72.3
gb-31	5	50.64	0.92	2.73	7.43	0.19	16.44	21.05	0.26	79.8
gb-31	6	51.19	0.55	1.63	9.99	0.29	15.23	20.74	0.27	73.1
gb-32	1	50.11	0.85	2.86	7.65	0.21	14.83	20.83	0.34	77.6
gb-32	2	52.00	0.83	2.45	7.45	0.27	15.42	21.78	0.31	78.7
gb-32	3	51.61	0.87	2.86	8.06	0.22	15.01	21.36	0.31	76.8
gb-34	41	52.23	0.46	1.54	8.36	0.47	15.78	20.70	0.39	77.1
gb-34	42	52.82	0.50	1.61	8.47	0.42	15.80	20.90	0.34	76.9
gb-34	44	51.98	0.50	1.44	8.83	0.38	15.14	20.75	0.30	75.3
gb-40	33	50.42	1.32	3.17	9.42	0.33	14.85	20.59	0.31	73.7
gb-40	34	50.37	1.33	3.21	9.55	0.18	15.07	20.54	0.30	73.8
gb-40	1	51.28	1.01	2.59	9.18	0.22	15.57	20.20	0.34	75.1
gb-40	2	50.30	1.31	3.28	9.47	0.23	15.00	20.28	0.36	73.8
gb-41	1	50.38	0.45	1.05	17.71	0.59	9.73	19.38	0.34	49.5
gb-41	2	50.27	0.55	1.28	16.62	0.55	10.61	19.44	0.33	53.2

gb-42	1	50.18	1.29	4.08	8.05	0.18	15.08	20.92	0.37	76.9
gb-42	2	51.88	0.96	2.09	9.46	0.31	15.42	20.02	0.39	74.3
gb-42	3	51.79	1.15	2.55	9.33	0.27	15.44	20.25	0.38	74.7
gb-42	4	51.64	1.02	2.21	9.15	0.22	15.62	19.96	0.41	75.3
gb-42	5	51.33	1.18	2.59	9.19	0.22	15.38	20.19	0.38	74.9
gb-42	6	51.21	1.03	3.47	7.34	0.16	15.70	21.27	0.36	79.2
gb-43	1	51.19	1.00	2.48	9.25	0.31	15.04	20.35	0.33	74.3
gb-43	2	49.76	1.43	3.83	8.99	0.18	14.71	20.94	0.38	74.5
gb-43	3	51.04	1.04	2.49	9.93	0.31	14.86	20.08	0.38	72.7
gb-43	4	49.47	1.58	3.95	9.55	0.27	14.17	20.46	0.40	72.6
gb-43	5	50.81	1.15	2.72	9.31	0.27	14.88	20.29	0.39	74.0
gb-43	6	49.58	1.47	3.97	8.66	0.14	14.62	20.93	0.37	75.1
gb-81	1	47.87	2.15	5.83	9.02	0.14	13.63	21.06	0.38	72.9
gb-81	2	49.67	1.68	3.87	9.61	0.23	14.27	20.74	0.38	72.6
gb-81	3	48.27	1.81	5.43	9.05	0.21	13.78	21.34	0.36	73.1
gb-82	1	51.78	0.05	0.30	15.40	0.43	10.75	21.16	0.31	55.4
gb-82	2	52.57	0.02	0.22	13.48	0.45	11.85	21.64	0.25	61.0
gb-82	3	52.40	0.28	0.69	12.34	0.44	13.43	20.34	0.28	66.0
gb-83	1	52.13	0.34	0.87	11.83	0.46	13.59	20.16	0.35	67.2
gb-84	1	51.44	0.76	1.85	10.46	0.36	15.29	19.71	0.34	72.3
gb-84	2	51.60	0.76	1.77	10.89	0.38	15.61	19.66	0.33	71.9
gb-84	3	51.85	0.64	1.60	11.33	0.49	15.14	19.43	0.38	70.4
gb-84	5	50.89	0.97	2.81	8.08	0.22	16.14	20.90	0.32	78.1
gb-84	6	51.18	0.81	1.92	10.48	0.37	15.68	19.99	0.33	72.7
gb-84	7	51.55	0.79	1.80	9.98	0.35	15.35	20.47	0.37	73.3
gb-84	8	50.27	1.26	3.66	8.61	0.15	15.27	21.41	0.38	76.0
gb-84	9	50.85	0.96	2.87	9.51	0.25	14.84	21.15	0.39	73.5
gb-84	10	50.12	1.21	3.68	8.65	0.18	15.34	20.71	0.38	76.0
gb-84	11	51.31	0.88	2.07	10.79	0.40	15.52	19.55	0.38	71.9
gb-84	12	52.51	0.16	0.57	11.51	0.62	14.00	21.11	0.28	68.4
gb-84	14	51.59	0.87	1.86	10.35	0.40	15.83	19.88	0.35	73.2
gb-84	15	51.67	0.87	1.82	10.42	0.38	15.51	19.98	0.34	72.6
gb-84	17	49.37	1.33	3.51	8.70	0.19	15.01	20.91	0.38	75.5
gb-84	18	50.73	0.90	1.89	10.55	0.40	15.32	19.63	0.38	72.1
gb-84	19	48.79	1.52	4.00	8.72	0.17	14.75	21.08	0.40	75.1
gb-84	20	48.15	1.65	4.53	8.66	0.17	15.06	20.57	0.37	75.6

Pillows:

p-41a	1	51.68	0.21	0.67	11.66	0.31	13.29	20.80	0.33	67.0
p-41a	2	51.18	0.40	1.25	10.56	0.29	13.66	21.11	0.32	69.7
p-41a	4	52.75	0.10	0.47	11.26	0.29	13.58	22.67	0.27	68.2

p-41b	2	49.69	1.54	3.47	11.14	0.35	14.42	20.07	0.36	69.8
p-41b	4	49.06	1.92	4.15	11.24	0.38	14.29	19.63	0.42	69.4
p-41b	5	51.84	0.20	0.47	15.66	0.64	11.73	19.91	0.40	57.2
p-41b	6	50.48	1.33	3.12	11.42	0.41	14.92	19.36	0.37	69.9
p-41b	7	51.72	0.67	2.21	10.39	0.46	14.65	20.42	0.58	71.5
p-41b	8	51.59	0.09	0.36	17.02	0.63	10.44	20.77	0.28	52.2
p-61a	1	46.87	2.27	5.97	10.20	0.32	13.56	20.28	0.49	70.3
p-61a	2	48.83	1.74	4.07	9.31	0.22	14.28	20.38	0.40	73.2
p-61a	3	49.03	1.60	4.65	8.38	0.17	14.58	20.72	0.39	75.6
p-61a	4	52.13	0.24	0.84	11.97	0.31	12.23	22.06	0.37	64.5
p-61b	1	47.26	2.25	4.98	10.17	0.24	14.11	19.97	0.43	71.2
p-61b	2	47.47	2.15	4.64	9.95	0.26	14.03	20.16	0.47	71.5
p-61b	3	49.15	1.63	3.53	9.40	0.27	14.82	20.54	0.40	73.7
p-61b	4	48.01	1.74	4.73	8.86	0.19	14.59	20.86	0.37	74.6
p-61b	5	49.87	1.36	2.94	9.54	0.27	15.54	19.92	0.31	74.4
p-61b	6	47.13	2.32	5.12	10.31	0.31	14.04	20.00	0.44	70.8
p-61b	7	47.71	2.00	4.71	9.76	0.26	14.23	20.29	0.41	72.2
p-62a	1a	52.38	0.17	0.54	12.08	0.35	13.08	21.24	0.31	65.9
p-62a	1b	52.71	0.15	0.54	12.17	0.35	13.03	21.32	0.36	65.6
p-62a	1c	52.80	0.27	0.80	10.99	0.41	13.67	21.29	0.41	68.9
p-62a	2	45.71	2.94	6.25	11.18	0.20	12.16	20.93	0.48	66.0
p-62a	3a	52.25	0.15	0.53	12.16	0.40	13.04	21.14	0.30	65.6
p-62a	3b	46.01	2.74	6.43	10.26	0.16	11.96	21.72	0.44	67.5
p-62a	3c	51.99	0.47	1.52	9.67	0.30	13.72	22.35	0.33	71.7
p-62a	3d	50.65	1.14	2.75	10.00	0.33	14.49	20.76	0.39	72.1
p-62a	4a	49.94	1.37	3.51	9.41	0.26	14.08	21.30	0.37	72.7
p-62a	4b	50.69	1.23	3.13	9.49	0.30	14.38	21.36	0.37	73.0
p-62a	4c	52.25	0.15	0.44	12.28	0.34	12.98	21.50	0.28	65.3
p-62a	4d	52.81	0.16	0.56	12.39	0.36	13.04	21.42	0.33	65.2
p-62a	5	52.58	0.14	0.70	11.39	0.30	13.01	22.44	0.29	67.1
p-62a	6	53.01	0.16	1.67	10.77	0.30	12.59	22.13	0.48	67.6
p-62a	7a	52.66	0.26	1.20	9.27	0.22	13.85	23.23	0.27	72.7
p-62a	7b	52.76	0.16	0.74	10.90	0.26	13.18	22.94	0.25	68.3
p-62a	7c	52.63	0.13	0.53	12.40	0.37	12.88	22.00	0.32	64.9
p-62a	7d	52.63	0.11	0.50	12.14	0.32	12.76	21.83	0.30	65.2
p-62b	1a	51.94	0.11	0.48	13.13	0.34	12.17	21.31	0.30	62.3
p-62b	1b	53.38	0.02	0.26	8.62	0.34	14.58	23.00	0.24	75.1
p-62b	2	47.94	1.89	5.57	9.33	0.23	14.16	19.86	0.41	73.0
p-62b	3a	51.14	0.98	2.29	9.13	0.25	15.96	19.69	0.30	75.7
p-62b	3b	48.42	1.79	4.67	9.65	0.19	13.74	20.99	0.44	71.7
p-62b	4a	53.17	0.04	0.27	9.35	0.26	13.91	22.93	0.20	72.6
p-62b	4b	52.43	0.14	0.49	12.41	0.39	12.67	21.17	0.35	64.5
p-62b	4c	52.58	0.15	0.50	12.55	0.45	12.62	21.19	0.34	64.2
p-62b	5	47.88	2.01	4.93	9.38	0.17	13.74	20.90	0.44	72.3
p-62b	6	52.13	0.25	0.75	12.35	0.55	13.27	20.32	0.35	65.7

p-66	1	49.52	1.48	3.60	9.45	0.22	14.85	20.74	0.36	73.7
p-66	2	52.23	0.29	0.74	13.63	0.48	13.22	20.17	0.30	63.3
p-66	3	51.73	0.18	0.47	14.70	0.44	11.78	20.80	0.33	58.8
p-66	4	51.36	0.94	2.09	9.92	0.27	16.45	19.16	0.27	74.7
p-66	5	49.49	1.55	3.40	10.82	0.23	14.63	19.87	0.37	70.0
p-66	6	51.67	0.15	0.38	14.71	0.43	11.87	20.68	0.32	59.0
p-66	7	49.52	1.31	3.75	8.99	0.22	15.34	20.32	0.38	75.2
p-66	8	51.54	0.22	0.68	13.84	0.39	11.92	20.99	0.39	60.5
p-66	9	51.62	0.20	0.69	14.28	0.53	12.40	20.41	0.32	60.7
p-66	10	51.54	0.17	0.37	14.82	0.50	11.12	21.33	0.33	57.2
p-66	11	46.71	1.99	4.34	10.89	0.27	13.71	18.99	0.35	69.2
p-66	12	47.14	1.49	3.78	10.14	0.28	14.53	19.32	0.34	71.9
p-69	1	49.22	2.07	4.24	10.66	0.25	13.69	19.83	0.61	69.6
p-69	2	48.86	1.87	4.41	10.77	0.25	14.13	19.46	0.35	70.0
p-69	3	49.15	1.39	4.18	8.76	0.23	14.79	20.24	0.39	75.1
p-69	4	49.78	1.33	3.99	8.51	0.15	14.87	20.63	0.34	75.7

Olivine Microprobe Analyses

Sample Analysis		SiO ₂	TiO ₂	Al ₂ O ₃	FeO	MnO	MgO	CaO	Fo
g-23	1	30.27	0.10	0.05	65.78	3.20	0.84	0.36	2.2
gb-32	1	54.42	0.43	1.07	15.50	0.39	26.97	1.32	75.6
gb-32	2	36.98	0.02	0.02	29.87	0.43	32.48	0.05	66.0
gb-32	3	37.24	0.02	0.00	25.37	0.42	35.42	0.06	71.3
gb-32	4	37.38	0.01	0.01	26.19	0.35	35.32	0.05	70.6
gb-32	5	37.23	0.02	0.01	26.87	0.45	34.73	0.04	69.7
gb-42	1	38.17	0.01	0.02	22.22	0.32	39.00	0.25	75.8
gb-42	2	36.66	0.03	0.04	31.75	0.58	31.55	0.21	63.9
gb-42	3	36.86	0.01	0.03	30.26	0.56	32.88	0.18	65.9
gb-42	4	36.94	0.02	0.03	29.45	0.54	33.19	0.23	66.8
gb-42	5	36.64	0.03	0.03	30.93	0.56	32.22	0.18	65.0
gb-42	6	37.41	0.00	0.02	26.86	0.48	35.85	0.11	70.4
gb-42	7	37.02	0.02	0.01	29.69	0.53	33.36	0.14	66.7
p-69	34	37.67	0.03	0.02	22.70	0.40	38.87	0.12	75.3

Amphibole Microprobe Analyses

Sample	Analysis	SiO ₂	TiO ₂	Al ₂ O ₃	FeO	MnO	MgO	CaO	Na ₂ O	K ₂ O
g-43	1	46.32	1.22	4.75	22.36	0.58	9.56	9.50	2.18	0.63
g-43	2	45.62	1.79	5.91	20.47	0.48	10.42	9.77	2.38	0.78
g-43	3	46.39	1.33	4.79	22.89	0.55	9.22	9.70	2.07	0.63
g-43	4	47.22	1.91	4.91	18.43	0.49	11.15	10.32	2.35	0.73
g-43	5	45.97	1.31	5.22	22.30	0.48	9.26	9.85	2.18	0.77
g-65	1	44.33	1.89	6.90	20.88	0.36	9.49	10.21	2.15	0.88
g-65	2	45.26	1.64	6.27	21.13	0.38	9.65	10.12	2.05	0.77

APPENDIX II. REPLICATE ANALYSES
INSTRUMENTAL NEUTRON ACTIVATION ANALYSIS

	p-61a		p-62b		p-62a		d-46		d-43		gb-30 avg (10)	std	%dev
	i	ii	i	ii	i	ii	i	ii	i	ii			
La	14.72	14.92	18.36	19.96	17.17	17.10	10.80	10.47	12.34	12.46	2.47	.06	2.4
Ce	38.7	35.3	48.5	50.7	43.2	41.9	27.8	27.0	32.4	33.0	7.22	.18	2.5
Nd	22.4	23.4	27.9	29.3	26.0	25.7	17.5	17.9	20.1	21.3	5.88	.30	5.1
Sm	5.73	5.66	7.72	7.62	6.61	6.65	5.34	5.12	5.43	5.31	2.01	.04	2.0
Eu	2.12	2.01	2.50	2.60	2.47	2.31	1.90	1.81	1.83	1.90	.96	.02	2.1
Tb	1.0	1.0	1.1	1.3	1.20	1.02	1.1	1.0	0.9	0.9	.4	.1	25
Yb	2.15	2.18	2.69	3.09	2.52	2.67	2.91	2.91	2.21	2.12	.94	.06	6.4
Lu	0.29	0.37	0.41	0.44	0.35	0.37	0.44	0.42	0.32	0.35	.13	.01	7.7
Hf	4.3	4.3	6.1	5.9	4.9	4.5	3.0	3.0	3.5	3.5	1.2	.10	8.3
Th	0.9	0.8	1.5	1.2	1.0	0.9	0.6	0.5	0.7	0.8	.2	.1	50
Ta	1.01	0.96	1.20	1.26	1.05	1.09	0.70	0.70	0.94	0.90	.20	.03	15
Cr	174	159	115	117	138	132	168	159	45.1	43.0	14.3	1.2	8.4
Co	46.5	45.6	40.1	41.4	45.9	44.9	50.7	39.7	43.1	43.1	71.9	1.8	2.5
Sc	30.6	29.3	30.0	30.7	33.3	32.1	40.9	39.7	29.9	30.1	49.6	1.1	2.2

Note: Sample gb-30 has the lowest abundances of incompatible elements analyzed in Austurhorn samples, hence the reported per cent deviations based on replicate analyses is maximized.

X-RAY FLUORESCENCE - MAJOR ELEMENTS

	BHVO-1 (71 analyses)	
	average	std
SiO ₂	50.32	.16
TiO ₂	2.76	.01
Al ₂ O ₃	13.86	.06
Fe ₂ O ₃	12.21	.02
MgO	7.21	.07
MnO	.17	.02
CaO	11.46	.09
Na ₂ O	2.36	.29
K ₂ O	.55	.02
P ₂ O ₅	.28	.003

X-RAY FLUORESCENCE - MAJOR ELEMENTS

	BHVO-1 (71 analyses)	
	average	std
SiO2	50.32	.16
TiO2	2.76	.01
Al2O3	13.86	.06
Fe2O3	12.21	.02
MgO	7.21	.07
MnO	.17	.02
CaO	11.46	.09
Na2O	2.36	.29
K2O	.55	.02
P2O5	.28	.003

- p-66: Glomerocrysts of plag + cpx + opaques. Local "pockets" of 2-5mm plag, cpx (sometimes altered to amphibole) but majority of sample is <1mm. Oxides acicular near contact with granophyre.

C. Felsic Samples

- g-1: Salmon granophyre. Tabular plag (3mm max) with granophyric matrix. Zoning over outer <1mm of plag, polysynthetic twinning rare. Minor cpx, locally altered to opaques + amphibole. Abundant allanite, minor biotite, epidote, chlorite.
- g-22: Granophyre. Two generations of plag: smaller (<2mm) are dusty throughout, and larger (2-5mm) dusty on outer margins only. "Dust" probably micron-scale intergrowth of quartz+ksp. Minor (5%) cpx, locally altered to amphibole + opaques. Local zoisite, epidote.
- g-23: Average 5-7mm plag and cpx. Cpx locally rosetta morphology, also acicular. Minor olivine. Plag generally turbid if <7mm; locally find granophyric intergrowths surrounding small plag crystals.
- g-41: No granophyre. Sample dominantly plag, with dusty mantles that appear to be K-feldspar. Minor cpx, often altered along cleavage.
- g-61: Salmon granophyre. Dusty mantles on tabular plag (<5mm), with cpx and opaques interstitial to large plag. Some cpx rimmed by amphibole.
- g-62: Average 5-8mm plag and cpx. Cpx locally rosetta morphology. Plag pervasively dusty on outer margins. Local quartz, hematite (after magnetite?).
- g-63: No granophyre. Tabular plag with interstitial quartz, K-feldspar and cpx with amphibole rims. Few opaques.
- g-64: No granophyre. Tabular to subhedral plag (2-4mm) with interstitial subhedral quartz, K-feldspar and cpx/amphibole. Opaques euhedral, locally altered to hematite.
- g-65: Spiky (1-2mm) plag and amphibole (~10-12%), with scattered tabular plag (2-4mm). Some amphiboles have cpx cores. Interstitial amph, opaques, feldspar.
- g-81: Grey granophyre. Plag 60-70%, pervasively dusty. Local granophyre, local K-feldspar mantles to plag crystals. Polysynthetic twinning absent. Cpx usually replaced by amphibole and opaques.
- g-82: Granophyre. Tabular plag with interstitial quartz, K-feldspar and opaques. No amphibole, cpx.
- g-83: No granophyre. Coarse (3-7mm) tabular plag, with interstitial quartz, K-feldspar and amphibole (after cpx). Abundant euhedral opaques, primarily as alteration products of cpx.

Appendix IV

Temperature and Oxygen Fugacity for Icelandic samples

Part A. Key to analyses plotted in text

Location	Sample	Temp	del f O ₂	-log f O ₂
Austurhorn	f-61	955	+1.37	9.89
	gb-32	701	+1.22	17.13
	gb-34 a	1099	+ .66	8.86
	gb-34 b	1098	+ .66	8.88
	gb-34 c	1127	+ .75	8.42
	gb-34 d	1084	+ .61	9.12
	gb-34 e	1064	+ .54	9.46
	gb-40	909	- .10	12.50
	p-67 a	742	+ .51	15.27
	p-67 b	763	+ .36	14.94
	p-67 c	762	+ .44	14.88
	p-67 d	749	+ .54	15.10
	p-67 e	755	+ .49	15.00
	p-67 f	767	+ .41	14.81
Askja	AS-162 a	945	+1.02	10.76
	AS-162 b	998	+ .85	10.10
	AS-162 c	949	+1.00	10.70
	AS-162 d	951	+1.05	10.63
	AS-162 e	1005	+ .87	9.96
	AS-162 f	955	+1.03	10.57
	AS-5 a	1200	+ .65	7.65
	AS-5 b	1158	+ .70	8.08
	AS-5 c	1160	+ .70	8.07
Eldfell	VE-111 a	1023	- .46	11.03
	VE-111 b	1027	- .46	10.97
	VE-119 1105	- .16	9.60	
Jan Mayen	69-p	749	- .73	15.55
	69-g	887	- .95	13.74
	48-m	927	+ .34	11.74
	63-m	784	-1.25	16.08
	146-p a	754	-1.70	17.21
	146-p b	975	- .29	11.58
	26-g a	920	- .91	13.12
	26-g b	925	- .88	12.99
	166-g	889	- .84	13.57
	27-lam	952	- .01	11.66

Sources of data: Askja Sigurdsson & Sparks, 1981
 Eldfell Jakobsson et al., 1973
 Jan Mayen Imsland, 1986

p=phenocryst, g=groundmass, m=microphenocryst, lam=sandwich lamellae
 del f O₂ = log units above (+) or below (-) QFM buffer

Part B. Magnetite-Ilmenite Geothermometry Comparison

Sample	PSM B&L ^a T	fO ₂	PSM A&L ^b T	fO ₂	THF S&L ^c T	fO ₂	THF A&L ^d T	fO ₂
HS-709a	975	-12.0	903	-13.9	1048	-10.8	1158	-9.3
HS-709b	1020	-11.0	949	-12.7	752	-17.7	802	-16.6
HS-713	915	-13.0	810	-15.9	665	-18.9	731	-18.2
HS-715	985	-11.8	923	-13.5	671	-18.6	729	-18.0
HS-729a	975	-11.2	837	-15.6	816	-16.0	878	-14.6
HS-729b	1000	-11.6	857	-15.0	863	-14.7	938	-13.3
HS-743a	1000	-11.5	913	-13.7	898	-13.8	972	-12.5
HS-734b	1020	-11.0	943	-12.8	901	-13.6	961	-12.5
HS-743	935	-12.7	791	-16.7	758	-17.4	804	-16.4

Key to analyses:

- a Usp, Ilm from Meyer (1984); Buddington & Lindsley (1964) geothermometer
- b Usp, Ilm from Meyer (1984); Andersen & Lindsley (1988) geothermometer
- c Usp, Ilm calculated by Furman; Spencer & Lindsley (1982) geothermometer
- d Usp, Ilm calculated by Furman; Andersen & Lindsley (1988) geothermometer

refer to text to note that all calculation schemes define a single T-f O₂ curve
all temperatures in degrees Centigrade

DOCUMENT LIBRARY

July 5, 1989

Distribution List for Technical Report Exchange

Attn: Stella Sanchez-Wade
Documents Section
Scripps Institution of Oceanography
Library, Mail Code C-075C
La Jolla, CA 92093

Hancock Library of Biology &
Oceanography
Alan Hancock Laboratory
University of Southern California
University Park
Los Angeles, CA 90089-0371

Gifts & Exchanges
Library
Bedford Institute of Oceanography
P.O. Box 1006
Dartmouth, NS, B2Y 4A2, CANADA

Office of the International
Ice Patrol
c/o Coast Guard R & D Center
Avery Point
Groton, CT 06340

Library
Physical Oceanographic Laboratory
Nova University
8000 N. Ocean Drive
Dania, FL 33304

NOAA/NESDIS Miami Library Center
4301 Rickenbacker Causeway
Miami, FL 33149

Library
Skidaway Institute of Oceanography
P.O. Box 13687
Savannah, GA 31416

Institute of Geophysics
University of Hawaii
Library Room 252
2525 Correa Road
Honolulu, HI 96822

Library
Chesapeake Bay Institute
4800 Atwell Road
Shady Side, MD 20876

MIT Libraries
Serial Journal Room 14E-210
Cambridge, MA 02139

Director, Ralph M. Parsons Laboratory
Room 48-311
MIT
Cambridge, MA 02139

Marine Resources Information Center
Building E38-320
MIT
Cambridge, MA 02139

Library
Lamont-Doherty Geological
Observatory
Columbia University
Palisades, NY 10964

Library
Serials Department
Oregon State University
Corvallis, OR 97331

Pell Marine Science Library
University of Rhode Island
Narragansett Bay Campus
Narragansett, RI 02882

Working Collection
Texas A&M University
Dept. of Oceanography
College Station, TX 77843

Library
Virginia Institute of Marine Science
Gloucester Point, VA 23062

Fisheries-Oceanography Library
151 Oceanography Teaching Bldg.
University of Washington
Seattle, WA 98195

Library
R.S.M.A.S.
University of Miami
4600 Rickenbacker Causeway
Miami, FL 33149

Maury Oceanographic Library
Naval Oceanographic Office
Stennis Space Center
NSTL, MS 39522-5001

Marine Sciences Collection
Mayaguez Campus Library
University of Puerto Rico
Mayaguez, Puerto Rico 00708

REPORT DOCUMENTATION PAGE	1. REPORT NO. WHOI-89-29	2.	3. Recipient's Accession No.
4. Title and Subtitle Evolution of Icelandic Central Volcanoes: Evidence from the Austurhorn Plutonic and Vestmannaeyjar Volcanic Complexes			5. Report Date September 1989
7. Author(s) Tanya Helen Furman			8. Performing Organization Rept. No. WHOI-89-29
9. Performing Organization Name and Address The Woods Hole Oceanographic Institution Woods Hole, Massachusetts 02543, and The Massachusetts Institute of Technology Cambridge, Massachusetts 02139			10. Project/Task/Work Unit No.
			11. Contract(C) or Grant(G) No. (C) (G)
12. Sponsoring Organization Name and Address The Office of Naval Research through the Massachusetts Institute of Technology			13. Type of Report & Period Covered Ph.D. Thesis
			14.
15. Supplementary Notes This thesis should be cited as: Tanya Helen Furman, 1989. Evolution of Icelandic Central Volcanoes: Evidence from the Austurhorn Plutonic and Vestmannaeyjar Volcanic Complexes. Ph.D. Thesis, MIT/WHOI, WHOI-89-29.			
16. Abstract (Limit: 200 words) <p>There are several aspects of Icelandic magmatism which are not predicted from its geographic position along the mid-Atlantic Ridge. Specifically, local occurrences of alkalic lavas and oversaturated silicic magmas are uncommon in a mid-ocean ridge setting. This study uses field, petrologic and geochemical data to understand the petrogenesis of these diverse lava types. Two areas have been investigated: the volcanic Vestmannaeyjar archipelago and the hypabyssal Austurhorn intrusive complex. Vestmannaeyjar is located at the tip of a transgressive ridge segment (the eastern neovolcanic zone); the most recent eruption in this area was Eldfell in 1973. Austurhorn is an evolved central volcano in southeastern Iceland which was active approximately 6-7 Ma and has been exhumed by glaciation. In both areas, the relative contributions of fractional crystallization and crustal melting to geochemical trends among cogenetic magmas have been assessed, and fractionation processes are found to dominate. Vestmannaeyjar moderate pressure (~8 kbar) fractionation of mantle-derived liquids can produce the observed range of erupted compositions. Radiogenic and stable isotope data support this scenario. At Austurhorn sampled mafic and felsic magmas differentiated at near surface conditions (<~2 kbars). The cumulus mineralogy of associated gabbros supports this model.</p>			
17. Document Analysis a. Descriptors			
1. Iceland			
2. petrology			
3. silicic			
b. Identifiers/Open-Ended Terms			
c. COSATI Field/Group			
18. Availability Statement Approved for publication; distribution unlimited.	19. Security Class (This Report) UNCLASSIFIED	21. No. of Pages 373	
	20. Security Class (This Page)	22. Price	